Journal of Double Star Observations

VOLUME 14 NUMBER 2 April 1, 2018

Inside this issue:

Inside this issue:

An Astrometric Observation of Binary Star System WDS 15559-0210 at the Great Basin Observatory

Lila Musegades[1,2], Cole Niebuhr[2], Mackenzie Graham[1,2], Andrew Poore[1], Rachel Freed[3,4], John W. Kenney, III[1], and Russell Genet[3,4]

1. Concordia University, Irvine, California
2. Global Science Directive, Las Vegas, Nevada
3. Cuesta College, San Luis Obispo, California
4. California Polytechnic State University, San Luis Obispo, California

Abstract: Researchers at Concordia University Irvine measured the position angle and separation of the double star system WDS 15559-0210 using a SBIG STX-16803 CCD camera on the PlaneWave 0.7-m CDK 700 telescope at the Great Basin Observatory. Images of the binary star system were measured using AstroImageJ software. Twenty observations of WDS 15559-0210 were measured and analyzed. The calculated mean resulted in a position angle of 345.95° and a separation of 5.94". These measurements were consistent with the previous values for this binary system listed in the Washington Double Star Catalog.

Introduction

Double stars are two stars that appear to be close together from Earth's perspective. Observations can be made over decades to determine whether double stars are gravitationally-bound binaries, (that is, physical pairs travelling together but not in a mutual orbit) or chance optical alignments of separate stars. If the star system is a binary, an orbit can be resolved and, if we know the distance to the system, the total system mass ("dynamical mass") can be computed. Knowing the stellar mass is critical to understanding the life cycle of the star (Genet 2016).

Binary star research is a new endeavor at Concordia University Irvine (CUI) and has great scientific potential and educational merit. In this pilot study, a student-led team at CUI made observations of WDS 15559-0210 using the remotely-controlled telescope (Figure 2) at the newly constructed Great Basin Observatory (GBO). The purpose of these observations was to introduce the student research team to astrometric data collection and analysis and to use the GBO as a research instrument to gather scientific data for use in double star astrometry. The GBO was constructed through the collaborative efforts of CUI, Southern Utah University, University of Nevada-Reno, Western Nevada College, Great Basin National Park, and the Great Basin National Park Foundation to support a vigorous program of astronomical research, education, and outreach. The observatory is located at Great Basin National Park, high in the mountains (6825 ft), and distant from any major city or population. The altitude, seclusion, and low-humidity of the desert allow for ideal dark-sky (21.32-21.48 mags/arcsecond^2) conditions required for obtaining high-quality observations (Great Basin Na-

Figure 1. The Concordia University Irvine Astronomy Research Team after the first in-person meeting. Left to right: Russell Genet, Rachel Freed, Lila Musegades, Mackenzie Graham, Andrew Poore, Michelle Caldwell, Selena Masson, Aludith Mayares, John Kenney, III, and Cole Niebuhr.

An Astrometric Observation of Binary Star System WDS 15559-0210 at the Great Basin Observatory

Figure 2. *The 0.7m CDK 700 PlaneWaveTelescope at the Great Basin Observatory in eastern Nevada celebrating its "first light" on 25 August 2016.*

Figure 3: Inside of the observatory dome at Great Basin Observatory in Great Basin National Park, Nevada.

tional Park, 2016).

The binary system WDS 15559-0210 was selected for study from the Washington Double Star catalog using the following parameters: the system was visible from the Great Basin Observatory, had a proposed period, a separation greater than 5", magnitude values less than seven, and a magnitude difference less than five. WSD 15559-0210 was selected because it had many previous data points, high-fidelity data gathered by CCD cameras, and it appeared to be veering off the 1973 calculated orbit. Thus a new data point would either contribute to the validation of the original orbit or provide important data for a needed recalculation.

Equipment

The Great Basin Observatory (GBO) is equipped with a PlaneWave 0.7-m CDK 700 telescope (Great Basin Observatory, 2016). The GBO utilizes a SBIG STX-16803 CCD camera that is attached to the telescope (STX-16803 2017). The images obtained from the observatory were analyzed with the db3.2.1 version of AstroImageJ, a public-domain image processing program, to measure separations and position angles (Collins et. al., 2017). It should be noted that a user account code is needed from nova.astrometry.net in order to use the plate solving capabilities of the program.

Image Analysis

On 18 June 2017, 20 images were taken by GBO using a 10-second exposure time and no filter. The images were then analyzed using AstroImageJ. In the software, the radius parameter under the "Plate Solving with Options" was set to 5 pixels, the "Radius of Object Aperture" setting was decreased from 30 to 6 pixels, and the "Centroid Aperture" feature was left on default. These settings allowed the program to identify the binary stars as two separate objects and orient measurements to the center point of each star.

A difficulty did arise using the "Plate Solve" method when both stars would be initially identified as objects but the secondary would be removed if the process was allowed to finish. This occurred because AstroImageJ would attempt to validate the automatically selected objects through astrometry.net; however, the information for both components were stored under the same entry causing AstroImageJ to only verify the primary star. It is for this reason that measurements were made after the objects were identified but before the validation process finished.

Results

Table 1 shows the results for position angle and separation for this study. The average position angle from this study was 354.95 ± 0.09°, and the average separation was 5.94 ± 0.04". The observations were made on 18 June 2017 or date 2017.4600.

Discussion

The 2012 Washington Double Star Catalog reports 205 observations for WDS 15559-0210 and, after the exclusion of incomplete entries and outliers greater than two standard deviations away from best fit, 161 of these past observations were plotted in conjunction with the new point in Figure 4 (Washington Double Star Catalog 2012). A reproduced orbit was provided for comparison by creating a trend line from data points

Table 1. Position angle and separation measurements made by the Concordia team from GBO data acquired on 18 June 2017.

Time Stamp	Position Angle	Separation	Time Stamp	Position Angle	Separation
6:00:43	355.63	6.02	6:10:36	354.25	5.73
6:01:54	355.17	5.91	6:11:55	355.58	5.64
6:02:53	355.26	5.91	6:13:00	354.34	5.93
6:03:48	354.79	5.97	6:14:00	354.41	5.96
6:04:46	354.73	5.99	6:15:05	355.10	6.25
6:05:46	354.93	5.95	6:16:11	355.16	6.22
6:06:44	354.78	5.72	6:17:11	354.73	5.70
6:07:43	354.56	5.82	6:18:15	355.54	6.08
6:08:38	355.46	5.87	6:19:16	354.99	5.95
6:09:36	354.86	5.93	6:20:14	354.70	5.94

	Position Angle	Separation
Mean	354.95	5.94
Standard Deviation	0.41	0.18
Standard Error of the Mean	0.09	0.04

derived from the WDS orbital plot. The observation from this study appears to fit well with the previous data and, as shown in Figure 4, the cumulative plot shows a deviation from the published orbit.

Conclusion

The new data generated by this study fits well with previous data and cumulatively show a deviation from the proposed orbit for the binary system WDS 15559-0210. Moreover, this study, the first of its type using

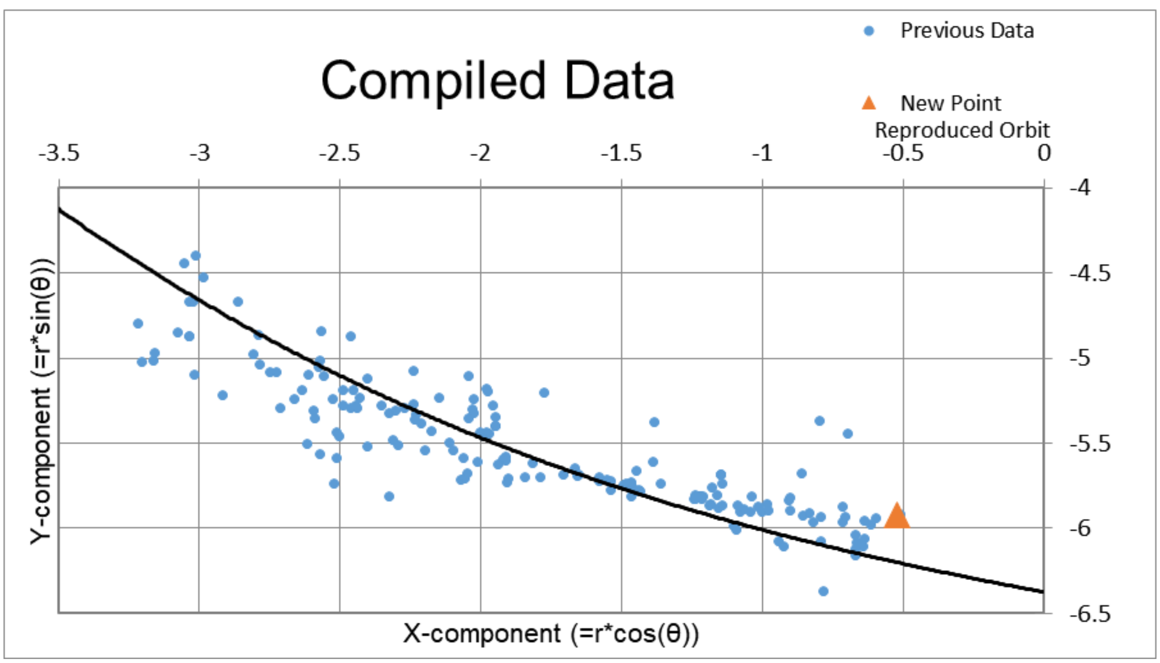

Figure 4. The new point gathered in this research, shown as an orange triangle, aligns with the path of the previous data points, shown as blue dots, provided by information in the WDS. The compiled data shows a trend away from the published orbit.

the GBO, also serves to verify the capabilities of this new telescope.

Acknowledgements

We would especially like to thank Paul Gardner, Observatory Systems, Pasadena, CA for his vital role in the construction and design of the GBO. In addition, we thank the Great Basin National Park and Great Basin National Park Foundation. We would also like to acknowledge Global Science Directive for its contribution to this study. We are grateful to Brian Mason for his providing previous observations from the Washington Double Star Catalog. We would also like to acknowledge Cuesta College for hosting the ASTR 299 Astronomy Research seminar. Finally, we would like to thank Richard Harshaw and Vera Wallen for their role as external reviewers.

References

Collins, K., Kielkopf, J., Stassun K., & Hessman, F., 2017, "AstroImageJ: Image Processing and Photometric Extraction for Ultra-Precise Astronomical Light Curves", *The Astronomical Journal*, **153**, 77-90. http://iopscience.iop.org/article/10.3847/1538-3881/153/2/77

Genet, R., Johnson, J., Buchheim, R., & Harshaw, R., 2016, *Small Telescope Astronomical Research Handbook*, Collins Foundation Press, Santa Margarita, California.

Great Basin National Park, 2016, retrieved July 23, 2017, from http://www.darksky.org/idsp/parks/greatbasin/

Great Basin Observatory, 2016, retrieved July 06, 2017, from http://planewave.com/great-basin-observatory/

STX-16803, (Diffraction Limited), retrieved July 11, 2017, from http://diffractionlimited.com/product/stx-16803/

The Washington Double Star Catalog, 2012, retrieved July 06, 2017, from http://www.usno.navy.mil/USNO/astrometry/optical-IR-prod/wds/WDS

CCD Astrometric Measurements of WDS 13513-3928 (HJ 4618) Using the iTelescope Network

Mattie Sanseverino[1], Nathan Bradshaw[1], Kathryn Chan[1], Vasundhara Sengupta[1], Nima Fariborzi[1], Grady Boyce[2], and Pat Boyce[2]

1. Westview High School, San Diego, California
2. Boyce Research Initiatives and Education Foundation (BRIEF)

Abstract: Astrometric measurements of WDS 13513-3928 were made using the iTelescope network. The position angle and separation of the two-star system were found to be 51.1 degrees and 28.3 arcseconds.

Introduction

WDS 13513-3928 (HJ 4618) was chosen from the Washington Double Star catalog (WDS) after meeting these specific selection criteria: right ascension between 12 and 18 hours, delta magnitude of 3 or less, separation sufficient to allow for each star to be separate on the image, and large changes in position angle (Theta) and distance between the pair's stars (Rho) as indicated by past observations. Its low declination made telescopes in Australia best suited for CCD imaging.

HJ 4618 was first observed by John Herschel in 1834 and has since been measured a total of ten times. This project added another data point to this set, to assist in future determination of whether the system is gravitationally bound or a visual double star.

Equipment and Method

HJ 4618 was measured from Australia's T32 wide deep field telescope from the iTelescope Network. T32 has a large CCD chip that allows the telescope to take wide pictures of the sky. The Planewave Ascension 200HR mount's accuracy does not require active guidance, thus decreasing the session setup time when imaging. The F/Ratio is f/6.8 and with a CCD 9um pixel size the resolution is 0.63 arcsecs per pixel.

CCD images were taken by Australia's T32 at epoch 2017.2450. with exposures of 80 ms and 160 ms for luminance and HA filters, 5 images in total. Each image was analyzed in MaximDL, where the PinPoint Astrometry function was used to set the World Coordinate System (WCS) right ascension and declination coordinates in the image for further processing. Mira Pro x64, a robust astrometry program, was used for measuring Theta and Rho of HJ 4618. Averages were found of the measurements.

The A and B stars were located and Mira was used to measure the separation distance from the stars' centroids and the separation angle of the pair. These measurements were recorded into Microsoft Excel to calculate statistics and plot the new data points visually as a graph relative to the previous measurements' points. Figures 1 and 2 show examples of CCD images that were analyzed in Mira, with the A and B stars labeled. Figure 1 is an example of an image taken with a luminance filter while Figure 2 was taken with a hydrogen-alpha filter.

Theta and Rho measurements from the CCD images, Table 1, are outlined along with basic statistics. These include the average and standard deviation of the measurements for position angle and separation distance as well as the standard errors for the averages. The historical measurements, including our 2017 measurements, are outlined in Table 2 and plotted in Figure 3.

Discussion

No measured values were omitted because our CCD images produced consistent values as the separation distances were far enough for the images to portray

(Text continues on page 203)

CCD Astrometric Measurements of WDS 13513-3928 HJ 4618 Using the iTelescope Network

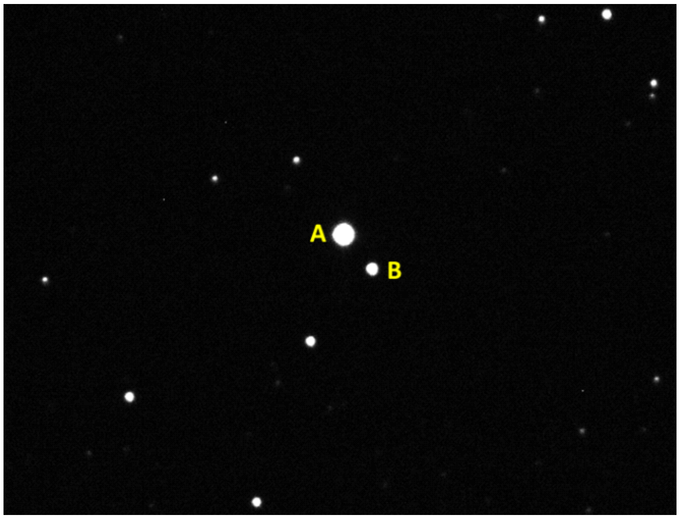

Figure 1. Luminance filter w/ 80s exposure.

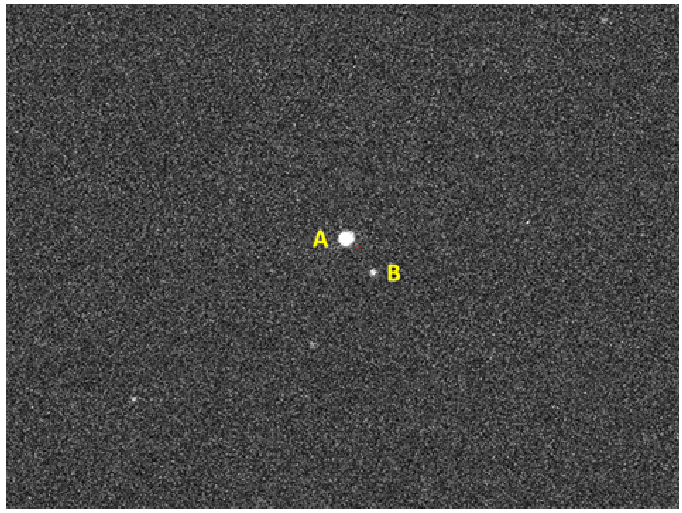

Figure 2. Hα filter with 160 s exposure.

Table 1. Theta and Rho for each Measurement

Image	Position Angle	Separation Distance
Image 1	51.27°	28.37"
Image 2	51.28°	28.34"
Image 3	50.66°	28.34"
Image 4	51.21°	28.42"
Image 5	51.30°	28.11"
Mean	**51.10°**	**28.30"**
Standard Deviation	**0.27°**	**0.12"**
Std. Error of Mean	**0.054°**	**0.024"**

Table 2. Historical Measurements from the WDS with this Paper's 2017 Measurements Included

Observation Date (year)	Position Angle	Separation Distance
1834.48	339.6°	12.00"
1907.49	18.5°	16.06"
1913.63	22.5°	17.67"
1920.17	25.4°	17.60"
1929.43	28.9°	18.27"
1959.46	38.5°	21.30"
1998.523	48.1°	25.92"
1999.29	48.4°	26.06"
2004.36	49.0°	26.74"
2010.5	50.1°	27.42"
2017	*51.1°*	*28.30"*

CCD Astrometric Measurements of WDS 13513-3928 HJ 4618 Using the iTelescope Network

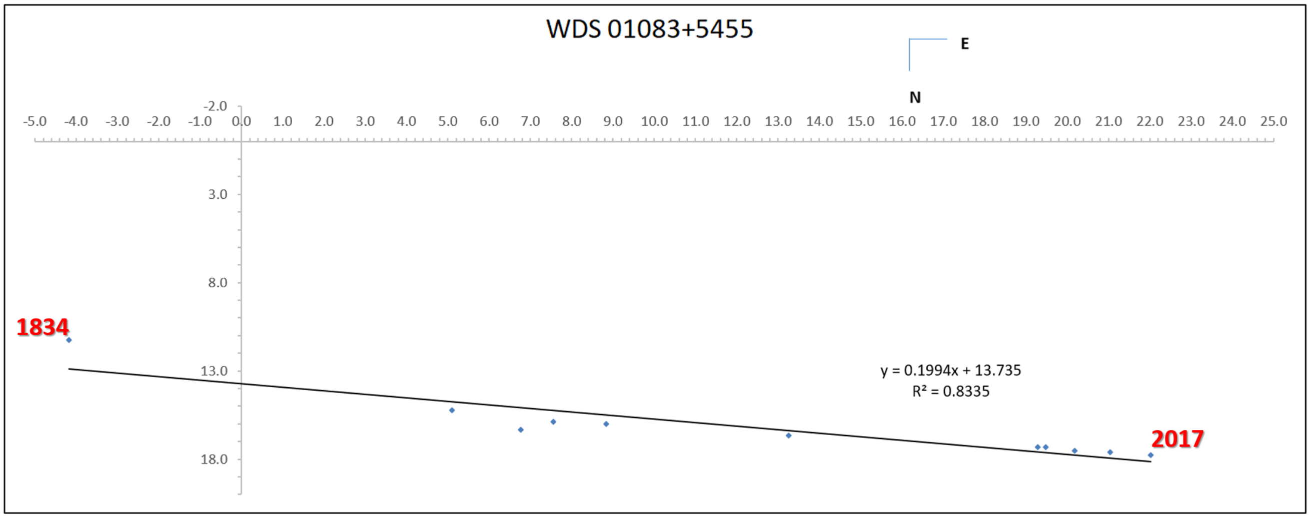

Figure 3. Plot of the historical measurements from 1834 through 2017 from Table 2. The axis are in arcseconds with the A component at the origin.

(Continued from page 201)

two distinct stars, not fused together. Figure 3 shows a graph of the historical position angle and distance measurements, converted into X and Y coordinates, from the data recorded in the WDS and the 2017 images. The first data point, labeled 1834, appears to be lacking in accuracy because it is visually spaced far away from the other points on the graph. However, the gap of time between this point and the chronological next point is 73.01 years while the mean gap in time between the next four measurements and their chronological neighbors is 7.313 years. The major difference in time gaps (73.01>>7.313) accounts for the visual separation in the graph, therefore reassuring the validity of the first data point. Plus, the 1834 measurement is consistent with the linear trend across the rest of the graph with the trend line (R^2) close to one indicating a near linear fit.

Conclusion

Our observed data is consistent with the WDS catalog as our measurements show a clear linear trend line similar to WDS. The data suggest that the pair could be an optical double.

Acknowledgements

We would like to thank the United States Naval Academy for providing access to historical measurement data through the Washington Double Star Catalog. In addition, we thank the Boyce Research Initiatives and Education (B.R.I.E.F) for allowing us to use the iTelescope robotic telescope system along with other software tools. In addition, we'd like to acknowledge the help of Mira Pro for accurate measurements of our binary star system.

References

Mason, B. and Hartkopf, W., 2015, The Washington Double Star Catalog, U.S. Naval Observatory. http://ad.usno.navy.mil/proj/WDS

Genet, R., Johnson, J., Buchheim, R., & Harshaw, R., 2016, *Small Telescope Astronomical Research Handbook*, Collins Foundation Press, Santa Margarita, California.

About the Authors: The primary authors are all students of Westview High School in San Diego, California and have a strong passion for astronomy. Their research was conducted as part of an Astronomy Research Seminar run by Boyce Research Initiatives and Education Foundation (BRIEF).

Refuting S 825AB System Classification through Astrometry and Gaia Satellite Data

Noah Lyman[1], Lila Musegades[2, 3], Edward Davis[4, 5], Micah Briney[5], Aaron Francis[5,] Cole Niebuhr[3], David Rowe[6], Richard Harshaw[7], and Russell Genet[5, 8]

1. University of California Santa Cruz, Santa Cruz, CA
2. Concordia University Irvine, Irvine, CA
3. Global Science Directive, Las Vegas, NV
4. Humboldt State University, Arcata, CA
5. Cuesta College, San Luis Obispo, CA
6. PlaneWave Instruments, CA
7. Brilliant Sky Observatory, Cave Creek, AZ
8. California Polytechnic University, San Luis Obispo, CA

Abstract: A student-led team of researchers studied double star S 825AB (WDS 23100+3651). Analysis of ten CCD images obtained by the Sierra Research Observatory yielded an average position angle of 318.37º and an average separation of 67.38". Comparing these results to published findings in the Washington Double Star Catalog and measurements taken from the European Space Agency's Gaia astrometry satellite, the team concluded that S 825AB is not a binary system.

Introduction

The term "double star" refers to any two stars that appear near to each other from the perspective of Earth. Although the stars may appear to be in close proximity, the components of the systems may actually be separated by great distances. The distance and masses of the components in three-dimensional space determines whether the system is a binary system, an optical double, or a common proper motion pair. A true binary system contains two stars that are physically bound and orbit around a common gravitational center. This is in contrast to optical double and common proper motion systems which are chance optical alignments but the component stars are not orbiting one another. Through repeated observations of these systems, taking place over many years, the nature of the stellar relationship can be determined.

A team of students from several institutions studied the suspected binary star system S 825AB (listed as WDS 23100+3651 in the Washington Double Star Catalog) by collecting new images and combining the data with past observations. S 825AB has been previously proposed as a binary system due to past findings suggesting the stars are gravitationally bound (Figure 1). The proposed orbit, however, did not coincide with recent observations. Data collected by the Gaia satellite from the European Space Agency (ESA) provides strong evidence that S 825AB is not a binary system. The purpose of this study was to make a new observation to determine the nature of S 825AB as a binary.

Procedures and Instrumentation

Previous data was collected on S 825AB from both the Washington Double Star Catalog (WDS) via the United States Naval Observatory and the Gaia Satellite Observations database from the European Space Agency. New data was obtained through Sierra Remote Observatory in California using a PlaneWave Instruments CDK217 Astrograph telescope and Apogee F16 KAF-16803 CCD camera. Instrument specifications are listed in Table 1. Ten images were captured and compiled on June 30, 2017 in order to measure current system positions.

The collected images were analyzed using AstroImageJ, a public domain image processing program based on the ImageJ software developed by the National Institutes of Health (Collins et al., 2017). AstroImageJ has the option to use "centroid apertures" within its measuring tools that automatically sets the

Refuting S 825AB System Classification through Astrometry and Gaia Satellite Data

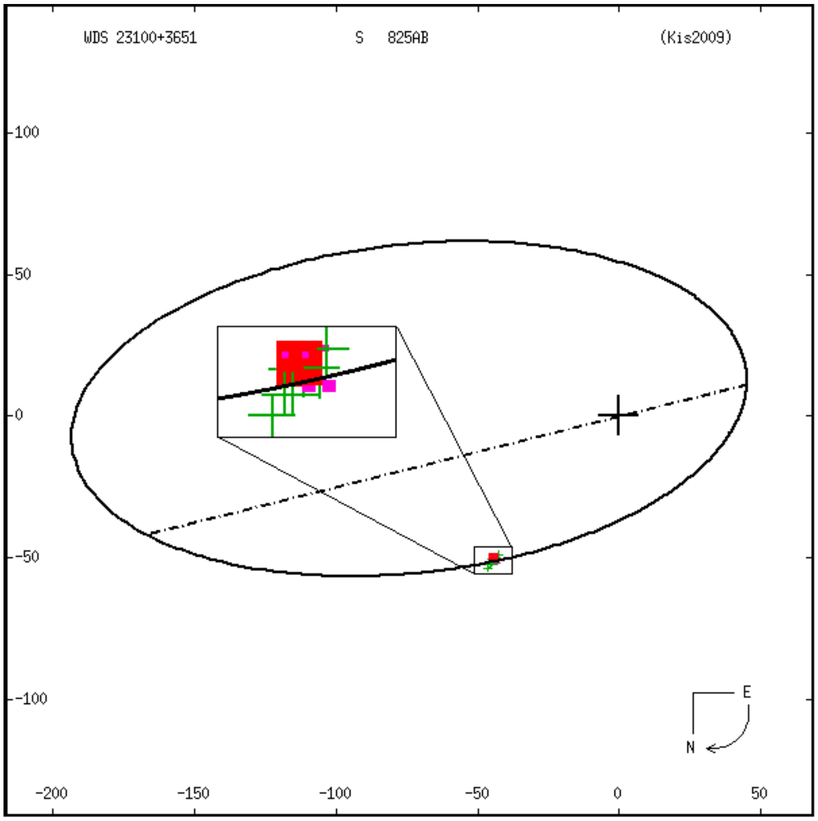

***Figure 1.** An orbital plot containing 38 previous observations of S 825AB provided by U.S. Naval Observatory.*

cursor to the center of the identified stars. This option reduces the human error involved in measuring the separation and position angle between the component stars. With the *Plate Solve* feature, the identity of the stars was confirmed and compass directions oriented via the online database astrometry.net, thus further validating the measurements.

Data and Results

Previous data was collected and compared from both the Washington Double Star Catalog and the Gaia Catalog. Of particular importance is the description of the proper motions of the individual stars in the double star system from the Gaia Satellite (Table 2). The data collected from Sierra Remote Observatory is displayed with data from each captured image (Table 3) and resulted in a combined position angle of 318.37±0.005° and a separation of 67.38±0.01".

Discussion

The results of this study combined with previous data demonstrate a nearly linear change in position between the two stars (Figure 2). Possible explanations of

(Text continues on page 207)

***Table 1:** Summary of Equipment Utilized with Specifications.*

Equipment	Specifications
Telescope	CDK17 OTA, IRF90 integrated rotator/focuser
Telescope mount	A200 mount with Sitech controller
Camera	Apogee F16M KAF-16803 based camera with filter wheel
Software	STI 1.4.2 mount interface, PWI 3.3.3 focuser/rotator interface, PWA 1.09 automation software, MaxIm DL Pro 5 camera interface, TeamViewer 12, Google Drive, db3.2.1 version AstroImageJ

Refuting S 825AB System Classification through Astrometry and Gaia Satellite Data

Table 2: *Selected data obtained from the ESA's Gaia astrometry satellite describing the location and movements of each component of the double star S 825AB*

Right Ascension (degree)	Declination (degree)	Parallax (milliarcsec)	Proper Motion RA (milliarcsec/year)	Proper Motion DE (milliarcsec /year)
347.5108173664	+36.8482827887	3.26	14.712	-2.267
347.4952824410	+36.8622777008	1.56	4.290	-0.004

Table 3. *Separation and position angle measurements from CCD images taken in this study including average value, standard deviation, and standard error of the mean.*

Observation	Position Angle (degrees)	Separation (arc seconds)
1	318.36	67.42
2	318.39	67.40
3	318.38	67.41
4	318.37	67.30
5	318.36	67.46
6	318.35	67.37
7	318.39	67.33
8	318.39	67.36
9	318.38	67.38
10	318.35	67.41
Mean	318.37	67.38
Std. Deviation	0.02	0.05
SE Mean	0.005	0.01

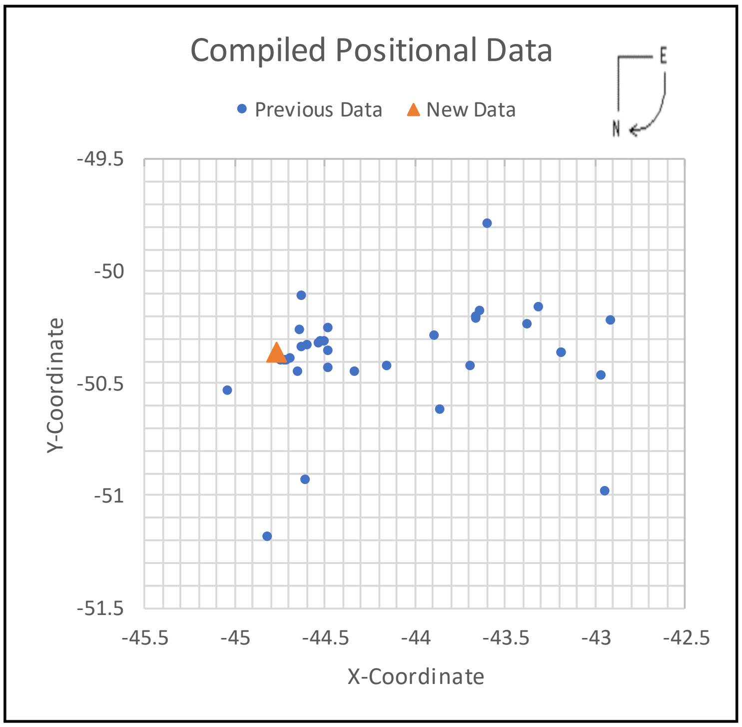

Figure 2. *A compilation of new and previous data plotted on a Cartesian Coordinate system for comparison (excluding statistical outliers).*

Refuting S 825AB System Classification through Astrometry and Gaia Satellite Data

(Continued from page 205)

these results are that the system exhibits an orbit with a prolonged period or that the components are not gravitationally-bound. Large differences in parallax and proper motion are reported in the Gaia catalog data set, suggesting that the components of the system are chance optical alignments rather than a gravitationally bound binary system.

Conclusion

This student-led study has successfully introduced several undergraduate researchers to the field of astrometry. The results show definitely that the double star S 825AB is not a binary system but rather an optical motion double star. The component stars move in a similar direction; however, it can be inferred that with the passage of time, the differences in proper motions will cause the pair's separation to widen.

Acknowledgements

We thank Planewave Instruments for their use in data collection. Our research was made possible with the following catalogs, databases, and support:

Washington Double Star Catalog maintained at the U.S. Naval Observatory.

The European Space Agency (ESA) mission Gaia (https://www.cosmos.esa.int/gaia), processed by the Gaia Data Processing and Analysis Consortium (DPAC, https://www.cosmos.esa.int/web/gaia/dpac/consortium). Funding for the DPAC has been provided by national institutions, in particular the institutions participating in the Gaia Multilateral Agreement.

VizieR catalogue access tool, CDS, Strasbourg, France. The original description of the VizieR service was published in A&AS 143, 23

Dr. Vera Wallen for review and formatting reference.

References

Collins, K., Kielkopf, J., Stassun, K., & Hessman, F., 2017. *AstroImageJ: Image Processing and Photometric Extraction for Ultra-Precise Astronomical Light Curves.* The Astronomical Journal, 153, 77-90. http://iopscience.iop.org/article/10.3847/1538-3881/153/2/77

Genet, R., Johnson, J., Buchheim, R., & Harshaw, R. 2016. Small Telescope Astronomical Research Handbook. Santa Margarita, CA: Collins Foundation Press.

Gaia Collaboration: T. Prusti, J. H. J. de Bruijne, A. G. A. Brown, A. Vallenari, C. Babusiaux, C. A. L. Bailer-Jones, U. Bastian, M. Biermann, D. W. Evans, et al. 2016b The Gaia mission. A&A 595, pp. A1.

Gaia Collaboration, A. G. A. Brown, A. Vallenari, T. Prusti, J. H. J. de Bruijne, F. Mignard, R. Drimmel, C. Babusiaux, C. A. L. Bailer-Jones, U. Bastian, et al. 2016a Gaia Data Release 1. Summary of the astrometric, photometric, and survey properties. A&A 595, pp. A2.

Mason, Brian. 2017. Washington Double Star Catalog. Astrometry Department, U.S. Naval Observatory. http://ad.usno.navy.mil/wds/

The Southern Double Stars of Carl Rümker II: Their Relative Rectilinear Motion

Roderick R. Letchford[1], Graeme L. White[2], Allan D. Ernest[3]

1. Vianney College Seminary, NSW Australia
rodvianey@yahoo.com.au
2. Astrophysics Group, Computational Engineering and Science Research Centre, University of Southern Queensland, Toowoomba, Australia QLD 4350
graemewhiteau@gmail.com
3. Charles Sturt University, NSW Australia
aernest@csu.edu.au

Abstract: A description of the relative rectilinear motion of double stars provides an important clue to the relationship of the components. The aim is to provide an objective method of obtaining Rectilinear Elements. We present a simplified method to calculate relative rectilinear motion, relying on the data obtained from the HIPPARCOS and GAIA DR1 missions, together with their uncertainties. As examples, we present the Rectilinear Elements of RMK 1, 3, 4, 5, 6, 8, 10, 11, 12, 17, 20, 25, 27, and 28.

1. Introduction

The description of the relative motion of the components of double stars in the form of rectilinear motion is the analysis of the (presumed) perceived linear motion of the secondary star relative to the primary. It is usually visualized as a straight line on a Cartesian plot where the primary star is the origin (0,0) position.

Such descriptions are an important tool in distinguishing between optical doubles and physical binaries, which in turn, have implications for stellar formation models. Relatively slow moving doubles may be either chance alignments of unrelated stars or very long period bound pairs. A comparison of the best-fit rectilinear motion and curved orbital motion should result in a clear distinction between these two types, since it is the variations from linearity that allows a sensitive identification of a Keplerian system.

We present here a portion of a continuing study of the double stars identified nearly two hundred years ago at Sir Thomas Brisbane's observatory at Parramatta, Australia (see paper 1, Letchford, White, and Ernest 2017, and references therein). In this study, and this paper, we present the rectilinear elements of pairs from the double star list of Rümker (Rümker 1832). Section 2 is our revised method for the computation of the elements of rectilear motion, and Section 3 presents the elements and the diagrammatic results for 14 of the 28 Rümker pairs.

2. Derivation of Rectilinear Elements

Rectilinear motion has been studied for many double star pairs, and a *Catalog of Rectilinear Elements* (CORE) is maintained by the USNO†. Utilizing the USNO method as a starting point, we see several ways that the CORE can be improved. Our improvements are designed to address:

1. The present conversion from polar to Cartesian coordinates is non-standard resulting in a plot that is East-West/North-South reversed relative to adopted orientation.
2. The quoted uncertainties for at least one of the computed parameters appear to be underestimated.
3. The weights associated with the individual observations are subjective.
4. The method used to arrive at the *Rectilinear Elements* (RE) is not stated in easily reproducible form.

We therefore propose an alternate procedure for rectilinear motion that eliminates each of the above inadequacies by (i) applying the convention in converting from polar to cartesian coordinates: $y = \rho \sin\theta$ and

† http://ad.usno.navy.mil/wds/lin1/lelements.html

The Southern Double Stars of Carl Rümker II: Their Relative Rectilinear Motion

$x = \rho\cos\theta$ where ρ is the separation of the primary and the secondary in arcseconds and θ is the precessed (to Equinox J2000.0) position angle, in degrees, initially given at the equinox of date (epoch), (ii) the calculation of the uncertainties following the standard definition,

$$\sigma_{f(x_i)} = \pm\sqrt{\sum\left(\frac{\partial f(x_i)}{\partial x_i}\sigma_{x_i}\right)^2}$$

and (iii) further modifications as discussed in section 2.1 below.

2.1 Adoption of Space-Based Data

The rectilinear elements in the CORE are the result of assigning weights to each observation (which, despite the best of efforts, always involves an element of subjectiveness), and then calculating the line of best fit based on historical observations. Instead we propose to avoid altogether the need for weighting by using only the positions observed by the HIPPARCOS (HIP) and GAIA (GAIA) space missions. These two positions offer uncertainties far smaller than is currently available with terrestrial measurements. HIPPARCOS positional uncertainties are approximately 5 milli-arcseconds (mas) and GAIA are 0.4 mas for the RMK stars in this paper. The line of motion can then be fitted to the two-point astrometric positions in an entirely objective fashion. This utilizes the most powerful data available for astrometric work; relegating the other ground-based and historic measures to a secondary "supportive" role.

The adoption of the HIPPARCOS positions for the individual stars comes, however, with a caveat that the HIPPARCOS mission had technical difficulties handling double stars within specific seperation and magnitude limits. Details of the limitations of the HIPPARCOS mission's handling of double stars are given in Lindegren et al. (1997), and analysis of data from that mission must be treated in light of that paper.

We give here in section 2 full derivations of all elements and their uncertainties.

2.2 Input Data

To compute the CORE elements, the following data are needed:

- The Right Ascension (RA) and Declination (DE) of the primary and secondary (1 and 2, respectively) stars from HIPPARCOS, together with their uncertainties.
- The Right Ascension (RA) and Declination (DE) of the primary and secondary (1 and 2, respectively) stars from GAIA DR1 (Gaia Data Release 1) together with their uncertainties.

The above data for the Rümker doubles in this paper are presented in Table 1.

HIPPARCOS and GAIA positions are both given in the International Celestial Reference System (ICRS), with the epoch of HIPPARCOS set at J1991.25 and those of GAIA DR1 at J2015.0. Alignment to the ICRS at epoch J1991.25 is estimated to be within 0.6 mas (Hilton and Hohenkerk, 2004). This is smaller than the uncertainties of positions of our RMK stars in the HIPPARCOS catalogue, and less than those associated with any transformation required for the ground-based observations, and so the differences in the definitions of ICRS can be safely ignored.

2.3 Computation of Rectilinear Elements

Let:

ΔRA	Difference in RA between the primary and secondary
ΔDE	Difference in DE between the primary and secondary
$RA1$	RA of primary
$DE1$	DE of primary
$RA2$	RA of secondary
$DE2$	DE of secondary
θ	Position angle
ρ	Separation
xh	x cartesian coordinate of HIP relative position of secondary
yh	y cartesian coordinate of HIP relative position of secondary
xg	x cartesian coordinate of GAIA relative position of secondary
yg	y cartesian coordinate of GAIA relative position of secondary
σ	Uncertainty of quantity

And so:

$$\Delta RA^{rad} = \left(RA2^{rad} - RA1^{rad}\right)\cos\left(DE1^{rad}\right)$$

$$\Delta DE^{rad} = DE2^{rad} - DE1^{rad}$$

Therefore, the position angle is:

$$\vartheta^{o} = \begin{cases} \frac{180}{\pi}\arctan 2\left[\Delta RA^{rad}, \Delta DE^{rad}\right] \\ \vartheta^{o} + 360^{o}, \text{ if } \vartheta^{o} < 0^{o} \\ \vartheta^{o} - 360^{o}, \text{ if } \vartheta^{o} > 360^{o} \end{cases}$$

and the separation is

$$\rho'' = \frac{360.180}{\pi}\sqrt{\left(\Delta RA^{rad}\right)^2 + \left(\Delta DE^{rad}\right)^2}$$

(Text continues on page 212)

The Southern Double Stars of Carl Rümker II: Their Relative Rectilinear Motion

Table 1: Data from the HIP (ICRS, epoch J1991.25) and GAIA DR1 (ICRS, epoch J2015.0) catalogues

RMK	HIP RA °	HIP DE °	HIP pmRA mas/yr	HIP pmDE mas/yr	GAIA RA °	GAIA DE °	GAIA pmRA mas/yr	GAIA pmDE mas/yr
	± mas	± mas	± mas/yr	± mas/yr	± mas	± mas	± mas/yr	± mas/yr
1 A	13.10213861	-69.50359643	3.81	-68.87	13.10221204	-69.50404326	4.040	-67.635
	1.73	1.78	1.84	2.14	0.288	0.161	0.115	0.111
1 B	13.11818630	-69.50273658	-2.47	-59.75	13.11823831	-69.50321341	3.265	-72.464
	15.63	14.16	11.60	12.41	0.376	0.247	0.325	0.312
3 A	64.41777199	-63.25549171	5.48	35.53	64.41785704	-63.25526588	5.837	34.244
	0.66	0.61	0.51	0.60	0.308	0.454	0.025	0.030
3 B	64.41790229	-63.25434505	5.02	28.29	64.41795947	-63.25413265	N/A	N/A
	4.04	4.13	1.68	2.17	0.113	0.124	N/A	N/A
4 A	66.05133135	-57.07115747	-104.32	-73.73	66.05005359	-57.07164998	-105.265	-74.750
	0.97	0.94	1.09	0.92	0.149	0.306	0.041	0.043
4 B	66.04872176	66.04872176	-99.63	-59.98	66.04751666	-57.07220024	N/A	N/A
	1.93	1.93	1.42	1.28	0.056	0.096	N/A	N/A
5 A	107.60195006	-55.58769155	-1.46	-9.42	107.60194970	-55.58776986	0.217	-12.031
	1.27	1.17	1.16	1.25	0.174	0.230	0.132	0.117
5 B	107.59949405	-55.58903491	-1.46	-9.42	107.59949880	-55.58911163	N/A	N/A
	2.13	2.18	1.16	1.25	0.058	0.108	N/A	N/A
6 A	110.08940661	-52.31188250	-35.17	147.45	110.08900990	-52.31091536	-36.881	146.689
	1.00	0.96	0.85	1.00	0.780	0.614	0.050	0.045
6 B	110.09119822	-52.30958151	-30.09	139.97	110.09085430	-52.30866713	N/A	N/A
	3.46	3.46	1.79	2.01	0.635	0.777	N/A	N/A
8 A	123.81647486	-62.91561677	-26.87	-10.95	123.81613060	-62.91569353	N/A	N/A
	0.60	0.55	0.62	0.57	0.270	0.327	N/A	N/A
8 B	123.81876212	-62.91520742	-26.87	-10.95	123.81845950	-62.91530189	N/A	N/A
	6.84	7.13	0.62	0.57	0.057	0.084	N/A	N/A
10 A	139.47917885	-69.80468837	-4.17	4.71	139.47903390	-69.80464588	-7.794	6.518
	2.16	2.22	2.55	2.08	0.254	0.233	0.063	0.069
10 B	139.48185926	-69.80195281	-12.53	8.73	139.48171690	-69.80191018	-6.978	6.315
	3.97	3.75	3.59	2.85	0.245	0.226	0.085	0.098

Table 1 concludes on next page.

The Southern Double Stars of Carl Rümker II: Their Relative Rectilinear Motion

Table 1 (conclusion): Data from the HIP (ICRS, epoch J1991.25) and GAIA DR1 (ICRS, epoch J2015.0) catalogues

RMK	HIP RA °	HIP DE °	HIP pmRA mas/yr	HIP pmDE mas/yr	GAIA RA °	GAIA DE °	GAIA pmRA mas/yr	GAIA pmDE mas/yr
	± mas	± mas	± mas/yr	± mas/yr	± mas	± mas	± mas/yr	± mas/yr
11 A	146.77557340	-65.07201888	-11.55	4.97	146.77536750	-65.07197603	N/A	N/A
	0.42	0.39	0.49	0.38	1.200	1.273	N/A	N/A
11 B	146.77819338	-65.07287694	-11.55	4.97	146.77800690	-65.07283570	N/A	N/A
	9.06	7.82	0.49	0.38	0.255	0.210	N/A	N/A
12 A	148.77381591	-69.18905000	-67.46	31.29	148.77258570	-69.18886855	-66.237	27.490
	0.68	0.63	0.85	0.66	0.341	0.307	0.033	0.031
12 B	148.76989518	-69.19119668	-67.46	31.29	148.76870420	-69.19102761	N/A	N/A
	6.18	5.28	0.85	0.66	0.141	0.128	N/A	N/A
17 A	203.01630920	-63.04189266	-1.40	-5.60	203.01623910	-63.04190578	-4.946	-2.433
	4.40	3.80	5.50	4.10	0.189	0.219	0.298	0.316
17 B	203.01589640	-63.03745126	16.30	23.90	203.01584320	-63.03747152	-4.610	-3.541
	6.10	6.00	8.20	7.50	0.236	0.322	0.344	0.378
20 A	236.97123090	-65.44218988	-27.98	-41.74	236.97076230	-65.44244124	-29.371	-38.218
	1.11	1.20	1.08	1.39	0.179	0.349	0.036	0.045
20 B	236.97189982	-65.44261411	-28.00	-34.83	236.97142560	-65.44284167	N/A	N/A
	2.01	2.08	1.32	1.59	0.086	0.175	N/A	N/A
25 A	303.73387783	-56.97624609	38.22	-96.11	303.73432470	-56.97686335	36.677	-93.431
	1.75	1.46	2.43	2.00	0.151	0.194	0.073	0.062
25 B	303.73563959	-56.97448410	38.22	-96.11	303.73606750	-56.97513412	N/A	N/A
	3.19	3.37	2.43	2.00	0.068	0.070	N/A	N/A
27 A	354.86635383	-46.63789839	22.44	40.99	354.86656960	-46.63766756	22.353	34.941
	1.04	0.81	0.94	0.65	0.323	0.436	0.038	0.033
27 B	354.86478545	-46.63777300	28.98	36.14	354.86503090	-46.63752002	N/A	N/A
	3.59	3.24	2.07	1.55	0.122	0.123	N/A	N/A
28 A	356.88918210	-60.51913771	34.80	-14.40	356.88942030	-60.51912624	17.492	2.075
	7.40	9.50	9.60	13.10	0.214	0.214	0.478	0.438
28 B	356.89237990	-60.51941088	20.20	8.70	356.89260510	-60.51940647	17.510	1.857
	9.20	12.40	12.10	17.10	0.207	0.205	0.472	0.431

The Southern Double Stars of Carl Rümker II: Their Relative Rectilinear Motion

and the above in Cartesian coordinates:

$$x" = \rho"\cos\left(\vartheta^{rad}\right)$$
$$y" = \rho"\sin\left(\vartheta^{rad}\right)$$

This has the effect that increasing x is in the direction of increasing North and increasing y is in the direction of increasing East.

The relative proper motions of the secondary in the x (xa) and y (ya) coordinates are:

$$xa^{"/yr} = \frac{xg" - xh"}{2015.0 - 1991.25}$$
$$ya^{"/yr} = \frac{yg" - yh"}{2015.0 - 1991.25}$$

The secondary position at $t = 0$ (not $t0$) on the x axis (xb) and y axis (yb) is:

$$xb" = xg" - xa".2015.0$$
$$yb" = yg" - ya".2015.0$$

So the time of closest approach ($t0$) and position ($x0$,$y0$) of secondary is:

$$t0^{yr} = \frac{xa.xb + ya.yb}{xa^2 + ya^2}$$
$$x0" = xa"(t0 - 2015.0) + xg"$$
$$y0" = ya"(t002015.0) + yg"$$
$$\vartheta 0 = \left\{ \begin{array}{l} \frac{180}{\pi}\arctan 2\left[y0, x0\right] \\ \vartheta^o + 360^o \quad \text{if } \vartheta^o < 0^o \\ \vartheta^o - 360^o \quad \text{if } \vartheta^o > 360^o \end{array} \right\}$$
$$\rho 0" = \sqrt{x0^2 + y0^2}$$

The seven Rectilinear elements ($x0$, xa, $y0$, ya, $t0$, $\theta 0$, $\rho 0$) thus calculated are defined in Section 3.1.

2.4 Uncertainties of the Rectilinear Elements

The uncertainties for the RA (σ_{RA}) and DE (σ_{DE}) of the HIP and GAIA positions are presented in the catalogues in milli-arcseconds (mas). Here, they are assumed to be in radians.

$$\sigma_{\Delta RA}^{rad} = \pm\sqrt{\left(\sigma_{RA2}^2 + \sigma_{RA1}^2\right)\cos^2\left(DE1\right) + \left(RA2 - RA1\right)^2 \sin^2\left(DE1\right)\sigma_{DE1}^2}$$

$$\sigma_{\Delta DE}^{rad} = \pm\sqrt{\sigma_{DE2}^2 + \sigma_{DE1}^2}$$

$$\sigma_{\vartheta}^{o} = \pm\frac{180}{\pi}\sqrt{\frac{\left(\Delta RA.\sigma_{\Delta DE}\right)^2 + \left(\Delta DE.\sigma_{\Delta RA}\right)^2}{\left(\Delta RA^2 + \Delta DE^2\right)^2}}$$

where $\frac{\partial\vartheta}{\partial\Delta RA} = \frac{\Delta DE}{\Delta DE^2 + \Delta RA^2}$ and $\frac{\partial\vartheta}{\partial\Delta DE} = -\frac{\Delta RA}{\Delta DE^2 + \Delta RA^2}$

so, $\sigma_{\vartheta}^2 = \left(\frac{\partial\vartheta}{\partial\Delta RA}\sigma_{\Delta RA}\right)^2 + \left(\frac{\partial\vartheta}{\partial\Delta DE}\sigma_{\Delta DE}\right)^2$, radians

$$\sigma_{\vartheta}^2 = \left(\frac{\partial\vartheta}{\partial\Delta RA}\sigma_{\Delta RA}\right)^2 + \left(\frac{\partial\vartheta}{\partial\Delta DE}\sigma_{\Delta DE}\right)^2, \quad \text{radians}$$

$$\sigma"_{\rho} = \pm\frac{3600.180}{\pi}\sqrt{\frac{\left(\Delta RA\,\sigma_{\Delta RA}\right)^2 + \left(\Delta DE\,\sigma_{\Delta DE}\right)^2}{\Delta RA^2 + \Delta DE^2}}$$

$$\sigma"_{x} = \pm\frac{3600.180}{\pi}\sqrt{\left[\cos\left(\vartheta^{rad}\right)\sigma_{\rho}^{rad}\right]^2 + \left[\rho^{rad}\sin\left(\vartheta^{rad}\right)\sigma_{\vartheta}^{rad}\right]^2}$$

$$\sigma"_{y} = \pm\frac{3600.180}{\pi}\sqrt{\left[\sin\left(\vartheta_{\rho}^{rad}\right)\right]^2 + \left[\rho^{rad}\cos\left(\vartheta^{rad}\right)\sigma_{\vartheta}^{rad}\right]^2}$$

$$\sigma"_{xa} = \pm\frac{3600.180}{\pi}\sqrt{\frac{\sigma_{xg}^2 + \sigma_{xh}^2}{23.75}}$$

$$\sigma"_{ya} = \pm\frac{3600.180}{\pi}\sqrt{\frac{\sigma_{yg}^2 + \sigma_{yh}^2}{23.75^2}}$$

$$\sigma"_{xb} = \pm\frac{3600.180}{\pi}\sqrt{\sigma_{xg}^2 + \left(2015.0\,\sigma_{xa}\right)^2}$$

$$\sigma"_{yb} = \pm\frac{3600.180}{\pi}\sqrt{\sigma_{yg}^2 + \left(2015.0\,\sigma_{ya}\right)^2}$$

$$\sigma"_{x0} = \pm\sqrt{\left[\left(t0 - 2015.0\right)\sigma_{xa}\right]^2 + \sigma_{xg}^2}$$

$$\sigma"_{y0} = \pm\sqrt{\left[\left(t0 - 2015.0\right)\sigma_{ya}\right]^2 + \sigma_{yg}^2}$$

$$\sigma"_{\vartheta 0} = \pm\frac{180}{\pi}\sqrt{\frac{\left(x0\,\sigma_{y0}\right)^2 + \left(y0\,\sigma_{x0}\right)^2}{\left(x0^2 + y0^2\right)^2}}$$

$$\sigma"_{\rho 0} = \pm\sqrt{\frac{\left(x0\,\sigma_{x0}\right)^2 + \left(y0\,\sigma_{y0}\right)^2}{x0^2 + y0^2}}$$

The uncertainty for t0 is much more complicated. Recall that:

$$t0^{yr} = \frac{xa\ xb + ya\ yb}{xa^2 + ya^2}$$

Then: $p = xa\ xb + ya\ yb$ and $q = xa2+ya2$, so that

$$t0 = \frac{p}{q}$$

Thus:

$$\sigma_{t0}^2 = \left(\frac{\partial t0}{\partial p}\sigma_p\right)^2 + \left(\frac{\partial t0}{\partial q}\sigma_q\right)^2$$

$$\sigma_{t0}^2 = \left(\frac{1}{q}\sigma_p\right)^2 + \left(\frac{p}{q^2}\sigma_q\right)^2$$

$$\sigma_p^2 = \left(\frac{\partial p}{\partial xa}\sigma_{xa}\right)^2 + \left(\frac{\partial p}{\partial xb}\sigma_{xb}\right)^2 + \left(\frac{\partial p}{\partial ya}\sigma_{ya}\right)^2 + \left(\frac{\partial p}{\partial yba}\sigma_{yb}\right)^2$$

$$\sigma_p^2 = \left(xb\ \sigma_{xa}\right)^2 + \left(xa\ \sigma_{xb}\right)^2 + \left(yb\ \sigma_{ya}\right)^2 + \left(ya\ \sigma_{yb}\right)^2$$

$$\sigma_q^2 = \left(\frac{\partial q}{\partial xa}\sigma_{xa}\right)^2 + \left(\frac{\partial q}{\partial xb}\sigma_{xb}\right)^2$$

$$\sigma_q^2 = \left(2xa\ \sigma_{xa}\right)^2 + \left(2ya\ \sigma_{ya}\right)^2$$

2.5 Ephemeris

With the rectilinear elements (REs) thus calculated, the equations derived can be used to compute the position angle (θ, PA in degrees) and separation (ρ in arcseconds) of the components at any epoch (t_{Eph}). Such computations can be used to establish positions for calibration pairs to be used in later observations.

$$x''_{Eph} = xa\left(t_{Eph} - 2015.0\right) + xg$$

$$y''_{Eph} = ya\left(t_{Eph} - 2015.0\right) + yg$$

$$\vartheta_{Eph}^o = \begin{cases} \frac{180}{\pi}\arctan 2\left(y_{Eph}, x_{Eph}\right) \\ \vartheta_{Eph}^o + 360^o, \text{ if } \vartheta_{Eph}^o < 0^o \\ \vartheta_{eph}^0 - 360^o, \text{ if } \vartheta_{Eph}^0 > 360^o \end{cases}$$

$$\rho''_{Eph} = \sqrt{x_{Eph}^2 + y_{Eph}^2}$$

2.6 Uncertainties of the Ephemeris

Note first that $\sigma_{tEph} = 0$, i.e. the uncertainty in the ephemeris date is zero.

$$\sigma''_{xEph} = \pm\sqrt{\left(\left(t_{Eph} - 2015.0\right)\sigma_{xa}\right)^2 + \sigma_{xg}^2}$$

$$\sigma''_{yEph} = \pm\sqrt{\left(\left(t_{Eph} - 2015.0\right)\sigma_{xa}\right)^2 + \sigma_{xg}^2}$$

$$\sigma_{Eph}^o = \pm\frac{180}{\pi}\sqrt{\frac{\left(x_{Eph}\ \sigma_{yEph}\right)^2 + \left(y_{Eph}\ \sigma_{xEph}\right)^2}{\left(x_{Eph}^2 + y_{Eph}^2\right)^2}}$$

$$\sigma''_{\rho Eph} = \pm\sqrt{\frac{\left(x_{Eph}\ \sigma_{xEph}\right)^2 + \left(y_{Eph}\ \sigma_{yEph}\right)^2}{x_{Eph}^2 + y_{Eph}^2}}$$

3. Application to the Rümker Double Stars

As stated in Section 1, this paper is a continuation of a series that retrospectively analyzes the double star observations from the private observatory built by Sir Thomas Brisbane in Parramatta, Australia, in 1822. The three astronomers associated with Parramatta observatory were Brisbane himself, and two employees: Carl Rümker and James Dunlop. This paper builds on our study of the double star catalog of Rümker (WDS designation RMK, see Letchford et al., 2017), and is undertaken with the aim of improving the data sets and our understanding of the quality of the associated historic data.

Again as stated (Section 2), we are working with the milli-arcsecond results from the space missions HIPPARCOS and GAIA, and present all ground-based and historic observations only as a starting point for a later study of the precision of such data.

HIPPARCOS and GAIA positions and proper motions are currently available for only 14 RMK pairs: 1, 3, 4, 5, 6, 8, 10, 11, 12, 17, 20, 25, 27, and 28 (i.e. 50% of the 28 pairs in the Rumker catalog). The Rectilinear Elements and their uncertainties for these pairs are given in Table 2. Following the USNO lead, we leave all digits from the computation rather than round off the elements and the uncertainties in the elements.

In addition, we have also adopted the 'one line' formatting of the CORE elements rather that utilizing the subscripted form (for example we use t0 for the date of closest approach rather than t_0) as seen in current references.

3.1 The Rectilinear Elements as defined in the CORE

- x0 - The RA position of the secondary (usually defines as the fainter) star relative to the primary (brightest) in the Cartesian frame centered on the primary, in units of arcseconds, at the time of closest approach, t0.

- xa - The RA proper motion of the secondary star relative to the primary in the Cartesian frame centered on the primary, in units of arcseconds per year.
- y0 - The Declination position of the secondary star relative to the primary in the Cartesian frame centered on the primary in units of arcseconds, at the time of closest approach, t0.
- ya - The Declination proper motion of the secondary star relative to the primary in the Cartesian frame centered on the primary, in units of arcseconds per year.
- t0 - The date of closest apparent approach of the two stars, in calendar years.
- θ0 - The Position Angle of the secondary star relative to the primary at time of closest approach, t0, in units of degrees measured from celestial North via East.
- ρ0 - The separation of the two stars in the Cartesian frame at the time of closest approach, t0, in units of arcseconds.

3.2 *The Rectilinear Motion as a Test for Binary Orbit*

The differentiation of an optical pair and a physically-bound binary system is a skill in its own right. For a pair to be bound, the relative motion of the stars as determined by astrometric means should show a curved orbital path (and the two stars should have the same parallax, appropriate radial velocities, and other physical and inferred properties). In contrast, the astrometric paths of the optical pairs will show no deviation from a straight line (although it is conceded that an orbit may present itself as a straight line under rare edge-on alignment of the orbit).

This analysis is, of course, made more difficult for wide, slow moving binary systems of great period. For all work of this type, there is no substitute for good quality (low uncertainty) data made over a long time baseline.

Also, well-defined relative proper motions can allow scale calibration for imaging systems and improvement in the determined proper motions of individual components.

3.3 *Explanation of Figures*

Plots of the Rümker doubles are given in Figures 1-28, presented in the Appendix. Historical data from the WDS have been incorporated into the figures and their position angles have been precessed from Equinox of date to J2000.0 and then converted to Cartesian coordinates. The WDS data for 1991.25 (HIP) were not precessed because they are already presented at Equinox J2000.0 and not at Equinox of date as the remaining WDS measures are presumed to be. Precessed WDS observations are prepepented in the plots by a '+'.

The HIP and GAIA positions are represented by a red circle and green square respectively. The dotted ellipses are the uncertainty ellipses for the t0 (unzoomed figure for each RMK pair). If they cannot be seen in the plots, it is because of the plot scale. Uncertainty ellipses for the HIP and GAIA were also plotted but in each case they are too small to see at the scales that are needed to represent all relevant data.

4 Notes on Individual Pairs.

RMK 1: Closing, secondary moving 4.69 ± 0.06 mas/yr a linear velocity along the line of best fit ($= \sqrt{(xa^2 + ya^2)}$). Proper motion data from both the HIP and GAIA missions are available. The red line is the rectilinear movement based on only HIP proper motions, the green line based on GAIA. The GAIA relative proper motion is similar to this paper; the HIP very different. The proper motions from the HIP data for RMK 1 is suspect, see note above re the limitation of the HIP data.

RMK 3: Closing, 2.79 ± 0.05 mas/yr. Primary is RMK 3AB and secondary is RMK 3B, between is RMK 3A or θ Ret. Proper motion available only from HIP and our own calculations.

RMK 4: Closing, 14.80 ± 0.03 mas/yr. Motion in close agreement with the relative proper motion as determined by HIPPARCOS.

RMK 5: Closing, 0.50 ± 0.07 mas/yr. Primary is itself a double (HD 55598 and CPD-55 1174B). Rümker secondary is CD-55 1708.

RMK 6: Closing, 9.38 ± 0.06 mas/yr. Primary is a spectroscopic binary. Close agreement between the determined rectilinear motion and that inferred by the HIP proper motion.

RMK 8: Widening, 3.93 ± 0.14 mas/yr.

RMK 10: Widening, 0.14 ± 0.10 mas/yr. Proper motion data from both the HIP and GAIA missions are available. The large uncertainty in t0 is due to: the extremely slow relative motion (the slowest of our sample); and the large separation (~10.4 arcseconds at J2015.0).

RMK 11: Widening: 1.26 ± 0.25 mas/yr.

RMK 12: Widening, 2.82 ± 0.12 mas/yr.

RMK 17: Closing, 1.59 ± 0.11 mas/yr. Disparate proper motions.

RMK 20: Closing, 3.62 ± 0.01 mas/yr. Similar proper motions.

(Text continues on page 217)

The Southern Double Stars of Carl Rümker II: Their Relative Rectilinear Motion

Table 2: Rectilinear Elements and their uncertainties, all ICRS

RMK	x0 "	xa "/yr	y0 "	ya "/yr	t0 yr	θ0 °	ρ0 "
	+/-	+/-	+/-	+/-	+/-	+/-	+/-
1	-4.63768	-0.00455	18.26516	-0.00115	3691.82472	104.24681	18.84474
	0.98846	0.00059	0.43580	0.00026	1027.75053	2.93110	0.48744
3	1.81763	-0.00204	-1.94640	-0.00190	3126.16037	313.04064	2.66313
	0.19615	0.00018	0.08739	0.00008	380.67083	3.34059	0.14833
4	1.51283	0.01353	-3.41838	0.00599	2273.13836	293.87220	3.73818
	0.02239	0.00009	0.01717	0.00007	30.87234	0.33146	0.01813
5	-1.60271	0.00024	0.88157	0.00044	15407.22262	151.18704	1.82916
	1.13936	0.00009	1.13873	0.00009	5901.71816	35.67360	1.13921
6	4.01399	-0.00800	6.55690	0.00490	2525.12668	58.52597	7.68798
	0.07207	0.00014	0.06016	0.00012	87.91699	0.51444	0.06363
8	2.65704	-0.00268	2.48239	0.00287	1550.42556	43.05369	3.63622
	0.12623	0.00027	0.08616	0.00019	248.17533	1.68162	0.10940
10	9.10521	0.00002	-1.42270	0.00014	-3012.00720	351.11925	9.21569
	5.90460	0.00017	3.46400	0.00010	101342.38340	22.01999	5.85827
11	-2.22133	-0.00024	-0.43684	0.00124	-1564.21086	191.12556	2.26388
	0.95782	0.00027	0.92232	0.00026	908.24950	23.37677	0.95652
12	-6.80683	-0.00188	-6.05101	0.00211	1500.33914	221.63586	9.10756
	0.09344	0.00018	0.08306	0.00016	301.12882	0.55229	0.08900
17	8.22116	-0.00108	7.66155	0.00116	9168.62396	42.98211	11.23774
	2.13949	0.00030	1.03391	0.00014	3433.77602	8.37729	1.71658
20	0.08279	0.00361	0.84265	-0.00035	2437.53812	84.38862	0.84671
	0.03475	0.00008	0.03093	0.00007	131.73156	2.34897	0.03097
25	-0.41727	-0.00497	1.32091	-0.00157	3352.66840	107.53102	1.38525
	0.17939	0.00013	0.15245	0.00011	197.22727	7.32583	0.15509
27	2.13848	0.00336	-2.32489	0.00309	2493.73377	312.60843	3.15883
	0.06756	0.00014	0.05244	0.00011	164.97803	1.10818	0.05985
28	-3.26241	-0.00107	3.60044	-0.00097	4120.86184	132.18019	4.85865
	1.35100	0.00064	0.59959	0.00028	3203.61894	12.72483	1.01011

The Southern Double Stars of Carl Rümker II: Their Relative Rectilinear Motion

Table 3: HIP and GAIA position data and Ephemeris, all ICRS.

RMK	1991.25	(HIP)	2015.0	(GAIA)	2020.0		2025.0		2030.0	
	θ °	ρ "	θ °	ρ "	θ °	ρ "	θ °	ρ "	θ °	ρ "
	+/-	+/-	+/-	+/-	+/-	+/-	+/-	+/-	+/-	+/-
1	81.29989	20.46414	81.58779	20.42096	81.64856	20.41193	81.70937	20.40293	81.77025	20.39395
	0.00069	0.00586	0.00001	0.00017	0.00824	0.00137	0.01643	0.00271	0.02465	0.00406
3	2.92738	4.13337	2.32927	4.08300	2.20148	4.07246	2.07302	4.06193	1.94389	4.05142
	0.00045	0.00417	0.00004	0.00047	0.00594	0.00100	0.01132	0.00183	0.01686	0.00269
4	245.73211	5.60185	248.24731	5.34520	248.80760	5.29255	249.37909	5.24043	249.96200	5.18883
	0.00038	0.00143	0.00006	0.00014	0.00543	0.00040	0.00971	0.00072	0.01434	0.00106
5	225.93633	6.95384	225.91055	6.94238	225.90511	6.93997	225.89966	6.93755	225.89422	6.93514
	0.00029	0.00199	0.00003	0.00019	0.00386	0.00047	0.00720	0.00087	0.01066	0.00129
6	25.45552	9.17420	26.63652	9.05461	26.88910	9.02992	27.14307	9.00542	27.39842	8.98109
	0.00027	0.00338	0.00008	0.00093	0.00633	0.00110	0.00929	0.00162	0.01281	0.00222
8	68.54127	4.02825	69.72832	4.06931	69.97514	4.07818	70.22090	4.08712	70.46557	4.09613
	0.00168	0.00391	0.00008	0.00017	0.01894	0.00101	0.03714	0.00198	0.05543	0.00296
10	18.68870	10.39617	18.70465	10.39768	18.70801	10.39800	18.71136	10.39832	18.71472	10.39864
	0.00020	0.00416	0.00001	0.00031	0.00316	0.00086	0.00605	0.00165	0.00900	0.00246
11	127.84868	5.03443	127.69577	5.06128	127.66379	5.06693	127.63187	5.07259	127.60003	5.07825
	0.00131	0.00567	0.00021	0.00089	0.01865	0.00163	0.03184	0.00279	0.04604	0.00404
12	212.97951	9.21250	212.56752	9.22284	212.48091	9.22507	212.39433	9.22733	212.30780	9.22961
	0.00037	0.00462	0.00002	0.00029	0.00542	0.00092	0.01051	0.00178	0.01566	0.00265
17	357.58727	16.00323	357.68222	15.97641	357.70225	15.97077	357.72229	15.96513	357.74235	15.95949
	0.00021	0.00710	0.00001	0.00039	0.00265	0.00154	0.00522	0.00301	0.00782	0.00450
20	146.76197	1.82595	145.45490	1.75013	145.16521	1.73429	144.87018	1.71850	144.56969	1.70275
	0.00084	0.00208	0.00013	0.00032	0.01556	0.00049	0.02706	0.00084	0.03965	0.00122
25	28.58665	7.22378	28.77798	7.10244	28.81910	7.07690	28.86051	7.05137	28.90223	7.02584
	0.00034	0.00336	0.00002	0.00019	0.00497	0.00067	0.00974	0.00131	0.01461	0.00195
27	276.64163	3.90289	277.95003	3.84026	278.23090	3.82733	278.51366	3.81450	278.79833	3.80176
	0.00085	0.00258	0.00012	0.00024	0.01244	0.00061	0.02213	0.00113	0.03245	0.00168
28	99.84728	5.75019	100.13696	5.73192	100.19818	5.72809	100.25949	5.72427	100.32087	5.72046
	0.00268	0.00632	0.00005	0.00015	0.03181	0.00152	0.06346	0.00303	0.09518	0.00454

The Southern Double Stars of Carl Rümker II: Their Relative Rectilinear Motion

(Continued from page 214)

RMK 25: Closing, 5.21 ± 0.03 mas/yr. Component A is a spectroscopic binary. X-ray source at 5.2" from component Aa.

RMK 27: Closing, 4.56 ± 0.07 mas/yr.

RMK 28: Closing, 1.44 ± 0.19 mas/yr.

5 Conclusions

Our method of describing the relative Rectilinear motion of double stars produces objective results. It eliminates a number of the problems we believe are associated with the current *Catalog of Rectilinear Elements* (CORE) maintained by the USNO (see Section 2). We present the Rectilinear Elements of RMK 1, 3, 4, 5, 6, 8, 10, 11, 12, 17, 20, 25, 27, and 28 based on the data obtained from the HIPPARCOS and GAIA missions.

Acknowledgments

This research has made use of:

- The *Aladin sky atlas* developed at CDS, Strasbourg Observatory, France.
- The *Washington Double Star Catalog* maintained by the USNO.
- The *Catalog of Rectilinear Elements* (CORE) maintained by the USNO. We wish to particularly thank Bill Hartkopf of the UNSO who gave the first author a copy of the fortran program from which data in the CORE is currently generated.
- The HIPPARCOS Catalogue (The Hipparcos and Tycho Catalogues (ESA 1997)) from VizieR†.
- The GAIA Catalogue (Gaia DR1 (Gaia Collaboration, 2016)) from VizieR††.

References

Letchford, Roderick R, Graeme L White, and Allan D Ernest. 2017. "The Southern Double Stars of Carl Rümker I: History, Identification, Accuracy." *Journal of Double Star Observations* 13 (2): 220–32. http://www.jdso.org/volume13/number2/Letchford_220-232.pdf.

Lindegren, L, F Mignard, S Söderhjelm, M Badiali, H.-H. Bernstein, Patricia Lampens, R Pannunzio, et al. 1997. "Double Star Data in the HIPPARCOS Catalogue." *Astronomy and Astrophysics* 323: L53–56. http://adsabs.harvard.edu/abs/1997A&A...323L..53L.

Rümker, Carl. 1832. *Preliminary Catalogue of Fixed Stars: Intended for a Prospectus of a Catalogue of the Stars of the Southern Hemisphere Included Within the Tropic of Capricorn : Now Reducing from the Observations Made in the Observatory at Paramatta*. Hamburg: Perthes and Besser. http://adsabs.harvard.edu/abs/1833AN.....10..377R.

† http://vizier.u-strasbg.fr/viz-bin/VizieR-3?-source=I/239/h_dm_com
††http://vizier.u-strasbg.fr/viz-bin/VizieR-3?-source=I/337/gaia

The Southern Double Stars of Carl Rümker II: Their Relative Rectilinear Motion

Appendix: Figures

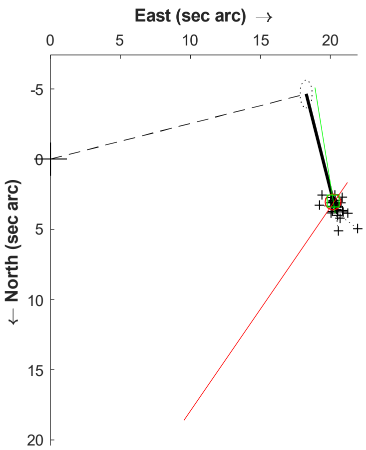

Figure 1. RMK 1

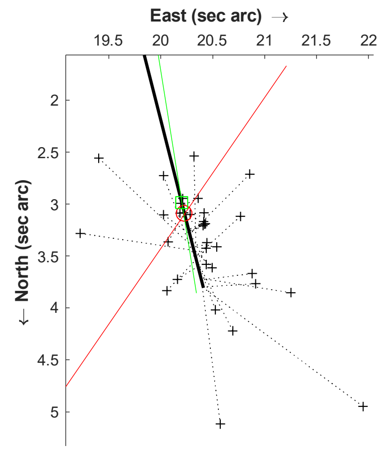

Figure 2. RMK 1 zoom

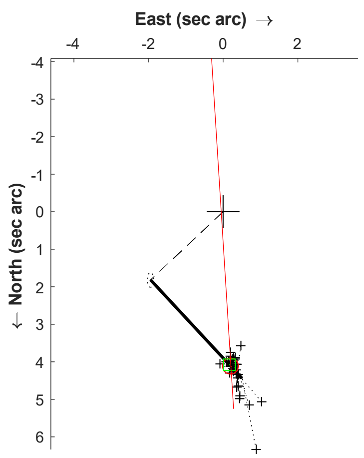

Figure 3. RMK 3

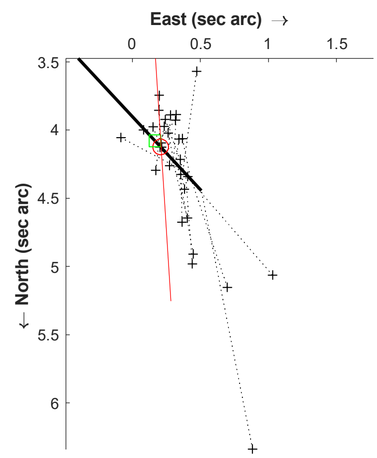

Figure 4. RMK 3 zoom

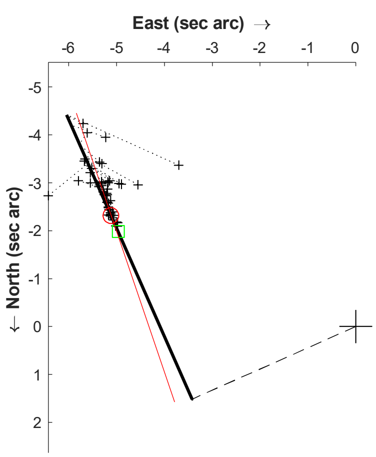

Figure 5. RMK 4

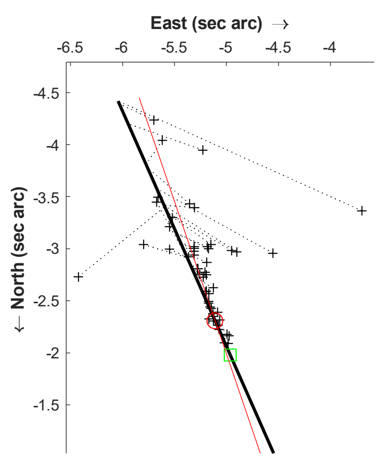

Figure 6. RMK 4 zoom

Appendix: Figures

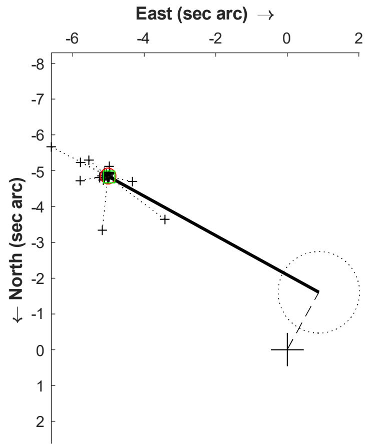

Figure 7. RMK 5

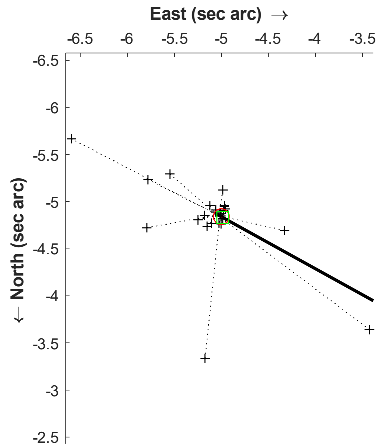

Figure 7. RMK 5 zoom

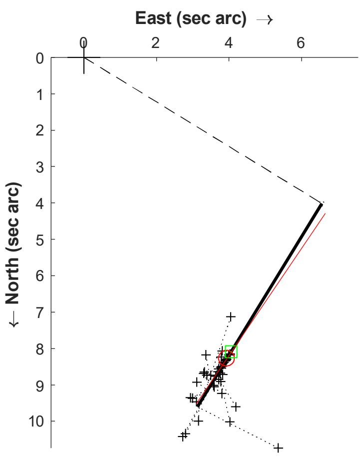

Figure 9. RMK 6

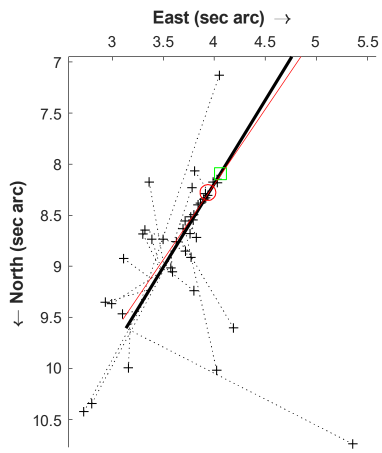

Figure 10. RMK 6 zoom

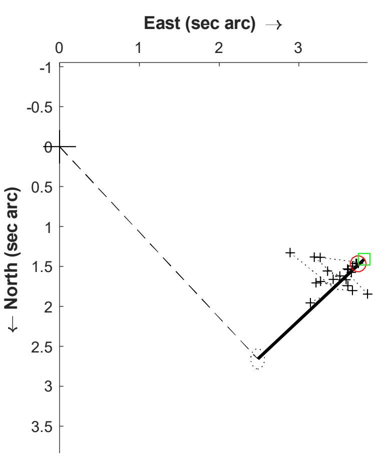

Figure 11. RMK 8

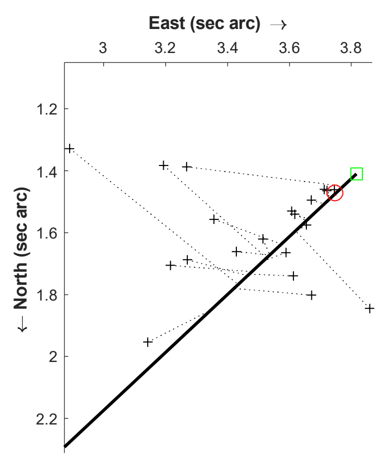

Figure 12. RMK 8 zoom

Appendix: Figures

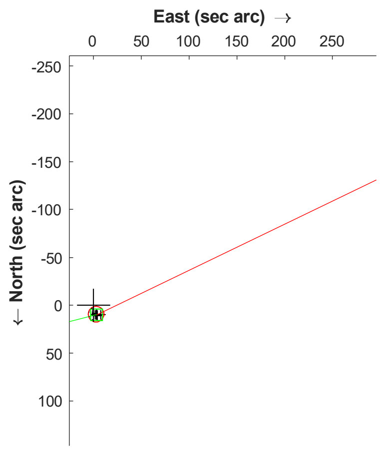

Figure 13. RMK 10

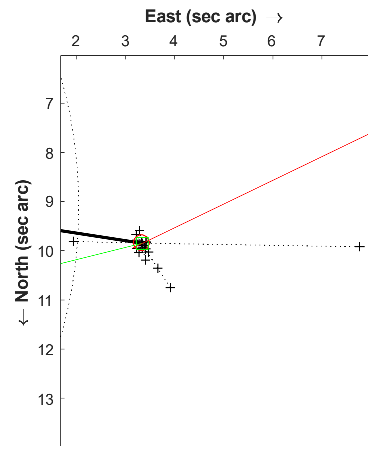

Figure 14. RMK 10 zoom

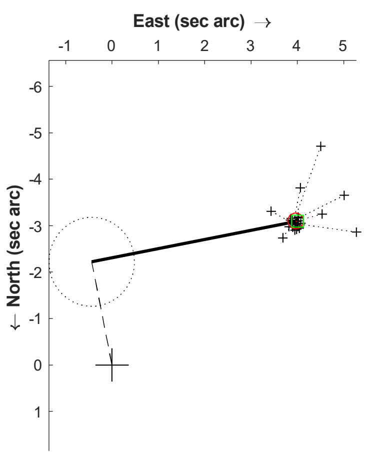

Figure 15. RMK 11

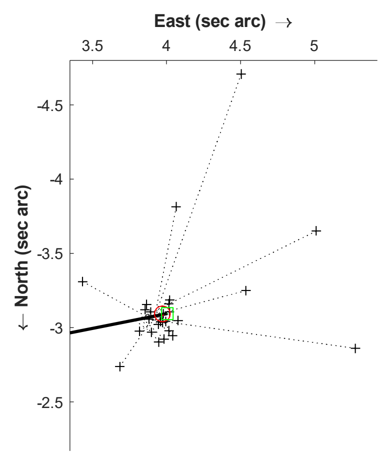

Figure 16. RMK 11 zoom

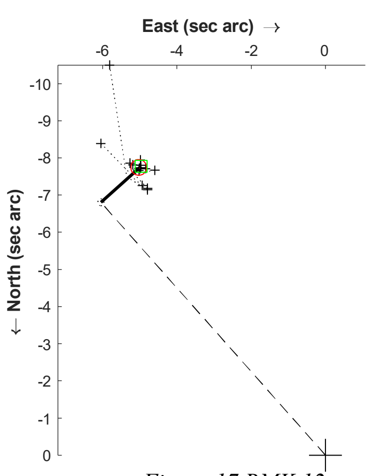

Figure 17 RMK 12

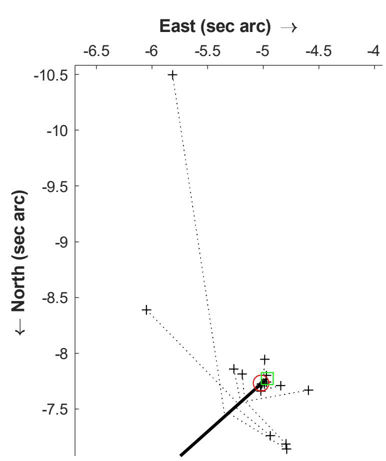

Figure 18. RMK 12 zoom

The Southern Double Stars of Carl Rümker II: Their Relative Rectilinear Motion

Appendix: Figures

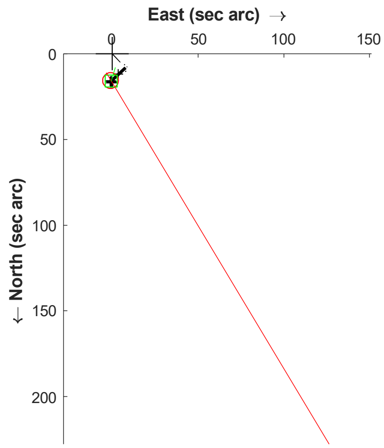

Figure 19. RMK 17

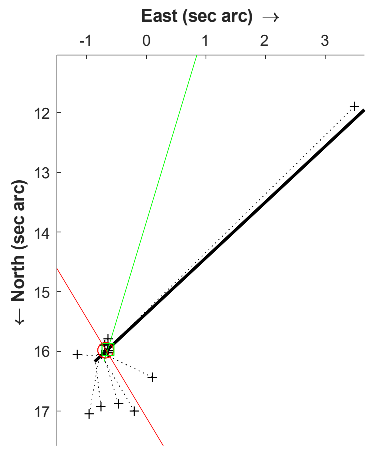

Figure 20. RMK 17 zoom

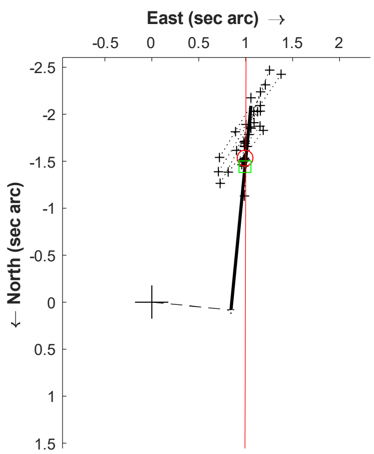

Figure 21. RMK 20

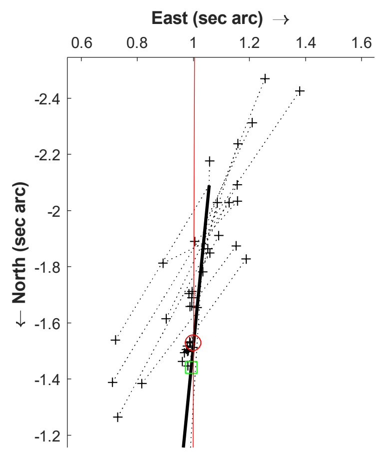

Figure 22. RMK 20 zoom

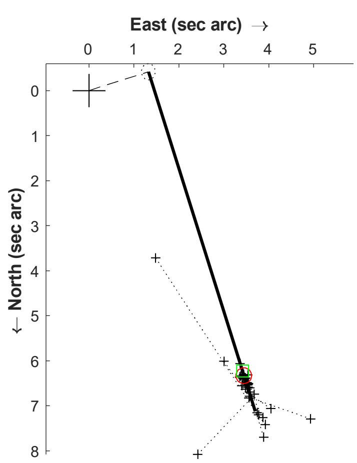

Figure 23 RMK 25

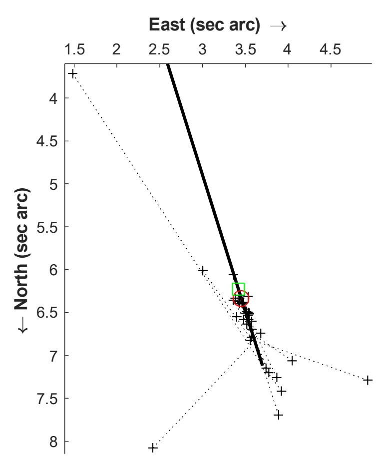

Figure 24. RMK 25 zoom

The Southern Double Stars of Carl Rümker II: Their Relative Rectilinear Motion

Appendix: Figures

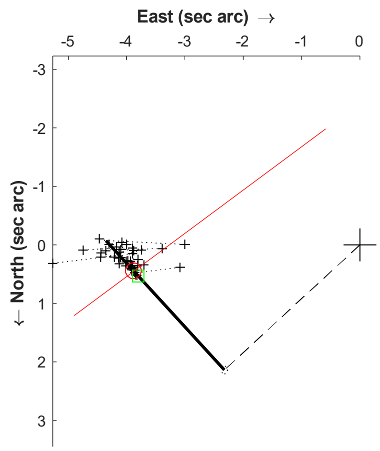

Figure 25. RMK 27

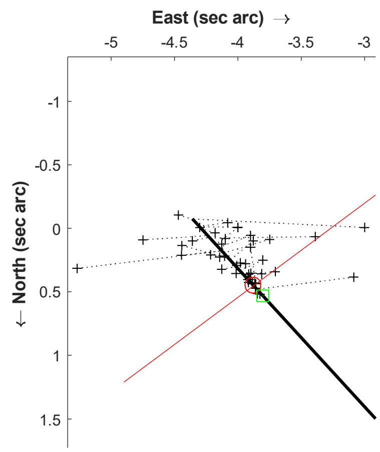

Figure 26. RMK 27 zoom

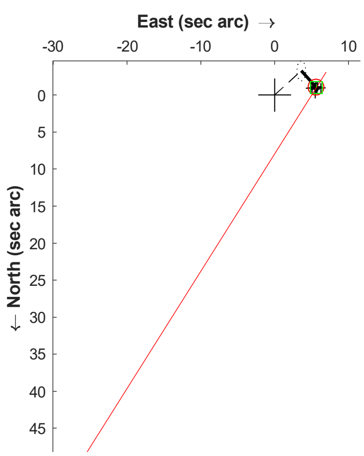

Figure 27. RMK 28

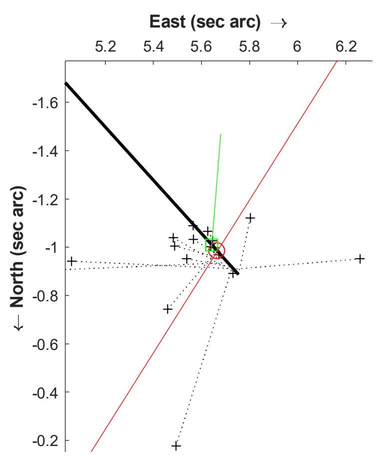

Figure 28. RMK 28 zoom

Speckle Interferometry with the OCA Kuhn 22" Telescope

Rick Wasson

Murrieta, California
ricksshobs@verizon.net

Abstract: Speckle interferometry measurements of double stars were made in 2015 and 2016, using the Kuhn 22-inch classical Cassegrain telescope of the Orange County Astronomers, a Point Grey Blackfly CMOS camera, and three interference filters. 272 observations are reported for 177 systems, with separations ranging from 0.29” to 2.9”. Data reduction was by means of the REDUC and Speckle Tool Box programs. Equipment, observing procedures, calibration, data reduction, and analysis are described, and unusual results for 11 stars are discussed in detail.

Introduction

Membership in the Orange County Astronomers (OCA), one of the largest and most active amateur astronomy clubs in the United States, has many privileges, not the least of which is access to the fine Kuhn 22-inch (0.56 meter) Cassegrain telescope, located at the club’s Anza observing site, with fairly dark skies at 4300 feet elevation, in the hills about 15 miles northeast of Mount Palomar Observatory. OCA member William Kuhn led a volunteer effort of many OCA members in designing and building the telescope, named after him. The observatory became operational in 1984, and has been used occasionally for research, particularly discovery of supernovae and asteroids. It is open to all club members and guests every month at new-moon star parties, for viewing all types of celestial wonders.

The combination of my long-time OCA membership, experience in observing double stars (Wasson, 2014), and the convenient Anza site located only 37 miles from my home, seemed a natural fit to attempt a new type of research - Speckle Interferometry - which would benefit greatly from a larger aperture than my own 12-inch telescope.

I was encouraged by a workshop on Speckle Interferometry presented by Russ Genet and Dave Rowe at the Society for Astronomical Sciences (SAS) meeting in June 2015.

From its inception in the 1970s until recently, Speckle Interferometry was practiced only by professional astronomers and graduate students, using specialized equipment at major observatories. The example shown in Figure 1 demonstrates the potential of Speckle Interferometry to improve measurement accuracy for close binaries, reducing uncertainty and eventually producing a high-quality orbit solution.

The technological revolution in small, sensitive, fast, moderately-priced CMOS cameras, now used extensively by amateurs to make exquisite planetary images, has also opened the Speckle imaging field to amateurs. The last piece of the puzzle, easy-to-use software for processing Speckle images, has only become available since 2010, making amateur Speckle Interferometry practical for the first time.

Why Observe Double Stars?

Everything we know about stars is based on observing their light with a range of instruments, to measure or derive their basic properties. The most fundamental property of any star is its mass, which determines how rapidly nuclear fusion proceeds in its core, and thus its intrinsic brightness and its life expectancy.

The only direct way to determine the mass of stars is by observing them in binary systems. Orbital velocity (measured by Doppler shift) and period are driven by the stars’ masses and distance apart. We need to know the apparent size of the orbit and its distance from us, to find the true physical size of the binary star orbit. Distance is measured most accurately by parallax; the Hip-

(Text continues on page 224)

Speckle Interferometry with the OCA Kuhn 22" Telescope

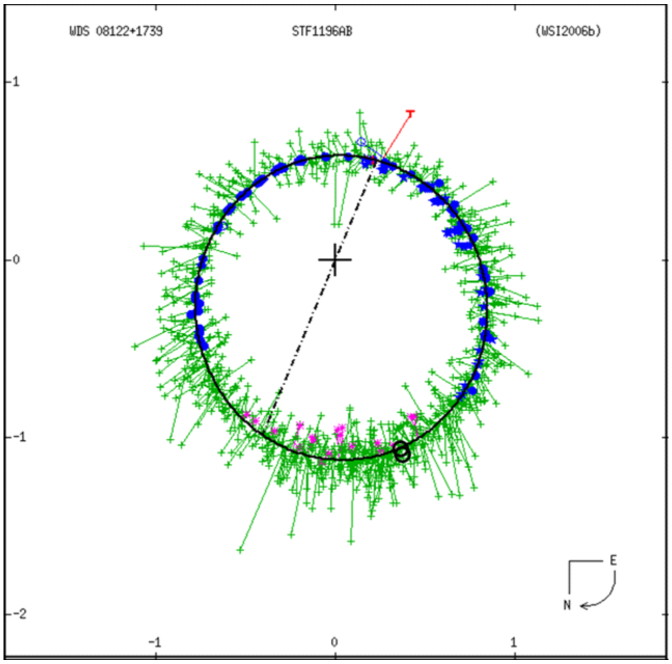

Figure 1. The orbit of STF1196AB, the brightest two components of the well-observed, multiple star system Zeta Cancri ("Tegmen"). These two stars (A and B) orbit each other in 59.6 years. The large + symbol represents the primary star. Solid blue dots (speckle interferometry) and small + symbols (visual micrometer) are measurements of the secondary star position. Note the improved precision (reduced scatter) of the speckle points as compared to visual observations. The ellipse is the best current orbit solution, giving extra weight to the speckle data. Lines from data points to the ellipse indicate the time on the orbit at which the data point was taken. The scales are in arc seconds. Two new speckle points from this paper are shown as black circles, added to the plot by the method of Buchheim, 2017.

parcos satellite of the 1990s made great improvements in distance accuracy, and the next-generation Gaia satellite is now in operation. That leaves the apparent orbit ellipse as the last measurement needed to define the stellar masses accurately.

Surprisingly, less than 60 binary star systems have *accurately* measured (definitive) orbits, so the quality of our models of stellar evolution hangs on this remarkably small sample! Many systems with large orbits are so slow that they have not completed a single orbit since measurements began (about 250 years ago by William Herschel), and many "fast" orbits appear so close together that they can only be resolved by very large telescopes. But many others, some having orbital periods of a few decades, are near enough that their separation can theoretically be resolved and measured by the Kuhn 22-inch aperture, for which the "Rayleigh limit" resolution is about 0.3 arc-sec; thus, the Kuhn 22-inch telescope has the potential to help refine the accuracy of stellar masses – among the most fundamental properties in astronomy!

The "Seeing" Problem

The theoretical angular resolution of any telescope depends only on the wavelength of light and the telescope aperture - the larger the aperture, the smaller and closer are details which can be resolved. But for telescopes larger than about 4 inches, atmospheric "seeing" begins to limit the resolution that can be achieved. The problem, of course, is that the sharp, diffraction-limited image of a star is continuously chopped up, shifted and smeared in random ways by small atmospheric cells of variable temperature, density and refraction index, creating an image that is blurred into the "seeing disk."

A most remarkable fact was discovered and demonstrated by Anton Labeyrie in 1970: the full-resolution information of a double star image still exists in the scrambled "seeing" disk! If very short exposures are taken to "freeze" the motion, each frame shows a pattern of small "speckles." This is the interference pattern of images formed by many, small, separate atmospheric cells, superimposed upon each other, swirling within the seeing disk. Constructive interference forms a bright speckle. Picture the moving pattern of light "speckles" on the bottom of a swimming pool, created by the wavy surface acting like a bunch of small, moving, tilting lenses.

The power of Speckle Interferometry is to recover almost all the information contained in a diffraction-limited image of a double star formed by the full telescope aperture. Fourier Transform analysis finds dimensional frequency information (spacing and orientation) from the speckle patterns of each frozen image; the information gathered from many images is then averaged. Those speckles related to the diffraction-limited image add together, while randomly positioned speckles do not. Quality is enhanced by observing a single reference star, nearby on the sky and near in time; deconvolution with the reference star helps cancel distortions which are common to both the single and double star images.

Equipment - Telescope

The Kuhn 22-inch telescope is an f/8 classical Cassegrain design on an equatorial fork mount. It has encoders on both axes, and "Go-To" capability using an older version of TheSky software (www.bisque.com). Although it was built decades ago, club members have upgraded and maintained it well. It can find most objects within a few arc minutes, well within a medium power eyepiece field. Tracking errors from frame to frame are usually smaller than the seeing movements caused by the atmosphere, which are stopped anyway by taking short exposures (typically 10 to 40 milliseconds), so the telescope is suitable for high magnification Speckle Interferometry.

Equipment - Camera

For all the observations in this paper, I used a Point Grey BlackFly 23S6M-C high-speed monochrome camera, having a Sony IMX249 CMOS detector with 5.86μ square pixels in a 1920x1200 array, and a global shutter (https://www.ptgrey.com). This camera was chosen because of its fairly large detector (11.2mm x 7.0mm), advertised low read noise (7e- rms), high Quantum Efficiency (82% peak at 500nm), high speed USB3.0 interface (more than 30 fps full frame), and moderate price ($495). A larger-than-usual CMOS detector was considered important for the following reasons:

1. Prior experience with my 12-inch Go-To Dobsonian telescope at home had shown that it may be difficult to acquire and track faint stars at high magnification required for speckle work, and the pointing and tracking performance of the 22" was unknown to me at the time.

2. I planned to investigate the sidereal drift method to calibrate images for orientation and plate scale (discussed in detail below), where a larger field, giving a longer drift, is helpful.

Equipment – Eyepiece Projection

High magnification is required in Speckle Interferometry, so that details of the distorted star images can be seen; individual speckles, which are comparable in size to the Airy disk, should each cover at least several pixels. Proper magnification is a balance between magnifying enough for adequate pixel sampling of the image, but not magnifying so much that S/N is low and fainter stars cannot be detected. I have had success with plate scales of about 0.07 arc-sec/pixel, so that the Airy Disk spans about 8 pixels, a value recommended by Dave Rowe (Rowe, 2016) based on simulation studies. For the Kuhn aperture and detector pixel size, this corresponds to about f/30. A spreadsheet was developed to estimate the magnification achieved for eyepiece projection or a Barlow lens.

For all the observations presented here, magnification was accomplished by eyepiece projection, using a Baader Hyperion 10mm eyepiece, T2 threaded adapters on the eyepiece and camera, and T2 projection tubes. Screw threads helped make a solid, rigid optical assembly. A flip mirror and 23mm illuminated reticle eyepiece were used to find, identify and center target stars. The cabling is clean and simple: a single 3-meter USB3.0 cable supplied 5VDC power to the camera and carried data to the laptop computer. My setup ready for speckle interferometry is shown in Figure 2.

Equipment - Filters

In early observations, a red filter was used to minimize color dispersion of the speckles. It was simply screwed into the $1^1/_4$-inch threads on the front of the Baader Hyperion eyepiece. After purchasing a ZWO manual filter wheel (https://www.zwo.com), additional filters were also used during each observing run.

Table 1 gives the filter characteristics. The filters are not members of any photometric standard series,

Figure 2. Left: Speckle Interferometry installation on the Kuhn 22" Telescope. A single blue USB3.0 cable connects the camera to the laptop on the white table at lower right. Right: Close-up of the simple finding and magnification optics: an illuminated reticle eyepiece is at top in the flip mirror; below are the Baader Hyperion 10mm eyepiece, projection tubes, and tiny (30mm cube) camera, attached to the blue USB3.0 cable. No filter wheel was used in this early configuration.

such as Johnson-Cousins or Sloan. However, these interference filters are similar in bandpass to some of the photometric standard filters, with significant advantages over colored glass: sharper cutoff, symmetric transmission profile, much better durability and lower price. If differential photometry of close binary stars becomes practical in the future, it is believed that the G and R filters, which are part of the Baader LRGB series for CCD imaging, will transform well to the standard photometric systems, because G has 50% transmission wavelengths very close to Johnson V, and R has the same 50% transmission width as Cousins R, but shifted about 15 nm farther red. The "IR742" filter is not a good match to any photometric filters, but was used in attempting to observe faint late-type stars. Unfortunately, the QE of the IMX249 CMOS detector is low in the near IR, only about 16% at 823nm. However, some recent Sony CMOS detectors have improved QE, even approaching that of back-illuminated CCDs.

Preparing for a Speckle Run

Double star targets were chosen by searching the Washington Double Star (WDS) Catalog, using the online tool developed by Tom Bryant (2015), by way of his web site. The search parameters generally employed were:

- 3.0" > Separation < 0.3" (0.3" is the approximate Rayleigh criterion for 22" aperture)
- Primary star brighter than magnitude 10
- Magnitude difference less than 3
- Declination between +70° and -30°
- Each search limited to a 2-hour RA window.

Within any given RA range, the WDS provides many candidates. Those with at least a preliminary orbit were preferentially selected, with the goal of adding quality speckle points to help refine the orbits. Other target stars included some late spectral types (K0 and later) and Hipparcos discoveries that have shown some movement. For each selected double star, the WDS data line was copied into an EXCEL spreadsheet. Multiple sheets, each containing targets in a 2-hour RA window, constituted a Master Target List workbook. Some spreadsheets were printed, to act as both the target list and log for hand-written notes at the telescope.

For some stars, more information was found at the Italian website Stelle-Doppie (Sordiglioni, 2016), including SAO number, orbital period, and current orbit ephemerides for separation and PA. The WDS orbit plots were also copied and hyper-linked into the spreadsheet for quick reference. For observations made after June 2016, the "master" spreadsheet was copied, then used as a computer log during the run, by editing recorded sequence numbers and notes into the spreadsheet in real time, eliminating the paper log.

I have found that the easiest way to identify target stars at the telescope is by SAO catalog number, so the SAO number of each target double star, and a nearby single "reference" star (used for deconvolution during data reduction) were added to the Master Target List spreadsheets. This was a time-consuming process, but saved observing time. Dave Rowe has recently developed a WDS search program WDS1.0 (Rowe, 2017) which searches the WDS catalog for double stars according to user-input parameters, but also has the very useful feature of listing all nearby SAO stars by magnitude, spectral type and distance from the double, thus saving a great deal of manual search time. The general faint limit of about 10th magnitude for SAO stars seems well suited to the 22" for my camera, magnification and typical 30-millisecond exposures; fainter stars are often buried in the noise, but there are plenty of suitably bright targets.

At the Telescope

Observing runs were made only about once per month, for convenience in scheduling, allowing choice of "good" nights, and giving plenty of time for data reduction. After following the checklist for opening the OCA observatory and preparing the Kuhn telescope and control computers, the Speckle Interferometry optical train is screwed together and installed in the Cassegrain 2-inch focuser. The cable from the camera is plugged into a USB3.0 port on the laptop, and the data acquisi-

Table 1. Filter characteristics. These interference filters typically have a sharp rise and fall of about 10 nm width, and a high, nearly constant transmission plateau (95+%). The "IR742" filter is a long-pass IR transmission filter; the asterisks indicate convolved characteristics: the filter transmission times the QE of the Sony IMX249 monochrome CMOS detector, as measured by Point Grey (https://www.ptgrey.com).

Filter	Manufacturer Name	50% Band Pass (nm)	Center Wavelength (nm)	Width (nm)	Peak Transition
G	Baader G (CCD)	495 - 575	534	80	96%
R	Baader R (CCD)	585 - 690	636	105	98%
IR742	Astronomik ProPlanet 742	740 – 1000 *	823 *	250 *	30% *

tion software FireCapture (Edelmann, 2015) is started. This program, designed primarily for planetary imaging, is used because it can handle many types of cameras and can output frames as FITS files, which is a convenient format for Speckle data reduction.

The telescope is slewed to a bright star, the star is centered in the illuminated reticle eyepiece, then focused and centered in the camera display screen, and "synced," to be sure TheSky software knows accurately where the telescope is pointing. The highly-magnified, turbulent image of the moderately bright star is focused until speckles become clearly visible on the laptop screen. Since the telescope truss tube is made of welded steel tubing, and the mirror is about 3 inches thick, focus can change slightly as the telescope cools through the evening. Re-focusing is needed when the speckles gradually become "soft" or smeared, or the star image shape appears distorted in a systematic way. Re-focus movements were very small, and the possible effect on image scale calibration was not investigated.

After selecting a target double star, typing in its SAO number, and clicking the "slew" command, the telescope comes to life, majestically but quietly "humming" its way toward the target, which is almost always seen in the eyepiece of the flip mirror. After centering in the illuminated reticle eyepiece, the star is always close to the center of the camera CMOS chip displayed on the laptop. The double star target is centered and a small "Region of Interest" (ROI) selected in FireCapture, usually a 512x512 pixel patch (about 40x40 arc-sec) near the center of the chip. With the filter, exposure and camera settings confirmed, FireCapture is ordered to record 1000 frames, and I watch as the star boils and dances for about 30 seconds, to be sure it doesn't drift too near an edge of the ROI field. Only bright and well-separated double stars (more than about 1 arc-sec) are obviously seen as double on the screen; a tight and/or faint companion is invisible in the seeing mess, but it is still there! 1000 frames are taken as a good sample of the random variations in speckle patterns produced by the atmosphere, to get an accurate average of the speckle spacing and orientation information.

The next target is a "reference" star, which is a nearby *single* star, used later for deconvolution in data reduction. All the same optical imperfections that affect the double star are captured in the reference star as well, including even focus and some atmospheric effects. By Fourier Transform "deconvolution," these small effects are cancelled from the double star data, greatly improving and sharpening the Autocorrelation end product.

Although only one sequence is required for a speckle measurement, several sequences may be taken, to provide improved S/N or statistical samples for defining uncertainty of the final measurement. More frames are generally better, especially for fainter, closer doubles.

Light passing through the atmosphere is affected by atmospheric dispersion: the atmosphere refracts different wavelengths by different amounts, forming a miniature spectrum at focus. This effect may be noticeable at very high magnification, and increases rapidly at large zenith angles. An atmospheric dispersion corrector (ADC) was not used for these observations, but "smearing" was minimized by using filters to restrict the wavelength range, and by usually limiting observations to stars within about 40 degrees of the zenith. Nevertheless, in some results, the "smearing" was noticeable, reducing the measurement accuracy somewhat.

Calibration

The Drift Calibration method was used to calibrate each night's data for Plate Scale and Camera Orientation on the sky. Multiple drifts were made throughout the night, usually on brighter reference stars, and the average results of all drifts were used to reduce all the speckle data for that night. This method applies only to equatorially-mounted telescopes, and no adjustments can be made which could change the magnification or rotate the camera.

To make a Calibration Drift sequence, a special ROI was used, having full E-W frame width (about 2½ arc-minutes) but only 300 pixels in N-S height; this ROI speeds up the frame rate and reduces hard drive storage space. A moderately bright star was moved to the east edge of the field, then the recording sequence was started and immediately the circuit breaker powering the telescope RA drive motor was turned off. After the star drifted at the sidereal rate from the eastern to the western edge of the field, the breaker was turned back on. The telescope was driven west with the hand paddle control until the star was again recovered. A drift typically takes about 10 seconds near the equator, and longer at higher declination. A series of several drifts was usually made with the same star. After the drift series was completed, TheSky was "synced" once more to re-establish accurate telescope pointing.

The sidereal drift path of the star describes the true east-west direction, distorted somewhat by the star bouncing around in the seeing disk, or possibly by a breeze moving the telescope, so the more drifts the better. The FireCapture acquisition software writes the computer clock time (to the nearest millisecond) to the FITS header of each frame. The exposures are short enough to stop the sidereal motion in each frame, as well as the seeing motion. Thus, the drift sequence records hundreds of star positions (seeing-distorted image centroid, in pixels) at known times. The least-squares slope of the star positions calibrates the rotation angle of the camera relative to the true east-west direction on the sky. Changes in star position versus time, and the known sidereal rate (a function only of star declination) are used to calculate the pixel scale calibration constant (arc-sec / pixel).

This drift analysis was originally done - very laboriously - in a spreadsheet, but is now part of the Speckle Tool Box (STB) data reduction program (Harshaw, Rowe, and Genet, 2017), making it *very much* easier, faster, and more accurate. Figure 3 is an example of one night's calibration data. Each drift sequence was first edited in REDUC (Losse, 2015) to delete frames having the star not in the field, or overlapping the edge. REDUC then calculated the camera rotation angle on the sky by least-squares fitting the star position from all valid frames. The same set of valid frames was then processed in STB, calculating both the drift angle and pixel scale factor, using the computer clock time written to the FITS header. For each drift, the camera angle results from REDUC and STB usually agree very closely: within a few hundredths of a degree.

Very rarely, a laptop clock "glitch" was found to occur. The cause may be either intensive processing by a program other than the FireCapture image acquisition program, or by an automatic clock update during sequence acquisition. The quad processors of the Intel i7-based laptop make such events very rare, but when they occur they are easily identified: there is a large effect on pixel scale, which depends on self-consistent time within the sequence, but no effect on the drift angle, which does not depend on time.

Data Reduction and Speckle Analysis

Speckle Interferometry data reduction is accomplished by Fourier Transform mathematical analysis of dimensional frequency information - that is, the spacing and orientation of the speckle patterns in every frame. It requires some intense "number crunching!" Processing includes taking Fast Fourier Transforms (FFT) of all 1000 individual frames in the binary star sequence, then averaging the results. The same operations are done for the sequence of single "reference" star frames. In "deconvolution," the average transform of the double is divided by that of the reference, tending to cancel aberrations and distortions that are common to both sets. The cancelling benefit can include optical aberrations (central obstruction, mirror imperfections, coma, focus errors, etc.), and even some atmospheric effects!

In the last step of processing, an inverse Fourier Transform is taken to give an "Auto-correlogram." Although it may look like a picture of the stars, it is no longer a real image. But the auto-correlogram still contains the near-diffraction-limited information from which measurements are made. An example is shown in Figure 4.

Fortunately, the "heavy lifting" of Fourier Transform math for speckle image processing has been implemented already, and is transparent to the user. At least two freeware programs for Speckle data reduction are available on-line to amateur astronomers, by request of the authors: REDUC (Losse, 2015) and Speckle Tool Box (STB) (Harshaw, Rowe, and Genet, 2017). STB1.05 was used for all position angle (PA) and separation measurements presented here.

STB marks the secondary peak chosen to measure PA and separation, with a purple "ship's wheel" symbol, as seen in Figure 4. Measurements are based on

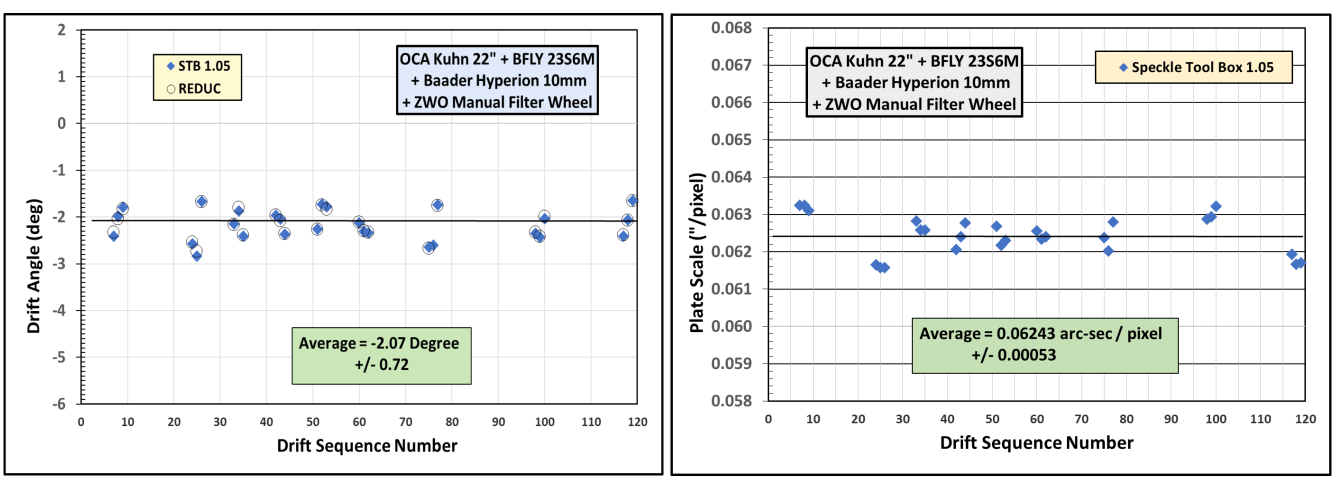

Figure 3. Results of Drift Calibration sequences during a Speckle run in November 2016, using the STB and REDUC programs. Left: Drift Angle. Right: Plate Scale.

calculation of the centroid of the secondary peak, to a small fraction of a pixel. Because the speckle images, and resulting auto-correlogram peaks, are over-sampled (typically ~8 pixels across the Airy disk), the centroid location is very accurate, yielding accurate measurements.

The STB default orientation is north down, east right like most reflecting telescopes show, and like the WDS orbit plots. However, I always orient my camera with north up and east left, as though looking at the sky with the pole up – it's just easier for my foggy brain to think about late at night - so my orientation is rotated 180 degrees. Therefore, I always choose the peak in the opposite quadrant, which gives the correct numerical PA value. The observer must be careful to select the peak consistent with actual image orientation. The same convention and care must also be used in interpreting the camera calibration angle from the STB Drift Calibration tool.

Speckle Measurement Uncertainty and Observation Quality

Quality of the speckle measurements was not rigorously evaluated. Usually only one sequence of 1000 frames was recorded, and no statistical information was calculated. For very faint systems, 2000 to 5000 frames were sometimes recorded, aiming to improve S/N - but even then, all the frames were processed as one sequence, yielding no statistics.

Standard deviation was calculated for calibration data, since many samples were acquired each night. Standard deviation of the camera drift angle for all nights ranged from 0.01 degree to 0.72 degree, with an average of 0.26 degree. Standard deviation of pixel scale ranged from 0.25% to 2.82%, with an average of 0.83%. Therefore, it is assumed that the *minimum* uncertainty of PA is roughly 0.3 degree, and the *minimum* uncertainty of separation is roughly 0.8%. The total uncertainty of the measurements, considering unknown error sources besides calibration, must be greater, perhaps more than twice these values. Therefore, the typical uncertainties of the measurements presented here are estimated to be roughly +/-1 degree for PA, and +/-0.01 arc-sec for separation.

A *qualitative* figure of merit was assigned to each measurement, as shown in Table 2, with values rated from 1 to 7. When measuring PA and separation in STB, the auto-correlograms of most doubles were bright and wide enough to yield very "solid," repeatable solutions. Observations with mild atmospheric dispersion, causing "smeared" auto-correlogram peaks, were assigned quality 2. For very close and/or faint doubles, the measurements were sometimes difficult. Values of 5 are not considered very accurate, because the secondary peak of the auto-correlogram was not clearly separated from the central peak, making its centroid location uncertain. Values of 6 are also unreliable because the faint secondary peak was distorted by, or not clearly distinguishable from, background noise. A value of 7 indicates that no reasonable measurement was possible. In Table 3, those measurements having poor quality of 5, 6 or 7 are flagged in color.

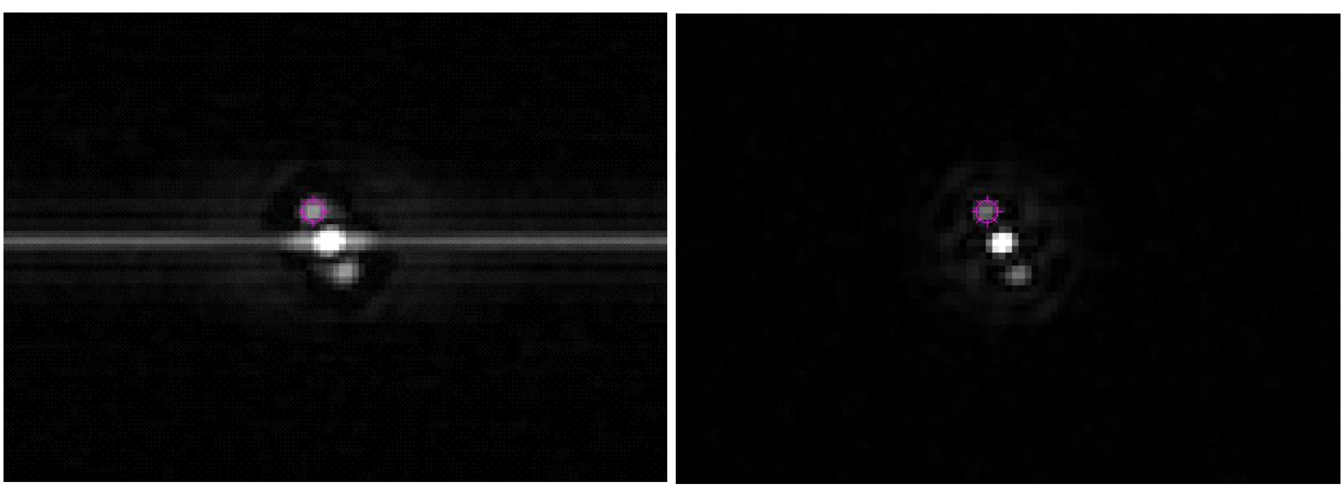

Figure 4. The Auto-correlogram of the binary star BU688AB, WDS magnitudes 8.1 and 8.6, observed with the Kuhn 22" and R filter on September 1, 2016. The bright central peak corresponds to the Airy disk of the primary star, always centered in the frame. The Fourier Transform process creates two equally valid peaks corresponding to the secondary star; they have the same separation, but are exactly 180 degrees apart. Selection of the correct one (purple "ship's wheel" symbol) is based on prior observation trends or an estimated orbit. Left: The horizontal line is an artifact of line pattern ("read") noise of the CMOS camera. Right: Employing the Interference and High Pass filtering features of STB cleans up the Auto-correlogram beautifully. The measured Separation was 0.406 arc-sec, PA=195.43 deg.

Speckle Interferometry with the OCA Kuhn 22" Telescope

Table 2. Qualitative Figure of Merit for Speckle Measurements. A Figure of Merit code number is given for each measurement in Table 3.

Figure of Merit	Notes Related to Quality of the Observations
1	Bright, clear Auto-correlogram. Solid measurement.
2	Some distortion of fringes or peaks, but measurement solid.
3	Close, but measurement clear, solid.
4	Companion faint, but measurement clear, solid.
5	Very close. Measurement uncertain.
6	Companion very faint. Measurement uncertain.
7	Companion too close or faint. Measurement NOT valid.

Double Star Separation and Position Angle Measurements

Speckle measurements were made from September 2015 through December 2016, observing with the OCA Kuhn 22-inch telescope approximately one night per month. A total of 177 double stars were observed in up to three filters, with separations ranging from 0.29 to 2.9 arc-seconds, and secondary WDS magnitudes from 5.5 to 9.9. The speckle measurements are presented in Table 3.

Discussion of Selected Double Stars

Many of the stars observed in Table 3 are binaries with at least a preliminary orbit. Some were found to have large Separation or PA O-C values, relative to the orbit ephemerides. In addition, a few stars had large movement from relatively few prior measures. Some of those, with O-C greater than 0.1" separation or 10 degrees PA, are discussed below.

The binary **00022+2705 BU733AB** (85 Peg) has a very high proper motion (+830-989) and short period (26.28 years). It was observed in the R filter at a separation of 0.309", barely above the Rayleigh criterion of 0.286". The night was marginal, with occasional high clouds, and the speckle solution centroid was uncertain (figure of merit 6). The results are shown in Figure 5.

The Hipparcos-Tycho satellite observed **02194 +6616 TDS2201** as double (PA=123.5 deg, separation=0.32") in 1991, but this remains the only prior observation. The current measure of Table 3, in the "R" filter, is PA=94.93 deg, separation=0.462". However, this observation was rated only as quality 6 (Table 2), because the companion was very faint, the secondary peaks were barely above the background noise, as seen in Figure 6, and the secondary peak centroid was uncertain. There was also a second pair of peaks, shown in the speckle auto-correlogram of Figure 6. The peak at 94 degrees was chosen because it was slightly stronger, closer to the Tycho value, and the "smeared" shape of

(Continued on page 236)

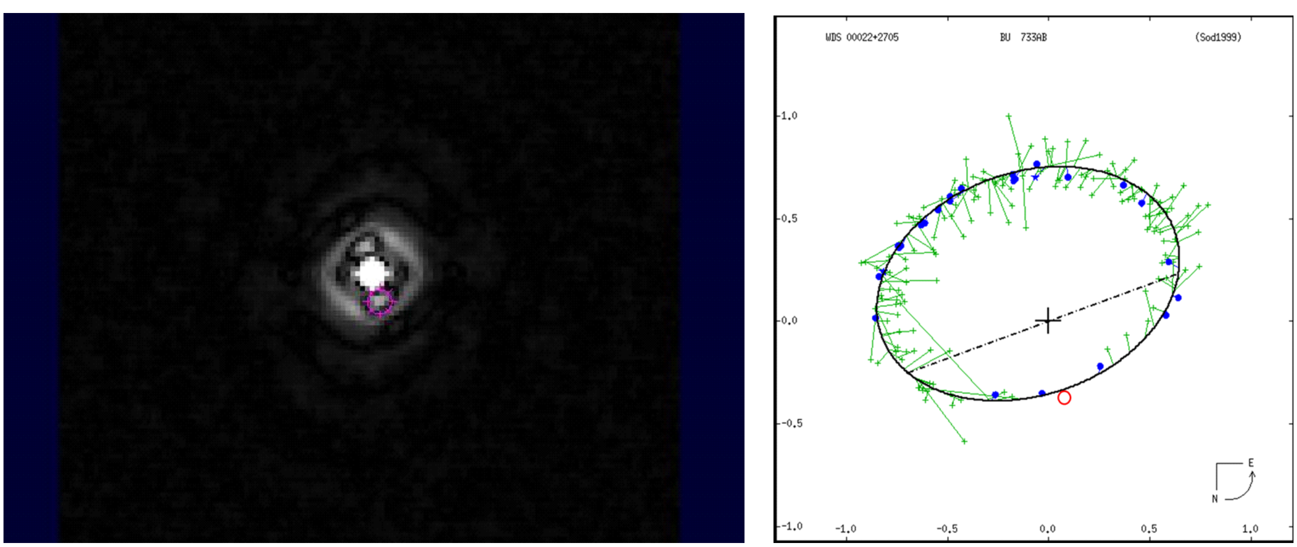

Figure 5. Left: BU733AB STB auto-correlogram. Right: Orbit plot from the WDS 6th Orbit Catalog, with the new speckle point

Table 3. Speckle measurements in 2015 and 2016, using the OCA Kuhn 22-inch telescope, Point Grey BlackFly-U3-23S6M-C CMOS camera, and interference filters. The columns are: observation date, WDS designation, WDS discovery designation, filter (Table 1), position angle observed (degrees), separation observed (arc-seconds), and qualitative figure of merit (Table 2).

Obs Date	WDS	Discovery	Filter	ThetaO	RhoO	Quality
2015.846	00014+3937	HLD60	R	166.72	1.328	4
2015.934	00022+2705	BU733AB	R	12.10	0.385	6
2015.846	00028+0208	BU281AB	R	159.74	1.579	1
2015.958	00049+3005	A1250AB	R	41.22	0.885	1
2016.843	00063+5826	STF 3062	G	359.36	1.528	1
2016.843	00063+5826	STF 3062	IR742	359.41	1.503	1
2015.934	00063+5826	STF3062	R	358.08	1.548	1
2016.843	00063+5826	STF 3062	R	359.40	1.509	1
2015.958	00065+1250	TDS1293	R	4.91	0.430	3
2016.843	00118+2825	BU 255	G	66.24	0.447	4
2016.843	00118+2825	BU 255	IR742	71.86	0.467	4
2016.843	00118+2825	BU 255	R	67.53	0.432	1
2016.843	00121+5337	BU 1026AB	G	321.12	0.355	4
2016.843	00121+5337	BU 1026AB	IR742	329.64	0.371	3
2016.843	00121+5337	BU 1026AB	R	323.19	0.338	5
2016.994	00308+4732	BU394AB	G	277.87	0.809	1
2016.994	00308+4732	BU394AB	IR742	277.62	0.789	2
2016.994	00308+4732	BU394AB	R	278.13	0.811	1
2016.994	00550+2338	STF73AB	G	331.58	1.145	1
2016.994	00550+2338	STF73AB	IR742	331.37	1.132	1
2016.994	00550+2338	STF73AB	R	331.44	1.144	1
2015.934	01006+4719	MAD1	R			7
2015.958	01006+4719	MAD1	R	1.27	0.836	1
2015.958	01014+1155	BU867	R	352.46	0.659	1
2015.846	01030+4723	STT21	R	175.23	1.294	1
2015.958	01097+2348	BU303	R	293.52	0.607	1
2015.846	01106+5101	BU235AaAb	R	140.41	0.835	1
2016.843	01234+5809	STF 115AB	G	158.45	0.403	1
2016.843	01234+5809	STF 115AB	IR742	160.43	0.448	1
2016.843	01234+5809	STF 115AB	R	158.82	0.405	1
2016.994	02037+2556	STF208AB	G	344.32	1.419	1
2016.994	02037+2556	STF208AB	IR742	344.30	1.413	1
2016.994	02037+2556	STF208AB	R	344.24	1.410	1
2016.994	02140+4729	STF228	G	303.39	0.653	1
2016.994	02140+4729	STF228	IR742	304.92	0.647	1
2016.994	02140+4729	STF228	R	303.77	0.654	1
2015.934	02186+4017	EGG2Aa,Ab	R			7
2015.958	02194+6616	TDS2201	R	94.93	0.462	6
2015.958	02211+4246	STF248	R	206.69	0.722	2
2015.934	02231+7021	MLR377AB	R	141.07	0.803	4
2016.994	02471+3533	BU9AB	G	217.19	0.925	4
2016.994	02471+3533	BU9AB	IR742	216.96	0.922	1
2016.994	02471+3533	BU9AB	R	217.31	0.925	4
2016.994	02572+0153	A2413	G	164.92	0.612	1
2016.994	02572+0153	A2413	IR742	174.36	0.495	6
2016.994	02572+0153	A2413	R	165.12	0.619	1
2016.994	02589+2137	BU525	G	274.01	0.551	1
2016.994	02589+2137	BU525	IR742			7
2016.994	02589+2137	BU525	R	274.56	0.536	1

Table 3 continues on next page.

Table 3 (continued). Speckle measurements in 2015 and 2016, using the OCA Kuhn 22-inch telescope, Point Grey BlackFly-U3-23S6M-C CMOS camera, and interference filters. The columns are: observation date, WDS designation, WDS discovery designation, filter (Table 1), position angle observed (degrees), separation observed (arc-seconds), and qualitative figure of merit (Table 2).

Obs Date	WDS	Discovery	Filter	ThetaO	RhoO	Quality
2016.917	03054+2515	STF346AB	G	256.32	0.464	1
2016.917	03054+2515	STF346AB	G	256.09	0.465	1
2016.994	03054+2515	STF346AB	G	255.97	0.450	1
2016.994	03054+2515	STF346AB	IR742	256.22	0.472	1
2016.917	03054+2515	STF346AB	R	257.36	0.462	1
2016.917	03054+2515	STF346AB	R	256.83	0.460	1
2016.994	03054+2515	STF346AB	R	255.97	0.445	1
2015.958	03101+2145	BU1030AB	R	101.93	0.833	1
2015.846	03122+3713	STF360	R	125.47	2.873	4
2015.846	03140+0044	STF367	R	130.71	1.240	6
2015.958	03158+5057	HU544	R	102.76	1.653	1
2015.846	03175+6540	STT52AB	R	56.33	0.484	1
2016.994	03177+3838	STT53AB	G	232.47	0.575	1
2016.994	03177+3838	STT53AB	IR742	232.85	0.568	1
2016.994	03177+3838	STT53AB	R	232.78	0.556	1
2015.846	03184-0056	AC2AB	R	261.84	1.190	1
2015.846	03212+2109	COU259	R	217.82	0.908	1
2015.846	03233+2058	STF381	R	108.45	1.080	1
2016.033	03307-0416	STF408	R	320.21	1.165	1
2015.958	03344+2428	STF412AB	R	351.54	0.766	1
2015.958	03346-3152	B53	R	228.21	1.445	6
2016.994	03350+6002	STF400AB	G	268.41	1.628	1
2016.994	03350+6002	STF400AB	IR742	268.63	1.603	1
2016.033	03350+6002	STF400AB	R	268.49	1.703	1
2016.994	03350+6002	STF400AB	R	268.46	1.612	1
2016.033	03356+3141	BU533AB	R	221.99	1.066	1
2015.958	03362+4220	A1535	R	346.00	0.746	1
2016.033	03362+4220	A1535	R	346.36	0.732	4
2016.033	03377+4807	HLD9AB	R			7
2015.846	03443+3217	BU535	R	20.45	1.052	1
2015.767	03463+2411	BU536AB	R			7
2016.994	03496-0220	YR23	G	294.77	0.355	3
2016.994	03496-0220	YR23	IR742	286.30	0.373	6
2016.994	03496-0220	YR23	R	295.69	0.369	1
2016.994	03503+2535	STT65	G	201.94	0.442	1
2016.994	03503+2535	STT65	IR742	200.86	0.464	1
2016.994	03503+2535	STT65	R	201.85	0.431	1
2016.917	04239+0928	HU304	G	29.54	0.325	2
2016.917	04239+0928	HU304	R	30.57	0.339	2
2016.112	04257-0214	BU 403	G	83.35	0.921	2
2016.112	04275-2427	I 413	G	330.90	0.729	2
2016.112	04279-2130	BU 184	G	247.89	1.917	2
2015.846	04301+1538	STF554	R	15.56	1.465	1
2015.934	04306-2301	HDS580	R			7
2016.112	04308+1609	PAT 11	G			7
2016.112	04316+3739	BU 789	G	323.37	0.919	1
2015.846	04334-1047	HDS592	R			7
2016.112	04349+3908	HU 1082	G	189.86	0.266	6
2016.112	05005+0506	STT 93	G	243.28	1.636	1
2016.112	05043-0602	A 481AB	G	281.77	0.413	3
2016.112	05055+1948	STT 95	G	295.61	0.955	1
2016.112	05059-1355	A 3009	G	274.09	1.226	2
2016.112	05079+0830	STT 98	G	288.94	0.956	1
2016.205	05131+2424	COU 468	G	32.63	0.576	1
2016.205	05135+0158	STT 517AB	G	240.87	0.731	1
2016.205	05140+5126	HU 821	G	171.77	0.826	1
2016.205	05181+0342	A 2639	G	277.24	0.942	1

Table 3 continues on next page.

Table 3 (continued). Speckle measurements in 2015 and 2016, using the OCA Kuhn 22-inch telescope, Point Grey BlackFly-U3-23S6M-C CMOS camera, and interference filters. The columns are: observation date, WDS designation, WDS discovery designation, filter (Table 1), position angle observed (degrees), separation observed (arc-seconds), and qualitative figure of merit (Table 2).

Obs Date	WDS	Discovery	Filter	ThetaO	RhoO	Quality
2016.205	05204-0522	HDS702AaAb	G	234.29	0.642	6
2016.033	05208+3329	COU1231	R	140.96	0.373	3
2016.205	05213+3529	COU 1535	G	99.52	0.359	6
2016.033	05219+3934	COU2037	R	141.98	0.375	3
2016.033	05525+4009	STF802AB	R			7
2015.958	06041+1101	J335	R	270.79	1.274	1
2016.112	06149+2230	BU 1008	G	256.56	1.847	1
2016.112	06221+5922	STF 881AB	G	149.29	0.638	1
2016.112	06256+2227	STT 139	G	257.42	0.791	1
2016.205	06336-1207	HU 43	G	308.30	0.897	1
2016.205	06345-1114	HO 234	G	4.49	0.617	1
2016.112	06364+2717	STT 149	G	279.03	0.752	1
2015.958	06425+6612	MLR318	R	309.13	1.717	1
2016.112	06455+2922	A 122	G	24.48	0.410	3
2016.205	06462+5927	STF 948AB	G	67.31	1.921	1
2016.112	06478+0020	STT 157	G	162.79	0.562	2
2016.205	06487+0737	A 2731AB	G	67.15	1.344	1
2016.205	06555+3010	STF 981	G	299.25	0.925	1
2016.033	06564+0957	HDS960	R	210.19	0.657	6
2015.846	06573+5825	STT159AB	R	235.11	0.710	2
2016.205	07001+4211	COU 2374	G	17.33	0.289	3
2016.033	07003+6720	HDS976	R	188.35	0.382	6
2016.205	07008+2716	BU 1022AB	G	32.10	0.327	3
2016.205	07018-1053	BU 573	G	307.55	0.880	1
2016.205	07028+1305	HO 342	G	88.54	1.201	1
2016.205	08005+0955	A 2954AB	G	337.54	0.647	1
2015.846	08010+2335	STF1171	R	325.80	2.046	4
2016.205	08013-2220	BU 333AB	G	43.15	1.651	2
2016.205	08024+0409	STF 1175	G	287.03	1.419	1
2015.846	08033+2616	STT186	R	76.23	1.077	2
2016.205	08044+1217	BU 581AB	G	214.85	0.353	3
2015.846	08122+1739	STF1196AB	R	19.12	1.120	1
2015.958	08122+1739	STF1196AB	R	18.69	1.153	1
2015.958	08122+1739	STF1196AC	R	61.65	6.345	1
2015.958	08122+1739	HUT1CaCb	R			7
2016.337	09006+4147	KUI 37AB	R	177.07	0.437	5
2016.337	09179+2834	STF 3121AB	R	15.90	0.412	1
2016.337	10279+3642	HU 879	R	226.83	0.543	3
2016.337	10426+0335	A 2768	R	243.68	0.648	1
2016.337	13157+5424	HDS 1858	R			7
2016.337	13166+1948	HDS1862AaAb	R	262.39	0.416	6
2016.337	13189+0341	HDS 1865	R	109.01	1.186	1
2016.337	13202+1534	HDS1870AaAb	R	270.14	0.426	5
2016.337	14426+1929	HU 575AB	R			7
2016.671	15038+4739	STF1909	G	71.27	0.739	1
2016.337	15038+4739	STF1909	R	70.56	0.779	1
2016.671	15038+4739	STF1909	R	71.38	0.743	1
2016.337	15360+3948	STT 298AB	R	185.40	1.194	1
2016.337	15371+2646	HDS2199	R			7
2016.337	15404+2123	HU 579	R			7
2016.337	16309+0159	STF 2055AB	R	42.20	1.373	1
2016.671	16413+3136	STF2084	G	125.51	1.303	1
2016.337	16413+3136	STF 2084	R	126.28	1.252	1
2016.671	16413+3136	STF2084	R	125.06	1.286	1
2016.671	16511+0924	STF2106AB	G	171.54	0.794	1
2016.671	16511+0924	STF2106AB	R	170.54	0.791	1
2016.337	16514+0113	STT 315	R	310.03	0.716	1
2016.337	16518+2840	STF 2107AB	R	104.93	1.436	1

Table 3 continues on next page.

Speckle Interferometry with the OCA Kuhn 22" Telescope

Table 3 (continued). Speckle measurements in 2015 and 2016, using the OCA Kuhn 22-inch telescope, Point Grey BlackFly-U3-23S6M-C CMOS camera, and interference filters. The columns are: observation date, WDS designation, WDS discovery designation, filter (Table 1), position angle observed (degrees), separation observed (arc-seconds), and qualitative figure of merit (Table 2).

Obs Date	WDS	Discovery	Filter	ThetaO	RhoO	Quality
2016.337	17053+5428	STF 2130AB	R	1.58	2.510	1
2016.337	17066+0039	BU 823AB	R	161.86	1.065	4
2016.337	17082-0105	A 1145	R	340.95	0.691	1
2016.671	17130+0745	STT325	G	295.54	0.364	5
2016.671	17130+0745	STT325	R	291.30	0.425	5
2016.337	17141+5608	STT 327	R			7
2016.337	17166-0027	A 2984	R	21.37	0.772	4
2016.761	17304-0104	STF 2173AB	G	142.33	0.646	2
2016.337	17304-0104	STF2173AB	R	143.42	0.661	1
2016.761	17304-0104	STF 2173AB	R	142.60	0.650	1
2016.337	17349+1234	MCY 4	R	235.45	0.537	6
2016.337	17386+5546	STF 2199	R	55.63	1.930	6
2016.671	17400-0038	BU631	G	82.18	0.321	5
2016.671	17400-0038	BU631	R	83.68	0.351	5
2016.671	17471+1742	STF2215	G	250.20	0.451	1
2016.671	17471+1742	STF2215	R	252.57	0.454	1
2016.671	17520+1520	STT338AB	G	162.63	0.846	1
2016.671	17520+1520	STT338AB	R	162.50	0.825	1
2016.671	17571+0004	STF2244	G	100.13	0.695	1
2016.671	17571+0004	STF2244	R	99.85	0.665	1
2016.337	18571+3451	HDS2685	R	199.81	0.550	6
2015.728	19487+1149	STF2583AB	R	105.21	1.487	1
2015.767	19553-0644	STF2597AB	R	99.58	0.720	6
2016.843	20020+2456	STT 395	G	127.04	0.771	1
2016.843	20020+2456	STT 395	IR742	126.75	0.773	1
2016.843	20020+2456	STT 395	R	127.00	0.765	1
2016.671	20320+2548	STF2695	G	259.00	0.359	5
2016.671	20320+2548	STF2695	R	259.47	0.381	5
2016.917	20375+1436	BU151AB	G	185.21	0.318	2
2016.917	20375+1436	BU151AB	G	185.47	0.317	2
2016.917	20375+1436	BU151AB	G	188.75	0.310	2
2016.671	20396+0458	KUI99AB	G	317.87	0.533	6
2016.671	20396+0458	KUI99AB	R	321.35	0.583	6
2016.761	20474+3629	STT 413AB	G	1.37	0.931	1
2016.761	20474+3629	STT 413AB	R	1.47	0.937	1
2016.761	20519+0544	A 613	G	319.94	0.670	4
2016.761	20519+0544	A 613	R	318.15	0.671	1
2016.761	20524+2008	HO 144	G	350.01	0.435	1
2016.761	20524+2008	HO 144	R	352.04	0.448	1
2016.843	21026+2141	BU 69AB	G	10.65	0.283	6
2016.843	21026+2141	BU 69AB	IR742			7
2016.843	21026+2141	BU 69AB	R	4.98	0.382	5
2016.761	21135+0713	BU 270AB	G	346.54	0.490	6
2016.761	21135+0713	BU 270AB	R	351.67	0.455	1
2016.671	21137+6424	H1-48	G	244.15	0.684	1
2016.671	21137+6424	H1-48	R	244.02	0.689	1
2016.671	21148+3803	AGC13	G	197.54	0.944	1
2016.671	21148+3803	AGC13	R	197.21	0.938	1
2016.671	21186+1134	BU163AB	G	257.16	0.903	1
2016.671	21186+1134	BU163AB	R	257.72	0.905	1
2015.767	21352+2124	BU74	R	337.73	0.979	1
2016.671	21395-0003	BU1212AB	G	302.30	0.314	1
2015.767	21395-0003	BU1212AB	R	301.17	0.336	3
2016.671	21395-0003	BU1212AB	R	298.07	0.371	5
2016.671	21426+4103	BU688AB	G	197.56	0.373	1
2016.671	21426+4103	BU688AB	R	195.43	0.406	1

Table 3 concludes on next page.

Speckle Interferometry with the OCA Kuhn 22" Telescope

Table 3 (conclusion). Speckle measurements in 2015 and 2016, using the OCA Kuhn 22-inch telescope, Point Grey BlackFly-U3-23S6M-C CMOS camera, and interference filters. The columns are: observation date, WDS designation, WDS discovery designation, filter (Table 1), position angle observed (degrees), separation observed (arc-seconds), and qualitative figure of merit (Table 2).

Obs Date	WDS	Discovery	Filter	ThetaO	RhoO	Quality
2016.671	21555+1053	BU75AB	G	25.80	1.052	1
2016.671	21555+1053	BU75AB	R	25.38	1.066	1
2015.767	22029+4439	BU694AB	R	5.95	1.018	1
2015.767	22044+1339	STF2854	R	83.71	1.601	1
2016.843	22057+3521	PRU 2	G			7
2016.843	22057+3521	PRU 2	IR742	4.05	0.453	6
2015.767	22057+3521	PRU2	R			7
2015.958	22057+3521	PRU 2	R			7
2016.843	22057+3521	PRU 2	R			7
2015.934	22365+5826	PRU3	R	5.14	0.365	5
2016.843	22388+4419	HO 295AB	G	336.10	0.318	1
2016.843	22388+4419	HO 295AB	IR742	336.12	0.360	5
2016.843	22388+4419	HO 295AB	R	336.29	0.325	3
2015.846	22400+0113	A2099	R	164.92	0.840	4
2016.843	22402+3732	HO 188	G	230.64	0.361	1
2016.843	22402+3732	HO 188	IR742			7
2016.843	22402+3732	HO 188	R	228.39	0.351	3
2015.846	22409+1433	HO296AB	R	51.59	0.465	1
2015.934	22437+4725	HDS3224	R			7
2015.846	22478-0414	STF2944AB	R	304.65	1.866	1
2015.958	22514+2623	HO482AB	R	13.36	0.518	2
2015.846	22514+6142	STF2950AB	R	275.20	1.182	1
2016.843	22520+5743	A 632	G	110.12	0.359	2
2016.843	22520+5743	A 632	IR742	108.31	0.378	5
2016.843	22520+5743	A 632	R	109.31	0.379	1
2016.843	22537+4445	BU 382AB	G	244.92	0.676	1
2016.843	22537+4445	BU 382AB	IR742	245.98	0.638	1
2016.843	22537+4445	BU 382AB	R	244.80	0.685	1
2015.934	23029+0738	HDS3282	R			7
2016.843	23072+6050	BU 180AB	G	133.02	0.544	4
2016.843	23072+6050	BU 180AB	IR742			7
2016.843	23072+6050	BU 180AB	R	134.06	0.541	4
2016.994	23176+1818	HU400	G	70.26	0.344	6
2016.994	23176+1818	HU400	IR742			7
2016.994	23176+1818	HU400	R	67.52	0.349	6
2016.761	23241+5732	STT 495	G	120.43	0.404	1
2016.761	23241+5732	STT 495	R	120.14	0.407	1
2016.843	23375+4426	STT 500AB	G	13.83	0.439	1
2016.843	23375+4426	STT 500AB	IR742	12.83	0.462	1
2016.843	23375+4426	STT 500AB	R	12.71	0.423	1
2015.728	23413+3234	BU858AB	R			7
2015.728	23420+2018	STT503AB	R	134.50	1.233	1
2015.846	23440+2922	AGC14	R	283.95	0.857	4
2016.843	23516+4205	STT 510AB	G	300.81	0.609	1
2016.843	23516+4205	STT 510AB	IR742	295.27	0.619	2
2016.843	23516+4205	STT 510AB	R	300.29	0.619	1
2016.994	23595+3343	STF3050AB	G	340.17	2.469	1
2016.994	23595+3343	STF3050AB	R	340.22	2.452	1
2016.994	23595+3343	STF3050AB	IR742	340.24	2.439	1
2016.994	23595+3343	STF3050AD?	G	38.67	4.280	4
2016.994	23595+3343	STF3050AD?	R	38.27	4.292	4
2016.994	23595+3343	STF3050AD?	IR742	37.85	4.315	4

the primary peak may indicate that the peaks above and below are artifacts of atmospheric dispersion, due to the zenith angle greater than 30 degrees. Additional observations are needed.

The Table 3 observation of **02231+7021 MLR377AB** is uncertain at best (figure of merit 6). The STB auto-correlogram in Figure 7 had the weakest secondary peaks of all the stars observed. Although these measured peaks were the brightest in the field, there are numerous other possible candidates which are likely just noise and not faint stars. In the orbit plot, even though the current observation continues the trend diverging from the premature orbit, it seems too far from the other points. The proper motions of the two components are the same, although they are small.

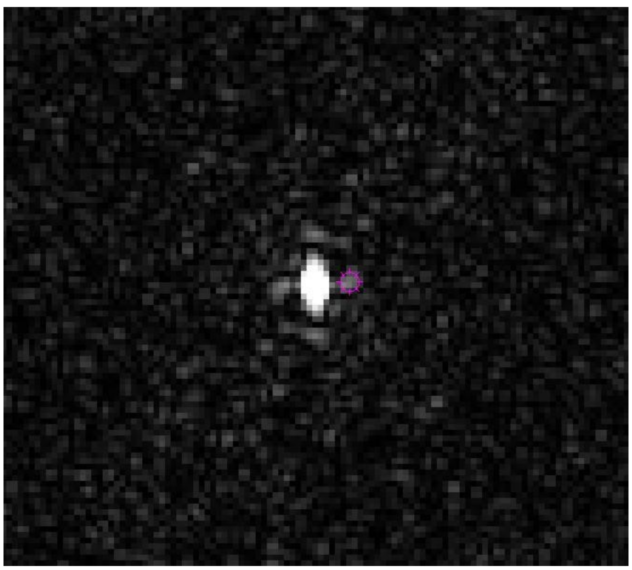

Figure 6. The STB auto-correlogram of TDS2201. The secondary peaks are barely above the background noise.

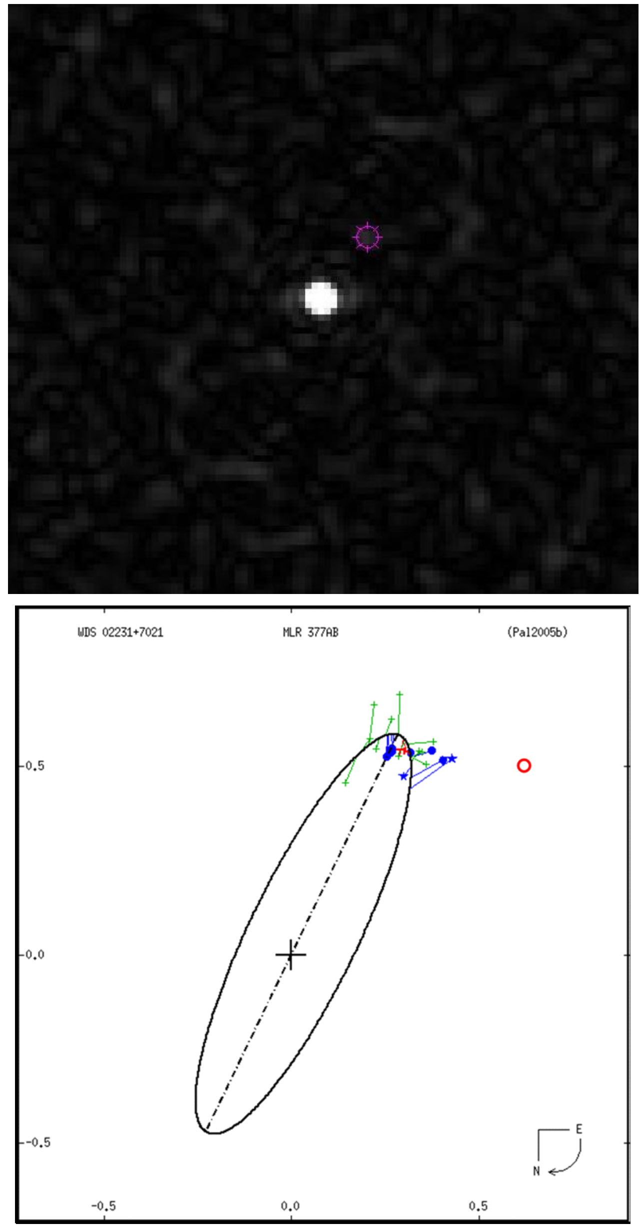

Figure 7. Top: The STB auto-correlogram of MLR377AB. Bottom: The position of the current uncertain measure (red circle) generally continues the diverging trend of earlier speckle points.

Speckle Interferometry with the OCA Kuhn 22" Telescope

The binary **03175+6540 STT52AB** has a Grade 4 orbital period of 350 years, but most of the recent speckle points are diverging from that orbit, shown in Figure 8, including the observation of Table 3. The speckle points show a roughly linear trend of increasing separation, so the period is likely much longer, but the earliest micrometer points (green +), and the same proper motion of both components, still demand that this is a binary.

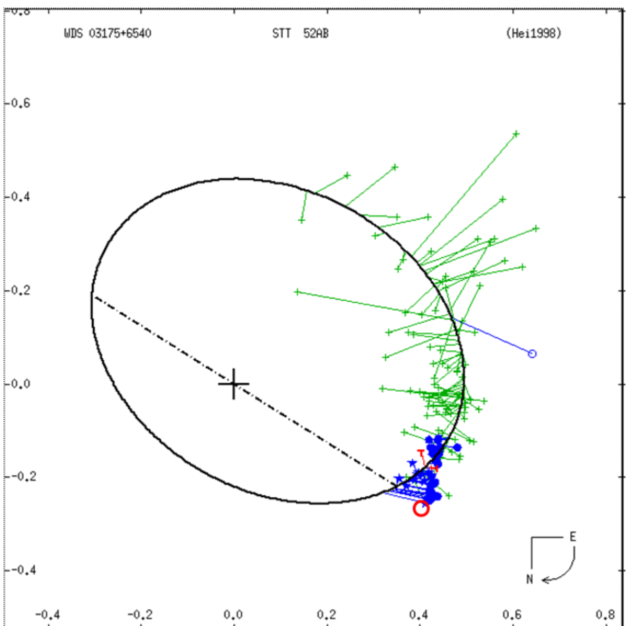

Figure 8. The orbit of binary star STT52AB, from the Washington Double Star 6th Orbit Catalog. The point from Table 3 is indicated by the red circle.

05208+3329 COU1231 was discovered visually by Paul Couteau in 1975 (Couteau, 1976). There are very few observations in the WDS archives, all of which are plotted in Figure 9. There were no observations from 1975 to 2000, then four speckle observations from 2000 to 2010. No other observations were available in the WDS. The current observation of Table 3 was in early 2016.

In the top-left part of Figure 9, all the points are plotted as given in WDS. However, the distribution of points seems peculiar - the discovery point (+) of Couteau, a very experienced observer, seems out of place, and the general trend shows little movement in the first 25 years, but fast closure in the most recent 6 years. For these reasons, all the speckle points from 2000 to 2016 were plotted with 180 degrees added to the PA, as shown in the top-right part of Figure 9. This distribution, which assumed that the observation of Couteau had the only correct PA quadrant because it was obtained visually, looks reasonable, suggesting a high-inclination orbit with a period on the order of only five or six decades.

To help clarify the situation, a request was made to Dave Rowe, who is developing a new bi-spectral tool for his Speckle Tool Box program, to do bi-spectral

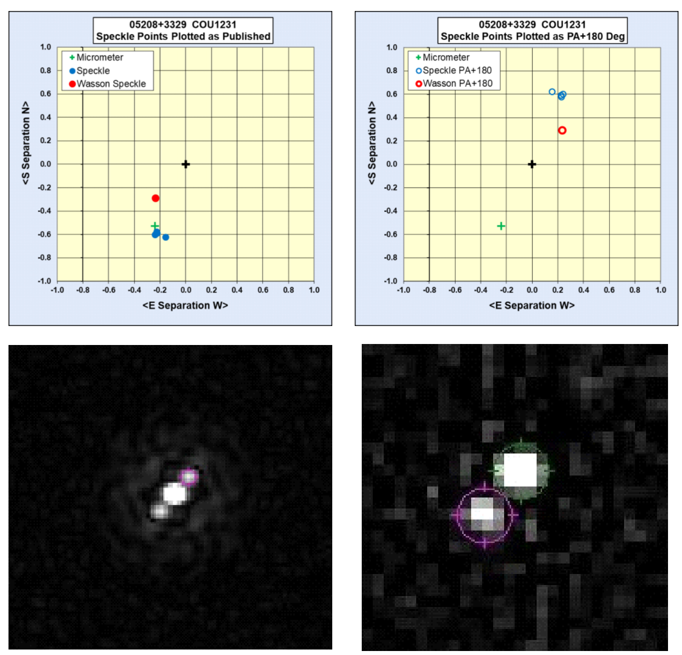

Figure 9. Upper Left: All observations of COU1231 from the WDS are plotted, together with the new point from Table 3, indicated by the solid red circle. (Note: north up, east left, as on the sky). Upper Right: Speckle points are plotted with 180 degrees added to the PA values from WDS and Table 3. Lower Left: The current auto-correlogram. Lower Right: The bispectrum image of COU1231, courtesy of Dave Rowe, clearly shows that the PA of the companion is in the second (southeast) quadrant.

analysis of my speckle images. The result (Rowe, 2017), shown at lower-right of Figure 9, confirms that the speckle PA observations are properly located in the second quadrant, as given in WDS.

06149+2230 BU1008 is a very bright semiregular variable (V=3.3-3.9) red giant (Eta Gem, M3.5I-II), 2.6 magnitudes brighter than its companion. All speckle points are diverging from the grade 5 preliminary orbit, including the Hipparcos/Tycho measures. The Table 3 measure continues that trend, as seen in Figure 10. Therefore, the period is likely longer than the 474-year orbit. However, since the motion so far seems roughly linear, the pair may also be only optical.

06256+2227 STT139: This pair was observed in February 2016 with the G filter, but the measured separation was larger than the WDS last observation and much larger than the orbit ephemerides. Figure 11 shows the WDS orbital plot, with the current point added. Only one other speckle point is available since the Hipparcos/Tycho observations. However, since emerging from periastron, the trend is clearly diverging into a wider orbit, just as the early micrometer points indicated before periastron. Perhaps the observations merit an updated orbit solution.

The class 2 orbit of **08044+1217 BU581AB**, with a period of 45 years, is now approaching a full revolution

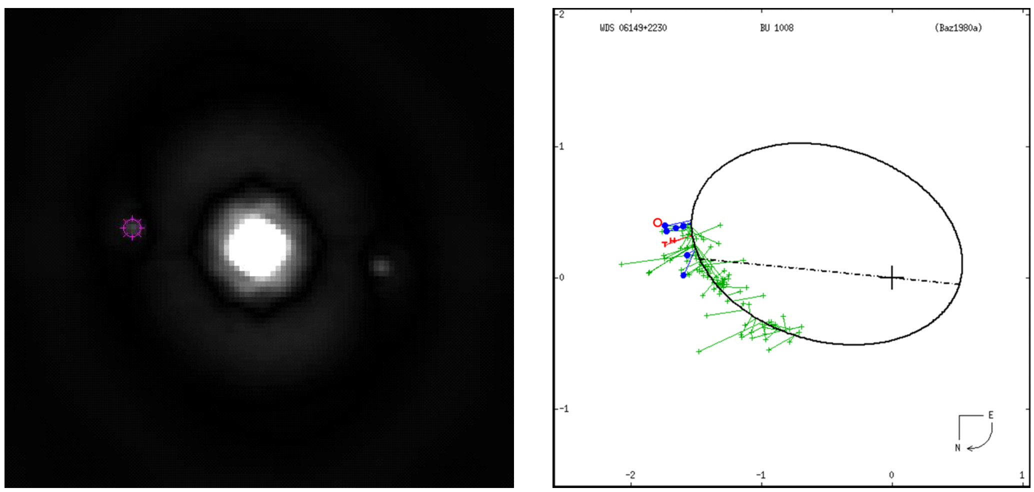

Figure 10. Left: The STB auto-correlogram of BU1008. Right: The position of the current measure (red circle) continues the generally diverging trend of the other speckle points.

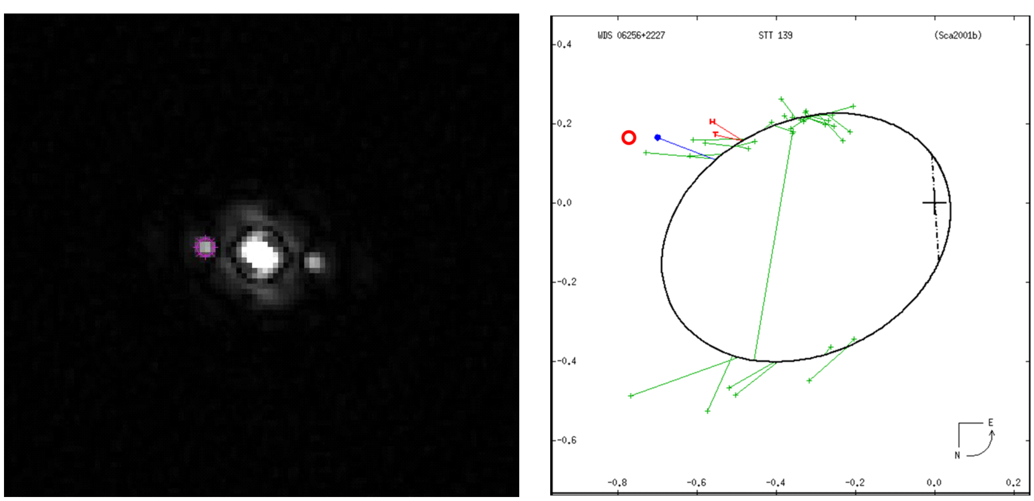

Figure 11. Left: STB auto-correlogram of STT139. Right: The current measure (red circle) supports a clear trend toward a larger orbit, based on the other speckle point, Hipparcos, Tycho, and early micrometer points.

of speckle measurements. The Table 3 measure, shown in Figure 12, is a little inside the orbit solution, but helps fill in the gap since the last WDS plotted speckle point in 2006. Two other recent speckle points from 2008 and 2010, are available in the WDS observation database, but not yet shown on its orbit plot. These were added to Figure 12 as blue circles. Additionally, an observation taken with the same OCA 22-inch telescope early in 2017, but with a different camera, is slightly outside the orbit line (black circle), and will be published later. This pair deserves more frequent speckle observations.

22365+5826 PRU3 is the very luminous variable *supergiant* star W Cephei, which pulsates from orange to red in color and has the strange spectral type K0Iapev. It has very small proper motion (-3, -2) and the huge distance, based on Hipparcos measurements, is over 100,000 light years. Although it is a spectroscopic binary, the visible companion, only 1.3 magnitudes fainter, is unlikely to be gravitationally bound, but is almost certainly a much nearer star. Therefore, the relative motion should be linear. Only two prior measures have been made, one by Hipparcos (1991) and one by speckle (1997). There were also two unresolved speckle observations on 2-meter telescopes (closer than 0.05") within 2 years of the successful speckle observation. It is possible that these may have failed because the primary variability increased the delta magnitude. The current observation in Table 3 is uncertain, but the PA which is more consistent with linear motion - moving farther apart in roughly the same direction – was selected for Table 3. If this trend is true, a few further observations should confirm it.

The binary **22409+1433 HO296AB** was observed in November 2015, chosen as a bright double with a well-known orbit, but challengingly close for the 22-inch. HO296AB, whose orbit it shown in Figure 13, is one of the few binaries which has a Grade 1 "definitive" orbit solution, meaning it has numerous accurate measurements over at least one full orbit. The period is 20.83 years, so the orbit has been fully covered by speckle measurements, begun in 1979 by Dr.

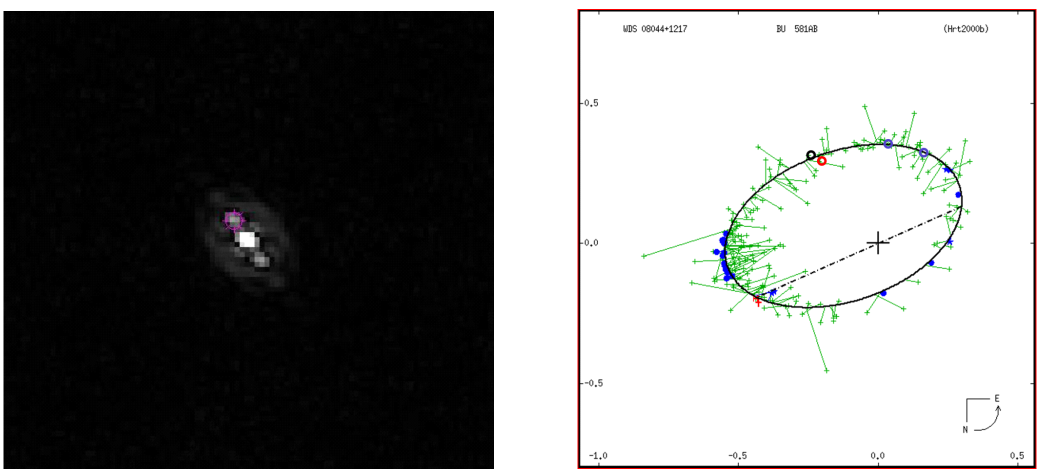

Figure 12. Left: STB autocorrelogram of BU581AB. Right: The measure of Table 3 (red circle) helps fill in the gap in speckle observations. Two additional speckle points which are in the WDS archive but not yet plotted, are shown as blue circles, while the black circle is a 2017 observation by the author.

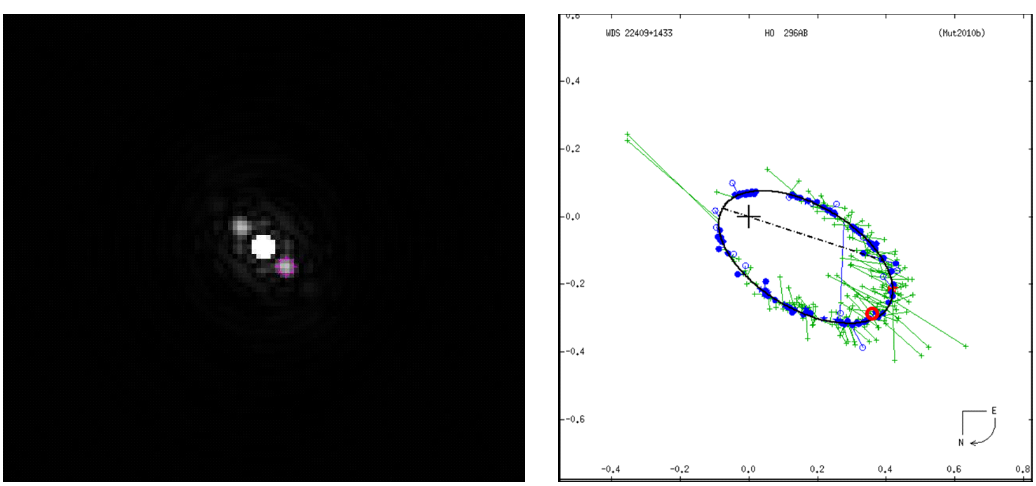

Figure 13. Left: STB autocorrelogram of HO296AB. Right: The point in Table 3 is the red circle at lower right, in reasonably good agreement with the Class 1 orbit.

Harold McAlister on the Kitt Peak 4-meter Mayall telescope. Almost all the other speckle observations were also made by professional astronomers with telescopes including the Kitt Peak 2.1m, WIYN 3.5m, Mt. Wilson 2.5m (100"), and the Discovery Channel 4.3m. In addition, near periastron, where the separation is less than 0.1 arc-second, measurements have been made with the Russian 6m telescope (speckle in 1983) and with the Palomar Test Bed Interferometer (2003 through 2008). Not until after I reduced the data and compared my measurement with the historical data of others, did I realize what distinguished company I had inadvertently joined.

The auto-correlograms of **23595+3343 STF3050** are shown in Figure 14, in all three filters of Table 1. The top row shows the AB components. However, the bottom row has been over-exposed to show an additional faint star at about 4.3" separation and 38 degrees PA, as given in Table 3. Of course, the PA of this object may be actually 180 degrees from Table 3.

This object cannot be the faint C component (magnitude 12.8), because WDS lists it about 80 arc-sec distant from A; therefore, this could be a new "D" component. However, this system has been very well observed in the past, with more than 600 published observations in the WDS archives. Therefore, it is extremely unlikely that this star, which is probably brighter than the C component, has been overlooked by all previous observers.

Indeed, a plot of the three measurements of Table 3, Figure 15, shows small but roughly linear motion, consistent with the order in which the exposure sequences were made: G, R, IR742. All sequences were 1000 exposures of 0.030 sec each. The mid-time of the R sequence was 50.4 sec after the mid-time of the G sequence, while the IR742 sequence was 45.2 sec after the R sequence. Therefore, the "new" component was moving about 0.044 arc-sec per minute toward the north-west (or south-east).

The faint object shows up in the double star autocorrelations, with and without using the reference star for deconvolution, and it does not appear in the reference autocorrelation alone; therefore, it is not an artifact from a faint companion near the reference star, as may sometimes occur. Although it was about 33 degrees north of the ecliptic, which is near zero declination at RA~24 hours, this object may be an interloping asteroid.

However, a cursory search found no asteroid with a well-known orbit near the double star at the time. Two

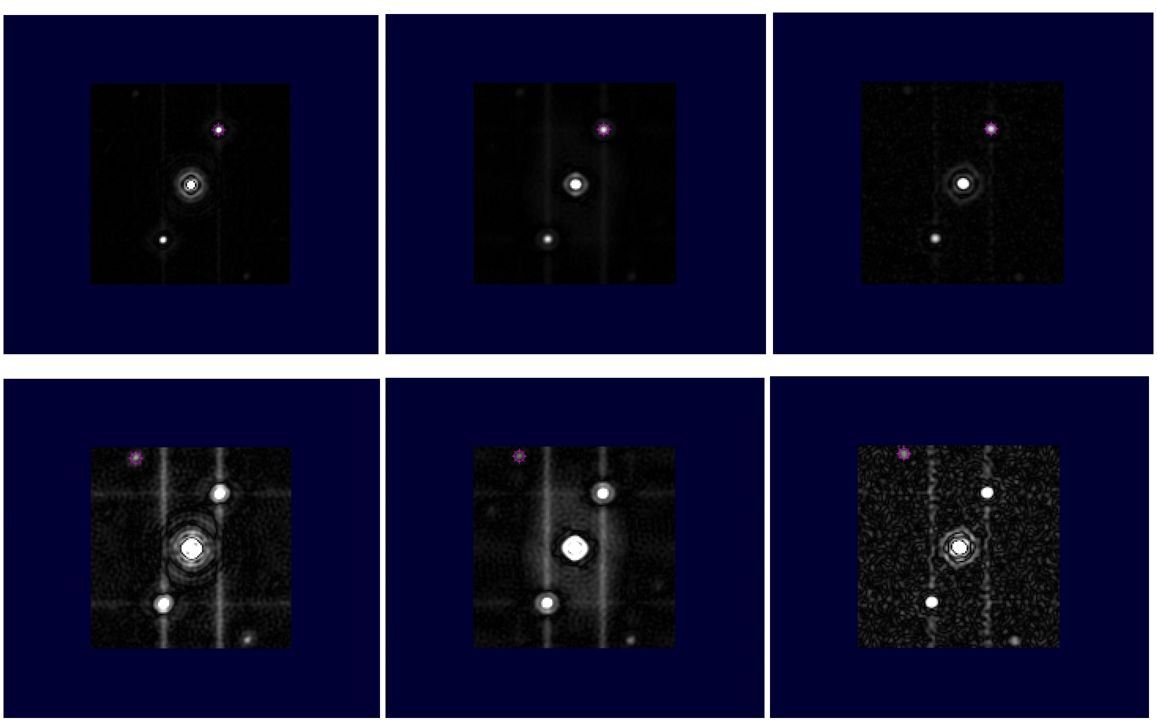

Figure 14. Top Row: STB auto-correlograms of STF3050AB in all three filters of Table 1: G (left), R (middle) and IR742-pass (right). Bottom Row: The same auto-correlograms, shown over-exposed to reveal an additional faint star. The vertical and horizontal streaks are artifacts probably caused by CMOS line pattern ("read") noise related to the bright B component. The STB interference filter can suppress line pattern noise related to the primary star, because it is always at the center of the field after FFT processing.

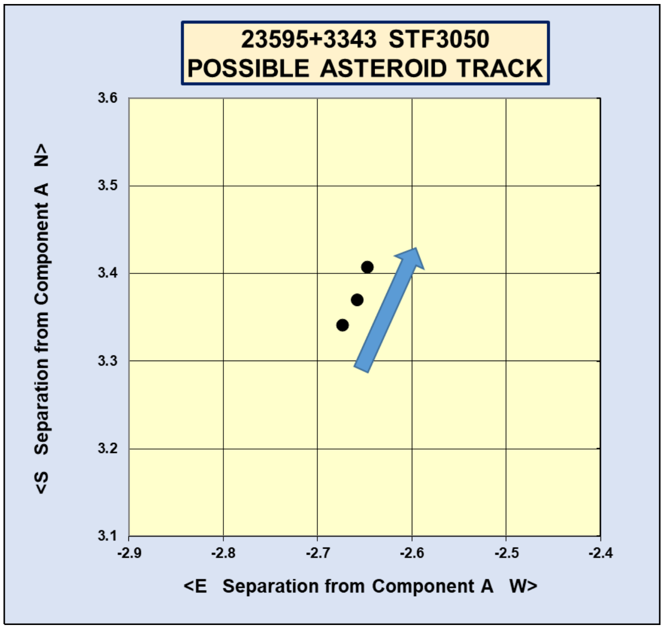

Figure 15. The Table 3 offsets (arc-seconds) of the "new" component of STF3050, relative to the A component, for the G, R and IR742 filter sequences. The arrow indicates the order of the three sets of exposures, and therefore, the direction of travel. Because of the speckle 180-degree ambiguity, the actual motion may be in the opposite direction.

other remote possibilities may be a small, near-earth asteroid, or an old geosynchronous satellite, out of fuel and drifting far from the original equatorial region. Unfortunately, this object remains a mystery.

Acknowledgements

The author is very grateful to OCA President Barbara Toy for her dedication and expertise in instructing new Star Members, and her custodianship of the Kuhn 22-inch Telescope, and to members of the Orange County Astronomers for support and maintenance of the Anza site facilities. He also thanks Dave Rowe, Russ Genet, and Bob Buchheim for their inspiration, correspondence, instruction, and assistance along the speckle journey.

This research has made use of the Washington Double Star Catalog, the 6th Orbit Catalog, and the Observation Catalog, all maintained at the U.S. Naval Observatory, and the author particularly thanks Brian Mason for providing all previous observation data for requested stars.

References

Bryant, Tom, 2015. http://mainsequence.org/html/wds/getListOfDoubles/listWithOrbits.html

Buchheim, R. K., 2017. *Journal of Double Star Observations*, **13**, 233-236, April, 2017.

Couteau, P., 1976. *A&AS*, **24**, 495.

Edelmann, Torsten, 2015. FireCapture2.4. http://firecapture.wonderplanets.de

Harshaw, Richard and Rowe, David and Genet, Russell, 2017. "The Speckle Toolbox: A Powerful Data Reduction Tool for CCD Astrometry." *Journal of Double Star Observations*, **13**, 52-67, January 1, 2017.

Losse, Florent, 2015. "REDUC 4.72." http://www.astrosurf.com/hfosaf.

Rowe, David A. and Genet, Russell M., 2015. "User's Guide to PS3 Speckle Interferometry Reduction Program." *Journal of Double Star Observations*, **11**, 266-276.

Rowe, David A., 2016. Yahoo Group speckleinterferometry@yahoo.com.

Rowe, David A., 2017. Private communication.

Sordiglioni, Gianluca, 2016. http://stelledoppie.goaction.it/index2.php?section=1.

Wasson, Rick, 2014. "Measuring Double Stars with a Dobsonian Telescope by the Video Drift Method." *Journal of Double Star Observations*, **10**, 324-341.

Astrometric Measurements of Triple Star System 15379+3006 STF 1963AB, STF 1963AC

Harker Russell[1], Lindsey Miller[1], Alexander Beltzer-Sweeney[1,2], Trey Shilts[1], and Irena Stojimirovic[1,2]

1 San Diego Mesa College, San Diego, California, USA
2 Boyce Research Initiative and Education Foundation (BRIEF)

Abstract: Research team PRSM reports astrometric measurements of the double star system WDS 15379+3006 (STF 1963AB, STF 1963AC) obtained using the iTelescope Network. By performing CCD astrometry, the team determined a position angle of 298.4° ± 0.1° with an angular separation of 05. 28" ± 0.1" for STF 1963AB, and a position angle of 116.1° ± 0.1° with an angular separation of 32.35" ± 0.1" for STF 1963AC. The angular separation and position angle have changed from previous measurements.

Introduction

The purpose of this paper was to select a double star system from the Washington Double Star Catalog (WDS) and observe it using CCD imaging. From the images, we could determine the position angle and separation between stars in the double system. The goal was to determine, based on the orbital plot, if the stars belong to the gravitationally bound system or they are not physically connected and just appear close together.

The star system was selected using the following criteria: a difference in magnitude of no more than 6, with both stars being brighter than 12 magnitudes. A minimum angular separation of 6 arc seconds was also required. In addition, the system must be observable in the spring. Enough historical data on the double star system must exist and will be combined with our measurements to determine if the system is a physical double or visual double star system. Despite the secondary star having a magnitude of 13.58, the triple star system STF1963AB/STF1963AC adhered to the rest of the requirements and the system was selected for observation, Figure 1.

STF1963AC is in the constellation of Corona Borealis and was first observed by Sherburne Wesley Burnham in 1908 (Mason 2017). There have been three more observations made since; the most recent was made in 2009. The separation in 1908 was 31 arc seconds (31”), and 32” in 2009. The position angle has remained virtually unchanged from 116° (Mason 2017).

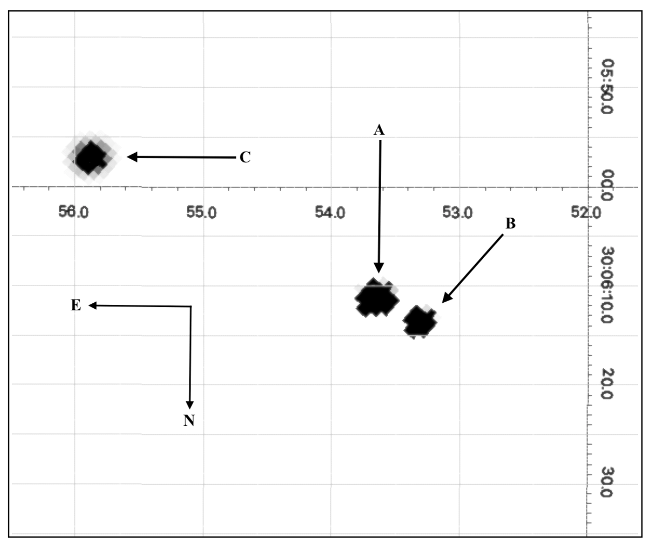

Figure 1. WDS 15379+3006 composite image of A B and C components serves to illustrate the relative positions of each; (WCS). This does not represent relative apparent luminance. The horizontal axis is right ascension (hours). Vertical axis is declination (degrees). Created with SAOImage DS9 (SAOImage, 2016).

The relative proper motion (rPM) is 0.19 arcseconds per year ("/yr)—a good indication that this system has potential to be a gravitationally linked binary star system (Stelle 2017).

The AB component of this system is also very interesting because the rPM is 0.43"/yr which could indicate no gravitational link. The primary star has a magnitude of 8.54 and the secondary star, a magnitude of 8.85. The first separation was 4.2" and the last separation was 5.1" (Mason 2017). The first position angle was 291° and the last position angle was 298°. One journal listing in particular mentions STF1963AB by an alternate identifier, HD 139569 in their Table 2, which listed stars with the following attributes:

The results for the most interesting objects… [their team] found a signature of periodic variations (rotational periods of activity cycles) in 19 stars. Whereas 10 stars show a clear overall trend in Hα with time. (Sissa, E., Gratton, R., Desidera, S., et al.).

The spectral class of primary star is F and the secondary star is a G class star (Stelle 2017). No orbital solutions had been made to date for either AB or AC relative motion. In the Table 1 we present some of the historical measurements of position angle (θ) and separation distance (ρ) as well as the technique codes for the method used to obtain them.

Equipment, Observations, And Data Analysis Procedures

The iTelescope Network's telescope T18 was used to take CCD images of STF1963AB and STF1963AC. This 0.32-meter f/8.0 reflector telescope is located at the AstroCamp Observatory in Nerpio, Spain (38° 09' North, 002° 19' West) and has a resolution of 0.72 arcseconds per pixel (Moore 2017). Four images were ordered. Two images made use of luminance filters—with exposure times of 30 and 60 seconds—and two used hydrogen-alpha filters—with exposure times of 30 and 90 seconds. All of these images were preprocessed (dark and flat subtraction) by the iTelescope data reduction pipeline. Optimal system altitude and time of observation were determined by the use of SkyX Pro software. Images were scheduled through Boyce-Astro, and taken 2017.229798.

Table 1. *Historical and present measurements for STF 1963 AC (WDS 15370+3006). The WDS (Mason 2017) technique Codes for Table 1 are as follows: Ma, Micrometer with refractor telescope; E2, 2MASS; Eu, UCAC3 or UCAC4; C, CCD image.*

WDS 15379+3006 AC			
Date of Observation	Angle (θ)	Separation (ρ)	Technique Code
1908.31	115.9	31.0	Ma
1998.25	116.3	32.09	E2
2002.154	116.0	31.85	Eu
2009.448	116.4	31.98	C
2017.333	116.09	32.35	C

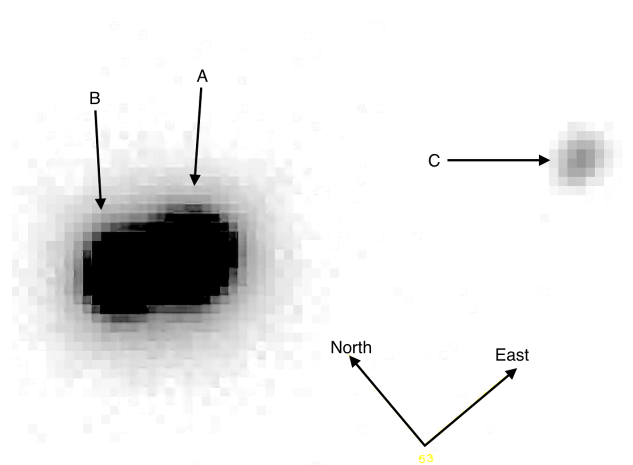

Figure 2. WDS 15379+3006 A B and C components. The purpose of this image is to show the relative apparent luminance of all system components with respect to each other and to demonstrate the difficulties that arose in determining the centroid of component-A when measuring ρ and θ of STF1963AB/ STF1963AC. This necessitated developing a way to double check measurements made in Mira64 that utilized automatic centroid detection (Mira, 2016).

Each image was received as a FITS file. Astrometry of images was performed using MaxImDL v6 software. In its astrometric measurements, MaxImDL finds all the stars in the image and matches them against cataloged positions for stars in that vicinity (by referencing the UCAC4 catalogue). The calculated mapping is stored as standardized World Coordinate System (WCS) values in the FITS header of each image file.

To analyze the separation (θ) and position angle (ρ) of the components in our triple system Mira64 was used. Due to STF1963AB having such a small Δ magnitude, and STF1963AC Δ magnitude being relatively large, see Figure 2, a process coined 'manual centroid detection' was developed by the team and used for measuring the position angle and separation in addition to the automatic centroid technique provided by Mira64.

The manual centroid detection was carried out as follows: The location of the primary star's (component A) centroid was determined by visual analysis of each pixel in the image, and the RA and Dec of the manually determined centroid was then recorded as shown in Mira64, Figure 3. The secondary star's centroid could then be determined, through the same methodology, while being able to adjust qualitative attributes of each

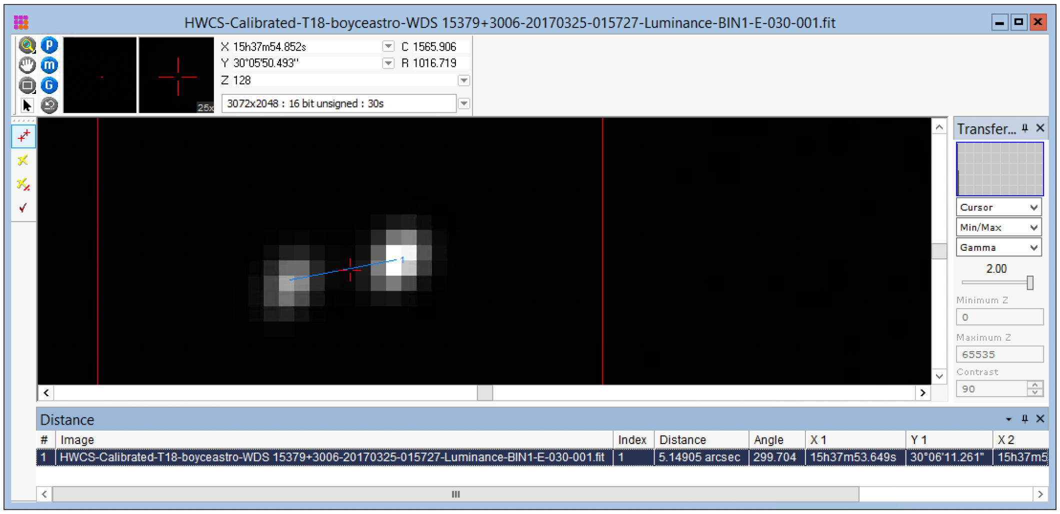

Figure 3. Resolved image of STF1963AB used to determine the coordinates (right ascension and declination) of the primary component-A centroid for use in our manual centroid detection and to measure separation distance (ρ) and position angle (θ) for the STF1963AB component. Differences in accuracy are highlighted in Table 3. This image is created with Mira64 (Mira, 2016).

image to optimally suit the luminance of the secondary star. Mira64's measurement tool was used by dragging the cursor from the previously determined coordinates of component A to the previously determined coordinates of the secondary star. This was done to acquire data points that were not biased by bleed from the nearby A and B components of the system, which the team believed may be biasing the auto centroid centering feature. This process was repeated in each image for all components. Mira64's auto centroid centering feature was also used for measuring separation distances and position angles.

Regarding the STF1963AC component measurements, both automatic and manual centroid detection, Figure 4, techniques had no significant difference between reported data. Both sets of data were, therefore, taken into account, Table 3, for statistical analysis to provide accurate resultant measurements. For STF1963AB, however, measurements made using manual centroid detection were selected for analysis, and this will be discussed in results section.

Using SAOImage DS9 (SAOImage 2016) we were

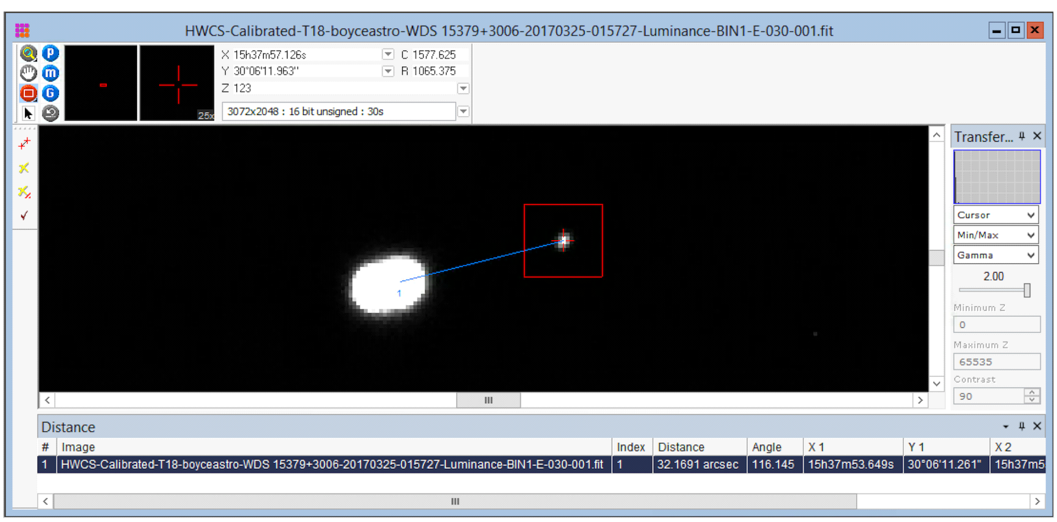

Figure 4. The same image as in Figure 3 after being adjusted to measure separation distance (ρ) and position angle (θ) of STF1963AC. The coordinates (right ascension and declination) of the primary component-A centroid, found using manual centroid technique, were used to ensure that our results would not be skewed by lack of resolution of STF1963AB once STF1963AC was made visible. This image is created with Mira64 (Mira, 2016).

able to check that detection of all three stars were significant with high signal-to-noise ratio using Luminance filter with both 30 and 60 and Hα 90 seconds exposure times. We have failed to detect C component in Hα image with 30 seconds exposure. Table 2 summarizes these findings and Figures 5 and 6 show relative quality of the data taken with these two different filters.

Results

The results of our measurements using both manual centroid and auto centroid techniques are summarized in Table 3. Filter and exposure times are noted as well.

AC Component

Standard deviation of the mean was 0.14 and 0.18 in position angle and separation distance respectively. Precision in the astrometric measurements taken were excellent, as evidenced by 0.07 and 0.05 standard deviation from the mean in separation distance and position angle respectively. Thus the major uncertainty in our data comes from the telescopic resolution of 0.72 arcsec/pixel.

Table 2. *Table of all images taken for PRSM and the signal-to-noise ratio for each component. Determined by using DS9 software to compare the average pixel intensity across the star with average pixel intensity of surrounding pixels (SAOImage, 2016).*

WDS 15379+3006 Signal:Noise Ratio			
Image	C	B	A
Lum 30 sec	58.511	69.739	105.818
Lum 60 sec	106.293	92.597	145.188
Ha 30 sec	NaN	65.600	87.836
Ha 90 sec	28.832	199.681	289.217

With respect to the AC component of WDS 15379+3006, PRSM measurement appears reasonable

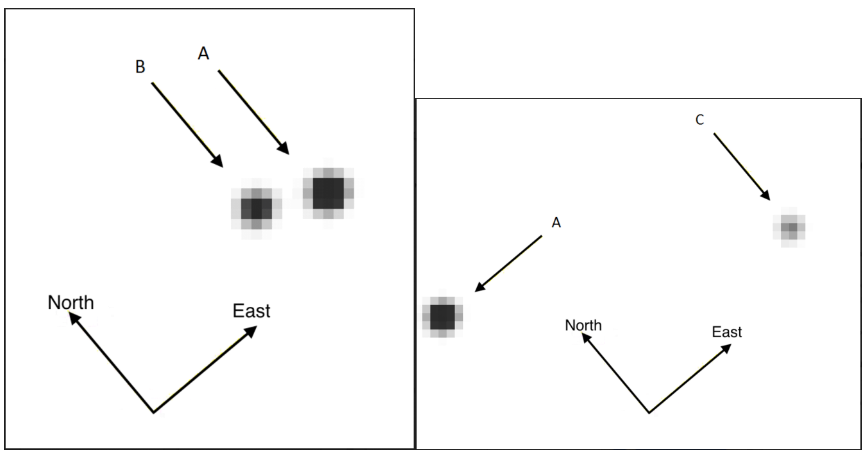

Figure 5. WDS 15379+3006, STF1963AB resolved (left) and STF1963AC resolved (right). These images were obtained using Luminance filter with an exposure of 60 seconds (Mira 2016).

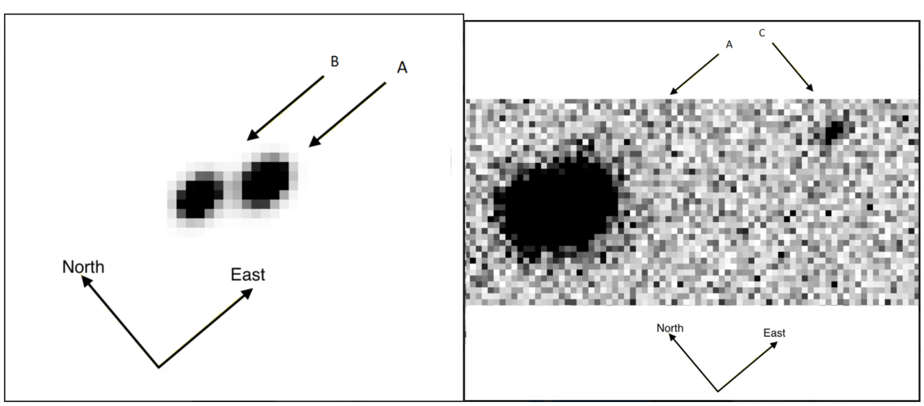

Figure 6. WDS 15379+3006, STF1963AB resolved (left) and STF1963AC (right). These images were obtained using Hα filter with an exposure of 90 seconds (Mira, 2016). As one can see, the A and B components readily bled into one another, necessitating the development of techniques other than automatic centroid detection for our measurements (detailed below).

Astrometric Measurements of Triple Star System15379+3006 STF 1963AB, STF 1963AC

Table 3. *Data table of all measurements taken of STF 1963 (AC and AB components). All measurements were used to tabulate average, median, standard deviation, and standard deviation of the mean, except those with labeled with a "*" which were omitted. These measurements were found to lie demonstrably outside of the trends outlined by previous measurements and those that used the Manual Centroid Detection techniques. Measurements of Separation (ρ) in STF1963AB were found to be significant when compared to trends (see Figure 11) and therefore the Automatic Centroid Measurements were omitted. Average values were used as results and plotted below.*

WDS 15379+3006					
* omitted from statistics and plots		AC component		AB component	
	Image filter (exposure time)	Separation (Rho)	Angle (Theta)	Separation (Rho)	Angle (Theta)
Auto Centroid	Luminance (30 sec)	32.5615	116.2550	4.2853*	298.0100
	Luminance (60 sec)	32.4889	116.1980	4.1497*	299.0020
	Hydrogen Alpha (30 sec)	NaN	NaN	4.2320*	299.2580
	Hydrogen Alpha (90 sec)	32.4194	115.9810	4.2540*	297.7390
Manual Centroid	Luminance (30 sec)	32.1691	116.1450	5.1491	299.7040
	Luminance (60 sec)	32.3999	115.8320	5.2204	298.3200
	Hydrogen Alpha (30 sec)	NaN	NaN	5.3799	297.2150
	Hydrogen Alpha (90 sec)	32.0435	116.1130	5.3677	297.6860
Statistical Analysis	Average:	32.3471	116.0873	5.2793	298.3668
	Median:	32.3999	116.1130	5.2204	298.0100
	Std Deviation:	0.1816	0.1419	0.0979	0.8139
	Std Deviation of the Mean:	0.0687	0.0536	0.0438	0.2713

when compared with historical measurements (see Figures 8 and 9) that will be explored in greater detail in the discussion section.

AB Component

With respect to the AB component of WDS 15379+3006, the astrometric measurement appears reasonable when compared with historical measurements, Figures 10 and 11. Standard deviation of the mean between all manual centroid measurements of this system were 0.8 and 0.1 in position angle and separation distance respectively, Table 3. Precision in the astrometric measurements taken were also excellent, as evidenced by 0.3 and 0.04 standard deviation from the mean in position angle and separation distance respectively.

While there was no significant difference in position angle determination between automatic versus manual centroid detection methods, Figure 11 demonstrates that a separation distance near four arc-seconds

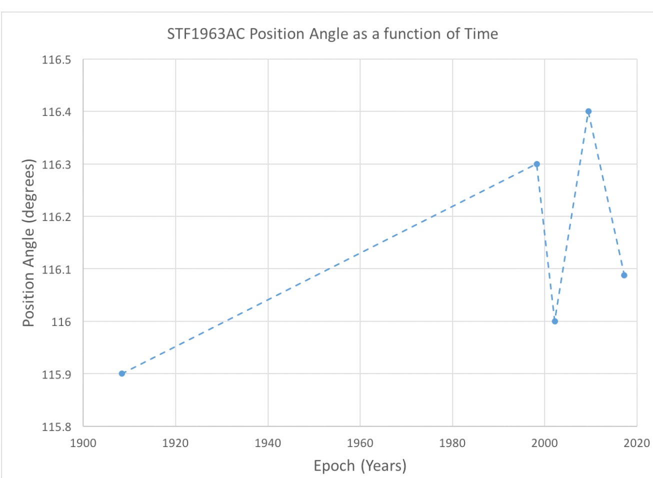

Figure 8. Graphical depiction of all measurements of position angle (to date) of STF1963AC with respect to time (epoch).

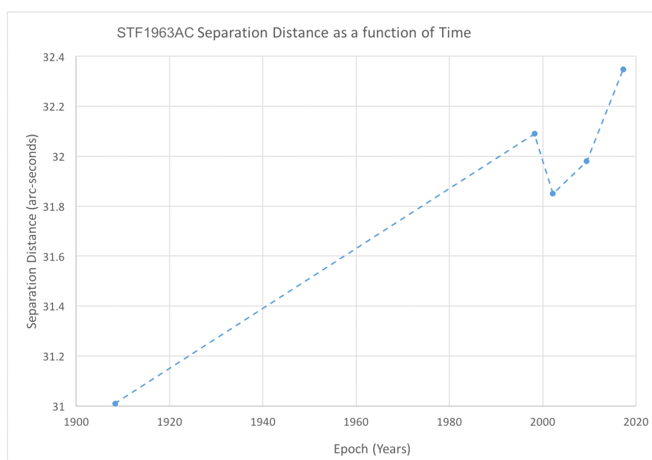

Figure 9. Graphical depiction of all measurements of separation distance (to date) of STF1963AC with respect to time (epoch).

Astrometric Measurements of Triple Star System15379+3006 STF 1963AB, STF 1963AC

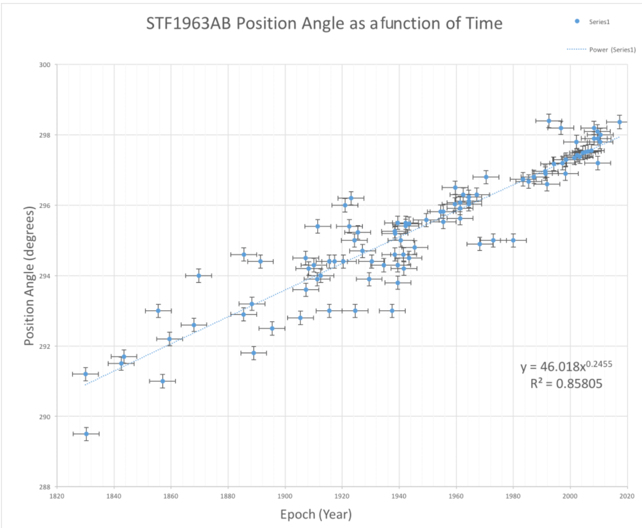

Figure 10. Graphical depiction of all historical measurements of position angle (to date) of STF1963AB with respect to time (epoch). One can see a linear trend, not indicative of an orbital binary. Outliers omitted.

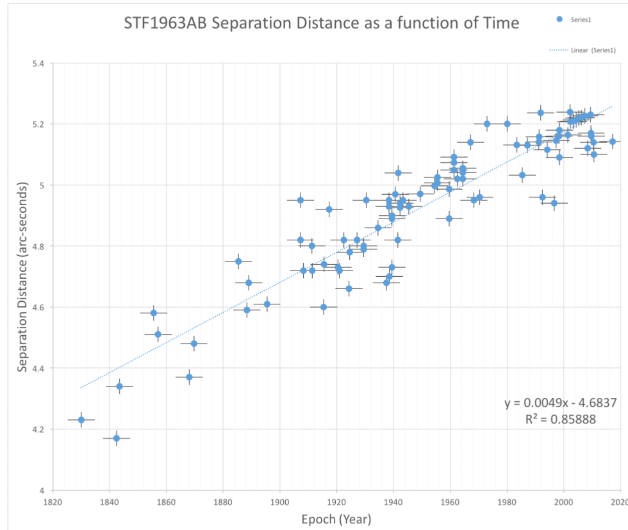

Figure 11. Graphical depiction of all measurements of separation distance (to date) of STF1963AB with respect to time (epoch). Again, one can see a linear trend, not indicative of an orbital binary. Outliers omitted.

clearly does not follow the historic trend outlined therein. Manual centroid detection methods, however, did yield precise measurements which fit this trend nicely. Furthermore, a significant difference between measurements which used manual centroid detection and those that used automatic centroid detection did occur, and the measurements which utilized manual centroid detection techniques had a high degree of precision with respect to one another between images (Table 3). For this reason, measurements of separation ascertained by utilizing automatic centroid detection were omitted from AB considerations.

Discussion

AC Component

When compared with historical observational data half a degree variation in position angle between measurements of 1908 and 2009 is seen. Somewhat zigzagged pattern in position angle changes is observed, Figure 8. The 2017 angular separation measurement shows 1.4 arc second change compared to the first historic measurement. Within the last twenty years of measuring the overall change in the separation angle is within our resolution limit, Figure 9. Thus, no reasonable trend could be ascertained by careful analysis of the position angle or separation distance with respect to their epoch.

Orbital plots of C component's position relative to A, Figure 12, does not yield any further evidence of a gravitational relationship between the two components either (Genet 2016). Although only five astrometric measurements have been contributed to-date they all show very good overall agreement, Figure 12 right panel, leading us to conclude that C component doesn't appear to move significantly with respect to the A component, Figure 12, left panel.

AB Component

When compared with historical observational data, this system shows consistency, Figures 10 and 11. Since the first measurements were taken in early 1800s the position angle has changes by eight degrees and the separation has changed by only one arc-second. This indicated that the distance between A and B stars has not change significantly in the last two hundred years while they did change position with respect to each other.

In the Figure 13, we have attempted to present orbital motion of component B with respect to the component A. In the left panel, the A component is found in the origin and all historic data for the motion of component B are plotted including our measurement. In the right panel we averaged measurements in 60-year bins to clarify any trends in motion. Although no elliptical orbit has yet been made available, more observations of this system, over some time, may be able to provide enough data to establish one. This statement is justified by an apparent curvature toward the north-northeast in the motion of component B with respect to the component A. A determination as to whether or not STF1963AB is an optical double or long-period gravi-

(Text continues on page 249)

Astrometric Measurements of Triple Star System15379+3006 STF 1963AB, STF 1963AC

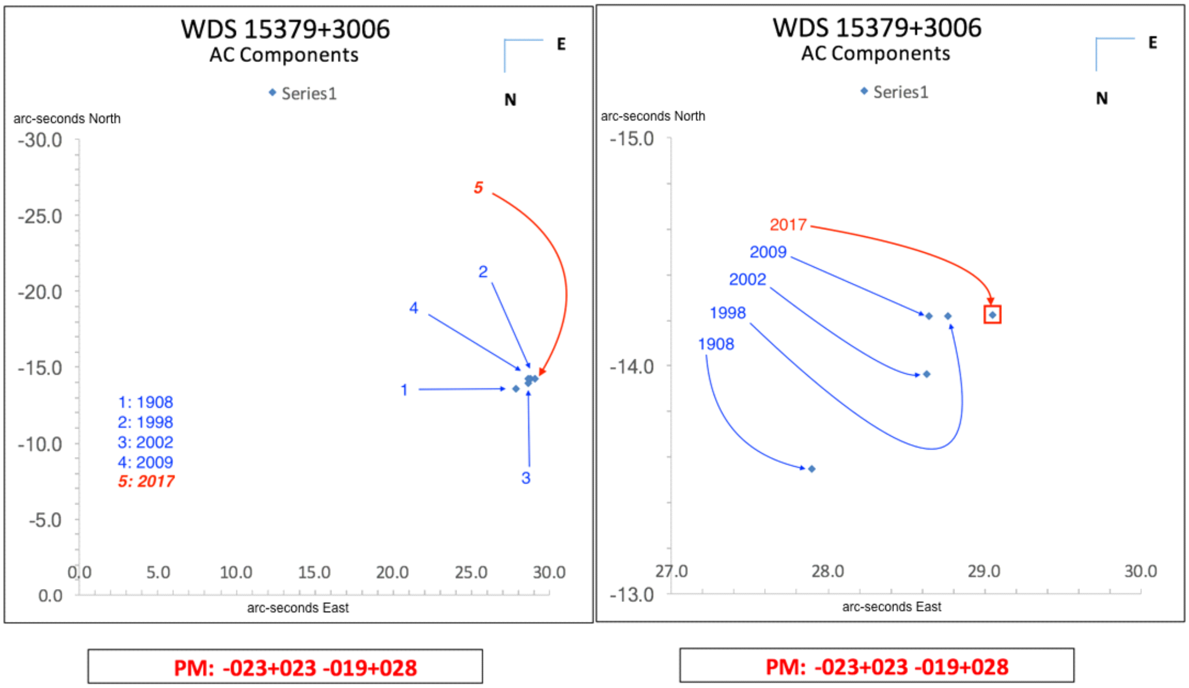

Figure 12. Graphical depiction of historical measurements (C component) and present measurement of STF1963AC. Team PRSM measurement appears in red, and by italicized text. In the left panel STF 1963's A component is at the coordinate system origin. In the right panel we zoom into the motion of C component to capture the positions relative to one another.

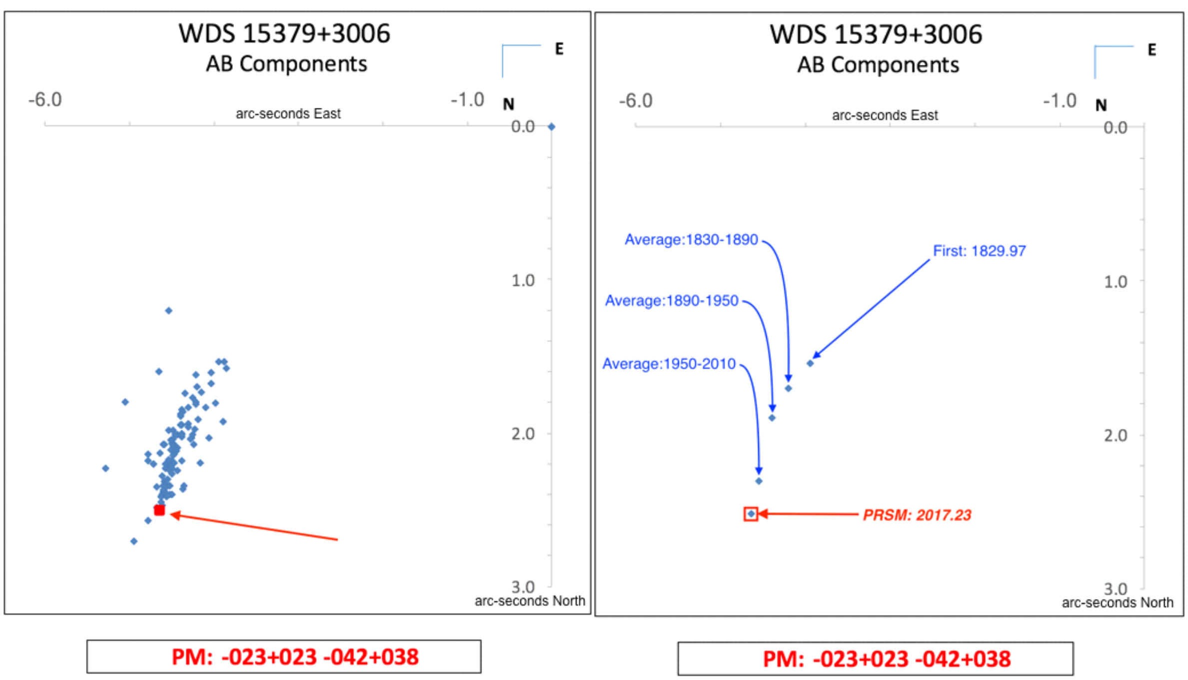

Figure 13. Graphical depiction of historical measurements and present measurement of STF1963AB. A component positioned at the origin (left panel). Team PRSM measurement appears as a red square, and indicated by an arrow. On the right panel graphical depiction of historical measurements, averaged in 60-year swaths of measurements to clarify any trends in motion. Team PRSM measurement appears and encircled by a red square, and italicized text.

Astrometric Measurements of Triple Star System15379+3006 STF 1963AB, STF 1963AC

(Continued from page 247)

tational binary is difficult to make as both of these can exhibit this overall linear behavior (Heintz 1978).

Conclusion

Precise measurements of WDS 15379+3006 (STF1963AB and STF1963AC) were obtained successfully from four CCD images taken by iTelescope networks T-18 telescope located in Nerpio, Spain. These measurements shall contribute to a large body of historical astrometric measurements of STF1963AB, and to the very few historical astrometric measurements of STF1963AC. STF1963AC shows no reasonable trends and it is the opinion of the authors that it is a visual double star system, and not a physical double star system as suggested by its low rPM.

Measurements of the STF1963AB component of WDS 15379+3006 show a linear trend, although there may be some reason to argue that a seemingly curved path of B with respect to the A exists and therefore is evidence for a long period gravitationally bound system, no orbital relationship was able to be ascertained at the time of this study.

Acknowledgements

The authors would like to thank the iTelescope Network for the use of their service and the United States Naval Observatory for providing historical measurement data. The authors would also like to thank the Boyce Research Initiative and Education Foundation (BRIEF) for their generous financial donation that allowed us to use the iTelescope robotic telescope system, remote server and software. Lastly, the authors thank Pat Boyce, Grady Boyce and Russell Genet for their guidance and expertise during the review of this paper.

References

Genet, R., Johnson, J., Buchheim, R., and Harshaw, R., 2016, *Small Telescope Astronomical Research Handbook.*

Hartkopf, W.I., Mason, B.D., and Wycoff, G.L., 2011, "Speckle interferometry at the U.S. Naval observatory", *The Astronomical Journal,* **3**, pp. 3.

Heintz, W.D., 1978, *Double Stars.* Dordrecht: D. Reidel Publishing Company, pp. 17-18.

Mason, B., "The Washington Double Star Catalog", 2017, Astrometry Department, U.S. Naval Observatory. http://ad.usno.navy.mil/wds/Webtextfiles/wdsnewframe3.html

MaxIm DL [Computer software], 2017, Diffraction Ltd., Retrieved from http://diffractionlimited.com/product/maxim-dl/.

Mira Pro x64 [Computer software], 2016, Mirametrics Inc., Retrieved from http://www.mirametrics.com/mira_pro_x64.php.

Moore, B.. 2017, iTelescope-T18-Medium Deep Space -Spain, iTelescope.Net Pty Lt. http://www.itelescope.net/telescope-t18/.

SAOImage DS9 [Computer software], 2016., Smithsonian Astrophysical Observatory., Cambridge, MA., Retrieved from http://ds9.si.edu/site/Download.html.

Sissa, E., Gratton, R., Desidera, S., Martinez Florensano, A.F., Bonfanti, A., Carolo, E., Vassollo, D., Claudi, R.U., Endl, M., and Cosentino, R., 2016, "Hα- activity and ages for stars in the SARG survey", *Astronomy and Astrophysics.* pp. 7-8.

SkyX Pro [Computer software], 2017, Software Bisque Inc., Retrieved from http://www.bisque.com/sc/media/24/default.aspx.

Stelle Doppie. 15379+3006 STF1963AC., 2017, http://stelledoppie.goaction.it/index2.php?menu=29&iddoppia=63379.

Analyzing the Proper Motion of Two Double Star Systems from Astrometric Measurements

Alex Falatoun[1], Janet Barrera[1], Anna de Neef [2], Aura Gonzalez[3], Jae Calanog[1], Pat Boyce[4], and Grady Boyce[4]

1. San Diego Miramar College, San Diego, California, USA
2. MiraCosta College, Oceanside, California, USA
3. San Diego Mesa College, San Diego, California, USA
4. Boyce Research Initiatives and Education Foundation (BRIEF), California, USA

Abstract: The iTelescope network was used to obtain astrometric measurements of double star systems WDS 12202-1408 (STF 1631) and WDS 12339+5522 (STI 2286). Through astrometric measurement softwares SAOImage DS9 and Mira Pro x64, a mean position angle for STF 1631 of 304.8° ± 0.9° and a mean separation 14.7" ± 0.2" was measured. For STI 2286, a newly measured mean position angle of 85.9° ± 0.9° and mean separation 11.5" ± 0.3" were obtained. The relative proper motion of 1631 shows that the system could be demonstrating a linear path or an approximately circular orbit with a period of ~1400 years. Parallax measurements of the secondary star will aid in classifying if this system is a physical or a visual pair. The proper motion of STI 2286 indicates that it could be a physical pair, featuring an orbit nearing a turning point. Follow-up observations in three to four year intervals will further validate or refute this claim and constrain the shape of a possible orbit.

Introduction

The Astronomy Research Seminar is a project offered by San Diego Miramar Community College for students to gain insight on how research is performed in the real world. This program allows students to learn about binary stars and the basics of astronomy. This project was supervised by Jae Calanog at Miramar College and was supported by the Boyce Research Initiatives and Education Foundation (BRIEF).

Double stars consist of any two stars in the sky within close proximity when viewed from Earth. Some double stars are physically associated or gravitationally bound to each other, commonly referred to as binary stars. However, it is also possible that some double stars are aligned by chance along our line of sight, appearing close to each other when observed but are actually hundreds or thousands of light years apart (Buchheim, 2015). A straightforward method of gathering evidence in order to classify a double star as a visual or a physical pair is to track their positions over time. If the position of each star is determined, the double star's position angle, θ, and separation distance, ρ, can be measured and one can effectively visualize the relative proper motion when compared with historical data.

For this research, the Washington Double Star Catalog (WDS) by Brian Mason (2012) was used to select two double star systems, WDS 12202-1408 (hereafter referred to as STF 1631) and WDS 12339+5522 (hereafter referred to as STI 2286). The double star systems were selected based on their visibility in the Northern Hemisphere during the spring semester (January - June). The WDS catalog was used to search for systems with a right ascension between 12 and 18 hours. In addition, a minimum separation of 6 arc seconds and a magnitude difference no greater than 6 was preferred. Both double star systems met the criteria and had less than 15 observations making them favorable to study because our research would provide valuable information for their classification.

The first star system was selected because it was labeled as a linear system yet the data presented did not seem to support that statement. This star system was discovered in 1831 by John Frederick Herschel, son of astronomer William Herschel. In 1816 Herschel was

Table 1. Historical measurements for STF 1631. Position angle is measured in degrees and separation distance in arcseconds.

WDS 12202-1408 (STF 1631)		
Epoch	**θ (°)**	**ρ (")**
1831.35	268.0	21.0
1900.34	278.3	15.63
1905.35	276.0	15.753
1906.32	277.5	15.926
1909.34	278.3	15.63
1930.42	283.0	15.29
1991.25	298.08	14.681
1991.25	292.7	14.665
1991.69	298.0	14.984
1998.29	300.0	14.73
2000.085	299.9	14.625

directed to continue his father's work and in 1820 became a member of the Astronomical Society. In addition to astronomy, John Herschel is known for many of his accomplishments in mathematics, chemistry, and photography (Lankford, 1997). The star system's observation history and data can be viewed in Table 1.

The second star system, STI 2286, had a noticeable difference in its position angle as well as its separation, which indicated significant movement away from the primary star. It was first observed in 1917 by astronomers at the Vatican Observatory Foundation (2015-2016), a few years after Pope Leo XIII re-founded the institution in 1891. He wanted to demonstrate that the Church was not against science, but instead, promoted it. Based on the information from the WDS catalog and the historical data, these systems seemed to be appropriate candidates to be binary systems. Observation history and data is outlined in Table 2.

The goal of this study was to measure the current separation distances and position angles from the selected double star systems. In obtaining these measurements, we can provide supporting evidence whether or not these systems are either physically associated or just aligned by chance along our line of sight.

Equipment, Observations, and Data Analysis Procedures

Equipment

iTelescope Network's T18 (Figure 1) is located at the AstroCamp Observatory in Nerpio, Spain. The attached charged coupled device (CCD) has a 100,000e- non anti-blooming gate and uses a Planewave CDK optical tube assembly on a Paramount PME externally guided mount. This telescope provides 0.73"/pixel resolution, and images were taken using an Astrodon Series E LRGB (Luminance, Red, Green, Blue) filters (Jenkins, 2003).

Table 2. Historical data for STI 2286. Position angle is measured in degrees and separation distance in arcseconds.

WDS 12339+5522 (STI 2286)		
Epoch	**θ (°)**	**ρ(")**
1917.28	176.7	5.7
1917.28	176.7	5.685
2000.26	80.0	10.18
2003.16	81.1	10.472
2006.408	82.3	10.84
2010.5	84.0	11.25

Figure 1. *The iTelescope Network's T18 used for the astrometric measurements of STF 1631 and STI 2286.*

Observations

The date of observation was chosen to align as closely as possible to a new moon phase in order to have the lowest luminosity from the moon as determined by the Staralt visibility tool (Sorensen, 2002). The first date of observation was in late March and the

Analyzing the Proper Motion of Two Double Star Systems from Astrometric Measurements

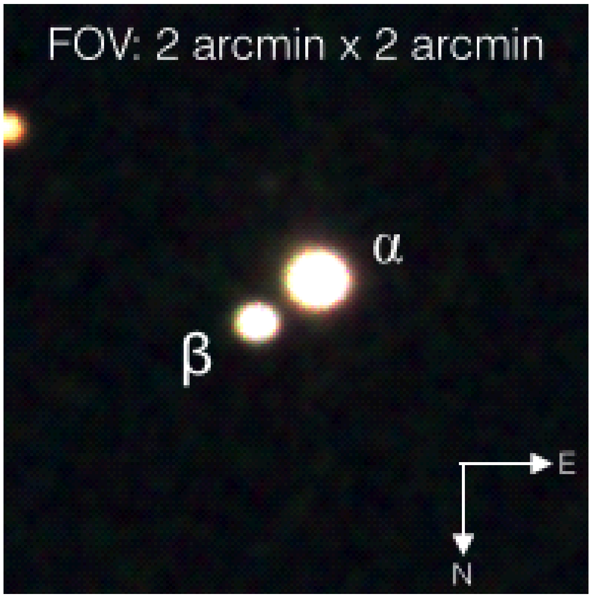

Figure 2. Three color image of STF 1631 with combined filters red, green and blue. Field of view is 2 arcmin x 2 arcmin.

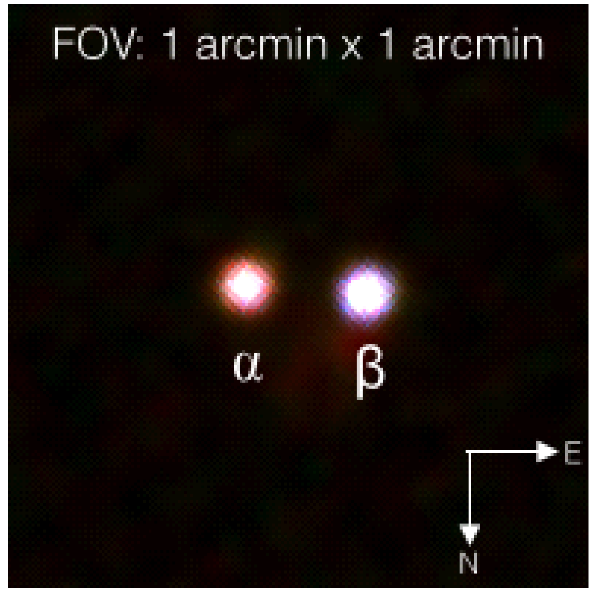

Figure 3. Three color image of STI 2286 with combined filters red, green and blue. Field of view is 1 arcmin x 1 arcmin.

second date of observation in early May.

Four images were taken in total of STF 1631 at 60 seconds exposures each, using a luminance, red, green and blue filter. Five images of STI 2286 were taken in total, two using a luminance filter for unbiased viewing at 60 and 120 second exposures, and one of each red, green, and blue filters, each with 60 second exposures. See Figures 2 and 3.

Analysis Procedures

All images were preprocessed (flat-fielded and dark subtracted) by the iTelescope network. The pixels that contained our double star systems were checked for counts to make sure that none of the images were oversaturated. After assessing the quality of the images, they were imported to MaximDL in order to assign World Coordinate System (WCS) positions using the Pinpoint Astrometry feature, which compares the image to the Naval Observatory's Catalog (UCAC4). The UCAC4 catalog matched 110 out of 148 catalog stars with an average residual of .1 arcseconds for STF 1631 and 104 out of 174 image stars with an average residual of .1 arcseconds for STI 2286.

The image analysis software SAOImage DS9 (referred to henceforth as DS9) was used to consistently measure the position angle (θ) and separation distance (ρ) for each image. First, a 7" circle was created using the Regions feature and placed over the A star, followed by a circle of the same radius around the B star. DS9's auto-centroiding feature was used to find the center of each star, which effectively calculates the weighted mean position of all the counts per pixel enclosed in the circle. The coordinates for the centroid of each star were recorded and then placed as endpoints of a line segment. The length of the line segment provided the separation distance in arcseconds and its orientation relative to some reference provided the position angle.

To further validate the measurements taken by SAOImage DS9, images were cross referenced with Mira Pro x64. Both results provided considerable overlap in each measurement, verifying the precision of each software.

Results

We list our astrometric measurements in Table 3 and Table 4 for STF 1631 and STI 2286, respectively. For the epoch, 2017.33, we measure STF 1631 at a mean position angle of 304.8° ± 0.9° and separation distance of 14.7" ± 0.2". For STI 2286, we measure a position angle of 85.9° ± 0.9° and separation distance, 11.5" ± 0.3". Assuming that the 1-σ uncertainties associated with the last measurement for STF 1631 (Hartkopf et al. 2013) and STI 2286 (Cutrie et al. 2012) are of the magnitude of the smallest significant figure listed, then one can conclude that both systems have exhibited a significant change in position between the primary and the secondary.

Discussion

Figure 4 shows an increasing trend in the position

Analyzing the Proper Motion of Two Double Star Systems from Astrometric Measurements

Table 3. Position angle, separation distance, and uncertainties for STF 1631

WDS 12202-1408 STF 1631					
Epoch	Number of Images	Mean θ (°)	σ_θ (°)	Mean ρ (″)	σ_ρ (″)
2017.33	4	304.8	0.9	14.7	0.2
2000.085	Last Measurement (Hartkopf, et al 2013)	299.9	0.5	14.6	0.1

Table 4. Position angle, separation distance, and uncertainties for STI 2286

WDS 12339+5522 STI 2286					
Epoch	Number of Images	Mean θ (°)	σ_θ (°)	Mean ρ (″)	σ_ρ (″)
2017.33	5	85.9	0.9	11.5	0.3
2010.5	Last Measurement (Cutrie et al 2012)	84.0	0.8	11.3	0.2

angle for STF 1631. It is difficult to determine whether the trend over the past ~200 years has been approximately linear, since we do not have knowledge of the uncertainties associated with the first measurement in 1831. We reach a similar conclusion when examining the longitudinal data associated with the separation distance (Figure 5). All subsequent measurements after the first observation show the separation distance to be slowly decreasing at a steady rate. Figure 6 shows the relative proper motion of STF 1631. If we treat the 1831 measurements as an outlier, then the subsequent data shows two possibilities: First, STF 1631 is a visual pair, with the primary and secondary exhibiting a high degree of relative proper motion. Second, STF 1631 is a binary system in an elliptical orbit, and the current set of data points are only a fraction of the orbital path. This could be indicative of a special case in which a circular orbit with a period of ~1400 years (determined assuming a constant rate of change in theta and estimating the time for the secondary star to complete 360 degrees around the primary), as explained by the separation remaining statistically constant since its last measurement, and a constant increase in position angle. In addition, we also note that the recent data release from the GAIA satellite (Arenou et al. 2017) provides a parallax measurement of the primary star and has an estimated distance of 109 ± 3 parsecs (~350 light years). If STF 1631 is indeed a binary system, then we would expect the secondary star to have a similar distance, therefore highlighting the importance of the secondary star's parallax measurement for future observations.

Figure 7 shows a peculiar measurement in STI 2286's initial position angle, measured by the Vatican Observatory in 1917. It is significantly larger and does not fit the trend of measurements in later years. We have explored different possibilities on how this measurement could have been so different, such as a North-South switch, a nearby star that could have been mistaken for the secondary, or an initial observation that was taken at the end of a period and subsequent observations were measured once the position angle had reset back to zero. None of these scenarios were able to reproduce the initial measured position angle. In addition, the initial separation distance measured also adds complexity to the issue (of disregarding the 1917 meas-

(Text continues on page 255)

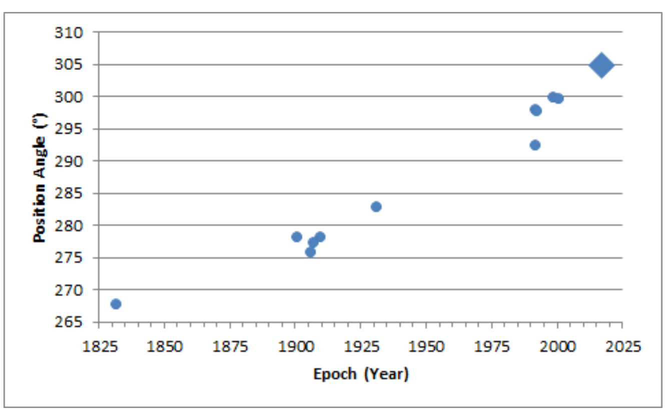

Figure 4. Position angle in degrees and epoch in years for STF 1631, including historical data and new measurement (large diamond). Since its observation, the position angle has steadily increased, which could indicate a constant angular velocity.

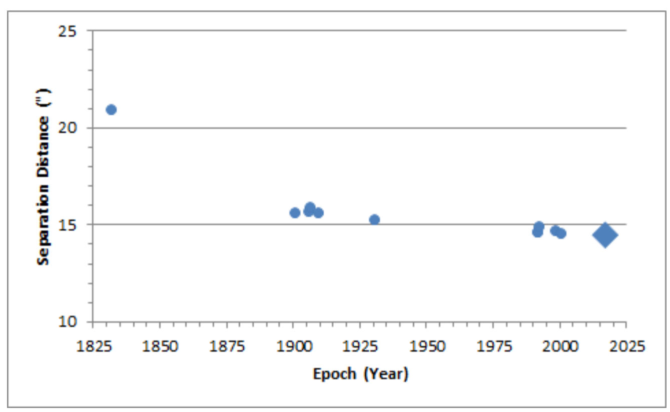

Figure 5. Graph of separation *distance in arcseconds and epoch in years for STF 1631, including historical data and new measurement (large diamond). Aside from the first observation, the separation distance appears to be steadily decreasing but could also be statistically constant if the uncertainties from previous measurements overlap with the more recent measurements.*

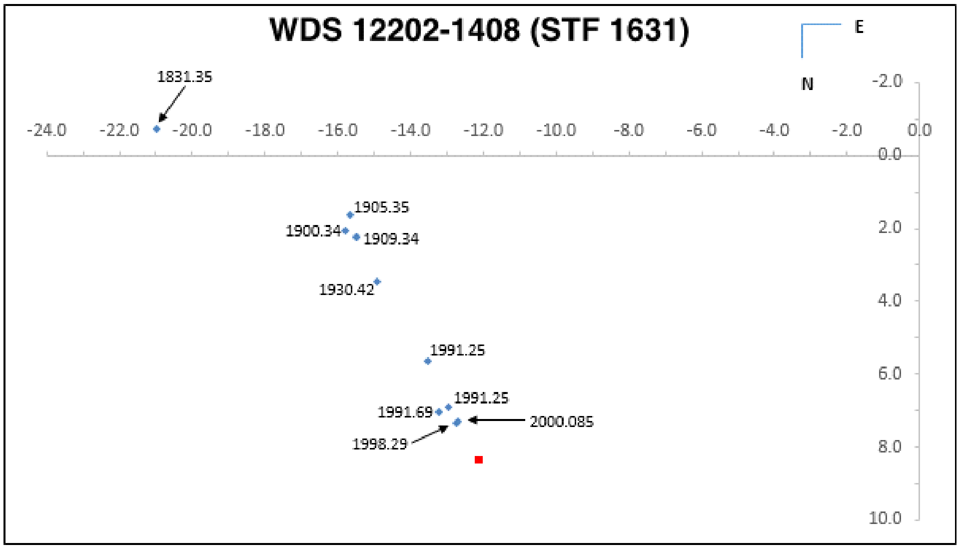

Figure 6. Relative proper motion plot of STF 1631, expressed as ΔRA vs. ΔDEC relative to the primary, placed at the origin. Subsequent measurements from Herschel show two possibilities: a linear solution, which would classify the system as a visual pair or a binary system with an approximately circular orbit, indicated by the steadily changing position angle and an approximately constant separation distance.

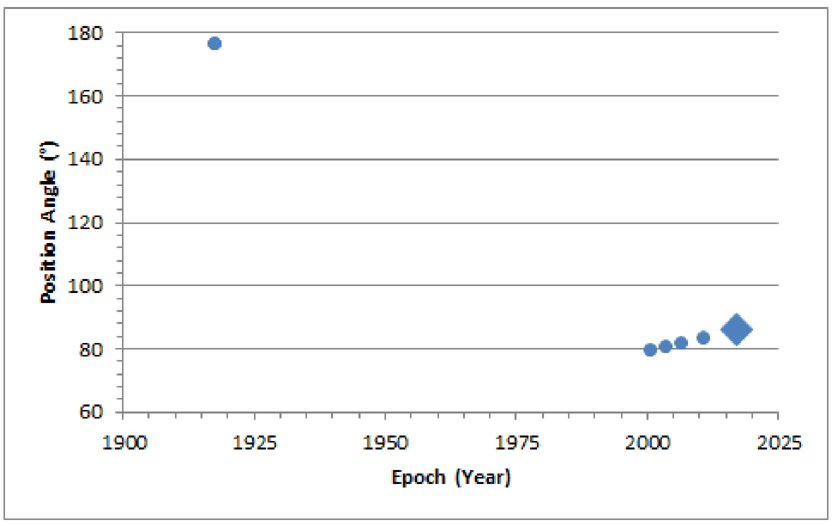

Figure 7. Graph of position angle in degrees and epoch for STI 2286, including historical data and new measurements (large diamond). The first observation in 1917 does not fit the trend displayed by subsequent measurements and is likely an outlier.

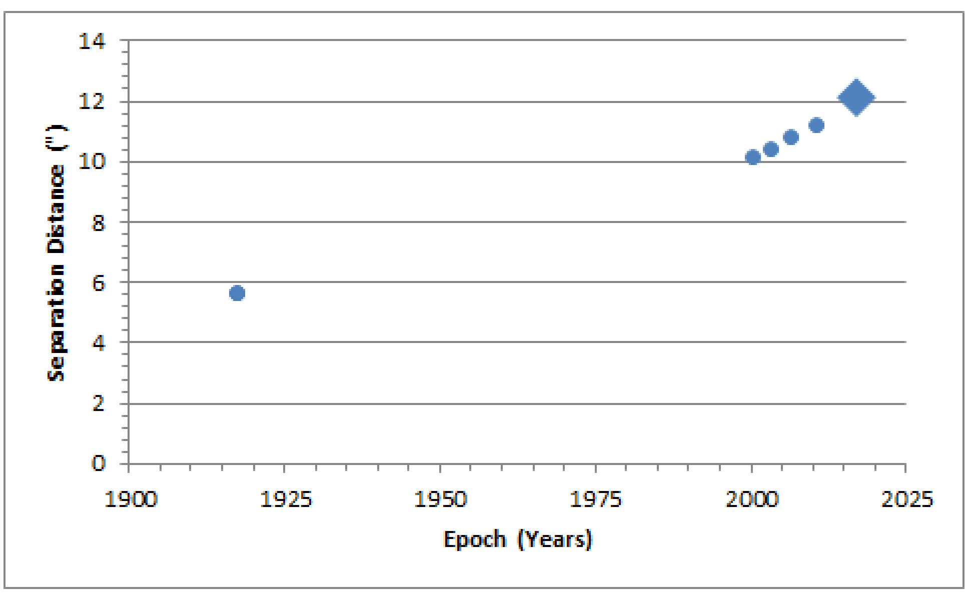

Figure 8. Graph of separation distance in arcseconds and epoch for STI 2286, including historical data and new measurements (large diamond). Subsequent measurements after 1917 show a steadily increasing separation distance.

Analyzing the Proper Motion of Two Double Star Systems from Astrometric Measurements

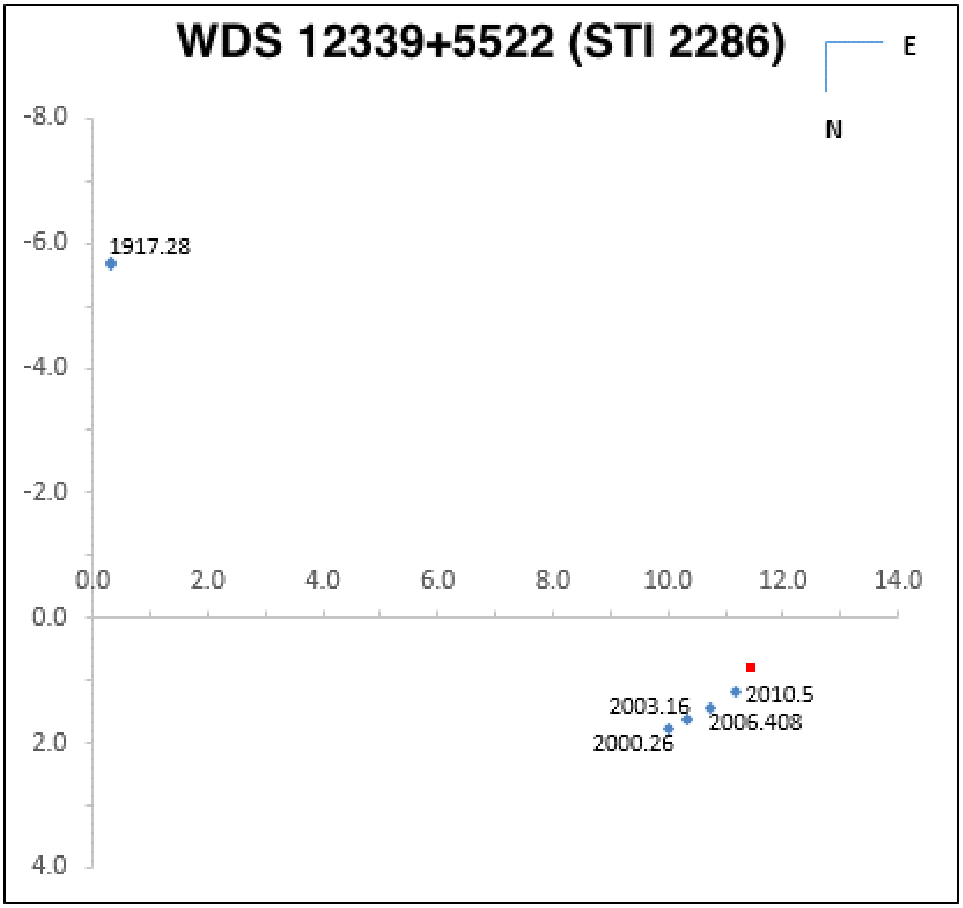

Figure 9. Relative proper motion plot of STI 2286, expressed as ΔRA vs. ΔDEC relative to the primary, placed at the origin. Excluding its first observation in 1917 (likely an outlier), STI 2286 follows a curved path that could indicate an orbit around the primary star.

(Continued from page 253)

urements) since it could be consistent with a nonlinear, increasing trend (Figure 8). If we choose to omit the 1917 measurements, then Figure 9 shows that the secondary's relative proper motion is exhibiting some curvature, consistent with an orbit around the primary. Furthermore, from the shape of the secondary's curved path, it looks to be that it might be nearing a turning point. Given that the historical data for STI 2286 listed in Table 2 shows that the position angle has been changing at a rate of 1-2° per every 3-4 years and its possible current stage in an elliptical orbit, follow-up observations of this double star system in those time intervals will provide critical longitudinal information in classifying whether or not this system is a physical or a visual double.

Conclusion

We have successfully measured the position angles and separation distances of the star systems, WDS 12202-1408 (STF 1631) and WDS 12339+5522 (STI 2286), using observations from iTelescope's T18 telescope. Both measurements showed a significant change in position from their last measurements. Our conclusions for each system are as follows:

1. The current set of data for STF 1631 currently shows a proper motion that could be linear or part of orbit with a small degree of eccentricity and a period of ~1400 years.
2. The first set of measurements for STF 2286 is likely an outlier. If we make this assumption, STF 2286 could represent a physical double star system with the secondary nearing a turning point. Observations every 3-4 years will prove very beneficial in constraining a possible orbit for this system.

Acknowledgements

This research was supported by the Boyce Research Initiatives and Education Foundation (BRIEF). We thank Brian D. Mason for past observations on both

STF 1631 and STI 2286 from the Washington Double Star Catalog.

We are grateful to the San Diego Community College for allowing us to hold meetings on campus. We also would like to thank the members of the Boyce Astro community for the resources and financial donations that have allowed us to carry out our research.

This work has made use of data from the European Space Agency (ESA) mission Gaia (https://www.cosmos.esa.int/gaia), processed by the Gaia Data Processing and Analysis Consortium (DPAC, https://www.cosmos.esa.int/web/gaia/dpac/consortium). Funding for the DPAC has been provided by national institutions, in particular the institutions participating in the Gaia Multilateral Agreement.

References

Arenou, F., et al., 2017, “Gaia Data Release 1. Catalogue Validation”, *Astronomy & Astrophysics*, **599**, 35.

Boyce, G. and Boyce, P. Boyce, Research Initiatives and Education Foundation (BRIEF), http://www.boyce-astro.org/home.html.

Buchheim, R., Johnson, J., Harshaw, R., & Gennet, R. (2015). Small Telescope Astronomical Research Handbook. Collins Foundation Press.

Cutri, R. M., et. al., 2012, WISE All-Sky Data Release (Cutri+ 2012), http://adsabs.harvard.edu/abs/2012yCat.2311....0C.

Jenkins, A., 2003, *iTelescope Network News – Remote Internet Telescope Network – Online Imaging & Telescope Hosting Service*, N., Mortillano and I. Musgrave, eds., http://www.itelescope.net/.

Lankford, J., 1997. *History of Astronomy: An Encyclopedia*, Garland Publishing Inc., New York.

Mason, Brian., 2012, *Washington Double Star Catalog.* Astronomy Department, United States Naval Observatory, http://ad.usno.navy.mil/proj/WDS/.

Sordiglioni, Gianluca, 2016, Stella Doppie Double Star Catalog, http://stelledoppie.goaction.it/.

Sorensen, P., Azzaro, M., Méndez, J., 2002, *Isaac Newton Group of Telescopes,* http://catserver.ing.iac.es/staralt/.

Vat. Obs. Foundation. 2015-2016. *Specola Vaticana History*, https://www.vofoundation.org/mission.

Hartkopf, William, Mason, Brian, Finch, Charlie, Zacharias, Norbert, Wycoff, Gary, and Hsu, Danley, “Double Stars in the USNO CCD Astrographic Catalog”, *The Astronomical Journal*, **146**, no. 4, 2013.

Measurements of 161 Double Stars With a High-Speed CCD: The Winter/Spring 2017 Observing Program at Brilliant Sky Observatory, Part 2

Richard Harshaw

Brilliant Sky Observatory, Cave Creek, AZ
rharshaw51@cox.net

Abstract: In the winter and spring of 2017, an aggressive observing program of measuring close double stars with speckle interferometry and CCD imaging was undertaken at Brilliant Sky Observatory, my observing site in Cave Creek, Arizona. A total of 596 stars were observed, 8 of which were rejected for various reasons, leaving 588 pairs. Of these, 427 were observed and measured with speckle interferometry, while the remaining 161 were measured with a CCD. This paper reports the results of the observations of the 161 CCD cases. A separate paper in this issue will report the speckle measurements of the 427 other pairs.

1. Introduction

The winter and spring of 2017 marks the start of the third observing season at Brilliant Sky Observatory using high-speed CCD imaging. Previous measurements have been reported in this journal by this author (Harshaw, A through G). This paper will continue the reports in that tradition.

2. Equipment Used

Brilliant Sky Observatory is equipped with a Celestron C-11 11-inch SCT telescope mounted on a Celestron CGEM-DX mount atop a PierTech adjustable pier. (See Figure 1.) The mount is controlled by a Lenovo desktop computer running TheSky 6.0.

The optical train consists of a Crayford focuser (locked in place so as not to affect focal length between observing sessions) which feeds into an Orion 1.25-inch flip mirror. One leg of the flip mirror unit—the acquisition leg—feeds a 25mm f/l illuminated reticle eyepiece with a single crosshair illuminated by a dimmable LED. The mount always places the target star within 5 arc minutes of the cross hair, so acquisition is fast and easy. The camera leg of the flip mirror unit feeds into a ZWO ASI290MM monochrome camera, known for its low read noise and excellent performance

Figure 1: The setup at Brilliant Sky Observatory

as a speckle camera. The camera has a 2x "Shorty Barlow" from Orion affixed to its mounting ring. Because only the lens and its mounting barrel from the Shorty Barlow are used, the actual multiplication of the Barlow is 1.5, resulting in a system focal ratio of 14.98 resulting in 7 pixels per arc second.

The focal length of the system, as well as pixel scale and camera orientation with respect to north, are all determined by multiple drifts (20 or more drifts per session) of a star near declination 45°. The drift star is edged to the east edge of the camera's field of view, the drive motor then turned off, and the star allowed to drift across the camera's field of view while the computer is recording the file as a series of FITS frames. These files are then analyzed in The Speckle ToolBox (STB) using the Drift Analysis function of STB.

Focus is achieved and maintained by a Feathertouch focuser controlled by a MicroTouch temperature-compensated focus controller, both obtained from Starizona, a telescope supply and service center located in Tucson, Arizona.

When doing CCD measurements, 1,000 frames are made of each star at as short an integration time as possible given the magnitudes of the two stars. Usually five such files are made of each star, but for fainter pairs, there may be fewer files made due to the longer exposure times required to accumulate 1,000 frames. For close CCD pairs (pairs that require more than 40 ms of integration time, even if rho is under the 5" criterion for speckle), a single star is also shot for deconvolution purposes.

Files are written to a 2TB portable USB3 hard drive, which is then taken into my office for analysis the next day using STB for data reduction and measurements.

Final results are then saved to a 5TB USB3 hard drive with a backup made to a second 5TB USB3 hard drive. The backup drive undergoes an incremental backup once a week.

3. Methodology

3a. Speckle or CCD?

The decision to make a file as a speckle interferometry case or a CCD case depends on two factors: the separation (rho) of the two stars and the magnitudes of the two stars.

To qualify for speckle interferometry, the pair must have a rho value of 5" or less (but on nights of very good seeing, this can be pushed up a bit, perhaps to 6"). Also, the stars must be bright enough to register in 40 ms or less.

Any pair wider than 5" and/or requiring integration times over 40ms is then recorded and processed as a CCD file.

3b. Using The Speckle Toolbox in Manual Mode.

Some of the stars in this report are described as "Manual solution with STB." When a pair is wide enough to produce three distinct star images in the autocorellogram (the primary flanked by symmetric images of the companion's power spectrum), STB has no difficulty in automatically locating and selecting the companion star (although sometimes, the observer must use the complementary image 180° from the one chosen by STB if theta is greater than 180°). But in cases where the power spectrum images of the stars are not distinct, or the frame is noisy, STB may not be able to automatically find the companion's image. In such cases, STB allows the user to manually select the companion's image by right clicking on it. In this report, all the pairs measured with "Manual solution" had distinct companion power spectrum images to select, but noise near the primary misled STB's automatic selection process.

3c. A New Method Code.

In the spring of 2017, I entered into correspondence with Brian Mason of the U. S. Naval Observatory (the curators of the Washington Double Star Catalog, or WDS) regarding the Su and Cu codes used in the WDS datarequest files. I was able to verify that the Su and Cu codes employed by the USNO were the same procedure I was doing with CCD cases using STB—that is, a pair too wide for speckle (or one requiring integration times over 40 ms) is measured with the autocorellogram generated by speckle reduction software, such as STB. In my experience, this yields slightly better results than lucky imaging alone and has become my method of choice for analyzing CCD images.

To accommodate this process, Mason agreed to a new code, "Cv", which means that the observer made the measurement of a CCD image using speckle reduction software. The official USNO description for Cv reads, "CCD imaging (speckle-style reduction)".

3d. Using the Most Accurate Proper Motions Available.

Until recently, the most accurate data sources for parallax and proper motion were rather limited in depth and scope. Also, the WDS often reports proper motions for one or both of the stars in a system without referencing the source of the measurement (See Harshaw 2017H). When reporting proper motions in this paper, I will indicate the source of the data by following the proper motion numbers with a letter — G for Gaia, U for UCAC5, or W for a proper motion listed in the WDS but for which the source is not known.

In Harshaw 2017H, I reported how the resultant of two proper motion vectors could be computed. I use that method in this paper to indicate when the proper motion vectors do not seem to agree with the observations of the pair.

For example, a pair with widely differing proper motions would be expected to exhibit a linear or nearly-linear track over time, and there are many examples of this in the WDS. However, there are also cases where pairs with widely differing proper motions show no apparent trend in the measurements at all — all of the data points tend to clump around a central point much like the random scattering of buckshot from a shotgun. When widely differing proper motion vectors are listed for a pair with a tight pattern of measurements like this, we may assume that one (or both) of the proper motion vectors is incorrect.

In correspondence with Norbert Zacharias, team leader for the UCAC5 catalog, I learned that Zacharias suggests that where data is available in both Gaia and UCAC5 that we use Gaia: "I recommend to use Gaia DR1 data, i.e. for those stars which are in the TGAS… keep in mind the UCAC data still has issues with poor charge transfer efficiency of the detector leading to magnitude (and field) dependent systematic errors at the about 2000 epoch. This could translate into about 1 to 2 mas/yr systematic errors for individual stars. But if the UCAC5 random errors on proper motions are small (order 1-2 mas/yr) while the TGAS proper motions are larger, you might want to take UCAC5 or a mean between TGAS and UCAC5… For stars not in TGAS, UCAC5 is a good option, although there are several other attempts to get proper motions with Gaia data and some other earlier data. See for example HSOY (update of PPMXL) or the GPS1 (derived from Pan-STARRS, SDSS and 2MASS). Then there is also the PMA (proper motion absolute) catalog based on 2MASS. They all have their pros and cons and are on about the same level of formal errors - nobody knows which is better in an absolute sense."

In many cases, Gaia has good proper motion data on only one of the stars in a double star system. Since the UCAC5 catalog has a much larger sampling of proper motions, it is common for a star without a proper motion value in Gaia to be listed in the UCAC5 data. When this was the case, I looked at the proper motion data in both catalogs for the star that was listed in both catalogs. If the UCAC5 proper motion vector was within 5 milli-arc seconds (mas) of the Gaia value, I assumed that the UCAC5 data for the second star would be on a par with Gaia (had Gaia listed it). However, if the difference in proper motions exceeded 5 mas, the UCAC5 data for the second star was not used.

3e. Using the Most Accurate Parallax Data Available.

Like the proper motion data, parallax data will be listed with attribution to its source. The format will be XX.XX ± 0.XX S, where the X's are the numbers of the parallax value (with ± 0.XX being the stated error estimate of the parallax) and S the source—H for Hipparcos, G for Gaia.

Most of the time, we only have parallax data on one of the stars in a double star system. In this report, only 34 of the 417 speckle measurements (8%) have parallax on both stars. For thESE CCD cases, the situation is slightly better — 22 out of 158 pairs (14%) have parallax on both stars.

Determining if two stars are close enough to be physical on the basis of parallax data alone is a bit tricky. Let's consider two of the stars in this report.

WDS 09371–1350 (BRT1909) has parallaxes for both stars shown in Gaia. For the primary, Gaia shows 1.76 ± 0.40 mas, while for the companion it shows 2.19 ± 0.93 mas. Thus the primary could have a parallax ranging from 1.36 up to 2.16 mas while the companion could range from 1.26 to 3.12 mas. So there is a considerable range of parallaxes for the stars that could be at the same distance from the earth. If we draw a diagram showing the parallaxes with their error estimates, we get a picture like Figure 2.

Whereas the two stars could clearly be at the same distance (as shown by the Region of Overlap), they

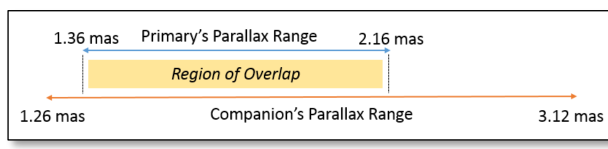

Figure 2: Parallax overlap of BRT1909

could also be at quite different distances. The Region of Overlap is 0.80 mas whereas the entire parallax range is 3.12 – 1.26 or 1.86 mas. So the range of overlap is equivalent to 0.80 / 1.86 or 43% of the total parallax space. Does this mean the stars have 43% chance of being at the same distance?

Unfortunately, no. The reason is that the probability of a star being at any given parallax value is not a linear function around the mean parallax value but rather a Gaussian distribution around the mean. The reported error estimate is one standard deviation. In a normal distribution, the first standard deviation from the mean contains 34.13% of the possible values, so there is a 68.26% chance that a star will be within its given parallax window. The actual math to compute a precise probability of two stars being at the same distance given their parallaxes is quite complicated. For our purposes, the percentage of overlap will serve as a reasonable indicator of a pair's likelihood of being at the same distance.

Let us consider a case where the stars clearly have no overlap in their parallaxes values. Let us look at WDS 10258+3237 (ES 432), a pair with given parallaxes of 4.00 ± 0.36 and 2.74 ± 0.49. Here is a diagram of

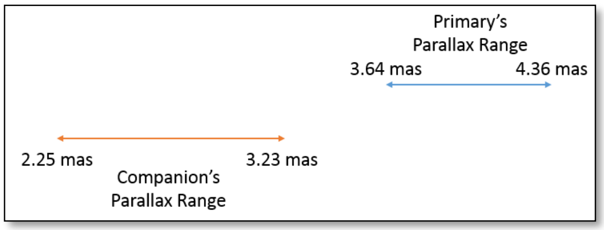

Figure 3: Parallax range of ES 432

the parallax data (Figure 3).

Clearly, there is no overlap between the parallax values of the stars in the system, so they are probably too far apart to be captured by their mutual gravitational forces.

In doing parallax calculations, if the error estimate of the parallax was 25% or more of the mean, the parallax was rejected as being unreliable.

Also, at the suggestion of William Hartkopf at the US Naval Observatory, I decided to use a weighted average of the parallax values for stars whose parallaxes could place them close enough in physical proximity to

$$PX_w = \frac{\left[(1 - PxA\ err\%) * PxA\right] + \left[(1 - PxB\ err\%) * PxB\right]}{\left[(1 - PxA\ err\%) + (1 - PxB\ err\%)\right]} \quad [1]$$

be physical. In such cases, the weighted parallax was computed as (Equation 1)

PX_w is the weighted parallax. *PxA err%* is the error in parallax for the primary star expressed as a percentage (Error / Parallax). Likewise for *PxB err%.*

Let's take an example. Consider the case of WDS 11272+1908 (KU 38), a pair for which Gaia lists parallax for both stars. For the primary, Gaia shows 6.18 ±

$$PX_w = \frac{\left[(1 - 0.38/6.18) * 6.18 + (1 - 0.42/6.23) * 6.23\right]}{\left[(1 - 0.38/6.18) + (1 - 0.42/6.23)\right]}$$
$$= 6.20$$

0.38 mas and for the companion, 6.23 ± 0.42 mas. The weighted parallax then works out to

Knowing the weighted parallax, it is a simple matter to divide 1 by the parallax in arc seconds (converting mas to arc seconds by multiplying the mas by 0.001). In this case, the distance would be 1 / 0.0062 = 161 parsecs.

3f. Estimating the minimum separation between the two stars.

When we have a parallax for each star, we can then compute the *minimum* separation between the two stars once we have the distance in parsecs. This is found by simply multiplying the distance (in parsecs) by the latest value for rho (in arc seconds). In the case of KU 38, the last value for rho in the WDS was listed as 5.90". Hence, the minimum separation between the two stars is 5.90 * 161 or 950 astronomical units (AU)–roughly 32 times the distance from the Sun to Neptune. This is a vast distance to be sure, but well within the realm of possibility for a binary star system.

This method will yield only the *minimum* separation in the two stars since we do not know the orientation of the stars relative to our line of sight. We are only seeing a projection of their distance on the sky's plane, and in all likelihood, one of the stars lies closer to earth than the other. As a result, we see one leg of a right triangle, while the stars are truly separated by the hypotenuse of that triangle.

A survey of the Sixth Orbit Catalog shows, that where we have the distance to a pair and can therefore compute the true separation of a binary system in AU, the true separations of stars (based on the semi-major axis of the orbit) run a range from 4.1 AU at the low end to 1,707 AU at the high end, with a mean of 281 AU. (These data are based on an analysis of 887 systems in the 6th Orbit Catalog.)

The data available to date suggests that true separations in binary stars will be, at most, in the low thousands of astronomical units. Of course, this is not to say that a true binary could not have a separation of 30,000 astronomical units or more, but only that our research so far makes such a wide pair highly unlikely. Obviously, the 6th Orbit Catalog represents a selection bias due to the fact that we only have good distance data and orbits on binary stars that are relatively close to us. Nonetheless, I would be highly suspicious of a given pair's odds of being a true binary if the separation between the two stars exceeds 3 or 4 thousand astronomical units.

4. Results

4a. The Results Tables.

The results of the winter and spring 2017 observing season at Brilliant Sky Observatory are presented in 11 tables as shown in Table 1. (The numbers indicate the number of pairs listed under each section.)

In Table 1, the number before the colon indicates the table number. CPM means common proper motion pairs (pairs where the proper motion vectors are both

Measurements of 161 Double Stars With a High-Speed CCD ...

Table 1: Results by Type of System

Type	CCD
CPM	3: 105
DPM	4: 21
LIN	5: 5
ORB	6: 4
SAB	n/a
UNK	7: 26

Table 2: Annual Differences in θ and ρ

Measurement Type	θ	ρ
Average Standard Error of the Means		
CCD	+0.015"	+0.000"
Average Raw Residuals		
CCD	+0.1°	+0.081"
Average Annual Change in q, r		
CCD	+0.01°	+0.011"

within 5 mas of each other, except where the proper motions are large, in which case the differences can be extended). DPM means the pair has different proper motions (more than 5 mas difference in both vector values). LIN means the pair is showing a linear pattern. ORB are pairs that have known orbits. SAB signifies short arc binaries, pairs that are showing an arc but for which there are not yet orbital solutions. And UNK stands for unknown—cases that do not fit any of the other categories.

4b. A Quick Check of Measurement Consistency.

A quick way to check consistency of one's measurements has traditionally been to compare the observer's measurement to the last measurement listed in the WDS (and obtained by a datarequest email to the USNO). The problem with this method is that if the last measurement was of uncertain value, the residual (difference between the observer's measurement and the last measurement on record) may be large, suggesting a poor measurement. Of course, the large residual may be due to a poor *prior* measurement. This will be seen in several cases in the tables that follow.

A more consistent method is to compute the average annual difference between the values of theta and rho from the last measurement on record to the observer's measurement, and then add all of the differences. The closer to zero each sum would be (theta and rho), the more consistent the measurements of the observer.

The reasoning is that for any large sample (and 578 pairs is probably a large enough sample), one would expect the changes in theta to be evenly divided between increasing theta (a + value for the difference) and decreasing theta (a – value); likewise for rho. In other words, there is a 50/50 chance that for any given pair, theta will increase over time or decrease, as will be the case for rho.

By computing the average *annual* change in theta and rho, one gets around those cases where the last measurement was made, say, 20 years ago and the residual seems very large. But if one computes the change in theta and rho per year over the 20 year window, the residuals become much smaller.

In computing annualized changes in theta and rho, I took the date of the observation minus the year of the last observation plus 0.5 (assuming an average measurement would be made mid-year), resulting in the number of years that have elapsed since the last measurement on file and the one I made. I then divided the raw residuals by this number of years to get the annual change.

I do this procedure for each night I observe and if the average annual change in theta exceeds 0.5° or rho exceeds 0.100", I assume there is a problem with the measurements that night (more than likely a calibration issue). If the cause of the error can be determined (for example, doing a drift calibration the next night without moving the camera from the night before), the correction will be applied to the measurements obtained and results reported. If the cause cannot be determined, or if even after finding the cause, the errors still lie outside the parameters I have set, I reject all the work for that night and try to get the measurements on a later night.

For all of the pairs in this report, the annual differences came to the values shown in Table 2. I also report in this table the average standard error of the mean and average raw residual.

Measurements of 161 Double Stars With a High-Speed CCD ...

4c. Format of the Tables.

The table column headings are as follows:

Date: date of the observation (Julian)

WDS No: the WDS number of the pair

Disc/Comp: discoverer and components

PM A: proper motion of the primary in mas per year. Source indicated by W for WDS, G for Gaia, or U for UCAC5

PM B: proper motion of the companion as for A

Last Yr: last year of measurement on file with the WDS

Last θ: the last value for θ reported

Last ρ: the last value for ρ reported

Msrs: Number of measures made on the night of observation

Measured θ ± err (°): the measured value of θ that night with the standard error of the mean, expressed in degrees

Measured ρ ± err ("): the measured value of ρ that night with the standard error of the mean, expressed in arc seconds

Resid θ: the difference between the observed value of θ and the last value on record

Resid ρ: the difference between the observed value of ρ and the last value on record

In the plot diagrams that accompany the notes, the historical data has been corrected for precession and the axis values are expressed in arc seconds.

Every pair that I measure has a plot of its measurements made from a WDS data request. Any measurement I make that lies far from the mean of the historical data is not reported, as there may be problems with calibration or even the measurement of the wrong star (surprisingly easy to do in a rich star field!).

In addition, some of the plots of the measurements presented in the "Notes" tables that follow each table of results contain a heavy orange line. This line is the PM vector that the stars should have followed if the displacement over its observed history is due only to a difference in proper motions. In some cases, the fit of the orange line to the data is so good as to virtually confirm the pair is linear. In other cases, the orange line is displayed on a small and dense packing of measurements, which would indicate a problem with one (or both) of the proper motion vectors.

(Text continues on page 274)

Table 3: Common Proper Motion Pairs Measured With the Cv Method

Date	WDS No	Disc/Comp	PM A	PM B	Last Yr	Last θ	Last ρ	Msrs	Measured θ ± err (°)	Measured ρ ± err (")	Resid θ	Resid ρ	Notes
2017.3288	09036-0225	HO 41AB	-024+002 G	-024+001 U	2011	71.8	3.90	5	71.7 ± 0.1	3.935 ± 0.001	-0.1	0.035	*
2017.3288	09042-1152	BRT3209	-020-012 U	-019-012 U	2000	173.7	4.07	5	174.8 ± 0.5	4.115 ± 0.039	1.1	0.045	
2017.3342	09319-1202	BRT2720	-009+009 U	-009+009 U	2010	64.1	3.70	2	63.7 ± 1.7	3.862 ± 0.001	-0.4	0.162	
2017.3342	09330-1411	BRT1908	-020-017 G	-022-015 W	2000	249.2	3.60	2	250.4 ± 0.6	3.632 ± 0.036	1.2	0.031	*
2017.3096	09357+5318	STF1366	-045-037 U	-046-038 U	2006	321.8	8.34	5	321.0 ± 0.0	8.262 ± 0.012	-0.8	-0.078	*
2017.3342	09371-1350	BRT1909	-000-006 G	+002-007 G	2010	252.1	3.65	2	252.2 ± 0.0	3.746 ± 0.031	0.1	0.096	*
2017.3342	09405-1509	J 1555	-015+001 G	-011+002 U	2010	292.8	8.18	4	292.8 ± 0.0	8.601 ± 0.002	0.0	0.421	*
2017.3397	09469-1121	BRT3211	-019-013 U	-019-012 U	2000	301.9	3.33	3	298.1 ± 0.6	3.378 ± 0.024	-3.8	0.048	*
2017.3342	09483-1448	BRT 575	-006+012 U	-006+012 U	2010	69.0	6.50	2	68.4 ± 1.4	6.539 ± 0.118	-0.6	0.039	
2017.3397	09497-1414	BRT2722	-021+005 G	-022+006 U	2005	97.0	5.40	3	93.2 ± 0.0	5.415 ± 0.005	-3.8	0.015	*
2017.3397	09549-1750	FEN 16	+025-033 U	+026-032 G	2010	155.3	4.51	3	154.8 ± 0.6	4.567 ± 0.039	-0.5	0.057	*
2017.3315	10025-0915	RST3674	-001+000 G	-004+001 U	2012	142.5	2.84	4	142.3 ± 0.1	2.866 ± 0.003	-0.2	0.026	*
2017.3315	10038+0125	BAL1435	-005-000 U	-005-001 U	2002	102.4	2.86	2	103.0 ± 0.4	2.879 ± 0.015	0.6	0.019	*
2017.3562	10057+8042	WFC 91	-009-017 G	-010-020 W	2011	272.0	8.40	4	271.1 ± 0.0	8.493 ± 0.009	-0.9	0.093	*
2017.3370	10066+2602	TDS 569	-008+003 G	-012+008 G	2001	90.4	2.28	4	89.3 ± 0.1	2.324 ± 0.002	-1.1	0.044	*
2017.3562	10090+6427	STF1407	-010-026 U	-007-022 U	2011	50.5	4.90	4	50.0 ± 0.2	4.935 ± 0.022	-0.5	0.035	
2017.3397	10135+3746	HJ 3322	-033+014 G	-034+015 U	2010	131.6	8.06	3	131.8 ± 0.3	8.059 ± 0.003	0.2	-0.001	*
2017.3397	10135+3928	STF1414	+001-001 G	+002-003 U	2012	94.2	3.94	4	93.9 ± 0.1	4.125 ± 0.003	-0.3	0.185	*
2017.3726	10216+4609	STF1425	+002-011 U	+006-009 U	2012	358.0	4.80	4	358.0 ± 0.1	4.828 ± 0.003	0.0	0.028	

Table 3 continues on next page.

Measurements of 161 Double Stars With a High-Speed CCD ...

Table 3 (continued). Common Proper Motion Pairs Measured With the Cv Method

Date	WDS No	Disc/Comp	PM A	PM B	Last Yr	Last θ	Last ρ	Msrs	Measured θ ± err (°)	Measured ρ ± err (")	Resid θ	Resid ρ	Notes
2017.3562	10232+6137	KR 36	+002-021 G	+003-022 G	2011	243.0	5.50	4	243.0 ± 0.0	5.637 ± 0.001	0.0	0.137	*
2017.3808	10233+4843	ES 917	+006-015 W	+006-015 W	2001	151.8	2.16	3	150.9 ± 0.1	2.046 ± 0.004	-0.9	-0.114	
2017.3370	10236+2617	A 1991	-081-010 W	-081-010 W	2012	189.2	1.47	4	188.8 ± 0.2	1.494 ± 0.004	-0.4	0.024	*
2017.3644	10245+3259	ES 2222	-020-000 G	-020-000 U	2010	290.0	8.20	3	290.7 ± 0.0	7.701 ± 0.002	0.7	-0.499	*
2017.3562	10248+6739	MLB 461	-019-001 G	-017-002 U	2007	249.3	6.58	3	252.5 ± 0.7	6.648 ± 0.030	3.2	0.068	*
2017.3644	10258+3237	ES 432	-033-004 G	-037-001 G	2002	163.3	2.92	3	162.9 ± 0.1	2.935 ± 0.012	-0.4	0.015	*
2017.3836	10283+4013	HJ 2531	+011-037 G	+009-040 U	2010	3.0	8.70	4	4.1 ± 0.0	8.647 ± 0.002	1.1	-0.053	*
2017.3342	10291+0342	BAL2841	-042-017 G	-042-017 U	2010	355.3	4.68	2	355.0 ± 0.2	4.663 ± 0.054	-0.3	-0.017	*
2017.3836	10308+4414	ES 1151	-009+000 G	-012+001 U	2002	298.1	2.58	4	299.5 ± 0.1	2.709 ± 0.005	1.4	0.129	*
2017.3260	10324+6800	HJ 3327	-119-059 G	-114-066 U	2010	100.3	3.22	5	99.1 ± 0.2	3.258 ± 0.017	-1.2	0.038	*
2017.3370	10335+1120	BU 1426	-042+032 G	-040+031 U	2002	201.6	2.60	4	200.3 ± 0.0	2.706 ± 0.002	-1.3	0.106	*
2017.3014	10341-1255	J 1567	-000-016 G	+001-017 U	2010	204.7	5.37	5	203.5 ± 0.1	5.432 ± 0.016	-1.2	0.062	*
2017.3014	10355-1756	HLD 107	-016+008 W	-016+008 W	2010	306.6	1.64	5	306.7 ± 0.3	1.589 ± 0.017	0.1	-0.051	*
2017.3014	10376-1921	HJ 4337	-020+006 G	-020+005 U	2010	73.0	9.45	5	71.4 ± 0.0	9.757 ± 0.006	-1.6	0.307	*
2017.3342	10389+0721	J 79	-040-031 G	-043-030 W	2005	133.2	1.56	2	131.7 ± 0.4	1.500 ± 0.000	-1.5	-0.060	*
2017.3644	10400+3505	ES 2164	-008-013 W	-008-013 W	2001	90.0	2.03	3	89.4 ± 0.4	1.895 ± 0.025	-0.6	-0.135	
2017.3342	10410+0336	J 1369	+128-132 W	+125-134 W	2010	121.0	7.40	2	120.5 ± 0.0	7.530 ± 0.055	-0.5	0.130	
2017.3644	10420+3005	TDS7425	+012-019 W	+012-019 W	1991	357.1	2.14	2	0.4 ± 0.7	1.921 ± 0.014	3.3	-0.219	*
2017.3370	10422+0054	BAL1440	-034-064 G	-036-063 U	2002	210.9	3.34	3	212.3 ± 0.1	3.324 ± 0.005	1.4	-0.016	*
2017.3644	10443+3739	ES 2634	+004-001 G	+005-001 U	2010	233.8	9.26	3	234.1 ± 0.0	9.522 ± 0.007	0.3	0.262	
2017.3288	10443-1731	RST3711	-073-020 G	-078-032 W	1999	96.6	2.29	5	97.9 ± 0.2	2.404 ± 0.003	1.3	0.114	*
2017.3288	10595-1430	A 1772	-045+002 G	-043+006 U	2011	212.7	3.68	5	212.8 ± 0.2	3.682 ± 0.025	0.1	0.002	*
2017.3370	11001-0657	A 134	+003-020 W	+003-020 W	2003	330.1	1.78	4	329.3 ± 0.4	1.867 ± 0.017	-0.8	0.087	
2017.3808	11004+5237	ES 722	-013+019 G	-013+017 U	2010	103.0	7.00	4	103.9 ± 0.0	8.386 ± 0.001	0.9	1.386	*
2017.3644	11068+2513	TDS7670	-014-043 G	-010-043 U	2002	359.2	2.32	3	359.1 ± 0.6	2.192 ± 0.087	-0.1	-0.128	*
2017.3370	11080+1012	J 81	-017-019 W	-017-019 W	2000	139.0	1.95	3	136.7 ± 0.3	1.944 ± 0.033	-2.3	-0.006	
2017.3836	11175+5900	ES 1786	-020-008 G	-020-008 U	2008	335.9	3.92	3	338.0 ± 0.0	4.144 ± 0.004	2.1	0.224	*
2017.4164	11183+6858	TDS 630	+030+022 W	+030+022 W	2005	242.0	2.14	3	239.2 ± 0.4	2.040 ± 0.028	-2.8	-0.100	*
2017.3808	11190+5118	WNC 3	+028+002 G	+030+005 U	2011	208.0	6.80	3	208.0 ± 0.0	6.713 ± 0.005	0.0	-0.087	*
2017.4164	11230+6443	AG 174 AB	-008-112 G	-013-110 W	2014	104.0	2.05	3	103.7 ± 0.1	2.112 ± 0.009	-0.3	0.062	*
2017.3644	11272+1908	KU 38	-041-017 G	-042-016 G	2010	54.0	5.90	4	53.8 ± 0.0	6.252 ± 0.005	-0.2	0.352	*
2017.3699	11323+3323	ES 2284	-020-028 U	-024-031 U	2001	77.5	3.03	3	76.2 ± 0.0	3.093 ± 0.003	-1.3	0.063	
2017.4164	11333+5748	KR 39AB	+027+006 G	+028+011 G	2011	151.0	10.10	4	151.9 ± 0.0	10.379 ± 0.014	0.9	0.279	*
2017.3726	11336+4445	LEO 34	+021-004 W	+021-004 W	2001	160.9	1.76	3	159.0 ± 0.1	1.669 ± 0.010	-1.9	1.669	*
2017.3726	11392+4910	STF1562	+016-037 G	+017-038 U	2010	270.0	16.20	3	269.7 ± 0.0	16.173 ± 0.005	-0.3	-0.027	*
2017.3699	11396+2657	STF1564	+001-004 G	+000-003 W	2010	87.0	5.20	4	86.6 ± 0.0	5.277 ± 0.002	-0.4	0.077	*

Table 3 continues on next page.

Measurements of 161 Double Stars With a High-Speed CCD ...

Table 3 (continued). Common Proper Motion Pairs Measured With the Cv Method

Date	WDS No	Disc/Comp	PM A	PM B	Last Yr	Last θ	Last ρ	Msrs	Measured θ ± err (°)	Measured ρ ± err (")	Resid θ	Resid ρ	Notes
2017.4164	11430+6421	STF1567	-011-003 G	+012+002 U	2014	85.0	3.45	4	84.3 ± 0.0	3.567 ± 0.003	-0.7	0.117	*
2017.3699	11461+3727	ES 1738	+003-018 W	+003-018 W	2001	163.2	1.91	3	163.6 ± 0.2	1.823 ± 0.010	0.4	-0.087	
2017.4027	11466+5710	STI2276	-035+009 G	-032+007 U	2010	9.0	11.40	3	9.7 ± 0.0	11.456 ± 0.002	0.7	0.056	*
2017.4027	11468+5951	KR 40	+024-020 G	+026-022 U	2003	274.0	3.30	4	274.5 ± 0.0	3.341 ± 0.002	0.5	0.041	*
2017.3699	11489+3342	KU 40	-006+000 G	-005-001 U	2002	184.2	2.89	4	184.5 ± 0.0	2.959 ± 0.005	0.3	0.069	*
2017.3699	11533+2019	STF1577	-023+004 G	-023+005 U	2011	10.0	8.40	3	9.6 ± 0.0	8.646 ± 0.004	-0.4	0.246	*
2017.4027	11543+5033	ES 724	-033-006 G	-032-003 G	2002	227.8	2.75	3	230.8 ± 0.1	2.720 ± 0.003	3.0	-0.030	*
2017.3644	11556+1654	KU 41	+011-021 G	+003-019 G	2011	68.0	5.10	4	67.7 ± 0.0	5.141 ± 0.008	-0.3	0.041	*
2017.3370	12029-1908	B 2536	-019+002 G	-018+001 G	2002	289.0	2.47	3	288.2 ± 0.5	2.576 ± 0.019	-0.8	0.106	*
2017.3644	12061+3850	STF1601	-028-063 G	-	2007	300.0	2.10	4	297.6 ± 0.1	2.010 ± .0.013	-2.4	-0.090	*
2017.3589	12126+3546	STF1613	+009+008 W	+009+008 W	2015	11.0	1.10	5	7.3 ± 0.2	1.168 ± 0.003	-3.7	0.068	*
2017.4055	12151+8349	WFC 124	-014-006 U	-014-008 G	2004	132.3	4.63	3	132.0 ± 0.0	4.663 ± 0.015	-0.3	0.033	*
2017.3808	12164+4444	A 1781	-032+002 G	-026+001 U	2007	301.8	2.84	3	303.0 ± 0.3	2.857 ± 0.015	1.2	0.017	*
2017.3808	12239+4441	ES 1155	+028+016 G	+027+012 U	2003	200.8	3.52	4	200.8 ± 0.5	3.594 ± 0.062	0.0	0.074	*
2017.3808	12242+4304	STF1638	+003+000 G	+004+002 U	2010	282.0	8.20	3	282.0 ± 0.0	8.293 ± 0.015	0.0	0.093	*
2017.4055	12285+8841	STF1717	-020-013 G	-019-012 G	2011	328.0	8.30	4	322.5 ± 0.1	8.316 ± 0.021	-5.5	0.016	*
2017.4055	12291+8525	LDS1752	-143+074 W	-154+046 W	1991	205.1	3.30	3	200.2 ± 0.6	3.156 ± 0.013	-4.9	-0.144	*
2017.3644	12295+2931	BU 1324AB	-001-007 G	+001-005 G	2014	224.0	2.20	4	223.7 ± 0.3	2.367 ± 0.011	-0.3	0.167	*
2017.3808	12334+3202	STF1653	-006-002 G	-004-003 U	2013	342.0	8.00	4	342.9 ± 0.0	8.027 ± 0.002	0.9	0.027	*
2017.3589	12360+1124	STF1661	-301-074 G	-302-073 W	2013	253.0	2.20	5	253.2 ± 0.0	2.322 ± 0.000	0.2	0.122	*
2017.3589	12388+1252	AG 343	-056+027 G	-057+026 U	2010	325.0	8.50	3	325.2 ± 0.0	8.501 ± 0.001	0.2	0.001	*
2017.3836	12439+4950	BEM 1	-003+006 G	-010+010 W	2010	202.0	9.40	3	203.9 ± 0.0	9.602 ± 0.015	1.9	0.202	*
2017.3808	12480+3420	AG 182	-007+010 W	-007+010 W	1996	189.8	2.34	4	190.4 ± 0.0	2.363 ± 0.001	0.6	0.023	
2017.3644	12587+2707	STF1700	-001+009 G	+006+007 U	2011	84.0	7.40	4	83.9 ± 0.0	7.439 ± 0.002	-0.1	0.039	*
2017.3808	13080+4907	HJ 2642	-031+045 G	-032+045 U	2010	177.0	9.00	3	177.5 ± 0.0	9.183 ± 0.006	0.5	0.183	*
2017.3644	13112+3050	STF1729AB-C	-38-013 U	-041-013 G	2011	276.0	8.70	2	275.5 ± 0.0	8.702 ± 0.009	-0.5	0.002	*
2017.4027	13174+5812	MLB 69	+006-014 G	+009-016 U	2004	40.2	4.02	3	39.6 ± 0.1	4.045 ± 0.004	-0.6	0.025	*
2017.3644	13208+3158	ES 308	-028+025 G	-031+029 G	2008	113.6	7.25	3	113.5 ± 0.0	7.360 ± 0.005	-0.1	0.110	*
2017.4027	13298+5905	ES 1790	+013-004 U	+012-004 U	2003	250.5	4.95	3	251.6 ± 0.0	4.996 ± 0.006	1.1	0.046	
2017.3562	13378+2819	HJ 3341AB	-140+035 G	-141+041 W	2000	190.8	2.30	3	189.6 ± 0.2	2.392 ± 0.003	-1.2	0.092	*
2017.3644	13490+3056	BRT 250	-028+043 U	-027+043 U	2010	136.0	5.50	3	137.4 ± 0.1	5.514 ± 0.001	1.4	0.014	
2017.3644	13525+2544	A 568	-004+011 G	-004+013 U	2003	320.7	2.55	3	321.3 ± 0.1	2.606 ± 0.002	0.6	0.056	*
2017.4466	14156+2255	ROE 74	+003+002 U	+004+002 U	2011	286.8	7.09	2	287.0 ± 0.0	7.118 ± 0.014	0.2	0.028	
2017.4493	14170+2412	STF1828	-004-006 G	-005-004 W	2013	159.2	2.09	4	159.2 ± 0.1	2.084 ± 0.001	0.0	-0.006	*
2017.4493	14197+2330	STF3083	+004+016 G	+001+014 U	2010	231.7	4.65	4	232.5 ± 0.0	4.794 ± 0.007	0.8	0.144	*
2017.4438	14207+1210	HO 541	-005+013 U	-003+011 U	2002	89.8	2.60	2	88.9 ± 0.2	2.622 ± 0.006	-0.9	0.022	
2017.4438	14217+1003	HEI 779	-019-014 U	-017-013 U	2002	102.8	2.77	2	103.5 ± 0.1	2.779 ± 0.011	0.7	0.009	

Table 3 continues on next page.

Measurements of 161 Double Stars With a High-Speed CCD ...

Table 3 (conclusion). Common Proper Motion Pairs Measured With the Cv Method

Date	WDS No	Disc/Comp	PM A	PM B	Last Yr	Last θ	Last ρ	Msrs	Measured θ ± err (°)	Measured ρ ± err (")	Resid θ	Resid ρ	Notes
2017.4438	14227+0039	J 439	-024-010 U	-025-010 U	2002	239.2	3.93	2	237.4 ± 0.2	3.917 ± 0.017	-1.8	-0.013	*
2017.4438	14229+0943	A 1103	-032+006 G	-032+005 U	2011	203.9	4.65	3	204.2 ± 0.0	4.726 ± 0.004	0.3	0.076	*
2017.4438	14244+1813	COU 62	-050-004 G	-050-005 G	2001	200.7	2.39	2	200.4 ± 0.1	2.397 ± 0.032	-0.3	0.007	*
2017.4438	14266+0208	HJ 1254	-137+091 W	-137+091 W	2011	62.8	6.02	3	63.1 ± 0.1	6.229 ± 0.002	0.3	0.209	
2017.4438	14317+0150	AG 195	-009+005 G	-008+002 W	2010	337.7	1.74	4	336.9 ± 0.2	1.866 ± 0.003	-0.8	0.126	*
2017.4493	14326+3522	ALI 130	-010+005 G	-011+005 U	2002	182.2	8.13	3	182.6 ± 0.0	8.17 ± 0.010	0.4	0.040	*
2017.4493	14353+2004	BRT2418	-000-066 G	+001-066 G	2001	195.2	3.70	3	194.8 ± 0.1	3.816 ± 0.001	-0.4	0.116	*
2017.4466	14430+1310	KU 48 AB	-004+066 W	-006+065 W	2010	136.7	6.45	4	137.6 ± 0.0	6.685 ± 0.003	0.9	0.235	
2017.4493	14533+3426	ES 311	+015-037 G	+017-039 U	2010	290.5	4.00	3	290.8 ± 0.0	4.021 ± 0.004	0.3	0.021	*
2017.4438	14544+0017	J 440	+009-009 G	+010-009 G	2000	220.7	2.55	2	219.9 ± 0.2	2.618 ± 0.004	-0.8	0.068	*
2017.4493	16065+5441	MLB 135	-003+003 G	-001+004 G	2011	96.1	3.52	3	96.1 ± 0.0	3.603 ± 0.000	0.0	0.083	*
2017.4493	16081+5605	STI2331	+004-061 U	+004-060 U	2010	18.0	5.40	2	18.9 ± 0.1	6.460 ± 0.52	0.9	1.060	
2017.4493	16140+5844	STI2334	+002-015 G	-004-014 U	2006	111.4	8.98	2	112.4 ±0.0	9.051 ± 0.004	1.0	0.071	*
2017.4493	16160+5718	STI2335	+020-052 U	+020-053 U	2010	149.0	9.80	2	151 ± 0.1	9.456 ± 0.026	2.0	-0.344	

Notes for Table 3

WDS Number	Parallax	Parallax Source	Distance (Parsecs)	Min Sep (AU)	Plot Figure	Comments
09036-0225 AB	3.44 ± 0.25	G	291	1,134	-	
09330-1411	4.48 ± 0.63	G	223	804	-	
09357+5318	10.47 ± 1.66	H	96	797	-	
09371-1350	A: 1.76 ± 0.40 B: 2.19 ± 0.93	G G	515	1,878	-	Weighted parallax of 1.94 mas used. There is a 58% overlap in the parallax windows. Likely physical pair.
09405-1509	2.07 ± 0.54	G	N/A	N/A	-	The error makes the parallax unusable.
09469-1121	-	-	-	-	-	Only 6 measurements. A third star of estimated magnitude 13 noted at 204.5°, 1.852".
09497-1414	2.40 ± 0.44	G	417	2,250	-	The high theta residual is due to the WSI2005 measure which appears to be well away from the mean.
09549-1750	B: 6.56 ± 0.64	G	152	169	-	
10025-0915	2.54 ± 0.62	G	394	1,102	-	
10038+0125	-	-	-	-	-	Only four measurements.
10057+8042	2.77 ± 0.30	G	361	3,043	-	
10066+2602	A: 2.46 ± 0.46 B: 2.13 ± 0.73	G G	432	995	-	Only 4 measurements. A weighted parallax (2.13 mas) was used; 40% overlap in the parallax windows. Probably physical.
10135+3746	6.30 ± 0.64	G	159	1,286	-	
10135+3928	2.46 ± 0.53	G	407	1,602	-	A weak trend is forming.
10232+6137	A: 2.51 ± 0.25 B: 2.48 ± 0.27	G G	401	2,188	-	Weighted parallax of 2.49 mas, with an 87% overlap in the parallax windows. Likely physical pair.
10236+2617	-	-	-	-	-	A weak trend is forming.

Measurements of 161 Double Stars With a High-Speed CCD ...

Notes for Table 3 continued

WDS Number	Parallax	Parallax Source	Distance (Parsecs)	Min Sep (AU)	Plot Figure	Comments
10245+3259	2.36 ± 0.58	G	424	3,475	-	
10248+6739	2.27 ± 0.44	G	250	2,907	-	
10258+3237	A: 4.00 ± 0.36 B: 2.74 ± 0.49	G G	250 365	730 1,066	-	There is no overlap in the parallax windows. The pair is probably not physical.
10283+4013	5.76 ± 0.25	G	174	1,502	-	
10291+0342	3.49 ± 0.37	G	287	1,129	-	The mean was used for the last measure. UPR2010.421 (the last measure on record) lies far from the mean; my measure is closer to the mean. A weak trend may be developing.
10308+4414	3.25 ± 0.36	G	308	800	-	
10324+6800	7.45 ± 0.26	G	134	432	-	
10335+1120	6.50 ± 0.40	G	154	400	-	There appear to be quadrant reversals on OL1932.23 and HEI1983.74. A quadrant flip may be the case for BLW1981.361.
10341-1255	2.45 ± 0.49	G	408	2.163	-	A very scattered group of 9 measurements.
10355-1756	-	-	-	-	-	Only 7 measurements. Manual solution with STB.
10422+0054	5.23 ± 0.55	G	191	631	-	Only 5 measurements.
10376-1921	4.39 ± 0.34	G	228	2,210	-	
10389+0721	7.82 ± 0.31	G	128	205	-	
	-	-	-	-	-	Only 2 measurements.
10443-1731	10.73 ± 0.46	G	93	213	-	A short (possibly linear) trend is forming.
10595-1430	6.52 ± 0.46	G	153	567	-	
11004+5237	3.68 ± 0.27	G	272	2,283	-	
11068+2513	2.82 ± 0.40	G	355	823	-	Only 5 measurements.
11175+5900	2.87 ± 0.24	G	348	1,366	-	
11183+6858	-	-	-	-	-	Only 2 measurements.
11190+5118	3.91 ± 0.25	G	256	1,731	-	
11230+6443 AB	7.01 ± 0.27	G	143	292	-	
11272+1908	A: 6.18 ± 0.38 B: 6.23 ± 0.42	G G	161	957	-	Weighted parallax (6.20 mas) used. There is a 91% overlap in the parallax windows. Likely physical pair.
11333+5748 AB	A: 9.55 ± 0.26 B: 9.91 ± 0.28	G G	103	1,033	-	Weighted parallax (9.73 mas) used. There is a 20% overlap in the parallax windows.
11336+4445					-	There appears to be a quadrant reversal for WOR1964.931.
11392+4910	11.72 ± 0.33	G	85	1,368	-	
11396+2657	1.22 ± 0.34	G	N/A	N/A	-	The error make the parallax unusable.
11430+6421	A: 3.91 ± 0.41 B: 3.89 ± 0.28	G H	256	885	-	Weighted parallax (3.90 mas) used. There is a 67% overlap in the parallax windows. Likely physical pair.
11466+5710	4.01 ± 0.97	G	249	2,840	-	
11468+5951	2.79 ± 0.24	G	358	1,184	-	
11489+3342	2.64 ± 0.26	G	379	1,095	-	

Measurements of 161 Double Stars With a High-Speed CCD ...

Notes for Table 3 continued

WDS Number	Parallax	Parallax Source	Distance (Parsecs)	Min Sep (AU)	Plot Figure	Comments
11533+2019	4.34 ± 0.31	G	230	1,933	-	
11543+5033	A: 3.67 ± 0.34 B: 3.39 ± 0.52	G G	283	778	-	Weighted parallax of 3.53 mas used. There is a 45% overlap in the parallax windows. Likely physical pair.
11556+1654	A: 9.27 ± 0.51 B: 8.53 ± 0.74	G G	112	577	-	Weighted parallax of 8.91 mas used. There is a 24% overlap in the parallax windows. With a significant difference in the proper motions, this pair might not be physical.
12029-1908	A: 2.22 ± 0.47 B: 3.01 ± 0.54	G G	381	953	1	Weighted parallax of 2.62 mas used. There is a 46% overlap in the parallax windows. Likely physical pair. Trend forming. Could be linear or edge-on short arc.
12126+3546	-	-	-	-	-	Rough trend starting to emerge.
12151+8349	B: 3.90 ± 0.30	G	256	278	-	Only 6 measurements.
12164+4444	4.97 ± 0.26	G	201	571	-	
12239+4441	3.94 ± 0.31	G	254	888	-	
12242+4304	2.94 ± 0.29	G	340	2,786	-	
12285+8841	A: 4.55 ± 0.25 B: 4.29 ± 0.23	G G	226	187	-	Weighted parallax of 4.42 mas was used. There is a 32% overlap in the parallax windows; possible physical pair.
12291+8525	-	-	-	-	-	Only 5 measurements.
12295+2931 AB	A: 5.19 ± 0.29 B: 5.28 ± 0.41	G G	191	470	-	Weighted parallax of 5.23 mas was used. There is a 76% overlap in the parallax windows; likely physical pair.
12334+3202	4.45 ± 0.36	G	225	1,775	-	
12360+1124	12.56 ± 0.26	G	80	185	-	
12388+1252	3.83 ± 0.34	G	261	2,219	-	
12439+4950	2.69 ± 0.27	G	372	3,564	-	
12587+2707	1.68 ± 0.28	G	595	4,399	-	
13080+4907	4.14 ± 0.24	G	242	2,207	-	
13112+3050 AB-C	B: 6.91 ± 0.26	G	145	150	-	
13174+5812	5.51 ± 0.39	G	181	726	-	
13208+3158	A: 2.43 ± 0.26 B: 1.43 ± 0.31	G G	412 699	-	-	There is no overlap in the parallax windows. Based on parallax, the pair is optical. But the proper motions are very similar, so we cannot yet rule on this pair.
13378+2819	6.79 ± 0.27	G	147	339	-	
13525+2544	3.31 ± 0.43	G	302	772	2	Strong linear trend.
14170+2412	0.97 ± 0.87	G	N/A	N/A	-	The error makes the parallax unusable.
14197+2330	9.00 ± 0.25	G	111	517	-	
14227+0039	-	-	-	-	3	Strong linear trend.
14229+0943	3.88 ± 0.30	G	258	1,198	-	
14244+1813	A: 5.2 ± 0.25 B: 5.47 ± 0.27	G G	187	450	-	Weighted parallax of 5.33 mas used. The parallax windows have a 32% overlap. May be physical.
14317+0150	1.71 ± 0.35	G	585	1,016	-	
14326+3522	2.54 ± 0.31	G	394	3,189	-	
14353+2004	A: 3.75 ± 0.27 B: 3.67 ± 0.29	G G	270	997	-	Weighted parallax of 3.71 mas used. There is a 42% overlap in the parallax windows. May be physical.
14533+3426	3.50 ± 0.29	G	286	1,143	-	
14544+0017	A: 1.45 ± 0.41 B: 1.41 ± 0.30	G G	N/A 709	N/A 1,809	-	The error on the primary's parallax makes it unusable, but be that as it may, the weighted parallax (which I would not suggest we use) is 1.43 mas. The parallax windows, under this assumption, have a 75% overlap. Probably physical.
16065+5441	A: 1.89 ± 0.28 B: 1.90 ± 0.38	G G	528	1,858	-	Weighted parallax of 1.89 mas used; the parallax windows have a 73% overlap. This pair is probably physical.
16140+5844	1.59 ± 0.26	G	629	5,660	-	
Mean AB Separation in AU				1,427		

Measurements of 161 Double Stars With a High-Speed CCD ...

Table 4: Different Proper Motion Pairs Measured With the Cv Method

Date	WDS No	Disc/Comp	PM A	PM B	Last Yr	Last q	Last r	Msrs	Measured θ ± err (°)	Measured ρ ± err (")	Resid θ	Resid ρ	Notes ?
2017.3288	09154-1955	I 826	-018+005 U	-009+010 U	1999	18.9	3.02	5	19.2 ± 0.1	3.065 ± 0.005	0.3	0.045	
2017.3315	09202-1346	TDS6485	-012+011 U	-015+003 U	2010	203.3	2.52	2	200.2 ± 1.6	2.553 ± 0.027	-3.1	0.033	*
2017.3315	09213-1207	TDS6501	-016-027 W	-021-006 W	2005	358.5	2.89	2	356.0 ± 0.2	3.143 ± 0.006	-2.5	0.253	*
2017.3315	10078+0715	HEI 755	-047-025 G	-028-014 W	2002	57.6	2.24	2	56.7 ± 0.5	2.293 ± 0.008	-0.9	0.053	*
2017.3562	10285+4733	HU 635	-028+007 G	-027+009 U	2010	174.0	4.00	4	173.5 ± 0.1	4.131 ± 0.008	-0.5	0.131	*
2017.3836	10369+4504	ES 1152	+034-038 W	+020+010 W	2012	349.0	2.83	3	349.3 ± 0.1	2.866 ± 0.005	0.3	0.036	*
2017.3288	10464-1259	BRT2725	+013-020 G	+015-014 U	2001	5.3	3.81	5	4.8 ± 0.3	4.090 ± 0.220	-0.5	0.280	*
2017.3370	10498+1805	A 2371	-022-004 G	-046+010 W	2012	321.0	2.50	4	320.2 ± 0.1	2.658 ± 0.002	-0.8	0.158	*
2017.3260	10538+7947	STF1471	+015+113 U	+004-077 U	2013	183.0	2.07	5	185.8 ± 0.5	2.167 ± 0.035	2.8	0.097	*
2017.3644	11128+2158	ELS 2	-003+008 W	+035+006 W	2002	88.1	3.65	3	89.2 ± 0.2	3.721 ± 0.021	1.1	0.071	*
2017.3288	11344+0407	J 86	-049-010 W	-014-008 W	2006	95.6	2.62	5	90.9 ± 0.3	2.407 ± 0.009	-4.7	-0.213	*
2017.3288	11348+0130	AG 175	+010-028 G	+012-018 W	2013	191.7	2.22	5	191.3 ± 0.2	2.261 ± 0.009	-0.4	0.041	*
2017.4164	11366+5608	STF1553	-179-091 G	-145-052 U	2010	166.0	6.20	4	165.1 ± 0.0	6.194 ± 0.009	-0.9	-0.006	*
2017.3288	11527+0701	HEI 506	-025-025 G	+000-017 W	2010	75.5	2.26	3	75.1 ± 0.1	2.334 ± 0.001	-0.4	0.074	*
2017.3836	12014+5600	STI2278	-005-003 G	-014-002 U	2006	297.8	4.84	2	298.5 ± 0.1	4.936 ± 0.001	0.7	0.096	*
2017.4027	12040+6429	STI 739	-001+010 G	-015+016 G	2010	245.0	9.80	3	246.0 ± 0.0	9.986 ± 0.002	1.0	0.186	*
2017.4027	12232+5621	MLB 67	-019-005 G	-001+000 U	2003	137.1	8.33	3	136.4 ± 0.1	8.496 ± 0.012	-0.7	0.166	*
2017.4027	12272+5519	MLB1076	-002-008 G	+007-021 U	2004	225.4	10.94	3	225.2 ± 0.0	11.057 ± 0.009	-0.2	0.117	*
2017.4055	12307+7518	DOO 55	+015-003 G	+017-003 W	2004	54.6	4.44	4	56.0 ± 0.0	4.476 ± 0.001	1.4	0.036	*
2017.4493	14317+3554	ALI 366	-026+020 G	-010+025 W	2008	285.5	6.70	3	284.8 ± 0.0	6.906 ± 0.006	-0.7	0.206	*
2017.4493	15018+5128	ES 739	-038+008 U	-022+037 G	2001	159.1	2.15	3	159.9 ± 0.0	2.121 ± 0.001	0.8	-0.029	*

Measurements of 161 Double Stars With a High-Speed CCD ...

Notes for Table 4

WDS Number	Parallax	Parallax Source	Distance (Parsecs)	Min Sep (AU)	Plot Figure	Comments
09202-1346	-	-	-	-	-	Only 4 measurements.
09213-1207	-	-	-	-	-	Only 4 measurements.
10078+0715	5.08 ± 0.78	G	197	441	-	Only 5 measurements.
10285+4733	5.21 ± 0.41	G	192	852	-	
10369+4504	-	-	-	-	4	The PM vector (344°, 8.4") does not align well to the recorded motion.
10464-1259	5.14 ± 0.99	G	195	739	-	
10498+1805	3.09 ± 0.53	G	324	845	5	The PM vector (300°, 2.8") does not fit the observations. Theta looks about right, but rho is far off.
10538+7947	-	-	-	-	6	The PM vector (183°, 34.3") is clearly incorrect. The historical data forms a very tight cluster. High residuals due to WSI2013, which appears to be off.
11128+2158	-	-	-	-	7	The PM vector (267°/3.9") does not match the observations.
11344+0407	-	-	-	-	8	The PM vector (87°, 3.4") does not fit the observations. This historical data only spans approximately 1".
11348+0130	4.87 ± 0.43	G	205	456	-	
11366+5608	21.18 ± 0.22	G	47	291	9	The PM vector does not comport with the history.
11527+0701	4.62 ± 0.50	G	216	498	-	
12014+5600	1.04 ± 0.24	G	962	4,615	-	
12040+6429	A: 1.04 ± 0.26 B: 3.86 ± 0.76	G G	769 216	-	10	The error in the primary's parallax makes that measurement unusable. There is no overlap of the proper motion windows either. The PM vector (317°, 2.28") comes close to matching the observations.
12232+5621	2.24 ± 0.43	G	446	3,705	11	The PM vector (74°, 1.7") comes close to the observations.
12272+5519	0.72 ± 0.31	G	N/A	N/A	-	The error in the proper motion makes it unusable.
12307+7518	2.97 ± 0.24	G	337	1,495	-	
14317+3554	3.24 ± 0.33	G	309	2,068	12	The PM vector is far larger than the measured motion. (73°, 1.26").
15018+5128	B: 3.33 ± 0.29	G	300	645	13	The PM vector (4.39" @ 200°) does not match the observations.
Mean AB Separation in AU				1,585		

Table 5: Linear Pairs Measured With the Cv Method

Date	WDS No	Disc/Comp	PM A	PM B	Last Yr	Last θ	Last ρ	Msrs	Measured θ ± err (°)	Measured ρ ± err (")	Resid θ	Resid ρ	Notes?
2017.3288	10409-1306	HDO 128	-027-024 G	-	2003	25.6	2.49	5	31.7 ± 0.1	3.028 ± 0.003	6.1	0.538	*
2017.3644	10441+3230	HJ 2543 AB	-057-029 G	-043-003 W	2001	32.3	2.03	4	32.9 ± 0.1	3.363 ± 0.012	0.6	1.333	*
2017.3315	10517-0340	HDS1551	-157+088 G	-020+006 W	2012	322.5	2.80	2	331.5 ± 0.1	1.969 ± 0.003	9.0	-0.831	*
2017.3397	10592+2423	BRT 157	-008-020 G	-006-015 U	2002	293.4	3.41	3	294.0 ± 0.1	3.424 ± 0.000	0.6	0.014	*
2017.4164	11589+6002	STI 736	+012-009 G	-014-004 U	2007	315.3	9.79	3	314.6 ± 0.0	9.691 ± 0.009	-0.7	-0.099	*

Notes for Table 5

WDS Number	Parallax	Parallax Source	Distance (Parsecs)	Min Sep (AU)	Plot Figure	Comments
10409-1306	5.64 ± 0.43	G	177	441	-	Linear solution by HRT 2011. Ephemerides: 32.8°, 3.064". Residuals: -1.1°, -0.036".
10441+3230 AB	11.03 ± 0.29	G	91	312	14	No linear solution yet. The PM vector (28°, 5.3") does not fit the observations very well.
10517-0340	11.33 ± 0.35	G	88	247	15	Very strong unsolved linear case. The PM vector (239°, 3.4") is a close fit to history, but not exact.
10592+2423	4.34 ± 0.35	G	230	783	16	This strongly linear case has no solution yet.
11589+6002	0.55 ± 0.24	G	N/A	N/A	17	The error makes the parallax unusable. Strong linear case without a solution yet.
Mean AB Separation in AU				446		

Table 6: Known Orbits Measured With the Cv Method

Date	WDS No	Disc/Comp	PM A	PM B	Last Yr	Last θ	Last ρ	Msrs	Measured θ ± err (°)	Measured ρ ± err (")	Resid θ	Resid ρ	Notes?
2017.3260	10110+7508	KUI 47	+219+264 G	+228+252 W	2012	121.0	1.84	5	121.1 ± 0.7	1.955 ± 0.039	0.1	0.115	*
2017.3589	12108+3953	STF1606	-092-025 W	-	2015	151.0	0.60	5	144.8 ± 0.4	0.627 ± 0.015	-6.2	0.027	*
2017.3370	12160+0538	STF1621	-320-066 W	-320-066 W	2010	42.7	1.52	4	46.4 ± 0.1	1.815 ± 0.004	3.7	0.295	*
2017.3589	12291+3123	STT 251	+148-041 W	+148-041 W	2015	61.0	0.70	5	60.7 ± 0.3	0.781 ± 0.001	-0.3	0.081	*

Notes for Table 6

WDS Number	Parallax	Parallax Source	Distance (Parsecs)	Min Sep (AU)	Plot Figure	Comments
10110+7508	47.5 ± 0.27	G	21	39	-	Orbit by HEI1994. Ephemerides: 124.7°, 1.850". Residuals: -3.6°, +0.105".
12108+3953	-	-	-	-	-	Orbit by MSN1999. Ephemerides: 146.4°, 0.545". Residuals: -1.6°, +0.082".
12160+0538	38.72 ± 3.68	H	26	39	-	Orbit by SOD1999. Ephemerides: 44.6°, 0.645". Residuals: +1.8°, +0.17".
12291+3123	5.76 ± 1.46	H	N/A	N/A	-	The error makes the parallax unusable. Orbit by SCA2003. Ephemerides: 61.2°, 0.676". Residuals: -0.5°, +0.105".
Mean AB Separation in AU				39		

Measurements of 161 Double Stars With a High-Speed CCD ...

Table 7: Unknown Cases Measured With the Cv Method

Note: These cases are called "unknown" because no proper motions are known, or only one proper motion is known.

Date	WDS No	Disc/Comp	PM A	PM B	Last Yr	Last q	Last r	Msrs	Measured q ± err (°)	Measured r ± err (")	Resid q	Resid r	Notes?
2017.3342	09383-1956	RST2645	-001-006 G	-	2008	274.4	2.13	1	271.8	2.106	-2.6	-0.024	*
2017.3342	09410-1250	RST3656	-015+013 G	-	2008	302.4	2.12	2	306.3 ± 0.5	2.206 ± 0.001	3.9	0.086	*
2017.3726	10129+4835	HU 632	-006+007 G	-	2001	66.6	3.12	4	64.6 ± 0.1	3.061 ± 0.001	-2.0	-0.059	*
2017.3370	10159+2746	COU 958	+089+062 G	-	2005	80.6	2.30	3	81.3 ± 0.2	2.345 ± 0.014	0.7	0.045	*
2017.3370	10173+1210	J 1126	+011-020 W	-	2001	307.5	2.26	4	307.0 ± 0.1	2.277 ± 0.005	-0.5	0.017	
2017.3644	10207+3719	ES 1639	-025-011 G	-	2010	132.0	2.27	3	133.3 ± 0.4	2.225 ± 0.010	1.3	-0.045	*
2017.3808	10241+4034	ES 1394	+015-077 W	-	2010	142.6	6.80	4	143.5 ± 0.0	6.697 ± 0.006	0.9	-0.103	
2017.3342	10300+0543	HEI 762	-001-002 G	-	2002	146.8	2.74	2	145.0 ± 1.2	2.623 ± 0.026	-1.8	-0.117	*
2017.3014	10380-1257	DOO 52AB	+007-024 W	-	2001	331.4	2.27	5	330.3 ± 0.1	2.394 ± 0.004	-1.1	0.124	*
2017.3370	11085-0721	TDS7694	-055+010 W	-	2002	43.5	2.73	3	67.7 ± 0.1	2.715 ± 0.008	24.2	-0.015	*
2017.3726	11303+4115	ES 1399	-031-046 W	-	2008	123.9	3.14	3	122.5 ± 0.2	3.151 ± 0.007	-1.4	0.011	*
2017.3699	11391+3225	ES 2412	-001-014 G	-	2002	321.7	2.39	3	319.6 ± 0.1	2.406 ± 0.006	-2.1	0.016	*
2017.3726	11431+4808	TDS 642	-045-028 G	-	1991	185.1	2.33	2	191 ± 0.0	2.27 ± 0.003	5.9	-0.060	*
2017.3288	11534+0340	STF1578	-050-029 W	-	2014	161.4	3.13	2	160.5 ± 0.3	3.148 ± 0.009	-0.9	0.018	
2017.3726	11556+4815	ES 923	+021-024 G	-	2003	215.9	2.38	3	218.1 ± 0.2	2.359 ± 0.008	2.2	-0.021	*
2017.3644	12061+3850	STF1601	-028-063 G	-	2007	300.0	2.10	4	297.6 ± 0.1	2.010 ± .0.013	-2.4	-0.090	*
2017.3808	12076+4813	COU1907	-036+028 G	-	2001	357.8	2.96	3	357.5 ± 0.1	2.899 ± 0.008	-0.3	-0.061	*
2017.3370	12158+0902	STF1620	-003-008 G	-	2000	81.1	2.19	5	81.5 ± 0.2	2.309 ± 0.007	0.4	0.119	*
2017.3370	12256-0818	RST3789	-043-001 W	-	2002	10.1	2.74	3	9.3 ± 0.4	2.726 ± 0.025	-0.8	-0.014	*
2017.3836	12412+4359	A 1850	-070+037 G	-	1999	49.0	2.86	4	50.3 ± 0.0	2.894 ± 0.005	1.3	0.034	*
2017.3808	12473+3357	AG 181	-002-010 W	-	2013	340.0	1.90	3	340.8 ± 0.0	2.258 ± 0.003	0.8	0.358	*
2017.3616	12483+1530	HEI 160	+050-031 G	-	2005	346.0	2.39	3	344.1 ± 0.0	2.425 ± 0.000	-1.9	0.035	*
2017.3808	14004+3658	STF1796	-018-004 G	-	2007	193.0	2.60	4	192.2 ± 0.1	2.609 ± 0.001	-0.8	0.009	*
2017.4493	14166+2328	BU 1441	+030+019 G	-	2002	78.5	3.56	4	79.5± 0.2	3.597 ± 0.002	1.0	0.370	*
2017.4438	14170-1626	HJ 1249AB	-017-004 W	-	1999	165.0	5.40	3	163.1 ± 0.2	5.212 ± 0.027	-1.9	-0.188	
2017.4493	14198+3016	TDS9165	+005-018 G	-	2002	172.9	3.03	3	174.1 ± 0.1	3.129 ± 0.000	1.2	0.099	*

Measurements of 161 Double Stars With a High-Speed CCD ...

Notes for Table 7

WDS Number	Parallax	Parallax Source	Distance (Parsecs)	Min Sep (AU)	Plot Figure	Comments
09383-1956	2.58 ± 0.40	G	388	826	-	
09410-1250	4.01 ± 0.61	G	249	529	-	
10129+4835	4.12 ± 0.35	G	243	752	-	Only 6 measurements.
10159+2746	11.83 ± 0.71	G	85	194	-	Just 7 measurements.
10207+3719	0.38 ± 0.99	G	N/A	N/A	-	The error makes the parallax unusable. A trend might be emerging.
10300+0543	2.12 ± 0.51	G	472	1,274	-	Only 3 measurements.
10380-1257	-	-	-	-	-	A linear trend is emerging.
11085-0721	-	-	-	-	-	Only 3 measurements. No other star near this position.
11303+4115	-	-	-	-	-	Only 6 measurements, but a linear trend is emerging.
11391+3225	2.43 ± 0.35	G	412	988	-	Only 5 measurements.
11431+4808	3.16 ± 0.28	G	316	736	-	Only 2 measurements.
11556+4815	2.55 ± 0.25	G	392	941	-	5 measurements.
12061+3850	13.11 ± 0.26	G	76	157	-	
12076+4813	8.67 ± 0.27	G	115	341	-	4 measurements.
12158+0902	3.50 ± 0.34	G	286	625	-	
12256-0818	-	-	-	-	-	Only 4 measurements.
12412+4359	4.95 ± 0.24	G	202	578	-	
12473+3357	-	-	-	-	-	Starting to show a linear trend.
12483+1530	5.19 ± 0.53	G	193	462	18	Strong linear trend.
14004+3658	3.90 ± 0.30	G	256	655	-	
14166+2328	4.33 ± 0.34	G	231	831	-	
14198+3016	2.68 ± 0.46	G	373	1,131	-	Only 4 measurements.
Mean AB Separation in AU				659		

Measurements of 161 Double Stars With a High-Speed CCD ...

(Continued from page 262)

5. Discussion

5.1. The Impact of GAIA and UCAC5 data.

The new data from GAIA (DR1) has been of huge benefit in the analysis of double star systems. PM analysis can bolster a pair's odds of being physical, or dispel it (if the parallaxes are greatly different).

In addition, the latest high-quality PM data from GAIA and the UCAC5 catalog can support a pair's claim to physicality (if the PMs are nearly the same) or suggest a linear or optical nature (if the PMs are greatly different).

The Winter/Spring 2017 observing program at Brilliant Sky Observatory revealed the following possibilities flowing from GAIA and UCAC5 data. (Table 8)

Table 8: Outcomes From GAIA/UCAC5

Physicality suggested by parallax	
Type	WDS Number
CPM	09371-1350
	10066+2602
	10232+6137
	11272+1908
	11333+5748 AB
	11430+6421
	11543+5033
	12029-1908
	12285+8841
	12295+2931 AB
	14244+1813
	14353+2004
	14544+0017 ?
	16065+5441
UNK	03401+3407 ?
Parallax suggests pair is not physical	
CPM	10258+3237
	11566+1654 ?
	13208+3158 ?
DPM	12040+6429
Proper motion does NOT account for observations (one or both PM values are incorrect)	
DPM	10369+4504
	10498+1805
	10538+7947
	11128+2158
	11344+0407
LIN	10441+3230 AB
Proper motion accounts for the observations	
DPM	12232+5621
Linear cases for which no solution is yet available	
LIN	10441+3230 AB
	10517-0340
	10592+2423
	11589+6002

6. Conclusion

We have already established in the pages of this Journal that small telescopes can do speckle interferometry of close pairs with a high degree of precision.

The results of the 2017 Winter and Spring observing program at Brilliant Sky Observatory show great promise for the addition of the new GAIA DR1 and UCAC5 parallax and proper motion data to our research as we continue to work on the WDS to determine which of its 140,000+ pairs are true binaries and which are optical or non-binary but physical pairs. I can only assume that when GAIA DR2 is released in April of 2018, our pursuit of true binaries will literally explode. We are in for some exciting times!

7. Acknowledgements

This paper has made extensive use of the Washington Double Star Catalog and the Sixth Orbit Catalog, both maintained by the U. S. Naval Observatory in Washington, D.C. The author is also indebted to Norbert Zacharias and William Hartkopf (both of the U. S. Naval Observatory) for their help and suggestions in private email communications.

8. References

Harshaw, Richard, 2015A, "Measurements of 2 Wide CPM Pairs with a CCD", *Journal of Double Star Observations,* **11**(4), 424-428.

Harshaw, Richard, 2016B, "CCD Measurements of 66 Rectilinear Pairs and Probable Rectilinear Pairs: The Autumn 2015 Observing Program at Brilliant Sky Observatory, Part 1", *JDSO*, **12**(4), 376-387.

Harshaw, Richard, 2016C, "CCD Measurements of 8 Double Stars with Binary Nature: The Autumn 2015 Observing Program at Brilliant Sky Observatory", *JDSO*, **12**(4), 388-393.

Harshaw, Richard, 2016D, "CCD Measurements of 141 Proper Motion Stars: the Autumn 2015 Observing Program at Brilliant Sky Observatory", *JDSO*, **12** (4), 393-399.

Harshaw, Richard, 2017E, "Quasi-Speckle Measurements of Close Double Stars With a CCD Camera", *JDSO*, **13**(1), 13-16.

Harshaw, Richard, 2017F, "The Winter 2015 Observing Program at Brilliant Sky Observatory: Report on the Measurement of 112 Pairs", *JDSO*, **13**(1), 17-24.

Harshaw, Richard, 2017G, "The Spring 2016 Observing Program of Brilliant Sky Observatory: Measurements of 313 Pairs", *JDSO*, **13**(1), 104-121.

Harshaw, Richard, 2017H, "When Things Don't Look Right: What Appear to be Proper Motion Discrepancies in the WDS", *JDSO*, **13**(4), 570-579.

Appendix. Plots of the Measurments Detailed in the Notes to the Tables.

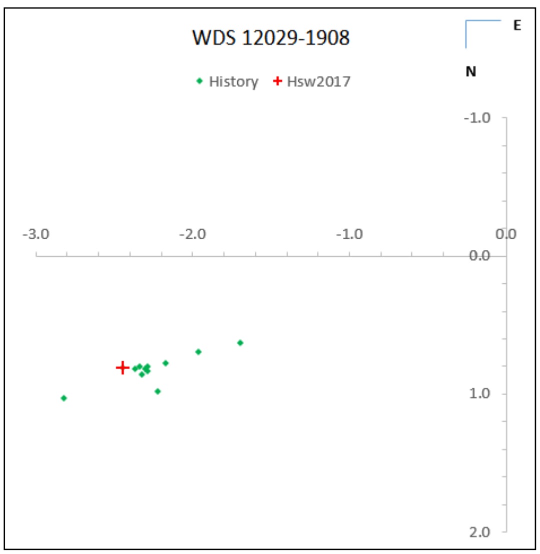

Figure 1. Plot of WDS 12029-1908

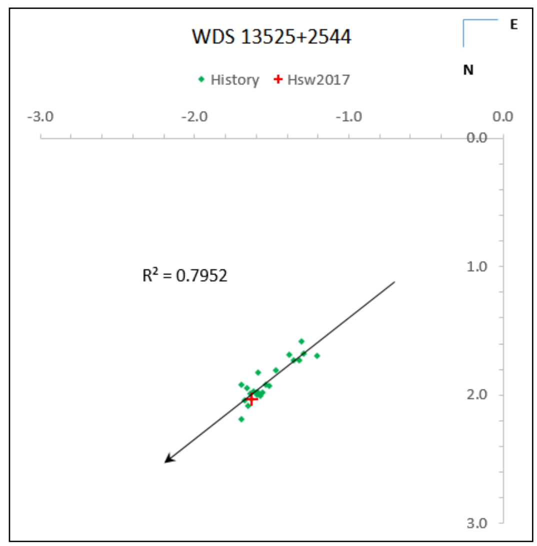

Figure 2. Plot of WDS 13525+2544

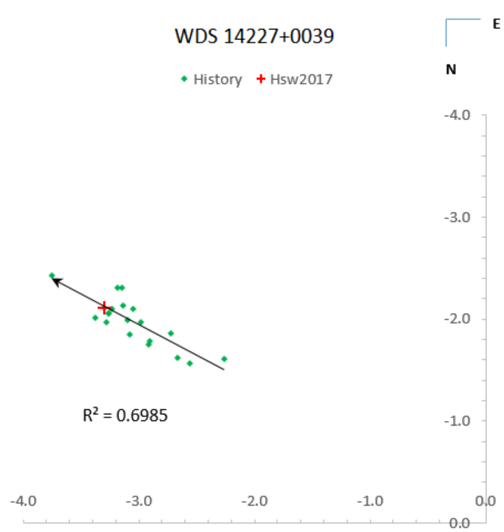

Figure 3. Plot of WDS 14227+0039.

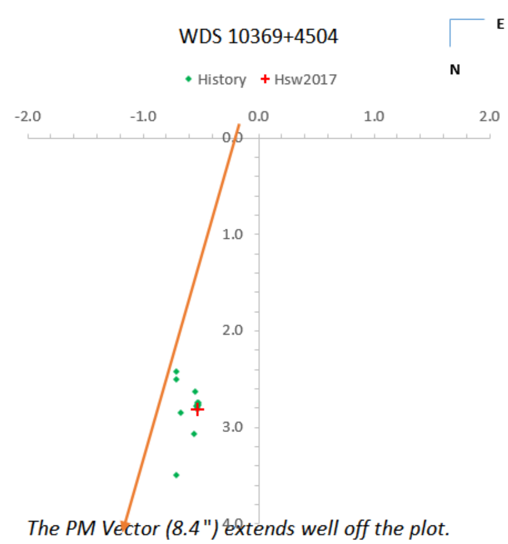

Figure 4. Plot of WDS 10369+4504

Measurements of 161 Double Stars With a High-Speed CCD ...

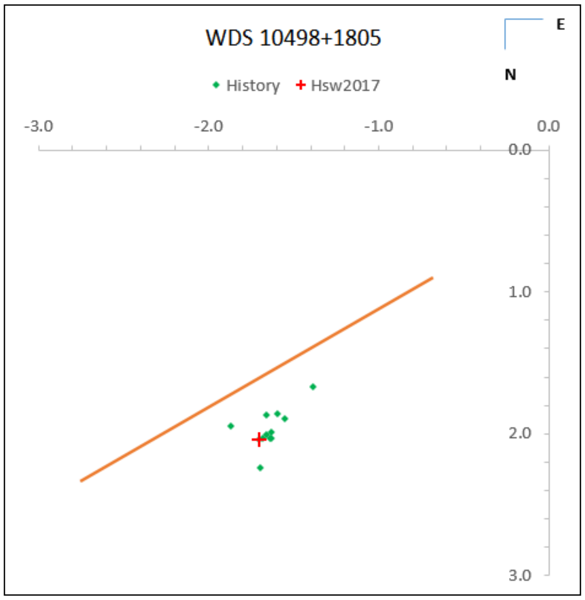

Figure 5. Plot of WDS 10498+1805.

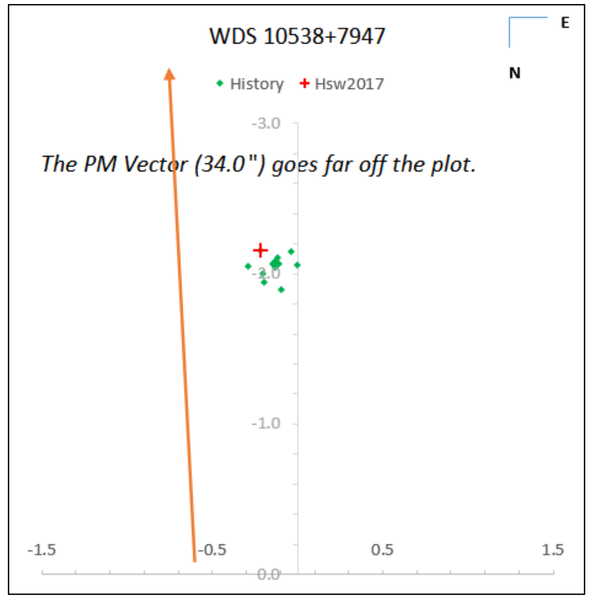

Figure 6. Plot of WDS 10538+7947.

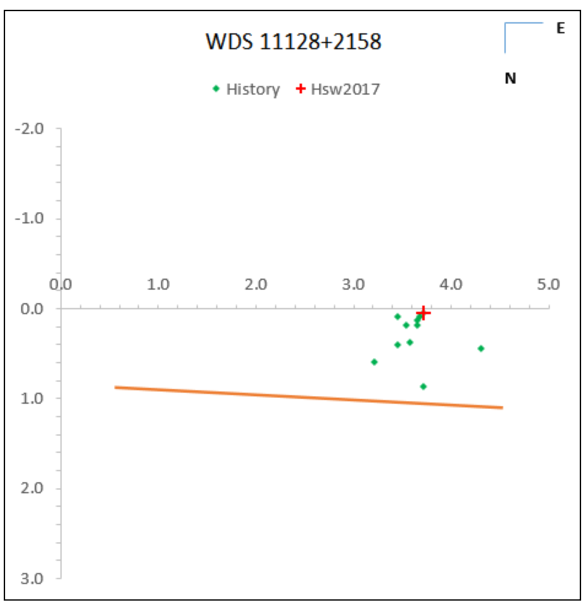

Figure 7. Plot of WDS 11128+2158.

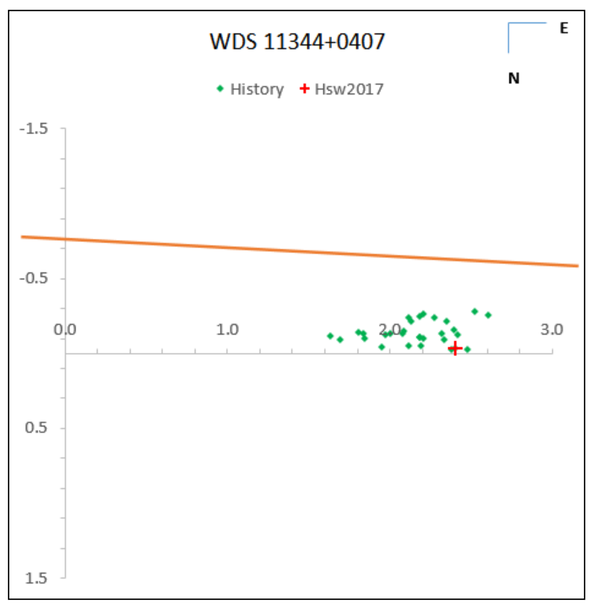

Figure 8. Plot of WDS 11344+0407 .

Measurements of 161 Double Stars With a High-Speed CCD ...

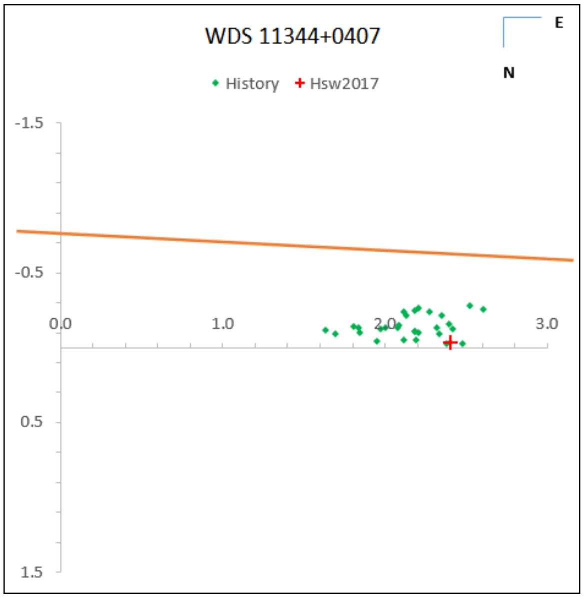

Figure 9. Plot of WDS 11344+0407.

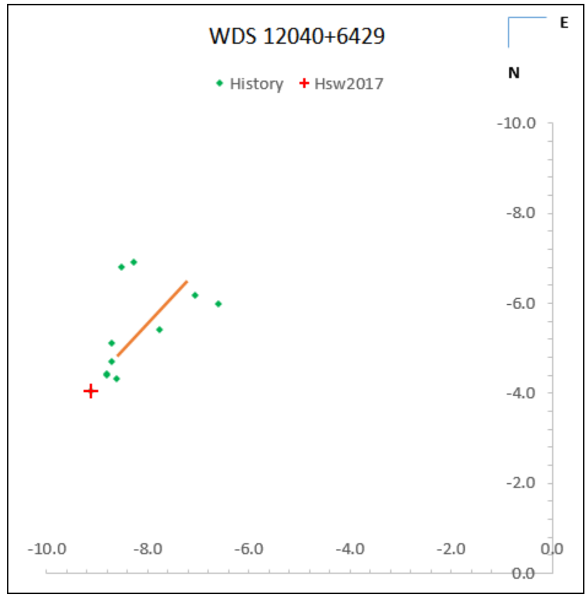

Figure 10. Plot of WDS 12040+6429.

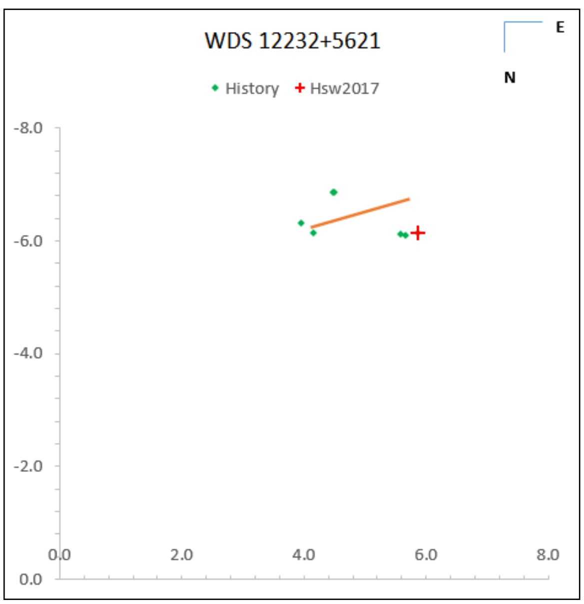

Figure 11. Plot of WDS 12232+5621.

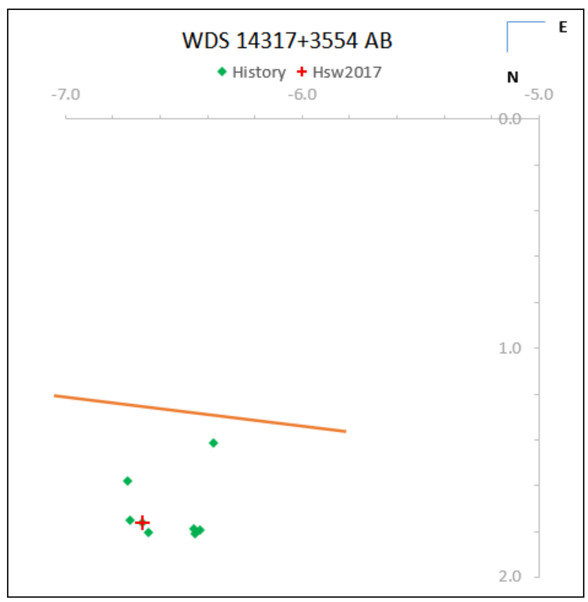

Figure 12. Plot of WDS 14317+3554 AB.

Measurements of 161 Double Stars With a High-Speed CCD ...

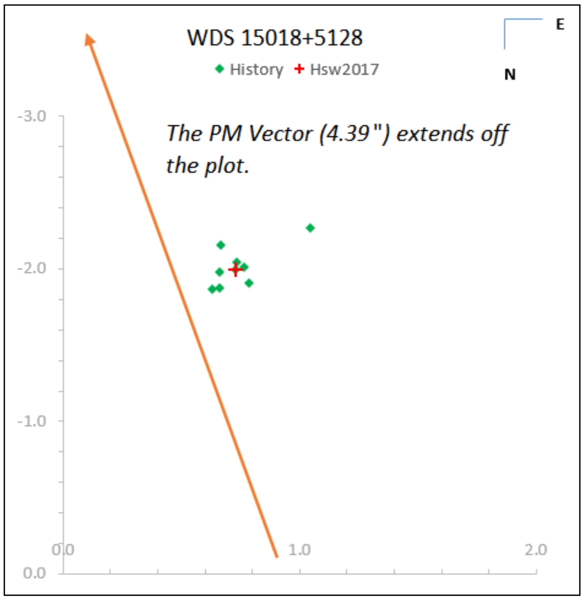

Figure 13. Plot of WDS 15018+5128.

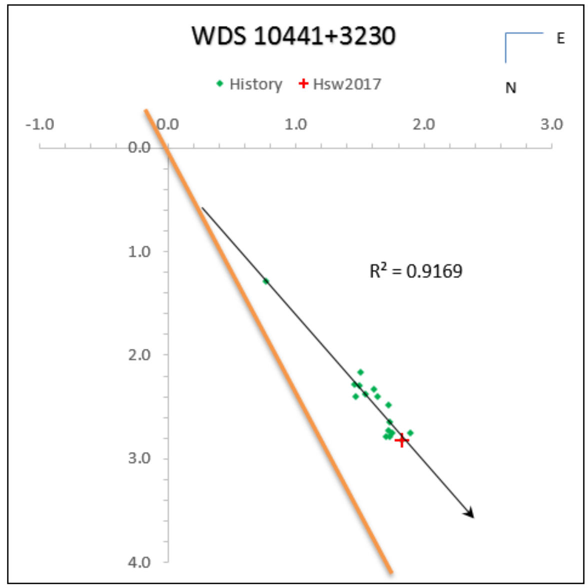

Figure 14. Plot of WDS 10441+3230.

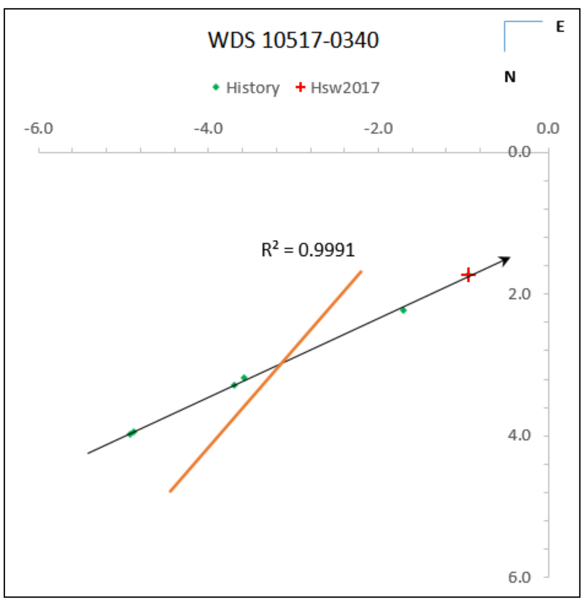

Figure 15. Plot of WDS 10517-0340.

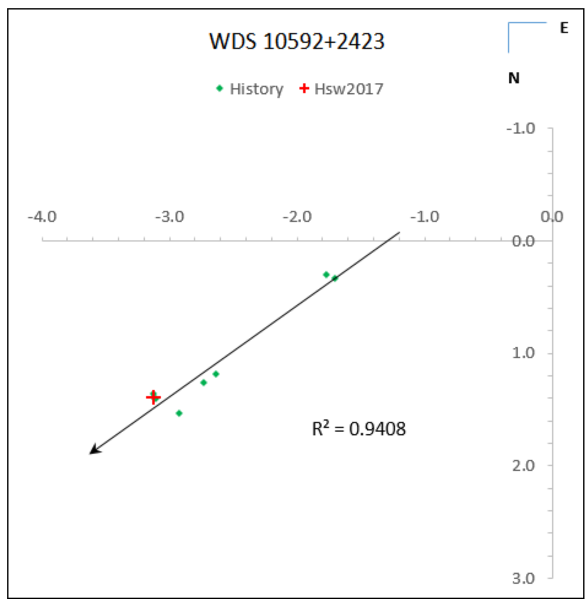

Figure 16. Plot of WDS 10592+2423.

Measurements of 161 Double Stars With a High-Speed CCD ...

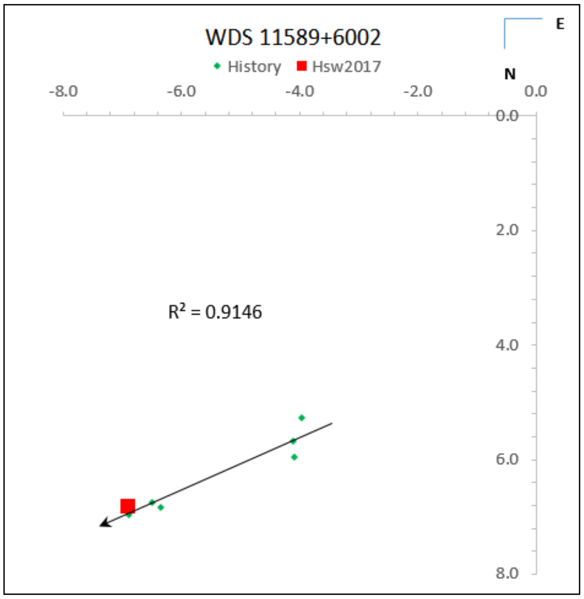

Figure 17. Plot of WDS 11589+6002.

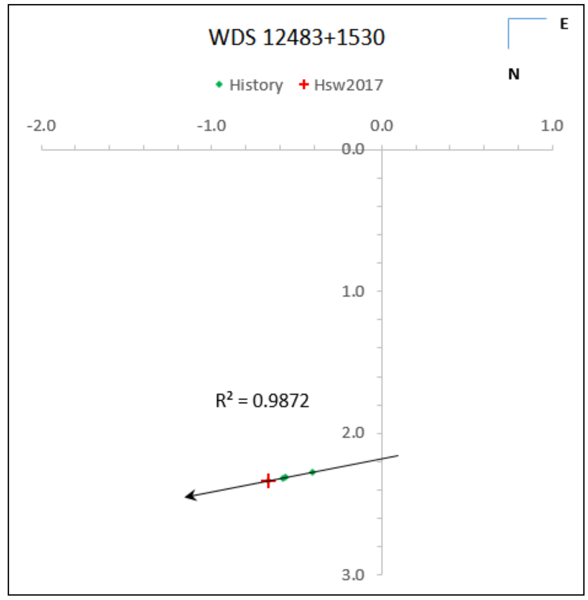

Figure 18. Plot of WDS 12483+1530.

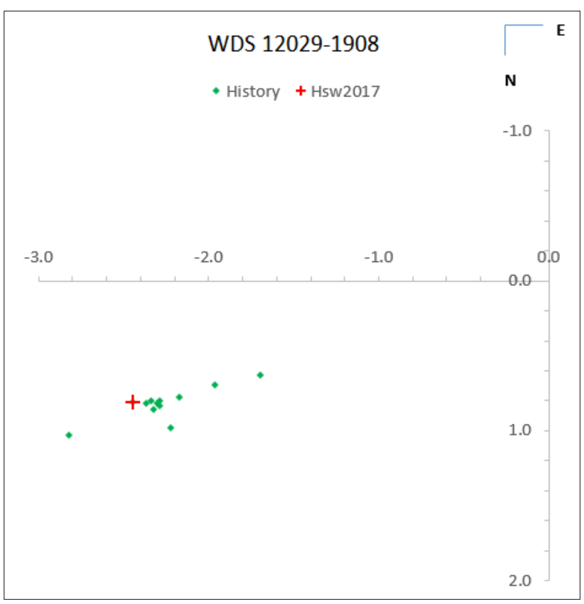

Figure 19. Plot of WDS 12029-1908.

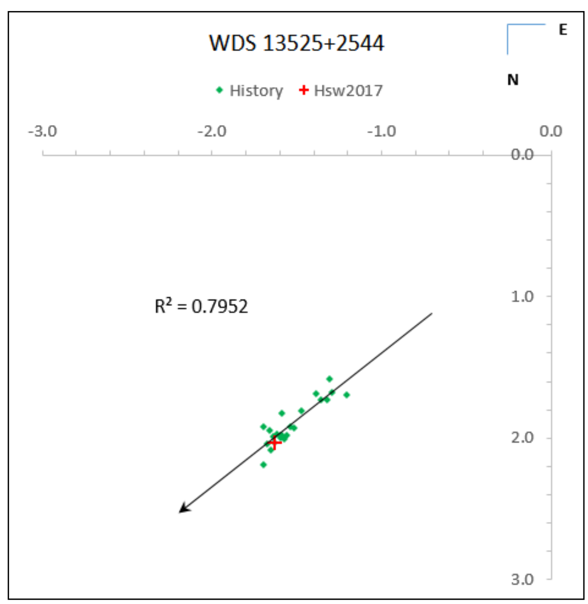

Figure 20. Plot of WDS 13525+2544.

Measurements of 161 Double Stars With a High-Speed CCD ...

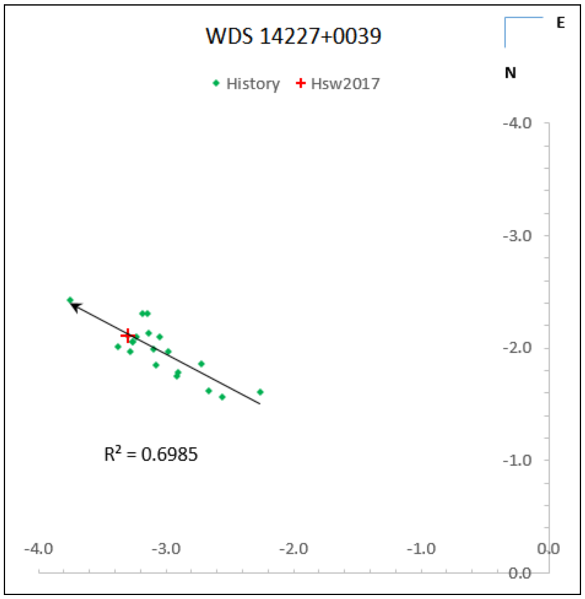

Figure 21. Plot of WDS 14227+0039.

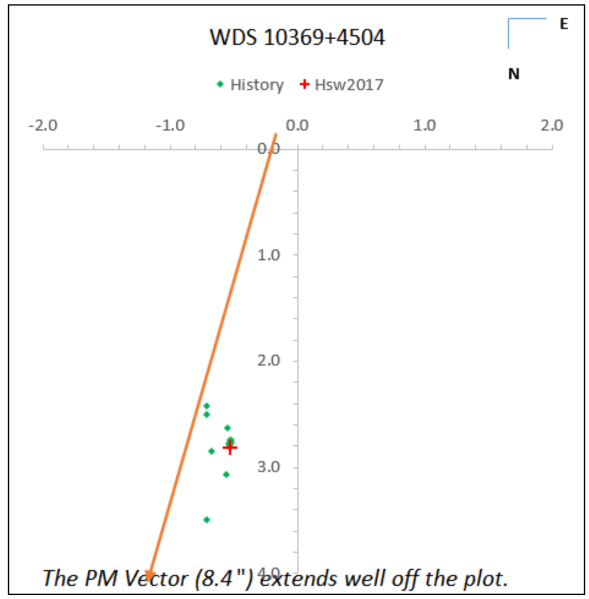

Figure 22. Plot of WDS 10369+4504.

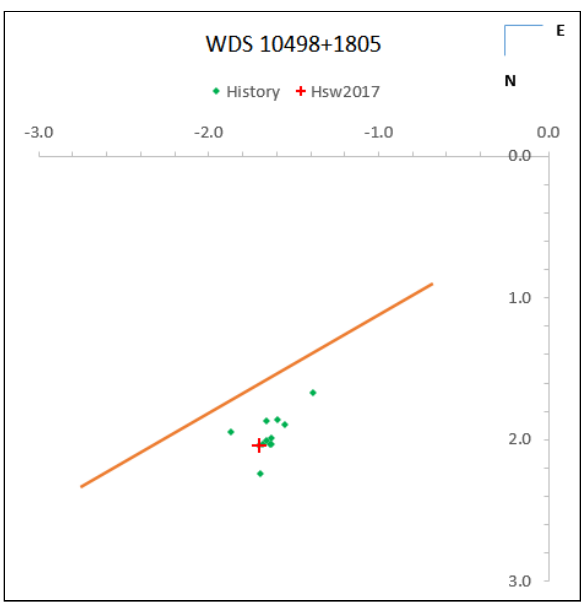

Figure 23. Plot of WDS 10498+1805.

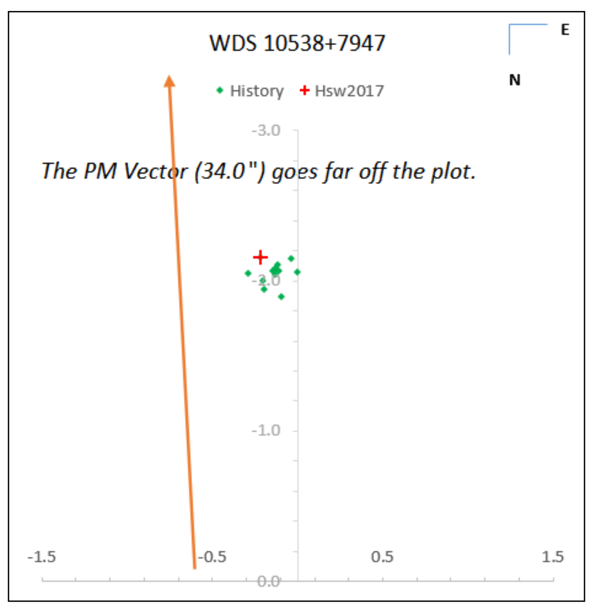

Figure 24. Plot of WDS 10538+7947.

Measurements of 161 Double Stars With a High-Speed CCD ...

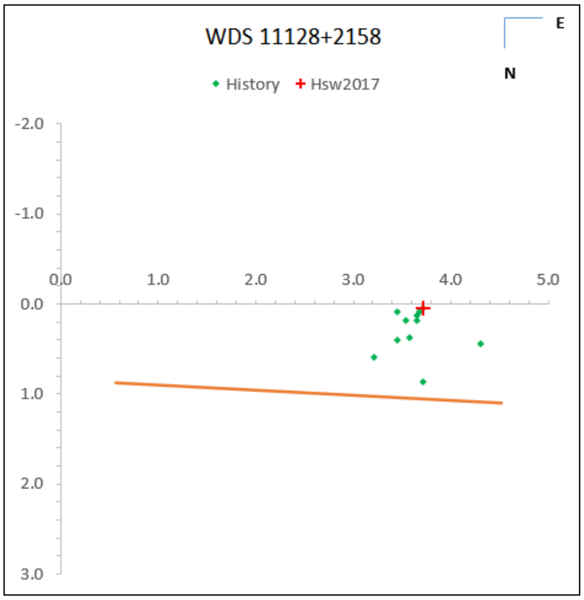

Figure 25. Plot of WDS 11128+2158.

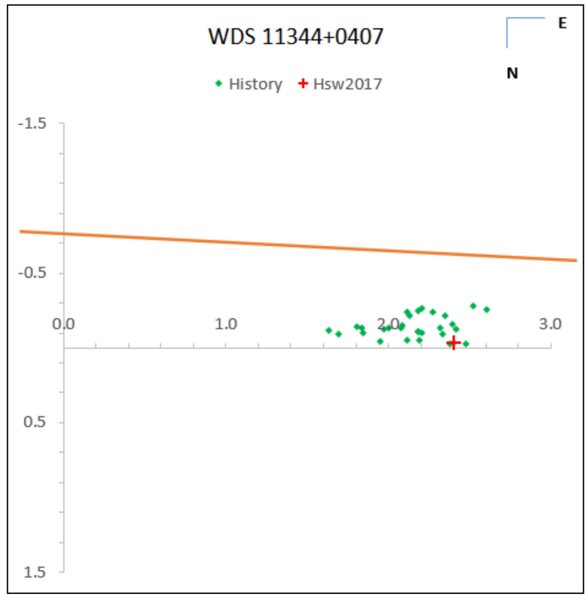

Figure 26. Plot of WDS 11344+0407.

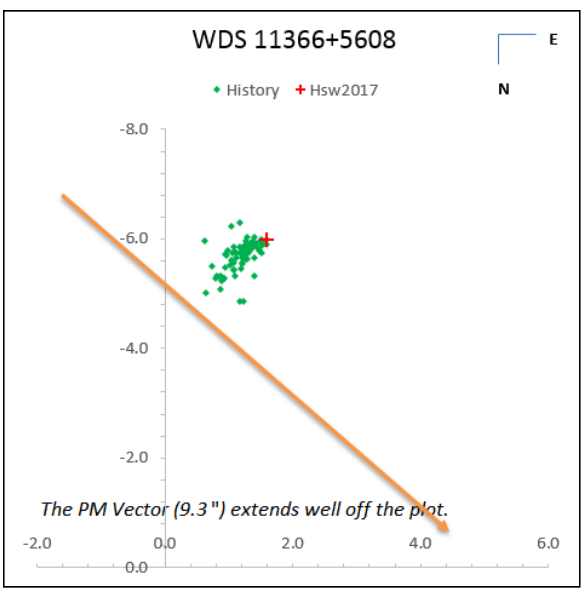

Figure 27. Plot of WDS 11366+5608.

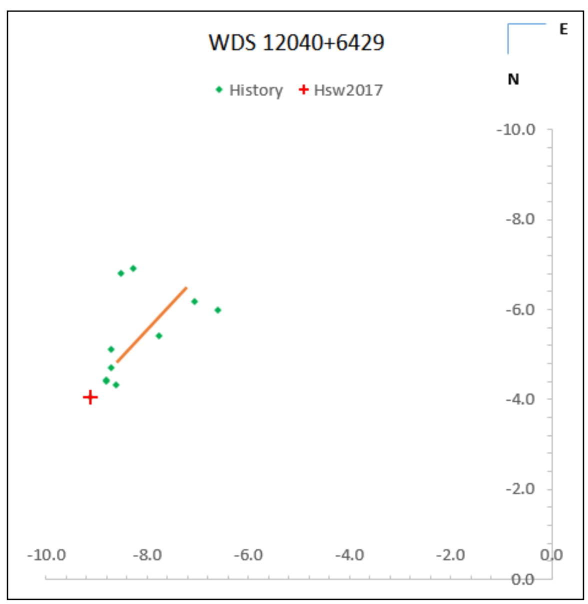

Figure 28. Plot of WDS 12040+6429.

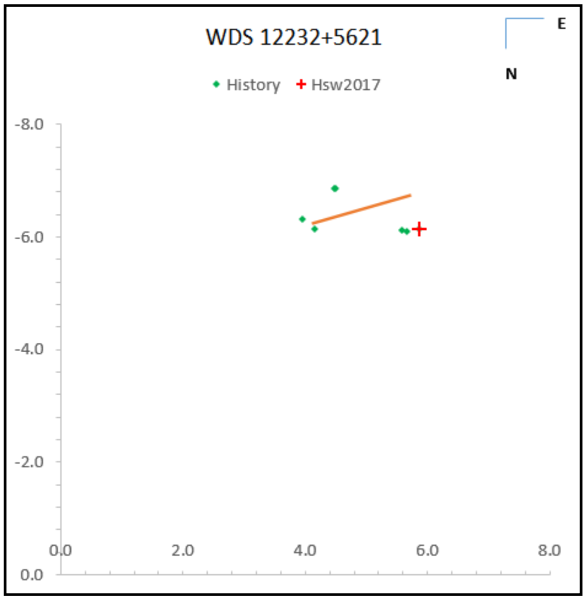

Figure 29. Plot of WDS 12232+5621.

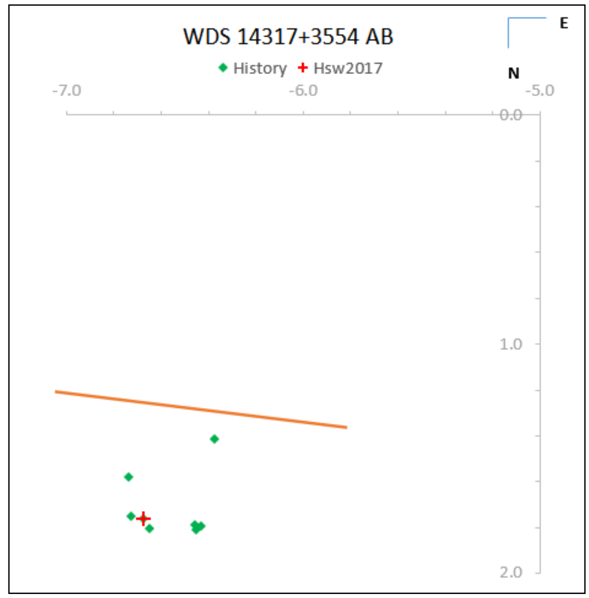

Figure 30. Plot of WDS 14317+3554 AB.

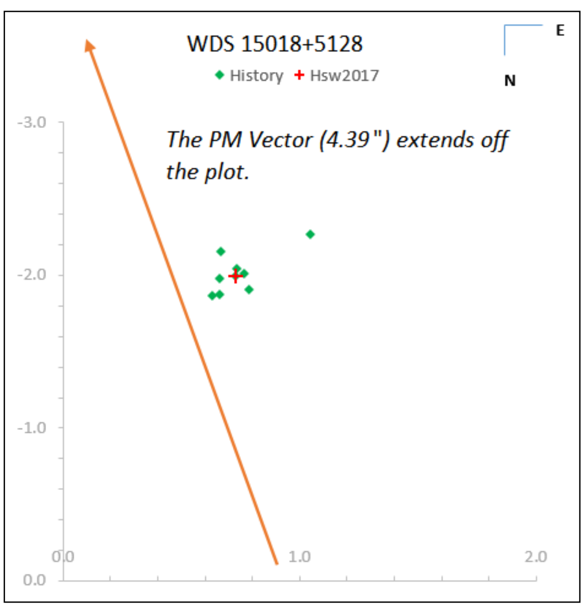

Figure 31. Plot of WDS 15018+5128.

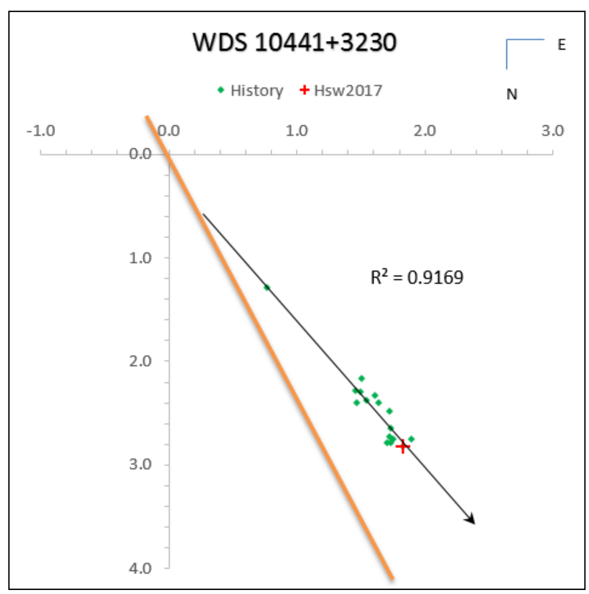

Figure 32. Plot of WDS 10441+3230.

Measurements of 161 Double Stars With a High-Speed CCD ...

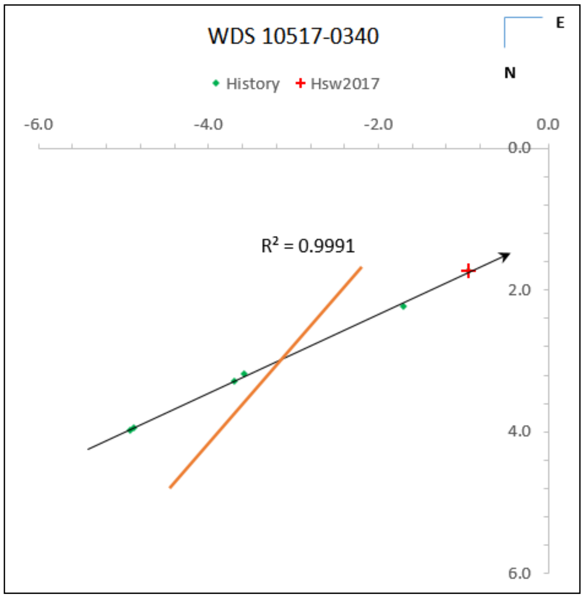

Figure 33. Plot of WDS 10517-0340.

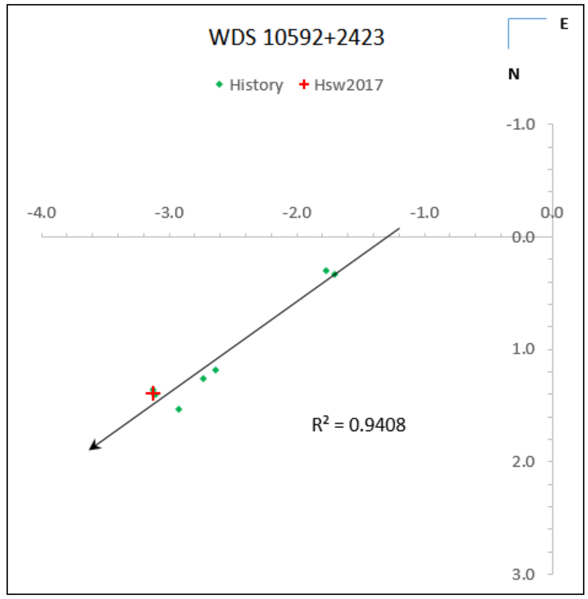

Figure 34. Plot of WDS 10592+2423.

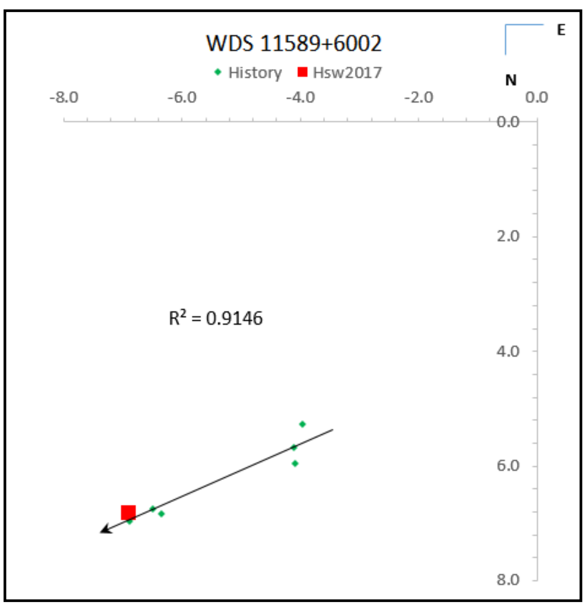

Figure 35. Plot of WDS 11589+6002.

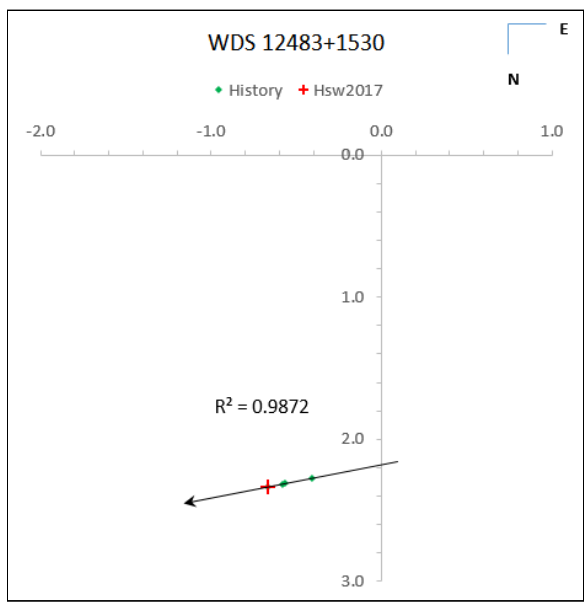

Figure 36. Plot of WDS 12483+1530.

Measurements of 427 Double Stars With Speckle Interferometry: The Winter/Spring 2017 Observing Program at Brilliant Sky Observatory, Part 1

Richard Harshaw

Brilliant Sky Observatory
Cave Creek, AZ
rharshaw51@cox.net

Abstract: In the winter and spring of 2017, an aggressive observing program of measuring close double stars with speckle interferometry and CCD imaging was undertaken at Brilliant Sky Observatory, my observing site in Cave Creek, Arizona. A total of 596 stars were observed, 8 of which were rejected for various reasons, leaving 588 pairs. Of these, 427 were observed and measured with speckle interferometry, while the remaining 161 were measured with a CCD. This paper reports the results of the observations of the 427 speckle cases. A separate paper in this issue will report the CCD measurements of the 161 other pairs.

1. Introduction

The winter and spring of 2017 marks the start of the third observing season at Brilliant Sky Observatory using speckle interferometry. Previous measurements have been reported in this journal by this author (Harshaw, A through G). This paper will continue the reports in that tradition.

2. Equipment Used

Brilliant Sky Observatory is equipped with a Celestron C-11 11-inch SCT telescope mounted on a Celestron CGEM-DX mount atop a PierTech adjustable pier. (See Figure 1.) The mount is controlled by a Lenovo desktop computer running TheSky 6.0.

The optical train consists of a Crayford focuser (locked in place so as not to affect focal length between observing sessions) which feeds into an Orion 1.25-inch flip mirror. One leg of the flip mirror unit—the acquisition leg—feeds a 25mm f/l illuminated reticle eyepiece with a single crosshair illuminated by a dimmable LED. The mount always places the target star within 5 arc minutes of the cross hair, so acquisition is fast and easy. The camera leg of the flip mirror unit feeds into a ZWO ASI290MM monochrome camera, known for its low read noise and excellent performance as a speckle camera. The camera has a 2x "Shorty Barlow" from Orion affixed to its mounting ring. Because only the lens and its mounting barrel from the Shorty

Figure 1: The setup at Brilliant Sky Observatory

Barlow are used, the actual multiplication of the Barlow is 1.5, resulting in a system focal ratio of 14.98.

The focal length of the system, as well as pixel scale and camera orientation with respect to north, are all determined by multiple drifts (20 or more drifts per session) of a star near declination 45°. The drift star is nudged to the east edge of the camera's field of view, the drive motor turned off, and the star allowed to drift across the camera's field of view while the computer is recording the file as a series of FITS frames. These files are then analyzed in The Speckle ToolBox (STB) using the Drift Analysis function of STB.

Focus is achieved and maintained by a Feathertouch focuser controlled by a MicroTouch temperature-compensated focus controller, both obtained from Starizona, a telescope supply and service center located in Tucson, Arizona.

Stars measured with speckle must have rho under 5" and be bright enough to permit both stars to appear with integration times at or under 40ms.

When doing speckle measurements, 1,000 frames are made of each star at as short an integration time as possible given the magnitudes of the two stars. Usually five such files are made of each star (especially for speckle). A nearby single star is then imaged (again, 1,000 frames) and is used for deconvolution of the speckle files captured.

Files are written to a 2TB portable USB3 hard drive, which is then taken into my office for analysis the next day using STB for data reduction and measurements.

Final results are then saved to a 5TB USB3 hard drive with a backup made to a second 5TB USB3 hard drive. The backup drive undergoes an incremental backup once a week.

3. Methodology

3a. Speckle or CCD?

The decision to make a file as a speckle interferometry case depends on two factors: the separation (rho) of the two stars and the magnitudes of the two stars.

To qualify for speckle interferometry, the pair must have a rho value of 5" or less (but on nights of very good seeing, this can be pushed up a bit, perhaps to 6"). Also, the stars must be bright enough to register in 40 ms or less.

Any pair wider than 5" and/or requiring integration times over 40ms is then recorded and processed as a CCD file.

3b. Using The Speckle Toolbox in Manual Mode.

Some of the stars in this report are described as "Manual solution with STB." When a pair is wide enough to produce three distinct star images in the autocorellogram (the primary flanked by symmetric images of the companion's power spectrum image), STB has no difficulty in automatically locating and selecting the companion star (although sometimes, the observer must use the complementary image 180° from the one chosen by STB if theta is greater than 180°). But in cases where the power spectrum images of the stars are not distinct, or the frame is noisy, STB may not be able to automatically find the companion's power spectrum. In such cases, STB allows the user to manually select the companion's power spectrum by right clicking on it. In this report, all the pairs measured with "Manual solution" had distinct companion power spectra to select, but noise near the primary misled STB's automatic selection process.

3c. Using the Most Accurate Proper Motions Available.

Until recently, the most accurate data sources for parallax and proper motion were rather limited in depth and scope. Also, the WDS often reports proper motions for one or both of the stars in a system without referencing the source of the measurement. (See Harshaw 2017H) When reporting proper motions in this paper, I will indicate the source of the data by following the proper motion numbers with a letter — G for Gaia, U for UCAC5, or W for a proper motion listed in the WDS but for which the source is not known.

In Harshaw 2017H, I reported how the resultant of two proper motion vectors could be computed. I use that method in this paper to indicate when the proper motion vectors do not seem to agree with the observations of the pair.

For example, a pair with widely differing proper motions would be expected to exhibit a linear or nearly-linear track over time, and there are many examples of this in the WDS. However, there are also cases where pairs with widely differing proper motions show no apparent trend in the measurements at all — all of the data points tend to clump around a central point much like the random scattering of buckshot from a shotgun. When widely differing proper motion vectors are listed for a pair with a tight pattern of measurements like this, we may assume that one (or both) of the proper motion vectors is incorrect.

In correspondence with Norbert Zacharias, team leader for the UCAC5 catalog, Zacharias suggested that where data is available in both Gaia and UCAC5 that we use Gaia:

> "I recommend to use Gaia DR1 data, i.e. for those stars which are in the TGAS… Keep in mind the UCAC data still has issues with poor charge transfer efficiency of the detector leading to magnitude (and field) dependent systematic errors at the

> about 2000 epoch. This could translate into about 1 to 2 mas/yr systematic errors for individual stars. But if the UCAC5 random errors on proper motions are small (order 1-2 mas/yr) while the TGAS proper motions are larger, you might want to take UCAC5 or a mean between TGAS and UCAC5… For stars not in TGAS, UCAC5 is a good option, although there are several other attempts to get proper motions with Gaia data and some other earlier data. See for example HSOY (update of PPMXL) or the GPS1 (derived from Pan-STARRS, SDSS and 2MASS). Then there is also the PMA (proper motion absolute) catalog based on 2MASS. They all have their pros and cons and are on about the same level of formal errors - nobody knows which is better in an absolute sense."

In many cases, Gaia has good proper motion data on only one of the stars in a double star system. Since the UCAC5 catalog has a much larger sampling of proper motions, it is common for a star without a proper motion value in Gaia to be listed in the UCAC5 data. When this was the case, I looked at the proper motion data in both catalogs for the star that was listed in both catalogs. If the UCAC5 proper motion vector was within 5 milli-arc seconds (mas) of the Gaia value, I assumed that the UCAC5 data for the second star would be on a par with Gaia (had Gaia listed it). However, if the difference in proper motions exceeded 5 mas, the UCAC5 data for the second star was not used.

3d. Using the Most Accurate Parallax Data Available

Like the proper motion data, parallax data will be listed with attribution to its source. The format will be XX.XX ± 0.XX S, where the X's are the numbers of the parallax value (with ± 0.XX being the stated error estimate of the parallax) and S the source—H for Hipparcos, G for Gaia.

Most of the time, we only have parallax data on one of the stars in a double star system. In this report, only 34 of the 417 speckle measurements (8%) have parallax on both stars.

Determining if two stars are close enough to be physical on the basis of parallax data alone is a bit tricky. Let's consider two of the stars in this report.

WDS 09371–1350 (BRT1909) has parallaxes for both stars shown in Gaia. For the primary, Gaia shows 1.76 ± 0.40 mas, while for the companion it shows 2.19 ± 0.93 mas. Thus the primary could have a parallax ranging from 1.36 up to 2.16 mas while the companion could range from 1.26 to 3.12 mas. So there is a considerable range of parallaxes where the stars could be at the same distance from the earth. If we draw a diagram showing the parallaxes with their error estimates, we get a picture like Figure 2.

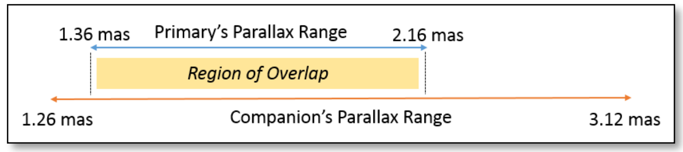

Figure 2: Parallax overlap of BRT1909

Whereas the two stars could clearly be at the same distance (as shown by the Region of Overlap), they could also be at quite different distances. The Region of Overlap is 0.80 mas whereas the entire parallax range is 3.12 – 1.26 or 1.86 mas. So the range of overlap is equivalent to 0.80 / 1.86 or 43% of the total parallax space. Does this mean the stars have a 43% chance of being at the same distance?

Unfortunately, no. The reason is that the probability of a star being at any given parallax value is not a linear function around the mean parallax value but rather a Gaussian distribution around the mean. The reported error estimate is one standard deviation. In a normal distribution, the first standard deviation from the mean contains 34.13% of the possible values, so there is a 68.26% chance that a star will be within its given parallax window (using 1 standard deviation on both sides of the mean). The actual math to compute a precise probability of two stars being at the same distance given their parallaxes is quite complicated. For our purposes, the percentage of overlap will serve as a reasonable indicator of a pair's likelihood of being at the same distance.

Let us consider a case where the stars clearly have no overlap in their parallaxes values. Let us look at WDS 10258+3237 (ES 432), a pair with given parallaxes of 4.00 ± 0.36 and 2.74 ± 0.49. Here is a diagram of the parallax data (Figure 3):

Clearly, there is no overlap between the parallax values of the stars in the system, so they are probably too far apart to be captured by their mutual gravitational forces.

In doing parallax calculations, if the error estimate of the parallax was 25% or more of the mean, the parallax was rejected as being unreliable.

Also, at the suggestion of William Hartkopf at the US Naval Observatory, I decided to use a weighted average of the parallax values for stars whose parallaxes

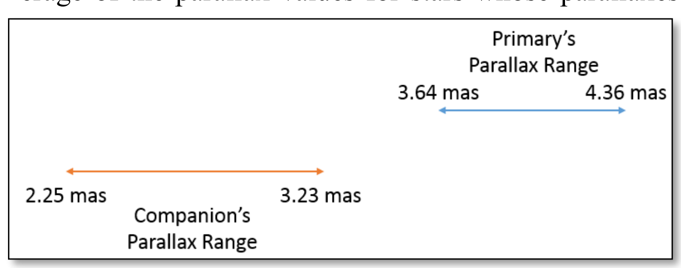

Figure 3: Parallax range of ES 432

Measurements of 427 Double Stars With Speckle Interferometry ...

could place them close enough in physical proximity to be physical. In such cases, the weighted parallax was computed as shown in Equation 1.

$$PX_w = \frac{\left[\left(1 - PxA\ err\%\right) * PxA\right] + \left[\left(1 - PxB\ err\%\right) * PxB\right]}{\left[\left(1 - PxA\ err\%\right) + \left(1 - PxB\ err\%\right)\right]} \quad [1]$$

PX_w is the weighted parallax. *PxA err%* is the error in parallax for the primary star expressed as a percentage (Error / Parallax). Likewise for *PxB err%.*

Let's take an example. Consider the case of WDS 11272+1908 (KU 38), a pair for which Gaia lists parallax for both stars. For the primary, Gaia shows 6.18 ± 0.38 mas and for the companion, 6.23 ± 0.42 mas. The weighted parallax then works out to

$$PX_w = \frac{\left[\left(1 - 0.38/6.18\right) * 6.18\right] + \left[\left(1 - 0.42/6.23\right) * 6.23\right]}{\left[\left(1 - 0.38/6.18\right) + \left(1 - 0.42/6.23\right)\right]}$$
$$= 6.20$$

Knowing the weighted parallax, it is a simple matter to divide 1 by the parallax in arc seconds (converting mas to arc seconds by multiplying the mas by 0.001). In this case, the distance would be 1 / 0.0062 = 161 parsecs.

3e. Estimating the minimum separation between the two stars.

When we have a parallax for each star, we can then compute the *minimum* separation between the two stars once we have the distance in parsecs. This is found by simply multiplying the distance (in parsecs) by the latest value for rho (in arc seconds). In the case of KU 38, the last value for rho in the WDS was listed as 5.90". Hence, the minimum separation between the two stars is 5.90 * 161 or 950 astronomical units (AU)— roughly 32 times the distance from the Sun to Neptune. This is a vast distance to be sure, but well within the realm of possibility for a binary star system.

This method will yield only the *minimum* separation between the two stars since we do not know the orientation of the stars relative to our line of sight. We are only seeing a projection of their distance on the sky's plane, and in all likelihood, one of the stars lies closer to earth than the other. As a result, we see one leg of a right triangle, while the stars are truly separated by the hypotenuse of that triangle.

This same procedure can be applied, of course, to pairs where the parallax to only one of the stars is known. In such cases, the minimum separation is a rough guide to the physicality of the system.

A survey of 888 systems from the Sixth Orbit Catalog where we have the distance to the pair and can therefore compute the true separation of a binary system in AU, the true separations of stars (based on the semi-major axis of the orbit) run a range from 4.1 AU at the low end to 1,707 AU at the high end, with a mean of 281 AU.

The data available to date suggests that true separations in binary stars will be, at most, in the low thousands of astronomical units. Of course, this is not to say that a true binary could not have a separation of 30,000 astronomical units or more, but only that our research so far makes such a wide pair highly unlikely. Obviously, the 6th Orbit Catalog represents a selection bias due to the fact that we only have good distance data and orbits on binary stars that are relatively close to us and with short enough periods to detect a short arc in the data when plotted on a graph. Such visual clues can then lead to an orbital solution. Nonetheless, I would be highly suspicious of a given pair's odds of being a true binary if the separation between the two stars exceeds 3 or 4 thousand astronomical units.

4. Results

4a. The Results Tables.

The speckle results of the winter and spring 2017 observing season at Brilliant Sky Observatory are presented in 6 tables as shown in Table 1. (The numbers indicate the number of pairs listed in each table.)

In Table 1, the number before the colon indicates the table number. CPM means common proper motion pairs (pairs where the proper motion vectors are both within 5 mas of each other, except where the proper motions are large, in which case the differences can be extended). DPM means the pair has different proper motions (more than 5 mas difference in both vector values). LIN means the pair is showing a linear pattern. ORB are pairs that have known orbits. SAB signifies short arc binaries, pairs that are showing an arc but for which there are not yet orbital solutions. And UNK

Table 1: Results by Type of System

Type	Speckle
CPM	3: 278
DPM	4: 21
LIN	5: 13
ORB	6: 79
SAB	7: 12
UNK	8: 24

stands for unknown—cases that do not fit any of the other categories.

4b. A Quick Check of Measurement Consistency.

A quick way to check consistency of one's measurements has traditionally been to compare the observer's measurement to the last measurement listed in the WDS (and obtained by a datarequest email to the USNO). The problem with this method is that if the last measurement was of uncertain value, the residual (difference between the observer's measurement and the last measurement on record) may be large, suggesting a poor measurement. Of course, the large residual may be due to a weak *prior* measurement. This will be seen in several cases in the tables that follow.

A more consistent method is to compute the average annual difference between the values of theta and rho from the last measurement on record to the observer's measurement, and then add all of the differences. The closer to zero each sum would be (theta and rho), the more consistent the measurements of the observer.

The reasoning is that for any large sample (and 427 pairs is probably a large enough sample), one would expect the changes in theta to be evenly divided between increasing theta (a + value for the difference) and decreasing theta (a – value); likewise for rho. In other words, there is a 50/50 chance that for any given pair, theta will increase over time or decrease, as will be the case for rho.

By computing the average *annual* change in theta and rho, one gets around those cases where the last measurement was made, say, 20 years ago and the residual seems very large. But if one computes the change in theta and rho per year over the 20 year window, the residuals become much smaller.

In computing annualized changes in theta and rho, I took the date of the observation minus the year of the last observation plus 0.5 (assuming an average measurement would be made mid-year), resulting in the number of years that have elapsed since the last measurement on file and the one I made. I then divided the raw residuals by this number of years to get the annual change.

I do this procedure for each night I observe and if the average annual change in theta exceeds 0.5° or rho exceeds 0.100", I assume there is a problem with the measurements that night (more than likely, a calibration issue). If the cause of the error can be determined (for example, doing a drift calibration the next night without moving the camera from the night before), the correction will be applied to the measurements obtained and results reported. If the cause cannot be determined, or if even after finding the cause, the errors still lie outside the parameters I have set, I reject all the work for that night and try to get the measurements on a later night.

Table 2: Annual Differences in θ and ρ

Measurement Type	θ	ρ
Average Standard Error of the Means		
Speckle	+0.4°	+0.2°
Average Raw Residuals		
Speckle	-0.1°	+0.000"
Average Annual Change in θ, ρ		
Speckle	-0.01°	-0.020"

For all of the pairs in this report, the annual differences came to the values shown in Table 2. I also report in this table the average standard error of the mean and average raw residual.

4c. Table Format.

The table column headings are as follows:

- Date: date of the observation (Julian)
- WDS No: the WDS number of the pair
- Disc/Comp: discoverer and components
- PM A: proper motion of the primary in mas per year. Source indicated by W for WDS, G for Gaia, or U for UCAC5
- PM B: proper motion of the companion as for A
- Last Yr: last year of measurement on file with the WDS
- Last θ: the last value for θ reported
- Last ρ: the last value for ρ reported
- Msrs: Number of measures made on the night of observation
- Measured θ ± err (°): the measured value of θ that night with the standard error of the mean, expressed in degrees
- Measured ρ ± err ("): the measured value of ρ that night with the standard error of the mean, expressed in arc seconds
- Resid θ: the difference between the observed value of θ and the last value on record
- Resid ρ: the difference between the observed value of ρ and the last value on record

In the plot diagrams that accompany the notes, the historical data has been corrected for precession and the axis values are expressed in arc seconds.

Every pair that I measure has a plot of its measurements generated from a WDS data request. Any measurement I make that lies far from the mean of the his-

Measurements of 427 Double Stars With Speckle Interferometry ...

torical data is not reported, as there may be problems with calibration or even the measurement of the wrong star (surprisingly easy to do in a rich star field!).

In addition, some of the plots of the measurements presented in the “Notes” tables that follow each table of results contain a heavy orange line. This line is the PM vector that the stars should have followed if the displacement over its observed history is due only to a difference in proper motions. In some cases, the fit of the orange line to the data is so good as to virtually confirm the pair is linear. In other cases, the orange line is displayed on a small and dense packing of measurements, which would indicate a problem with one (or both) of the proper motion vectors.

(Text continues on page 315)

Table 3: Common Proper Motion Pairs (CPM) Measured With Speckle

Date	WDS No	Disc/Comp	PM A	PM B	Last Yr	Last θ	Last ρ	Msrs	Measured θ ± err (°)	Measured ρ ± err (")	Resid θ	Resid ρ	Notes?
2017.0822	02123+2357	STF 226AB	+135-169 U	+130-160 W	2009	231.9	1.76	5	230.9 ± 0.0	1.755 ± 0.002	-1.0	-0.005	*
2017.0822	02214+0853	BU 8	+000-015 W	+000-015 W	2008	224.7	1.53	5	224.0 ± 0.1	1.632 ± 0.012	-0.7	0.102	*
2017.0767	02233-0749	HO 313AB	+013-024 W	+013-024 W	2012	75.9	2.13	5	73.3 ± 0.2	2.279 ± 0.012	-2.6	0.149	
2017.0795	02244+1130	STF 261	+000+003 G	-001+005 U	2008	252.0	2.90	5	253.6 ± 0.3	2.831 ± 0.015	1.6	-0.069	*
2017.0822	02327+0620	STF 276	+023-095 W	+023-095 W	2011	274.0	1.70	5	275.6 ± 0.0	1.839 ± 0.002	1.6	0.139	
2017.0795	02389+1526	AG 43	-016-011 U	-018-012 U	2008	61.8	2.97	5	63.3 ± 0.2	2.857 ± 0.023	1.5	-0.113	
2017.0822	02411+1848	STF 291AB	-003-013 G	-002-013 W	2016	117.1	3.31	5	117.2 ± 0.1	3.366 ± 0.012	0.1	0.056	*
2017.0795	02429-0629	A 452	+066-057 G	+059-064 W	2006	112.5	1.80	5	114.5 ± 0.1	1.891 ± 0.020	2.0	0.091	*
2017.0795	02447-0158	STF 303	-009-004 G	-010-005 U	2003	180.9	5.79	5	182.8 ± 0.1	5.841 ± 0.010	1.9	0.051	*
2017.0795	02527+0628	STF 323	+022-013 W	+022-013 W	2012	278.3	2.71	5	280.3 ± 0.1	2.719 ± 0.035	2.0	0.009	*
2017.0795	03051+2755	STF 342	-009-038 U	-002-027 W	2008	303.9	3.20	5	304.2 ± 0.1	3.399 ± 0.006	0.3	0.199	*
2017.0822	03088+3528	STF 352	+032-031 G	+032-030 W	2011	359.5	3.79	4	358.7 ± 0.0	3.898 ± 0.001	-0.8	0.108	*
2017.0795	03242+1733	STF 383	+016-048 U	+014-053 W	2010	120.2	5.33	5	120.8 ± 0.0	5.562 ± 0.010	0.6	0.232	*
2017.0767	03258-1304	HU 21	+008-000 G	+003+001 W	1999	36.8	1.39	5	37.8 ± 0.5	1.458 ± 0.015	1.0	0.068	*
2017.0795	03312+1947	STF 403	+031+037 G	+034+024 W	2012	171.4	2.29	5	172.7 ± 0.1	2.296 ± 0.010	1.3	0.006	*
2017.0822	03446+3551	HO 504	+009-011 W	+009-011 W	2009	192.4	1.11	5	193.1 ± 0.1	1.105 ± 0.005	0.7	-0.005	
2017.0767	03545-1243	HLD 67	-009-016 G	-017-011 W	2009	149.8	2.78	5	146.8 ± 0.1	2.885 ± 0.006	-3.0	0.105	*
2017.0795	03554+1738	BU 85	-000-005 G	-002-005 W	2010	216.5	3.96	5	216.6 ± 0.0	4.037 ± 0.003	0.1	0.077	*
2017.0822	04024-0700	STF 489	-009+024 G	-010+027 U	2010	197.2	3.08	5	196.5 ± 0.0	3.078 ± 0.005	-0.7	-0.002	*
2017.1507	04059+1058	STF 491	-002-074 G	-004-072 W	2010	96.8	2.90	5	96.5 ± 0.0	2.843 ± 0.001	-0.3	-0.057	*
2017.1507	04160+0027	STF 517	+024-021 G	+024-022 W	2012	8.0	3.29	5	6.6 ± 0.3	3.248 ± 0.002	-1.4	-0.042	*
2017.1507	04409+0058	STF 583AB	+000-001 G	+000-001 W	2012	327.5	5.45	5	326.9 ± 0.0	5.757 ± 0.001	-0.6	0.307	*
2017.1507	04448+0517	STF 589AB	-118-045 G	-122-058 W	2011	277.0	4.70	5	276.1 ± 0.0	4.669 ± 0.001	-0.9	-0.031	*
2017.1507	04551-0033	STF 614AB-C	+003+002 G	-001+002 W	2010	69.1	4.39	5	68.5 ± 0.0	4.420 ± 0.001	-0.6	0.030	*
2017.1507	04561+0908	BU 405	-005-004 W	-005-004 W	2015	290.7	1.65	5	290.1 ± 0.1	1.772 ± 0.001	-0.6	0.122	*

Table 3 continues on next page.

Measurements of 427 Double Stars With Speckle Interferometry ...

Table 3 (continued): Common Proper Motion Pairs (CPM) Measured With Speckle

Date	WDS No	Disc/Comp	PM A	PM B	Last Yr	Last θ	Last ρ	Msrs	Measured θ ± err (°)	Measured ρ ± err (")	Resid θ	Resid ρ	Notes?
2017.1616	05030-0840	STF 636	-012-003 W	-012-003 W	2013	103.2	3.60	5	103.6 ± 0.0	3.669 ± 0.001	0.4	0.069	*
2017.1644	05041+0257	A 2632	+000-006 W	+000-006 W	2016	300.0	0.90	5	303.3 ± 0.3	0.901 ± 0.004	3.3	0.001	
2017.1644	05079+0824	STF 643	+023-061 G	+018-061 G	2010	124.4	2.38	5	124.9 ± 0.0	2.448 ± 0.004	0.5	0.068	*
2017.1616	05110-0146	BU 885	+006-001 W	+006-001 W	2006	196.1	0.64	5	198.3 ± 0.4	0.601 ± 0.013	2.2	-0.039	*
2017.1671	05118+0102	STF 652	-001-017 W	-001-017 W	2015	180.0	1.60	5	179.6 ± 0.1	1.668 ± 0.002	-0.4	0.068	*
2017.1616	05125-0302	A 51	+000-008 W	+000-008 W	2009	104.3	1.48	5	105.0 ± 0.2	1.486 ± 0.003	0.7	0.006	
2017.1616	05147-0704	STF 667	-008-008 G	-009-010 W	2004	316.2	4.22	5	315.7 ± 0.0	4.284 ± 0.003	-0.5	0.064	*
2017.1671	05152+0826	STF 664	+015-036 G	+011-039 W	2011	177.2	4.66	5	176.3 ± 0.0	4.702 ± 0.001	-0.9	0.042	*
2017.1671	05159+0345	A 2638	-006-021 W	-006-021 W	2016	279.0	0.90	5	280.3 ± 0.1	0.961 ± 0.003	1.3	0.061	
2017.1616	05162-0329	BU 318	-002-001 W	-002-001 W	1997	261.6	0.62	5	264.3 ± 1.1	0.643 ± 0.010	2.7	0.023	*
2017.1671	05177+0441	STF 678AB	+017-032 G	+013-030 W	2009	102.6	3.62	5	103.4 ± 0.0	3.594 ± 0.001	0.8	-0.026	*
2017.1616	05204-0805	BU 190AB	-000-063 G	+000-065 W	2001	328.2	0.66	5	326.3 ± 0.5	0.706 ± 0.009	-1.9	0.046	*
2017.1616	05217-0203	STF 693	-001+010 G	-002+010 W	2008	10.5	3.49	5	10.7 ± 0.0	3.511 ± 0.003	0.2	0.021	*
2017.1671	05231+0103	STF 700	+001-006 G	+003-007 W	2015	6.9	4.73	5	3.9 ± 0.0	4.788 ± 0.001	-3.0	0.058	*
2017.1616	05231-0806	A 486	-003+005 W	-003+005 W	1997	71.3	0.63	5	73.2 ± 0.7	0.750 ± 0.029	1.9	0.120	*
2017.1507	05236-1025	STN 10	-002+005 W	-002+005 W	2006	120.6	0.85	5	120.4 ± 0.6	1.096 ± 0.025	-0.2	0.246	
2017.1671	05252+0155	STF 708	+002-007 W	+002-007 W	2010	321.1	2.69	5	321.1 ± 0.0	2.772 ± 0.001	0.0	0.072	*
2017.1671	05265+0256	STF 712AB	-002-006 W	-002-006 W	2012	66.4	3.16	5	65.9 ± 0.0	3.157 ± 0.001	-0.5	-0.003	*
2017.1644	05291-0201	D 8AB	-001-020 W	+003-023 W	2010	49.0	4.80	5	47.7 ± 0.1	5.711 ± 0.004	-1.3	0.911	
2017.1671	05312+0318	STF 729AB	+000-006 W	+000-006 W	2015	27.0	1.90	5	25.5 ± 0.0	1.849 ± 0.002	-1.5	-0.051	*
2017.1644	05314-0206	STF 731AB	+001+001 W	-001+000 W	2006	327.2	4.94	5	327.0 ± 0.1	4.830 ± 0.008	-0.2	-0.110	*
2017.1644	05331-0143	STF 734AB	-001-007 W	-001-007 W	2008	357.3	1.65	5	355.3 ± 0.0	1.614 ± 0.003	-2.0	-0.036	
2017.1644	05345-0429	BU 13	-009-007 W	-009-007 W	1991	141.9	0.96	5	144.1 ± 0.5	0.830 ± 0.002	2.2	-0.130	
2017.1644	05347-0424	STF 743	-006-004 W	-006-004 W	2012	282.0	1.80	5	283.2 ± 0.0	1.852 ± 0.003	1.2	0.052	
2017.1644	05355-0422	STF 750	+004+001 W	+004+001 W	2014	60.1	4.10	5	59.6 ± 0.0	4.238 ± 0.002	-0.5	0.138	*
2017.1671	05381-0011	STF 757AB	-001-008 W	-001-008 W	2010	239.4	1.45	5	239.3 ± 0.1	1.525 ± 0.003	-0.1	0.075	*
2017.1507	05457-1447	A 3018	-002-048 W	-002-048 W	1998	294.2	0.75	5	303.3 ± 0.6	0.707 ± 0.018	9.1	-0.043	*
2017.1507	05484-1842	HJ 3799	-011+002 W	-011+002 W	2008	152.4	3.79	5	151.4 ± 0.2	3.781 ± 0.008	-1.0	-0.009	
2017.1616	05495-1234	HDS 783	-001+005 W	-001+005 W	2000	167.2	1.70	4	168.6 ± 0.1	1.944 ± 0.011	1.4	0.244	
2017.1616	05514-1139	A 2512	-008-004 W	-008-004 W	1991	279.0	1.13	5	275.3 ± 0.3	0.999 ± 0.008	-3.7	-0.131	*
2017.1507	06041-1541	SKI 2	-010+014 W	-006+007 W	1999	171.9	5.50	5	170.8 ± 0.3	5.293 ± 0.027	-1.1	-0.207	
2017.2137	06049-0243	STF 839AB	-003-006 G	-002-005 G	2004	289.1	4.94	5	288.1 ± 0.1	5.100 ± 0.005	-1.0	0.160	*
2017.2137	06074-0400	STF 850AB	-004-010 G	-004-010 G	2008	17.8	2.02	5	15.2 ± 0.1	2.171 ± 0.004	-2.6	0.151	*
2017.1616	06114-1650	A 3022	-013-006 W	-013-006 W	2008	359.9	1.04	5	357.6 ± 0.4	1.098 ± 0.018	-2.3	0.058	
2017.1507	06167-1203	BU 18	-012-035 G	-015-039 W	1993	284.5	1.81	5	286.0 ± 0.2	1.872 ± 0.014	1.5	0.062	*

Table 3 continues on next page.

Table 3 (continued): Common Proper Motion Pairs (CPM) Measured With Speckle

Date	WDS No	Disc/Comp	PM A	PM B	Last Yr	Last θ	Last ρ	Msrs	Measured θ ± err (°)	Measured ρ ± err (")	Resid θ	Resid ρ	Notes?
2017.1644	06217-1424	HU 1241AB	-016+008 W	-016+008 W	1996	81.4	0.83	5	79.7 ± 0.4	0.766 ± 0.004	-1.7	-0.064	
2017.1644	06238-1947	BU 568	-004+003 W	-004+003 W	2005	153.0	0.79	5	155.2 ± 0.9	0.849 ± 0.015	2.2	0.059	*
2017.1644	06252-1056	BU 569	-002-013 W	-002-013 W	1991	117.1	1.69	5	115.0 ± 0.1	1.675 ± 0.005	-2.1	-0.015	*
2017.1507	06372-1415	HLD 80	-002+002 G	-001+002 G	2011	311.9	4.03	5	310.6 ± 0.0	4.090 ± 0.003	-1.3	0.060	*
2017.1507	06420-1600	BU 19	-004+002 G	-002+004 W	1999	168.5	3.95	5	166.9 ± 0.1	3.797 ± 0.009	-1.6	-0.153	*
2017.1644	06484-1326	STF 971AB	-010-009 W	-010-009 W	2008	323.0	1.20	5	323.0 ± 0.2	1.237 ± 0.001	0.0	0.037	*
2017.1644	06488-1613	BU 20	+009-049 G	+011-049 W	2002	27.2	3.29	5	26.7 ± 0.1	3.315 ± 0.005	-0.8	0.025	*
2017.2137	06573-1005	A 514	-025+014 W	-025+014 W	1991	101.4	1.39	5	103.0 ± 0.2	1.465 ± 0.004	1.6	0.075	*
2017.2137	06584-1011	A 515	-009+004 W	-009+004 W	1991	313.0	1.68	5	314.7 ± 0.1	1.708 ± 0.004	1.7	0.028	
2017.2712	08019-0333	A 539	-009-001 W	-009-001 W	2005	19.6	0.75	5	21.3 ± 1.3	0.663 ± 0.005	1.7	-0.087	
2017.2712	08042-0151	BU 903	-006-005 G	-002-012 W	1991	33.6	1.72	5	34.0 ± 0.0	1.649 ± 0.001	0.4	-0.071	*
2017.2986	08046+5445	STF1172	-018-017 G	-018-014 W	1995	243.6	1.66	5	243.5 ± 0.0	1.746 ± 0.001	-0.1	0.086	*
2017.2877	08091+3714	HU 849	-035-042 G	-035-040 W	2008	283.1	1.17	5	282.5 ± 0.1	1.255 ± 0.002	-0.6	0.085	*
2017.2712	08092-0642	BU 583	-003-009 W	-003-009 W	2010	71.3	1.83	5	70.7 ± 0.0	1.844 ± 0.001	-0.6	0.014	
2017.2740	08101+0403	AG 150	+022-001 G	+018-001 G	2010	30.3	5.00	5	30.0 ± 0.1	5.085 ± 0.004	-0.3	0.085	*
2017.2712	08109-0455	A 335	-011-003 G	-015-006 W	1991	125.9	1.43	5	127.2 ± 0.1	1.512 ± 0.002	1.3	0.082	*
2017.2795	08127+2933	STF1197	-008+005 W	-008+005 W	2015	99.5	1.83	5	99.9 ± 0.1	1.783 ± 0.001	0.4	-0.047	
2017.2795	08136+1023	BU 204	-008+010 W	-008+010 W	2004	292.0	0.80	5	291.0 ± 0.9	0.773 ± 0.003	-1.0	-0.027	*
2017.2740	08138+0159	BU 1244	+043-056 W	+043-056 W	2005	10.8	0.98	5	5.8 ± 0.1	1.033 ± 0.001	-5.0	0.053	*
2017.2795	08138+1538	PRT 3	-022+045 W	-022+045 W	2015	339.7	1.50	5	338.7 ± 0.0	1.506 ± 0.002	-1.0	0.006	
2017.2712	08140-1740	HU 1249	+026-028 W	+026-028 W	2003	122.2	0.73	5	124.2 ± 1.7	0.910 ± 0.012	2.0	0.180	*
2017.2986	08296+5203	HDS1213 AaAb	-087+025 W	-087+025 W	2015	323.0	0.90	5	321.8 ± 0.0	1.019 ± 0.001	-1.2	0.119	*
2017.2986	08298+5112	STF1225	+004+001 G	+003-002 G	2008	189.4	3.68	5	192.3 ± 0.0	3.759 ± 0.001	2.9	0.079	*
2017.2740	08330+0958	A 2895	+007-037 W	+007-037 W	1991	57.3	0.81	5	55.9 ± 1.3	0.768 ± 0.021	-1.4	-0.042	
2017.2712	08331-1257	A 2365	-005+006 W	-005+006 W	2005	282.1	1.29	5	282.3 ± 0.7	1.363 ± 0.007	0.2	0.073	
2017.2740	08339+0135	STF1243	-002-004 W	-002-004 W	2008	233.2	1.74	5	232.8 ± 0.0	1.724 ± 0.001	-0.4	-0.016	
2017.2986	08342+5655	STF1235	-014-029 G	-014-033 W	1996	85.4	1.50	5	88.3 ± 0.2	1.529 ± 0.005	2.9	0.029	*
2017.2795	08421+2501	J 1110	-046-018 G	-042-021 G	2012	41.6	3.36	5	41.5 ± 0.0	3.424 ± 0.001	-0.1	0.064	*
2017.2877	08432+3849	BU 209	+036+016 G	+035+008 W	2012	8.3	1.25	5	8.2 ± 0.1	1.278 ± 0.001	-0.1	0.028	*
2017.2795	08437+1654	A 2546	+019-007 W	+019-007 W	2010	215.5	1.70	5	218.6 ± 0.1	1.243 ± 0.001	3.1	-0.457	*
2017.2795	08444+1555	A 2472	-002-016 W	-002-016 W	2012	262.7	0.80	5	260.8 ± 0.2	0.810 ± 0.001	-1.9	0.010	*
2017.2712	08453-0236	STF1270	+001-010 G	+004-013 W	2013	264.4	4.61	5	264.5 ± 0.3	4.699 ± 0.004	0.1	0.089	*
2017.2740	08461+0748	J 735	-097+054 G	-099+053 W	2014	339.7	2.79	5	339.2 ± 0.3	2.818 ± 0.013	-0.5	0.028	*
2017.2877	08466+3829	STF1259	-049-059 G	-050-058 U	2010	341.5	5.00	5	340.5 ± 0.0	5.102 ± 0.004	-1.0	0.102	*
2017.2740	08482+0235	BU 335	-023-037 G	-023-038 W	2013	265.5	2.74	5	264.6 ± 0.0	2.607 ± 0.004	-0.9	-0.133	*

Table 3 continues on next page.

Measurements of 427 Double Stars With Speckle Interferometry ...

Table 3 (continued): Common Proper Motion Pairs (CPM) Measured With Speckle

Date	WDS No	Disc/Comp	PM A	PM B	Last Yr	Last θ	Last ρ	Msrs	Measured θ ± err (°)	Measured ρ ± err (")	Resid θ	Resid ρ	Notes?
2017.2877	08500+3935	STF1279	+073-007 G	+073-015 W	2013	87.0	1.25	5	87.4 ± 0.1	1.277 ± 0.002	0.4	0.027	*
2017.2877	08505+2308	AG 157	-047+013 U	-045+016 G	2013	75.2	2.27	5	74.8 ± 0.0	2.295 ± 0.001	-0.4	0.022	*
2017.2877	08508+3504	STF1282AB	-174+114 W	-174+114 W	2014	277.6	3.50	5	277.8 ± 0.0	3.518 ± 0.003	0.2	0.018	*
2017.2740	08512+0820	PER 1	-005-006 W	-005-006 W	2015	353.7	0.84	5	350.0 ± 0.4	0.838 ± 0.017	-3.7	-0.002	
2017.2712	08516-0711	BU 587AB	-053-017 W	-053-017 W	2003	120.6	1.15	5	121.2 ± 0.6	1.186 ± 0.023	0.6	0.036	*
2017.2712	08518-1108	SCJ 11	-005-002 W	-005-002 W	2008	353.2	2.16	5	353.0 ± 0.0	2.282 ± 0.002	-0.2	0.122	
2017.2712	08538-0035	STF1292AB	-043+044 G	-043+043G	2004	188.1	5.93	5	188.5 ± 0.2	6.082 ± 0.003	0.4	0.152	*
2017.2740	08542-0846	BU 24	-009+001 G	-012-003 W	2014	174.8	1.17	5	174.0 ± 0.2	1.179 ± 0.002	-0.8	0.009	*
2017.2986	08548+4335	STF1289	-057-153 G	-055-154 W	2015	7.0	3.70	5	6.6 ± 0.0	3.700 ± 0.001	-0.4	0.000	*
2017.2740	08549-0749	BU 103	-008-002 G	-002-005 W	2014	74.6	3.22	5	71.9 ± 0.1	3.008 ± 0.005	-2.7	-0.212	*
2017.2986	08561+4341	STF3120	+014-005 W	+014-005 W	2015	1.0	1.40	5	0.7 ± 0.0	1.393 ± 0.001	-0.3	-0.007	*
2017.2795	08571+1045	A 2968	-034-027 W	-034-027 W	2015	132.4	1.11	5	132.3 ± 0.0	1.177 ± 0.002	-0.1	0.067	
2017.2740	08598-0607	RST4427	-001-017 W	-001-017 W	1991	340.6	0.57	5	334.0 ± 0.3	0.588 ± 0.009	-6.6	0.018	*
2017.2877	09016-0832	A 3071	-070-025 W	-070-025 W	2004	335.3	1.27	5	336.1 ± 0.3	1.318 ± 0.006	0.8	0.048	*
2017.2877	09020+0240	BU 211	-006-003 G	-005-010 W	2006	268.4	1.10	5	268.2 ± 0.1	1.125 ± 0.002	-0.2	0.025	*
2017.3096	09033+4740	HU 720	-017-011 W	-017-011 W	2015	140.0	0.70	5	135.6 ± 0.3	0.781 ± 0.011	-4.4	0.081	*
2017.3096	09071+3037	AG 162	+029-039 G	+030-039 G	2007	106.8	4.01	5	106.6 ± 0.1	4.114 ± 0.013	-0.2	0.104	*
2017.3260	09080+8102	STF1284	-054-016 U	-050-031 W	2012	167.8	2.58	5	168.3 ± 0.1	2.484 ± 0.003	0.5	-0.096	*
2017.2877	09095+0256	STT 197	-016-037 W	-016-037 W	2000	66.3	1.43	5	64.5 ± 0.1	1.438 ± 0.001	-1.8	0.008	*
2017.2740	09101-1507	A 3073	-014-001 G	-026-010 W	1991	347.0	1.80	5	348.9 ± 0.6	1.856 ± 0.005	1.9	0.056	*
2017.3096	09103+5223	STF1312	-012-014 G	-014-014 W	2010	149.0	4.50	5	148.2 ± 0.0	4.766 ± 0.004	-0.8	0.266	*
2017.2740	09118-1649	BU 336	-017+005 W	-017+005 W	1991	239.3	1.79	5	240.0 ± 0.1	1.933 ± 0.003	0.7	0.143	*
2017.2877	09122-0729	A 2972	-037+014 U	-038+015 U	2011	340.5	4.26	5	340.6 ± 0.1	4.363 ± 0.004	0.1	0.103	
2017.3014	09127+1632	STF1322	+002-006 G	+001-003 W	2015	53.0	1.72	5	53.4 ± 0.2	1.748 ± 0.001	0.4	0.028	*
2017.2986	09149+0413	BU 455	+039-050 W	+039-050 W	2002	69.3	1.84	5	68.1 ± 0.0	1.845 ± 0.000	-1.2	0.005	*
2017.2877	09161-0821	BU 212	-047-000 G	-043-011 W	2011	198.4	1.60	5	198.0 ± 0.0	1.627 ± 0.002	-0.4	0.027	*
2017.2877	09168-0050	RST4906	-011-003 W	-011-003 W	1991	153.4	0.73	5	154.0 ± 0.2	0.842 ± 0.013	0.6	0.112	*
2017.2740	09186-1712	A 3076	+000-001 W	+000-001 W	2003	282.8	1.04	5	285.2 ± 0.3	1.071 ± 0.014	2.4	0.031	
2017.3096	09188+3648	STF1334AB	-033-124 W	-	2014	223.6	2.54	5	223.0 ± 0.1	2.620 ± 0.005	-0.6	0.080	
2017.2795	09188-1025	A 125AB	-022+004 G	-020+001 W	2012	30.9	3.02	5	30.4 ± 0.0	3.048 ± 0.003	-0.5	0.028	*
2017.3260	09208+6121	STF1331AB	-016+010 W	-016+010 W	2010	151.9	0.90	5	152.5 ± 0.4	0.941 ± 0.019	0.6	0.041	*
2017.3096	09210+3643	STF1339	-003+009 W	-003+009 W	2015	65.0	1.40	5	64.9 ± 0.2	1.485 ± 0.008	-0.1	0.085	
2017.3014	09233+2211	AG 165	-008+000 W	-008+000 W	2015	15.2	1.27	5	15.5 ± 1.2	1.381 ± 0.071	0.3	0.111	
2017.3096	09235+3908	STF1344	-014-032 G	-020-030 W	2014	103.2	3.72	5	102.9 ± 0.0	3.815 ± 0.002	-0.3	0.095	*
2017.3014	09239+2754	STT 201AB	-005-040 W	-005-040 W	2015	207.0	1.24	5	206.1 ± 0.4	1.373 ± 0.021	-0.9	0.133	*

Table 3 continues on next page.

Measurements of 427 Double Stars With Speckle Interferometry ...

Table 3 (continued): Common Proper Motion Pairs (CPM) Measured With Speckle

Date	WDS No	Disc/Comp	PM A	PM B	Last Yr	Last θ	Last ρ	Msrs	Measured θ ± err (°)	Measured ρ ± err (")	Resid θ	Resid ρ	Notes?
2017.3096	09256+5401	STF1346AB	-036-022 G	-038-023 W	2014	315.3	5.77	5	314.0 ± 0.0	5.762 ± 0.004	-1.3	-0.008	*
2017.2877	09269-0315	A 128	-041-028 W	-041-028 W	1997	262.5	1.30	5	262.1 ± 0.3	1.335 ± 0.004	-0.4	0.035	
2017.3014	09277+1545	STF1353	-022-019 U	-020-019 U	2010	126.0	3.26	5	125.1 ± 0.3	3.315 ± 0.020	-0.9	0.055	*
2017.2877	09296-0307	BU 591	-002-004 G	+000-006 W	1997	30.4	0.86	5	28.6 ± 0.2	0.967 ± 0.009	-1.8	0.107	*
2017.3096	09300+4216	A 1985	-029-039 W	-029-039 W	2015	24.0	1.60	5	23.2 ± 0.0	1.670 ± 0.002	-0.8	0.070	*
2017.2795	09310-1544	BU 339	-047+025 W	-047+025 W	2001	247.3	1.25	5	248.8 ± 0.1	1.211 ± 0.007	1.5	-0.039	*
2017.2986	09315+0128	STF1365	-011-030 W	-011-030 W	2012	157.1	3.44	5	156.4 ± 0.1	3.456 ± 0.002	-0.7	0.016	*
2017.2795	09338-1020	A 131AB	-091-001 W	-091-001 W	2014	324.3	0.90	5	323.6 ± 0.5	0.954 ± 0.043	-0.7	0.054	
2017.2795	09400-1710	STN 19AB	+001-019 U	-002-022 U	2012	263.9	2.71	5	261.9 ± 0.3	2.791 ± 0.035	-2.0	0.081	
2017.2795	09415-1829	BU 214AB	+007-010 W	+007-010 W	2002	243.0	3.62	5	242.1 ± 0.1	3.749 ± 0.011	-0.9	0.129	*
2017.3096	09450+4314	STF1376AB	-009-119 W	-008-100 G	2014	310.0	5.30	5	309.3 ± 0.1	5.371 ± 0.007	-0.7	0.071	
2017.3260	09460+7643	STF1373	-009-119 W	-008-100 G	2012	135.5	1.89	5	137.1 ± 0.2	2.168 ± 0.003	1.6	0.278	*
2017.3096	09476+5057	HU 630	+008-005 U	+005-001 U	2013	72.6	2.24	5	74.0 ± 0.1	2.200 ± 0.001	1.4	-0.040	
2017.3260	09509+5812	KR 33	-014-083 W	-014-083 W	2005	213.4	2.06	5	214.0 ± 0.2	2.082 ± 0.006	0.6	0.022	
2017.3014	09521+1628	STF1390AB	-004+002 W	-004+002 W	2010	206.9	2.22	5	206.6 ± 0.3	2.223 ± 0.023	-0.3	0.003	
2017.3260	09551+6854	STF1386AB	-010-002 G	-006-001 W	2012	110.5	2.10	5	110.7 ± 0.3	2.183 ± 0.013	0.2	0.083	*
2017.3096	09572+4554	STF1394	-024-086 G	-025-085 W	2013	249.2	4.59	5	250.5 ± 0.0	4.525 ± 0.004	1.3	-0.065	*
2017.3260	09591+8023	STF1380	+003-003 W	+003-003 W	1991	25.8	1.65	5	21.6 ± 0.7	1.736 ± 0.028	-4.2	0.086	*
2017.2959	10040+3239	HU 631	-039+005 W	-039+005 W	2015	255.1	0.70	5	257.5 ± 0.1	0.800 ± 0.001	2.4	0.100	*
2017.2959	10056+3105	STF1406	-045-013 W	-045-013 W	2015	221.0	0.80	5	219.1 ± 0.1	0.728 ± 0.009	-1.9	-0.072	*
2017.3315	10076+0621	WEI 23	+006+002 U	+010-001 U	2011	314.6	3.33	5	314.3 ± 0.0	3.396 ± 0.001	-0.3	0.066	
2017.2959	10114+7302	STF1408	+014+014 G	+013+015 U	2011	13.3	3.71	5	12.7 ± 0.0	3.782 ± 0.002	-0.6	0.072	*
2017.2822	10151+1907	STF1417	-031-005 W	-018+001 W	2013	77.2	2.33	5	76.6 ± 0.0	2.376 ± 0.001	-0.6	0.046	*
2017.3397	10163+3309	HU 634	+003+018 W	+003+018 W	2010	169.3	1.95	5	169.4 ± 0.1	1.984 ± 0.003	0.1	0.034	
2017.2822	10180+1711	A 2369	-004+001 G	-003+002 W	2010	296.7	1.09	5	295.7 ± 0.5	1.031 ± 0.007	-1.0	-0.059	*
2017.2822	10181+2731	STF1421	+001-020 G	+001-020 W	2012	330.9	4.54	5	330.3 ± 0.0	4.601 ± 0.002	-0.6	0.061	*
2017.2795	10206-1621	HLD 103	+023-024 G	-019-024 W	2001	344.0	1.76	5	343.3 ± 0.1	1.738 ± 0.007	-1.0	-0.022	*
2017.2959	10234+2630	A 1990	-001+001 W	-001+001 W	2015	290.5	1.48	5	290.1 ± 0.0	1.511 ± 0.000	-0.4	0.031	*
2017.2795	10256+0847	STF1431	-013-002 G	-011-005 W	2012	73.7	3.56	5	73.5 ± 0.0	3.586 ± 0.001	-0.2	0.026	*
2017.2959	10260+5237	STF1428	-125-040 G	-131-044 W	2012	87.4	2.88	5	88.3 ± 0.0	2.810 ± 0.003	0.9	-0.066	*
2017.2959	10321+8136	TDS 594	-049-045 U	-051-043 U	2011	104.2	2.86	5	103.0 ± 0.1	2.894 ± 0.002	-1.2	0.034	*
2017.2959	10333+3740	STF1443	+011-075 G	+010-079 U	2010	160.1	5.43	5	160.7 ± 0.0	5.313 ± 0.008	0.6	-0.117	*
2017.2822	10336+1513	STF1446	+012-007 G	+012-008 U	2013	250.5	5.50	5	249.6 ± 0.0	5.601 ± 0.003	-0.9	0.101	*
2017.2959	10338+2321	STF1447	-046-005 G	-047-004 W	2011	124.4	4.44	5	123.9 ± 0.0	4.463 ± 0.001	-0.5	0.023	*
2017.2795	10391-1735	HLD 108AB	-004-002 W	-004-002 W	2005	26.5	0.97	5	22.8 ± 0.1	0.981 ± 0.004	-3.7	0.011	

Table 3 continues on next page.

Measurements of 427 Double Stars With Speckle Interferometry ...

Table 3 (continued): Common Proper Motion Pairs (CPM) Measured With Speckle

Date	WDS No	Disc/Comp	PM A	PM B	Last Yr	Last θ	Last ρ	Msrs	Measured θ ± err (°)	Measured ρ ± err (")	Resid θ	Resid ρ	Notes?
2017.2959	10402+3824	STF1459	-027-015 G	-028-016 W	2014	152.1	5.33	5	152.2 ± 0.0	5.423 ± 0.004	0.1	0.093	*
2017.2822	10417+1044	STT 227	+020-001 W	+020-001 W	2010	2.9	0.89	5	1.9 ± 0.2	0.903 ± 0.003	-1.0	0.013	*
2017.2959	10447+2042	STF1468	+040-012 G	+038-012 U	2010	334.5	4.24	4	333.5 ± 0.0	4.265 ± 0.001	-1.0	0.025	*
2017.2795	10462-0546	STF1470	-015+005 G	-022+002 W	2005	193.7	1.40	5	190.8 ± 0.2	1.459 ± 0.004	-2.9	0.059	*
2017.2959	10473+2235	STT 228	-037-001 W	-037-001 W	2015	170.4	0.62	5	169.9 ± 0.7	1.650 ± 0.003	-0.5	1.035	*
2017.3315	10512-0906	BU 111AB	-003-001 G	-004+001 G	2013	4.8	3.40	5	4.2 ± 0.1	3.282 ± 0.004	-0.6	-0.118	*
2017.2795	10575-1105	A 1770AB-C	-011+018 W	-011+018 W	2012	8.7	4.51	5	8.0 ± 0.1	4.561 ± 0.002	-0.7	0.051	*
2017.3397	11023+3049	STF1501	-047-042 W	-047-042 W	2015	186.0	1.30	5	184.5 ± 0.1	1.317 ± 0.002	-1.5	0.017	*
2017.3616	11024+8313	STF1479	-025-021 W	-022-013 W	2011	25.4	4.46	5	24.7 ± 0.3	4.588 ± 0.013	-0.7	0.128	*
2017.3397	11050+3825	HO 378	-065-031 W	-065-031 W	2015	236.0	1.00	5	236.6 ± 0.0	1.092 ± 0.002	0.6	0.092	*
2017.3397	11137+4105	HO 50	-014+016 G	-014+016 W	2003	35.1	3.03	5	35.0 ± 0.1	3.005 ± 0.001	-0.1	-0.025	*
2017.3397	11151+3735	STT 232AB	+003-005 W	+003-005 W	2014	246.0	0.70	5	243.2 ± 0.6	0.604 ± 0.004	-2.8	-0.096	*
2017.3315	11154+2734	STF1521	-035+001 G	-036+001 W	2013	96.3	3.65	5	97.6 ± 0.0	3.705 ± 0.006	1.3	0.055	*
2017.3616	11156+5947	STF1519	-029-015 G	-027-018 W	2015	290.0	1.40	5	289.0 ± 0.9	1.485 ± 0.019	-1.0	0.085	*
2017.3562	11195+4728	STF1525	-003-008 G	-004-005 W	2010	174.0	4.00	5	173.2 ± 0.1	2.285 ± 0.006	-0.8	-1.715	*
2017.3616	11328+6004	KR 38	+004+004 G	+009+005 U	2014	52.3	2.78	5	52.6 ± 0.5	2.802 ± 0.013	0.3	0.022	*
2017.4027	11329+5525	A 1593	-025-003 G	-026-002 U	2011	255.0	4.00	5	255.4 ± 0.0	4.177 ± 0.003	0.4	0.177	*
2017.3562	11332+4927	HU 727	-023-021 W	-023-021 W	2014	205.0	1.20	5	205.2 ± 0.0	1.253 ± 0.001	0.2	0.053	
2017.3315	11367+2128	STF1558AB	-061-030 W	-061-030 W	2010	165.1	1.28	5	168.2 ± 0.1	1.265 ± 0.008	3.1	-0.015	*
2017.3562	11371+4040	A 1996	-016+013 W	-016+013 W	2014	190.0	2.00	5	188.9 ± 0.2	1.988 ± 0.001	-1.1	-0.012	*
2017.3616	11388+6421	STF1559	+018+006 W	+018+006 W	2013	322.9	1.96	5	323.6 ± 0.0	1.974 ± 0.005	0.7	0.014	*
2017.2795	11438+1831	BRT2412	-147+010 G	-157-004 W	2015	291.9	4.95	5	290.9 ± 0.1	4.886 ± 0.008	-1.0	-0.064	*
2017.3562	11517+4449	HJ 842	-067-010 G	-067-011 W	2010	88.6	3.15	5	88.9 ± 0.0	3.104 ± 0.011	0.3	-0.046	*
2017.3397	11529+3050	STF1576	-067+024 G	-066+026 W	2013	241.1	5.18	5	241.2 ± 0.0	5.369 ± 0.002	0.1	0.189	*
2017.3562	11551+4629	STF1579AB-C	-010-003 W	-010-003 W	2014	42.0	3.90	5	41.8 ± 0.1	3.882 ± 0.005	-0.2	-0.018	*
2017.3726	11561+4533	STF1581	-024-006 G	-026-007 W	2012	169.9	2.39	5	170.6 ± 0.0	2.459 ± 0.003	0.7	0.069	*
2017.3397	11563+3527	STT 241	-097+010 G	-085-023 W	2011	145.5	1.83	5	146.6 ± 0.1	1.830 ± 0.006	1.1	0.000	*
2017.3616	11598+5324	STT 243	-044-020 W	-044-020 W	2015	8.0	1.10	5	8.2 ± 0.0	1.169 ± 0.001	0.2	0.069	
2017.3397	12005-1517	A 2162	-026+023 G	-026+0221 W	1999	151.9	1.41	5	149.4 ± 0.4	1.716 ± 0.019	-2.5	0.306	*
2017.4055	12120+6836	STF1611	+006-003 G	+004-002 W	2000	5.0	1.80	5	4.1 ± 0.0	1.890 ± 0.001	-0.9	0.090	*
2017.3616	12137+7826	HU 891	-001-087 G	+002-075 W	1999	13.0	2.73	5	12.0 ± 0.1	2.808 ± 0.002	-1.0	0.078	*
2017.3726	12167+3004	AG 176	+010-068 G	+011-064 U	2001	185.3	2.65	5	183.7 ± 0.1	2.336 ± 0.005	-1.6	-0.314	*
2017.3836	12189+5622	STF1630	-011-013 W	-011-013 W	2004	169.0	2.40	5	171.1 ± 0.0	2.542 ± 0.001	2.1	0.142	
2017.3562	12207+2255	STF1634	-072-029 W	-072-029 W	2014	147.2	5.08	5	147.3 ± 0.0	5.380 ± 0.011	0.1	0.300	*
2017.3397	12217+0333	HU 737	+028-057 G	+028-057 U	2013	56.6	2.64	5	55.8 ± 0.1	2.648 ± 0.010	-0.8	0.008	*

Table 3 continues on next page.

Measurements of 427 Double Stars With Speckle Interferometry ...

Table 3 (continued): Common Proper Motion Pairs (CPM) Measured With Speckle

Date	WDS No	Disc/Comp	PM A	PM B	Last Yr	Last θ	Last ρ	Msrs	Measured θ ± err (°)	Measured ρ ± err (")	Resid θ	Resid ρ	Notes?
2017.3836	12257+4444	STF1642	-071-005 G	-072-004 W	2012	179.4	2.53	5	179.6 ± 0.1	2.488 ± 0.004	0.2	-0.042	*
2017.3397	12311+0207	AG 178	-008-014 W	-008-014 W	2005	284.2	1.33	5	285.5 ± 0.4	1.314 ± 0.005	1.3	-0.016	
2017.3616	12321+7449	STF1654	-010-008 G	-010-007 W	2006	22.8	3.77	5	22.5 ± 0.0	3.834 ± 0.000	-0.3	0.064	*
2017.3589	12396+6440	STF1667AB	+017-010 W	+017-010 W	2015	38.0	1.10	5	40.2 ± 0.1	1.244 ± 0.003	2.2	0.144	
2017.3836	12406+4017	HJ 2617AB	-020+062 G	-020+063 W	2010	2.0	5.70	5	2.5 ± 0.0	5.762 ± 0.004	0.5	0.062	*
2017.3589	12427+3349	STF1672	+000-006 G	+004-004 U	2013	313.0	4.30	5	312.7 ± 0.1	4.393 ± 0.015	-0.3	0.093	*
2017.3397	12438+0733	STF1674	+001+009 W	+001+009 W	2013	173.5	2.38	5	172.9 ± 0.0	2.322 ± 0.003	-0.6	-0.058	*
2017.3836	12460+4949	STF1679AB	+013+003 G	+013+001 U	2013	207.0	5.90	5	208.0 ± 0.0	5.909 ± 0.004	1.0	0.009	*
2017.3397	12533+1310	HU 894	+003-029 W	+003-029 W	2011	145.2	1.19	5	143.1 ± 0.1	1.237 ± 0.002	-2.1	0.047	*
2017.3589	12563+5406	STF1695AB	-062-002 W	-087+003 W	2015	282.0	3.60	5	280.6 ± 0.1	3.867 ± 0.004	-1.4	0.267	*
2017.3616	12564-0057	STT 256	+027-092 W	+027-092 W	2013	101.0	1.10	5	100.7 ± 0.0	1.057 ± 0.001	-0.3	-0.043	*
2017.3589	12574+3022	STF1696	-022-006 G	-020-006 W	2014	203.2	3.53	5	203.7 ± 0.1	3.651 ± 0.004	0.5	0.121	*
2017.3644	12587+2728	STF1699	-122-104 G	-128-103 W	2014	8.0	1.70	5	8.7 ± 0.1	1.650 ± 0.023	0.7	-0.050	*
2017.3616	12592+8256	STF1720	-018+001 W	-018+001 W	2009	329.3	1.62	5	329.4 ± 0.0	1.701 ± 0.001	0.1	0.081	
2017.4055	13007+7343	HJ 2633	-038-111 G	-043-112 G	2013	90.3	4.67	5	91.4 ± 0.0	4.633 ± 0.001	1.1	-0.037	*
2017.4027	13026+5625	KR 41	+022+012 G	-025+008 U	2003	333.8	3.68	5	334.0 ± 0.0	3.614 ± 0.002	0.2	-0.066	*
2017.4247	13034-0626	BU 928AB	-021-023 W	-	2011	318.8	2.41	5	318.7 ± 0.1	2.523 ± 0.006	-0.1	0.113	
2017.4055	13048+7302	BU 799AB	-019+010 W	-017+013 W	2013	265.1	1.39	5	266.9 ± 0.3	1.343 ± 0.012	1.8	-0.047	*
2017.4055	13128+4030	A 1606	-062+007 W	-062+007 W	2012	16.8	1.27	5	16.8 ± 0.1	1.297 ± 0.003	0.0	0.270	
2017.4055	13166+5034	STT 263	-045+023 W	-051+031 W	2011	135.8	1.72	5	137.9 ± 0.0	1.735 ± 0.004	2.1	0.015	*
2017.3562	13207+0257	STF1734	-060-012 W	-060-012 W	2014	174.0	1.10	5	173.1 ± 0.6	1.069 ± 0.011	-0.9	-0.031	*
2017.3562	13243+0124	STF1742	-026-014 W	-026-014 W	2012	356.0	0.90	5	357.0 ± 0.1	0.940 ± 0.001	1.0	0.040	*
2017.4164	13261+3509	A 1855	+005+020 G	+001+020 U	2011	291.5	3.58	5	290.9 ± 0.1	3.691 ± 0.006	-0.6	0.111	*
2017.4055	13288+5956	STF1752AB	-084+031 W	-084+031 W	2010	107.9	0.97	5	107.4 ± 0.3	0.973 ± 0.005	-0.5	0.003	*
2017.4164	13324+3649	STF1755	-019-022 G	+018-020 W	2012	129.9	4.21	5	129.6 ± 0.0	4.185 ± 0.005	-0.3	-0.025	*
2017.4055	13341+6746	STF1767	-180+021 G	-180+019 U	2013	344.5	4.22	5	344.8 ± 0.0	4.143 ± 0.010	0.3	-0.077	*
2017.3644	13344+2617	STF1760	+010+001 G	+009+001 U	2007	64.0	8.70	5	64.2 ± 0.0	8.824 ± 0.001	0.2	0.124	*
2017.3644	13346+3308	BU 933AB	+049-055 G	+049-054 W	2011	22.0	2.70	5	22.7 ± 0.1	2.827 ± 0.003	0.7	0.127	*
2017.4027	13354+5955	KR 42	-071+023 G	-070+022 G	2011	215.4	3.73	5	216.6 ± 0.0	3.723 ± 0.002	1.2	-0.007	*
2017.4055	13356+4939	AG 190	+007-002 G	+007-006 G	2011	12.8	2.56	5	13.3 ± 0.0	2.619 ± 0.003	0.5	0.059	*
2017.4055	13367+6947	STF1771	-019+032 W	-019+032 W	2013	82.9	1.79	5	82.8 ± 0.1	1.786 ± 0.004	-0.1	-0.004	*
2017.4164	13368+0650	A 1611	-048+002 W	-048+002 W	2010	121.7	0.86	5	120.7 ± 1.0	0.885 ± 0.011	-1.0	0.025	*
2017.4055	13377+5043	STF1770	-012+004 G	-016+004 W	2012	126.0	1.77	5	123.0 ± 0.2	1.669 ± 0.006	-3.0	-0.101	*
2017.4027	13509+4422	A 1613AB	-075+031 U	-076+028 U	2011	260.7	3.10	5	261.4 ± 0.1	3.136 ± 0.004	0.7	0.036	*
2017.4164	13563+0517	STT 273AB	+045-059 W	+045-059 W	2014	112.2	1.01	5	111.7 ± 0.4	0.972 ± 0.002	-0.5	-0.038	*

Table 3 continues on next page.

Measurements of 427 Double Stars With Speckle Interferometry ...

Table 3 (continued): Common Proper Motion Pairs (CPM) Measured With Speckle

Date	WDS No	Disc/Comp	PM A	PM B	Last Yr	Last θ	Last ρ	Msrs	Measured θ ± err (°)	Measured ρ ± err (")	Resid θ	Resid ρ	Notes?
2017.4055	13571+3426	BU 937	-040+020 W	-040+020 W	2011	135.3	1.03	5	136.6 ± 0.1	1.052 ± 0.003	1.3	0.022	*
2017.4164	13591+2549	STF1793	+011-005 G	+004-003 W	2015	241.3	4.64	5	242.0 ± 0.0	4.854 ± 0.002	0.7	0.214	*
2017.4164	14033+0557	HWE 29AB	-103+009 W	-103+009 W	2012	235.8	1.28	5	235.2 ± 0.1	1.421 ± 0.000	-0.6	0.014	*
2017.4466	14101+2636	STF1808AB	-173-055 W	-173-055 W	2011	81.0	2.60	5	82.8 ± 0.1	2.624 ± 0.001	1.8	0.024	*
2017.4247	14116+2802	STF1810	-027+047 G	-026+044 W	2013	183.7	2.36	5	183.7 ± 0.0	2.392 ± 0.000	0.0	0.032	*
2017.4411	14143+3356	STF1818	-108+029 G	-104+028 U	2013	330.1	5.50	5	330.5 ± 0.0	5.473 ± 0.003	0.4	-0.027	*
2017.4247	14158+1018	STF1823AB-C	+119-193 U	+119-193 W	2012	147.0	3.84	5	146.7 ± 0.0	3.933 ± 0.001	-0.3	0.093	
2017.4164	14203+0835	STT 281	+014-022 W	+014-022 W	2010	165.6	1.50	5	165.6 ± 0.4	1.456 ± 0.006	0.0	-0.044	
2017.4164	14270+0341	STF1842	-052-069 W	-057-090 W	2010	198.0	2.74	5	197.0 ± 0.0	2.743 ± 0.001	-1.0	0.003	*
2017.4411	14279+2123	HO 543	+042-095 G	-044-095 U	2010	236.9	4.59	5	237.5 ± 0.0	4.669 ± 0.000	0.6	0.079	*
2017.4027	14339+5514	STF1860	-011+014 W	-011+014 W	2011	112.3	0.99	5	112.3 ± 0.1	1.045 ± 0.004	0.0	0.055	*
2017.4466	14363+1924	STF3087	-004-008 W	-004-008 G	2005	222.1	2.25	5	222.9 ± 0.3	2.378 ± 0.007	0.8	0.128	*
2017.4466	14403+1206	HWE 34	-056-005 G	-054-005 G	2012	12.8	2.58	5	12.4 ± 0.1	2.599 ± 0.008	-0.4	0.019	*
2017.4247	14417+0932	STF1866	-050+024 W	-050+024 W	2010	203.5	0.74	5	205.0 ± 0.3	0.742 ± 0.003	1.5	0.002	*
2017.4027	14436+3745	STF1875	-024+052 U	-024+050 G	2012	128.1	3.04	5	129.4 ± 0.1	3.085 ± 0.001	1.3	0.045	
2017.4247	14471+0058	STF1881	-028-029 W	-028-029 W	2011	0.3	3.44	5	0.0 ± 0.0	3.462 ± 0.001	-0.3	0.022	*
2017.4466	14524+1757	A 2071	-029-012 W	-029-012 W	2011	270.0	1.40	5	272.9 ± 0.1	1.295 ± 0.021	2.9	-0.105	*
2017.4411	14531+7811	HU 908AB	-013-002 G	-011-002 W	2012	237.3	1.52	5	236.3 ± 0.3	1.590 ± 0.008	-1.0	0.070	*
2017.4027	14545+3406	STF1891	-067+044 G	-067+045 W	2010	246.6	3.58	4	247.8 ± 0.0	3.519 ± 0.001	1.2	-0.061	*
2017.4027	14584+4403	STF1896AB	-061-068 G	-058-069 W	2013	277.0	4.05	5	277.6 ± 0.0	4.091 ± 0.002	0.6	0.041	*
2017.4493	15058+5841	A 1114	-020+034 W	-020+034 W	2010	285.6	1.22	5	286.1 ± 0.4	1.225 ± 0.005	0.5	0.005	
2017.4247	15087-0059	STF3090AB	+030-096 W	+030-096 W	2010	286.3	0.62	5	287.2 ± 0.7	0.627 ± 0.024	0.9	0.007	*
2017.4438	15126+1523	STF1917	-005-009 G	-008-012 U	2011	232.9	2.52	5	232.6 ± 0.1	2.448 ± 0.008	-0.3	-0.072	*
2017.4438	15138+1427	STF1923AB	-056-012 G	-054-014 W	2010	11.6	4.64	5	11.3 ± 0.2	4.841 ± 0.008	-0.3	0.201	*
2017.4247	15227-1654	HU 307	-012-001 G	-014+000 W	1999	2.7	2.94	5	2.4 ± 0.0	2.959 ± 0.001	-0.3	0.019	*
2017.4466	15257+2638	STF1941	+016-005 G	-018-007 W	2014	212.0	1.40	5	212.2 ± 0.0	1.397 ± 0.002	0.2	-0.003	*
2017.4247	15264+0822	A 1119	-012-002 W	-012-002 W	2012	178.5	1.57	5	179.7 ± 0.9	1.796 ± 0.026	1.2	0.226	*
2017.4247	15276+0522	STF1943	-031-028 G	-031-031 W	2014	148.0	4.93	5	147.2 ± 0.2	5.093 ± 0.025	-0.8	0.163	*
2017.4466	15300+2530	STF1950	-004+007 W	-005+008 W	2013	91.3	3.37	5	91.8 ± 0.0	3.338 ± 0.002	0.5	-0.032	*
2017.4493	15361+4849	HU 652	-020-012 W	-020-012 W	2011	185.1	1.12	5	185.9 ± 0.0	1.158 ± 0.001	0.8	0.038	*
2017.4493	15361+5531	A 1124	-001+055 G	-003+056 W	2012	143.2	1.38	5	143.3 ± 0.2	1.458 ± 0.003	0.1	0.078	*
2017.4247	15391-0834	STF3094	-102-016 G	-108-024 W	2010	297.4	2.49	5	296.4 ± 0.0	2.575 ± 0.001	-1.0	0.085	*
2017.4466	15398+2117	AG 197	+022-024 G	+021-026 U	2010	126.7	3.11	5	126.8 ± 0.0	3.183 ± 0.006	0.1	0.073	*
2017.4247	15443-1943	HU 654	-029-024 W	-029-024 W	1991	11.7	1.08	5	14.2 ± 0.8	1.079 ± 0.021	2.5	-0.001	
2017.4438	15453+0432	AG 198	+003-015 W	+002-016 W	2013	144.4	2.25	5	144.3 ± 0.1	2.249 ± 0.005	-0.1	-0.001	*

Table 3 concludes on next page.

Measurements of 427 Double Stars With Speckle Interferometry ...

Table 3 (conclusion): Common Proper Motion Pairs (CPM) Measured With Speckle

Date	WDS No	Disc/Comp	PM A	PM B	Last Yr	Last θ	Last ρ	Msrs	Measured θ ± err (°)	Measured ρ ± err (")	Resid θ	Resid ρ	Notes?
2017.4247	15470-1908	HU 656	-004-009 U	-004-009 W	2002	16.9	1.36	5	15.0 ± 0.8	1.484 ± 0.007	-1.9	0.124	
2017.4247	15492-0314	STF1974	-007-002 G	-006-001 G	2009	158.7	2.43	5	157.7 ± 0.2	2.467 ± 0.021	-1.0	0.370	*
2017.4493	15499+4247	STF1982	-032+025 G	-033+027 U	2008	298.0	4.94	5	299.5 ±0.1	4.903 ±0.002	1.5	-0.037	*
2017.4466	15509+1911	A 2078	-015-016 W	-015-016 W	2010	166.3	1.09	5	165.3 ± 0.2	1.14 ± 0.008	-1.0	0.050	*
2017.4247	15589-0304	STF3101	-237+042 G	-237-042 W	2009	73.4	2.22	5	72.7 ± 0.0	2.200 ± 0.001	-0.7	-0.020	*
2017.4438	16179-0724	A 23	-013-006 W	-013-006 W	1999	69.6	1.89	5	71.6 ± 0.3	1.95 ± 0.011	2.0	0.060	
2017.4438	16394-0306	BU 820AB	-060+039 G	-059+040 W	2010	235.2	4.25	5	234.6 ± 0.1	4.414 ± 0.003	-0.6	0.164	*
2017.4438	16462-1721	SKI 10	-023-017 G	-027-017 U	2014	84.8	3.37	5	84.0 ± 0.3	3.434 ± 0.008	-0.8	0.064	*

Notes to Table 3 (CPM Pairs)

WDS Number	Parallax	Parallax Source	Distance (Parsecs)	Min Sep (AU)	Plot Figure	Comments
02123+2357AB	27.3 ± 1.19	H	37	65	4	The PM vector (331°, 1.8"), shown as an orange line on the plot, is a rough fit to data.
02214+0853	8.31 ± 0.81	H	120	184	-	
02244+1130	5.39 ± 0.29	G	186	529	-	
02429-0629	8.13 ± 0.27	G	123	221	5	A short arc might be forming.
02447-0158	3.94 ± 0.26	G	254	1,469	-	Very tight clustering of data on the plot.
02527+0628	5.10 ± 0.90	H	196	531	-	Tight grouping.
03051+2755	-	-	-	-	-	The PM vector (32°, 2.3") does not fit the observations. This suggests that one (or both) of the PM vectors may be wrong. All of the measurements (except one from 1914) fall within a 0.5" region.
03088+3528	7.83 ± 0.34	G	128	484	-	
03242+1733	9.49 ± 3.48	H	N/A	N/A	-	The Hipparcos parallax has an error that exceeds 25%.
03258-1304	2.63 ± 0.42	G	380	529	-	
03312+1947	9.2 ± 0.32	G	109	249	-	The PM vector (193°, 2.4") is right for theta, but twice the value for rho. The data plot is showing an emerging trend that may lead to a short arc binary.
03545-1243	1.95 ± 0.73	G	N/A	N/A	-	The Gaia parallax has an error that exceeds 25%.
03554+1738	3.79 ± 0.25	G	264	1,045	-	
04024-0700	10.91 ± 0.23	G	92	282	-	
04059+1058	7.98 ± 0.42	G	125	363	-	
04160+0027	7.11 ± 0.35	G	141	462	-	
04409+0058AB	3.71 ± 0.41	G	270	1,469	-	
04448+0517AB	25.56 ± 0.24	G	39	178	6	This pair is trending towards a short arc binary.
04551-0033AB-C	2.87 ± 0.27	G	648	1,530	-	
05030-0840	5.31 ± 0.69	G	188	678	-	

Measurements of 427 Double Stars With Speckle Interferometry ...

Notes to Table 3 (CPM Pairs) continued

WDS Number	Parallax	Parallax Source	Distance (Parsecs)	Min Sep (AU)	Plot Figure	Comments
05079+0824	A: 18.91 ± 0.28 B: 18.67 ± 0.48	G G	53	127	-	A weighted parallax (18.79 mas) was used. The parallax bars overlap 51%. Given the nearly identical proper motions (of moderately high value), this pair is probably physical.
05118+0102	5.12 ± 1.07	H	195	328	-	
05147-0704	2.59 ± 0.46	G	386	1,629	-	
05152+0826	10.32 ± 0.30	G	97	452	-	
05162-0329	5.09 ± 1.14	H	196	132	-	
05177+0441 AB	5.21 ± 0.24	G	192	696	-	
05204-0805 AB	6.10 ± 0.37	G	164	108	-	Tight grouping of data points, but a trend may be starting to form.
05217-0203	4.17 ± 0.26	G	240	839	-	
05231+0103	3.52 ± 0.51	G	284	1,403	-	
05231-0806	4.43 ± 0.89	H	2,326	142	7	A very strong trend is emerging in the data.
05252+0155	1.84 ± 1.10	H	N/A	N/A	-	Hipparcos parallax is not usable (error too large).
05265+0256 AB	6.86 ± 0.89	H	146	461	-	
05312+0318 AB	2.87 ± 0.84	H	N/A	N/A	-	Hipparcos parallax is not usable (error too large).
05314-0206 AB	2.49 ± 0.27	H	N/A	N/A	-	Hipparcos parallax is not usable (error too large).
05355-0422	2.77 ± 0.82	H	N/A	N/A	-	Hipparcos parallax is not usable (error too large).
05381-0011 AB	3.72 ± 1.25	H	N/A	N/A	-	Hipparcos parallax is not usable (error too large).
05457-1447					8	Trend forming.
05495-1234					-	Only 4 measurements.
05514-1139	2.71 ± 0.88	H	N/A	N/A	-	Hipparcos parallax is not usable (error too large).
06041-1541	B: 3.28 ± 0.92	H	N/A	N/A	-	Hipparcos parallax is not usable (error too large).
06049-0243 AB	A: 2.27 ± 0.28 B: 2.52 ± 0.38	G G	418	2,065	-	A weighted parallax (2.39 mas) was used. The overlap in the parallaxes is 98%. This pair is probably physical. But no trend can yet be seen in the data plot; the past measurements are all very tightly clustered together.
06074-0400 AB	A: 4.53 ± 0.27 B: 4.04 ± 0.27	G G	233	471	-	A weighted parallax (4.29 mas) was used. The overlap in the parallaxes is only 5%. Yet Gaia has identical proper motions for this pair. Despite the weak indicator provided by the parallaxes, the pair does indeed appear to be physical.
06167-1203	6.98 ± 0.45	G	143	260	-	
06238-1947	2.43 ± 0.59	H	412	325	-	
06252-1056	5.37 ± 1.01	H	186	314	-	
06372-1415	A: 5.63 ± 0.31 B: 5.69 ± 0.27	G G	177	712	-	A weighted parallax (5.66 mas) was used. There is an overlap of 98% in the parallax windows. Given that these two stars have the same (albeit small) proper motion, they are most likely a physical pair. However, the plot of the measurements shows a very tight clustering with no apparent trend showing.
06420-1600	2.47 ± 0.40	G	405	1,599	-	
06484-1326 AB	7.75 ± 0.78	H	129	156	-	

Notes to Table 3 (CPM Pairs) continued

WDS Number	Parallax	Parallax Source	Distance (Parsecs)	Min Sep (AU)	Plot Figure	Comments
06488-1613	5.57 ± 0.31	G	180	591	-	
06573-1005	18.29 ± 0.25	G	55	79	-	
08042-0151	3.54 ± 0.62	G	282	486	-	Tightly grouped data plot.
08046+5445	2.44 ± 0.29	G	410	680	-	
08091+3714	12.39 ± 0.37	G	81	100	-	
08101+0403	A: 7.30 ± 0.63 B: 4.67 ± 0.30	G G	137 214			There is absolutely no overlap in the parallax windows. On the basis of parallax alone, this pair would not be physical, as the stars are (by parallax) 77 parsecs apart. Yet the proper motion data suggests a physical connection. This star needs more observations, but not on a frequent schedule. 114 years of observations yields a cluster of data that fits inside a 0.50" circle.
08109-0455	2.96 ± .049	G	338	483	9	A trend (perhaps short arc binary?) is emerging.
08136+1023	5.70 ± 1.07	H	175	140	-	
08138+0159	7.02 ± 0.67	H	142	140	10	This pair is one of those cases where the last measurement produces a high residual. The data plot shows an emerging short arc.
08140-1740	-	-	-	-	11	Very interesting case. This pair is showing a very strong linear pattern, but given the identical proper motions, we may be seeing a nearly edge-on short arc orbit (a large orbit would appear linear as the companion passes the primary). The R^2 value shown on the chart is generated by Excel using the Trend Line function and represents the fit of the trend line to the data. 1.00 is a perfect fit, and this system is showing an R^2 value of 0.9569, an extremely high correlation. Note, however, that Excel assigns equal weight to all of the data in the sample, something that would not actually be done when analyzing an orbit (or linear case).
08296+5203AaAb	-	-	-	-	-	Only 5 measurements.
08298+5112	A: 4.62 ± 0.49 B: 3.85 ± 0.24	G G	216 260	-	-	There is no overlap in the parallax windows.
08342+5655	5.17 ± 0.33	G	193	290	12	This pair may be starting to exhibit a short arc.
08421+2501	A: 5.91 ± 0.37 B: 5.94 ± 0.38	G G	169	567		A weighted parallax of 5.92 mas was used. There is a 98% overlap in the parallax windows. Given the nearly identical (and significant) proper motions, this pair is most likely physical.
08432+3849	7.72 ± 0.93	G	130	161	-	
08437+1654	-	-	-	-	13	Linear trend, R^2 = 0.8735. This pair could be an edge-on short arc binary.
08444+1555	-	-	-	-	-	Evn1980.159 appears to be a quadrant reversal.
08453-0236	12.51 ± 0.32	G	80	369	-	Very tight grouping of measurements.
08461+0748	13.64 ± 0.34	G	73	205	-	
08466+3829	4.71 ± 0.26	G	212	1,062	-	Very tight grouping of measurements.
08482+0235	7.30 ± 0.33	G	133	375	-	Very tight grouping of measurements.
08500+3935	7.87 ± 0.54	G	127	159	14	Trend forming. PM vector (180°, 1.5") does not fit observations.
08505+2308	B: 5.45 ± 0.50	G	183	417	-	A trend is beginning to emerge.

Measurements of 427 Double Stars With Speckle Interferometry ...

Notes to Table 3 (CPM Pairs) continued

WDS Number	Parallax	Parallax Source	Distance (Parsecs)	Min Sep (AU)	Plot Figure	Comments
08508+3504 AB	18.41 ± 0.26	G	54	190	-	
08516-0711 AB	7.31 ± 0.60	H	137	157	-	
08538-0035 AB	A: 6.22 ± 0.50 B: 5.20 ± 0.32	G G	161 192	-	-	The stars are probably not physical. But the proper motions are identical. Puzzling case.
08542-0846	2.44 ± 0.24	G	410	480	-	
08548+4335	18.55 ± 0.29	G	54	201	-	
08549-0749	3.97 ± 0.30	G	252	811	-	Manual solution with STB. (Companion star had to be selected manually since STB's automatic detection routine failed to find it.)
08561+4341	4.80 ± 1.03	H	208	280	-	
08598-0607	-	-	-	-	-	Only 5 measurements.
09016-0832	-	-	-	-	-	There appear to be several quadrant reversals among the measurements: A 1918.28, A 1922.98, A 1931.72, B 1937.27, Wor 1980.254 and Wor 1983.156.
09020+0240	4.71 ± 0.53	G	212	234	-	A vague trend seems to be shaping up.
09033+4740	6.56 ± 1.49	H	152	111	-	
09071+3037	A: 6.32 ± .038 B: 6.26 ± 0.44	G G	159	638	-	Weighted parallax (6.29 mas) used. 85% overlap in the parallax values.
09080+8102	4.06 ± 0.61	H	246	635	15	Trend emerging. PM vector (195°, 2.8") does not match the observations.
09095+0256	6.07 ± 0.66	H	165	236	-	
09101-1507	3.39 ± 0.44	G	295	532	-	
09103+5223	2.47 ± 0.34	G	405	2,000	16	Trend forming.
09118-1649	-	-	-	-	17	Trend forming.
09127+1632	3.49 ± 0.35	G	287	516	-	
09149+0413	3.21 ± 1.16	H	N/A	N/A	-	The error in the Hipparcos parallax is too large to make the measurement usable.
09161-0821	4.78 ± 0.42	G	209	335	-	
09168-0050	-	-	-	-	18	Short but pronounced linear trend. May be a nearly edge-on short arc binary?
09188-1025 AB	5.98 ± 0.46	G	167	505	-	
09208+6121 AB	4.84 ± 1.15	H	207	185	-	
09235+3908	5.16 ± 0.49	G	194	721	-	
09239+2754 AB	6.40 ± 1.01	H	156	191	-	
09256+5401 AB	5.56 ± 0.32	G	180	1,038	-	High residual due to CTT2014.282 having higher theta than the mean. My measurement plots well with the mean.
09277+1545	-	-	-	-	-	Phl1934.12 appears to be a quadrant reversal.
09296-0307	2.94 ± 0.27	G	340	313	-	
09300+4216	7.39 ± 1.14	H	135	213	19	Trending linear, but with identical proper motions, this may be a short piece of an arc. Cll1980 appears to be a quadrant reversal.
09310-1544	7.59 ± 0.96	H	132	165	-	This pair may be starting to show a short arc. Very rough and difficult to be sure.
09315+0128	10.45 ± 1.29	H	96	329	-	

Measurements of 427 Double Stars With Speckle Interferometry ...

Notes to Table 3 (CPM Pairs) continued

WDS Number	Parallax	Parallax Source	Distance (Parsecs)	Min Sep (AU)	Plot Figure	Comments
09415-1829	18.09 ± 1.86	H	55	55	-	Scattered grouping. Is Tok2010 a measurement of the wrong star?
09450+7643	A: 7.67 ± 1.11 B: 8.78 ± 0.29	H G	121	229	-	A weighted parallax of 8.26 mas was used, and the parallax windows have a 10% overlap. Probably a physical pair, despite the significant difference in proper motions. Cll 1979.999 looks like a quadrant reversal.
09551+6854AB	6.33 ± 0.26	G	158	332	-	A weak trend is starting to show.
09572+4554	14.05 ± 0.41	G	71	327	-	
09591+8023	4.57 ± 0.77	H	219	360	-	
10040+3239	13.08 ± 1.03	H	76	64	-	
10056+3105	4.66 ± 1.50	H	N/A	N/A	20	The error is too large to make the Hipparcos parallax usable. A short arc is forming.
10114+7302	7.48 ± 0.27	G	134	496	-	
10151+1907	-	-	-	-	21	Tight grouping. The PM vector (65°, 2.6") does not fit the observations.
10180+1711	1.78 ± 0.62	G	N/A	N/A	-	The error in the parallax measurement makes the parallax unusable.
10181+2731	3.77 ± 0.28	G	265	1,205	-	Tight grouping with five wide outliers.
10206-1621	4.76 ± 0.66	G	210	370	-	
10234+2630	-	-	-	-	22	Definite trend developing.
10256+0847	6.08 ± 0.29	G	164	587	-	
10260+5237	12.62 ± 0.51	G	79	221	23	Definite trend forming.
10321+8136	-	-	-	-	-	Only 4 measurements.
10333+3740	7.03 ± 0.24	G	142	772	-	
10336+1513	5.85 ± 0.79	G	171	940	-	Tight grouping.
10338+2321	6.70 ± 0.40	G	149	663	-	
10402+3824	3.14 ± 0.27	G	318	1,697	-	Tight grouping.
10417+1044	-	-	-	-	-	May be trending to a short arc binary.
10447+2042	7.81 ± 0.29	G	128	549	-	
10462-0546	2.62 ± 0.92	G	N/A	N/A	24	The error is too large to make the parallax usable. The PM vector (247°, 1.3") matches observations closely. The may be a QR in BAB1933.26.
10473+2235	6.32 ± 1.20	H	158	97	25	Manual solution. The data may be starting to reveal a short arc.
10512-0906AB	A: 5.20 ± 0.45 B: 4.42 ± 0.50	G G	208	706	-	Weighted parallax of 4.82 mas. There is a 10% overlap in the error windows. Given the CPM, this pair is probably physical.
10575-1105AB-C	-1.10 ± 3.04	H	N/A	N/A	-	The error is too large to make the parallax usable.
11023+3049	-	-	-	-	26	Strong trend developing.
11024+8313	7.59 ± 1.13	H	132	588	-	The PM vector (21°, 1.5") does not align well with the observations. The data cluster fits inside a 0.5" region.
11050+3825	7.35 ± 1.05	H	136	147	27	A strong trend is developing.
11137+4105	8.24 ± 0.23	G	121	368	-	
11151+3735AB	3.18 ± 1.17	H	N/A	N/A	-	The error is too large to make the parallax usable.
11154+2734	8.06 ± 0.59	G	124	453	-	
11156+5947	4.58 ± 0.23	G	218	317	-	Starting to develop a loose trend in the data plot.
11195+4728	3.97 ± 0.29	G	252	574	-	
11328+6004	3.45 ± 0.55	G	290	806	-	
11329+5525	4.23 ± 0.25	G	236	957	-	
11388+6421	4.74 ± 0.57	H	211	413	28	
11438+1831	19.78 ± 0.30	G	51	250	-	
11517+4449	6.06 ± 0.22	G	165	520	-	

Notes to Table 3 (CPM Pairs) continued

WDS Number	Parallax	Parallax Source	Distance (Parsecs)	Min Sep (AU)	Plot Figure	Comments
11529+3050	6.38 ± 0.25	G	157	812	-	
11551+4629AB-C	4.72 ± 0.58	H	212	784	-	
11561+4533	3.55 ± 0.38	G	282	672	-	
11563+3527	7.41 ± 0.40	G	135	247	-	Scattered data plot that is beginning to converge on a trend.
12005-1517	7.89 ± 0.43	G	127	179	-	Weak trend may be starting to emerge.
12120+6836	4.9 ± 0.55	G	204	376	-	
12137+7826	8.12 ± 0.29	G	123	336	29	The PM vector (14°, 1.2") does not match the observations.
12167+3004	14.36 ± 0.30	G	70	185	-	
12207+2255	3.50 ± 1.16	H	N/A	N/A	-	The error makes the parallax unusable.
12217+0333	10.36 ± 0.32	G	97	255	-	
12257+4444	4.93 ± 0.30	G	203	513	-	
12321+7449	4.17 ± 0.23	G	240	904	-	
12406+4017AB	15.39 ± 0.29	G	65	373	-	
12427+3349	3.66 ± 0.23	G	273	1,123	-	
12438+0733	5.01 ± 1.64	H	N/A	N/A	-	The error makes the parallax unusable.
12460+4949AB	5.21 ± 0.26	G	192	1,138	-	
12533+1310	-	-	-	-	30	Strong trend forming.
12563+5406AB	11.54 ± 0.51	H	87	329	31	Tight grouping. The PM vector (281°, 4.9") is clearly off.
12564-0057	12.56 ± 1.26	H	80	84	-	The data plot shows a scattered early history that is beginning to converge on a trend. (This convergence is due to better measurement techniques over the years.)
12574+3022	5.16 ± 0.23	G	194	684	-	
12587+2728	11.20 ± 0.41	G	89	148	32	This pair may be starting to reveal an arc.
13007+7343	A: 7.67 ± 1.11 B: 8.78 ± 0.29	G H	143	666	-	A weighted parallax (7.01 mas) was used. However, the error windows only share a 29% overlap. Yet given the large and common proper motions, this pair is most likely physical.
13026+5625	9.94 ± 0.26	G	101	372	-	
13048+7302	8.32 ± 0.49	G	120	167	33	Strong trend emerging.
13166+5034	-	-	-	-	34	Solid trend emerging.
13207+0257	7.38 ± 0.66	H	136	151	-	The trend in the plot shows a tightening of the measurements.
13243+0124	9.06 ± 0.81	H	110	104	-	
13261+3509	9.10 ± 0.26	G	110	393	-	
13288+5956	13.62 ± 0.65	G	73	71	-	The data plot is showing a convergence, but an arc is not yet emerging.
13324+3649	3.49 0.29	G	287	1,205	-	The PM vector (87°, 6.7") is clearly not correct.
13341+6746	13.48 ± 0.25	G	74	313	-	
13344+2617	8.02 ± 0.32	G	125	1,087	-	
13346+3308AB	9.10 ± 0.30	G	110	301	35	Short arc emerging?

Measurements of 427 Double Stars With Speckle Interferometry ...

Notes to Table 3 (CPM Pairs) continued

WDS Number	Parallax	Parallax Source	Distance (Parsecs)	Min Sep (AU)	Plot Figure	Comments
13354+5955	A: 11.11 ± 0.23 B: 11.19 ± 0.23	G G	90	335	-	A weighted average parallax (11.15 mas) was used. The parallax windows have a 50% overlap, with B's window being totally contained inside A's. Given the substantial common proper motion, this pair is likely physical.
13356+4939	A: 4.60 ± 0.27 B: 4.64 ± 0.44	G G	216	554	-	The weighted Gaia parallaxes (4.62 mas) were used. The parallax windows show a 39% overlap, with A's window being totally contained in B's. Given the small but almost identical proper motions, this pair is likely physical.
13367+6947	10.19 ± 0.95	H	98	176	-	
13368+0650	4.18 ± 1.79	H	N/A	N/A	-	The error is too large to make the parallax usable. A weak trend is beginning to emerge.
13377+5043	2.05 ± 0.52	G	N/A	N/A	-	The error is too large to make the parallax usable.
13509+4422AB	5.05 ± 0.23	G	198	614	-	
13563+0517	18.22 ± 3.81	H	55	55	-	
13571+3426	7.12 ± 1.56	H	140	144	-	
13591+2549	5.09 ± 0.30	G	196	912	36	The PM vector (286°, 1.4") does not match the observations.
14033+0557AB	-	-	-	-	37	Definite trend is showing.
14101+2636 AB	B: 13.86 ± 0.28	G	72	187	-	
14116+2802	8.80 ± 0.26	G	114	368	-	This pair may be starting to exhibit a short arc.
14143+3356	11.82 ± 0.24	G	85	465	-	
14270+0341	10.92 ± 1.59	H	92	251	38	Tight group. The PM vector (193°, 3.9") is far from the observations.
14279+2123	10.69 ± 0.26	G	94	429	-	
14339+5514	6.57 ± 0.77	H	152	151	-	
14363+1924	B: 7.46 ± 0.27	G	134	139	-	Madler's 1854.31 measurement looks like an error.
14403+1206	A: 4.09 ± 0.27 B: 4.1 ± 0.35	G G	244	630	-	Weighted parallax (4.09 mas) used, with an overlap in the parallax windows of 79%. Combined with the rather high common proper motion, this pair is physical.
14417+0932	2.19 ± 5.27	H	N/A	N/A	-	The error makes the parallax unusable.
14436+3745	B: 4.10 ± 0.24	G	244	259	-	
14471+0058	7.52 ± 1.62	H	133	457	-	
14524+1757	-	-	-	-	-	Definite trend is starting to emerge.
14531+7811AB	14.73 ± 0.23	G	68	103	-	Weak trend may be forming.
14545+3406	9.93 ± 0.61	G	101	361	-	
14584+4403AB	9.30 ± 0.33	G	108	435	-	
15087-0059AB	14.17 ± 2.78	H	71	44	39	Strong trend emerging, but impossible to tell yet if it is linear or short arc. Given the CPM nature, it is probably a small segment of a long arc.
15126+1523	7.89 ± 0.25	G	127	319	-	
15138+1427AB	7.03 ± 0.27	G	142	660	-	
15227-1654	2.73 ± 0.25	G	366	1,075	-	
15257+2638	5.61 ± 0.69	G	178	244	-	
15264+0822	-	-	-	-	40	May be in the early stages of showing a short arc.
15276+0522	A: 8.64 ± 0.69 B: 12.47 ± 0.50	G G	116 80	-	-	Based on parallax, the stars are 36 parsecs apart and thus clearly not physical. But with nearly identical proper motions, this pair presents an enigma. Is it physical or not?
15300+2530	1.68 ± 0.28	G	595	2,006	-	
15361+4849	6.88 ± 1.11	H	145	163	-	A weak pattern is starting to emerge.
15361+5531	7.17 ± 0.25	G	139	193	-	

Measurements of 427 Double Stars With Speckle Interferometry ...

Notes to Table 3 (CPM Pairs) conclusion

WDS Number	Parallax	Parallax Source	Distance (Parsecs)	Min Sep (AU)	Plot Figure	Comments
15391-0834	7.28 ± 0.75	G	137	342	41	The PM vector (217°, 1.8") does not fit the observations.
15398+2117	3.54 ± 0.25	G	282	879	-	
15453+0432	4.98 ± 0.30	G	201	452	-	A definite trend is emerging, but it is not possible yet to detect an arc. This pair may be involved in a large and nearly edge-on orbit.
15492-0314	A: 7.15 ± 0.27 B: 6.70 ± 0.33	G G	144	351	-	Weighted parallax (6.96 mas) used. The parallax windows overlap only 14%. Yet the proper motions are similar. Evidence suggests this is an optical pair, but more or better data is needed.
15499+4247	4.24 ± 0.23	G	236	1,165	-	
15509+1911	2.69 ± 1.40	H	N/A	N/A	-	The error makes the parallax unusable.
15589-0304	13.85 ± 0.24	G	72	160	-	
16394-0306AB	5.52 ± 0.26	G	181	770	-	
16462-1721	8.94 ± 0.28	G	112	377	-	
Mean AB separation in AU				504		

Table 4: Different Proper Motion Pairs (DPM) Measured With Speckle

Date	WDS No	Disc/Comp	PM A	PM B	Last Yr	Last θ	Last ρ	Msrs	Measured θ ± err (°)	Measured ρ ± err (")	Resid θ	Resid ρ	Notes?
2017.0822	02062+2507	STF 212	-020+029 U	-012-011 W	2010	161.0	1.90	5	160.4 ± 0.0	1.961 ± 0.001	-0.6	0.061	
2017.0767	02087-0026	STF 218	-042-013 W	-008-001 W	2009	248.0	4.90	5	245.7 ± 0.1	4.983 ± 0.009	-2.3	0.083	*
2017.0795	02341-0538	STF 280	+032+030 U	+004+095 U	2012	346.0	3.70	5	347.3 ± 0.3	3.612 ± 0.013	1.3	-0.088	*
2017.0767	03244-1400	BU 12	+031-016 U	+008+006 W	2001	280.6	2.40	5	277.8 ± 0.3	2.302 ± 0.020	-2.8	-0.098	*
2017.0822	03354+3341	STF 413	-052+040 U	+019-006 G	2010	124.7	2.38	5	124.3 ± 0.0	2.410 ± 0.001	-0.4	0.030	*
2017.0822	03581-0454	HLD 70	+029-013 G	-045-010 W	2008	273.5	3.47	5	272.0 ± 0.1	3.504 ± 0.005	-1.5	0.034	*
2017.0822	04222-0441	STF 536	+008+001 G	-007-009 W	2008	190.1	1.51	5	190.8 ± 0.2	1.561 ± 0.003	0.7	0.051	*
2017.2137	06512-1126	HLD 83	-017+037 W	+002-015 W	1999	163.1	2.88	5	161.4 ± 0.2	2.883 ± 0.020	-1.7	0.003	*
2017.2137	06561-1403	STF 997 AB	+000-011 W	-002+007 W	2011	343.9	2.88	5	343.0 ± 0.1	2.851 ± 0.015	-0.9	-0.029	*
2017.2740	08054+0550	STF1182	-011-006 G	-010-022 U	2010	73.7	4.69	5	73.4 ± 0.1	4.767 ± 0.009	-0.3	0.077	*
2017.2986	08298+5112	STF1225	+004+001 G	+003-002 G	2008	189.4	3.68	5	192.3 ± 0.0	3.759 ± 0.001	2.9	0.079	*
2017.2740	08555-0758	STF1295	+006-026 G	-034+005 U	2014	4.3	4.09	5	3.5 ± 0.0	4.068 ± 0.005	-0.8	-0.022	*
2017.3096	09051+3931	AG 160	+089+028 G	+018-025 W	2009	60.0	3.95	5	59.4 ± 0.1	3.908 ± 0.007	-0.6	-0.042	*
2017.3096	09136+4659	STF1318	-008+001 W	-011-015 W	2013	228.3	2.63	5	228.1 ± 0.0	2.632 ± 0.001	-0.2	0.002	*
2017.2795	09318-1126	HU 127	+008+000 G	+022+003 W	1991	85.6	0.89	5	84.9 ± 0.2	0.881 ± 0.002	-0.7	-0.009	*
2017.3014	09556+0806	AG 170	-058-069 G	-009-019 W	2005	43.3	1.65	5	42.5 ± 0.5	1.692 ± 0.060	-0.8	0.042	*
2017.4027	10406+4209	STF1460	-014+030 W	+003-002 W	2013	162.0	3.80	5	162.6 ± 0.0	3.818 ± 0.002	0.6	0.018	*
2017.2795	10533-1045	A 132	-012+004 U	-012-007 U	2011	201.0	4.41	5	200.3 ± 0.0	4.404 ± 0.008	-0.7	-0.006	
2017.4247	13376-0752	STF1763 AB	-011+001 U	-026-010 W	2010	39.1	2.66	5	38.6 ± 0.0	2.694 ± 0.000	-0.5	0.034	*
2017.4247	14083+2112	STF1804	-004-004 W	+002-004 W	2014	14.1	4.88	5	13.3 ± 0.2	4.843 ± 0.009	-0.8	-0.037	
2017.4411	14568+7050	STF1905	+032-025 G	-052 -077 U	2012	160.0	2.80	5	161.3 ± 0.0	2.815 ± 0.004	1.3	0.015	*
2017.4466	15208+3459	HO 62	+016-005 W	-043+019 W	2014	103.2	1.47	5	103.4 ± 0.1	1.526 ± 0.002	0.2	0.056	*

Notes to Table 4 (DPM Pairs)

WDS Number	Parallax	Parallax Source	Distance (Parsecs)	Min Sep (AU)	Plot Figure	Comments
02087-0026	7.98 ± 0.32	G	125	614	-	
02341-0538	5.62 ± 1.22	H	178	653	42	The PM vector (337°, 12.8") clearly does not reflect the motion.
03244-1400	-	-	-	-	43	The PM vector (313°, 4.1") does not fit observations at all. One (or both) of the PM values is questionable. This pair looks to be CPM from the data plot.
03354+3341	6.05 ± 0.44	G	165	393	44	The PM vector (237°, 15.5") does not match the observations at all.
03581-0454	6.66 ± 0.24	G	150	526	45	The PM vector (272°, 9.3") is clearly not correct.
04222-0441	8.21 ± 0.27	G	122	183	46	Trend emerging. The PM vector (236°, 3.2") does not fit the observed motion.
06512-1126	-	-	-	-	47	The PM vector (200°, 6.48") is clearly incorrect.
06561-1403 AB	2.62 ± 0.58	H	382	1,503	48	The PM vector (354°, 3.3") is clearly wrong.
08054+0550	3.86 ± 0.49	G	259	1,215	49	Weak trend. The PM vector (184°, 2.9") does not fit the observations.
08555-0758	10.74 ± 0.58	G	93	381	-	The PM vector (308°, 11.7") is far from the observations.
09051+3931	6.44 ± 0.34	G	155	613	50	Tight grouping. The PM vector (233°, 10.3") is clearly incorrect.
09136+4659	19.07 ± 0.98	H	52	138	51	Trend forming. The PM vector (191°, 3") does not fit the observations.
09318-1126	-0.88 ± 0.97	G	N/A	N/A	-	The parallax is not usable. A short trend is forming.
09556+0806	-24.82 ± 0.63	G	N/A	N/A	-	The parallax is not usable.
10406+4209	5.38 ± 1.00	H	186	699	-	A linear pattern is emerging.
13376-0752 AB	5.11 ± 0.80	H	196	521	52	The PM vector (4.22" @ 234°) is clearly incorrect.
14568+7050	13.14 ± 0.25	G	76	213	53	Linear trend. The PM vector (201°, 10") is clearly incorrect.
15208+3459	5.61 ± 0.69	G	178	238	-	Trend may be emerging.
Mean AB separation in AU				564		

Measurements of 427 Double Stars With Speckle Interferometry ...

Table 5: Linear Pairs Measured With Speckle

Date	WDS No	Disc/Comp	PM A	PM B	Last Yr	Last θ	Last ρ	Msrs	Measured θ ± err (°)	Measured ρ ± err (")	Resid θ	Resid ρ	Notes?
2017.0767	02493-1033	STF 315	+099-020 U	+099-039 W	2013	164.9	1.30	5	164.2 ± 0.1	1.427 ± 0.005	-0.7	0.127	*
2017.0767	03061-1326	BU 527 AB	+000-018 U	-020+013 W	1998	98.1	1.28	5	96.8 ± 0.2	1.406 ± 0.022	-1.3	0.126	*
2017.0822	03401+3407	STF 425	-135-018 U	-070+006 G	2012	60.4	1.94	5	58.2 ± 0.0	1.92 ± 0.001	-2.2	-0.020	*
2017.1507	04257-0214	BU 403	+058+003 W	+058+003 W	2015	83.3	0.95	5	82.2 ± 0.4	0.916 ± 0.014	-1.1	0.916	*
2017.1644	05245-0224	DA 5 AB	+003-001 W	-	2015	76.5	1.81	5	77.5 ± 0.1	1.827 ± 0.003	1.0	0.017	*
2017.1671	05269+0039	LEO 2	+006-013 G	+005-011 G	2002	85.4	2.87	5	85.9 ± 0.5	3.243 ± 0.006	0.5	0.373	*
2017.2986	08194+5627	STF1205	+004+020 W	+004+020 W	2016	166.0	1.70	5	166.2 ± 0.3	1.801 ± 0.005	0.2	0.101	*
2017.2712	08430-0242	HO 355	-016-028 W	-016-028 W	2005	159.3	0.66	5	152.4 ± 0.1	0.805 ± 0.004	-6.9	0.145	*
2017.2986	08593+3457	STF1296	+016+001 G	+011-002 G	2015	76.0	1.80	5	76.3 ± 0.0	1.753 ± 0.001	0.3	-0.047	*
2017.3014	09521+0249	A 2561 AB	-058-007 G	-088+018 W	2005	309.5	1.06	5	309.0 ± 0.1	1.138 ± 0.009	-0.5	0.078	*
2017.2959	10029+6847	STF1400 AB	-030-022 G	-031-022 W	2011	225.8	3.25	5	224.8 ± 0.2	3.564 ± 0.006	-1.0	0.314	*
2017.3315	11406+2102	STF1566	-009-020 G	-010-024 W	2011	350.0	2.42	5	349.1 ± 0.0	2.366 ± 0.004	-0.9	-0.054	*
2017.4027	14497+4843	STF1890	-078+097 W	-078+097 W	2013	46.3	2.58	5	46.7 ± 0.1	2.614 ± 0.004	0.4	0.034	*

Notes to Table 5 (Linear Pairs)

WDS Number	Parallax	Parallax Source	Distance (Parsecs)	Min Sep (AU)	Plot Figure	Comments
02493-1033	17.45 ± 0.95	H	57	74	-	Linear solution by HRT2013. Ephemerides predict 165°, 1.337". Residuals: -0.8°, +0.090".
03061-1326 AB	8.04 ± 0.98	H	124	159	54	Strong linear pattern, no solution yet.
03401+3407	A: 21.73 ± 0.84 B: 22.90 ± 0.73	H G	45	87	55 and 56	The distance and separation assume a weighted parallax of 22.32 mas, with a 16% overlap in the parallax windows. This pair could be physical, but a linear solution by FMR2014 yields ephemerides of 59.8°, 1.755". Curiously, another solution by GnR2015 yields the same ephemerides. The residuals for either case are -1.6°, +0.165".
04257-0214	23.4 ± 1.04	H	43	40	-	Linear solution by HRT2012 for which the ephemerides project 83.2°, 0.951". The residuals are -1.0°, -0.035".
05245-0224 AB	3.34 ± 0.07	H	N/A	N/A	-	The error in the parallax makes it unusable. Linear solution by HRT2012. Ephemerides predict 77.2°, 1.815". Residuals are +0.3°, +0.012".
05269+0039	A: 4.30 ± 0.22 B: 3.94 ± 0.23	G G	233 254	667 728	-	There is no overlap in the parallax windows. There are only six measurements, but a definite linear trend is beginning to emerge.
08194+5627	-	-	-	-	57	No solution yet. A strong linear pattern is forming.
08430-0242	6.37 ± 1.39	H	157	108	-	A moderately strong linear pattern is emerging. The R^2 value is 0.6707.
08593+3457	A: 10.12 ± 0.26 B: 10.65 ± 0.44	G G	96	179	58	A weighted parallax of 10.38 mas was used. The parallax windows have a 19% overlap.
09521+0249 AB	27.71 ± 0.72	G	36	40	59	The PM vector (310°, 3.6") is too long but it does have the correct theta. This is a strong linear case without a solution.
10029+6847 AB	13.9 ± 0.23	G	72	234	-	Linear solution by HRT2011. Ephemerides predict 225.0°, 3.525". Residuals of -0.2°, +0.039". However, this pair has identical proper motions. Is this then a short arc binary? Manual solution with STB.
11406+2102	8.38 ± 0.99	G	119	289	-	Linear solution by HRT2011. The ephemerides predict 350.5°, 2.377". The residuals are -1.4°, -0.011".
14497+4843	14.58 ± 0.51	G	69	177	-	Linear solution by HRT2011. The ephemerides predict 45.8°, 2.576". The residuals are +0.9°, +0.038".
Mean AB separation in AU				139		

Measurements of 427 Double Stars With Speckle Interferometry ...

Table 6: Known Orbit Pairs Measured With Speckle

Date	WDS No	Disc/Comp	PM A	PM B	Last Yr	Last θ	Last ρ	Msrs	Measured θ ± err (°)	Measured ρ ± err (")	Resid θ	Resid ρ	Notes?
2017.0795	02020+0246	STF 202AB	+042-011 W	+042-011 W	2012	266.0	1.70	5	264.5 ± 0.3	1.941 ± 0.007	-1.5	0.241	*
2017.0822	02037+2556	STF 208AB	+127+012 G	+134+010 W	2012	343.0	1.38	5	343.8 ± 0.5	1.410 ± 0.009	0.8	0.030	*
2017.0767	02158-1814	HTG 1	-036-119 G	-052-135 W	2014	162.5	1.97	5	164.1 ± 0.2	2.020 ± 0.024	1.6	0.050	*
2017.0822	02475+1922	STF 305AB	+118-160 W	+118-159 G	2012	306.5	3.60	5	306.5 ± 0.1	3.675 ± 0.004	0.0	0.075	*
2017.0822	03122+3713	STF 360	+069-017 U	-030-027 U	2011	125.6	2.79	5	124.3 ± 0.0	2.931 ± 0.001	-1.3	0.141	*
2017.0822	03356+3141	BU 533AB	+067+003 W	+061-000 G	2012	220.9	1.05	5	220.4 ± 0.1	1.048 ± 0.001	-0.5	-0.002	*
2017.1507	04199+1631	STT 79	+114-030 W	-	2012	358.1	0.51	5	3.3 ± 1.5	0.525 ± 0.021	5.2	0.015	*
2017.1644	05005+0506	STT 93	+035-038 W	+035-038 W	2014	243.5	1.61	5	243.6 ± 0.0	1.632 ± 0.003	0.1	0.022	*
2017.1644	05079+0830	STT 98	+022-061 W	+022-061 W	2015	286.0	0.90	5	286.1 ± 0.2	0.952 ± 0.004	0.1	0.052	*
2017.1671	05135+0158	STT 517AB	+007+002 W	+007+002 W	2014	243.0	0.69	5	240.2 ± 0.6	0.693 ± 0.004	0.2	0.003	*
2017.1616	05239-0052	WNC 2A-BC	-007+001 G	-005-009 W	2016	159.6	3.00	5	158.3 ± 0.0	3.166 ± 0.003	-0.5	0.166	*
2017.1671	05308+0557	STF 728	+005-042 W	+005-042 W	2013	44.9	1.28	5	43.4 ± 0.1	1.279 ± 0.002	-1.5	-0.001	*
2017.1671	05407-0157	STF 774AB	+004+003 W	+004+003 W	2013	167.1	2.36	5	165.9 ± 0.2	2.377 ± 0.013	-1.2	0.017	*
2017.1671	05417-0254	BU 1052	+054+017 W	+054+017 W	2013	185.2	0.62	5	186.9 ± 0.5	0.636 ± 0.007	1.7	0.006	*
2017.1644	06336-1207	HU 43	-048-215 W	-048-215 W	2010	307.6	0.79	5	308.1 ± 0.2	0.864 ± 0.005	0.5	0.074	*
2017.2740	08024+0409	STF1175	+066-103 G	+065-105 W	2012	285.1	1.42	5	286.6 ± 0.0	1.477 ± 0.001	1.5	0.057	*
2017.2712	08061-0047	A 1971	+087-064 W	+087-064 W	2014	2.8	0.96	5	2.2 ± 0.1	0.976 ± 0.001	-0.6	0.016	*
2017.2877	08095+3213	STF1187	+016-096 U	+033-008 W	2013	20.4	2.96	5	19.4 ± 0.0	3.103 ± 0.002	-1.0	0.148	*
2017.2712	08213-0136	STF1216	-009-028 W	-009-028 W	2013	304.8	0.53	5	306.7 ± 0.6	0.535 ± 0.017	1.9	0.005	*
2017.2795	08369+2315	AG 154	-109-107 W	-109-107 W	2011	1.2	2.62	5	0.5 ± 0.0	2.688 ± 0.003	-0.7	0.068	*
2017.2740	08507+0752	VDK 3	-069+009 W	-	2010	168.4	1.39	5	185.0 ± 0.2	1.146 ± 0.004	16.6	-0.244	*
2017.2986	09273+0614	STF1355	-178-151 W	-178-151 W	2016	355.0	1.70	5	354.7 ± 0.0	1.808 ± 0.001	-0.3	0.108	*
2017.3096	09414+3857	STF1374AB	+083-136 W	-	2014	310.0	2.70	5	311.0 ± 0.1	2.842 ± 0.002	1.0	0.142	*
2017.2822	10131+2725	STT 213	-050-123 W	-050-123 W	2015	121.7	1.07	5	120.8 ± 0.3	1.091 ± 0.006	-0.9	0.021	*
2017.2822	10200+1950	STF1424AB	+311-153 W	+306-161 W	2015	127.0	4.69	5	125.5 ± 0.1	4.776 ± 0.006	-1.5	0.176	*
2017.2795	10205+0626	STF1426AB	-007-044 W	-007-044 W	2014	312.0	0.94	5	313.3 ± 0.4	0.903 ± 0.001	1.3	-0.037	*
2017.2795	10217-0946	BU 25	+009-040 W	-	2015	130.2	1.55	5	128.6 ± 0.0	1.535 ± 0.001	-1.6	-0.015	*
2017.2822	10269+1713	STT 217	-042-067 W	-042-067 W	2015	146.3	0.73	5	146.5 ± 0.2	0.818 ± 0.001	0.2	0.088	*
2017.2822	10397+0851	STT 224AB	-105+006 W	-105+006 W	2014	135.2	0.49	5	135.4 ± 1.2	0.550 ± 0.014	0.2	0.060	*
2017.2959	10480+4107	STT 229	-021-003 W	-021-003 W	2013	259.8	0.63	5	256.3 ± 0.9	0.714 ± 0.008	-3.5	0.084	*
2017.2795	11000-0328	STF1500	+064+031 W	+064+031 W	2014	300.0	1.35	5	298.8 ± 0.0	1.345 ± 0.002	-1.2	-0.005	*
2017.3808	11080+5249	STF1510	-062-003 G	-072+003 W	2008	330.0	5.40	5	328.2 ± 0.0	5.586 ± 0.005	-1.8	0.186	*
2017.3562	11136+5525	A 1353	-037+007 W	-037+007 W	2013	209.8	0.57	5	210.9 ± 0.8	0.600 ± 0.010	1.1	0.030	*
2017.2795	11137+2008	STF1517AB	-388-125 W	-388-125 W	2015	315.7	0.71	5	314.4 ± 0.3	0.710 ± 0.002	-1.3	0.000	*
2017.3562	11390+4109	STT 237AB	-082-034 G	-081-038 W	2015	245.0	2.10	5	242.8 ± 0.1	2.042 ± 0.007	-2.2	-0.058	*
2017.3562	11520+4805	HU 731	-217+047 W	-217+047 W	2013	307.6	1.14	5	307.2 ± 0.5	1.211 ± 0.005	-0.4	0.071	*

Table 6 concludes on next page.

Measurements of 427 Double Stars With Speckle Interferometry ...

Table 6 (conclusion): Known Orbit Pairs Measured With Speckle

Date	WDS No	Disc/Comp	PM A	PM B	Last Yr	Last θ	Last ρ	Msrs	Measured θ ± err (°)	Measured ρ ± err (")	Resid θ	Resid ρ	Notes?
2017.3562	11520+4805	HU 731	-217+047 W	-217+047 W	2013	307.6	1.14	5	307.2 ± 0.5	1.211 ± 0.005	-0.4	0.071	*
2017.3562	12244+2535	STF1639AB	-013-013 W	-013-013 W	2015	323.0	1.80	5	323.6 ± 0.0	1.851 ± 0.001	0.6	0.051	*
2017.3562	12272+2701	STF1643AB	+096-229 W	+085-240 W	2014	4.0	2.70	5	3.4 ± 0.2	2.747 ± 0.008	-0.6	0.047	*
2017.3397	12306+0943	STF1647	+051-058 W	+051-058 W	2015	248.0	1.20	5	248.7 ± 0.1	1.306 ± 0.005	0.7	0.106	*
2017.3562	12372+2112	STF1663	-012-023 W	-012-023 W	2014	66.0	0.70	5	65.4 ± 1.6	0.537 ± 0.018	-0.6	-0.163	*
2017.3589	12533+2115	STF1687AB	-048-027 W	-048-027 W	2015	198.0	1.20	5	198.8 ± 0.3	1.145 ± 0.020	0.8	-0.055	*
2017.4164	13120+3205	STT 261	+026-007 G	+015-006 W	2014	337.6	2.53	5	337.9 ± 0.0	2.669 ± 0.004	0.3	0.139	*
2017.4164	13235+2914	HO 260	-468+245 W	-468+245 W	2012	86.0	1.62	5	88.6 ± 0.0	1.684 ± 0.003	2.6	0.064	*
2017.4247	13237-0043	A 2489	-053-023 W	-053-023 W	2010	189.9	0.84	5	188.1 ± 0.1	0.998 ± 0.018	-1.8	0.158	*
2017.4247	13343-0019	STF1757AB	-219+021 W	-219+021 W	2014	137.3	1.70	5	141.1 ± 0.0	1.702 ± 0.000	3.8	0.002	*
2017.4164	13375+3618	STF1768AB	-095+023 G	-085+002 W	2014	97.4	1.81	5	94.9 ± 0.2	1.703 ± 0.010	-2.5	-0.107	*
2017.4164	13461+0507	STF1781AB	-093-028 G	-103-035 W	2014	193.1	0.99	5	195.1 ± 0.2	1.047 ± 0.009	2.0	0.057	*
2017.4164	13491+2659	STF1785	-427-090 W	-471-092 W	2015	189.7	2.66	5	187.1 ± 0.1	2.902 ± 0.006	-2.6	0.242	*
2017.4055	13577+5200	A 1614	+236-007 W	+236-007 W	2013	300.4	1.43	5	299.5 ± 0.1	1.426 ± 0.003	-0.9	-0.004	*
2017.4027	14131+5520	STF1820	-342-002 W	-350-018 W	2012	121.7	2.49	5	124.1 ± 0.0	2.799 ± 0.001	2.4	0.309	*
2017.4027	14203+4830	STF1834	-073-013 G	-073-014 W	2013	102.6	1.64	5	104.5 ± 0.0	1.667 ± 0.000	1.9	0.037	*
2017.4411	14336+3535	STF1858AB	-193+064 W	-192+058 W	2013	37.9	3.05	5	38.4 ± 0.0	3.078 ± 0.002	0.5	0.028	*
2017.4027	14380+5135	STF1863	-056+007 W	-056+007 W	2013	59.2	0.65	5	58.9 ± 0.1	0.665 ± 0.002	-0.3	0.015	*
2017.4027	14407+3117	STF1867	-050-063 W	-050-063 W	2013	353.7	0.70	5	354.9 ± 0.4	0.674 ± 0.004	1.2	-0.026	*
2017.4247	14525+1844	BU 31AB	-026+198 W	-026+198 W	2013	220.3	2.06	5	221.7 ± 0.0	1.986 ± 0.000	1.4	-0.074	*
2017.4027	14455+4223	STT 285AB	-067+054 W	-067+054 W	2013	83.6	0.50	5	78.6 ± 0.1	0.533 ± 0.003	-5.0	0.033	*
2017.4247	14463+0939	STF1879AB	+071-266 U	+071-266 W	2014	84.6	1.73	5	81.1 ± 0.0	1.746 ± 0.001	-3.5	0.016	*
2017.3808	14464-0723	STF1876AB	-150+103 W	-150+103 W	2013	113.3	1.27	5	115.2 ± 0.1	1.256 ± 0.010	1.9	-0.014	*
2017.4247	14489+0557	STF1883	+027-125 U	-008-089 W	2013	278.2	0.98	5	277.4 ± 0.0	1.045 ± 0.001	-0.8	0.065	*
2017.4027	14515+4456	STT 287	-013-039 W	-013-039 W	2013	0.0	0.65	5	4.9 ± 0.5	0.575 ± 0.028	4.9	-0.075	*
2017.4247	14534+1542	STT 288	-020+030 W	-020+030 W	2014	159.7	0.98	5	159.0 ± 0.0	1.008 ± 0.001	-0.7	0.028	*
2017.4493	15038+4739	STF1909	-444+010 W	-374+039 W	2014	66.1	1.13	5	74.9 ± 0.2	0.656 ± 0.002	8.8	-0.474	*
2017.4466	15183+2650	STF1932AB	+093+071 W	+088+077 W	2014	264.0	1.56	5	266.9 ± 0.1	1.639 ± 0.001	2.9	0.079	*
2017.4438	15277+0606	STF1944	-002-036 W	-002-036 W	2013	295.2	0.66	5	292.5 ± 1.1	0.702 ± 0.010	-2.7	0.042	*
2017.4438	15348+1032	STF1954AB	-005+000 U	+008-017 U	2014	172.7	3.62	5	172.2 ± 0.1	4.097 ± 0.005	-0.5	0.477	*
2017.4466	15360+3948	STT 298AB	-483+028 W	-455+051 W	2014	185.8	1.18	5	186.2 ± 0.0	1.22 ± 0.004	0.4	0.040	*
2017.4466	15405+1840	A 2076	-019+019 W	-019+019 W	2012	185.1	0.73	5	186 ± 0.3	0.742 ± 0.005	0.9	0.012	*
2017.4493	15413+5959	STF1969	-223+160 G	-220+165 W	2013	29.0	1.01	5	31.5 ± 0.2	1.073 ± 0.007	2.5	0.063	*
2017.4247	15559-0210	STF1985	-091-062 G	-089-061 W	2013	353.1	5.92	5	354.1 ± 0.0	6.062 ± 0.003	1.0	0.142	*

Measurements of 427 Double Stars With Speckle Interferometry ...

Notes to Table 6 (Known Orbits)

All ephemerides were computed with an Excel spreadsheet prepared by Jack Drummond (April, 2014). The number after the term "Orbit" is the orbit's grade. True Separation computed from orbital elements (semi-major axis).

WDS Number	Parallax	Parallax Source	Distance (Parsecs)	True Sep (AU)	Plot Figure	Comments
02020+0246 AB	21.66 ± 1.06	H	46	340	-	Orbit (4) by PRU2017. The ephemerides predict 262.1°, 1.834" and the residuals are +2.4°, +0.107".
02037+2556 AB	18.2 ± 0.46	G	55	76	-	Orbit (3) by HEI1996. The ephemerides predict 346.5°, 1.492". The residuals are -2.7°, -0.082".
02158-1814	42.52 ± 0.53	G	24	52	-	Orbit (4) by TOK2015. The ephemerides are 163.1°, 1.736". The residuals are +1.0°, +0.284".
02475+1922 AB	A: 29.8 ± 0.82 B: 29.88 ± 0.27	H G	34	78	-	Orbit (4) by MSN2014. There is a 50% overlap in the parallax windows. The ephemerides predict 306.0°, 3.726". The residuals are +0.5°, -0.051".
03122+3713	25.05 ± 1.50	H	40	146	60 61 (Orb) 62 (Lin)	Orbit (5) by WSI2004. The ephemerides predict 125.7°, 2.857", while the residuals are -1.4°, -0.027". Curiously, there is also a linear solution by HRT2011. The ephemerides predict 124.9°, 2.919", while its residuals are -0.6°, +0.012". My measurement seems to favor the linear solution over the orbit. The PM vector (264°, 18.2") is far too long for the orbital solution.
03356+3141 AB	B: 11.32 ± 0.37	G	88	87	-	Orbit (5) by ZIR2015. The ephemerides predict 221°, 1.027" while the residuals are -0.6°, +0.021".
04199+1631	-	-	-	-	-	Orbit (2) by SOD1999. The ephemerides predict 4.3°, 0.561" while the residuals are -0.50°, -0.036".
05005+0506	17.98 ± 1.51	H	56	102	-	Orbit (4) by WSI2015. The ephemerides predict 1.550". The residuals are +0.0°, +0.082".
05079+0830	15.47 ± 1.89	H	65	65	63	Orbit (2) by SCA2008. The ephemerides predict 291.2°, 0.932". The residuals are -5.1°, +0.020".
05135+0158 AB	4.71 ± 0.85	H	212	163	-	Orbit (4) by TOK2014. The ephemerides predict 240.4°, 0.687" while the residuals are -0.2°, +0.006".
05239-0052 A-BC	18.75 ± 0.47	G	53	153	-	Orbit (5) by FMR2013. Ephemerides: 158.5°, 3.096". Residuals: -1.4°, +0.070".
05308+0557	10.77 ± 0.64	H	93	149	-	Orbit (4) by USN1999. Ephemerides: 44.4°, 1.315". Residuals: -1.0°, -0.036".
05407-0157 AB	4.43 ± 0.64	H	226	617	-	Orbit (5) by HOP1967. Ephemerides: 166.4°, 2.197". Residuals: -0.5°, +0.180".
05417-0254	12.39 ± 0.87	H	81	56	-	Orbit (3) by HRT2010. Ephemerides: 183.7°, 0.584". Residuals: +3.2°, +0.052".
06336-1207	11.8 ± 20.90	H	N/A	N/A	-	The error makes the parallax unusable. Orbit (5) by HEI1993. Ephemerides: 312.0°, 0.860". Residuals: -3.9°, +0.004".
08024+0409	24.21 ± 0.44	G	41	124	-	Orbit (5) by OLE2001. Ephemerides: 290.4°, 1.386". Residuals: -3.8°, +0.091".
08061-0047	9.86 ± 3.72	H	N/A	N/A	-	The magnitude of the error makes the parallax unusable. Orbit (5) by TOK2015. Ephemerides: 359.0 °, 0.819". Residuals: +3.2°, +0.157".
08095+3213	15.46 ± 1.23	H	65	198	-	Orbit (5) by OLE2001. Ephemerides: 20.4°, 2.955". Residuals: -1.0°, +0.148".
08213-0136	-	-	-	-	-	Orbit (3) by TOK2014. Ephemerides: 307.6°, 0.521". Residuals: -0.9°, +0.014". Manual solution with STB.
08369+2315	24.04 ± 2.97	H	42	131	-	Orbit (5) by HRT2011. Ephemerides: 0.9°, 2.670". Residuals: -0.4°, +0.018".
08507+0752	-	-	-	-	64	Orbit (4) by WSI2006. Ephemerides: 181.4°, 1.063". Residuals: +3.6°, +0.083". The last few measures appear to be veering off the predictions.
09273+0614	18.41 ± 1.23	H	54	94	-	Orbit (4) by LIN2011. Ephemerides: 354.5°, 1.810". Residuals: +0.2°, -0.002".
09414+3857 AB	19.5 ± 0.83	H	51	163	-	Orbit (5) by LIN2013. Ephemerides: 310.4°, 2.817". Residuals: +0.6°, +0.025".
10131+2725	13.93 ± 1.22	H	72	71	-	Orbit (4) by SCA2008. Ephemerides: 120.8°, 1.071". Residuals: +0.0°, -0.020".
10200+1950 AB	25.07 ± 0.52	H	40	124	-	Orbit (4) by PKO2014. (Two orbits with the apparent motion parameters method.) Ephemerides: 126.2°, 4.627". Residuals: -0.7°, +1.149".

Measurements of 427 Double Stars With Speckle Interferometry ...

Notes to Table 6 (Known Orbits) *continued*

All ephemerides were computed with an Excel spreadsheet prepared by Jack Drummond (April, 2014). The number after the term "Orbit" is the orbit's grade. True Separation computed from orbital elements (semi-major axis).

WDS Number	Parallax	Parallax Source	Distance (Parsecs)	True Sep (AU)	Plot Figure	Comments
10205+0626 AB	6.68 ± 1.99	H	N/A	N/A	-	The error makes the parallax unusable. Orbit (5) by NOV2006. Ephemerides: 312.5°, 0.912". Residuals: +0.8°, -0.009".
10217-0946	16.68 ± 1.18	H	60	110	-	Orbit (5) by ZIR2012. Ephemerides: 130.5°, 1.566". Residuals: -1.9°, -0.031".
10269+1713	11.8 ± 1.44	H	85	40	-	Orbit (3) by SCA2015. Ephemerides: 148.4°, 0.782". Residuals: -1.9°, +0.036".
10397+0851 AB	-	-	-	-	-	Orbit (3) by HRT2010. Ephemerides: 135.3°, 0.496". Residuals: +0.1°, +0.054". Manual solution with STB.
10480+4107	6.04 ± 0.96	H	166	104	-	Orbit (4) by ALZ1998. Ephemerides: 257.4°, 0.637". Residuals: -1.1°, +0.077". Manual solution with STB.
11000-0328	18.66 ± 0.86	H	54	182	-	Orbit (5) by HRT2013. Ephemerides: 299.9°, 1.336". Residuals: -1.1°, +0.009".
11080+5249	17.54 ± 0.26	G	57	450	-	Orbit (5) by KIS2012. Ephemerides: 328.3°, 5.461". Residuals: -0.1°, +0.125".
11136+5525	-	-	-	-	-	Orbit (3) by DOC2015. Ephemerides: 209.0 °, 0.537". Residuals: +1.9°, +0.063". Manual solution with STB.
11137+2008 AB	18.35 ± 0.96	H	54	123	-	Orbit (4) by FMR2011. Ephemerides: 316.3°, 0.694". Residuals: -1.9°, +0.016".
11390+4109 AB	12.24 ± 0.40	G	82	374	-	Orbit (5) by USN2002. Ephemerides: 244.4°, 2.033". Residuals: -1.6°, +0.009".
11520+4805	20.16 ± 3.04	H	50	59	-	Orbit (4) by HRT2008. Ephemerides: 307.9°, 1.171". Residuals: -0.7°, +0.040".
12244+2535 AB	11.08 ± 0.59	H	90	110	-	Orbit (4) by OLE2006. Ephemerides: 323.2°, 1.823". Residuals: +0.4°, +0.028".
12272+2701 AB	36.75 ± 0.90	H	27	73	-	Orbit (4) by WSI2004. Ephemerides: 4.0°, 2.745". Re-siduals: -0.6°, +0.002".
12306+0943	10.81 ± 0.90	H	93	405	-	Orbit (4) by HOP1970. Ephemerides: 251.4°, 1.243". Residuals: -2.7°, +0.063". There appear to be quadrant reversals on L 1902.35, FUR 1902.40, POS 1903.27, BOW 1904.30, and PHL 1923.07.
12372+2112	5.34 ± 1.09	H	187	131	-	Orbit (5) by ZIR2013. Ephemerides: 68.0°, 0.636". Residuals: -2.6°, -0.099". Manual solution with STB.
12533+2115 AB	11.52 ± 0.87	H	87	103	-	Orbit (4) by DRU2014. Ephemerides: 197.4°, 1.158". Residuals: +1.4°, -0.013".
13120+3205	13.68 ± 0.28	G	73	131	65 (Hsw) 66 (Kis) 67 (Hrt)	Interesting case - Kiselev derived an orbit whereas Hartkopf found a linear solution. Orbit (4) by KIS2012. Ephemerides: 338.5°, 2.582". Residuals: +0.6°, +0.087". Linear solution by HRT2011. Ephemerides not available.
13235+2914	53.97 ± 2.13	H	19	40	-	Orbit (3) by ZIR2013. Ephemerides: 87.1°, 1.626". Residuals: +1.5°, +0.058".
13237-0043	10.96 ± 4.13	H	N/A	N/A	-	The error makes the parallax unusable. Orbit (5) by WSI2004. Ephemerides: 191.6°, 0.945". Residuals: -3.5°, +0.053".
13343-0019 AB	37.68 ± 1.30	H	27	75	-	Orbit (4) by HEI1988. Ephemerides: 138.6°, 1.755". Residuals: +2.5°, -0.053"
13375+3618 AB	18.39 ± 0.99	G	54	55	-	Orbit (3) by SOD1999. Ephemerides: 95.2°, 1.697". Residuals: -0.3°, +0.006".
13461+0507 AB	13.96 ± 0.58	G	72	72	-	Orbit (3) by ALZ2007. Ephemerides: 194.5°, 0.975". Residuals: +0.6°, +0.072".
13491+2659	-	-	-	-	68	Orbit (2) by HEI 1988. Ephemerides: 185.5°, 2.937". Residuals: +1.6°, -0.035".
13577+5200	18.92 ± .76	H	53	45	-	Orbit (3) by RAO2014. Ephemerides: 301.6°, 1.486". Residuals: -2.1°, -0.060".
14131+5520	26.14 ± 0.90	G	38	135	-	Orbit (4) by KIY1998. Ephemerides: 122.4°, 2.265". Residuals: +1.7°, +0.146".
14203+4830	14.06 ± 0.34	G	71	72	-	Orbit (3) by WSI2015. Ephemerides: 103.8°, 1.580". Residuals: +0.7°, +0.097".
14336+3535 AB	25.34 ± 0.24	G	39	187	-	Orbit (5) by ZIR2015. Ephemerides: 37.8°, 3.029". Residuals: +0.6°, +0.049".

Measurements of 427 Double Stars With Speckle Interferometry ...

Notes to Table 6 (Known Orbits) *conclusion*

All ephemerides were computed with an Excel spreadsheet prepared by Jack Drummond (April, 2014). The number after the term “Orbit” is the orbit’s grade. True Separation computed from orbital elements (semi-major axis).

WDS Number	Parallax	Parallax Source	Distance (Parsecs)	True Sep (AU)	Plot Figure	Comments
14380+5135	11.67 ± 1.36	H	86	93	-	Orbit (4) by ZIR2013. Ephemerides: 60.3°, 0.649". Residuals: -1.4°, +0.016".
14407+3117	8.55 ± 1.73	H	117	141	-	Orbit (5) by ZIR2013. Ephemerides: 353.7°, 0.662". Residuals: +1.2°, +0.012".
14525+1844	20.65 ± 1.08	H	48	-	-	Orbit (5) by HRT2014. Ephemerides: 221.2°, 2.012". Residuals: +0.5°, 0.026".
14455+4223 AB	-	-	-	-	-	Orbit (2) by SCA2015. Ephemerides: 82.2°, 0.498". Residuals: -3.6°, +0.035".
14463+0939 AB	23.14 ± 1.26	H	43	48	-	Orbit (3) by MSN1999. Ephemerides: 83.1°, 1.720". Residuals: -2.0°, -1.720".
14464-0723 AB	-	-	-	-	-	Orbit (5) by USN2002. Ephemerides: 112.6°, 1.247". Residuals: +2.6°, +0.009".
14489+0557	17.99 ± 1.82	H	56	45	-	Orbit (2) by WSI2015. Ephemerides: 277.1 248/0.988". Residuals: +0.3°, +0.057".
14515+4456	16.91 ± 0.86	H	59	54	-	Orbit (4) by HEI1997. Ephemerides: 0.6°, 0.721". Residuals: +4.3°, -0.146".
14534+1542	20.99 ± 0.93	H	48	65	-	Orbit (4) by HEI1998. Ephemerides: 158.8°, 1.016". Residuals: +0.2°, +0.028".
15038+4739	79.95 ± 1.56	H	13	48	-	Orbit (2) by ZIR2011. Ephemerides: 66.7°, 1.02". Residuals: +8.2°, -0.364".
15183+2650 AB	27.29 ± 0.34	G	37	45	-	Orbit (2) by SCA2015 . Ephemerides: 265.1°, 1.622". Residuals: +1.8°, +0.017".
15277+0606	5.1 ± 1.29	H	N/A	N/A	-	The error makes the parallax unusable. Orbit (5) by ZIR2015. Ephemerides: 294.0°, 0.620". Residuals: -1.5°, +0.082". Manual solution with STB.
15348+1032 AB	14.3 ± 0.75	G	70	268	-	Orbit (4) by WSI2004. Ephemerides: 172.1°, 3.977". Residuals: +0.1°, +0.120".
15360+3948 AB	-	-	-	-	-	Orbit (1) by SOD1999. Ephemerides: 183.6°, 1.194". Residuals: +2.6°, +0.026".
15405+1840	3.23 ± 1.74	H	N/A	N/A	-	The error makes the parallax unusable. Orbit (4) by ZIR2014. Ephemerides: 185.4°, 0.729". Residuals: +0.6°, +0.013".
15413+5959	16.19 ± 0.25	G	62	63	-	Orbit (4) by RAO1999. Ephemerides: 29.4°, 0.957". Residuals: +2.1°, +0.116".
15559-0210	26.19 ± 0.40	G	38	264	-	Orbit (5) by HOP1973. Ephemerides: 354.9°, 6.281". Residuals: -0.8°, -0.219".
Mean AB separation in AU				136		

Measurements of 427 Double Stars With Speckle Interferometry ...

Table 7: Short Arc Pairs Measured With Speckle

Date	WDS No	Disc/Comp	PM A	PM B	Last Yr	Last θ	Last ρ	Msrs	Measured θ ± err (°)	Measured ρ ± err (")	Resid θ	Resid ρ	Notes?
2017.1507	04518+0115	BU 748	+009+004 G	+007+009 G	2010	70.0	2.80	5	69.0 ± 0.0	3.019 ± 0.001	-1.0	0.219	*
2017.1671	05181+0342	A 2639	-061+002 W	-061+002 W	2016	273.0	0.90	5	277.2 ± 1.6	0.846 ± 0.002	4.2	-0.054	*
2017.2795	08033+2616	STT 186	-014-009 W	-014-009 W	2012	73.7	0.99	5	73.4 ± 0.1	1.004 ± 0.001	-0.3	0.014	*
2017.2795	08136+1051	STF1202	+005-070 G	-	2011	306.2	2.70	5	303.8 ± 0.0	2.700 ± 0.003	-2.4	0.000	*
2017.2877	09193-0933	A 126	-050-001 W	-050-001 W	2014	121.6	1.09	5	122.3 ± 0.1	1.164 ± 0.004	0.7	0.074	*
2017.3014	09290+1917	COU 936	+026+033 W	+026+033 W	2012	226.3	0.88	5	225.8 ± 1.1	0.956 ± 0.017	-0.5	0.076	*
2017.2986	09500+0148	A 2560	-034-010 W	-034-010 W	2005	17.4	1.13	5	17.8 ± 0.1	1.122 ± 0.008	0.4	-0.008	*
2017.3260	09513+6037	STF1381	-018+088 W	-018+088 W	2015	186.2	0.80	5	187.3 ± 0.1	0.798 ± 0.005	1.1	-0.002	*
2017.3315	10069-0143	HDO 125	-072+023 G	-078+019 W	2012	190.0	2.70	5	190.3 ± 0.0	2.875 ± 0.003	0.3	0.267	*
2017.3397	11431+3715	HU 1135	-026-014 W	-026-014 W	2014	336.0	0.70	5	334.1 ± 0.2	0.742 ± 0.001	-1.9	0.042	*
2017.3589	12409+0850	STF1668	-013-030 W	-013-030 W	2009	187.0	1.10	5	186.8 ± 0.0	1.129 ± 0.001	-0.2	0.029	*
2017.4247	14165+2007	STF1825	-136-095 G	-131-084 W	2012	153.6	4.33	5	152.7 ± 0.1	4.425 ± 0.020	-0.9	0.095	

Notes to Table 7 (Short Arc Binaries, or SABs)

WDS Number	Parallax	Parallax Source	Distance (Parsecs)	Min Sep (AU)	Plot Figure	Comments
04518+0115	A: 12.69 ± 0.35 B: 14.46 ± 0.47	G G	79 69	-	69	There is no overlap in the parallax windows.
05181+0342	7.78 ± 1.76	H	129	100	70	
08033+2616	5.31 ± 1.04	H	188	187	71	Trend line does not "orbit" the primary star.
08136+1051	14.42 ± 0.35	G	69	187	-	
09193-0933	-	-	-	-	72	Trend line does not "orbit" the primary star.
09290+1917	12.03 ± 1.20	H	83	73	73	Trend line does not "orbit" the primary star.
09500+0148	4.40 ± 1.26	H	N/A	N/A	-	The parallax error makes the parallax unusable. Early case of showing a weak arc.
09513+6037	5.26 ± 2.19	H	N/A	N/A	74	The parallax error makes the parallax unusable.
10069-0143	10.4 ± 0.33	G	96	274	-	Weak arc is forming.
11431+3715	-	-	-	-	-	Early case of a weak arc forming. The R^2 value is very high (0.9463), but the motion of the companion has only traversed 0.5".
12409+0850	8.26 ± 0.85	H	121	137	-	Weak arc forming.
14165+2007	29.68 ± 0.47	G	34	146	75	
Mean AB Separation in AU				158		

Table 8: Unknown Cases Measured With Speckle
Note: These cases are called "unknown" because no proper motions are known, or only one proper motion is known.

Date	WDS No	Disc/Comp	PM A	PM B	Last Yr	Last θ	Last ρ	Msrs	Measured θ ± err (°)	Measured ρ ± err (")	Resid θ	Resid ρ	Notes?
2017.0795	02593-0615	A 454	+072+005 W	-	2010	132.1	3.89	5	134.3 ± 0.3	3.957 ± 0.033	2.2	0.067	
2017.0822	03384+1736	A 2420	-009-005 G	-	2008	268.9	2.08	5	267.6 ± 0.1	1.990 ± 0.004	-1.3	-0.090	*
2017.1507	04581+0141	STF 622	+058-003 G	+062-003 G	2010	162.0	2.40	5	161.4 ± 0.0	2.537 ± 0.001	-0.6	0.137	*
2017.1644	05063+0257	AG 89	+002-016 G	-	2006	178.8	2.31	5	178.5 ± 0.1	2.325 ± 0.002	-0.3	0.015	*
2017.1616	05099-0906	A 483AB	+002+001 G	-003+002 G	2009	58.0	3.95	5	58.5 ± 0.0	3.846 ± 0.002	0.5	-0.104	*
2017.1616	05129-0347	BRT 534	-001-002 G	-001-003 G	2000	171.9	4.16	5	171.8 ± 0.0	4.247 ± 0.004	-0.1	0.087	*
2017.2137	05589-0120	STF 826	+001-007 W	-	2010	132.6	1.99	5	132.2 ± 0.2	2.014 ± 0.011	-0.4	0.024	
2017.2137	06025-0222	STF 836	-005-011 W	-	2013	25.5	1.99	5	23.6 ± 0.1	1.967 ± 0.004	-1.9	-0.023	
2017.1644	06116-1727	A 3023	-010-020 G	-	2002	327.3	2.20	5	328.4 ± 0.0	2.316 ± 0.001	1.1	0.116	*
2017.1507	06249-1943	HO 339	-034+018 G	-	2005	191.8	5.29	5	191.2 ± 0.0	5.359 ± 0.007	-0.6	0.069	*
2017.2795	08413+1916	KU 32	-036-012 G	-	2000	165.4	2.16	5	164.7 ± 0.0	2.178 ± 0.001	-0.7	0.018	*
2017.2795	08515+1208	STF1287AB	-020-030 G	-	2012	87.0	2.18	5	86.1 ± 0.0	2.187 ± 0.003	-0.9	0.007	*
2017.2795	08521+0428	STF1290	-006-002 G	-	2009	325.1	2.77	5	324.7 ± 0.0	2.775 ± 0.003	-0.4	0.005	*
2017.2877	09012+0245	STF1302AB	-062+021 G	-	2009	236.3	2.71	5	233.3 ± 0.1	2.745 ± 0.005	-3.0	0.035	*
2017.2795	09463-1627	A 3079	-008-012 W	-	2000	122.4	2.73	5	123.8 ± 0.1	2.799 ± 0.011	1.4	0.069	
2017.3315	10314-0226	A 1350	-086-017 G	-	2008	317.2	2.59	5	316.0 ± 0.1	2.600 ± 0.003	-1.2	0.010	*
2017.2822	10350+0839	STF1450	-054-003 W	-	2013	155.8	2.11	5	155.7 ± 0.1	2.160 ± 0.004	-0.1	0.050	*
2017.3315	11245+2037	STF1537	-001+005 G	-	2013	358.3	2.28	5	358.1 ± 0.1	2.298 ± 0.004	-0.2	0.018	*
2017.3616	12168+7009	STF1626	+056+001 G	-	2005	4.8	2.16	5	2.0 ± 0.0	2.133 ± 0.000	-2.8	-0.027	*
2017.4247	14301+0617	STF1853	-024+027 U	-	2011	81.5	2.86	5	82.4 ± 0.0	2.858 ± 0.000	0.9	-0.002	
2017.4411	14450+2704	STF1877AB	-042+014 W	-	2014	343.4	2.90	5	344.8 ± 0.1	2.930 ± 0.011	1.4	0.030	*
2017.4247	15479-0519	STF3096	+027+004 G	+028+007 G	2011	77.2	3.73	5	76.1 ± 0.0	3.725 ± 0.001	-1.1	-0.005	*
2017.4247	15509-0902	STF 3097	-153-103 W	-	2009	188.1	3.95	5	187.2 ± 0.0	4.001 ± 0.001	-0.9	0.051	
2017.4438	16120-1928	BU 120AB	-010-025 W	-	2014	1.9	1.33	5	1.8 ± 0.5	1.514 ± 0.012	-0.1	0.184	*

Measurements of 427 Double Stars With Speckle Interferometry ...

Notes to Table 8 (Unknown Cases)

WDS Number	Parallax	Parallax Source	Distance (Parsecs)	Min Sep (AU)	Plot Figure	Comments
03384+1736	2.31 ± 0.32	G	433	902	-	
04581+0141	A: 10.42 ± 0.32 B: 9.84 ± 0.42	G G	99	254	-	Weighted parallax (10.13 mas) used. There is a 16% overlap in the parallax windows.
05063+0257	4.06 ± 0.27	G	246	569	-	
05099-0906	A: 3.15 ± 0.28 B: 3.12 ± 0.27	G G	319	1,260	-	A weighted parallax of 3.13 mas was used. There is a 90% overlap in the parallax windows.
05129-0347	A: 2.56 ± 0.29 B: 2.97 ± 0.28	G G	361	1,502	-	Weighted parallax (2.77 mas) used. There is a 20% overlap in the parallax windows.
06116-1727	1.64 ± 0.51	G	N/A	N/A	-	The error makes the parallax unusable.
06249-1943	16.54 ± 0.23	G	60	320	-	
08413+1916	5.00 ± 0.69	G	200	432	-	DAL2005.274 looks like a quadrant flip (90° west).
08515+1208 AB	5.58 ± 0.35	G	179	391	-	A trend appears to be forming.
08521+0428	6.75 ± 0.49	G	148	410	-	
09012+0245 AB	12.84 ± 0.30	G	78	211	-	Linear trend forming.
10314-0226	10.69 ± 0.94	G	91	242	-	
10350+0839	7.61 ± 0.67	H	131	277	-	
11245+2037	10.44 ± 0.27	G	96	218	-	
12168+7009	5.81 ± 0.22	G	172	372	-	
14450+2704 AB	16.10 ± 0.66	G	62	180	-	
15479-0519	A: 16.62 ± 0.3 B: 16.8 ± 0.24	G G	60	223	-	Weighted parallax of 16.71 mas. 100% overlap in the parallax windows. Pair is probably physical.
16120-1928 AB	-	-	-	-	-	A linear trend is forming.
Mean AB Separation in AU				485		

Measurements of 427 Double Stars With Speckle Interferometry ...

(Continued from page 289)

5. Discussion

5.1— The Impact of GAIA and UCAC5 data.

The new data from GAIA (DR1) has already been of huge benefit in the analysis of double star systems. PM analysis can bolster a pair's odds of being physical, or dispel it (if the parallaxes are greatly different).

In addition, the latest high-quality PM data from GAIA and the UCAC5 catalog can support a pair's claim to physicality (if the PMs are nearly the same) or suggest a linear or optical nature (if the PMs are greatly different).

The Winter/Spring 2017 observing program at Brilliant Sky Observatory revealed the following possibilities flowing from GAIA and UCAC5 data. (Table 9).

5.2— The Mean Separations and Projected Orbital Periods of the Stars by Type.

In addition to the possible new classifications arising from GAIA and UCAC5 data, it is also interesting to compare the mean separation of the two stars in cases where the distance is known (either for both stars, or it is assumed that both stars lie at the distance indicated by the one parallax on record). A survey of the data in the Notes to Tables 3 to 8 yields the data summarized in Table 10.

In the case of the known orbits, the mean orbital velocity may be calculated by using the orbital elements of the solution and solving for the perimeter of an ellipse, and then dividing that result by the orbital period.

$$p = \pi\left(a+b\right)\sum_{n=0}^{\infty}\binom{0.5}{n}^{2} h^{n} \qquad [2]$$

The perimeter of an ellipse is given by the infinite series (Equation 2):

$$b = ax\sqrt{1-e^{2}} \qquad [3]$$

In orbital solutions, we know the semi-major axis

Table 10: Mean AB Separation in AU

Type of Pair	Mean AB Sep in AU
CPM	504
DPM	564
LIN	139
ORB	136
SAB	158
UNK	485

Table 9: Outcomes From GAIA/UCAC5

Physicality suggested by parallax	
Type	WDS Number
CPM	05079+0824
	06049-0243 AB
	06074-0400AB ?
	06372-1415
	08421+2501
	09071+3037
	09300+4216
	09450+7643 ?
	13007+7343
	13354+5955
	13356+4939
	14403+1206
	15087-0059 AB
	15453+0432 ?
	15492-0314 ?
LIN	08593+3457
UNK	04581+0141
	05099-0906
	05129-0347
	15479-0519
Proper Motion accounts for observations (probable optical pairs)	
CPM	02123+2357 AB ?
	03312+1947 ?
	10462-0546
Proper Motion does NOT account for observations (one or both PM values are incorrect)	
CPM	08500+3935
	08538-0035 AB
	09080+8102
	10151+1907
	11024+8313
	12137-7826
	13324+3649
	14270+0341
	15391-0834
DPM	02341-0538
	03244-1400
	03354+3341
	03581-0454
	04222-0441
	06512-1126
	06561-1403
	08054+0550
	08555-0758
	09051+3931
	09136+4659
	13376-0752 AB
	14568+7050
Parallax suggests optical pair (different distances)	
CPM	08101+0403
	15276+0522
LIN	05269+0039
SAB	04518+0115
Probable Linear Cases without solutions	
CPM	08140-1740
	08437+1654 ?
LIN	03061-1326 AB
	08194+5627
	08430-0242
	09521+0249 AB

Measurements of 427 Double Stars With Speckle Interferometry ...

(a) and the eccentricity (e). From these, we can compute the semi-minor axis (b) by using the expression (Equation 3):

If we substitute the expression $(a\text{-}b)^2/(a+b)^2$ for h in

$$p=\pi(a+b)\left(1+\frac{1}{4}h+\frac{1}{64}h^2+\frac{1}{256}h^3+\frac{1}{16384}h^4\ldots\right) \quad [4]$$

Equation 2, this conveniently expands into a series Excel can handle and gives a very accurate answer after the fourth expansion (Equation 4):

By determining the length of the semi-major axis in AU, that value can then be used to convert the total perimeter from arc seconds to AU.

This exercise shows us that the average orbital velocity of the 51 known orbits in this observing program (for which we have good parallax data) is 35,267 km/hour or 9.80 km/sec. (The earth's mean orbital speed around the sun is 29.8 km/sec for comparison. The mean orbital speed of Neptune, a planet that is at a distance typical of many of the closer known binaries, is 5.43 km/sec.)

A plot of the results, showing the mean orbital velocity in red, is shown in Figure 4.(The y-axis maximum value is 40,000 km/hr and axis divisions are in 5,000 km/hr increments.)

The spread in orbital velocities spans a wide range, from 0.76 km/sec for the slowest pair (WDS 02020+0246 = STF 202AB) to the highest value of 51.70 km/sec for the fastest pair (WDS 10269+1713 = STT 217). The standard deviation of the 51 velocities was 8.43 km/sec, so this data is not of highly consistent quality. However, by matching the separation in the stars in AU from Table 10 to the nearest matching semi-major axis from the known orbits and using the orbital velocity of that pair as representative of the stars in the classes of Table 10, we can derive a rough estimate of periods of the stars of Table 10 to see if the velocity computations are consistent, and they are.

Considering only the CPM, SAB and UNK cases (since DPMs are most likely either pairs that are not physical or pairs with one or both proper motions in question, and LIN cases are linear and hence not likely to be physical), we get the following orbital period estimates (Table 11).

Since all of these estimates are well within the bounds of the 51 orbital cases, it would appear that the GAIA parallax data used to derive these projected periods is reasonably accurate. (The 51 orbital cases had a mean period of 1,104 years, with a minimum of 140 years and a maximum of 6,600 years.)

Table 11: Orbital Velocity Estimates of the 2017 Program Stars

Type of Pair	Projected orbital period, years
CPM	897
SAB	293
UNK	863

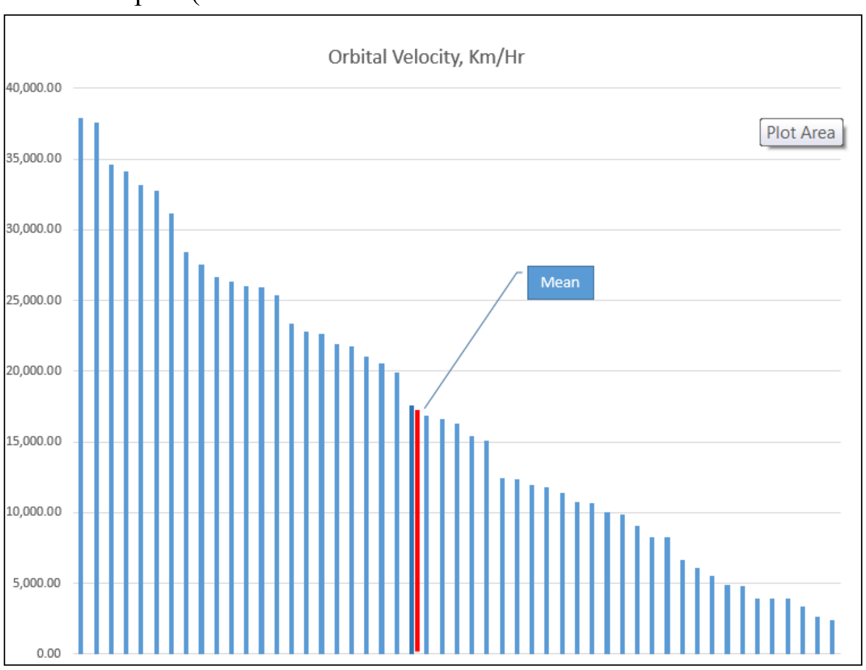

Figure 4: Spread of orbital velocity (km/hr) for known orbits in the 2017 observing program.

Measurements of 427 Double Stars With Speckle Interferometry ...

5.3— Analysis of 888 Orbits from the Sixth Orbit Catalog.

After the findings presented in section 5.2, I decided to investigate a larger sample of orbits. I downloaded the Sixth Orbit Catalog from the U. S. Navy's web site and selected only those pairs for which we had good parallax data ("good" defined as parallaxes from Hipparcos or GAIA). 888 pairs met this criterion.

I did the calculations detailed in section 5.2, and

$$Min\ Sep = (1-e)a$$

$$Max\ Sep = (1+e)a$$

added two new factors— the minimum separation of the stars (in AU) and the maximum separation (in AU). These values are derived from

The results of my analysis are shown in Table 12.

For comparison, the maximum velocity of the 51 orbits in this paper was 51.70 km/sec; the minimum velocity was 0.76 km/sec; and the mean velocity was 8.43 km/sec. The mean semi-major axis of the 51 orbits was 118.04 AU (slightly over twice that of the Sixth Catalog pairs); the mean semi-minor axis was 112.41 (roughly three times the Sixth Catalog); and the mean perimeter in AU was 955 (roughly three times the value of the Sixth Catalog pairs). Obviously, there are many pairs analyzed in the Sixth Orbit Catalog that are much closer than the pairs studied in this observing program (indeed, the closest pair being Mu Ori AaAb, a pair separated by only 0.08 AU, with a period of only 4.447585 days). In fact, many of the Sixth Orbit Catalog pairs in this analysis are far too close to resolve in an 11-inch telescope.

Of equally great importance, however, is the distribution of true A-B separations (in AU) that can be derived from the Sixth Orbit Catalog analysis. A histogram of the data is shown in Figure 76 (at the end of this paper). The surprising thing about this graph is how fast the distance between stars in known binaries drops off with increasing rho. 87.38% of the 888 pairs are less than 100 AU apart, and the widest pair analyzed (WDS 05407-0157, ζ Ori) was 615.80 AU apart. This would suggest caution regarding any computed separation that exceeds a few thousand AU.

Table 12: Orbital Velocity Estimates of 888 Known Orbits

Max Velocity, km/sec	211.17
Min Velocity, km/sec	0.13
Mean Velocity, km/sec	9.80
Mean semi-minor axis, AU	43.30
Mean semi-major axis, AU	54.57
Mean minimum sep, AU	62.32
Mean maximum sep, AU	83.22
Mean perimeter, "	6.432
Mean perimeter, AU	312.00

Of course, the Sixth Orbit Catalog also represents a heavily biased sample to date— it contains, almost by default, pairs that have short enough orbital periods to display meaningful data that leads to orbital solutions. It may well be that there are binaries with periods in the tens of thousands (or even hundreds of thousands) of years, but for such pairs, the change in relative position of the two stars will be barely detectable even over time frames of centuries.

It would make an interesting student project to run a set of simulations of hypothetical binaries in which pairs of different masses are compared, probable orbital velocities computed, and the binding force of gravity between the two is estimated. If the orbital velocity results in a centripetal force that exceeds the binding energy, it would be highly unlikely for the two stars to be a true binary.

Finally, Figure 5 shows the strong relationship between the semi-major axis (in AU) and the orbital peri-

$$Period = 1.3444 \times Sep^{0.6827}$$

od. An equal-weight trend line has been established by Excel and shows a best-fit correlation of 0.8331. The equation of that trend line is shown as

where S*ep* is the semi-major axis in AU and *Period* is the orbital period in years.

5.4— Comparison of AB Separation for the DPM pairs to All Other Classes.

When we compare the minimum AB separation for the stars for the DPM classes to all other classes, an obvious fact emerges: the mean separations for these stars is the greatest for any class of double star observed in the Winter/Spring 2017 program (564 AU). This is only slightly higher than the mean separation for the CPM pairs (504 AU), but considerably higher than those for the known orbits (136) and the short arc binaries (which may become orbits eventually, at 158 AU).

The widest DPM pair (WDS 06561-1403) came in at 1,503 AU, while the closest pair (WDS 09136+4659) was at 138 AU. The minimum AB separation for the orbital pairs in the observing program was 14 AU while the maximum was 533. Granted, this is a biased selection as we are dealing with close pairs (under 5"), but it would seem that pairs with separations in the thousands

Measurements of 427 Double Stars With Speckle Interferometry ...

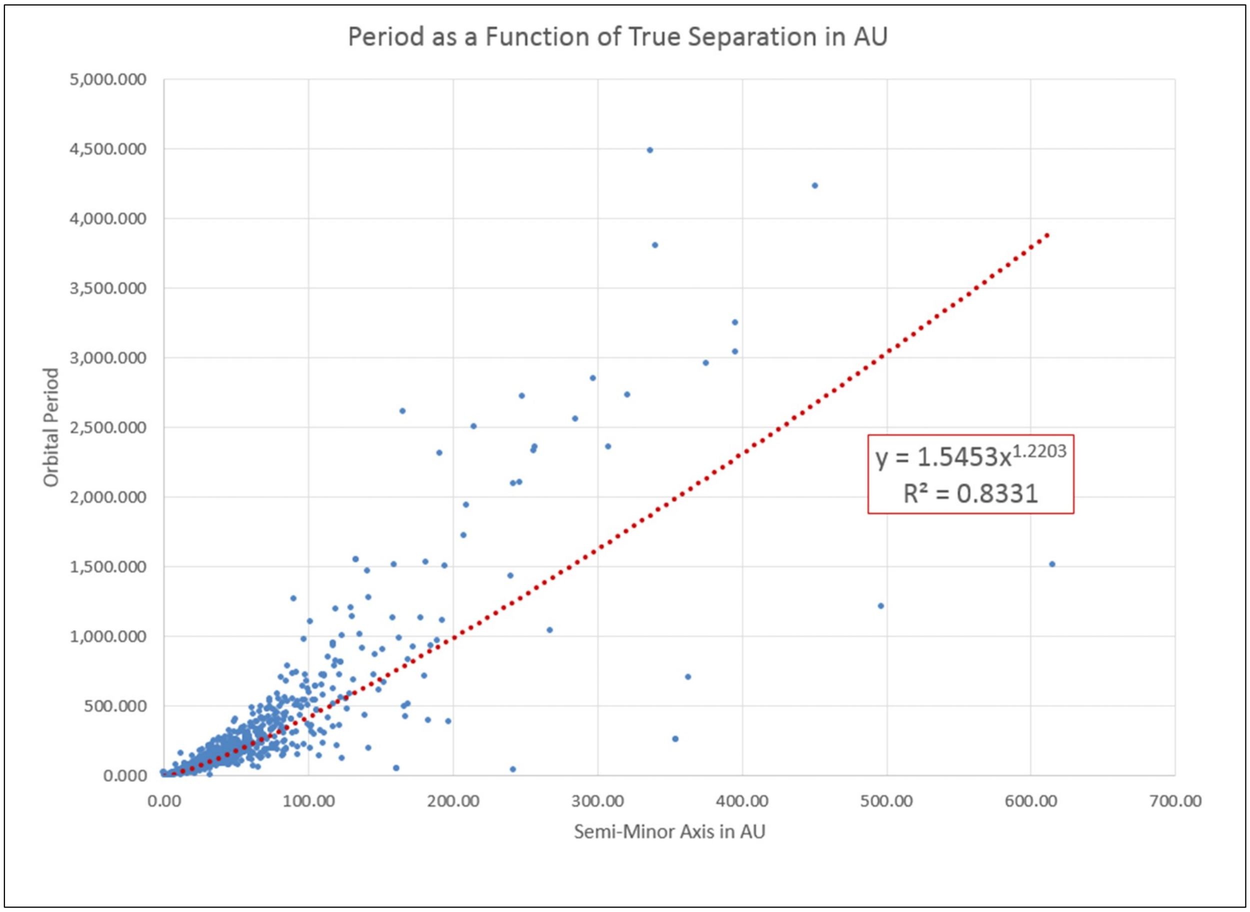

Figure 5. The relationship between the Semi-major axis (in AU) and the Orbital Period (in years)

of AU may not be very stable, if they exist as true binaries at all.

6. Conclusion

We have already established in the pages of this Journal that small telescopes can do speckle interferometry of close pairs with a high degree of precision.

The results of the 2017 Winter and Spring observing program at Brilliant Sky Observatory show great promise for the addition of the new GAIA DR1 and UCAC5 parallax and proper motion data to our research as we continue to work on the WDS to determine which of its 140,000+ pairs are true binaries and which are optical or non-binary but physical pairs. I can only assume that when GAIA DR2 is released in April of 2018, our pursuit of true binaries will literally explode. We are in for some exciting times!

7. Acknowledgements

This paper has made extensive use of the Washington Double Star Catalog and the Sixth Orbit Catalog, both maintained by the U. S. Naval Observatory in Washington, D.C. The author is also indebted to Norbert Zacharias and William Hartkopf (both of the U. S. Naval Observatory) for their help and suggestions in private email communications.

8. References

Harshaw, Richard, 2015, “A. Measurements of 2 Wide CPM Pairs with a CCD”, *Journal of Double Star Observations,* **11** (4), 424-428.

Harshaw, Richard, 2016 B, “CCD Measurements of 66 Rectilinear Pairs and Probable Rectilinear Pairs: The Autumn 2015 Observing Program at Brilliant Sky Observatory, Part 1”, *JDSO*, **12** (4), 376-387.

Harshaw, Richard, 2016 C, “CCD Measurements of 8 Double Stars with Binary Nature: The Autumn 2015 Observing Program at Brilliant Sky Observatory”, *JDSO*, **12** (4), 388-393.

Harshaw, Richard, 2016 D, “CCD Measurements of 141 Proper Motion Stars: the Autumn 2015 Observing Program at Brilliant Sky Observatory”, *JDSO*, **12** (4), 393-399.

Harshaw, Richard, 2017 E, “Quasi-Speckle Measurements of Close Double Stars With a CCD Camera”, *JDSO*, **13** (1), 13-16.

Harshaw, Richard, 2017 F, “The Winter 2015 Observing Program at Brilliant Sky Observatory: Report on the Measurement of 112 Pairs”, *JDSO*, **13** (1), 17-24.

Harshaw, Richard, 2017 G, “The Spring 2016 Observing Program of Brilliant Sky Observatory: Measurements of 313 Pairs”, *JDSO*, **13** (1), 104-121.

Harshaw, Richard, 2017 H, “When Things Don’t Look Right: What Appear to be Proper Motion Discrepancies in the WDS”, *JDSO*, **13** (4), 570-579.

Appendix: Plots of Special Cases Detailed in the Notes

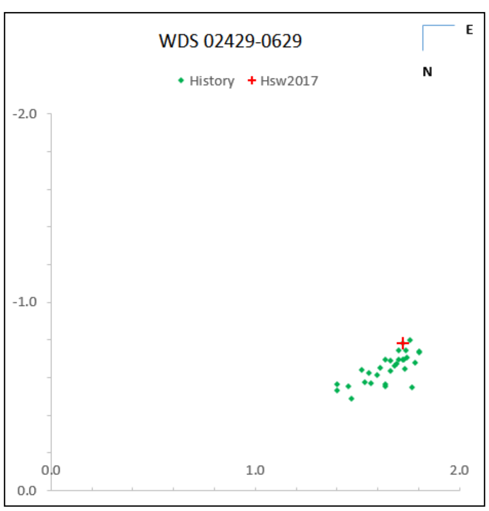

Figure 4: Plot of WDS 02429-0629.

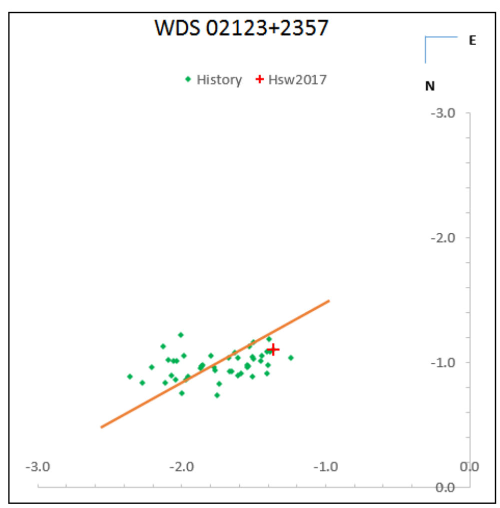

Figure 5: Plot of WDS 02123+2357.

Measurements of 427 Double Stars With Speckle Interferometry ...

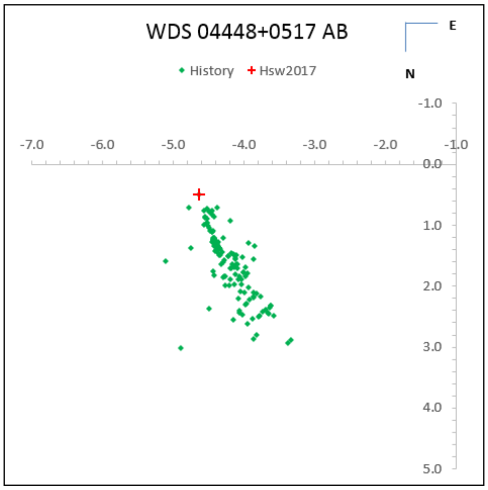

Figure 6. Plot of WDS 04448+0517 AB.

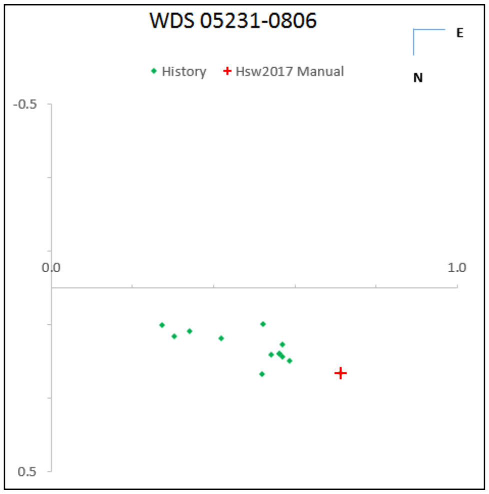

Figure 7. Plot of WDS 05231-0806..

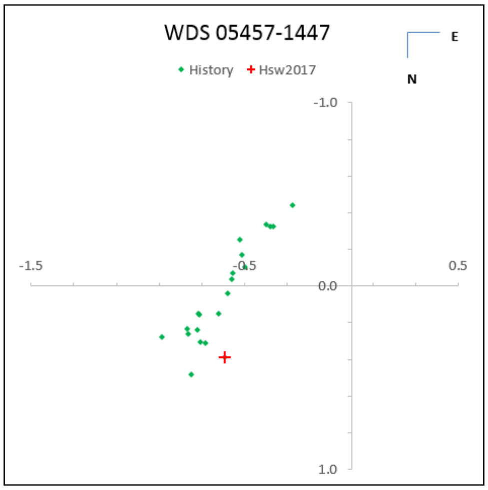

Figure 8. Plot of WDS 05231-0806..

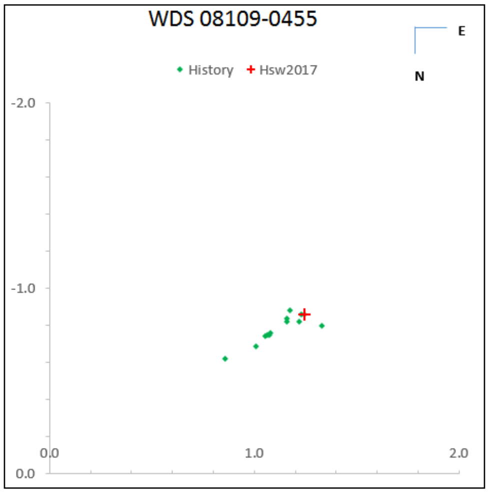

Figure 9. Plot of WDS 08109-0455.

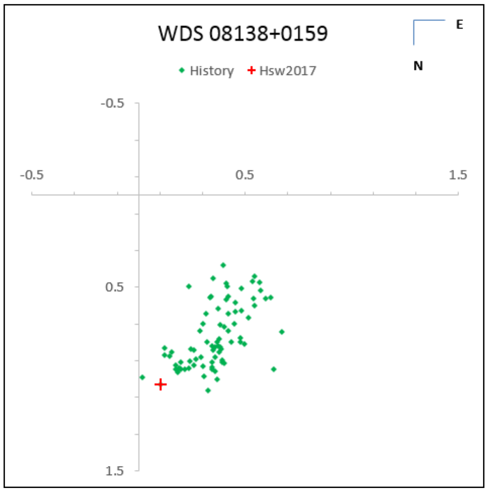

Figure 10. Plot of WDS 08138+0159

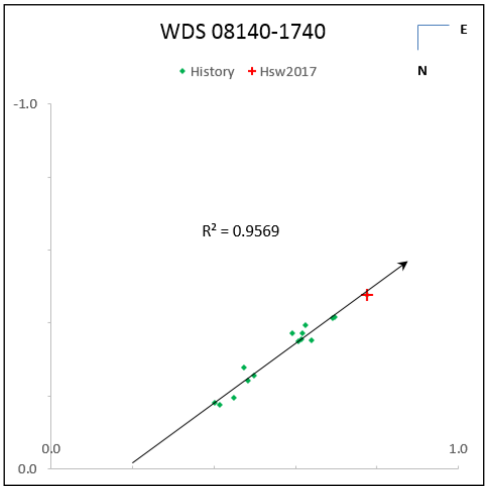

Figure 11. Plot of WDS 08140-1740.

Measurements of 427 Double Stars With Speckle Interferometry ...

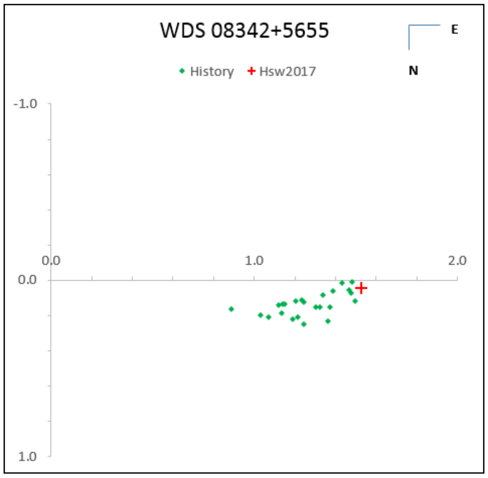

Figure 12. Plot of WDS 08342+5655.

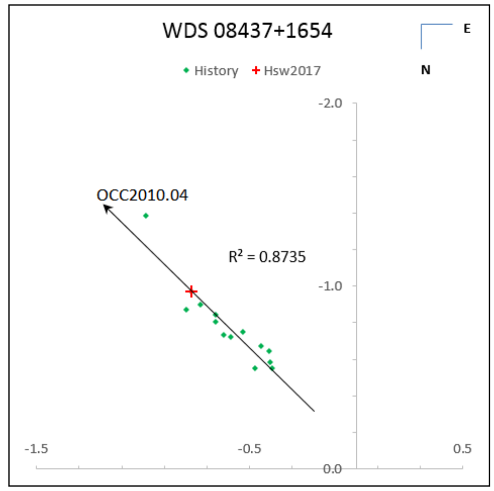

Figure 13. Plot of WDS 08437+1654.

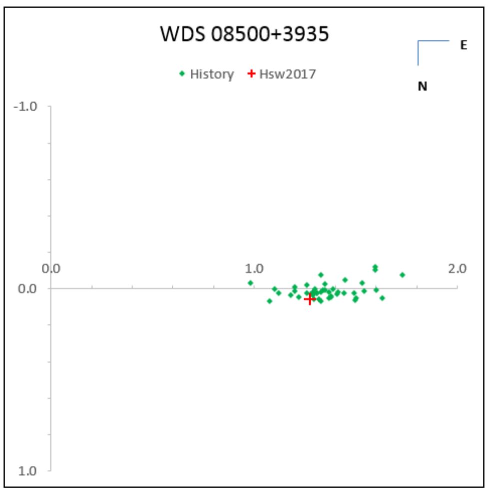

Figure 14. Plot of WDS 08500+3935.

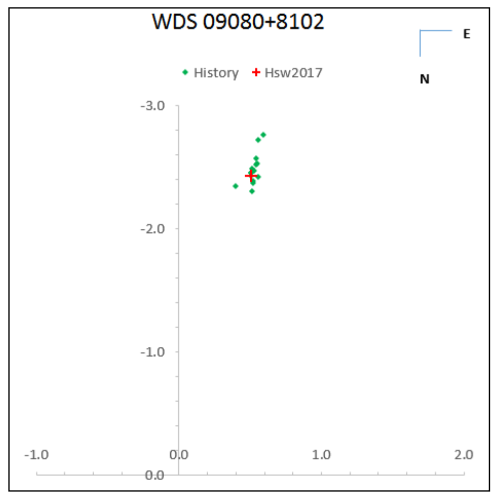

Figure 15. Plot of WDS 09080+8102.

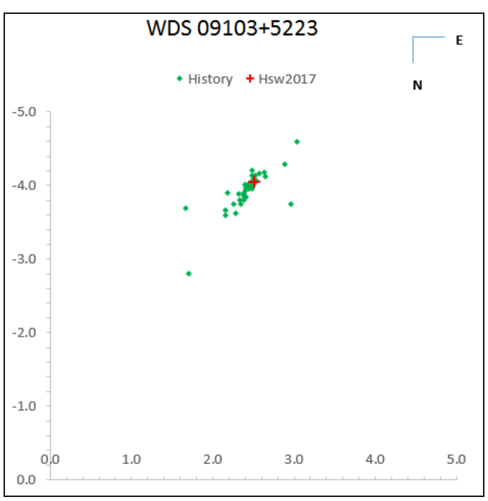

Figure 16. Plot of WDS 09103+5223

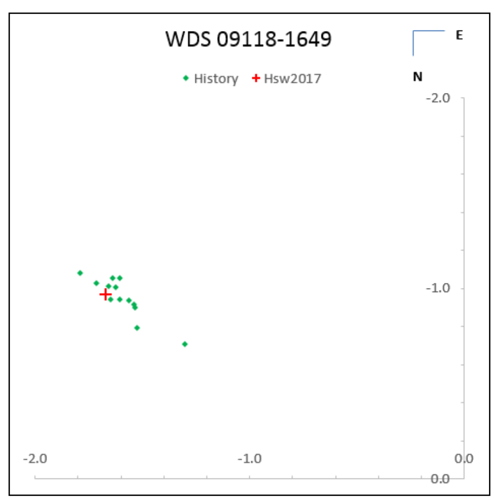

Figure 17. Plot of WDS 09118-1649.

Measurements of 427 Double Stars With Speckle Interferometry ...

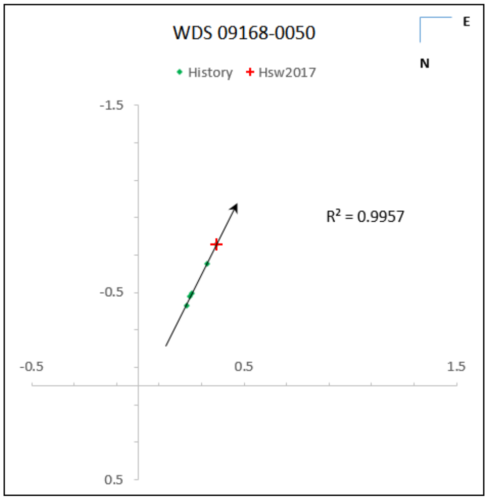

Figure 18. Plot of WDS 09168-0500.

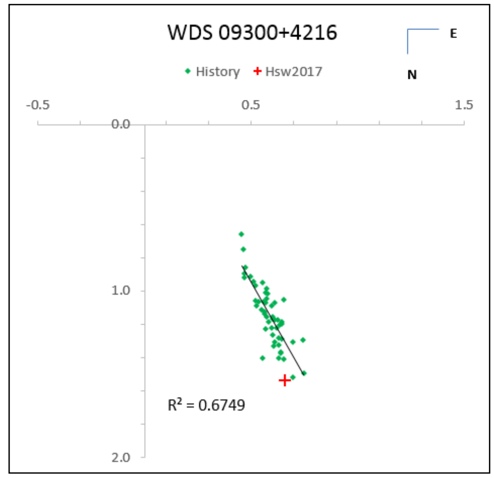

Figure 19. Plot of WDS 09300+4216.

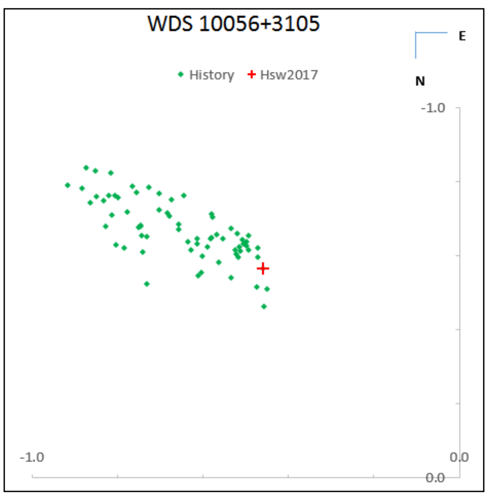

Figure 20. Plot of WDS 10056+3105.

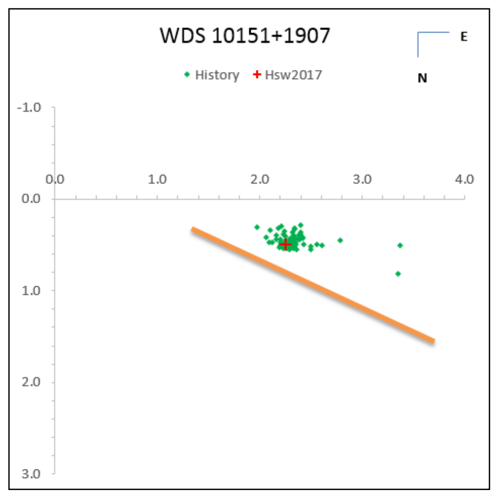

Figure 21. Plot of WDS 10151+1907.

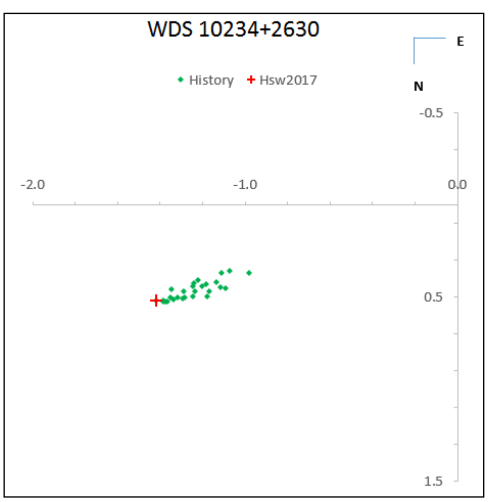

Figure 22. Plot of WDS 10234+2630

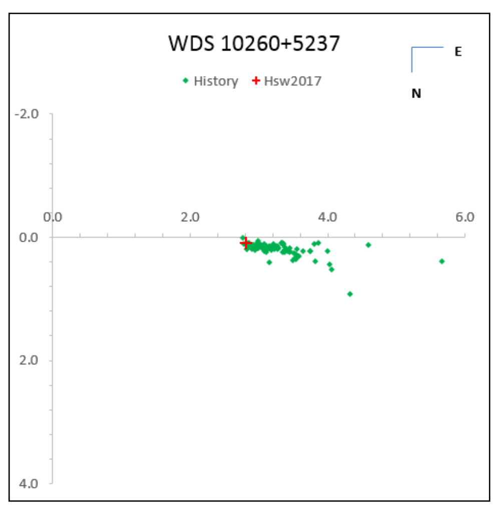

Figure 23. Plot of WDS 10260+5237.

Measurements of 427 Double Stars With Speckle Interferometry ...

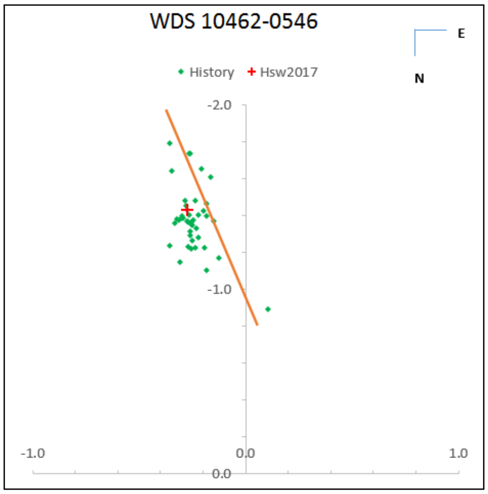

Figure 24. Plot of WDS 10642-0546.

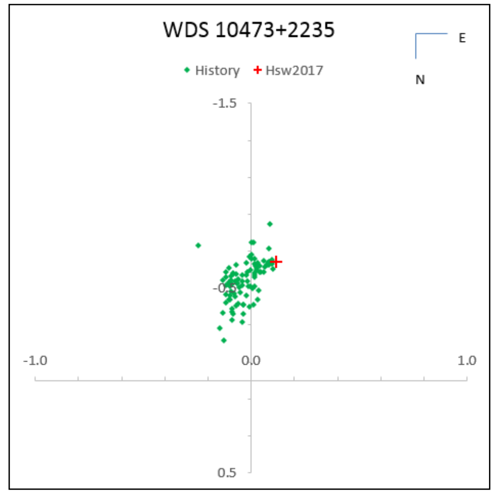

Figure 25. Plot of WDS 10473+2235.

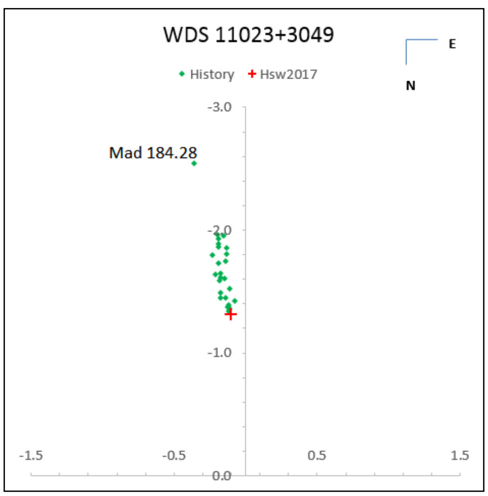

Figure 26. Plot of WDS 11023+3049.

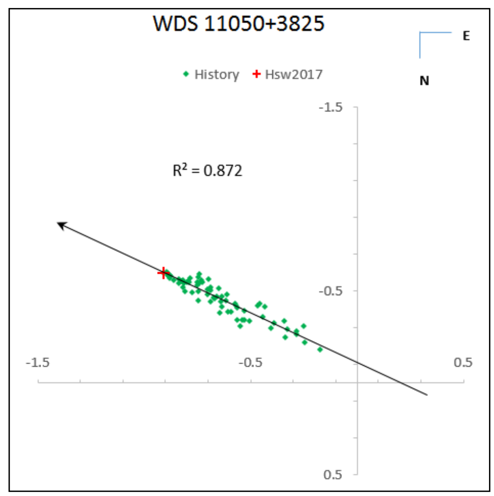

Figure 27. Plot of WDS 11050+3825.

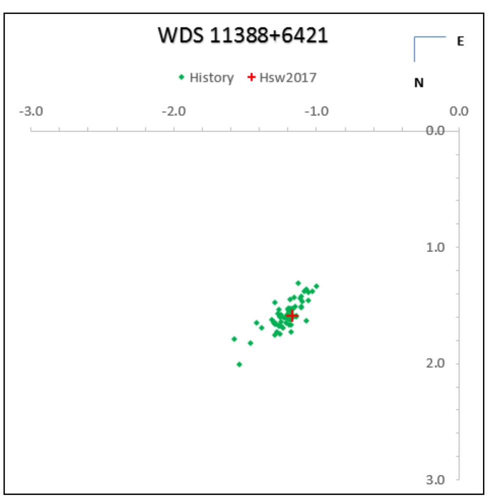

Figure 28. Plot of WDS 11388+6421.

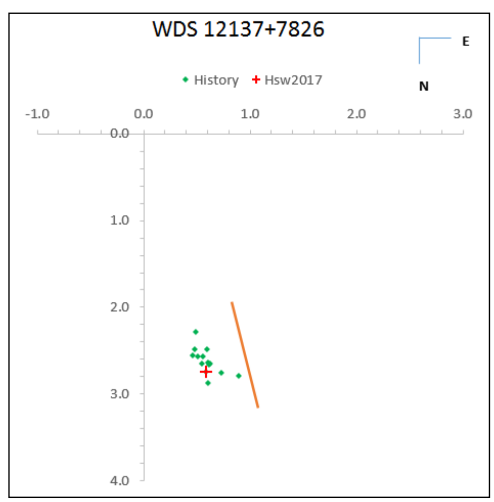

Figure 29. Plot of WDS 12137+7826.

Measurements of 427 Double Stars With Speckle Interferometry ...

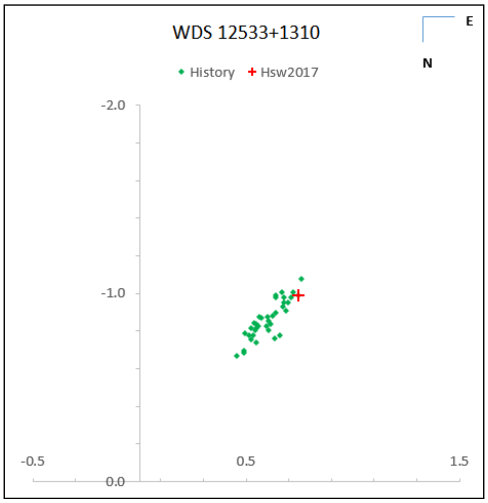

Figure 30. Plot of WDS 12533+1310.

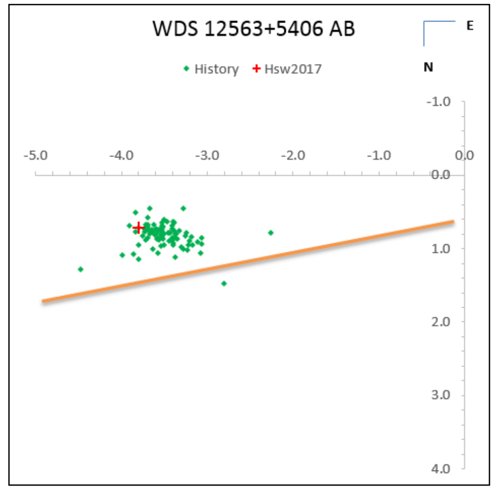

Figure 31. Plot of WDS 12563+5460 AB.

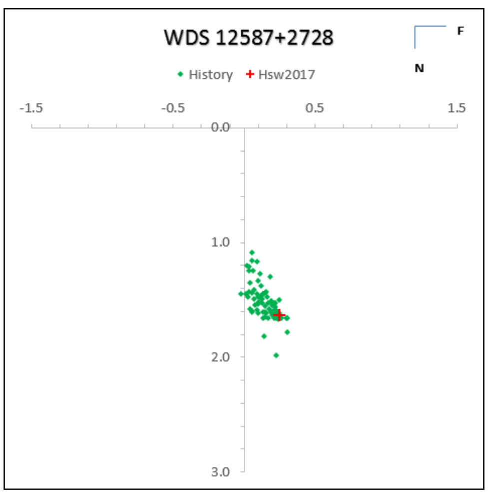

Figure 32. Plot of WDS 12587+2728.

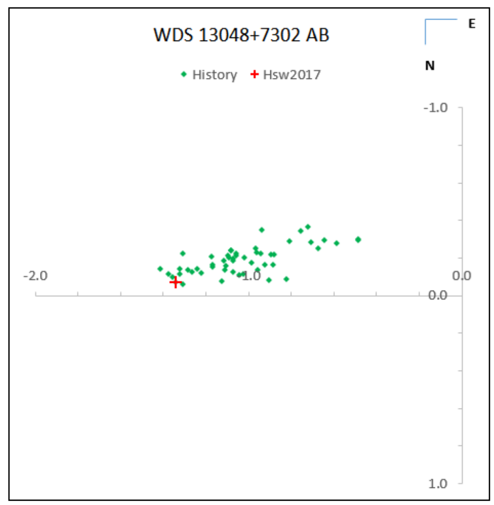

Figure 33. Plot of WDS 13048+7302.

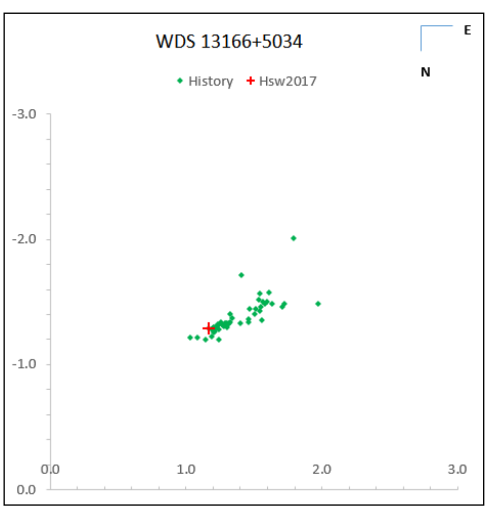

Figure 34. Plot of WDS 13166+5034.

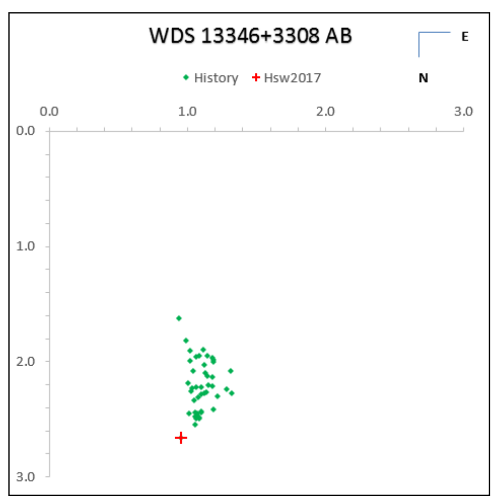

Figure 35. Plot of WDS 13346+3308.

Measurements of 427 Double Stars With Speckle Interferometry ...

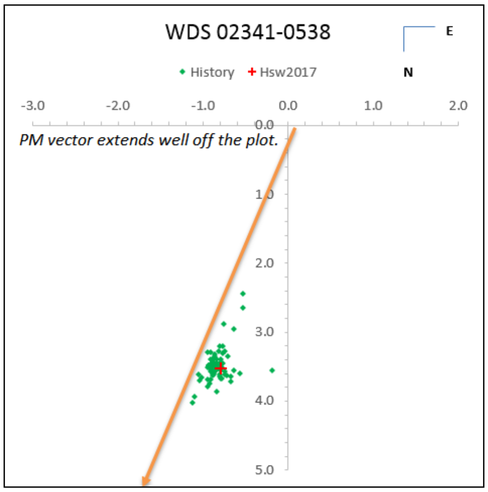

Figure 42. Plot of WDS 02341-0538

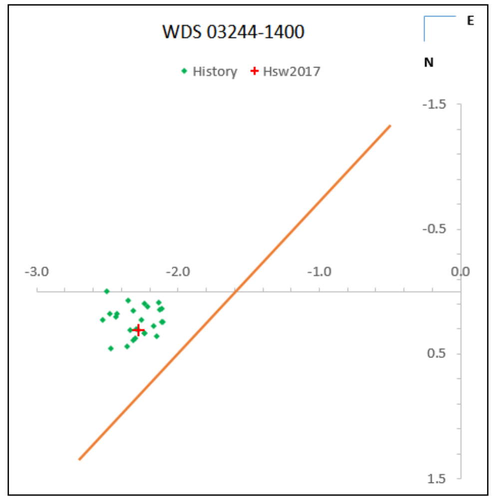

Figure 43. Plot of WDS 03244-1400.

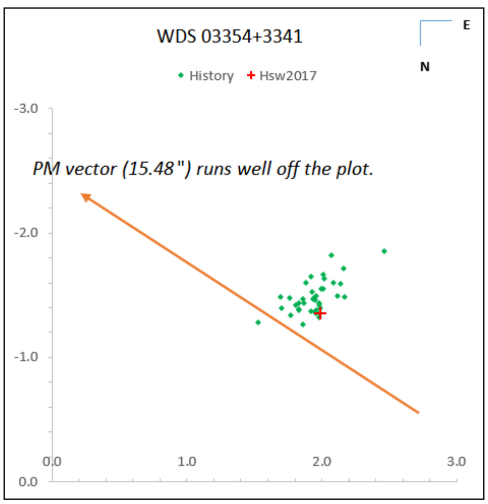

Figure 44. Plot of WDS 03354+3341.

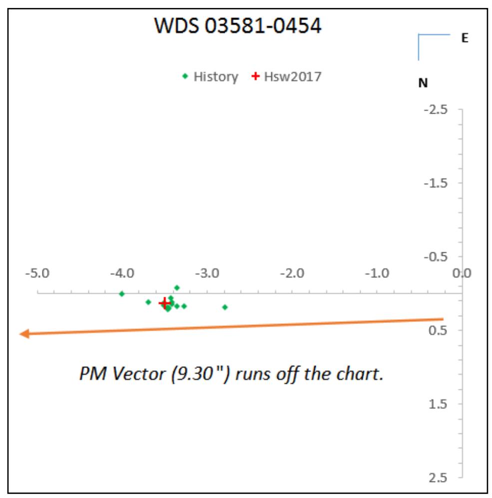

Figure 45. Plot of WDS 03581-0454.

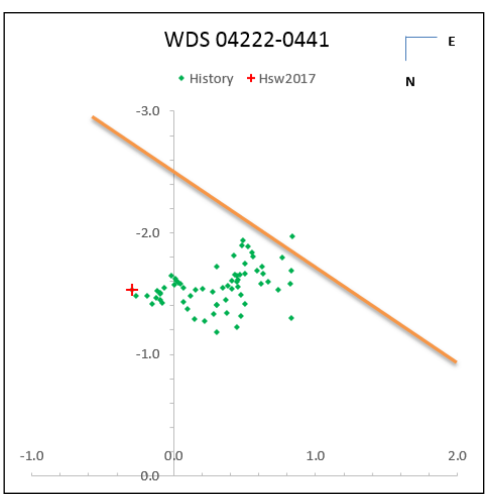

Figure 46. Plot of WDS 04222-0441.

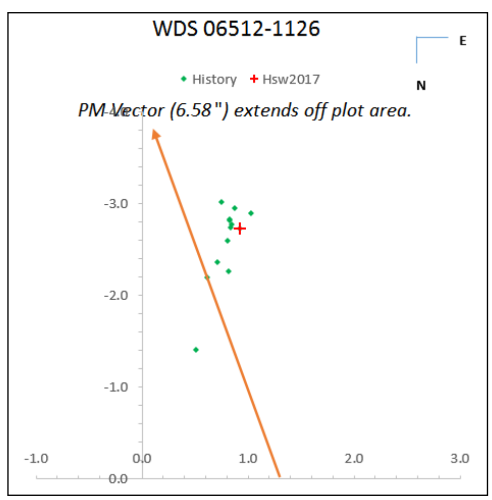

Figure 47. Plot of WDS 06512-1126.

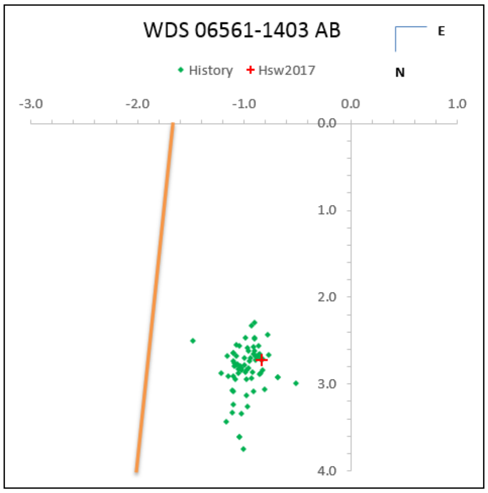

Figure 48. Plot of WDS 06561-1403

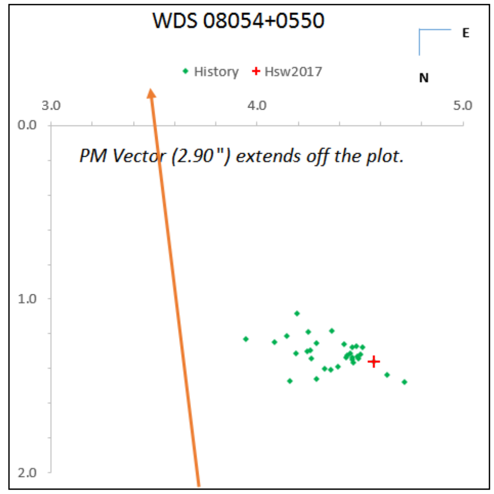

Figure 49. Plot of WDS 08054+0550.

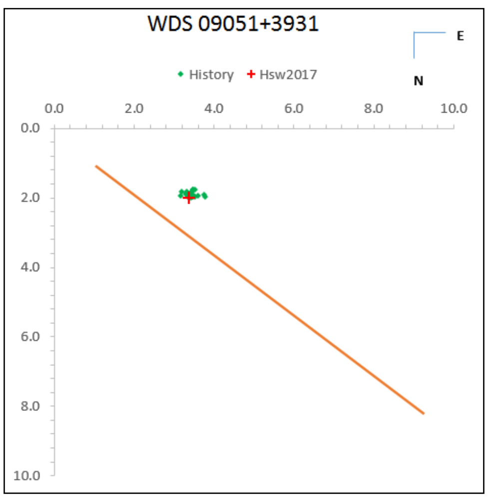

Figure 50. Plot of WDS 03354+3341.

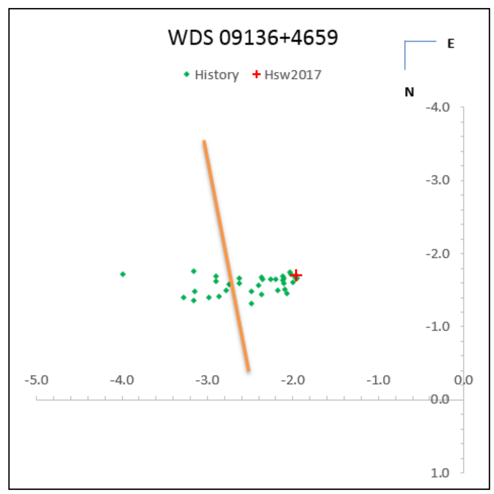

Figure 51. Plot of WDS 09136+4659.

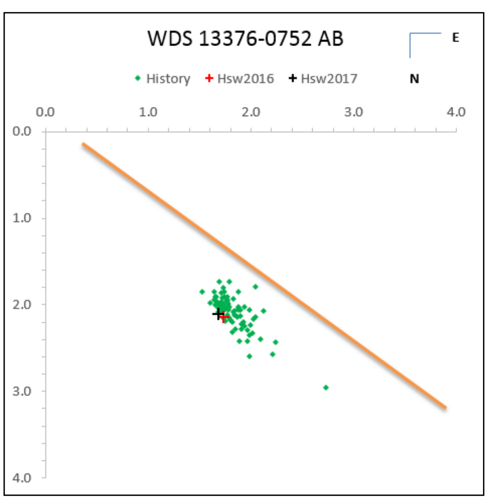

Figure 52. Plot of WDS 13376-0752.

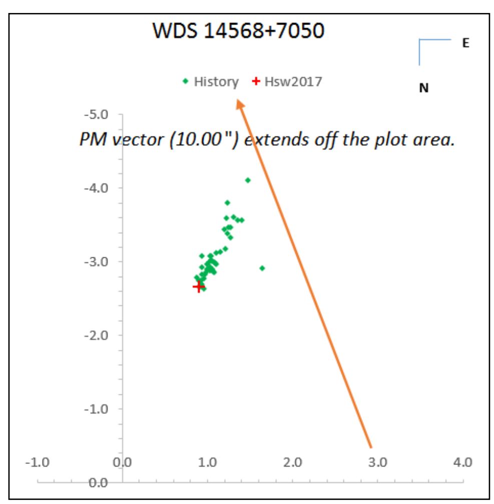

Figure 53. Plot of WDS 14568+7050.

Measurements of 427 Double Stars With Speckle Interferometry ...

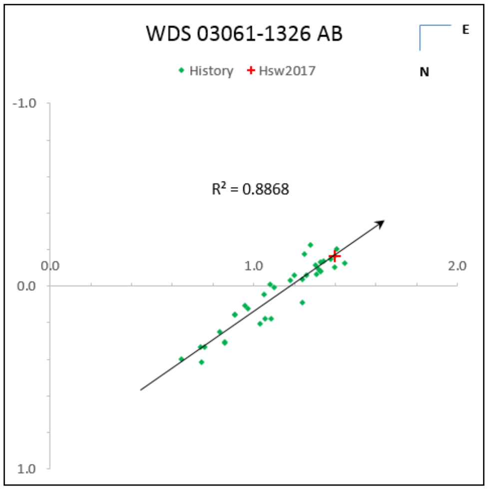

Figure 54. Plot of WDS 03061-1326 AB.

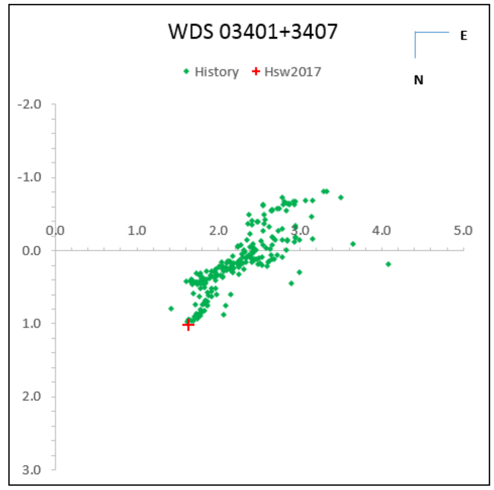

Figure 55. Plot of WDS 03401+3407.

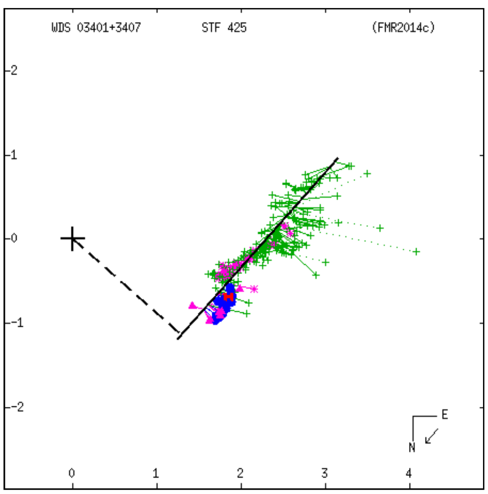

Figure 56. Linear solution of WDS 03401+3407 by FMR2014..

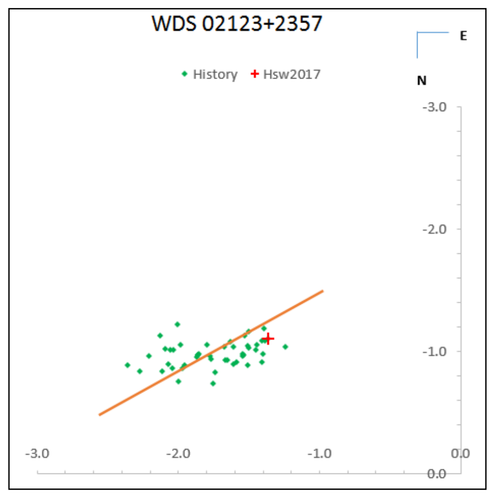

Figure 57. Plot of WDS 02123+2357.

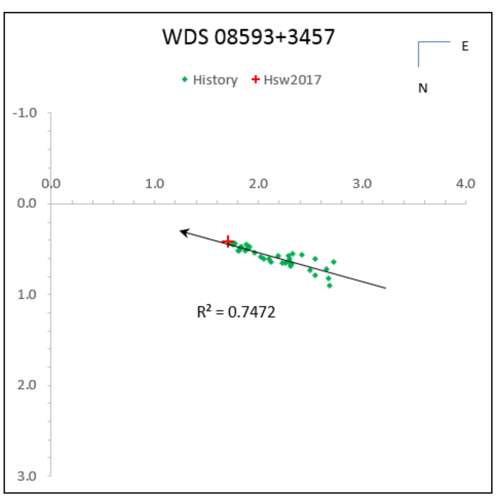

Figure 58. Plot of WDS 08593+3457.

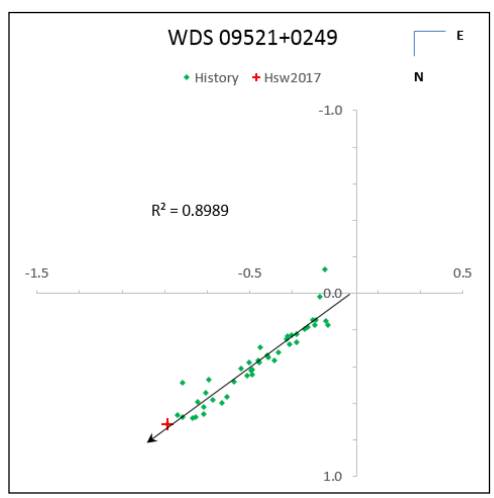

Figure 59. Plot of WDS 09521+0249.

Measurements of 427 Double Stars With Speckle Interferometry ...

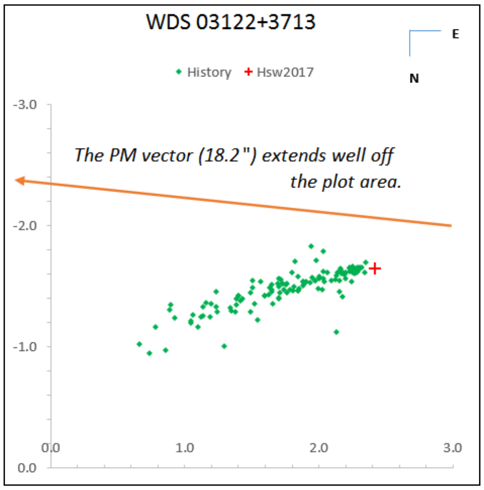

Figure 60. Plot of WDS 03122+3713.

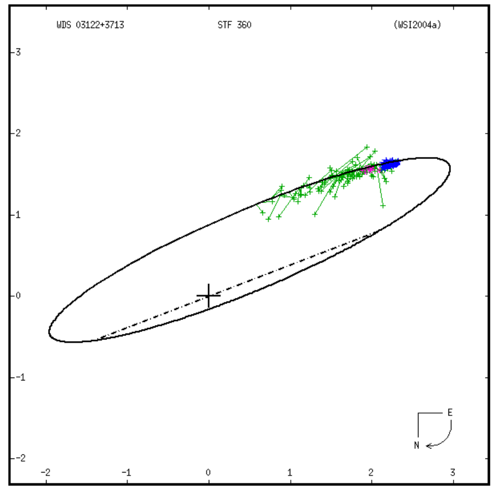

Figure 61. Orbital solution of WDS 03122+3713.

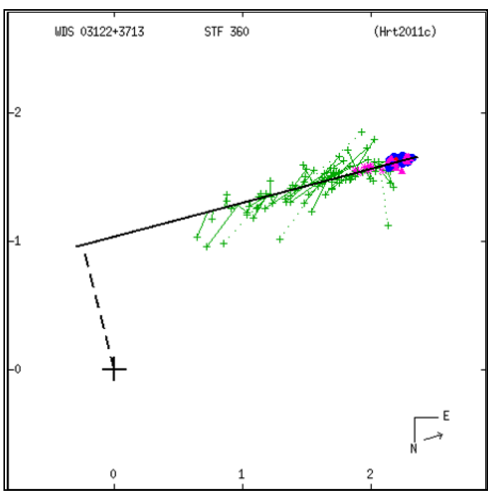

Figure 62: Linear solution of WDS 03122+3713.

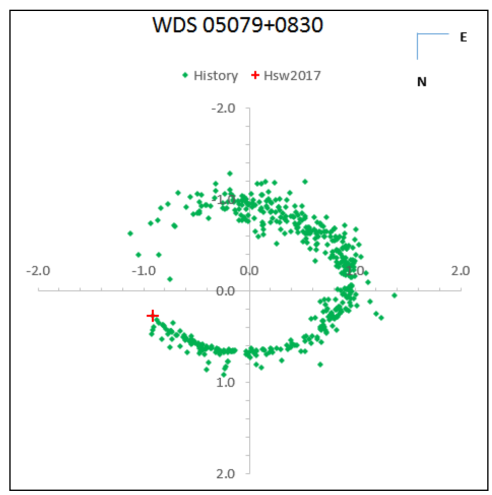

Figure 63. Plot of WDS 05079+0830.

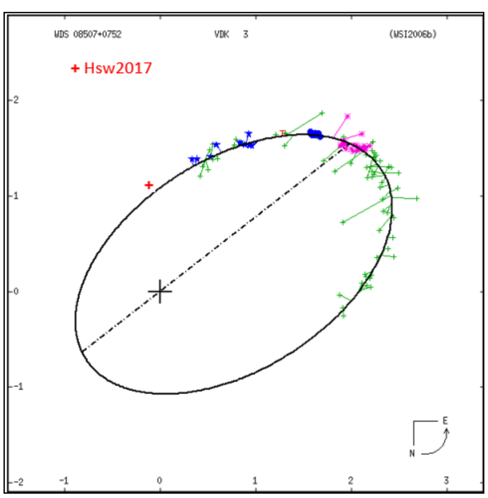

Figure 64. Plot of WDS 08507+0752.

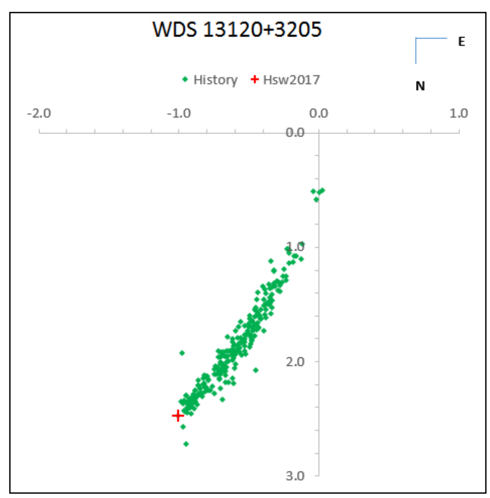

Figure 65. Plot of WDS 13120+0830.

Measurements of 427 Double Stars With Speckle Interferometry ...

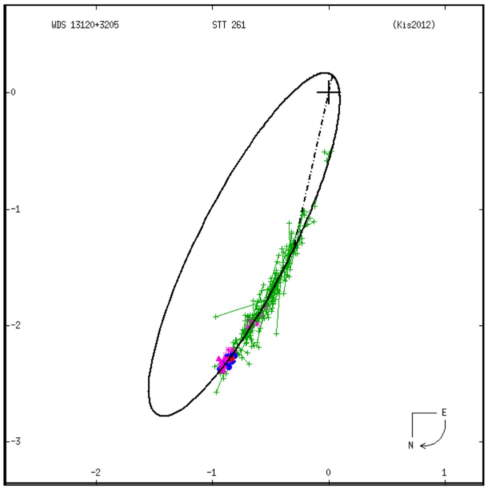

Figure 66: Kiselev's orbit for WDS 13120+3205.

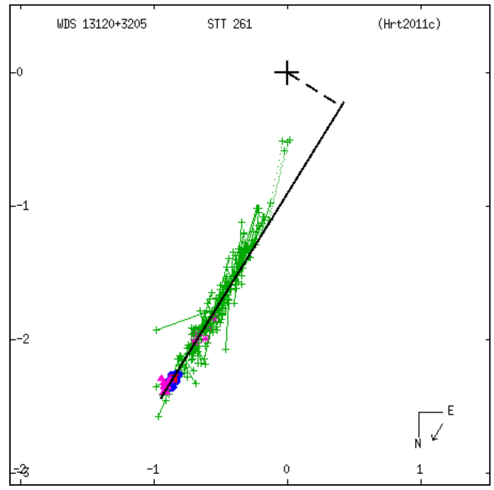

Figure 67: Hartkopf's linear solution for WDS 13120+3205 .

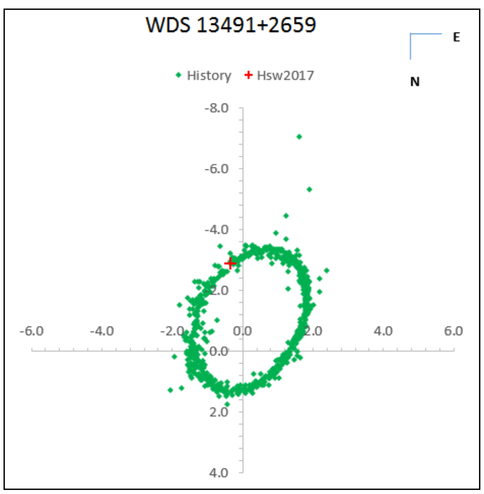

Figure 68: Plot of WDS 13491+2659.

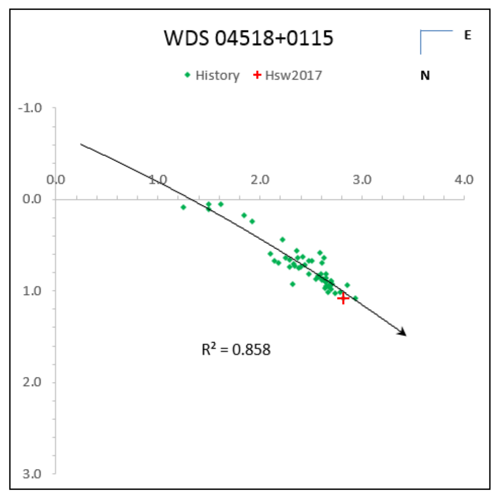

Figure 69. Plot of WDS 04518+3205.

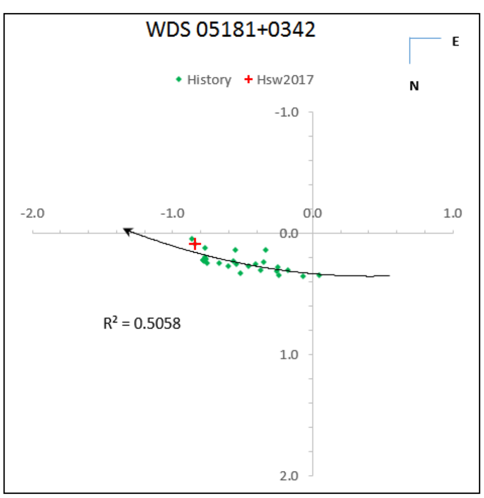

Figure 70. Plot of WDS 05181+0342.

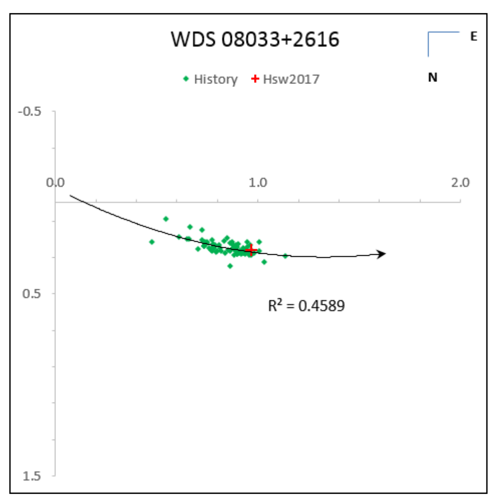

Figure 71. Plot of WDS 08033+2616.

Measurements of 427 Double Stars With Speckle Interferometry ...

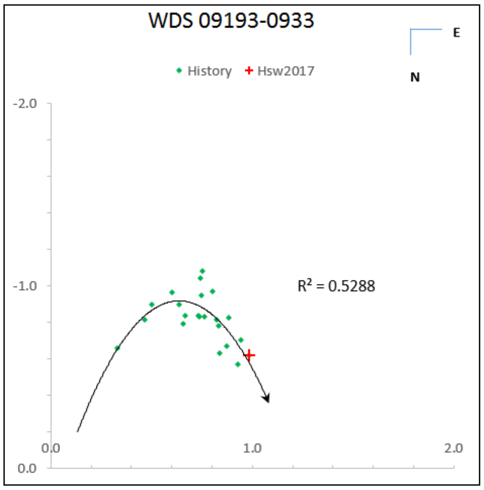

Figure 72: Plot of WDS 09193-0933.

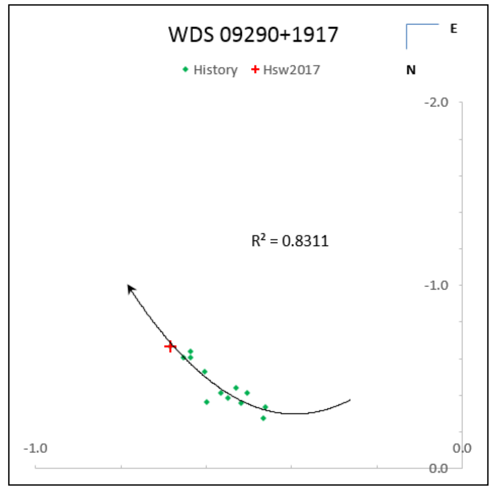

Figure 73. Plot of WDS 09290+1917.

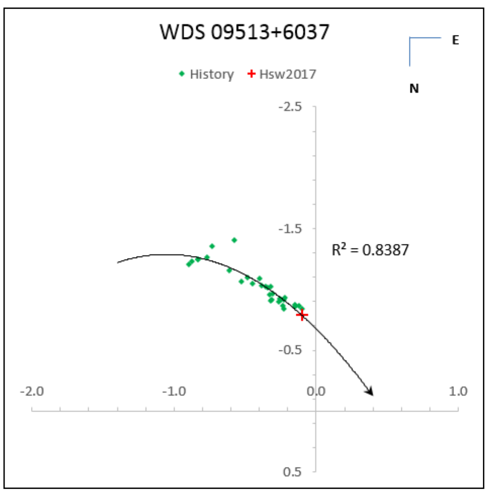

Figure 74. Plot of WDS 09513+6037.

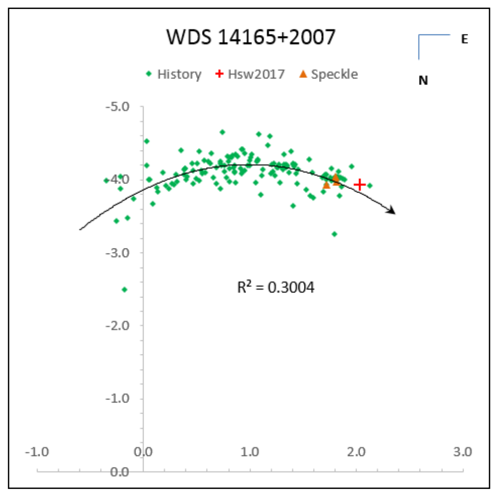

Figure 75. Plot of WDS 14165+2007.

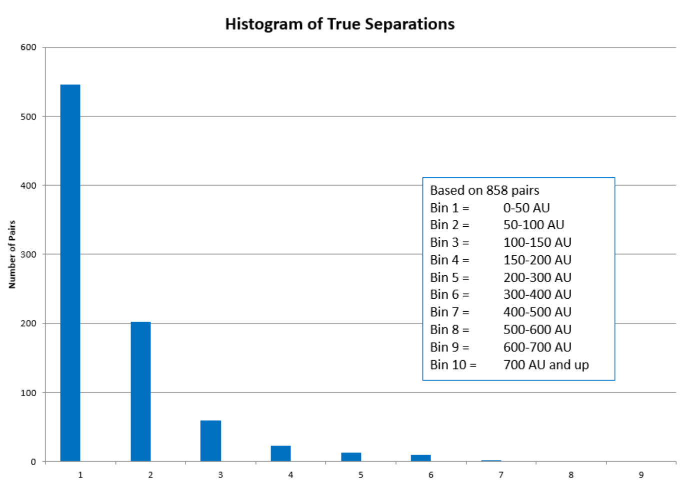

Figure 76: Histogram of A-B Separations (in AU) from the Sixth Orbit Catalog

A Simple Method for Reproducing Orbital Plots for Illustration Using Microsoft Paint and Microsoft Excel

Cole Niebuhr

Global Science Directive - Las Vegas, NV
Concordia University Irvine – Irvine, CA

Abstract: Papers published in the astronomical community, particularly in the field of double star research, often contain plots that display the positions of the component stars relative to each other on a Cartesian coordinate plane. Due to the complexities of plotting a three-dimensional orbit into a two-dimensional image, it is often difficult to include an accurate reproduction of the orbit for comparison purposes. Methods to circumvent this obstacle do exist; however, many of these protocols result in low-quality blurred images or require specific and often expensive software. Here, a method is reported using Microsoft Paint and Microsoft Excel to produce high-quality images with an accurate reproduction of a partial orbit.

Introduction

Accurate orbital reproductions are often difficult and time-consuming requiring advanced software coupled with a thorough knowledge of the program. Many of these methods do not translate well into Microsoft Excel graphs and attempts often result in low-quality images instead of high-quality plots. To this end, a method was developed that allows for high-quality reproductions to be made in Microsoft Excel using data extracted from images with Microsoft Paint. For purposes of illustration, recent work published on the binary star WDS 15559-0210 will be reproduced.

Methods

An orbital plot and the represented data points were obtained from the Washington Double Star Catalog (WDS) maintained by the United States Naval Observatory (ref: Washington Double Star Catalog). The data points were filtered (Musegades et al 2017) and plotted in MS Excel (Figure 1). The orbital plot was opened in MS Paint and the image was cropped to only include the third (lower left) quadrant. This placed the origin of the plot in the upper right corner of the image corresponding to pixel (230,0) as read in the cursor position readout at the bottom left corner of the MS Paint screen (Figure 2). Using the cursor position, 0 arcseconds(″) corresponded with 0-pixels and -5″ with 160 pixels. This means that, for this image, 1″ is equivalent to 32 pixels. This was an important conversion factor needed for plotting the orbit in MS Excel.

Next, using the cursor position readout, five points were collected from the orbit itself and the corresponding pixels recorded in MS Excel. Two additional points were collected for the endpoints of the orbit as determined by the window range desired for the graph. Each of the points was subtracted from the identified origin so that the new coordinate was in terms of distance from the origin. These values were made negative in order to correspond with the third quadrant. The points were converted to arcseconds with the conversion factor mentioned above.

For this equation, Q is the quadrant multiplier (-1

$$(x_{excel}, y_{excel}) = \left(Q_x * C.F. * \left|x_{origin} - x_n\right|, Q_y * C.F. \left|y_{origin} - y_n\right|\right)$$

for both x and y in Quadrant Three), C.F. is the conversion factor (1/32 for this example), and includes the pixel coordinates for the origin (230, 0)

These points, now in arcseconds from the origin,

$$(x_{excel}, y_{excel}) = \left(-\frac{1}{32} * \left|230 - x_n\right|, -\frac{1}{32} * \left|0 - y_n\right|\right)$$

were added to the MS Excel graph (Figure 3). Finally, as shown in Figure 4, a polynomial trend line of the extracted data points was added and the points were rendered invisible (Format Data Series – Marker Option – None).

(Text continues on page 333)

A Simple Method for Reproducing Orbital Plots for Illustration Using Microsoft Paint and Microsoft Excel

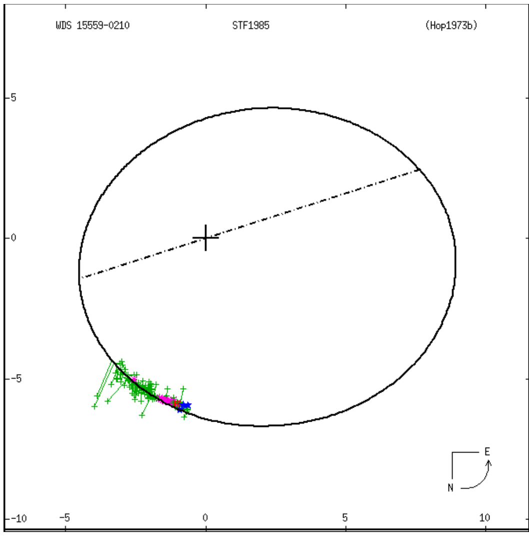

Figure 1. Two-dimensional orbital plot of WDS 15559-0210 (left) with the data points provided by the WDS plotted in Microsoft Excel (below).

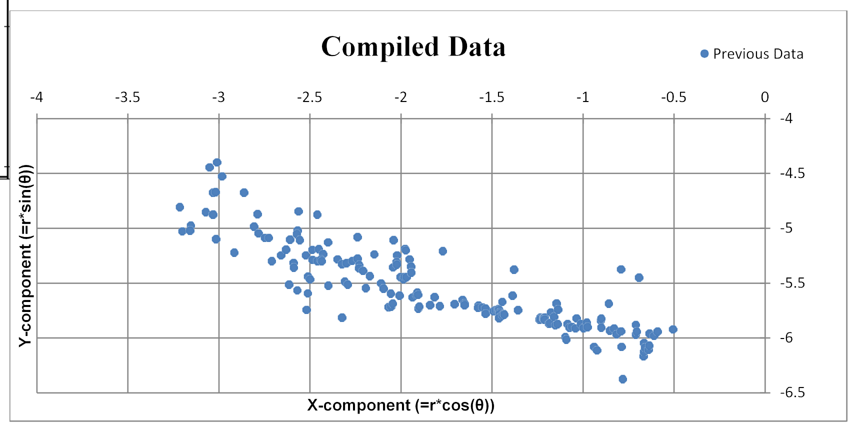

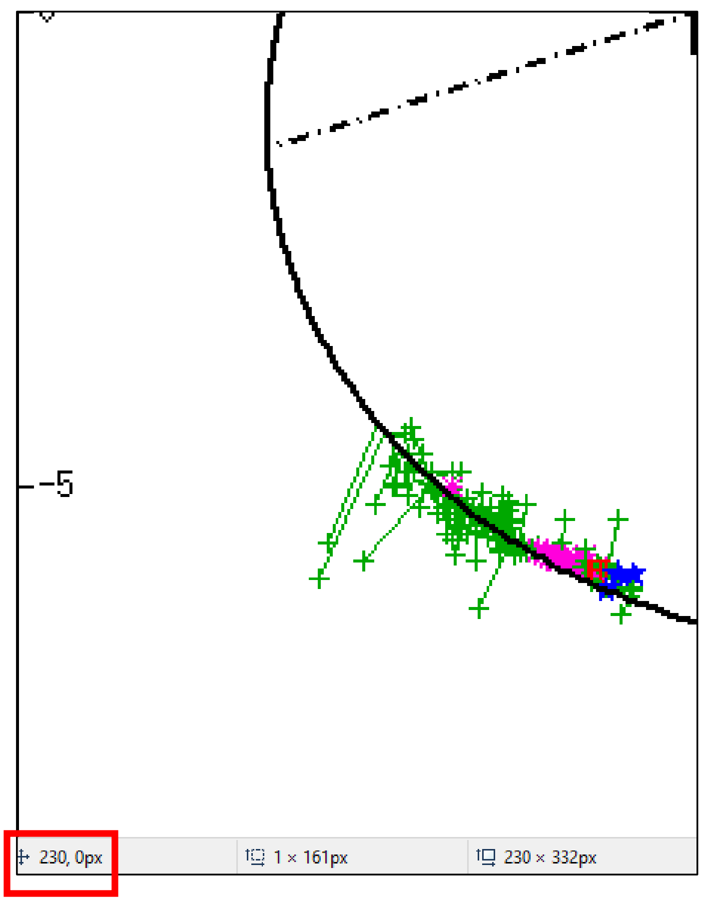

Figure 2. The orbital plot cropped to only include Quadrant Three. This places the origin of the orbit at pixel (230, 0) in the MS Paint Screen. Cursor position is shown in the bottom left corner of the screen and is highlighted in the figure with a red box.

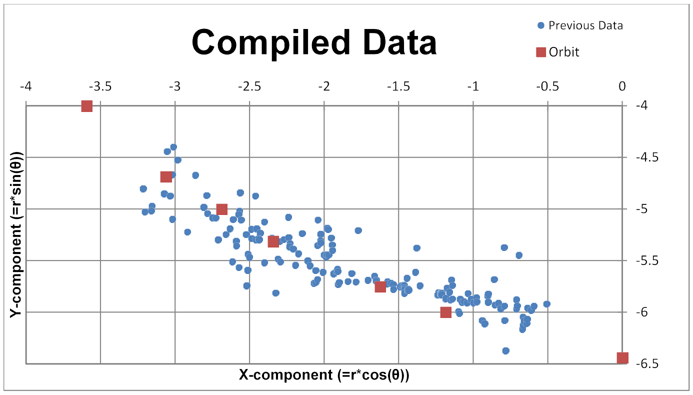

Figure 3. The points extracted from the published orbit (in pixels) were converted to arcseconds and plotted with the previous data points.

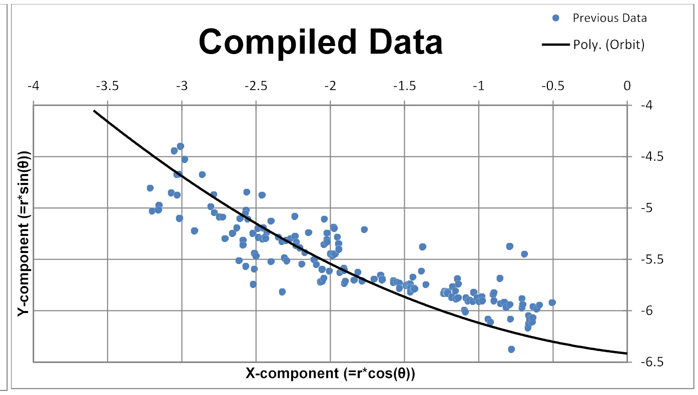

Figure 4. The "final product" where a reproduced orbit using the trend line feature is included with the previous data points for comparison.

(Continued from page 331)

Discussion

This method has many advantages but is not without limitation. The advantages include the low price, accessibility, and ease of use of the MS Paint software and MS Excel. The resultant plot is not completely accurate, but it does serve as a good approximation sufficient for illustrating small arcs of an orbit. As seen in Figure 5, the 2nd- through 5th-order polynomial trend lines quickly lose fidelity to the orbit once the domains of the functions move beyond the preselected data points. Within the scope of the selected data, however, the trend lines and published orbit overlap together nearly identically.

Acknowledgements

It is a pleasure to thank Brian Mason from the United States Naval Observatory for supplying the historic data collected in the Washington Double Star Catalog. Thanks are also due to Richard Harshaw, John Kenney, and Vera Wallen for their services as external reviewers.

References

Musegades, L., Niebuhr, C., Graham M., Poore, A., Freed, R., Kenney J., Genet, R., 2017, "An Astrometric Observation of Binary Star System WDS 15559-0210 at the Great Basin Observatory", *Journal of Double Star Observations*, **14**(2), 197 (this issue).

The Washington Double Star Catalog, 2012, Retrieved July 06, 2017, from http://www.usno.navy.mil/USNO/astrometry/optical-IR-prod/wds/WDS

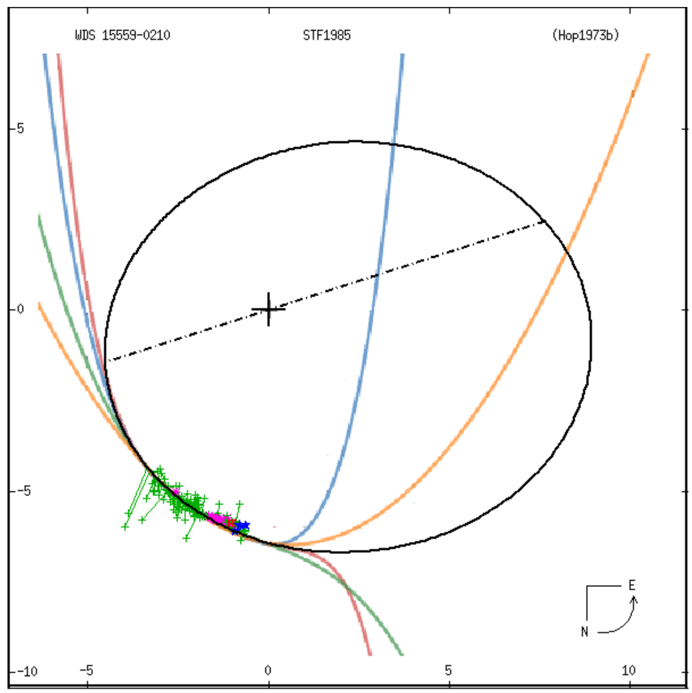

Figure 5. MS Excel trend lines plotted for comparison with the published orbit (black). The plots includes ~~s~~ 2nd, 3rd, 4th, and 5th order polynomial trend lines (colored). The graphs were produced with the Desmos software and MS Paint was used to paste the graphs onto the orbital plot by aligning the origin of the two images.

Astrometric Measurements and Proper Motion Analysis For WDS 11582 +0335 HJ 1204

Erica Edwards[1], Jose R. Garcia II[1], Cheyenne Terronez[1], Melanie Stuart[1], Jae Calanog[1], Pat Boyce[2], and Grady Boyce[2]

1. Miramar College, San Diego, California, USA
2. Boyce Research Initiatives and Education Foundation (BRIEF), California, USA

Abstract: We obtained and analyzed CCD images of the double star system WDS 11582 +0335 (HJ 1204) using the iTelescope network and a variety of specialized software. WCS coordinates were attached to each image, and the separation distance (ρ) and mean position angle (θ) were measured at ρ = 7.9" ± 0.03" and θ = 59.3º ± 0.2º. These results were compared to historical data, dating back ~200 years and we find that HJ 1204 is currently exhibiting a linearly decreasing ρ and a constant θ. This suggests that HJ 1204 could be a visual double or an edge-on binary. Follow-up spectroscopic observations should resolve the two possibilities.

Introduction

Double stars are two stars that appear close to each other when observed from Earth. Some double stars are gravitationally bound, referred to as binary stars, and some are apparent, simply aligned by chance in our line of sight. By observing double stars over time, we can track their relative proper motion, which can aid in distinguishing between gravitationally bound and apparent, or visual double star systems.

The goal of our research is to provide current astrometric measurements of separation distance (ρ) and position angle (θ) for one double star system, known by its Washington Double Star (WDS) identifier, 11582+0335 HJ 1204 and hereafter referred to as HJ 1204 (Figure 1). Cumulative data on the system will ultimately show presence or absence of observed motion - evidence which distinguishes between visual doubles and gravitationally bound systems. Binary and multi-star systems are of broader scientific interest because by analyzing their orbits stellar mass can be determined, offering insight into the life cycle and death of the star. We also learn from binary systems that the laws of gravitation apply to distant stellar and solar systems and are therefore a universal property of mass.

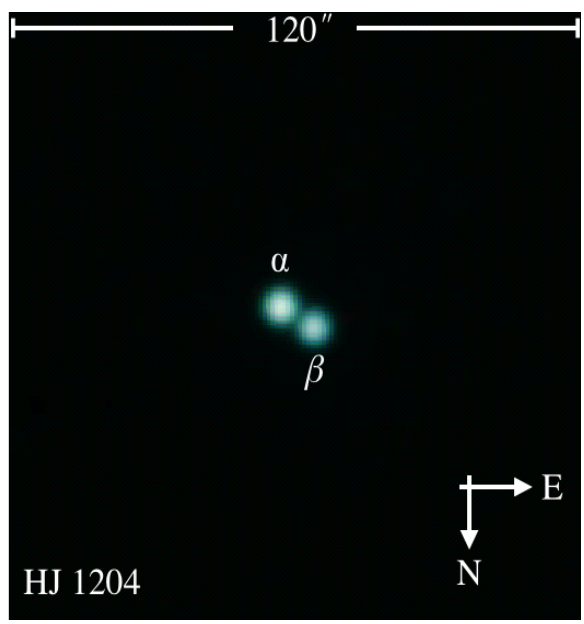

Figure 1: False color image of HJ 1204. North is down, east is right. The primary star is labeled α and the secondary star is labeled β. The image size shown is 120" x 120".

We selectively choose a double star system that fit our search parameters: right ascension and declination such that the pair are observable from approximately ~35° north latitude during the astronomical spring season, with a previously measured ρ between the primary (α) and secondary (β) stars of 7" and a magnitude dif-

Astrometric Measurements and Proper Motion Analysis For WDS 11582 +0335 HJ 1204

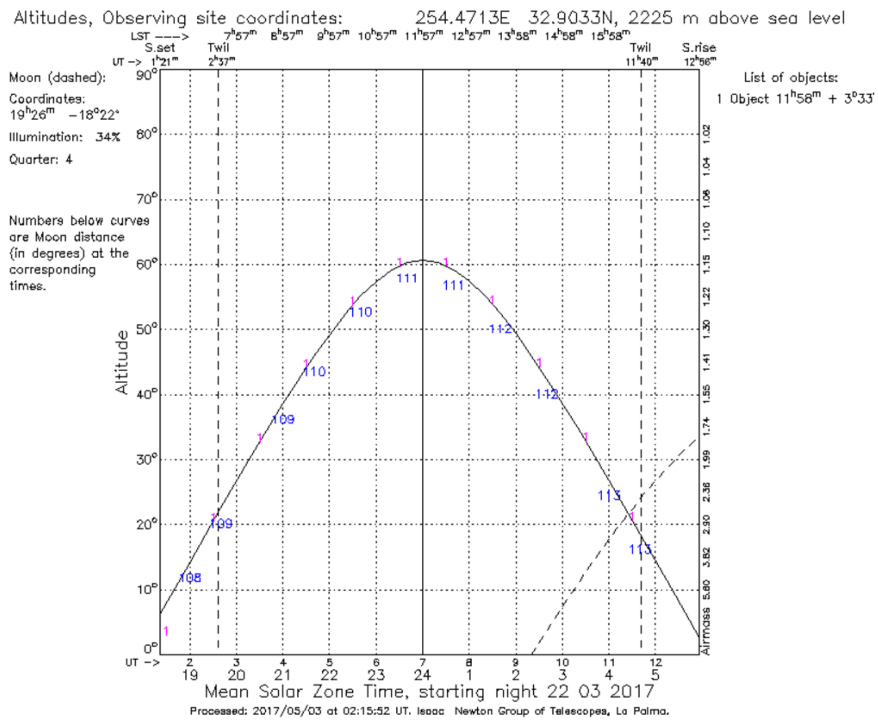

Figure 2. Graphical representation of HJ 1204's relative path through the night sky. The Object Visibility plot shows altitude above horizon (°) vs. time (hours), which was useful in determining an appropriate date and time to observe the pair. The curve indicates HJ 1204's path with numerical figures in blue representing relative distance from the Moon in degrees.

ference (Δm) between α and β of less than 1. The double star system HJ 1204 was an ideal candidate for observation, located in the Virgo constellation.

This system was first observed in 1828 by English astronomer Sir John Frederick William Herschel (1792-1871), who first recorded ρ = 15" and θ = 125°. The latter measurement is inconsistent with subsequent measurements, and Herschel's records indicate he was unsure about the orientation (Herschel, 1831). We have noted when this data point has been adjusted or omitted for the sake of consistency (see Discussion). Since 1828 there have been 13 observations, the most recent was a large sky survey in 2014 (Cvetkovic et al. 2015), with a ρ = 8" and θ = 59°, and a difference in magnitude of 0.44.

Methods and Equipment

We utilized the iTelescope network and requested images from two telescopes, T11 and T24, located in Mayhill, New Mexico and Auberry, California respectively. Both telescopes are equipped with cameras classified as CCD, or Charged Coupled Device technology (Table 3). The CCD camera has had a tremendous impact on astronomical imaging and spectroscopy since the 1980's. Deep space imaging is complicated by conditions of low light, noise, and cosmetics, however the CCD's high quantum efficiency (a ratio of the number of charge carriers collected by the solar cell to the number of incident photons) is 80-90% at peak in optical and is greatly advantageous over past observation methods (O'Connell, 2015). Figures 6 and 7 support the notion that measurements became more accurate with use of CCD. The T11 is a Planewave CDK20 equipped with a FLI ProLine PL1102M CCD and has a pixel scale of 0.81"/pixel. The T24 is a Planewave CDK24 equipped with an FLI Proline PL09000 CCD camera and has a pixel scale of 0.62"/pixel. We selected the telescopes based on geographic location, sub-arcsecond resolution, and equipment performance.

Observations were performed during times when HJ 1204 was approximately ~52° above the horizon in order to minimize atmospheric effects. Figure 2 shows the system's visibility curve for March 22, 2017 (ING, 2017). Eight images were taken on March 22, 2017 via the T11 (2 in luminance, 2 in Hα, 2 in green, and 2 in blue) and three images were taken April 24, 2017 via the T24 (1 in luminance, 1 in Hα, and 1 in blue). The flat-fielded and dark subtracted images were processed

Astrometric Measurements and Proper Motion Analysis For WDS 11582 +0335 HJ 1204

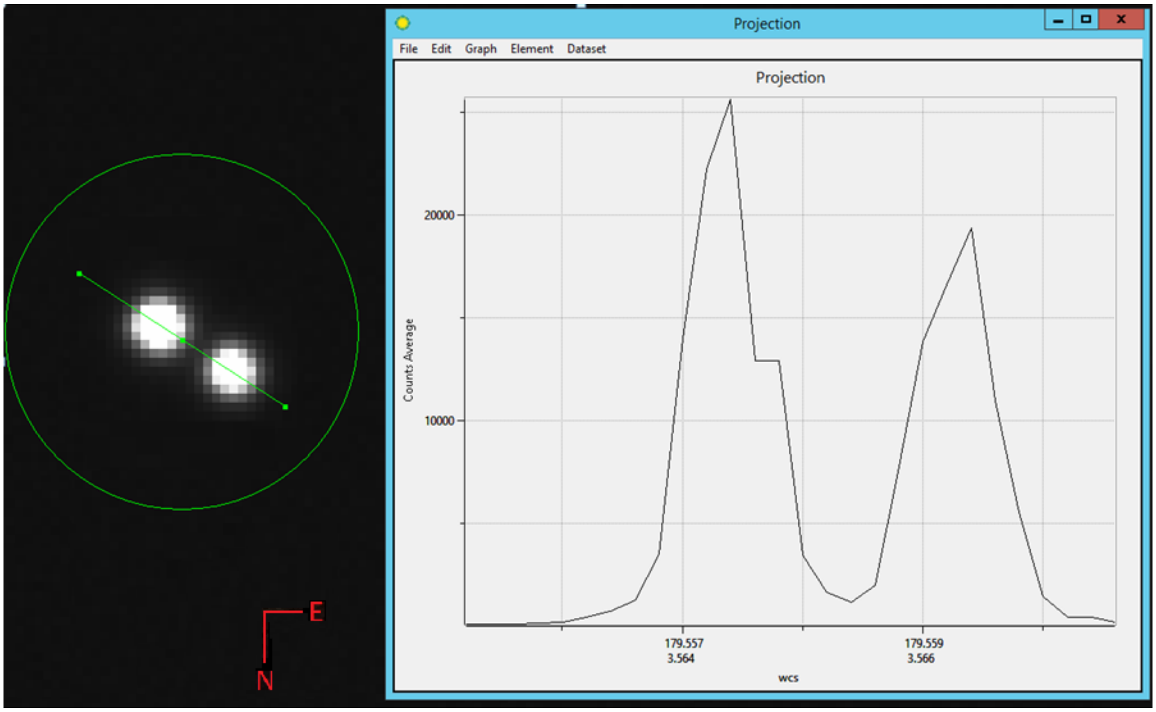

Figure 3. Quality analysis for one of eleven images taken of HJ 1204. The figure is a screenshot, using SAO Image DS9 software. The stellar image on the left is from the first set of images and shows the projection tool as a line segment that crosses the highest pixel value of each star. The graph on the right relays electron counts vs. pixel location (in WCS degree coordinates). The shape of the graph indicates a quality image, as the electron saturation for each star is less than half of the full-well limit of the T11 CCD, which is 60,000 electrons per pixel.

by the iTelescope Network's data reduction pipeline and downloaded.

In order to verify the quality of each image, we used SAO Image DS9 software's projection tool to display a graph of pixel count vs. position (Figure 3). By observing the peak count and the overall shape of the histogram, we were able to check that no saturation or unusual artifacts were present in the pixels associated with our double star system.

We used Maxim DL software to attach WCS coordinates to the image pixels. The U.S. Naval Observatory CCD Astrograph Catalog (UCAC4) was used as the WCS reference catalog for pattern recognition. Coordinates are determined by aligning known positions of stars within the image's field-of-view. A total of 867 imaged and catalog stars were used to fit WCS coordinates, with an average root-mean-square of 0.1".

To measure separation distance and position angle, each image was analyzed using Mira Pro software's point-to-point tool that connects a line between the centroids of the α and β stars (Figure 4). Mira Pro measures the centroid position by performing a Gaussian fit with a specified radius. The process is repeated several times on each image to ensure consistent results.

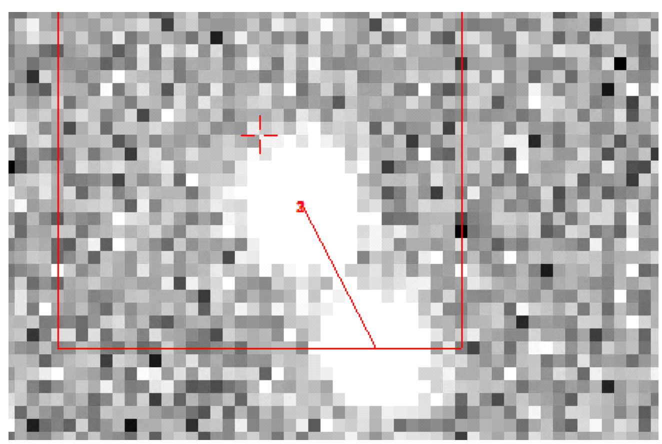

Figure 4. Astrometric analysis for one of eleven images taken of HJ 1204. This image was analyzed in Mira Pro. The red line depicts the point-to-point tool connecting the centroid of the primary to the centroid of the secondary star. Several red lines are superimposed, indicating the measured centers are consistently located to provide accurate measurements.

Results

Two sets of images were taken at separate locations, 31 days apart. The data sets are consistent with each other, indicating that the system exhibited negligi-

Astrometric Measurements and Proper Motion Analysis For WDS 11582 +0335 HJ 1204

Table 1. Recent data sets for observations of HJ 1204. *Position angle and separation distance are recorded for each telescope and epoch. For comparison, the most recent measurements taken in 2014 from the Rozhen Observatory in Bulgaria are listed in blue at bottom. Consistent with historical data, HJ 1204 currently exhibits a linearly decreasing ρ and a constant θ.*

Astrometric Results for HJ 1204		
T11 Telescope (8) Images Filters: (2) Luminance, (2) Hα, (2) G, (2) B		
Epoch 2017.2224	**θ(°)**	**ρ (")**
Mean	59.3	7.92
Standard Deviation	0.2	0.03
Standard Error of Mean	0.08	0.01
T24 Telescope (3) Images Filters: (1) Luminance, (1) Hα, (1) B		
Epoch 2017.3114	**θ(°)**	**ρ (")**
Mean	59.3	7.9
Standard Deviation	0.1	0.2
Standard Error of Mean	0.07	0.1
Epoch: 2014.2543 (Bulgaria)	59.3	8.01

ble movement between these two times. The results also concur with the trend exhibited by historical data.

Table 1 shows measurements from both observations along with the most recent for comparison. The average position angle calculated from the first set of images taken from the T11 telescope is 59.3º ± 0.2º, and separation of 7.9" ± 0.03" For the images obtained from the T24 telescope, we calculated a position angle of 59.3º ± 0.1º and a separation of 7.9"± 0.2" We note that we are unable to compare the statistical significance of our results with the last observation (Cvetkovic et al. 2015), since no uncertainties were reported with their measurements.

A full summary of historical astrometric data for HJ 1204 is shown along with present results in Table 2, and the method of measurement for each observation is further detailed in Table 3, with an implication that astrometric data for HJ 1204 may become more precise as a result of advanced technology.

Separation distance and position angle are plotted over time, shown in Figure 5 and Figure 6 respectively. The separation between α and β appears to be decreasing and supports a linear trend, with the two stars getting closer at a rate of 0.0375" per year.

The evolution of relative orientation between α and β features an obvious outlier of 125 degrees, recorded by Herschel in 1828. According to his remarks, Herschel was unsure about the correct orientation of north and south. Based on subsequent measurements including our own, we conclude this data point is likely an orientation error. If we adjust this record to reflect a reversed north and south, the result is 55 degrees, shown as an adjusted data point on the orbital plot (Figure 7) and the plot showing position over time (Figure 6). Once adjustments are made, α and β exhibit a position angle that has remained approximately con-

Table 2. Historical data for HJ 1204. Observer code indicates author and year of publication. The technique code (Table 3) identifies the type of technical equipment associated with each observation. Delta t in years is shown to note two significant periods of no observations following the initial observation and the 1913 observation.

Historical Data for HJ 1204					
Observation Date	**θ(°)**	**ρ (")**	**Δt (yrs)**	**Observer Code**	**Technique Code**
1828	125	15	N/A	HJ_1831	Mb
1903.3	62.2	12.042	75.3	Gau1926a	Pa
1910.34	60.4	12.009	7.04	WFC1998	Pa
1912.481	60.9	11.91	2.141	Fox1915	Ma
1913.34	61	11.76	0.859	Doo1923	Ma
2000.319	59.7	8.541	86.979	UC_2013	Eu
2000.91	59.6	8.48	0.591	TMA2003	E2
2006.315	59.4	8.32	5.405	Wly2007	C
2011.2379	59.43	8.06	4.9229	Pal2013	C
2012.3114	59.41	8.14	1.0735	Cve2015	C
2013.2843	59.32	8.05	0.9729	Cve2016	C
2014.2543	59.3	8.01	0.97	Cve2016	C
2017.2224	59.25	7.92	2.7457	N/A	C
2017.3114	59.3	7.9	N/A	N/A	C

Table 3. Expanded technique codes from those listed in Table 2.

Technique Code	Method of Measurement
Ma	Micrometer with Refractor
Mb	Micrometer with Reflector
Pa	Photographic technique, with astrograph
Eu	U.S. Naval Observatory CCD Astrograph Catalog (UCAC4)
E2	Two Micron All-Sky Survey (2MASS)
C	Charged Coupled Device (CCD)

Astrometric Measurements and Proper Motion Analysis For WDS 11582 +0335 HJ 1204

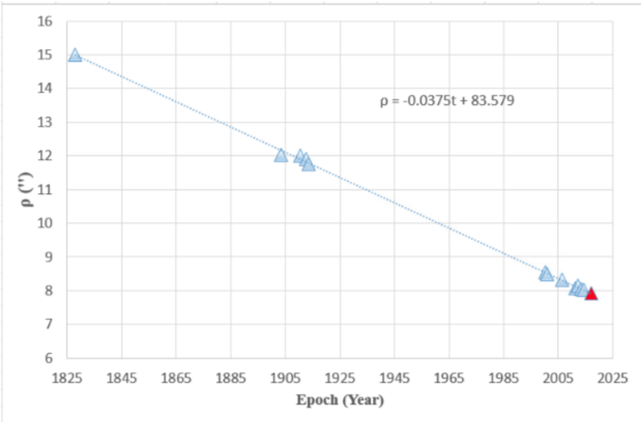

Figure 5. The graph represents the separation distance between α and β stars in arc seconds over time. Our 2017 measurement for ρ is shown as a darkened triangle at bottom right. Thirteen measurements over nearly two centuries show the distance between the stars is decreasing, and the data supports a linear trend, expressed in algebraic form. The linear fit suggests HJ 1204 is a visual double rather than gravitationally bound.

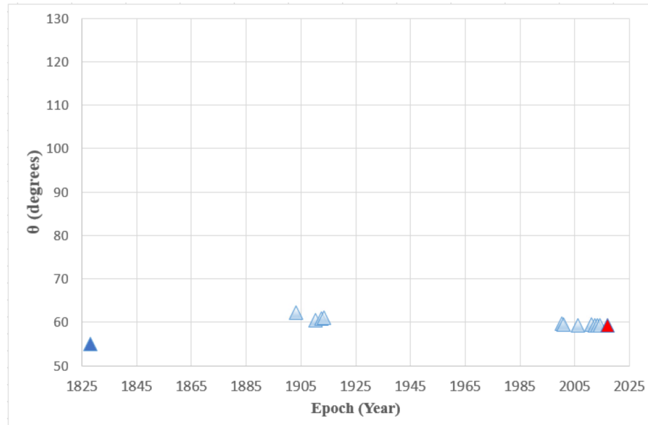

Figure 6. HJ 1204's change in position over time. Hershel's initial measurement in 1828 of 125° (darkened blue marker) at bottom left has been adjusted to reflect reversed poles. Our 2017 data points are combined at bottom right (darkened red marker). The vertical axis is degrees from north, the horizontal axis is time.

stant over the past 200 years.

The trends shown in Figure 5 and 6 are reflected in the orbital plot, with the secondary directly approaching the primary, positioned at the origin (Figure 7). The current set of data supports a linear solution for HJ 1204, where the relative proper motion will eventually cause these two stars to be completely aligned along our line of sight. If this is indeed the case, we would expect them to be aligned in ~2200 years, given the current rate at which the separation distance is decreasing. If this happens and given the right conditions, HJ 1204 might demonstrate an extremely rare and exotic strong gravitational lensing event (Einstein, 1936), producing multiple images of background star, lensed by the foreground star.

Another less likely possibility is that the primary

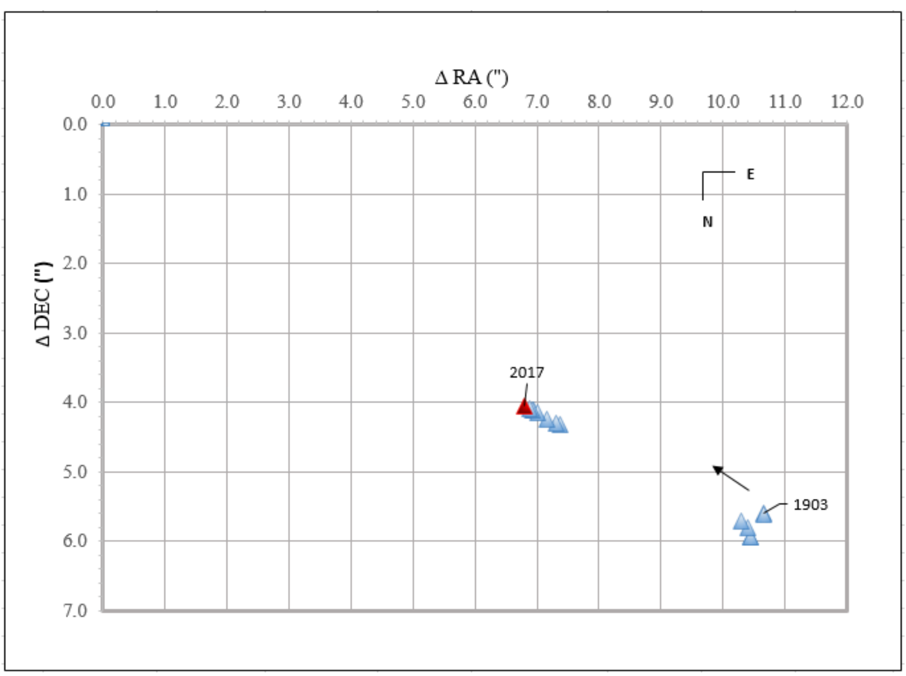

Figure 7. *The graph shows relative declination and relative right ascension with respect to the origin, where the primary star is placed. The data shows a generally linear motion where the position is changing at a constant rate, which would suggest a linear solution. Our 2017 result (Table 2) is shown as a darkened triangle. Herschel's 1828 data point is omitted for consistency.*

Astrometric Measurements and Proper Motion Analysis For WDS 11582 +0335 HJ 1204

and secondary are physically associated and is being observed edge-on, making HJ 1204 an ideal candidate for spectroscopic observations. In addition, having spectroscopic data would also determine physical distances for both stars, which will allow observers to correctly classify whether the HJ 1204 is a physical or a visual double. If HJ 1204 is a spectroscopic binary, we would expect it to have a period in the order of thousands of years, given that the slope in Figure 5 has remained constant for ~200 years.

Conclusion

We obtained and processed CCD images to measure the separation distance and position angle for HJ 1204. Our results are consistent with historical data. Over a timespan of ~200 years, the separation distance is linearly decreasing and cumulative changes in position angle are small enough to consider it constant. The current set of results show two possibilities: HJ 1204 could be aligned by chance or it could be an edge-on binary system. Spectroscopic follow-up observations would be necessary in order to arrive at a resolution.

Acknowledgements

The authors warmly thank Dr. Jae Calanog for his insightful contributions to this research paper, as well as B.R.I.E.F. for use of their remote server and funding of the project. The authors also thank the United States Naval Observatory for providing timely historical data and the iTelescope Network for use of their service.

References

Baillaud, R., *Annales de l'Observatoire de Besançon*, 1943. Vol 3, p72.

Cvetkovic, Z., Pavlovic, R., and Boeva, S., "CCD measurements of double and multi-star systems at NAO Rozhen". *Astronomical Journal,* 2015, 151, 58C.

Doolittle, E., Pub. University of Pennsylvania 4, Pt. 2, 1923

Einstein, A., *Science*, 1936, 84, 506

Fox, P., Ann. Dearborn Obs. 1, 1, 1915

Gauchet, P.L., Ann. Shanghai Obs. Zo-Se 14, 131, 1926

Hartkopf, W.I., Mason, B.D., Finch, C.T., Zacharias, N., Wycoff, G.L., & Hsu, D., Astronomical Journal, 146, 76, 2013 (UC 301 - 5058)

Herschel, J.F.W., 1831. *Memoirs of the Royal Astronomy*, Vol 4 p344

Pavlovic, R., Cvetkovic, Z., Boeva, S., Vince, O. & Stojanovic, M., Astronomical Journal 146, 52, 2013.

Urban, S.E., Corbin, T.E., Wycoff, G.L., Martin, J.C., Jackson, E.S., Zacharias, M.I., & Hall, D.M., Astronomical Journal 115, 1212, 1998 (Astrographic Cat. 2000).

Wiley, E.O. "Neglected Double Observations for 2016, No. 2", Journal of Double Star Observations, Vol 3, 63, 2007.

CCD Study of WDS 15098-0445

Rachel Banister[1], Nikki Arman[1], Kendra Kleber[1], and Grady Boyce[2]

1. Better Education for Women in Science and Engineering (BE WiSE)
2. Boyce Research Initiatives and Educational Foundation (BRIEF)

Abstract: Astrometric measurements of WDS 15098-0445 were obtained using the iTelescope Network. The distance between the A and B components was found to be 26.314" and the position angle was found to be 35.197°. The distance between the A and C components was found to be 607.927" and the position angle was found to be 217.868°. The change in the AC pair is consistent with past data, which indicates it is an optical double. The change in the AB pair indicates it is also an optical double.

Introduction

WDS 15098-0445 is a triple star system in which the AB pair was first measured in 1999 and the AC pair was first measured in 1920. The AB and AC pairs have discoverer codes of OSO and LDS, respectively, which identify the original measurements. This star system was selected for research from the Washington Double Star Catalog (WDS) because it possessed the following characteristics: The AB pair had few measurements and had not been measured since 1999, the AC pair had first been measured in 1920 and most recently measured in 2000, and was listed as an optical double (Mason & Hartkopf, 2012). These characteristics were desired because the researchers wanted to provide more data for a system that had been overlooked. Additionally, because the AC pair was an optical double and initial research using the online double star search engine, Stelle Doppie, indicated that the A star is a "high proper motion star" (SiMBADWeb), the researchers hypothesized that the AB pair was also an optical double.

The AB pair, with three measurements spanning a period of four years (1995-1999), has shown relatively high changes in position angle (Theta) and separation (Rho) for stars separated by a Rho of 20 arcseconds (20"). Over a period of 80 years, the separation of the AC pair has changed by 64", with an average change of almost an arcsecond per year. The measurements from this paper show significant movement since 2000 for both pairs.

Materials and Procedure

The AB components have a differential magnitude of 5 while the AC components have similar magnitudes. Given the differential magnitudes and separations, many of the iTelescope Network's telescopes were suitable imaging platforms. Additionally, because the declination of the system is near the celestial equator, all iTelescope locations were able to image this double star.

iTelescope T3, a one-shot color imaging system located in Nerpio, Spain, was chosen to image both pairs. In the original set of images, the B component was not visible, thus the images were not usable. The second set of images was obtained using the Mayhill, New Mexico Telescope 11 (T11) in the iTelescope network. The imaging session utilized hydrogen-alpha, red, and luminance filters. All components of the system were visible using the T11.

Images were downloaded from the iTelescope FTP site and imported into MaximDL to calibrate each pixel in the images with the World Coordinate System (WCS) Right Ascension and Declination. The WCS calibrated images were imported into Mira Pro x64 to measure Theta and Rho values. This data was then imported into Microsoft Excel to organize each measure and for statistical analysis.

Data and Results

Both the AB and AC pairs were successfully captured in seven images. Tables 1 and 2 provide the meas-

CCD Study of WDS 15098-0445

Table 1. Mira Pro measurement of the AB pair of WDS 15098-0445

AB Pair	Position Angle (degrees)	Separation (arc seconds)
Individual Measurements	35.47	26.29
	35.30	26.29
	35.20	26.29
	35.74	26.29
	34.52	26.24
	34.98	26.36
	35.18	26.44
Mean	35.20	26.31
Std. Dev.	0.385	0.385
Std. Error of Mean	0.146	0.025

Table 2. Mira Pro measurement of the AC pair of WDS 15098-0445

AC Pair	Position Angle (degrees)	Separation (arc seconds)
Individual Measurements	217.863	608.15
	217.868	608.18
	217.868	608.17
	217.864	607.95
	217.863	607.66
	217.874	607.69
	217.877	607.69
Mean	217.868	607.93
Std. Dev.	0.006	0.244
Std. Error of Mean	0.002	0.092

urements for each image individually as well as the mean, standard deviation, and standard error of the mean. The precision afforded via the Maxim and Mira software provides measurements to three significant figures. These were included in the Tables; however, to match historical measurements the values were rounded to match the precision of the WDS Catalog in Tables 3 and 4.

Discussion

AB Pair

The primary star in the AB pair is referenced by many catalogs, with SiMBAD specifically identifying the star as WOLF 1137, named after German Astronomer Max Wolf who compiled a catalog of over 1,500 low-luminosity, high proper motion stars, of which this star is the 1,137th in that catalog (SimBAD Web).

The first recorded data for this pair is from the Hipparcos mission in 1991 in which the location and magnitude of the A component was measured (HIPPARCOS). Osorio & Martin measured the AB pair in their paper, *A CCD Imaging Search for Wide Metal-Poor Binaries* (Osorio & Martin, 1995). The last reported measurement was recorded in 1999 by the Two-Micron All Sky Survey (2MASS).

Locating the AB pair in the T11 images was difficult due to the large difference in magnitude between the stars. There were a few candidate stars close to A, but none with a similar Theta and Rho to the last reported measurement. To locate the B component, ALADIN was used to obtain the image from 1999 from the 2MASS survey to compare with the Theta and Rho measurements of 51.7^o and 21.0" in the WDS (see Figure 1) (ALADIN).

After the B component was located, the 2017 T11 images indicated a Theta of 35.2^o and Rho of 26.4", a change of 16.5^o and 5.4" (see Figure 2). Measuring

Table 3. Historical data for the AB pair.

Epoch	Position Angle (degrees)	Separation (arcseconds)
1995	20.19	56.8
1999	20.99	51.6
1999	21.06	51.5
2017	*35.19*	*26.3*

Table 4. Historical data for the AC pair.

Epoch	Position Angle (degrees)	Separation (arcseconds)
1920.	225.00	677.0
1991.25	-	677.0
1999.20	217.30	614.04
1999.44	217.10	612.8
2000.268	217.30	613.5
2017	217.86	607.9

CCD Study of WDS 15098-0445

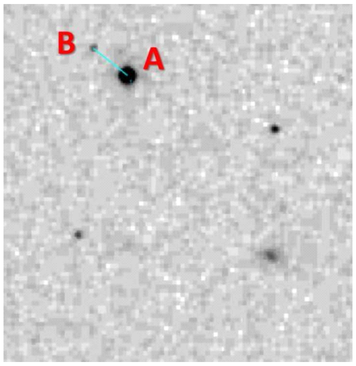

Figure 1. 2MASS image of AB from epoch 1999.

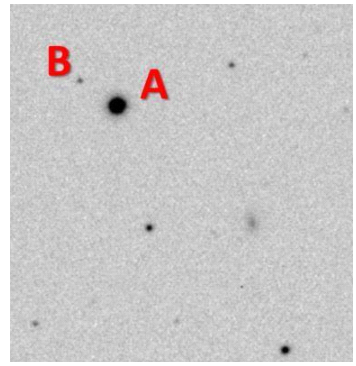

Figure 2. 2017 T11 image of AB from epoch 1999.

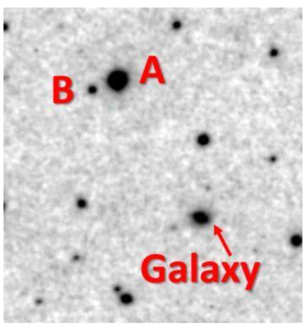

Figure 3. 1955 Palomar Sky Survey image from ALADIN.

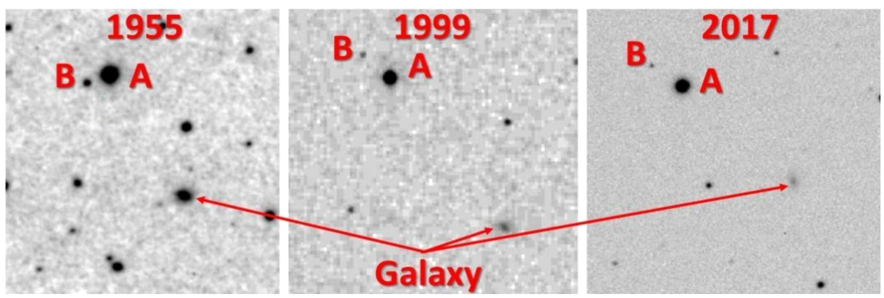

Figure 4. 1955-2017 image comparison

such a significant change in only 18 years raised doubt as to whether the 2017 T11 images correctly imaged the B component. To determine an accurate position for B, ALADIN was again consulted to obtain older images (ALADIN).

ALADIN provided access to the Palomar Sky Survey from 1955. This image was downloaded and imported into Mira to measure the star field. At first review, the area surrounding the AB pair did not resemble the previous images (see Figure 3). To establish the precise location of the B star in each image, a fixed background galaxy was used as a reference from which a galaxy-to-B component Theta and Rho measurement could be made. This measurement was then compared to the position of the B component in the 1999 and 2017 images with consistent results. Thus, the location of B was firmly established and the measurements from the 2017 T11 epoch were confirmed.

Reviewing the images obtained from ALADIN and the 2017 epoch, Figure 4 illustrates the motion of the primary A star against the background stars. Given its proper motion, the distance and angle changes, and the consistent position of B, it can be concluded that WDS 15098-0445 is an optical double and not a physically bound binary star.

AC Pair

The WDS notes indicate that the AC component (Figure 5) has already been established as an optical double (Mason and Hartkopf, 2012). The A component, as discussed above, is observed to have high proper

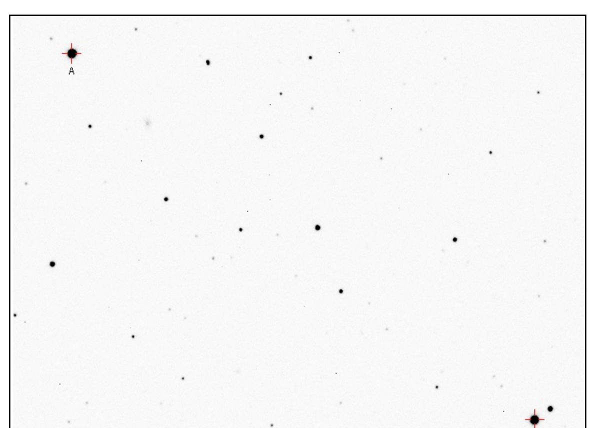

Figure 5. 2017 T11 image of the AC components.

motion which accounts for the historical Theta and Rho changes. The data from the 2017 images was consistent with the conclusion that the AC pair is an optical double.

Conclusion

The high proper motion of the A star accounts for the historical changes in Theta and Rho for both components. Through the use of a stationary background galaxy over short time frames, the position of the B component was correctly identified. From the historical data and the images obtained from ALADIN and 2017, we conclude that the AB pair is an optical double. The changes in the AC components were consistent with historical data.

Acknowledgements

We would like to thank the Boyce Research Initiatives and Education (B.R.I.E.F.) for guiding us in our research and writing, and for providing us with access to the iTelescope Network. We would also like to thank the United States Naval Observatory for access to the Washington Double Star Catalog and the historical data it provided. We would additionally like to acknowledge that this publication makes use of data products from the Two Micron All Sky Survey, which is a joint project of the University of Massachusetts and the Infrared Processing and Analysis Center, funded by the National Aeronautics and Space Administration and the National Science Foundation.

References

"2MASS First Incremental Data Release" *The Two Micron All Sky Survey at IPAC,* 20 Dec. 1999 https://www.ipac.caltech.edu/2mass/releases/first/index.html.

HIPPARCOS:

"Wolf 1137" *Hipparcos Main Catalog*, 28 Aug. 2012 https://heasarc.gsfc.nasa.gov/W3Browse/all/hipparcos.html.

Mason, B., & Hartkopf, W. 2012, *The Washington Double Star Catalog*. Astrometry Department, U.S. Naval Observatory, http://ad.usno.navy.mil/proj/WDS/

Osorio, Maria R. Zapatero, and E. L. Martin, "A CCD Imaging Search for Wide Metal-Poor Binaries", *Cornell University Astrophysics*, arXiv, 24 Feb. 2004, https://arxiv.org/abs/astro-ph/0402310.

SiMBADWeb:

"Wolf 1137" *SIMBAD Astronomical Database*, 26 Aug. 2017, http://simbad.u-strasbg.fr/simbad/sim-id?Ident=%402605833&Name=Wolf%2B1137&submit=submit.

Jonckheere Double Star Photometry – Part X: Hercules

Wilfried R.A. Knapp

Vienna, Austria
wilfried.knapp@gmail.com

Abstract: If any double star discoverer is in urgent need of photometry then it is Jonckheere. There are over 3000 Jonckheere objects listed in the WDS catalog and a good part of them with magnitudes obviously far too bright. This report covers 28 of the in total 82 Jonckheere objects in the constellation Hercules selected by a quick WDS data check for being potentially listed with questionable magnitudes. At least one image per object was taken with V-filter to allow for visual magnitude measurement by differential photometry. All objects were additionally checked for common proper motion and two qualify indeed as potential CPM pairs.

Introduction

As follow up to the report on J-objects I submitted so far I selected this time the J-objects in Hercules. To concentrate on the objects most in need of photometry I checked in the next step all objects for potentially suspect data – this process reduced the objects to check more in detail to 29. This does not mean that the data for the eliminated J-objects in Her are to be considered correct in all cases but the comparison of the given magnitudes with the UCAC4 fmag values suggests at least that any potential errors should be rather small.

Results of Photometry and Catalog Checking

For all but one of the selected J-objects one single image was taken with iTelescope iT24 with V-filter and 3s exposure time. The single image random effects seem less significant for the measured magnitudes as a magnitude error of ~0.1 or even a bit larger seems negligible in comparison with the Jonckheere objects often given magnitude errors in the range of up to 2 magnitudes. The images were then plate solved with Astrometrica using the URAT1 catalog with reference stars in the Vmag range of 8.5 to 14.5 giving not only RA/Dec coordinates but also photometry results for all reference stars used including an average dVmag error. The J-objects were then located in the center of the image and astrometry/photometry was then done by the rather comfortable Astrometrica procedure with point and click at the components delivering RA/Dec coordinates and Vmag measurements based on all reference stars used for plate solving. In one case, I had to take additional images with a different telescope to avoid issues with image quality.

The measurement results are given in Table 1 with the following structure:

- J# gives the number of the J-object
- RA/Dec gives the position in the HH:MM:SS/DD:MM:SS format for both components
- dRA and dDEc give the average plate solving error for RA and Dec in arcseconds
- Sep gives separation in arcseconds in the data lines calculated as

$$Sep = \sqrt{\left[\left(\cos\left(RA_1 - RA_2\right)\cos\left(Dec_1\right)\right)^2 + \left(Dec_2 - Dec_1\right)^2\right]}$$

  in radians
- ErrSep gives the calculated error range for Sep as

$$ErrSep = \sqrt{dRA^2 + dDec^2}$$

- PA gives position angle in degrees in the data lines calculated as

$$PA = \arctan\left[\frac{\left(RA_2 - RA_1\right)\cos\left(Dec_1\right)}{Dec_2 - Dec_1}\right]$$

  in radians depending on quadrant
- ErrPA = position angle error estimation in degrees

calculated as

$$ErrPA = \arctan\left(\frac{ErrSep}{Sep}\right)$$

assuming the worst case that *ErrSep* points perpendicular to the separation vector
- Mag gives Vmag for both components according to plate solving
- Err_Mag = magnitude error estimation calculated as

$$ErrMag = \sqrt{dVmag^2 + \left[2.5\log\left(1+1/SNR\right)\right]^2}$$

- SNR as signal to noise ratio for the given object
- dVmag as average magnitude plate solving error
- Date gives the Julian observation epoch (instead of the Bessel epoch used up to 2017 in the WDS catalog)
- N gives the number of images used
- Notes indicate the telescope used, number of images with exposure time, and additional comments if considered necessary.

In an additional step, I checked all objects for common proper motion using the UCAC5 catalog data when available. Table 2 lists the found data for the J objects in question and the assessment if the proper motion data allows for common proper motion using the following structure:

First row:
- J# gives the number of the J-object
- RA/Dec gives the GAIA DR1 position as given in the UCAC5 catalog in degrees for the primary
- Sep gives separation in arcseconds in the data lines calculated as

$$Sep = \sqrt{\left[\left(\cos\left(RA_1 - RA_2\right)\cos\left(Dec_1\right)\right)^2 + \left(Dec_2 - Dec_1\right)^2\right]}$$

in radians
- PA gives position angle in degrees in the data lines calculated as

$$PA = \arctan\left[\frac{\left(RA_2 - RA_1\right)\cos\left(Dec_1\right)}{Dec_2 - Dec_1}\right]$$

in radians depending on quadrant
- M1(G) and M2(G) give the GAIA DR1 Gmag values for both components as given in the UCAC5 catalog
- pmRA1, pmDec1/pmRA2, pmDec2 give the UCAC5 proper motion data and e_pm1/2 gives the total pm data error for both components
- Ap gives the GAIA aperture diameter (calculated for a corresponding surface with the used rectangular aperture)
- Me gives the observation method
- Date gives the GAIA DR1 observation epoch
- CPM Rat gives the CPM rating according to Knapp and Nanson 2017 (see Appendix A)
- Source/Notes gives the reference to the used catalog and additional comments on the objects

Second row:
- RA/Dec gives the UCAC5 position in degrees for the primary (from UCAC images re-reduced with TGAS reference stars)
- Sep gives separation in arcseconds in the data lines calculated as

$$Sep = \sqrt{\left[\left(\cos\left(RA_1 - RA_2\right)\cos\left(Dec_1\right)\right)^2 + \left(Dec_2 - Dec_1\right)^2\right]}$$

in radians
- PA gives position angle in degrees in the data lines calculated as before.
- Ap gives the used UCAC5 aperture
- Me gives the observation method
- Date gives the UCAC5 observation epoch (average from the used images)
- Source/Notes gives UCAC5 as used catalog and additional comments on the objects if necessary.

Summary

A good part of the listed J-objects in Hercules shows the expected significant magnitude difference compared with the WDS catalog data. Further, only two of these objects qualify as solid or at least good CPM candidates based on a rating scheme using UCAC5 proper motion data with the caveat that several objects are with at least one component not covered by UCAC5.

(Text continues on page 352)

Table 1: Measurement results for J objects in Her

J#		RA	Dec	dRA	dDec	Sep	Err Sep	PA	Err PA	Mag	Err Mag	SNR	dVmag	Date	N	Notes
98	A	18:33:12.263	17:28:33.74	0.08	0.07	3.928	0.106	146.883	1.550	10.324	0.110	173.98	0.11	2017.467	1	iT24 1x3s. Touching star disks
	B	18:33:12.413	17:28:30.45							11.894	0.111	73.55				
103	A	18:42:23.866	14:03:15.31	0.09	0.09	5.718	0.127	164.502	1.275	8.959	0.110	303.21	0.11	2017.467	1	iT24 1x3s. Touching star disks
	B	18:42:23.971	14:03:09.80							12.166	0.112	47.72				
399	A	16:23:11.312	23:41:16.97	0.06	0.07	4.931	0.092	49.997	1.071	10.168	0.080	204.53	0.08	2017.467	1	iT24 1x3s
	B	16:23:11.587	23:41:20.14							12.514	0.082	58.90				
400	A	16:44:06.847	42:02:39.67	0.06	0.06	5.945	0.085	173.761	0.818	12.075	0.071	88.49	0.07	2017.467	1	iT24 1x3s. SNR B <20
	B	16:44:06.905	42:02:33.76							14.889	0.102	14.27				
469	A	18:50:24.772	12:43:33.61	0.08	0.09	2.773	0.120	110.920	2.487	11.812	0.081	81.47	0.08	2017.467	1	iT24 1x3s. Touching star disks
	B	18:50:24.949	12:43:32.62							12.796	0.086	33.47				
532	A	18:54:51.539	12:59:59.89	0.09	0.10	4.420	0.135	3.792	1.744	11.056	0.081	113.60	0.08	2017.467	1	iT24 1x3s
	B	18:54:51.559	13:00:04.30							12.658	0.084	41.71				
738	A	16:41:30.635	21:47:29.57	0.07	0.09	1.969	0.114	247.924	3.314	11.813	0.095	36.11	0.09	2017.467	1	iT24 1x3s.Overlapping star disks
	B	16:41:30.504	21:47:28.83							11.724	0.094	37.91				
740	A	17:03:14.600	34:58:55.70	0.07	0.07	2.826	0.099	224.088	2.006	10.239	0.080	196.82	0.08	2017.467	1	iT24 1x3s. Touching star disks
	B	17:03:14.440	34:58:53.67							10.926	0.080	124.08				
752	A	18:25:07.654	16:47:44.25	0.11	0.11	4.630	0.156	256.128	1.924	10.863	0.091	78.65	0.09	2017.467	1	iT24 1x3s
	B	18:25:07.341	16:47:43.14							12.035	0.095	34.06				
757	A	18:02:15.397	38:04:10.50	0.12	0.11	3.170	0.163	327.050	2.940	11.879	0.073	52.78	0.07	2017.467	1	iT24 1x3s. Touching star disks
	B	18:02:15.251	38:04:13.16							12.456	0.035	30.55				
799	A	18:36:59.774	19:10:17.73	0.12	0.10	2.641	0.156	77.535	3.385	11.488	0.081	72.69	0.08	2017.467	1	iT24 1x3s. Touching star disks
	B	18:36:59.956	19:10:18.30							11.882	0.082	55.19				
1032	A	17:26:48.230	22:37:43.12	0.10	0.10	4.119	0.141	350.324	1.967	11.253	0.111	64.38	0.11	2017.467	1	iT24 1x3s. Touching star disks
	B	17:26:48.180	22:37:47.18							11.568	0.112	47.32				
1033	A	17:26:59.379	22:43:42.44	0.10	0.10	6.312	0.141	247.654	1.283	10.791	0.090	116.61	0.09	2017.467	1	iT24 1x3s
	B	17:26:58.957	22:43:40.04							12.212	0.093	50.16				
1071	A	18:42:20.344	14:06:36.03	0.09	0.09	5.089	0.127	66.983	1.433	13.118	0.110	303.21	0.11	2017.467	1	iT24 1x3s. Same image as J103
	B	18:42:20.666	14:06:38.02							13.843	0.112	47.72				
1127	A	18:00:36.903	30:13:24.59	0.08	0.11	2.862	0.136	341.244	2.721	12.544	0.073	55.38	0.07	2017.467	1	iT24 1x3s. Touching star disks
	B	18:00:36.832	30:13:27.30							12.729	0.074	43.12				
1132	A	18:06:37.776	20:14:20.98	0.10	0.11	3.275	0.149	134.849	2.599	12.021	0.121	63.42	0.12	2017.467	1	iT24 1x3s. Touching star disks
	B	18:06:37.941	20:14:18.67							12.719	0.125	32.02				

Table 1 continues on next page.

Table 1 (continues). Measurement results for J objects in Her

J#		RA	Dec	dRA	dDec	Sep	Err Sep	PA	Err PA	Mag	Err Mag	SNR	dVmag	Date	N	Notes
1133	A	18:32:06.920	13:59:16.35	0.11	0.10	2.237	0.149	124.280	3.802	12.257	0.092	55.03	0.09	2017.467	1	iT24 1x3s. Touching/ overlapping star disks. The WDS listed epoch 2000 meas- urement of this double with 0.55" separation has to be in error
	B	18:32:07.047	13:59:15.09							12.887	0.095	35.41				
1170	A	18:34:02.651	12:20:16.56	0.11	0.11	4.546	0.156	120.247	1.960	11.127	0.101	89.50	0.10	2017.467	1	iT24 1x3s
	B	18:34:02.919	12:20:14.27							13.044	0.108	26.30				
1197	A	18:33:50.895	12:21:15.88	0.09	0.10	2.290	0.135	180.367	3.362	13.515	0.136	27.59	0.13	2017.467	1	iT24 1x3s. Touching/ overlapping star disks
	B	18:33:50.894	12:21:13.59							13.329	0.134	35.04				
1218	A	18:05:03.407	38:29:55.26	0.06	0.05	2.969	0.078	166.743	1.507	12.171	0.081	19.39	0.06	2017.578	10	iT18 10x3s. SNR B<10
	B	18:05:03.465	38:29:52.37							13.628	0.137	8.29				
	A	18:05:03.407	38:29:55.25	0.06	0.07	3.062	0.092	166.701	1.725	12.187	0.051	122.96	0.05	2017.691	5	iT24 5x6s. Touching star disks
	B	18:05:03.467	38:29:52.27							13.636	0.054	56.25				
1278	A	18:56:30.080	15:56:10.46	0.11	0.12	2.284	0.163	97.547	4.076	11.778	0.101	62.88	0.10	2017.467	1	iT24 1x3s. Touching/ overlapping star disks
	B	18:56:30.237	15:56:10.16							12.356	0.104	36.34				
2098	A	17:56:40.229	15:41:09.93	0.12	0.11	4.292	0.163	130.197	2.172	12.779	0.114	37.31	0.11	2017.467	1	iT24 1x3s
	B	17:56:40.456	15:41:07.16							12.952	0.114	33.74				
2124	A	18:15:19.617	20:11:56.77	0.10	0.11	3.861	0.149	348.220	2.205	11.664	0.151	78.23	0.15	2017.467	1	iT24 1x3s
	B	18:15:19.561	20:12:00.55							13.242	0.157	22.50				
2912	A	18:29:17.376	17:41:51.70	0.11	0.11	6.771	0.156	143.175	1.316	11.231	0.160	93.25	0.16	2017.467	1	iT24 1x3s
	B	18:29:17.660	17:41:46.28							13.976	0.167	22.32				
2913	A	18:29:23.427	21:43:16.72	0.10	0.11	2.515	0.149	113.923	3.382	12.128	0.122	49.94	0.12	2017.467	1	iT24 1x3s. Touching/ overlapping star disks
	B	18:29:23.592	21:43:15.70							12.640	0.123	36.73				

Table 1 concludes on next page.

Table 1 (conclusionn). Measurement results for J objects in Her

J#		RA	Dec	dRA	dDec	Sep	Err Sep	PA	Err PA	Mag	Err Mag	SNR	dVmag	Date	N	Notes
2924	A	18:46:04.863	18:15:40.16	0.11	0.12	3.637	0.163	69.395	2.563	12.179	0.113	40.95	0.11	2017.467	1	iT24 1x3s. Touching star disks
	B	18:46:05.102	18:15:41.44							12.623	0.117	26.95				
2931	A	18:55:17.751	18:16:07.11	0.12	0.11	5.257	0.163	143.024	1.774	13.154	0.115	30.35	0.11	2017.467	1	iT24 1x3s. Touching star disks. Curious mag difference compared with WDS suggests object mismatch
	B	18:55:17.973	18:16:02.91							11.849	0.111	59.49				
3268	A	17:58:22.742	18:14:13.52	0.11	0.10	3.970	0.149	215.547	2.145	13.338	0.116	29.51	0.11	2017.467	1	iT24 1x3s
	B	17:58:22.580	18:14:10.29							13.779	0.117	26.92				
3324	A	16:29:51.725	24:52:37.50	0.11	0.08	2.224	0.136	60.349	3.500	11.899	0.091	85.20	0.09	2017.467	1	iT24 1x3s. Touching/ overlapping star disks
	B	16:29:51.867	24:52:38.60							12.672	0.094	42.28				

Explanations regarding the content of the Notes column:

"Touching star disks" indicates that the rims of the star disks are touching and that the measurement results might be a bit less precise than with clearly separated star disks

"Touching/Overlapping star disks" indicates that the star disks overlap to the degree of an elongation and that the measurement results is probably less precise than with clearly separated star disks

"SNR <20" indicates that the measurement result might be a bit less precise than desired due to a low SNR value but this is already included in the calculation of the magnitude error range estimation

"SNR <10" indicates that the measurement result is probably a bit less precise than desired due to a very low SNR value but this is already included in the calculation of the magnitude error range estimation

"Image quality questionable" or similar indicates rather large average errors for the reference stars used for plate solving for different reasons (mostly atmospheric influences). But this is at least to some degree already included in the calculation of the error range estimation

Table 2. J objects in Her being checked for being potentially CPM pairs

J#	RA	Dec	Sep "	PA °	M1(G)	M2(G)	pmRA1	pmDec1	e_pm1	pmRA2	pmDec2	e_pm2	Ap	Me	Date	CPM Rat	Source/Notes
98	278.30109970	17.4760136	4.00	146.8	10.25	11.65	-1.80	-7.40	1.70	-3.60	-7.10	3.39	0.96	Hg	2015.000	CACB	GAIA DR1. PM data from UCAC5 catalog. Rather optical
	278.30110670	17.4760411	4.02	146.5									0.20	Eu	2001.575		UCAC5
103	280.59944330	14.0542281	5.71	164.5	8.80	11.68	1.80	-13.70	2.40	-1.10	-14.80	8.49	0.96	Hg	2015.000	CBCB	GAIA DR1. PM data from UCAC5 catalog. Rather optical
	280.59943640	14.0542794	5.71	164.1									0.20	Eu	2001.486		UCAC5
399	245.79716030	23.6880494	4.99	49.8	9.77	12.31	-11.80	-4.70	1.70	-14.30	-3.20	2.83	0.96	Hg	2015.000	CCCB	GAIA DR1. PM data from UCAC5 catalog. Obviously optical
	245.79720850	23.6880669	5.00	50.2									0.20	Eu	2001.530		UCAC5
400	251.02855940	42.0443631	5.88	175.8	11.82	14.39	-17.80	-10.10	1.98	10.70	-11.40	4.10	0.96	Hg	2015.000	CCCB	GAIA DR1. PM data from UCAC5 catalog. Obviously optical
	251.02864310	42.0443983	5.85	179.3									0.20	Eu	2002.480		UCAC5
469	282.60319190	12.7260114	3.04	109.3	11.70	13.01	-2.30	-8.70	2.12	-0.40	-24.40	7.50	0.96	Hg	2015.000	CCCB	GAIA DR1. PM data from UCAC5 catalog. Obviously optical
	282.60320080	12.7260442	2.96	105.5									0.20	Eu	2001.455		UCAC5
532	283.71471690	12.9999708	4.52	5.9	10.83	12.40	-3.00	-0.20	1.41	-4.60	-1.10	1.63	0.96	Hg	2015.000	CCCC	GAIA DR1. PM data from UCAC5 catalog. Obviously optical
	283.71472860	12.9999717	4.54	6.2									0.20	Eu	2001.463		UCAC5
738	250.37771581	21.7915261	2.17	247.5	11.70	11.58							0.96	Hg	2015.000		GAIA DR1. No UCAC5 (nor 2MASS or URAT1) objects for B available
740	255.81079420	34.9821197	2.82	226.2	10.08	10.94	9.70	23.40	1.70	-4.50	5.20	2.97	0.96	Hg	2015.000	CCCB	GAIA DR1. PM data from UCAC5 catalog. Obviously optical
	255.81075270	34.9820375	2.53	227.2									0.20	Eu	2002.355		UCAC5
752	276.28188140	16.7956228	4.63	258.3	10.36	11.81	12.70	9.30	1.70	-2.90	-8.90	3.39	0.96	Hg	2015.000	CCCB	GAIA DR1. PM data from UCAC5 catalog. Opposite pm direction, obviously optical
	276.28183190	16.7955881	4.38	260.9									0.20	Eu	2001.565		UCAC5
757	270.56413610	38.0696086	3.47	323.2	11.60	12.67	5.70	2.60	1.84	6.10	6.40	2.83	0.96	Hg	2015.000	CCCB	GAIA DR1. PM data from UCAC5 catalog. Obviously optical
	270.56411140	38.0695997	3.43	322.7									0.20	Eu	2002.605		UCAC5
799	279.24927280	19.1715997	2.70	71.9	11.06	12.45	-3.30	-4.20	1.56	4.80	0.80	3.68	0.96	Hg	2015.000	CBCB	GAIA DR1. PM data from UCAC5 catalog. Obviously optical
	279.24928580	19.1716153	2.57	72.5									0.20	Eu	2001.604		UCAC5
1032	261.7009142	22.6286114	4.05	350.3	11.08	11.38	-18.00	23.00	1.56	-17.50	23.90	1.84	0.96	Hg	2015.000	AABB	GAIA DR1. PM data from UCAC5 catalog. Solid CPM candidate
	261.70098690	22.6285261	4.04	350.2									0.20	Eu	2001.619		UCAC5
1033	261.74743440	22.7284850	6.52	246.8	10.05	11.83	-3.80	-12.90	1.56	-12.90	-15.90	3.39	0.96	Hg	2015.000	CCCB	GAIA DR1. PM data from UCAC5 catalog. Obviously optical
	261.74744980	22.7285331	6.40	246.8									0.20	Eu	2001.618		UCAC5

Table 2 continues on next page.

Table 2 (continued). J objects in Her being checked for being potentially CPM pairs

J#	RA	Dec	Sep "	PA °	M1(G)	M2(G)	pmRA1	pmDec1	e_pm1	pmRA2	pmDec2	e_pm2	Ap	Me	Date	CPM Rat	Source/Notes
1071	280.58475810	14.1100147	5.14	67.6	12.80	13.01	-0.80	-10.00	1.70	-1.80	-2.50	1.84	0.96	Hg	2015.000	CCCB	GAIA DR1. PM data from UCAC5 catalog. Obviously optical
	280.58476110	14.1100522	5.12	68.7									0.20	Eu	2001.484		UCAC5
1127	270.15380810	30.2234269	2.93	337.3	12.48	12.77	38.70	-95.00	1.98	11.40	-38.20	2.69	0.96	Hg	2015.000	CCBA	GAIA DR1. PM data from UCAC5 catalog. Very different pm speed, obviously optical
	270.15365080	30.2237606	2.14	338.4									0.20	Eu	2002.357		UCAC5
1132	271.65743330	20.2390786	3.26	139.6	11.90	12.64	-17.10	-5.00	1.70	-17.50	-6.20	1.84	0.96	Hg	2015.000	BABB	GAIA DR1. PM data from UCAC5 catalog. Potential CPM candidate
	271.65750110	20.2390969	3.25	139.3									0.20	Eu	2001.606		UCAC5
1133	278.02883920	13.9877994	2.24	124.2	12.19	12.87	-6.60	-4.00	1.56	-6.00	-5.70	1.84	0.96	Hg	2015.000	CBCB	GAIA DR1. PM data from UCAC5 catalog. Rather optical
	278.02886440	13.9878144	2.22	123.8									0.20	Eu	2001.483		UCAC5
1170	278.51097720	12.3379464	4.73	118.4	10.37	12.50	-1.70	-0.70	1.70	4.20	14.00	2.12	0.96	Hg	2015.000	CCCB	GAIA DR1. PM data from UCAC5 catalog. Obviously optical
	278.51098390	12.3379492	4.76	121.0									0.20	Eu	2001.449		UCAC5
1197																	No UCAC5/GAIA DR1 objects available
1218	271.26417785	38.4986744	3.00	164.2	11.93	13.32							0.96	Hg	2015.000		GAIA DR1. M1 and M2 are G-band. No UCAC5 (nor 2MASS or URAT1) objects for B available
1278																	No UCAC5/GAIA DR1 objects available
2098	269.16760780	15.6860886	4.17	130.1	12.40	12.38	1.00	-6.60	1.56	3.60	-11.10	1.56	0.96	Hg	2015.000	CCCB	GAIA DR1. PM data from UCAC5 catalog. Obviously optical
	269.16760390	15.6861133	4.10	129.7									0.20	Eu	2001.508		UCAC5
2124	273.83176330	20.1990036	3.96	346.5	11.10	13.19	-6.60	10.30	1.56	-6.50	9.70	5.37	0.96	Hg	2015.000	AACB	GAIA DR1. PM data from UCAC5 catalog. Good CPM candidate with the caveat of a rather large pm error for B
	273.83178930	20.1989656	3.96	346.5									0.20	Eu	2001.615		UCAC5
2912	277.32242610	17.6976403	6.34	142.2	10.59	13.43	0.50	-2.80	1.56	-3.20	-3.10	2.12	0.96	Hg	2015.000	CCCC	GAIA DR1. PM data from UCAC5 catalog. Obviously optical
	277.32242420	17.6976508	6.36	141.8									0.20	Eu	2001.579		UCAC5
2913	277.34753640	21.7212992	3.14	117.5	11.58	12.66	-0.50	-12.00	1.56	1.40	-11.80	1.56	0.96	Hg	2015.000	CACB	GAIA DR1. PM data from UCAC5 catalog. Rather optical
	277.34753840	21.7213436	3.12	117.8									0.20	Eu	2001.639		UCAC5

Table 2 concludes on next page.

Jonckheere Double Star Photometry – Part X: Hercules

Table 2 (conclusion). J objects in Her being checked for being potentially CPM pairs

J#	RA	Dec	Sep "	PA °	M1(G)	M2(G)	pmRA1	pmDec1	e_pm1	pmRA2	pmDec2	e_pm2	Ap	Me	Date	CPM Rat	Source/Notes
2924	281.52035250	18.2609917	3.71	66.1	11.79	12.29	0.60	-1.20	1.63	21.40	-46.70	1.70	0.96	Hg	2015.000	ACCB	GAIA DR1. PM data from UCAC5 catalog. Obviously optical. Fast proper motion of B changes Sep and PA over time noticeable
	281.52035030	18.2609961	3.77	55.8									0.20	Eu	2001.583		UCAC5
2931	283.82393060	18.2686453	5.60	143.3	12.46	11.63	-3.60	-20.10	1.70	-5.60	-58.90	1.56	0.96	Hg	2015.000	CCBB	GAIA DR1. PM data from UCAC5 catalog. Obviously optical
	283.82394470	18.2687203	5.21	139.6									0.20	Eu	2001.583		UCAC5
3268	269.59482000	18.2370367	3.98	219.5	12.95	13.33	-4.50	-3.60	1.70	-5.60	-2.40	1.84	0.96	Hg	2015.000	CBCB	GAIA DR1. PM data from UCAC5 catalog. Rather optical
	269.59483750	18.2370503	3.98	219.1									0.20	Eu	2001.586		UCAC5
3324	247.46542810	24.8770486	2.61	55.2	11.76	12.68	-11.60	14.60	1.56	-10.30	19.00	1.84	0.96	Hg	2015.000	CCBB	GAIA DR1. PM data from UCAC5 catalog. Rather optical
	247.46547580	24.8769942	2.57	56.1									0.20	Eu	2001.557		UCAC5

Jonckheere Double Star Photometry – Part X: Hercules

(Continued from page 345)

References

Buchheim, Robert – 2008, CCD Double-Star Measurements at Altimira Observatory in 2007, Journal of Double Star Observations, Vol. 4 No. 1 Page 27-31

Knapp, Wilfried; Nanson, John – 2017, A new concept for counter-checking of assumed CPM pairs, Journal of Double Star Observing, Vol. 13 No 1 pp. 31-51

Acknowledgements:

The following tools and resources have been used for this research:

2MASS catalog
2MASS images
AAVSO APASS
AAVSO VPhot
Aladin Sky Atlas v9.0
Astrometrica v4.10.0.427
AstroPlanner v2.2
iTelescope:
iT24: 610mm CDK with 3962mm focal length. Resolution 0.625 arcsec/pixel. V-filter. No transformation coefficients available. Located in Auberry, California. Elevation 1405m
iT18: 318mm CDK with 2541mm focal length. CCD: SBIG-STXL-6303E. Resolution 0.73 arcsec/pixel. V-filter. No transformation coefficients available. Located in Nerpio, Spain. Elevation 1650m
GAIA DR1 catalog
MaxIm DL6 v6.08
POSS images
SDSS DR9 and DR7 catalogs
SDSS images
SIMBAD
UCAC4 catalog
UCAC5 catalog
URAT1 catalog
VizieR
Washington Double Star Catalog

Appendix A

CPM rating scheme according to Knapp/Nanson 2017 with extensions:

Four rating factors are used: Proper motion vector direction, proper motion vector length, size of position error in relation to proper motion vector length and relationship separation to average proper motion speed:

- Proper motion vector direction rating: “A” for within the error range identical direction, “B” for similar direction within the double error range and “C” for outside
- Proper motion vector length rating: “A” for within the error range identical length, “B” for similar length within the double error range and C for outside
- Error size rating: “A” for error size of less than 5% of the proper motion vector length, “B” for less than 10% and “C” for a larger error size
- Rating for relation separation to average proper motion speed: “A” for less than 100 years, “B” for 100 to 1000 years and “C” for above.

To compensate for (depending on the selected objects and available catalogs) excessively large position errors resulting an “A” rating despite rather high deviations absolute upper limits are applied regardless calculated error size:

- Proper motion vector direction: Max. 2.86° difference for an “A” and 5.72° for a “B”
- Proper motion vector length: Max. 5% difference for an “A” and 10% for a “B”

Modification for cases of very small position errors (when for example using SDSS9 instead of 2MASS or directly proper motion data from GAIA DR1 or UCAC5) with the consequence that the requirements to get an A or even B CPM rating get unreasonable hard:

- The from the position error resulting error estimation for proper motion vector direction and length is in this case calculated as root mean square from both position errors (instead of so far only the larger 2MASS one)
- If the PM vector direction difference is larger than this calculated “allowed” error but still less than 0.5° then an “A” is given, a “B” is given for larger than 0.5 but less than 1 degree, and a “C” is given if above
- If the PM vector length difference is larger than this calculated “allowed” error but still less than 0.5% then an “A” is given, a “B” is given for larger than 0.5 but less than 1 percent, and a “C” is given if above.

The Double Star Orbit Initial Value Problem

Hagan Hensley

Stanford Online High School, Stanford, California

Abstract: Many precise algorithms exist to find a best-fit orbital solution for a double star system given a good enough initial value. Desmos is an online graphing calculator tool with extensive capabilities to support animations and defining functions. It can provide a useful visual means of analyzing double star data to arrive at a best guess approximation of the orbital solution. This is a necessary requirement before using a gradient-descent algorithm to find the best-fit orbital solution for a binary system.

Introduction

Many double stars have hundreds of past observations showing an obvious curved pattern in the motion of the secondary relative to the primary, suggesting an orbit. By determining the precise orbital parameters of a double star system based on past observations, it is possible to predict where the secondary should be relative to the primary at any point in the future. Knowing the orbital parameters of binary systems in aggregate can provide valuable insight into the processes of binary star system dynamics. Waiting for the system to complete a full orbit before coming to conclusions about its orbital parameters is ideal, but would often take hundreds if not thousands of years. Therefore it is essential to make accurate determinations of a binary system's orbital parameters based on observations over only a small portion of the orbit.

Since a binary system orbit takes seven parameters to describe, the search space for finding a best-fit orbit is seven-dimensional and very computationally expensive to search using conventional methods. There are more efficient ways of finding a best-fit orbital solution, but all with the requirement that they must start with a fairly good best-guess initial value for the solution in order to converge in a reasonable amount of time. For this reason it is important to be able to arrive at good initial values for the orbital parameters before actually using any fitting algorithm.

Parameters of an Orbital Solution

Any double star orbit can be described uniquely by 7 orbital parameters, shown in Table 1 and described in "Keplerian Elements in Detail" (see references), slightly modified for a double star system instead of an Earth-orbiting body.

Table 1: The 7 parameters of an Orbital Solution

Parameter	Definition
a	Semi-major axis in arcseconds
e	Eccentricity of orbit
ω	Argument of periapsis, measured CCW from north
θ_m	Mean anomaly at epoch (default 2000). A time-dependent parameter
i	Inclination, measured in degrees from being face on looking down from above, where "above" means that the secondary is moving counterclockwise around the primary.
Ω	Longitude of ascending node, measured CCW from north
p	Orbital period of secondary. A time-dependent parameter, necessary when the mass of the primary is unknown

Normally, the semi-major axis is measured as a physical distance. However, since the distance to the double star system is not necessarily known, it is not possible to convert an observed separation into a physical separation. Normally, there are just six orbital parameters; the seventh, p, is not included. Here, p is necessary because the stars' mass and physical separation are unknown, so we can't calculate p from the semi-major axis with Kepler's 3rd law like we normally would. Knowing p and a gives us information about the ratio of the stars' mass and physical separation, using Kepler's 3rd law.

We can use these seven parameters to calculate the expected observed position of the secondary relative to the primary (in rectangular coordinates) at any given time based on a certain orbit.

Calculation of Expected Position

In any best-fitting algorithm, there must be some way to quantify the goodness of fit parameter to be optimized. In this case, the best-fit orbital solution is that which minimizes the sum of squares of the residuals. The calculated values to be compared to the observed values for determination of weighted residuals are found as such, as detailed by Giesen (2017):

First, we calculate the position of the secondary on the orbital plane, using a, e, ω, θ, and n. We also need the value of t, or time from epoch. This calculation will tell us where we should expect to see the secondary if we were looking at its orbit face-on, with 0 inclination.

Mean anomaly M represents the position angle that the secondary would be at on the orbital plane if it swept out its orbit at a uniform rate with respect to angle instead of following Kepler's 2nd law, but with the same orbital period. The expected mean anomaly at time t can be calculated as $\theta + nt$.

The next step is to solve Kepler's equation to find the eccentric anomaly E from the mean anomaly M. The eccentric anomaly represents the position angle of the secondary on the orbital plane measured not from the focus of the ellipse but the center of the ellipse. E and M should be thought of as intermediate values for the sake of simplification of the calculation, not as representing physical angles in the binary system.

Kepler's equation gives a simple relationship between M and E: $M = E - e \sin E$. This equation cannot be solved algebraically for E (except in the special case where $e = 0$, a circular orbit). The most computationally efficient way to solve it, and the way it is typically solved, is using Newton's method, starting by inverting the equation. For a first guess, we set

$$E = M + \sin M$$

Then, for three to four iterations, we apply Newton's method, repeatedly setting

$$E_{new} = E - \frac{E - e\sin E - M}{1 - e\cos E}$$

This should give us a satisfactory approximation of E, accurate to several decimal places.

From the eccentric anomaly E, we can now find the x and y coordinates of the secondary on its orbital plane, treating the argument of periapsis as the x axis.

$$x = a\cos E - ae; \qquad y - a\sqrt{1-e^2}\,\sin E$$

Converting this to polar coordinates gives the true anomaly and true separation. Lastly, we apply a rotation matrix by an angle equal to the inclination about the axis of Ω, and set the resulting z coordinate to 0, giving the projected position of the secondary.

Method 1: Visualization

Desmos is an online graphing calculator tool with extensive capabilities to support animations and defining functions. Using the orbital parameters and the calculations described above, it is possible to graph a projection of an orbit in *Desmos*. One issue is that *Desmos* cannot define functions, such as the Newton's method approximation of eccentric anomaly, recursively in terms of themselves. Therefore the recursion must be done indirectly, by defining each successive iteration as its own function. Despite limitations on processing power required to make the graph run smoothly, the iterative method shown in Equation 1 is repeated to 4 iterations without slowing things down. This means it is satisfactory for e < 0.95.

$$E_2(m) = E_1(m) - \frac{E_1(m) - e_o\left[E_1(m)\right] - m}{1 - e_o\cos\left[E_1(m)\right]} \qquad [1]$$

An iterative approximation of E(m) using Newton's method, as shown in Desmos. This step is repeated to calculate E_3, E_4, et cetera.

Figure 1 is a plot based on randomly generated sample data representative of a possible orbit with observations perturbed slightly from their calculated locations, getting closer as time goes on, shown with residuals. The sliders on the left hand side can be adjusted to modify the orbital parameters, and the residuals will be adjusted in turn. The eccentricity e was defined as e_o, so *Desmos* didn't think it was the number e. The solution shown in Figure 1 has an R^2 value of 0.97.

Changing the time-dependent parameters, θ_m and p, can have a large effect on the residuals while not changing the shape of the orbit. Figure 2 shows the same orbit with an incorrect value of p, and an R^2 value of -0.13:

3D Visualization

With some more manipulation, it is possible to get *Desmos* to display a 3-dimensional visualization of the orbit and residuals, which can further help build intuition for the effects of altering the various elements. The orbit in purple is the orbit as we observe it from Earth, which appears as projected onto a plane perpendicular to our line of sight. The orbit in red is the actual orbit of

(Text continues on page 356)

The Double Star Orbit Initial Value Problem

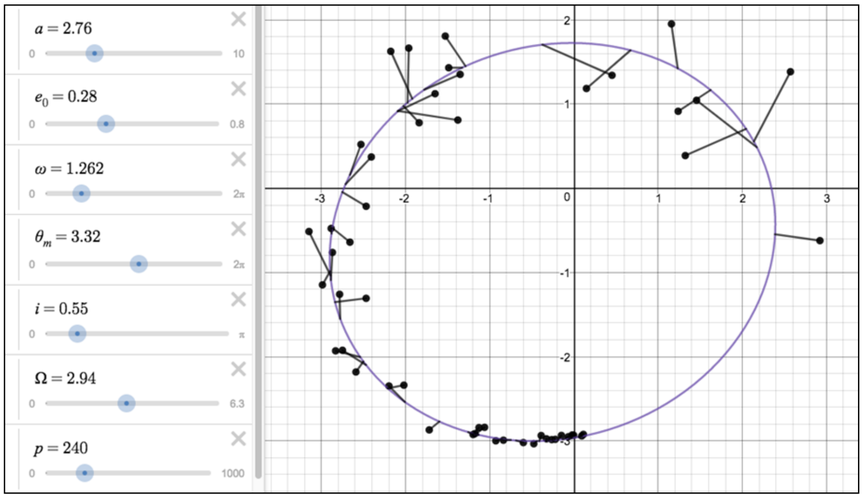

Figure 1: An orbital solution as shown in Desmos: from https://www.desmos.com/calculator/skxwjseto5

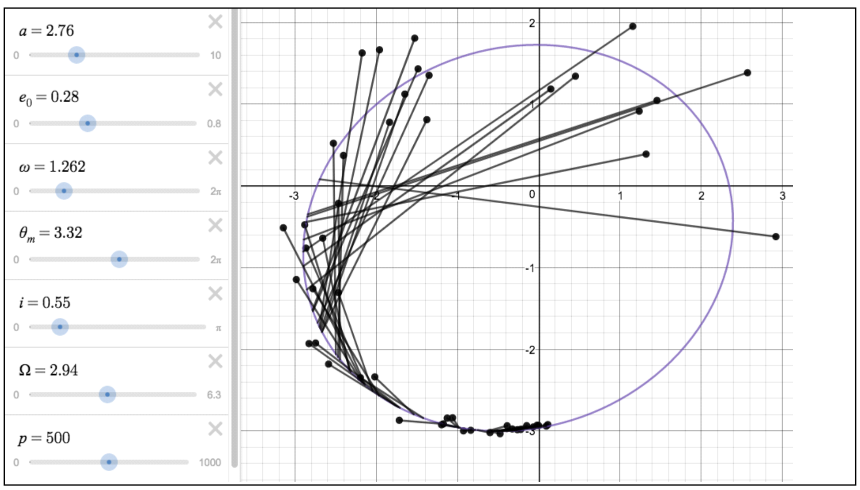

Figure 2: The same sample data with an incorrect value of p and the same other parameters, showing very different residuals.

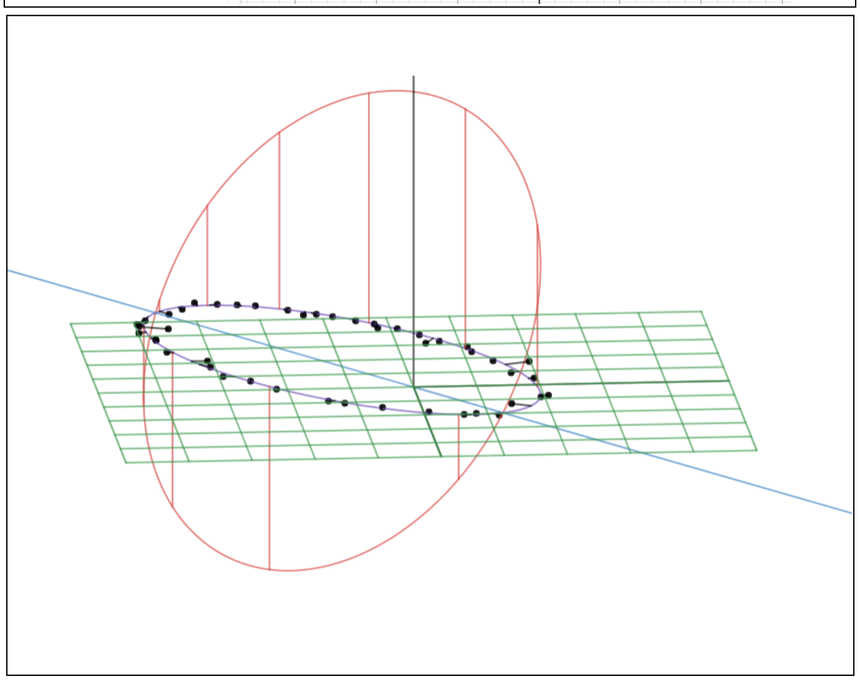

Figure 3. Selected points from the past observations of a real binary system, fitted manually using the 3d visualization tool.

The Double Star Orbit Initial Value Problem

(Continued from page 354)

the secondary, which can be seen to extend above and below the projected orbital plane in green. The blue line represents the line of nodes. Figure 3 shows an example of this method using 50 randomly selected data points for the Grade 1 system WDS 18055+0230

Manually finding a best guess for some parameters

By careful analysis of the data, we can come to an initial best guess for some of the parameters. For a large enough arc, we can use the sample data to get a fairly good approximation of the orbital period p. In the above data, for example, the position angles appear to traverse a full 360 degrees approximately once every 90 years, which can be used as a good guess at p. Because inclination is defined such that an inclination of 0 corresponds to CCW motion of the secondary, we can use the direction of the secondary's motion around the primary to constrain the value of i: CCW motion means that i must be between 0 and $\pi/2$, while CW motion means that i must be between $\pi/2$ and π (such that we are viewing the orbit 'from behind'). By playing around with the sliders, it becomes fairly simple to arrive at a good approximation of all the orbital parameters by trying to minimize the residuals visually.

Testing

This method was tested on 10 grade 1 orbits and four grade 2 orbits. On six of the grade 1 orbits and all of the grade 2 orbits, manually fitting an orbit to the data gives orbital elements very similar to the official values and can be done within just a few minutes. The other four grade 1 orbits exhibited some inconsistencies in the data points, as it appeared that some points had position angles flipped by 90 or 180 degrees from the correct values.

Implication

Given the success and ease of fitting randomly chosen data points from known orbits, this method holds promise for fitting previously unknown orbits.

Conclusion

Desmos can provide a useful visual means of arriving at a best guess of the seven orbital parameters for a set of observational data. This best guess can then be fed into a gradient descent algorithm or something similar to arrive at an optimized orbital solution.

Acknowledgements

This research has made use of the Washington Double Star Catalog maintained at the U.S. Naval Observatory. Special thanks to Russ Genet and Richard Harshaw for their encouragement.

Counter-Check of CBL Double Stars for being Physical Pairs

Wilfried R.A. Knapp

Vienna, Austria
wilfried.knapp@gmail.com

Abstract: This report counter-checks a random sample of CBL objects for the probability of being physical pairs using TGAS proper motion and parallax data finding most of them common proper motion pairs indeed but only in one case with some probability for gravitational relationship

Introduction

The WDS catalog contains (starting with the first Caballero JDSO report in 2009) per August 2017 about 600 CBL objects – most of them V-coded as assumed physical pairs by means of common proper motion. The TGAS subset of GAIA provides PM and Plx data for stars already covered in the Tycho and Hipparcos catalogs (Michalik at al. 2015) with some overlap for a part of the CBL objects. As a random CBL objects sample, I selected 23 objects with ~12mag secondaries. Next step was then to identify these objects in the 2MASS images and load the GAIA DR1 data to check the PM values for common proper motion using the CPM assessment model from Knapp and Nanson 2017. The results for the selected CBL objects are given in Table 1.

To make the CPM assessment more transparent the proper motion vector attributes direction and length and the differences are given in Table 2 as well as the TGAS Plx data with a calculation of the distance between the components for three cases with an assessment of the probability of an existing gravitational relationship:

- Best case: The Plx values are assumed the largest possible value within the given error range – the distance is then simply the part of the circumference with a radius given by this Plx
- Realistic case: Using the given GAIA DR1 values Plx1 and Plx2 – this adds to the best case the distance of the Plx data calculated approximately using the Pythagorean theorem
- Worst case: The given Plx errors work to full extent giving the largest possible distance – again calculated approximately using Pythagoras.

The assessment of a potential gravitational relationship between the components is then based on a quite simple approach assuming average means Sun like star mass with a then assumed gravitational "border" at the outer rim of the Oort cloud at ~100,000 AU. If the "realistic" distance between the components is therefore less than 200,000 AU then a potential gravitational relationship is assumed to be present with a high probability because of the overlapping Oort clouds (for details see Appendix B).

Summary

From 23 total objects, only 2 are to be considered probably not CPM pairs, confirming the assumed high quality of the CBL objects. Eleven objects did not allow for an assessment of gravitational relationship due to missing GAIA DR1 Plx data for at least one component. From the remaining 12 objects, only one can be considered physical in terms of at least some probability of gravitational relationship. All other pairs save 2, have a very small probability of being physical. And 2 objects are, with the given measurements, outside of any possibility of gravitational relationship (however, this does not exclude the possibility of common origin from the same molecular cloud).

(Text continues on page 361)

Table 1. CPM Rating for the selected CBL objects

Description of table contents:
- Header line: Gives the WDS catalog data available for the selected object with year of last observation in the Date column, for one object without WDS data the Tycho II data is given
- Data line:
-- RA and Dec give the coordinates from the used catalog in decimal degrees format as these values are directly usable for calculating Sep and PA
- Sep gives separation in arcseconds calculated from the coordinates of both components as SQRT(((RA2-RA1)*cos(Dec1))^2+(Dec2-Dec1)^2) in radians (Buchheim 2008)
-- PA gives position angle in degrees calculated from the coordinates of both components as arctan((RA2-RA1)*cos(Dec1))/(Dec2-Dec1)) in radians depending on quadrant (Buchheim 2008)
-- M1 and M2 give GAIA DR1 Gmags or in case of URAT1 Vmags if available
-- pmRA1 and pmDE1 with e_pm1 give the proper motion data for A and pmRA2, pmDE2 and e_pm2 for B
-- Ap indicates in the aperture used (calculated circular surface diameter)
-- Me indicates the WDS code for the used observation method
-- Date is the Julian observation epoch
-- CPM Rat gives the rating of the CPM assessment based on comparison of the given PM data (description see Appendix A)
-- Source/Notes finally indicates the used catalog and gives additional comments and explanations if considered necessary

Name	RA	Dec	Sep	PA	M1	M2	pmRA1	pmDec1	e_pm1	pmRA2	pmDec2	e_pm2	Ap	Me	Date	CPM Rat	Source/Notes
CBL 130	07:08:55.240	-11:23:29.6	48.0	31	11.29	12.27	-7	-73							2010		WDS07089-1123
	107.2301783	-11.39187011	48.002	31.114	11.096	11.988	-3.60	-74.25	1.909	-4.76	-71.55	1.963	0.96	Hg	2015.0	AAAB	GAIA DR1. PM data from GAIA DR1 catalog. Solid CPM candidate
CBL 114	00:32:19.100	-21:50:33.7	49.7	209	11.62	12.26	60	-1							2010		WDS00323-2151
	8.079834197	-21.84265497	49.714	208.503	11.436	12.032	60.57	-0.09	1.724	63.13	4.89	1.127	0.96	Hg	2015.0	CBAB	GAIA DR1. PM data from GAIA DR1 catalog. Rather optical
CBL 47	10:59:33.138	+23:15:47.1	19.9	183	11.08	12.22	44	-38							2013		WDS10596+2316
	164.8882947	23.2628989	19.808	182.982	10.602	11.750	42.40	-40.30	1.414	41.70	-39.50	1.414	0.96	Hg	2015.000	AAAB	GAIA DR1. PM data from UCAC5 catalog. Solid CPM candidate
CBL 112	05:55:36.199	+45:01:15.7	8.1	74	11.44	12.11	17	-68							2002		WDS05556+4501
	88.9009386	45.0207906	8.064	73.531			17.34	-68.64	5.75	17.67	-72.04	5.75	0.2	Eu	2013.603	AABB	URAT1. PM data calculated from position comparison with 2MASS. Solid CPM candidate
CBL 170	18:27:24.763	+21:51:53.4	26.6	160	10.31	12.08									2010		WDS18274+2152
	276.8531292	21.8650538	26.596	160.014	10.027	11.532	-14.24	54.36	1.265	-15.78	53.82	1.338	0.96	Hg	2015.0	AAAB	GAIA DR1. PM data from GAIA DR1 catalog. Solid CPM candidate
CBL 56	13:21:51.651	+55:54:04.2	25.1	77	9.33	12.05	-66	-4							2010		WDS13219+5554
	200.4647731	55.9011578	25.068	76.646		12.051	-73.07	6.68	5.88	-71.28	-2.22	5.87	0.2	Eu	2013.697	CABB	URAT1. PM data calculated from position comparison with 2MASS. Rather optical
CBL 178	20:33:53.247	-27:10:17.3	52.0	40	9.46	12.05									2010		WDS20339-2710
	308.4722226	-27.17185331	52.047	39.939	9.117	11.355	70.39	-85.20	0.088	70.84	-86.59	2.456	0.96	Hg	2015.0	AAAB	GAIA DR1. PM data from GAIA DR1 catalog. Solid CPM candidate
CBL 147	13:17:35.429	-11:57:01.3	24.1	345	11.23	12.02	-82	36							2013		WDS13176-1157
	199.3972222	-11.9501914	24.296	344.748	10.917	11.586	-85.20	35.40	1.628	-84.80	36.10	1.628	0.96	Hg	2015.000	AAAB	GAIA DR1. PM data from UCAC5 catalog. Solid CPM candidate
CBL 185	21:54:22.589	-44:09:46.4	18.0	74	10.97	12.01	20	-92							2010		WDS21544-4410
	328.5942328	-44.1632639	17.990	73.727	10.621	11.490	18.40	-88.90	1.273	18.20	-88.10	1.414	0.96	Hg	2015.000	AAAB	GAIA DR1. PM data from UCAC5 catalog. Solid CPM candidate

Table 1 concludes on the next page.

Counter-Check of CBL Double Stars for being Physical Pairs

Table 1(conclusion). CPM Rating for the selected CBL objects

Name	RA	Dec	Sep	PA	M1	M2	pmRA1	pmDec1	e_pm1	pmRA2	pmDec2	e_pm2	Ap	Me	Date	CPM Rat	Source/Notes
CBL 130	07:08:55.240	-11:23:29.6	48.0	31	11.29	12.27	-7	-73							2010		WDS07089-1123
CBL 115	00:55:33.210	-43:16:11.7	28.2	135	12.04	11.96	13	-86							2010		WDS00556-4316
	13.89617105	-43.27578229	28.193	314.525	11.681	11.812	14.08	-84.16	0.530	13.03	-85.10	0.531	0.96	Hg	2015.0	BBAB	GAIA DR1. PM data from GAIA DR1 catalog. Good CPM candidate
CBL 150	14:12:31.781	-30:06:17.7	31.3	217	11.32	11.95	-65	-16							2010		WDS14125-3006
	213.1320539	-30.1049925	31.264	216.472	11.002	11.743	-67.50	-19.40	1.556	-65.80	-18.80	1.556	0.96	Hg	2015.000	AAAB	GAIA DR1. PM data from UCAC5 catalog. Solid CPM candidate
CBL 57	13:54:51.370	+51:22:49.9	27.0	110	11.21	11.94	-55	22							2010		WDS13549+5123
	208.7136953	51.3805889	26.987	109.713	11.074	11.798	-53.90	18.80	1.980	-54.10	20.90	1.980	0.96	Hg	2015.000	AAAB	GAIA DR1. PM data from UCAC5 catalog. Solid CPM candidate
CBL 125	05:23:39.979	-38:18:48.1	24.0	194	11.98	11.93	30	39							2010		WDS05237-3819
	80.91474483	-38.31966402	24.023	13.465	11.691	11.749	26.58	41.91	1.602	26.97	40.75	1.250	0.96	Hg	2015.0	AAAB	GAIA DR1. PM data from GAIA DR1 catalog. Solid CPM candidate
CBL 129	07:03:08.450	-73:50:13.9	51.4	140	11.18	11.90	-3	59							2010		WDS07031-7350
	105.7851094	-73.8369683	51.334	140.088	10.969	11.614	-6.30	60.10	1.273	-5.10	60.70	1.273	0.96	Hg	2015.000	AAAB	GAIA DR1. PM data from UCAC5 catalog. Solid CPM candidate
CBL 136	10:32:03.301	-30:28:05.5	14.5	30	11.52	11.87	34	-38							2010		WDS10321-3028
	158.0139037	-30.46835253	14.484	29.584	11.276	11.465	34.30	-39.37	1.387	34.01	-38.97	1.026	0.96	Hg	2015.0	AAAB	GAIA DR1. PM data from GAIA DR1 catalog. Solid CPM candidate
CBL 172	18:41:25.437	-44:32:30.6	36.4	53	10.92	11.84	15	-46							2010		WDS18414-4433
	280.3560762	-44.54203407	36.251	53.431	10.740	11.621	16.64	-47.35	10.71	18.02	-54.18	5.84	0.96	Hg	2015.0	ACCC	GAIA DR1. M1 and M2 are G-band. PM data calculated from position comparison with 2MASS. Difference in PMVL too large to be considered a good CPM candidate
CBL 139	11:35:52.050	-40:40:36.4	20.0	247	11.92	11.82	-89	14							2010		WDS11359-4041
	173.9595911	-40.67886858	20.052	67.312	11.634	11.667	-87.41	13.80	1.153	-88.12	14.09	1.293	0.96	Hg	2015.0	AAAB	GAIA DR1. PM data from GAIA DR1 catalog. Solid CPM candidate
CBL 140	11:53:22.089	-67:07:05.6	36.1	119	10.63	11.77	-9	-55							2010		WDS11534-6707
	178.341913	-67.11842477	36.105	119.261	10.371	11.317	-8.94	-54.66	0.772	-8.67	-56.34	0.914	0.96	Hg	2015.0	ABAB	GAIA DR1. PM data from GAIA DR1 catalog. Good CPM candidate, difference in PMVL might indicate an orbit
CBL 177	20:06:03.950	-41:37:36.5	23.7	9	11.56	11.77	56	-51							2010		WDS20061-4138
	301.5167418	-41.62699058	23.727	8.935	11.205	11.595	52.05	-51.90	1.397	51.63	-50.36	2.046	0.96	Hg	2015.0	AAAB	GAIA DR1. PM data from GAIA DR1 catalog. Solid CPM candidate
CBL 165	17:59:53.978	-45:17:20.7	14.3	193	11.12	11.77	8	-46							2010		WDS17599-4517
	269.9749319	-45.28932788	14.246	192.908	10.865	11.389	6.30	-55.50	3.989	7.09	-51.25	8.377	0.96	Hg	2015.0	ABCB	GAIA DR1. PM data from GAIA DR1 catalog. Rather large PM error range, difference in PMVL might indicate an orbit
CBL 182	21:16:13.423	-40:40:51.9	31.3	152	11.28	11.74	43	-24							2010		WDS21162-4041
	319.0561483	-40.68119	31.279	151.653	11.214	11.608	43.80	-23.30	1.414	44.20	-23.30	1.414	0.96	Hg	2015.000	AAAB	GAIA DR1. PM data from UCAC5 catalog. Solid CPM candidate
CBL 134	10:15:08.030	-65:26:11.0	31.2	305	11.32	11.72	-59	15							2010		WDS10151-6526
	153.7828343	-65.43634137	31.083	304.604	11.073	11.479	-59.73	13.21	1.265	-61.02	11.78	1.206	0.96	Hg	2015.0	AAAB	GAIA DR1. PM data from GAIA DR1 catalog. Solid CPM candidate
CBL 128	06:38:17.670	+18:28:24.6	55.8	64	11.46	11.71	-74	-71							2010		WDS06383+1828
	99.5732433	18.4733886	55.816	63.628	10.878	11.055	-76.10	-22.40	1.697	-75.70	-21.60	1.697	0.96	Hg	2015.000	AAAB	GAIA DR1. PM data from UCAC5 catalog. Solid CPM candidate

Table 2. PM evaluation data and Plx Rating for the selected TGAS objects

Description of the table content:
- Name: Object WDS discoverer ID or Tycho catalog ID
- PMVD: Proper motion vector direction in degrees for A and B and delta AB
- PMVL: Proper motion vector length for A and B and delta AB derived from GAIA DR1 pm values
- Plx: Parallax A and B end parallax error A and B from GAIA DR1
- Dist AB min: "Best case" distance between the components in AU assuming largest possible equal Plx
- Dist AB Plx: "Realistic case" approx. distance between the components in AU according the given GAIA DR1 parallax values
- Dist AB max: "Worst case" approx. maximum distance between the components in AU according to the given GAIA DR1 Plx values with full error range applied in opposite directions
- Plx Rating for potential gravitational relationship (see Appencix B):
-- "A" for a "realistic" distance less than 200,000 AU (assuming average mass stars like our sun with then overlapping Oort clouds), "B" for less than 300,000 AU (with some probability for a smaller distance within the given Plx error range), "C" for above but with still less than 200,000 AU in "best case" and "D" for larger even in "best case"
-- For relation Plx error to Plx value with "A" for less than 5%, "B" for less than 10% and "C" for less than 15% and "D" above

Name	PMVD A	PMVD B	ΔPMVD	PMVL A	PMVL B	ΔPMVL	Plx A	Plx B	e_Plx A	e_Plx B	Dist AB min	Dist AB Plx	Dist AB max	Plx Rat	Notes
CBL 130	182.78	183.80	1.03	74.33	71.71	2.62	4.10	4.46	0.41	0.38	10,644	4,060,874	13,281,909	CB	Probability for gravitational relationship very small to near zero
CBL 114	90.08	85.57	4.51	60.57	63.32	2.74	3.79	2.57	0.51	0.33	8,240,356	25,835,793	44,114,870	DC	Zero probability for gravitational relationship
CBL 47															No Plx data for B available
CBL 112															No Plx data for A available
CBL 170	345.32	343.66	1.67	56.19	56.08	0.11	6.16	6.35	0.27	0.25	4,136	1,001,930	3,767,330	CA	Probability for gravitational relationship rather small
CBL 56															No Plx data for A available
CBL 178	140.43	140.71	0.28	110.52	111.87	1.35	11.69	11.82	0.55	0.74	4,252	194,111	2,093,383	AB	Good probability for gravitational relationship
CBL 147															No GAIA DR1 Plx data for A and B
CBL 185															No GAIA DR1 Plx data for B
CBL 115	170.50	171.30	0.79	85.33	86.09	0.76	4.11	4.23	0.23	0.23	6,496	1,423,763	6,913,466	CB	Probability for gravitational relationship rather small
CBL 150															No GAIA DR1 Plx data for A
CBL 57															No GAIA DR1 Plx data for A and B
CBL 125	32.39	33.50	1.11	49.63	48.87	0.76	3.97	4.06	0.22	0.23	5,734	1,151,770	6,923,721	CB	Probability for gravitational relationship rather small
CBL 129															No GAIA DR1 Plx data for A and B
CBL 136	138.94	138.89	0.05	52.21	51.72	0.49	4.26	4.61	0.48	0.42	3,056	3,676,139	13,560,774	CC	Probability for gravitational relationship very small
CBL 172															No GAIA DR1 Plx data for A
CBL 139	278.97	279.08	0.11	88.49	89.24	0.74	4.04	3.05	0.34	0.53	1,868,662	16,677,527	34,809,614	DC	Zero probability for gravitational relationship
CBL 140	189.29	188.75	0.53	55.39	57.00	1.61	11.79	11.52	0.25	0.29	3,057	410,057	1,235,704	CA	Very small but some probability for gravitational relationship
CBL 177	134.91	134.29	0.63	73.50	72.12	1.38	4.74	4.90	0.58	0.81	4,460	1,420,960	13,459,735	CC	Probability for gravitational relationship very small
CBL 165	173.52	172.13	1.39	55.86	51.74	4.12	5.45	5.75	0.30	0.24	2,478	1,974,656	5,616,678	CA	Probability for gravitational relationship very small
CBL 182															No GAIA DR1 Plx data for B
CBL 134	282.47	280.92	1.55	61.18	62.15	0.97	6.48	6.21	0.28	0.30	4,775	1,383,993	4,388,532	CA	Probability for gravitational relationship very small
CBL 128															No GAIA DR1 Plx data for B

Counter-Check of CBL Double Stars for being Physical Pairs

References

Buchheim, Robert – 2008, CCD Double-Star Measurements at Altimira Observatory in 2007, Journal of Double Star Observations, Vol. 4 No. 1 Page 28

Knapp, Wilfried R.A. and Nanson, John – 2017, A new concept for counter-checking of assumed CPM pairs, Journal of Double Star Observations, Vol. 13 No. 2 Page 139

Caballero, Rafael – 2009, Finding New Common Proper-Motion Binaries by Data Mining, Journal of Double Star Observations, Vol. 5 No. 3 Page 156

Acknowledgements:

The following tools and resources have been used for this research:

- Washington Double Star Catalog
- GAIA DR1 Catalog including TGAS
- UCAC5 catalog
- Aladin Sky Atlas v9.010
- VizieR
- AstroPlanner v2.2

Appendix A - Description of the CPM rating procedure:

- Four rating factors are used: Proper motion vector direction, proper motion vector length, size of position error in relation to proper motion vector length according to Knapp and Nanson 2017 with extension for relation separation to proper motion speed
- Proper motion vector direction ratings: “A” for identical direction within the error range (given by assuming the worst case of the position error pointing in right angle to the PM vector), “B” for similar direction within the double error range, and “C” for outside
- Proper motion vector length ratings: “A” for identical length within the error range (given by assuming the worst case of the position error pointing in the direction if the PM vector), “B” for similar length within the double error range, and C for outside
- Error size ratings: “A” for error size of less than 5% of the proper motion vector length, “B” for less than 10%, and “C” for a larger error size
- Relation separation to proper motion speed: "A" for less than 100 years, "B" for less than 1000 years and "C" for above

- To compensate for excessively large position errors resulting in an “A” rating despite rather high deviations an absolute upper limit is applied regardless of calculated error size:
- Proper motion vector direction: Max. 2.86° difference for an “A” and 5.72° for a “B”
- Proper motion vector length: Max. 5% difference for an “A” and 10% for a “B”

- To compensate for any overly small error “allowance” (result of a combination of very small position error with large PM vector length) the following exceptions are applied:
- If the PM vector direction difference is larger than this calculated “allowed” error but still less than 0.5° then an “A” is given, a “B” is given for larger than 0.5 but less than 1 degree, and a “C” is given if above
- If the PM vector length difference is larger than this calculated “allowed” error but still less than 0.5% then an “A” is given, a “B” is given for larger than 0.5 but less than 1 percent, and a “C” is given if above

Appendix B - Description of the Plx rating procedure:

- Two rating factors are used: Distance between the components calculated from the given Plx data and relationship of given Plx error in comparison with the given Plx data
- Distance rating: “A” for distance less than 200,000 AU assuming average star mass means Sun like and an assumed gravitational relationship border with Oort cloud distance, “B” for a distance of less than 300,000 AU, “C” for distance larger than 300,000 AU but best case scenario less than 200,000 AU and “D” if distance larger 300,000 AU even in best case
- Plx error rating: “A” less than 5%, “B” less than 10%, “C” less than 15% and “D” larger than 15% PM error size in relation to the given PM data

Neglected Northern Hemisphere Binary Star Systems with Updated Separations and Position Angles

Hannah Gulick and Robert Mutel

The University of Iowa
Iowa City, Iowa

Abstract: We observed 58 widely-separated (ρ > 3") northern hemisphere neglected binary star systems listed in theWashington Double Star catalog. Our goal was to obtain current separations and position angles of binaries that had not been observed in years or decades, and compare them with historical data. For each system, we fit Gaussian models to each component to determine the celestial coordinates and the corresponding position angles and angular separations of the binary. We combined these data with proper motions for each component from the recently-published UCAC5 catalog to determine the likelihood that each system was a true binary. We found that 29 candidate binaries were likely bona fide binaries, while 17 systems had large proper motion differences between components and were therefore deemed unlikely to be binaries. The remaining 12 systems had no proper motion listed.

1. INTRODUCTION

A comprehensive list of binary systems is the Washington Double Star [hereafter WDS] catalog, which is maintained by the U.S. Naval Observatory (1). The catalog include a list of “neglected” binary systems, consisting of unconfirmed binaries as well as systems which have not been observed for many years.

These systems provide a fertile research area for observers with small dedicated telescopes, as their properties can only be deduced by combining careful synoptic measurements with historical observations. This, in turn, can be used to create an aggregate database spanning many years. As an example, consider two solar-mass stars in a visual binary system with an angular separation 3" at a distance 100 pc. This system has an orbital period more than 1,000 yr, i.e. an annual position angle change less than 0.3 yr. Therefore, well-spaced observations are required over several decades to adequately sample the slow changes in position angle and angular separation.

In this paper, we report on observations of 59 visual doubles with angular separations exceeding 3" from the Northern Neglected WDS list. For all targets, we also retrieved proper motions from the recently-published UCAC5 proper motion catalog (2) based on GAIA data release 1. By combining our observation with proper motions for each component, we categorized the likelihood that each system is truly binary.

2. OBSERVATIONS

The observations were made using the Iowa Robotic Observatory (3) in southern Arizona. The IRO is a fully robotic telescope consisting of a 0.51 m f/6.8 Cassegrain reflector, a 2Kx2K back-thinned CCD imaging camera, and a 12-position filter wheel. We used a Sloan r' filter with exposure times between 1–3 sec depending on the apparent magnitude of the target stars. The observations were made at epoch 2017 March 30. Both nights had good observing conditions with clear skies and FWHM seeing between 1.8" – 2.0". Prior to analysis, each image had both CCD calibration (bias subtraction, dark-subtraction, flat-fielding) and a WCS astrometric solution (4) applied automatically.

3. DATA ANALYSIS

We fit circular Gaussian model profiles to each component using a downhill-simplex algorithm (Python library Scipy.optimize). For example, Figure 1 shows the double 05210+3728AB with overlaid contours from the Gaussian fits to each component. Using the derived centroid coordinates, we calculated the resulting binary

Neglected Northern Hemisphere Binary Star Systems with Updated Separations and Position Angles

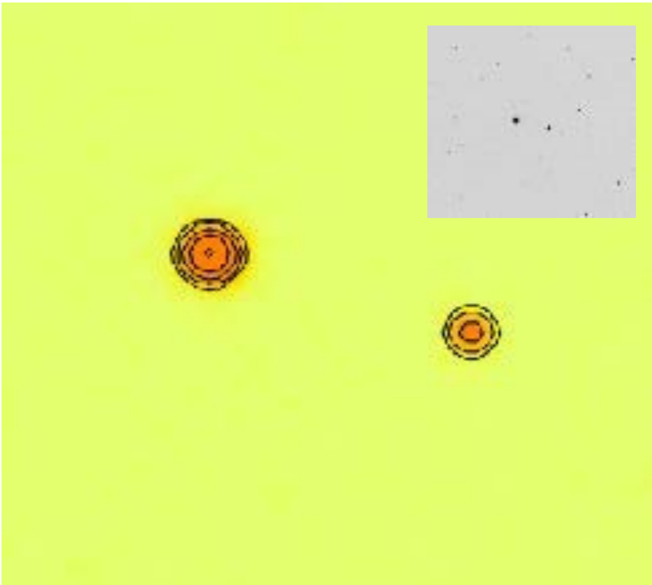

Figure 1. Image of binary system 05210+3728AB on March 2017 showing overlaid contours from Gaussian fits to primary (A) and secondary (B) components. Inset shows the location of 05210+3728 in 3' x 3' field.

angular separation (ρ) and position angle (φ). We also calculated the magnitude difference between primary and secondary components using the model-fit Gaussian peak amplitudes (a_p, a_s) and the expression,

$$\Delta m = 2.51 \log\left(\frac{a_s}{a_p}\right) \quad (1)$$

Stars in systems with a separation less than ~6" were deemed too close to reliably fit Gaussian model components due to component brightness overlap. For these systems we determined component centroid coordinates visually using the image display program DS9. This method did not yield peak amplitude, so magnitude difference was not calculated.

The uncertainties in ρ and φ were calculated in the following manner. We estimated that model-fit centroid positions had a 1σ uncertainty ±0.15 arcsec based on comparison of the fitted centroids with cataloged positions of field stars (e.g., Sloan Digital Sky Survey). Using standard error propagation analysis, the resulting uncertainties in the separation and position angle are,

$$\sigma_\rho = 2\sigma = 0.3" \quad (2)$$

$$\sigma_\varphi = \frac{\sigma_\rho}{\rho} \quad \text{radians.} \quad (3)$$

Most target binaries had angular separations between 3" – 30", so the resulting position angle uncertainty was in the range 0.6° – 6°.

4. RESULTS

We determined the angular separations, position angles, and Sloan r' magnitude differences for 59 neglected binary systems at the heliocentric Julian date of 2457842. These are listed in Tables 1–2 along with measured J2000 coordinates of each primary component and proper motions from the UCAC5 proper motion catalog (2). The latter were used to categorize each system as a bona fide binary with high or low confidence, as described below.

For any binary, there will be two velocity components contributing to each component's total proper motion on the sky: the center of mass proper motion and the contribution from the component's orbital velocity in the binary system. For the long-period binaries considered in this survey, orbital speeds are a few km/s or less, corresponding to a differential angular speed between components $\Delta\mu_{orb} \lesssim 10$ mas/yr for systems at a distance 100 pc, and correspondingly less at greater distance. Hence, if the proper motion difference in either right ascension or declination significantly exceeds this value, it is increasingly unlikely that the system is a true binary.

For Tables 1 and 2, columns are organized as: WDS listed binary system name, right ascension and declination of primary components at epoch J2000, difference in magnitude (secondary magnitude minus primary magnitude), observed position angle, change in position angle from 2017 to last cataloged position angle, observed angular separation, change in angular separation from 2017 to last cataloged separation, magnitude of the proper motion vector difference between primary and secondary stars, proper motion uncertainties of primary and secondary stars, heliocentric Julian date, and number of nights observed. Table 3 is organized the same as tables 1 and 2, but omits the columns for the magnitude of the proper motion vector difference between primary and secondary stars and the proper motion uncertainties of primary and secondary stars.

We assigned each binary a high confidence or low confidence label based on the proper motion difference between the primary and secondary stars. These are listed in Tables 1 and 2 respectively. To be considered a high confidence binary system, the proper motion difference between components in each coordinate must be less than three times the larger of the proper motion uncertainty in that coordinate or 10 mas (to account for

(Text continues on page 366)

Table 1. High Confidence Binaries

Name	RA+Dec	Δm	ϕ	Δϕ	ρ	Δρ	Δμ	σ_μ	Date	N
03467+4241 FOX 134	034645.013 +423927.45	1.2	107.7 ± 2.8	3.7	5.9 ± 0.2	-0.2	3.16	18.41, 9.68	2457842.612	1
04260+4515 ES 567BC	042602.179 +451359.98	0.2	128.1 ± 3.0	-1.9	8.1 ± 0.2	0.0	3.08	11.51, 21.19	2457842.616	1
04477+3446 HJ 349	044740.621 +344622.89	-0.4	266.7 ± 1.6	-0.3	10.4 ± 0.3	0.0	1.42	24.2, 30.85	2457842.621	1
04484+4611 HJ 2239	044810.874 +461119.81	1.1	163.7 ± 2.8	0.7	13.6 ± 0.2	0.5	0.85	34.46, 46.02	2457842.622	1
05177+3757 SEI 156	051742.932 +375613.07	0.1	244.0 ± 2.1	2.0	24.8 ± 0.3	-0.1	2.55	15.87, 13.57	2457842.627	1
05210+3728 SEI 203AB	052058.510 +372830.81	2.1	251.2 ± 1.3	0.2	21.5 ± 0.2	0.0	9.43	27.42, <0.01	2457842.630	1
05231+3802S EI 225	052308.984 +380138.25	-0.8	88.0 ± 0.4	0.0	26.2 ± 0.3	0.0	3.05	18.41, 6.69	2457842.631	1
05275+3425 TOB 35	052729.322 +342502.64	0.7	328.4 ± 2.9	-0.4	21.2 ± 0.2	0.4	0.30	46.02, 50.00	2457842.632	1
05279+4441 ES 1377	052754.793 +444108.24	N/A	185.0 ± 5.7	-0.8	4.0 ± 0.2	-0.4	3.92	34.46, 13.57	2457842.633	1
05385+3201 J 901	053832.826 +320124.28	N/A	143.2 ± 8.2	-5.6	2.8 ± 0.3	-0.1	2.10	8.08, 46.02	2457842.635	1
05399+5145 ES 893	053956.724 +514518.05	0.5	225.0 ± 3.3	0.0	7.2 ± 0.2	0.0	3.27	15.87, 42.08	2457842.637	1
05497+3146 SEI 391AC	054939.523 +314629.74	0.7	140.3 ± 2.6	0.3	27.5 ± 0.3	-1.4	6.58	0.02, 0.03	2457842.639	1
05498+3127 SEI 392	054948.887 +312637.03	0.8	309.1 ± 4.0	2.1	8.7 ± 0.3	0.1	0.78	34.46, 38.21	2457842.641	1
05499+2259 POU 789	054953.621 +225847.66	1.6	251.3 ± 2.6	-0.7	12.7 ± 0.3	0.0	6.53	24.20, 21.19	2457842.641	1
05523+3442 GYL 87	055214.353 +344120.96	0.5	327.2 ± 4.4	0.4	10.3 ± 0.3	-0.6	1.53	46.02, 18.41	2457842.643	1
05525+3235 SEI 424	055230.662 +323440.52	0.7	265.7 ± 1.0	0.7	13.1 ± 0.2	-0.2	1.42	27.42, 24.20	2457842.654	1
05553+2023 J 1914	055515.816 +202322.20	0.7	256.2 ± 2.1	6.2	7.8 ± 0.2	3.8	0.80	27.43, 50.00	2457842.656	1
05557+3127 SEI 440	055542.074 +312701.17	0.8	333.0 ± 2.6	-1.0	13.9 ± 0.2	0.2	2.10	46.02, 18.41	2457842.657	1
05559+3104 SEI 442	055548.964 +310422.81	1.2	186.5 ± 2.1	1.5	25.1 ± 0.2	-0.2	7.11	42.07, <0.01	2457842.660	1
05585+2727 J 252	055825.581 +272201.36	1.2	318.5 ± 3.8	-0.5	5.2 ± 0.2	-0.3	2.05	15.87, 18.41	2457842.660	1
05589+3143 SEI 450	055852.536 +314229.21	-0.2	178.0 ± 1.9	-1.8	28.8 ± 0.2	-0.6	5.08	1.79, 4.46	2457842.660	1
06138+3509 GCB 16	061407.230& 350532.36	0.1	184.4 ± 4.1	-0.6	6.4 ± 0.2	-2.0	1.03	38.21, 30.86	2457842.664	1
06162+2051 J 1054	061610.209 +205127.90	N/A	138.8 ± 7.5	-0.2	3.3 ± 0.3	0.3	2.20	46.02, 8.08	2457842.665	1
06279+3715 MLB 1028	062758.609 +371444.64	3.2	297.5 ± 2.3	7.8	7.9 ± 0.2	1.6	5.30	42.09, 13.57	2457842.669	1
06301+2756 J 2428	063003.892 +275749.44	N/A	178.9 ± 5.7	28.9	4.0 ± 0.2	0.0	1.77	21.19, 24.20	2457842.670	1
06368+2335 GCB 20	063621.872 +233818.56	0.5	229.2 ± 3.0	2.2	8.2 ± 0.2	0.2	0.22	46.02, 46.02	2457842.672	1
06442+3822 J 665	064405.904 +382233.01	2.8	66.5 ± 3.0	-1.4	7.6 ± 0.3	-0.8	2.55	8.08, 24.20	2457842.647	1
08036+4739 PKO 8	080346.120 +473905.06	0.1	249.8 ± 2.8	-0.2	11.7 ± 0.3	3.9	0.54	46.02, 42.07	2457842.653	1
08334+3348 MLB 838	083325.805 +335017.90	0.0	18.2 ± 6.8	-0.8	4.8 ± 0.3	0.6	3.22	6.69, 42.07	2457842.657	1

Neglected Northern Hemisphere Binary Star Systems with Updated Separations and Position Angles

Table 2. Low Confidence Binaries

Name	RA+Dec	Δm	ϕ	Δϕ	ρ	Δρ	Δμ	σ_μ	Date	N
03493+2424 HL 30AB	034916.805 +242346.35	3.9	13.4 ± 1.2	1.4	69.8 ± 0.2	-2.4	57.03	<0.01, <0.01	2457842.612	1
04020+6231 SLE 43AD	040158.322 +623050.42	2.2	277.9 ± 1.5	-1.1	19.9 ± 0.2	0.8	16.05	<0.01, <0.01	2457842.614	1
04076+3804 ALC 1AE	040734.354 +380428.37	0.0	99.6 ± 0.1	N/A	746.0 ± 0.2	26.0	68.04	<0.01, <0.01	2457842.613	1
04125+3538 HJ 341	041231.205 +354359.23	0.2	333.4 ± 2.6	2.4	13.8 ± 0.2	1.0	12.25	24.20, <0.01	2457842.615	1
05179+3724 SEI 162	051754.782 +372336.09	1.6	223.5 ± 3.6	-0.5	24.1 ± 0.4	2.9	28.62	<0.01, 0.02	2457842.627	1
05161+3632 SEI 132	051606.174 +363141.65	-0.1	113.6 ± 2.8	-5.6	25.0 ± 0.2	0.4	9.51	<0.01, <0.01	2457842.626	1
05380+3643 SEI 358	053758.715 +364234.70	0.6	196.8 ± 3.6	0.8	17.8 ± 0.3	-0.4	9.97	6.68, <0.01	2457842.637	1
05463+3152 SEI 384	054616.199 +315220.59	1.5	175.4 ± 4.1	-0.6	13.9 ± 0.3	0.2	11.15	<0.01, <0.01	2457842.639	1
06050+2913 MLB 750	060458.089 +291122.01	0.9	236.5 ± 3.2	-0.5	6.6 ± 0.2	0.3	10.67	0.07, <0.01	2457842.663	1
06125+2025 J 1926	061227.013 +202437.67	N/A	0.2 ± 5.8	5.2	6.1 ± 0.2	5.0	46.35	<0.01, <0.01	2457842.663	1
06204+2331 J 1822	062037.252 +232819.31	0.5	2.9 ± 3.9	-1.1	7.0 ± 0.2	2.0	23.90	<0.01, <0.01	2457842.665	1
06335+6712 MLB 457	063335.777 +671138.78	N/A	307.2 ± 5.9	18.2	4.5 ± 0.3	-1.7	22.61	<0.01, <0.01	2457800.678	1
06383+2427 HO 625AC	063818.901 +242701.71	4.4	352.2 ± 1.4	-0.8	50.5 ± 0.2	0.4	42.47	1.07, 0.02	2457842.674	1
07208+3151 SEI 478	072051.463 +315102.00	N/A	16.6 ± 5.5	-8.2	4.2 ± 0.2	-1.8	23.36	2.27, <0.01	2457842.650	1
09251+2933 BU 1423AC	092507.977 +293249.02	2.7	51.7 ± 0.6	-0.3	155.2 ± 0.2	0.8	47.79	<0.01, <0.01	2457842.682	1
09390+3017 ARY 51	093859.331 +301631.56	0.7	273.0 ± 0.2	0.0	118.7 ± 0.2	-0.9	37.89	<0.01, 5.48	2457842.692	1
11125+3549 STTA108BD	111244.285 +354947.96	0.0	247.8 ± 0.7	19.9	159.9 ± 0.4	7.0	245.82	<0.01, <0.01	2457842.759	1

Table 3. Systems without UCAC5 Proper Motion

Name	RA+Dec	Δm	ϕ	Δϕ	ρ	Δρ	Date	N
03267+4110 J 889	032646.903 +410850.52	N/A	61.0 ± 9.2	-36.0	2.1 ± 0.3	-0.8	2457842.609	1
03495+5239 ES 12DE	034924.675 +524019.45	N/A	223.9 ± 9.0	-6.1	2.4 ± 0.3	-0.3	2457842.611	1
04113+2630 LDS5514BC	041113.457 +262952.35	0.0	305.2 ± 2.3	5.2	11.0 ± 0.2	0.0	2457842.614	1
05119+3631 SEI 93	051149.163 +363028.70	N/A	146.7 ± 5.5	21.7	3.9 ± 0.2	-0.7	2457842.625	1
05225+6011 LEO 11	052232.232 +601123.64	N/A	215.6 ± 6.4	4.6	2.9 ± 0.2	-0.5	2457842.631	1
06212+2108 S 513BE	062110.309 +210745.216	1.7	327.8 ± 1.5	0.8	40.6 ± 0.2	-0.5	2457842.666	1
06214+3402 MLB1044	062126.528 +340155.550	1.3	126.0 ± 3.1	1.0	7.4 ± 0.2	0.5	2457842.667	1
06377+6129 BUP 91AC	063741.334 +612854.14	-0.2	92.3 ± 0.2	-1.7	397.5 ± 0.4	17.6	2457842.673	1
07018+6617 MLB 400	070140.898 +661654.20	N/A	214.0 ± 9.9	24.0	2.1 ± 0.3	0.0	2457842.647	1
07059+3603 STF1013	070551.903 +360255.17	N/A	56.6 ± 4.6	1.6	4.4 ± 0.2	-0.3	2457842.649	1
08010+3454 MLB 932	080101.534 +345310.10	0.7	56.0 ± 4.8	4.0	4.6 ± 0.3	0.2	2457842.652	1
10432+3849 MLB 933	104316.264 +384840.83	N/A	246.1 ± 5.0	-1.9	3.5 ± 0.2	-0.1	2457842.738	1

(Continued from page 363)

possible orbital motion contribution).

Twelve candidate systems did not have proper motions listed for both the primary and secondary star. These systems are listed in Table 3, where their binary status is indeterminate due to the lack of knowledge on their proper motions.

4. ACKNOWLEDGEMENTS

Recognition for observation and data analysis collaboration goes to Brandon Schuemann and Darean Witt.

This research used the Washington Double Star Catalog, maintained at the U.S. Naval Observatory, and the VizieR and SIMBAD databases, both maintained at CDS, Strasbourg, France. This research was supported by the National Science Foundation under grant No. 1517412.

5. REFERENCES

[1]Washington Double Star Catalog, United States Naval Observatory. http://ad.usno.navy.mil/wds/wdstext.html

[2] Zacharias, N. Finch, C. and Frouard, J. 2017, "UCAC5: New Proper Motions Using Gaia DR1", *AJ*, **53**,166.

[3]Iowa Robotic Observatory. http://astro.physics.uiowa.edu/iro

[4] Greisen, E. and Calabretta, M. 2002, "Representations of world coordinates in FITS", *A.A.*, **395**,1075.

CPM Pairs from LSPM so Far Not WDS Listed – Part IV

Wilfried R.A. Knapp
Vienna, Austria
wilfried.knapp@gmail.com

John Nanson
Star Splitters Double Star Blog
Manzanita, Oregon
jnanson@nehalemtel.net

Abstract: The LSPM catalog (Lepine and Shara 2005) is a rich source for CPM pairs we thought already exhausted – but as we found during research for our report "A New Concept for Counter-Checking of Assumed CPM Pairs" (Knapp and Nanson 2017), there are still many potential CPM pairs indicated in LSPM not listed in the WDS catalog. After our first three reports on about 100 such objects (Knapp and Nanson 2017 - CPM pairs from LSPM so far not WDS listed – Part I/II/III), this report with 30 additional potential common proper motion pairs is presented here.

Introduction

Similar to our first three reports on common proper motion pairs not listed so far in the WDS the selection from LSPM was done by sorting all LSPM objects by RA and then checking if the next LSPM object is nearer than 30 arc-seconds and so far not included in the WDS catalog. As a second criterion we selected all objects with an altitude suitable for imaging during the time of the research for this report with the intention of taking images with V- and I-filters in order to be able to determine as far as possible not only RA/Dec coordinates, separation, position angle, magnitudes and proper motion values, but also the spectral class range of all components according to the V-I color index.

Since GAIA DR1 coordinates are now available for most of the selected objects our most important CPM check analysis was done on the basis of comparison of 2MASS to GAIA DR1 positions. Because proper motion data listed directly in GAIA is still scarce and thus not available for both components of our objects, it was necessary to do our own calculations, which allowed a CPM rating according to Knapp/Nanson 2017 (see description Appendix A).

We also checked as many other sources as possible via Aladin for data for these CPM candidates beginning with visual comparison of POSS I and POSS II images. If the Aladin centroid feature did not work (as was usually the case) we then resorted to visual estimation of the centroids to determine separation, position angle and proper motion from POSS I to POSS II. Next came the check of other existing catalog data for the given field of view, especially URAT1, SDSS, WISE, UCAC4 and GSC.

Besides measuring Vmags in our own images we tried also to get the visual magnitudes for each of the components from the various catalogs we used.

When the 2MASS data with J- and K-band values were available, we used a spreadsheet to estimate Vmags with formulas found on the website of Bruce Gary (http://brucegary.net/dummies/method0.html) provided -0.1 < (J-K) < 1.0. For SDSS objects fainter than 15mag in g-band we estimated Vmag as (gmag+rmag)/2 based on advice from Brian Skiff that this might work rather well.

Spectral class data was scarce in the available catalogs so as already mentioned we had to resort to deriving the spectral class of the objects in question using the B-V color index provided we had these values listed in the same catalog. For this purpose we used a table provided by the Space Telescope Science Institute (http://www.stsci.edu/~inr/intrins.html).

Additionally we took images with I-filter to get Icmags to be able to estimate the spectral class range of the components on base of own image material again using the above mentioned table.

The image processing followed our usual procedure: Stacking with AAVSO VPhot, plate solving and measuring positions and Vmags with Astrometrica using URAT1 as reference catalog and calculating Sep and PA with the formulas provided by Buchheim 2008. Due to the faintness of some objects we had to use exposure times up to 300 seconds and even then some components were too faint to be resolved. The I-filter images were first also plate solved with URAT1 as reference catalog for the astrometry results and then again plate solved using Astrometrica with USNO B1 as reference catalog for Ic-mags for the I-band photometry results.

In total we got in this way an observation history of each object beginning in most cases in the year ~1950 with POSS I and ending in 2017 with own new images.

Results of Our Research

In Table 1 we present for the selected objects as much data as we could find in the catalogs available to us including our own measurements based on images taken with remote telescope iT24. Given below is a description of the table content per column:

- Name gives the discoverer ID of the selected object with a running number in the header line
- RA and Dec give the recent precise coordinates of the A component (if available from GAIA DR1) in the header line in the traditional HH:MM:SS DD:MM:SS format and in the data lines for the sources referred to in the Notes column in decimal degrees format as these values are directly usable for calculating Sep and PA
- Sep gives separation in arcseconds in the data lines calculated as

$$Sep = \sqrt{\left[\left(\cos\left(RA_1 - RA_2\right)\cos\left(Dec_1\right)\right)^2 + \left(Dec_2 - Dec_1\right)^2\right]}$$

  in radians
- PA gives position angle in degrees in the data lines calculated as

$$PA = \arctan\left[\frac{\left(RA_2 - RA_1\right)\cos\left(Dec_1\right)}{Dec_2 - Dec_1}\right]$$

  in radians depending on quadrant
- M1 and M2 give measured Vmags in the header line for A and B and if available also in the data lines where we had often to resort to estimated values based on calculation from the J- and K-band values if available
- pmRA1 and pmDE1 with e_pm1 give the proper motion data for A and pmRA2, pmDE2 and e_pm2 for B in the header line as well as in the data lines calculated by comparison of positions between catalogs or directly from the catalogs (specified in the Notes column)
- Spc1 and Spc2 give the spectral class range for A and B usually based on the V-I color index taking into consideration also the error range of the measured Imags
- Ap indicates in the data lines the aperture used for the observation listed (for GAIA calculated equivalent circular surface diameter) and Me indicates the WDS code for the used observation method
- Date is the Julian epoch of the (averaged) observation date given in the data lines
- CPM Rat gives the rating of the CPM assessment based on comparison of positions (in most cases between 2MASS and GAIA DR1 if available) in the header line and the corresponding data line
- Source/Notes finally indicates in the header line the LSPM ID and the overall assessment for the object in question and in the data lines the source used (images and catalogs) and additional explanations if considered necessary.

Summary

From 30 objects checked for CPM

- 22 objects received a solid or at least good CPM candidate rating based on position comparison, in most cases between 2MASS and GAIA DR1 (according to the method presented in Knapp/Nanson 2017)
- 4 objects could not be rated due to missing precise catalog positions for calculating CPM speed and direction – but in all cases visual evidence by comparing existing image material strongly suggested CPM
- 3 objects got a CPM rating for being most certainly not CPM
- 1 object remained unclear due to even missing visual evidence.

The issue of I-band photometry and using it for estimating the spectral class range was handled similarly to our part II&III report.

Follow Up

This report is our last one on this topic although we are convinced that there might be a lot more CPM pairs hidden in the LSPM catalog but with separations larger than 30 arcseconds thus not covered by our selection criterion up to this limit.

But we found in our image material for this report a number of WDS objects and will provide historical re-

(Text continues on page 385)

CPM Pairs from LSPM so Far Not WDS Listed – Part IV

Table 1: Research results for potential common proper motion pairs found in the LSPM catalog. Headline object position based on the most precise J2000 coordinates currently available for A (in most cases from the GAIA DR1 catalog)

Name	RA	Dec	Sep	PA	M1	M2	pmRA1	pmDec1	e_pm1	pmRA2	pmDec2	e_pm2	Spc1	Spc2	Ap	Me	Date	CPM Rat	Source/Notes
KPP n+1	05 44 41.239	21 20 51.39			15.27	18.00	-112.23	111.30	5.39	-112.22	112.60	4.96	>M4	>M4				AAAC	J0544+2120: Solid CPM candidate
	86.17387500	21.34600000	5.813	222.294											1.20	Pp	1951.849		POSS I.O estimates
	86.17216667	21.34736111	4.751	222.555			-123.92	106.01		-108.81	123.32				1.20	Pp	1998.072		POSS II.N estimates. PM estimates based on comparison with POSS I.O
	86.17240200	21.34707800	5.720	224.514	13.88	15.43									1.30	E2	1997.883		2MASS. M1 and M2 estimated from J- and K-band
	86.17187360	21.34755720	5.704	224.706	15.2		-113.20	110.30		-112.10	110.60				0.20	Eu	2013.616		URAT1
	86.17182909	21.34760721	5.704	224.669	14.08	16.09	-112.23	111.30	5.39	-112.22	112.60	4.96			0.96	Hg	2015.000	AAAC	GAIA DR1. M1 and M2 are G-band. PM data calculated from position comparison with 2MASS
	86.17172917	21.34767222	6.060	227.934	15.27	18.00									0.61	C	2017.081		iT24 1x60s V-filter
	86.17174583	21.34765556	5.563	223.878	12.66	14.55							>M4	>M4	0.61	C	2017.081		iT24 1x60s I-filter. Spc based on V-I color index
NSN n+1	06 11 56.179	33 25 43.03			14.98	18.60	133.37	-421.46	6.24	129.49	-412.57	6.20	>M4	M2->M4				AAAA	J0611+3325: Solid CPM candidate. M2 estimated, might be much fainter
	92.98300000	33.4308889	12.146	188.893											1.20	Pp	1999.057		POSS II.N estimates
	92.98329600	33.4307140	12.397	189.922	12.44	16.22									1.30	E2	1999.967		2MASS. M1 and M2 estimated from J- and K-band
	92.98390000	33.4291211	12.314	190.198	14.95		133.37	-421.46	6.24	129.49	-412.57	6.20			0.20	Eu	2013.609	AAAA	URAT1. PM data calculated from position comparison with 2MASS
	92.98405000	33.4286361			14.93										0.61	C	2017.084		iT24 1x60s V-filter. No resolution of B, has to be fainter than 18.5Vmag
	92.98410417	33.4287139	12.309	189.779	11.65	15.81							>M4	>M4	0.61	C	2017.076		iT24 1x60s I-filter. Spc based on V-I color index
																			Neither GAIA DR1 nor UCAC5/SDSS/WISE object for B available. Also no resolution of B in POSS I images
KPP n+2	06 12 20.450	37 21 07.32			16.13	17.48	-3.31	-130.34		0.00	-127.57		>M4	>M4					J0612+3721: Blinking POSS images suggests solid common proper motion
	93.08520833	37.35488889	2.412	185.674											1.20	Pp	1954.006		POSS I.O estimates
	93.08516667	37.3535833	2.303	182.968			-3.31	-130.34		0.00	-127.57				1.20	Pp	1990.066		POSS II.J estimates. PM estimates based on comparison with POSS I.O
	93.08521035	37.3520332	3.414	186.362	14.69	16.65									0.96	Hg	2015.000		GAIA DR1. M1 and M2 are G-band
	93.08506667	37.3519278	2.890	180.236	16.13	17.48									0.61	C	2017.209		iT24 1x300s V-filter. Heavily overlapping star disks
	93.08518333	37.3519194	3.100	179.339	13.47	14.51							>M4	>M4	0.61	C	2017.327		iT24 2x300s I-filter. Touching/overlapping star disks. Spc based on V-I color index
																			Neither 2MASS nor URAT1, UCAC5, SDSS or WISE object for B available

Table 1 continues on next page.

CPM Pairs from LSPM so Far Not WDS Listed – Part IV

Table 1 (continued). Research results for potential common proper motion pairs found in the LSPM catalog. Headline object position based on the most precise J2000 coordinates currently available for A (in most cases from the GAIA DR1 catalog)

Name	RA	Dec	Sep	PA	M1	M2	pmRA1	pmDec1	e_pm1	pmRA2	pmDec2	e_pm2	Spc1	Spc2	Ap	Me	Date	CPM Rat	Source/Notes
NSN n+2	06 38 52.448	22 55 11.29			13.43	17.05	-143.37	-312.03	5.70	-152.51	-313.39	5.70	>M4	>M4				AAAA	J0638+2255: Solid CPM candidate
	99.72125	22.92580556	3.922	173.934											1.20	Pp	1949.900		POSS I.O estimates
	99.71920833	22.9215	4.502	178.241			-141	-323		-146.76	-335.36				1.20	Pp	1997.908		POSS II.N estimates. PM estimates based on comparison with POSS I.O
	99.71923200	22.9212040	4.792	173.245	11.85	14.75									1.30	E2	1998.833		2MASS. M1 and M2 estimated from J- and K-band
	99.71853295	22.9198028	4.799	175.026	12.07	15.58	-143.37	-312.03	5.70	-152.51	-313.39	5.70			0.96	Hg	2015.000	AAAA	GAIA DR1. M1 and M2 are G-band. PM data calculated from position comparison with 2MASS
	99.71843333	22.9196306	4.692	175.947	13.43	17.05									0.61	C	2017.209		iT24 1x300s V-filter. SNR B <20. Heavily overlapping star disks
	99.71848333	22.9196417	4.876	177.239	10.58	13.91							>M4	>M4	0.61	C	2017.084		iT24 1x180s I-filter. SNR B <20. Heavily overlapping star disks. Spc based on V-I color index
KPP n+3	06 44 39.062	28 55 26.32			14.05	16.28	194.37	-10.10	5.68	188.74	-14.20	5.68	M2-M4	M3-M4				AAAA	J0644+2855: Solid CPM candidate
	101.15866667	28.9241111	4.561	239.717											1.20	Pp	1953.933		POSS I.O estimates
	101.16120833	28.9240000	4.561	233.704			191	-10		198	-19				1.20	Pp	1995.797		POSS II.N estimates. PM estimates based on comparison with POSS I.O
	101.16175800	28.9240230	5.625	234.698	12.88	14.63									1.30	E2	1998.762		2MASS. M1 and M2 estimated from J- and K-band
	101.16275963	28.9239774	5.738	234.683	13.00	15.00	194.37	-10.10	5.68	188.74	-14.20	5.68			0.96	Hg	2015.000	AAAA	GAIA DR1. M1 and M2 are G-band. PM data calculated from position comparison with 2MASS
	101.16288750	28.9239389	5.590	238.749	14.05	16.28									0.61	C	2017.076		iT24 1x60s V-filter
	101.16289583	28.9239944	5.796	235.773	11.88	13.86							M2-M4	M3-M4	0.61	C	2017.076		iT24 1x60s I-filter. Spc based on V-I color index
NSN n+3	06 46 00.821	52 14 11.26			15.97	16.15							K5-M0	K7-M1					J0646+5214: DSS and 2MASS images show elongation but none of the checked catalogs showed an object for B. Comparison POSS I:O and II.J images shows clearly common proper motion
	101.50370833	52.2395000	2.102	357.495											1.20	Pp	1954.148		POSS I.O estimates
	101.50370833	52.2380278	2.108	355.000			0.00	-143.31		-2.48	-143.31				1.20	Pp	1991.131		POSS II.N estimates. PM estimates based on comparison with POSS I.O
	101.50342083	52.2364611	2.301	357.941	15.97	16.15									0.61	C	2017.209		iT24 1x300s V-filter. Overlapping star disks
	101.50340000	52.2363556	2.381	358.231	14.56	14.55							K5-M0	K7-M1	0.61	C	2017.209		iT24 1x300s I-filter. Overlapping star disks
KPP n+4	06 54 37.555	17 08 03.57			15.22	16.36	-79.01	-141.89	7.18	-78.68	-143.10	7.18	M1-M3	M3-M4				AAAA	J0654+1708: Solid CPM candidate
	103.65787500	17.1371667	3.031	8.157											1.20	Pp	1951.849		POSS I.O estimates
	103.65687500	17.1348056	3.229	7.654			-71.64	-177.01		-71.64	-172.85				1.20	Pp	1999.868		POSS II.N estimates. PM estimates based on comparison with POSS I.O
	103.65684300	17.1349470	3.692	8.250	13.12	11.73									1.30	E2	2000.854		2MASS. M1 and M2 estimated from J- and K-band
	103.65648118	17.1343261	3.674	8.373	14.08	15.18	-79.01	-141.89	7.18	-78.68	-143.10	7.18			0.96	Hg	2015.000	AAAA	GAIA DR1. M1 and M2 are G-band. PM data calculated from position comparison with 2MASS
	103.65641667	17.1341917	3.768	6.992	15.22	16.36									0.61	C	2017.084		iT24 1x180s V-filter. Touching star disks
	103.65640000	17.1342417	3.334	8.157	13.61	14.36							M1-M3	M3-M4	0.61	C	2017.076		iT24 1x60s I-filter. Touching star disks

Table 1 continues on next page.

Table 1 (continued). Research results for potential common proper motion pairs found in the LSPM catalog. Headline object position based on the most precise J2000 coordinates currently available for A (in most cases from the GAIA DR1 catalog)

Name	RA	Dec	Sep	PA	M1	M2	pmRA1	pmDec1	e_pm1	pmRA2	pmDec2	e_pm2	Spc1	Spc2	Ap	Me	Date	CPM Rat	Source/Notes
NSN +4	06 59 03.303	56 31 00.57			15.64	18.57	-32.61	-139.66	5.31	-33.89	-138.09	5.31	K7-M1	M2-M4				AAAA	J0659+5631: Solid CPM candidate
	104.76458333	56.5192500	9.017	82.352											1.20	Pp	1954.072		POSS I.O estimates
	104.76370833	56.5174722	8.935	82.282			-40.56	-149.37		-42.49	-149.37				1.20	Pp	1996.919		POSS II.N estimates. PM estimates based on comparison with POSS I.O
	104.76402500	56.5174450	8.622	82.684	14.88	16.72									1.30	E2	1999.011		2MASS. M1 and M2 estimated from J- and K-band
	104.76376245	56.5168247	8.605	82.501	14.75	17.15	-32.61	-139.66	5.31	-33.89	-138.09	5.31			0.96	Hg	2015.000	AAAA	GAIA DR1. M1 and M2 are G-band. PM data calculated from position comparison with 2MASS
	104.76374167	56.5167556	8.380	84.522	15.64	18.57									0.61	C	2017.209		iT24 1x300s V-filter. SNR B <20
	104.76369167	56.5167611	8.703	84.594	14.06	16.31							K7-M1	M2-M4	0.61	C			iT24 1x60s I-filter. SNR B <20
KPP n+5	07 05 26.916	34 00 16.06			13.19	17.94	-62.12	-191.02		-73.08	-170.45		M1-M3	F1-G8					J0705+3400: DSS image shows the secondary but not 2MASS and none of the checked catalogs but GAIA DR1 showed an object for B. Comparison POSS I:O to II.J images suggests clearly common proper motion
	106.36279167	34.0075000	7.730	150.087											1.20	Pp	1953.862		POSS I.O estimates
	106.36208333	34.0056944	6.937	149.874			-62.12	-191.02		-73.08	-170.45				1.20	Pp	1987.890		POSS II.J estimates. PM estimates based on comparison with POSS I.O
	106.36215056	34.0044621	7.179	150.642	12.29	17.83									0.96	Hg	2015.000		GAIA DR1. M1 and M2 are G-band
	106.36215000	34.0043889	7.221	150.266	13.19	17.94									0.61	C	2017.084		iT24 1x180s V-filter. SNR B <20
	106.36210417	34.0043528	6.378	151.594	11.18	17.51							M1-M3	F1-G8	0.61	C	2017.209		iT24 1x300s I-filter. Touching star disks. SNR B <10. Spc based on V-I color index
NSN n+5	07 21 43.377	25 54 58.82			10.11	13.53	58.15	-164.33		29.08	-164.33		K2-K5	>M4					J0721+2555: No catalog data for CPM assessment available. Comparison POSS images suggests common proper motion
	110.429125	25.91922222	5.688	95.043											1.20	Pp	1954.970		POSS I.O estimates
	110.42979167	25.9175278	4.614	96.221			58.15	-164.33		29.08	-164.33				1.20	Pp	1992.090		POSS II.N estimates. PM estimates based on comparison with POSS I.O
	110.43036800	25.9171160	3.354	87.785	10.06										1.30	E2	1998.888		2MASS. M1 estimated from J- and K-band
	110.43073750	25.9163389	4.778	88.441	10.11	13.53									0.61	C	2017.084		iT24 1x180s V-filter. Heavily overlapping star disks
	110.43070833	25.9163583	4.252	87.979	9.12	10.98							K2-K5	>M4	0.61	C	2017.076		iT24 1x60s I-filter. Heavily overlapping star disks. Spc based on V-I color index

Table 1 continues on next page.

Table 1 (continued). Research results for potential common proper motion pairs found in the LSPM catalog. Headline object position based on the most precise J2000 coordinates currently available for A (in most cases from the GAIA DR1 catalog)

Name	RA	Dec	Sep	PA	M1	M2	pmRA1	pmDec1	e_pm1	pmRA2	pmDec2	e_pm2	Spc1	Spc2	Ap	Me	Date	CPM Rat	Source/Notes
KPP n+6	07 23 20.006	25 36 09.88			16.56	18.45	-103.30	-218.28	5.01	-105.36	-219.07	5.44	M1-M3	M2->M4				AAAA	J0723+2536: Solid CPM candidate
	110.8352083	25.60658333	5.315	39.516											1.20	Pp	1954.970		POSS I.O estimates
	110.83391667	25.6042222	5.230	38.373			-113	-229		-117	-229				1.20	Pp	1992.090		POSS II.N estimates. PM estimates based on comparison with POSS I.O
	110.83389900	25.6037710	5.571	38.273	15.9	17.4									1.30	E2	1998.066		2MASS. M1 and M2 estimated from J- and K-band
	110.83377300	25.6035930	5.520	38.137	16.58	18.62	-132.99	-208.34	27.59	-146.71	-218.87	29.97			2.50	Es	2001.142	ABCA	SDSS DR9. M1 and M2 are gmag+rmag/2 (used when gmag > 15.0). PM data calculated from position comparison with 2MASS
	110.83336020	25.6027442	5.539	38.074	15.60	17.37	-103.30	-218.28	5.01	-105.36	-219.07	5.44			0.96	Hg	2015.000	AAAA	GAIA DR1. M1 and M2 are G-band. PM data calculated from position comparison with 2MASS
	110.83332917	25.6026056	5.179	35.809	16.56	18.45									0.61	C	2017.209		iT24 1x300s V-filter. SNR B <20
	110.83342500	25.6026833	5.179	36.925	14.49	16.28							M1-M3	M2->M4	0.61	C	2017.076		iT24 1x60s I-filter. SNR B <20. Spc based on V-I color index
NSN n+6	07 30 22.917	27 16 07.25			11.85	17.08	34.06	-199.43	5.43	68.11	-248.59	5.84	G8-K4	K4-K7				CCAA	J0730+2716: Seems rather optical despite significant very fast proper motion of both components
	112.5946667	27.27219444	5.602	349.025											1.20	Pp	1953.124		POSS I.O estimates
	112.59516667	27.2698889	5.015	347.719			41	-213		41	-228				1.20	Pp	1992.090		POSS II.N estimates. PM estimates based on comparison with POSS I.O
	112.59532300	27.2695480	6.252	345.202	11.9	17.1									1.30	E2	1998.066		2MASS. M1 and M2 estimated from J- and K-band
	112.59537400	27.2693830	6.198	344.366		16.30	53.01	-192.96	27.56	29.11	-217.52	29.95			2.50	Es	2001.145	CBCA	SDSS DR9. M1 and M2 are gmag+rmag/2 (used when gmag > 15.0). PM data calculated from position comparison with 2MASS.
	112.59548940	27.2686819	5.343	348.622	11.86		34.06	-199.43	5.43	68.11	-248.59	5.84			0.20	Eu	2013.777	CCAA	URAT1. PM data calculated from position comparison with 2MASS
	112.59549167	27.2685222	5.365	346.637	11.85	17.08									0.61	C	2017.075		iT24 1x60s V-filter. SNR B <10. Heavily overlapping star disks
	112.59545417	27.2685000	5.741	340.461	11.05	15.78							G8-K4	K4-K7	0.61	C	2017.075		iT24 1x60s I-filter. SNR B <10. Heavily overlapping star disks. Spc based on V-I color index
KPP n+7	07 34 25.791	23 15 30.28			15.58	17.24	-230.22	-136.24	5.80	-225.98	-135.95	5.80	M3->M4	M3->M4				AAAA	J0734+2315: Solid CPM candidate
	113.6115	23.26105556	4.694	35.953											1.20	Pp	1954.970		POSS I.O estimates
	113.60841667	23.2592500	4.744	27.699			-226	-144		-239	-135				1.20	Pp	2000.027		POSS II.N estimates. PM estimates based on comparison with POSS I.O
	113.60865000	23.2590580	5.181	32.995	13.9	15.3									1.30	E2	1997.924		2MASS. M1 and M2 estimated from J- and K-band
	113.60746139	23.2584118	5.225	33.631	14.28	15.87	-230.22	-136.24	5.80	-225.98	-135.95	5.80			0.96	Hg	2015.000	AAAA	GAIA DR1. M1 and M2 are G-band. PM data calculated from position comparison with 2MASS
	113.60732083	23.2583000	5.473	37.184	15.58	17.24									0.61	C	2017.076		iT24 1x60s V-filter. SNR B <10. Identification of B a bit difficult due to a fore- or background star involved
	113.60728750	23.2583167	4.942	38.453	13.16	14.83							M3->M4	M3->M4	0.61	C	2017.076		iT24 1x60s I-filter. Touching star disks with B obviously optical double. SNR B <20. Spc based on V-I color index

Table 1 continues on next page.

Table 1 (continued). Research results for potential common proper motion pairs found in the LSPM catalog. Headline object position based on the most precise J2000 coordinates currently available for A (in most cases from the GAIA DR1 catalog)

Name	RA	Dec	Sep	PA	M1	M2	pmRA1	pmDec1	e_pm1	pmRA2	pmDec2	e_pm2	Spc1	Spc2	Ap	Me	Date	CPM Rat	Source/Notes
NSN +7	07 35 26.945	+48 14 33.16			11.66	16.86	94.35	-189.03	6.09	-24.46	20.81	10.75	M0-M2	G8-K4				CCCB	J0735+4814: Not a CPM candidate.
	113.8595420	48.2454170	6.703	1.708											1.2	Pp	1953.122		POSS I.O estimates.
	113.8611320	48.2438870			11.69										1.2	Pp	1991.820		GSC 2.3. M1 is GSC 2.3 Vmag, secondary not identified.
	113.8616740	48.2433400	6.677	349.406	11.10										1.3	E2	1999.857		2MASS. M1 estimated from J- and K-band, M2 not shown in 2MASS data.
	113.8608750	48.2435560	7.943	349.126			103.00	-166.00		63.00	-140.00				1.2	Pp	1999.863		POSS II.N estimates. PM estimates based on comparison with POSS I.O. Secondary very difficult to identify and separate in both POSS images.
	113.8617910	48.2431900	7.763	345.111	11.90	16.90									2.5	Es	2003.886	CCCB	SDSS DR9. Vmags estimated from (gmag+rmag)/2.
	113.8621914	48.2426403	9.831	342.752	11.70		90.08	-182.92	6.70	-32.39	22.26	11.80	K7		0.2	Eu	2013.642	CCCB	URAT1. M1 is URAT1 Vmag. SPC1 is URAT1 V-I value. PM data calculated from position comparison with 2MASS.
	113.8622699	48.2425449	10.200	342.738	10.75	16.47	103.32	-208.97	51.28	10.46	-7.60	0.26			0.96	Hg	2015.000	CCCB	GAIA DR1. M1 and M2 are G-band. PM data calculated from position comparison with SDSS DR9.
	113.8622699	48.2425449	10.200	342.738	10.75	16.47	94.35	-189.03	6.09	-24.46	20.81	10.75			0.96	Hg	2015.000	CCCB	GAIA DR1. M1 and M2 are G-band. PM data calculated from position comparison with 2MASS.
	113.8623292	48.2424417	10.846	342.083	11.66	16.86									0.61	C	2017.076		iT24 1x60s V-filter
	113.8623667	48.2424528	10.149	343.884	9.82	16.03							M0-M2	G8-K4	0.61	C	2017.076		iT24 1x60s I-filter. SNR B <20. Spc based on V-I color index
																			Notes: Secondary not identified in WISE, neither of the components is identified in UCAC5.
KPP n+8	07 48 35.903	+37 12 9.47			10.41								K7-M1						J0748+3712: No conclusion possible due to absence of secondary in all databases consulted with the exception of 2MASS.
	117.1498090	37.2037510	5.867	91.758	10.20	13.30									1.3	E2	1998.272		2MASS. M1 and M2 estimated from J- and K-band
	117.1498300	37.2036290			10.64								>M4		1.2	Pp	2000.000		GSC 2.3. M1 is GSC 2.3 Vmag, Spc1 is GSC 2.3 B-V value. Secondary not identified in GSC 2.3.
	117.1495978	37.2026306			9.86		-39.10	-241.00							0.2	Eu	2002.021		UCAC5 with GAIA coordinates. Secondary not identified. M1 is from J and K values. PmRA1 and pmDec1 are from UCAC5 data.
	117.1497750	37.2034994			9.81										0.2	Eu	2002.021		UCAC5 coordinates used here. M1 is UCAC5 Gmag value.
	117.1496850	37.2029780			10.16										0.4	Hw	2010.500		WISE. M1 is from G-band value. Secondary not identified in WISE.
	117.1496017	37.2026961			10.43								K5		0.2	Eu	2013.943		URAT1. M1 is URAT1 Vmag. SPC1 is URAT1 B-V value. Secondary not identified in URAT1.
	117.1495978	37.2026307			9.81		-40.07	-239.06							0.96	Hg	2015.000		GAIA DR1. Secondary not identified in GAIA DR1. M1 is G-band, pmRA1 and pmDec1 data are GAIA DR1 values listed in Aladin.

Table 1 continues on next page.

CPM Pairs from LSPM so Far Not WDS Listed – Part IV

Table 1 (continued). Research results for potential common proper motion pairs found in the LSPM catalog. Headline object position based on the most precise J2000 coordinates currently available for A (in most cases from the GAIA DR1 catalog)

Name	RA	Dec	Sep	PA	M1	M2	pmRA1	pmDec1	e_pm1	pmRA2	pmDec2	e_pm2	Spc1	Spc2	Ap	Me	Date	CPM Rat	Source/Notes
	117.1495333	37.2024806			10.41										0.61	C	2017.209		iT24 1x300s V-filter. No resolution of B
	117.1494958	37.2024667			8.83								K7-M1		0.61	C	2017.209		iT24 1x300s I-filter. No resolution of B. Spc based on V-I color index
																			Notes: There are five markers for the primary in SDSS-DR9, located 482 mas apart, so there's no way to be sure which is the primary - all values are similar - and the secondary is not identified. Not possible to locate secondary in the POSSI and POSSII images.
NSN n+8	07 51 01.841	+40 06 6.48			16.60	18.96	-126.61	-157.92	5.07	-122.78	-154.09	5.07	>M4	>M4				AAAA	J0751+4006: Solid CPM candidate.
	117.7604580	40.1044440	7.769	187.638											1.2	Pp	1953.198		POSS I.E estimates.
	117.7589620	40.1030200	7.107	185.782	15.68	17.86									1.2	Pp	1986.905		GSC 2.2. M1 and M2 are GSC 2.2 Rmags. Note: The GSC 2.2 Rmags are identical to the GSC 2.3 Fmags.
	117.7589620	40.1030200	7.107	185.782	16.27	17.86									1.2	Pp	1986.905		GSC 2.3. M1 is GSC 2.3 Vmag, M2 is GSC 2.3 Fmag.
	117.7584380	40.1025350	7.431	186.233	14.70	16.20									1.3	E2	1998.272		2MASS. M1 and M2 estimated from J- and K-band
	117.7581250	40.0124440	7.100	180.000			-150.00	-168.00		-126.00	-154.00				1.2	Pp	1999.172		POSS II.N estimates. PM estimates based on comparison with POSS I.E.
	117.7583310	40.1024470	7.373	185.680	16.68	19.04									2.5	Es	2000.244		SDSS DR9. M1 and M2 are gmag+rmag/2 (used when gmag > 15.0).
	117.7583310	40.1024470	7.373	185.680	16.68	19.04	-149.39	-160.62	43.02	-110.30	-135.07	43.02			2.5	Es	2000.244	BCCA	SDSS DR9. M1 and M2 are gmag+rmag/2 (used when gmag > 15.0). PM data calculated from position comparison with 2MASS.
	117.7576689	40.1018011			14.71		-103.30	-146.50							0.2	Eu	2002.118		UCAC5 with GAIA coordinates. Secondary not identified in UCAC5. M1 is from J and K values. PmRA1 and pmDec1 are from UCAC5 data.
	117.7581522	40.1023253			15.04										0.2	Eu	2002.118		UCAC5 coordinates used here. Secondary not identified. M1 is UCAC5 Gmag value.
	117.7578630	40.1020400	7.032	185.573	14.70	16.20	-132.10	-148.60	9.90	-121.70	-116.20	21.70			0.4	Hw	2010.500	BCCA	WISE. M1 from WISE J and K magnitudes. PM data calculated from position comparison with 2MASS.
	117.7576872	40.1018531	7.352	185.746	14.71	16.16	-132.98	-157.90	5.46	-128.28	-153.09	5.45			0.2	Eu	2013.828	AAAA	URAT1. M1 and M2 from URAT1 J and K values. PM data calculated from position comparison with 2MASS.
	117.7576688	40.1018012	7.361	185.791	15.04	16.97	-126.61	-157.92	5.07	-122.78	-154.09	5.07			0.96	Hg	2015.000	AAAA	GAIA DR1. M1 and M2 are G-band. PM data calculated from position comparison with 2MASS.
	117.7575292	40.1016639	7.558	186.450	16.60	18.96									0.61	C	2017.209		iT24 1x300s V-filter
	117.7575542	40.1018056	7.365	186.350	13.86	15.78							>M4	>M4	0.61	C	2017.075		iT24 1x60s I-filter. SNR B <20. Spc based on V-I color index

Table 1 continues on next page.

CPM Pairs from LSPM so Far Not WDS Listed – Part IV

Table 1 (continued). Research results for potential common proper motion pairs found in the LSPM catalog. Headline object position based on the most precise J2000 coordinates currently available for A (in most cases from the GAIA DR1 catalog)

Name	RA	Dec	Sep	PA	M1	M2	pmRA1	pmDec1	e_pm1	pmRA2	pmDec2	e_pm2	Spc1	Spc2	Ap	Me	Date	CPM Rat	Source/Notes
																			Notes: Secondary not identified in WISE, M1 J and K data in WISE appears to be unreliable since it results in a visual equivalent magnitude of 7.136. Only one object identified in URAT1, which doesn't appear to be either component based on URAT1 PM data.
KPP n+9	07 54 4.665	+13 05 53.48			15.50	16.09	170.41	-231.51	8.81	182.58	-241.61	6.06	G5-K3	K5-M0				BCAB	J0754+1305: Very difficult pair due to 13th magnitude star which overwhelms the 15th magnitude LSPM primary to the extent that most surveys fail to pick up the primary. Possibly a better PM candidate than the rating indicates.
						15.43				178.20	-247.50				0.2	Eu	2000.923		UCAC5. Primary not identified in UCAC5. M2 is UCAC5 Gmag, pmRA2 and pmDec2 are UCAC5 PM data.
	118.5189490	13.0988340	11.457	225.287	16.30	16.20									2.5	Es	2004.941		SDSS DR7. Vmags estimated from (gmag+rmag)/2. Three super-imposed objects at both primary and secondary positions, took the northernmost of the primary and used the object with the same epoch at the secondary location.
	118.5189590	13.0988730	11.571	224.916	16.10	16.20									2.5	Es	2004.951		SDSS DR9. M1 and M2 are gmag+rmag/2 (used when gmag > 15.0). Five superimposed objects at both primary and secondary locations, took the northernmost in each case (with same epoch).
	118.5194374	13.0981878	11.442	224.496	15.63	15.43	170.41	-231.51	8.81	182.58	-241.61	6.06			1.0	Hg	2015.000	BCAB	GAIA DR1. M1 and M2 are G-band. PM data calculated from position comparison with SDSS DR7.
	118.5194374	13.0981878	11.442	224.496	15.63	15.43	166.92	-245.48	6.76	181.88	-242.33	0.16			0.96	Hg	2015.000	CCAB	GAIA DR1. M1 and M2 are G-band. PM data calculated from position comparison with SDSS DR9.
	118.5192792	13.0982639	11.311	220.035	15.50	16.09									0.61	C	2017.076		iT24 1x60s V-filter. Star disk A overlaps with background star
	118.5196458	13.0979972	11.729	227.194	14.78	14.61							G5-K3	K5-M0	0.61	C	2017.076		iT24 1x60s I-filter. Star disk A overlaps with background star. Spc based on V-I color index
																			Notes: Primary not identified in 2MASS, WISE, GSC 2.2 and 2.3, and URAT1. Not possible to detect primary in POSSI and POSSII images - south-easterly motion of secondary is obvious, but no indication of an object moving south-easterly across the face of the 13th magnitude star that overwhelms the primary.

Table 1 continues on next page.

CPM Pairs from LSPM so Far Not WDS Listed – Part IV

Table 1 (continued). Research results for potential common proper motion pairs found in the LSPM catalog. Headline object position based on the most precise J2000 coordinates currently available for A (in most cases from the GAIA DR1 catalog)

Name	RA	Dec	Sep	PA	M1	M2	pmRA1	pmDec1	e_pm1	pmRA2	pmDec2	e_pm2	Spc1	Spc2	Ap	Me	Date	CPM Rat	Source/Notes
NSN n+9	08 58 10.034	+52 27 14.55			17.04	17.56	-130.92	-135.43	5.59	-131.43	-130.54	5.59	>M4	>M4				AAAA	J0858+5227: Solid CPM candidate.
	134.5453750	52.4559170	5.480	288.071											1.2	Pp	1954.146		POSS I.E estimates.
	134.5432620	52.4549340	5.542	280.516	16.90	17.57									1.2	Pp	1991.110		GSC 2.3. M1 and M2 are GSC 2.3 Vmag values.
	134.5426250	52.4550830	5.126	281.250			-141.00	-70.00		-137.00	-87.00				1.2	Pp	1997.908		POSS II.J estimates. PM estimates based on comparison with POSS I.E.
	134.5427150	52.4546130	5.742	280.329	15.20	15.60									1.3	E2	1999.825		2MASS. M1 and M2 estimated from J- and K-band.
	134.5426720	52.4546280	5.773	281.001	17.10	17.70									2.5	Es	2000.245		SDSS DR9. M1 and M2 are gmag+rmag/2 (used when gmag > 15.0).
	134.5418925	52.4540978	5.756	280.956	15.56	15.22	-129.97	-133.59	6.11	-130.15	-128.96	6.11			0.2	Eu	2013.708	AAAA	URAT1. M1 and M2 from URAT1 J and K values. PM data calculated from position comparison with 2MASS.
	134.5418093	52.4540421	5.763	281.041	15.52	16.00	-128.26	-142.94	0.19	-127.58	-142.79	0.19			0.96	Hg	2015.000	AAAA	GAIA DR1. M1 and M2 are G-band. PM data calculated from position comparison with SDSS DR9.
	134.5418093	52.4540421	5.763	281.041	15.52	16.00	-130.92	-135.43	5.59	-131.43	-130.54	5.59			0.96	Hg	2015.000	AAAA	GAIA DR1. M1 and M2 are G-band. PM data calculated from position comparison with 2MASS.
	134.5415583	52.4539611	5.596	282.802	17.04	17.56									0.61	C	2017.084		iT24 1x180s V-filter
	134.5417708	52.4539750	5.728	281.071	14.16	14.77							>M4	>M4	0.61	C	2017.076		iT24 1x60s I-filter. Spc based on V-I color index
																			Notes: Primary not identified in WISE. Neither of the components is identified in UCAC5.
KPP n+10	09 14 44.527	+18 06 15.48			15.89	19.20	-131.44	-94.38	5.89	-129.93	-94.32	5.89	M2-M4	M1-M3				AAAA	J0914+1806: Solid CPM candidate. M2 estimated as being 0.1 magnitude fainter than faintest stars resolved in V-filter image.
	138.6880000	18.1060000	11.300	112.917											1.2	Pp	1950.214		POSS I.O estimates.
	138.6861250	18.1051390	11.547	115.660			-150.00	-73.00		-150.00	-87.00				1.2	Pp	1990.088		POSS II.N estimates. PM estimates based on comparison with POSS I.O.
	138.6862500	18.1047450	11.177	112.258	16.08	19.37									1.2	Pp	1997.187		GSC 2.3. M1 is GSC 2.3 Vmag, M2 is GSC 2.3 f.mag.
	138.6861830	18.1047460	10.932	113.317	14.50	17.40									1.3	E2	1998.031		2MASS. M1 and M2 estimated from J- and K-band.
	138.6859340	18.1045600	10.915	113.293	16.00	20.60									2.5	Es	2005.053		SDSS DR9. M1 and M2 are gmag+rmag/2 (used when gmag > 15.0).
	138.6855836	18.1043353	10.977	113.052	15.80	17.42	-130.36	-93.97	6.36	-129.05	-93.97	6.48	>M4		0.2	Eu	2013.610	AAAA	URAT1. M1 is URAT1 Vmag, M2 is from URAT1 J and K values. Spc1 is URAT1 B-V value. PM data calculated from position comparison with 2MASS.
	138.6855312	18.1043011	10.955	113.258	14.66	18.30	-138.57	-93.69	0.16	-134.62	-94.66	3.02			0.96	Hg	2015.000	BBAA	GAIA DR1. M1 and M2 are G-band. PM data calculated from position comparison with SDSS DR9.
	138.6855312	18.1043011	10.955	113.258	14.66	18.30	-131.44	-94.38	5.89	-129.93	-94.32	5.89			0.96	Hg	2015.000	AAAA	GAIA DR1. M1 and M2 are G-band. PM data calculated from position comparison with 2MASS.

Table 1 continues on next page.

CPM Pairs from LSPM so Far Not WDS Listed – Part IV

Table 1 (continued). Research results for potential common proper motion pairs found in the LSPM catalog. Headline object position based on the most precise J2000 coordinates currently available for A (in most cases from the GAIA DR1 catalog)

Name	RA	Dec	Sep	PA	M1	M2	pmRA1	pmDec1	e_pm1	pmRA2	pmDec2	e_pm2	Spc1	Spc2	Ap	Me	Date	CPM	Source/Notes
	138.6854333	18.1042194			15.89										0.61	C	2017.210		iT24 1x300s V-filter. No resolution of B, has to be fainter than 19.1Vmag
	138.6854667	18.1042667	10.942	112.514	13.66	17.11							M2-M4	M1-M3	0.61	C	2017.210		iT24 1x300s I-filter. Spc based on V-I color index. Vmag2 estimated 19.2
																			Notes: Neither of the components is identified in UCAC5 and WISE.
NSN n+10	09 25 27.696	+21 02 31.22			14.53	19.60	-138.70	-76.95	6.02	-146.97	-75.47	6.02	K7-M1	M3->M4				AAAB	J0925+2102: Solid CPM Candidate. M2 estimated as being 0.1 magnitude fainter than faintest stars resolved in V-filter image.
	141.3672500	21.0436940	17.760	17.904											1.2	Pp	1951.090		POSS I.E estimates.
	141.3657500	21.0425830	17.654	15.642			-118.00	-94.00		-134.00	-91.00				1.2	Pp	1999.205		POSS II.F estimates. PM estimates based on comparison with POSS I.E.
	141.3660550	21.0423600	17.341	14.566	14.27	19.20									1.2	Pp	1999.209		GSC 2.3. M1 is GSC 2.3 Vmag, M2 is GSC 2.3 f.mag.
	141.3659800	21.0423070	17.394	14.293	13.90	17.30									1.3	E2	2000.914		2MASS. M1 and M2 estimated from J- and K-band
	141.3657950	21.0422230	17.432	14.169	14.80	20.40									2.5	Es	2005.047		SDSS DR9. M1 and M2 are gmag+rmag/2 (used when gmag > 15.0).
	141.3656100	21.0421410	17.494	14.299	13.90	17.30	-132.00	-63.50	11.40	-129.20	-53.10	20.10			0.4	Hw	2010.332	BACB	WISE. M1 and M2 from WISE J and K magnitudes. PM data calculated from position comparison with 2MASS.
	141.3654563	21.0420264	17.412	14.069	14.92	17.32	-135.81	-77.97	6.55	-139.64	-74.80	6.51	>K4		0.2	Eu	2013.912	AAAB	URAT1. M1 is URAT1 Vmag, M2 is from URAT1 J and K values. Spc1 is URAT1 B-V value. PM data calculated from position comparison with 2MASS.
	141.3653985	21.0420059	17.385	13.903	13.66	18.35	-133.84	-78.51	7.27	-142.85	-81.12	7.85			0.96	Hg	2015.000	BCAB	GAIA DR1. M1 and M2 are G-band. PM data calculated from position comparison with SDSS DR9.
	141.3653985	21.0420059	17.385	13.903	13.66	18.35	-138.70	-76.95	6.02	-146.97	-75.47	6.02			0.96	Hg	2015.000	AAAB	GAIA DR1. M1 and M2 are G-band. PM data calculated from position comparison with 2MASS.
	141.3653333	21.0419028			14.53										0.61	C	2017.209		iT24 1x300s V-filter. No resolution of B, has to be fainter than 19.5Vmag
	141.3653333	21.0419528	17.309	14.473	12.79	17.09							K7-M1	M3->M4	0.61	C	2017.209		iT24 1x300s I-filter. Spc based on V-I color index. Vmag2 estimated 19.6
																			Notes: Neither of the components is identified in UCAC5.
KPP n+11	09 47 43.251	+38 20 08.27			16.71	17.53	103.82	-298.99	5.07	104.24	297.76	5.07	>M4	>M4				AAAA	J0947+3820: Solid CPM candidate.
	146.9280000	38.3412220	4.929	291.420											1.2	Pp	1953.106		POSS I.O estimates
	146.9293400	38.3376020	5.267	291.534	15.62	16.29									1.2	Pp	1992.094		GSC 2.3. M1 and M2 are GSC 2.3 f.mag values.
	146.9292920	38.3374170	5.115	289.413			85.00	-320.00		80.00	-323.00				1.2	Pp	1997.166		POSS II.J estimates. PM estimates based on comparison with POSS I.O.
	146.9295970	38.3370210	5.376	291.282	14.90	15.40									1.3	E2	1998.255		2MASS. M1 and M2 estimated from J- and K-band.

Table 1 continues on next page.

CPM Pairs from LSPM so Far Not WDS Listed – Part IV

Table 1 (continued). Research results for potential common proper motion pairs found in the LSPM catalog. Headline object position based on the most precise J2000 coordinates currently available for A (in most cases from the GAIA DR1 catalog)

Name	RA	Dec	Sep	PA	M1	M2	pmRA1	pmDec1	e_pm1	pmRA2	pmDec2	e_pm2	Spc1	Spc2	Ap	Me	Date	CPM	Source/Notes
	146.9297780	38.3366220	5.373	291.540	16.80	17.60									2.5	Es	2002.999		SDSS DR9. M1 and M2 are gmag+rmag/2 (used when gmag > 15.0).
	146.9300320	38.3360650	5.321	290.061			101.70	-285.00	12.00	102.70	-295.50	17.60			0.4	Hw	2010.331	AABA	WISE. J and K magnitudes not listed in WISE. PM data calculated from position comparison with 2MASS.
	146.9301661	38.3357169	5.337	291.238	14.95	15.62	103.00	-300.90	5.44	104.83	-300.87	5.42			0.2	Eu	2013.889	AAAA	URAT1. M1 and M2 from URAT1 f.mag values. PM data calculated from position comparison with 2MASS.
	146.9302127	38.3356303	5.377	291.513	15.33	16.00	102.27	-297.48	0.13	101.92	-297.57	0.24			0.96	Hg	2015.000	AAAA	GAIA DR1. M1 and M2 are G-band. PM data calculated from position comparison with SDSS DR9.
	146.9302127	38.3356303	5.377	291.513	15.33	16.00	103.82	-298.99	5.07	104.24	297.76	5.07			0.96	Hg	2015.000	AAAA	GAIA DR1. M1 and M2 are G-band. PM data calculated from position comparison with 2MASS.
	146.9303333	38.3354778	5.317	290.246	16.71	17.53									0.61	C	2017.084		iT24 1x180s V-filter. SNR B <20
	146.9302917	38.3350583	5.422	289.276	13.69	14.37							>M4	>M4	0.61	C	2017.076		iT24 1x60s I-filter. Spc based on V-I color index
																			Notes: Neither of the components is identified in UCAC5.
NSN n+11	09 54 39.40	+24 27 54.07			19.00		-191.64	-26.29	49.23	-191.35	-26.86	50.02	>M4					ABCA	J0954+2427: Possible PM candidate,but limited ability to reach a conclusion because secondary not identified in 2MASS, URAT1, and GAIA DR1. POSSI and POSSII data promising, but certainly not conclusive.
	148.6695000	24.4658060	4.460	199.676											1.2	Pp	1955.216		POSS I.E estimates.
	148.6675000	24.4653330	4.366	200.118			-153.00	-40.00		-153.00	-37.00				1.2	Pp	1990.209		POSS II.J estimates. PM estimates based on comparison with POSS I.E.
	148.6677960	24.4652080	4.740	194.944	18.30										1.2	Pp	1990.737		GSC 2.3. M1 is GSC 2.3 Vmag, no Vmag or f.mag shown for secondary.
	148.6669950	24.4651080	4.828	197.089	18.98	20.54	-191.64	-26.29	49.23	-191.35	-26.86	50.02			2.5	Es	2004.957	ABCA	SDSS DR9. M1 and M2 are gmag+rmag/2 (used when gmag > 15.0). PM data calculated from position comparison with GSC 2.3.
	148.6664914	24.4650306			16.26		-193.60	-40.50							0.2	Eu	2013.714		URAT1. M1 is from URAT1 J and K values, PM data is directly from URAT1 data. Secondary not identified in URAT1.
	148.6664176	24.4650203			17.13										0.96	Hg	2015.000		GAIA DR1. M1 is from GAIA G-band. Secondary not identified in GAIA.
	148.6663417	24.4650333			19.00										0.61	C	2017.210		iT24 1x300s V-filter. SNR A <10. No resolution of B, has to be fainter than 19.5Vmag
	148.6663375	24.4649889			15.34								>M4		0.61	C	2017.210		iT24 1x300s I-filter. No resolution of B, has to be fainter than 18.9 Imag. Spc based on V-I color index
																			Notes: Secondary not identified in 2MASS and WISE, neither of the components is identified in UCAC5.

Table 1 continues on next page.

CPM Pairs from LSPM so Far Not WDS Listed – Part IV

Table 1 (continued). Research results for potential common proper motion pairs found in the LSPM catalog. Headline object position based on the most precise J2000 coordinates currently available for A (in most cases from the GAIA DR1 catalog)

Name	RA	Dec	Sep	PA	M1	M2	pmRA1	pmDec1	e_pm1	pmRA2	pmDec2	e_pm2	Spc1	Spc2	Ap	Me	Date	CPM Rat	Source/Notes
KPP n+12	10 01 19.938	+36 27 22.67			18.23	18.32	93.20	-160.27	9.95	89.12	-161.94	9.95	M0-M2	K7-M1				AABB	J1001+3627: Good PM candidate. Measures consistent in showing a slight disparity in motion in RA.
	150.3307500	36.4590560	5.001	1.382											1.2	Pp	1955.194		POSS I.E estimates. Secondary overlapping nearby star making it hard to identify centroid, PM results open to question.
	150.3322700	36.4574670	5.164	1.510	18.09	18.48							K2	K2	1.2	Pp	1988.949		GSC 2.3. M1 and M2 are GSC 2.3 Vmag values. Spc1 and Spc2 are GSC 2.3 V-N values.
	150.3325360	36.4570430	5.411	0.858	17.70	17.80									1.3	E2	1998.272		2MASS. M1 and M2 estimated from J- and K-band.
	150.3324170	36.4571670	5.101	1.355			113.00	-159.00		113.00	-157.00				1.2	Pp	1998.326		POSS II.N estimates. PM estimates based on comparison with POSS I.E.
	150.3326860	36.4568130	5.375	0.370	18.50	18.80	85.20	-166.54	29.08	78.03	-151.51	29.08			2.5	Es	2003.086	ABCA	SDSS DR9. M1 and M2 are gmag+rmag/2 (used when gmag > 15.0). PM data calculated from position comparison with GSC 2.3.
	150.3330700	36.4563169	5.367	359.743	17.74	17.81	98.21	-166.03	10.57	91.58	-168.89	10.58			0.2	Eu	2014.012	AABB	URAT1. M1 and M2 from URAT1 J and K values. PM data calculated from position comparison with 2MASS.
	150.3330745	36.4562983	5.383	0.136	17.49	17.76	94.41	-155.53	2.35	92.57	-154.86	2.38			0.96	Hg	2015.000	ABAB	GAIA DR1. M1 and M2 are G-band. PM data calculated from position comparison with SDSS DR9.
	150.3330745	36.4562983	5.383	0.136	17.49	17.76	93.20	-160.27	9.95	89.12	-161.94	9.95			0.96	Hg	2015.000	AABB	GAIA DR1. M1 and M2 are G-band. PM data calculated from position comparison with 2MASS.
	150.3329750	36.4562306	5.659	8.954	18.23	18.32									0.61	C	2017.081		iT24 1x60s V-filter. SNR A and B <20
	150.3330375	36.4561806	5.441	1.143	16.44	16.63							M0-M2	K7-M1	0.61	C	2017.081		iT24 1x60s I-filter. Spc based on V-I color index
																			Notes: Secondary not identified in WISE, neither of the components is identified in UCAC5.
NSN n+12	10 23 15.586	+54 40 06.51			15.86	17.73	-66.05	-77.45	7.25	-68.91	-74.85	7.25	>M4	>M4				AABA	J1023+5440: Solid CPM candidate.
	155.8164580	54.6698610	8.754	258.802											1.2	Pp	1955.075		POSS I.O estimates.
	155.8154170	54.6690280	8.821	259.549			-51.00	-70.00		-53.00	-68.00				1.2	Pp	1997.346		POSS II.J estimates. PM estimates based on comparison with POSS I.O.
	155.8155390	54.6687900	8.988	258.658	14.76	16.70									1.2	Pp	1998.299		GSC 2.3. M1 and M2 are GSC 2.3 f.mag values.
	155.8154140	54.6687970	8.833	258.051	14.50	15.90									1.3	E2	2000.073		2MASS. M1 and M2 estimated from J- and K-band
	155.8153250	54.6687720	8.863	258.306	15.90	17.90									2.5	Es	2001.967		SDSS DR9. M1 and M2 are gmag+rmag/2 (used when gmag > 15.0).
	155.8149406	54.6684758			14.63		-66.10	-77.50							0.2	Eu	2003.123		UCAC5 with GAIA coordinates. Secondary not identified in UCAC5. M1 is from UCAC5 Gmag value. PmRA1 and pmDec1 are from UCAC5 data.

Table 1 continues on next page.

Table 1 (continued). Research results for potential common proper motion pairs found in the LSPM catalog. Headline object position based on the most precise J2000 coordinates currently available for A (in most cases from the GAIA DR1 catalog)

Name	RA	Dec	Sep	PA	M1	M2	pmRA1	pmDec1	e_pm1	pmRA2	pmDec2	e_pm2	Spc1	Spc2	Ap	Me	Date	CPM Rat	Source/Notes
	155.8153175	54.6687317			15.56		-66.10	-77.50							0.2	Eu	2003.123		UCAC5 coordinates used here. Secondary not identified. M1 is UCAC5 f.mag value. PmRA1 and pmDec1 are from UCC5 data.
	155.8151230	54.6685940	8.765	259.612	14.50	15.90	-59.10	-71.30	10.70	-57.10	-47.10	19.80			0.4	Hw	2010.326	CCCB	WISE. M1 and M2 from WISE J and K magnitudes. PM data calculated from position comparison with 2MASS.
	155.8149631	54.6685119	8.873	258.317	15.77	15.90	-68.31	-74.68	7.87	-71.72	-72.31	7.87	K7		0.2	Eu	2013.820	AABA	URAT1. M1 is URAT1 Vmag, M2 is visual estimate from URAT1 J and K values; Spc1 is URAT1 B-V value. PM data calculated from position comparison with 2MASS.
	155.8149405	54.6684759	8.867	258.354	14.63	16.27	-61.43	-81.80	0.11	-61.83	-81.31	0.33			0.96	Hg	2015.000	AAAA	GAIA DR1. M1 and M2 are G-band. PM data calculated from position comparison with SDSS DR9.
	155.8149405	54.6684759	8.867	258.354	14.63	16.27	-66.05	-77.45	7.25	-68.91	-74.85	7.25			0.96	Hg	2015.000	AABA	GAIA DR1. M1 and M2 are G-band. PM data calculated from position comparison with 2MASS.
	155.8148083	54.6684806	8.915	259.335	15.86	17.73									0.61	C	2017.155		iT24 1x180s V-filter
	155.8148125	54.6684806	8.982	257.265	13.21	14.79							>M4	>M4	0.61	C	2017.081		iT24 1x60s I-filter. Spc based on V-I color index
KPP n+13	10 34 49.131	+01 58 40.54			14.71	14.78	125.03	-150.88	5.70	123.58	-151.00	5.70	M1-M3	M1-M3				AAAB	J1034+0158: Solid CPM Candidate.
	158.7021250	1.9807222	8.762	124.974											1.2	Pp	1952.079		POSS I.O estimates
	158.7038900	1.9788790	8.888	124.742	13.67	13.68									1.2	Pp	1991.050		GSC 2.3. M1 and M2 are GSC 2.3 f.mag values.
	158.7040417	1.9787222	8.640	125.361			161.00	-168.00		158.00	-168.00				1.2	Pp	1995.091		POSS II.J estimates. PM estimates based on comparison with POSS I.O.
	158.7041930	1.9785520	8.989	124.940	13.60	13.80									1.3	E2	2000.106		2MASS. M1 and M2 estimated from J- and K-band
	158.7041430	1.9785340	8.984	124.935	14.80	14.90	97.95	-133.65	51.76	104.53	-142.17	51.76			2.5	Es	2000.343	ABCB	SDSS DR9. M1 and M2 are gmag+rmag/2 (used when gmag > 15.0). PM data calculated from position comparison with GSC 2.3.
	158.7045610	1.9781410	8.812	124.927	13.60	13.80	128.60	-143.80	12.60	114.30	-134.30	11.50			0.4	Hw	2010.399	ABBB	WISE. M1 and M2 from WISE J and K magnitudes. PM data calculated from position comparison with 2MASS.
	158.7046803	1.9779633	9.000	125.068	14.18	13.79	125.68	-151.92	6.08	124.57	-152.41	6.04	>M4		0.2	Eu	2014.110	AAAB	URAT1. M1 is URAT1 Vmag, M2 is visual estimate based on URAT1 J and K magnitudes, Spc1 is URAT1 B-V value. PM data calculated from position comparison with 2MASS.
	158.7047106	1.9779278	8.972	125.028	13.70	13.75	139.32	-148.90	1.16	138.19	-149.26	1.30			0.96	Hg	2015.000	AAAC	GAIA DR1. M1 and M2 are G-band. PM data calculated from position comparison with SDSS DR9.
	158.7047106	1.9779278	8.972	125.028	13.70	13.75	125.03	-150.88	5.70	123.58	-151.00	5.70			0.96	Hg	2015.000	AAAB	GAIA DR1. M1 and M2 are G-band. PM data calculated from position comparison with 2MASS.
	158.7048000	1.9778278	9.000	125.295	14.71	14.78									0.61	C	2017.305		iT24 1x60s V-filter
	158.7048250	1.9778694	8.986	125.669	12.59	12.65							M1-M3	M1-M3	0.61	C	2017.305		iT24 1x60s I-filter. Spc based on V-I color index
																			Notes: Neither of the components is identified in UCAC5.

Table 1 continues on next page.

Table 1 (continued). Research results for potential common proper motion pairs found in the LSPM catalog. Headline object position based on the most precise J2000 coordinates currently available for A (in most cases from the GAIA DR1 catalog)

Name	RA	Dec	Sep	PA	M1	M2	pmRA1	pmDec1	e_pm1	pmRA2	pmDec2	e_pm2	Spc1	Spc2	Ap	Me	Date	CPM Rat	Source/Notes
NSN n+13	11 11 09.689	+02 21 06.80			16.14	19.20	-150.62	-143.33	8.24	-151.51	-143.44	8.98	>M4	M2->M4				AAAA	J1111+0221: Solid CPM candidate. M2 estimated as being 0.1 magnitude fainter than faintest stars resolved in V-filter image.
	167.7924170	2.3548610	7.830	282.539											1.2	Pp	1955.285		POSS I.E estimates.
	167.7910000	2.3530000	7.901	284.663			-119.00	-157.00		-110.00	-150.00				1.2	Pp	1995.151		POSS II.F estimates. PM estimates based on comparison with POSS I.E.
	167.7911910	2.3526890	7.883	285.088	15.13	19.45									1.2	Pp	1995.154		GSC 2.3. M1 and M2 are GSC 2.3 f.mag values.
	167.7909820	2.3524660	8.036	283.973	14.20	17.20									1.3	E2	2000.234		2MASS. M1 and M2 estimated from J- and K-band.
	167.7903706	2.3518881			14.62		-154.90	-139.40							0.2	Eu	2000.262		UCAC5 with GAIA coordinates. M1 is UCAC5 Gmag value. Secondary not identified. PmRA1 and pmDec1 are from UCAC5 data.
	167.7910053	2.3524589			14.21		-154.90	-139.40							0.2	Eu	2000.262		UCAC5 coordinates used here. M1 is from J and K values. Secondary not identified. PmRA1 and pmDec1 are from UCAC5 data.
	167.7909700	2.3524270	8.119	284.534	16.20	20.90									2.5	Es	2000.979		SDSS DR9. M1 and M2 are gmag+rmag/2 (used when gmag > 15.0).
	167.7905740	2.3520690	8.003	282.153	14.20	17.20	-144.10	-140.30	70.80	-146.50	-165.40	45.80			0.4	Hw	2010.423	BBCA	WISE. M1 and M2 from WISE J and K magnitudes. PM data calculated from position comparison with 2MASS.
	167.7904069	2.3519192	8.011	284.352	16.21	17.16	-155.93	-140.74	1.80	-152.18	-148.47	5.11	K7		0.2	Eu	2013.805	BAAA	URAT1. M1 is URAT1 Vmag, M2 is visual estimate from URAT1 J and K magnitudes; Spc1 is URAT1 B-V value. PM data calculated from position comparison with SDSS DR9.
	167.7904069	2.3519192	8.011	284.352	16.21	17.16	-150.62	-143.33	8.24	-151.51	-143.44	8.98	K7		0.2	Eu	2013.805	AAAA	URAT1. M1 is URAT1 Vmag, M2 is visual estimate from URAT1 J and K magnitudes; Spc1 is URAT1 B-V value. PM data calculated from position comparison with 2MASS.
	167.7902042	2.3518306			16.14										0.61	C	2017.324		iT24 1x300s V-filter. No resolution of B, has to be fainter than 19.1Vmag
	167.7902958	2.3517139	7.075	287.182	13.41	16.87							>M4	M2->M4	0.61	C	2017.324		iT24 1x300s I-filter. Touching star disks. Spc based on V-I color index with Vmag2 assumed 19.2
																			Notes: Secondary not identified in GAIA DR1.
KPP n+14	11 39 58.062	+34 54 21.18			15.15	17.23	176.72	-141.90	9.13	178.10	-143.32	9.13	>M4	>M4				AAAB	J1139+3454: Solid CPM candidate.
	174.9885420	34.9083890	8.275	101.149											1.2	Pp	1950.365		POSS I.E estimates.
	174.9905420	34.9072220	7.773	101.127			138.00	-98.00		127.00	-96.00				1.2	Pp	1998.326		POSS II.N estimates. PM estimates based on comparison with POSS I.E.
	174.9911550	34.9064770	8.120	99.467	14.73	16.91									1.2	Pp	1999.346		GSC 2.3. M1 and M2 are GSC 2.3 Vmag values.
	174.9910420	34.9064640	8.247	100.360	13.60	15.30									1.3	E2	2000.262		2MASS. M1 and M2 estimated from J- and K-band.

Table 1 continues on next page.

CPM Pairs from LSPM so Far Not WDS Listed – Part IV

Table 1 (continued). Research results for potential common proper motion pairs found in the LSPM catalog. Headline object position based on the most precise J2000 coordinates currently available for A (in most cases from the GAIA DR1 catalog)

Name	RA	Dec	Sep	PA	M1	M2	pmRA1	pmDec1	e_pm1	pmRA2	pmDec2	e_pm2	Spc1	Spc2	Ap	Me	Date	CPM Rat	Source/Notes
	174.9919242	34.9058831			13.87		160.50	-143.20							0.2	Eu	2002.071		UCAC5 with GAIA coordinates. M1 is UCAC5 Gmag value. Secondary not identified. PmRA1 and pmDec1 are from UCAC5 data.
	174.9912211	34.9063975			13.57		160.50	-143.20							0.2	Eu	2002.071		UCAC5 coordinates used here. M1 is from J and K values. Secondary not identified. PmRA1 and pmDec1 are from UCAC5 data.
	174.9913410	34.9063250	8.257	100.500	15.20	17.30									2.5	Es	2004.283		SDSS DR9. M1 and M2 are gmag+rmag/2 (used when gmag > 15.0).
	174.9917660	34.9061210	8.079	101.125	13.60	15.30	210.80	-121.80	10.40	192.50	-129.30	20.80			0.4	Hw	2010.401	BABB	WISE. M1 and M2 from WISE J and K magnitudes. PM data calculated from position comparison with 2MASS.
	174.9918436	34.9059411	8.250	100.350	13.57	15.32	174.92	-139.14	9.94	176.11	-139.85	10.00			0.2	Eu	2013.753	AAAB	URAT1. M1 and M2 estimated from URAT1 J and K values. PM data calculated from position comparison with 2MASS.
	174.9919242	34.9058831	8.271	100.478	13.87	15.76	160.65	-148.45	0.13	162.00	-148.39	0.27			0.96	Hg	2015.000	AAAB	GAIA DR1. M1 and M2 are G-band. PM data calculated from position comparison with SDSS DR9.
	174.9919242	34.9058831	8.271	100.478	13.87	15.76	176.72	-141.90	9.13	178.10	-143.32	9.13			0.96	Hg	2015.000	AAAB	GAIA DR1. M1 and M2 are G-band. PM data calculated from position comparison with 2MASS.
	174.9920875	34.9057806	8.135	100.124	15.15	17.23									0.61	C	2017.305		iT24 1x60s V-filter
	174.9920333	34.9058111	8.284	100.573	12.08	13.89							>M4	>M4	0.61	C	2017.305		iT24 1x60s I-filter. Spc based on V-I color index
NSN n+14	11 50 38.865	+31 42 23.61			11.90	15.54	-230.13	-12.00	10.13	-230.10	-7.95	10.13	K0-K4	K3-K5				AAAA	J1150+3142: Solid CPM candidate.
	177.6667080	31.7068610	4.577	257.380											1.2	Pp	1955.274		POSS I.E estimates.
	177.6632020	31.7066140	4.611	250.243	13.30										1.3	E2	1998.187		2MASS. M1 estimated from J- and K-band, M2 J and K data appears to be unreliable since it results in a visual equivalent magnitude of 7.136.
	177.6630420	31.7068060	4.624	249.758			-263.00	-5.00		-260.00	-19.00				1.2	Pp	1998.209		POSS II.N estimates. PM estimates based on comparison with POSS I.E.
	177.6619386	31.7065581			12.68		-235.30	-26.50							0.2	Eu	2001.441		UCAC5 with GAIA coordinates. M1 is UCAC5 Gmag value. Secondary not identified. PmRA1 and pmDec1 are from UCAC5 data.
	177.6629806	31.7066578			13.32		-235.30	-26.50							0.2	Eu	2001.441		UCAC5 coordinates used here. M1 is from J and K values. Secondary not identified. PmRA1 and pmDec1 are from UCAC5 data.
	177.6627520	31.7066320	4.580	250.533	14.10	18.70									2.5	Es	2004.316		SDSS DR9. M1 and M2 are gmag+rmag/2 (used when gmag > 15.0).
	177.6619387	31.7065579	4.588	251.041	12.68	16.53	-233.14	-24.95	7.81	-235.09	-21.61	7.81			0.96	Hg	2015.000	BBAA	GAIA DR1. M1 and M2 are G-band. PM data calculated from position comparison with SDSS DR9.
	177.6619387	31.7065579	4.588	251.041	12.68	16.53	-230.13	-12.00	10.13	-230.10	-7.95	10.13			0.96	Hg	2015.000	AAAA	GAIA DR1. M1 and M2 are G-band. PM data calculated from position comparison with 2MASS.

Table 1 continues on next page.

CPM Pairs from LSPM so Far Not WDS Listed – Part IV

Table 1 (continued). Research results for potential common proper motion pairs found in the LSPM catalog. Headline object position based on the most precise J2000 coordinates currently available for A (in most cases from the GAIA DR1 catalog)

Name	RA	Dec	Sep	PA	M1	M2	pmRA1	pmDec1	e_pm1	pmRA2	pmDec2	e_pm2	Spc1	Spc2	Ap	Me	Date	CPM Rat	Source/Notes
	177.6616792	31.7067611	4.976	256.401	11.90	15.54									0.61	C	2017.330		iT24 1x300s V-filter. Heavily overlapping star disks. SNR B <10
	177.6617000	31.7067389	4.969	256.737	11.02	14.41							K0-K4	K3-K5	0.61	C	2017.330		iT24 1x300s I-filter. Overlapping star disks. SNR B <20. Spc based on V-I color index
																			Notes: Secondary not identified in GSC 2.3 and WISE, M1 J and K data in WISE appears to be unreliable since it results in a visual equivalent magnitude of 7.136. Only one object identified in URAT1, which doesn't appear to be either component based on URAT1 PM data.
KPP n+15	12 07 03.579	+00 12 51.35			15.36	20.88	-172.32	25.40	6.73	-170.31	19.83	6.73	M2-M4	>M4				AAAA	J1207+0012: Solid CPM candidate.
	181.7677080	0.2137500	6.958	187.431											1.2	Pp	1955.296		POSS I.E estimates.
	181.7657500	0.2142220	7.031	191.070			-165.00	40.00		-175.00	40.00				1.2	Pp	1996.287		POSS II.F estimates. PM estimates based on comparison with POSS I.E.
	181.7658970	0.2140850	7.093	192.456	14.35	18.67									1.2	Pp	1996.290		GSC 2.3. M1 and M2 are GSC 2.3 f.mag values.
	181.7657090	0.2141180	7.358	193.064	15.40	20.30									2.5	Es	1999.221		SDSS DR9. M1 and M2 are gmag+rmag/2 (used when gmag > 15.0).
	181.7656240	0.2141590	7.302	193.543	14.20	17.40									1.3	E2	2000.134		2MASS. M1 and M2 estimated from J- and K-band.
	181.7649125	0.2142639			14.19		-184.20	35.30							0.2	Eu	2000.392		UCAC5 with GAIA coordinates. M1 is UCAC5 Gmag value. Secondary not identified. PmRA1 and pmDec1 are from UCAC5 data.
	181.7656597	0.2141208			14.18		-184.20	35.30							0.2	Eu	2000.392		UCAC5 coordinates used here. M1 is from J and K values. Secondary not identified. PmRA1 and pmDec1 are from UCAC5 data.
	181.7649672	0.2142397	7.347	193.186	15.31	17.38	-173.93	21.37	7.36	-173.19	17.60	7.43			0.2	Eu	2013.659	AAAA	URAT1. M1 is URAT1 Vmag, M2 estimated from URAT1 J and K values. PM data calculated from position comparison with 2MASS.
	181.7649124	0.2142639	7.376	193.167	14.19	18.03	-181.74	33.28	0.17	-182.81	32.37	3.66			0.96	Hg	2015.000	AAAA	GAIA DR1. M1 and M2 are G-band. PM data calculated from position comparison with SDSS DR9.
	181.7649124	0.2142639	7.376	193.167	14.19	18.03	-172.32	25.40	6.73	-170.31	19.83	6.73			0.96	Hg	2015.000	AAAA	GAIA DR1. M1 and M2 are G-band. PM data calculated from position comparison with 2MASS.
	181.7647208	0.2143444	7.077	194.861	15.36	20.88									0.61	C	2017.330		iT24 1x300s V-filter. Barely resolved, SNR B <5
	181.7646417	0.2144056	7.532	188.474	13.15	16.90							M2-M4	>M4	0.61	C	2017.330		iT24 1x300s I-filter. SNR B <20. Spc based on V-I color index
																			Notes: Secondary not identified in WISE.

Table 1 concludes on next page.

CPM Pairs from LSPM so Far Not WDS Listed – Part IV

Table 1 (conclusion). Research results for potential common proper motion pairs found in the LSPM catalog. Headline object position based on the most precise J2000 coordinates currently available for A (in most cases from the GAIA DR1 catalog)

Name	RA	Dec	Sep	PA	M1	M2	pmRA1	pmDec1	e_pm1	pmRA2	pmDec2	e_pm2	Spc1	Spc2	Ap	Me	Date	CPM Rat	Source/Notes
NSN n+15	12 45 22.960	+01 01 04.58			13.15	16.76	-199.25	-20.02	10.19	-189.78	-16.12	10.19	K5-K7	M3->M4				AABA	J1245+0101: Solid CPM candidate.
	191.3487920	1.0182500	5.636	334.802											1.2	Pp	1956.202		POSS I.O estimates.
	191.3462920	1.0182780	5.456	333.908			-211.00	2.00		-211.00	-2.00				1.2	Pp	1996.235		POSS II.N estimates. PM estimates based on comparison with POSS I.O.
	191.3464040	1.0180160	5.650	330.956	13.10	15.40									1.3	E2	2001.048		2MASS. M1 and M2 estimated from J- and K-band.
	191.3461310	1.0179660	5.711	330.967	13.30	16.90									2.5	Es	2006.331		SDSS DR9. M1 and M2 are gmag+rmag/2 (used when gmag > 15.0).
	191.3457369	1.0179475	5.663	331.449	13.14	15.42	-190.81	-19.60	11.29	-189.55	-16.97	11.39	K4-K5		0.2	Eu	2013.578	AABA	URAT1. M1 is URAT1 Vmag, M2 estimated from URAT1 J and K values. Spc1 is URAT1 B-V value (midway between K4 and K5). PM data calculated from position comparison with 2MASS.
	191.3456666	1.0179384	5.694	331.279	12.64	15.56	-192.83	-11.45	11.43	-188.76	-11.41	11.68			0.96	Hg	2015.000	ACBA	GAIA DR1. M1 and M2 are G-band. PM data calculated from position comparison with SDSS DR9.
	191.3456666	1.0179384	5.694	331.279	12.64	15.56	-199.25	-20.02	10.19	-189.78	-16.12	10.19			0.96	Hg	2015.000	AABA	GAIA DR1. M1 and M2 are G-band. PM data calculated from position comparison with 2MASS.
	191.3455083	1.0179639	5.134	333.638	13.15	16.76									0.61	C	2017.305		iT24 1x60s V-filter. SNR B <10
	191.3455500	1.0179222	5.845	332.825	11.79	14.33							K5-K7	M3->M4	0.61	C	2017.305		iT24 1x60s I-filter. Spc based on V-I color index
																			Notes: Secondary not identified in GSC 2.3 and WISE, neither of the components is identified in UCAC5.

CPM Pairs from LSPM so Far Not WDS Listed – Part IV

(Continued from page 368)

search and measurements for these in a separate paper.

References:

Buchheim, R., 2008, "CCD Double-Star Measurements at Altimira Observatory in 2007", *Journal of Double Star Observations*, **4**(1), 28: Formulas for calculating Separation and Position Angle from the RA/ Dec coordinates

Knapp W. and Nanson J., 2017, "A New Concept for Counter-Checking of Assumed CPM Pairs", *JDSO*. **13**(1), 31-51.

Knapp W. and Nanson J., 2017, "CPM Pairs from LSPM so Far Not WDS Listed – Part I", *JDSO*, **13** (2), 140-161.

Knapp W. and Nanson J., 2017, "CPM pairs from LSPM so far not WDS listed – Part II, *JDSO*, **13** (4), 447-464.

Knapp W. and Nanson J., 2017, "CPM pairs from LSPM so far not WDS listed – Part III", JDSO, **13** (4), 538-552.

Acknowledgements:

The following tools and resources have been used for this research:

- Washington Double Star catalog
- 2MASS All Sky catalog
- iTelescope: Images were taken with iT24: 610mm CDK with 3962mm focal length. CCD: FLI-PL09000. Resolution 0.62 arcsec/pixel. V-filter. Located in Auberry. California. Elevation 1405m
- AAVSO APASS
- GAIA DR1 catalog
- UCAC4 catalog
- URAT1 catalog
- WISE catalog
- SDSS catalog
- IGSL catalog
- LSPM catalog
- Aladin Sky Atlas v9.0
- SIMBAD, VizieR
- AstroPlanner V2.2
- NASA/ IPAC Infrared Science Archive
- Astrometrica 4.10.1.432

Appendix A

Description of the CPM assessment scheme according to Knapp/Nanson 2017 with extensions

Four rating factors are used: Proper motion vector direction, proper motion vector length, size of position error in relation to proper motion vector length and relationship of proper motion speed to angular separation:

- Proper motion vector direction ratings: "A" for within the error range of identical direction, "B" for similar direction within the double error range, and "C" for outside
- Proper motion vector length ratings: "A" for within the error range of identical length, "B" for similar length within the double error range, and C for outside
- Error size ratings: "A" for error size of less than 5% of the proper motion vector length, "B" for less than 10%, and "C" for a larger error size
- Relationship PM speed to angular separation: "A" for less than 100 years, "B" for less than 1000 years and "C" for above

To compensate for excessively large position errors resulting in an "A" rating despite rather high deviations an absolute upper limit is applied regardless of calculated error size:

- Proper motion vector direction: Max. 2.86° difference for an "A" and 5.72° for a "B"
- Proper motion vector length: Max. 5% difference for an "A" and 10% for a "B"

In some cases we could use SDSS DR9 coordinates instead of 2MASS with much smaller position errors with the consequence that the requirements to get an A or even B CPM rating were unreasonably hard so we had to modify our process somewhat:

- The position error resulting from the error estimation for proper motion vector direction and length is in this case calculated as root mean square from both position errors (instead of for only the larger 2MASS one)
- If the PM vector direction difference is larger than this calculated "allowed" error but still less than 0.5° then an "A" is given, a "B" is given for larger than 0.5 but less than 1 degree, and a "C" is given if above
- If the PM vector length difference is larger than this calculated "allowed" error but still less than 0.5% then an "A" is given, a "B" is given for larger than 0.5 but less than 1 percent, and a "C" is given if above.

Appendix B

The following Table 2 gives the plate solving errors for the used iT24 images and error information derived therefrom for the measurements provided in Table 1 and also the measured positions for both components:

Table 2. Error estimations for the in table 1 provided measurements for the given objects:
dRA and dDec = average RA and Dec plate solving errors in arcseconds
Err_Sep = separation error estimation in arcseconds calculated as SQRT(dRA^2+dDec^2)
Err_PA = position angle error estimation in degrees calculated as arctan (Err_Sep/Sep) assuming the worst case that Err_Sep points perpendicular to the separation vector
dmag as average mag plate solving error (Vmag for images with made V-filter and Imag for images made with I-filter)
*Err_Mag = magnitude error estimation calculated as SQRT(dVmag^2+(2.5*LOG10(1+1/SNR))^2)*
SNR as signal to noise ratio for the given object

Name		RA	Dec	dRA	dDec	Err Sep	Err PA	Err Mag	SNR	dmag	Date	Notes
J0544+2120	A	05 44 41.215	21 20 51.62	0.080	0.090	0.120	1.138	0.052	76.45	0.050	2017.081	iT24 1x60s V-filter. SNR B <20
	B	05 44 40.893	21 20 47.56					0.112	10.33			
	A	05 44 41.219	21 20 51.56	0.090	0.080	0.120	1.240	0.120	111.16	0.120	2017.081	iT24 1x60s I-filter. Spc based on V-I color index
	B	05 44 40.943	21 20 47.55					0.124	36.62			
J0611+3325	A	06 11 56.172	33 25 43.09	0.130	0.110	-	-	0.101	80.28	0.100	2017.209	iT24 1x300s V-filter. No resolution of B, has to be fainter than 18.5Vmag
	B	-	-					-	-			
	A	06 11 56.185	33 25 43.37	0.110	0.120	0.163	0.758	0.121	98.38	0.120	2017.076	iT24 1x60s I-filter. SNR B <20. Spc based on V-I color index
	B	06 11 56.018	33 25 31.24					0.129	22.43			
J0612+3721	A	06 12 20.416	37 21 06.94	0.120	0.120	0.170	3.361	0.092	58.74	0.090	2017.209	iT24 1x300s V-filter. Heavily overlapping star disks
	B	06 12 20.415	37 21 04.05					0.101	22.94			
	A	06 12 20.444	37 21 06.91	0.110	0.120	0.163	3.006	0.121	86.34	0.120	2017.327	iT24 2x300s I-filter. Touching/ overlapping star disks
	B	06 12 20.447	37 21 03.81					0.121	62.23			
J0638+2255	A	06 38 52.424	22 55 10.67	0.100	0.120	0.156	1.907	0.051	134.58	0.050	2017.209	iT24 1x300s V-filter. Heavily overlapping star disks. SNR B <20
	B	06 38 52.448	22 55 05.99					0.090	14.06			
	A	06 38 52.436	22 55 10.71	0.110	0.110	0.156	1.827	0.111	91.46	0.110	2017.084	iT24 1x180s I-filter. SNR B <20. Heavily overlapping star disks. Spc based on V-I color index
	B	06 38 52.453	22 55 05.84					0.133	14.19			
J0644+2855	A	06 44 39.093	28 55 26.18	0.120	0.120	0.170	1.739	0.061	90.07	0.060	2017.076	iT24 1x60s V-filter
	B	06 44 38.729	28 55 23.28					0.079	20.41			
	A	06 44 39.095	28 55 26.38	0.120	0.110	0.163	1.609	0.121	95.44	0.120	2017.076	iT24 1x60s I-filter. Spc based on V-I color index
	B	06 44 38.730	28 55 23.12					0.125	29.84			
J0646+5214	A	06 46 00.821	52 14 11.26	0.120	0.110	0.163	4.046	0.112	55.65	0.110	2017.209	iT24 1x300s V-filter. Overlapping star disks
	B	06 46 00.812	52 14 13.56					0.112	47.20			
	A	06 46 00.816	52 14 10.88	0.130	0.110	0.170	4.091	0.142	45.61	0.140	2017.209	iT24 1x300s I-filter. Overlapping star disks. Spc based on V-I color index
	B	06 46 00.808	52 14 13.26					0.142	44.37			
J0654+1708	A	06 54 37.540	17 08 03.09	0.110	0.120	0.163	2.474	0.073	50.54	0.070	2017.084	iT24 1x180s V-filter. Touching star disks
	B	06 54 37.572	17 08 06.83					0.084	22.77			
	A	06 54 37.536	17 08 03.27	0.130	0.120	0.177	3.038	0.142	47.80	0.140	2017.076	iT24 1x60s I-filter. Touching star disks. Spc based on V-I color index
	B	06 54 37.569	17 08 06.57					0.145	28.37			

Table 2 continues on next page.

CPM Pairs from LSPM so Far Not WDS Listed – Part IV

Table 2 (continued). Error estimations for the in table 1 provided measurements for the given objects

Name		RA	Dec	dRA	dDec	Err Sep	Err PA	Err Mag	SNR	dmag	Date	Notes
J0659+5631	A	06 59 03.298	56 31 00.32	0.070	0.080	0.106	0.727	0.051	103.84	0.050	2017.209	iT24 1x300s V-filter. SNR B <20
	B	06 59 04.306	56 31 01.12					0.077	17.94			
	A	06 59 03.286	56 31 00.34	0.130	0.110	0.170	1.121	0.112	55.91	0.110	2017.076	iT24 1x60s I-filter. SNR B <20. Spc based on V-I color index
	B	06 59 04.333	56 31 01.16					0.141	11.83			
J0705+3400	A	07 05 26.916	34 00 15.80	0.110	0.090	0.142	1.128	0.051	146.52	0.050	2017.084	iT24 1x180s V-filter. SNR B <20
	B	07 05 27.204	34 00 09.53					0.082	16.27			
	A	07 05 26.905	34 00 15.67	0.100	0.110	0.149	1.335	0.120	184.16	0.120	2017.209	iT24 1x300s I-filter. Touching star disks. SNR B <10. Spc based on V-I color index
	B	07 05 27.149	34 00 10.06					0.256	4.33			
J0721+2555	A	07 21 43.377	25 54 58.82	0.120	0.120	0.170	2.034	0.081	92.85	0.080	2017.084	iT24 1x180s V-filter. Heavily overlapping star disks
	B	07 21 43.731	25 54 58.95					0.088	29.09			
	A	07 21 43.370	25 54 58.89	0.110	0.100	0.149	2.002	0.101	84.89	0.100	2017.076	iT24 1x60s I-filter. Heavily overlapping star disks. Spc based on V-I color index
	B	07 21 43.685	25 54 59.04					0.105	34.76			
J0723+2536	A	07 23 19.999	25 36 09.38	0.120	0.110	0.163	1.800	0.092	61.61	0.090	2017.209	iT24 1x300s V-filter. SNR B <20
	B	07 23 20.223	25 36 13.58					0.134	10.47			
	A	07 23 20.022	25 36 09.66	0.120	0.110	0.163	1.800	0.116	29.57	0.110	2017.076	iT24 1x60s I-filter. SNR B <20. Spc based on V-I color index
	B	07 23 20.252	25 36 13.80					0.134	13.66			
J0730+2716	A	07 30 22.918	27 16 06.68	0.100	0.110	0.149	1.587	0.120	109.56	0.120	2017.075	iT24 1x60s V-filter. SNR B <10. Heavily overlapping star disks
	B	07 30 22.825	27 16 11.90					0.176	7.91			
	A	07 30 22.909	27 16 06.60	0.090	0.080	0.120	1.202	0.120	111.77	0.120	2017.075	iT24 1x60s I-filter. SNR B <10. Heavily overlapping star disks. Spc based on V-I color index
	B	07 30 22.765	27 16 12.01					0.163	9.30			
J0734+2315	A	07 34 25.757	23 15 29.88	0.110	0.100	0.149	1.556	0.058	37.33	0.050	2017.076	iT24 1x60s V-filter. SNR B <10. Identification of B a bit difficult due to a fore- or background star involved
	B	07 34 25.997	23 15 34.24					0.123	9.14			
	A	07 34 25.749	23 15 29.94	0.110	0.110	0.156	1.803	0.121	82.86	0.120	2017.076	iT24 1x60s I-filter. Touching star disks with B obviously optical double. SNR B <20. Spc based on V-I color index
	B	07 34 25.972	23 15 33.81					0.147	12.38			
J0735+4814	A	07 35 26.959	48 14 32.79	0.110	0.110	0.156	0.822	0.050	160.95	0.050	2017.075	iT24 1x60s V-filter
	B	07 35 26.625	48 14 43.11					0.068	23.11			
	A	07 35 26.968	48 14 32.83	0.110	0.110	0.156	0.878	0.130	116.94	0.130	2017.076	iT24 1x60s I-filter. SNR B <20. Spc based on V-I color index
	B	07 35 26.686	48 14 42.58					0.164	10.45			
J0748+3712	A	07 48 35.888	37 12 08.93	0.050	0.060	-	-	0.040	354.40	0.040	2017.209	iT24 1x300s V-filter. No resolution of B
	B	-	-					-	-			
	A	07 48 35.879	37 12 08.88	0.060	0.070	-	-	0.140	307.49	0.140	2017.209	iT24 1x300s I-filter. No resolution of B. Spc based on V-I color index
	B	-	-					-	-			
J0751+4006	A	07 51 01.807	40 06 05.99	0.080	0.110	0.136	1.031	0.043	69.54	0.040	2017.209	iT24 1x300s V-filter
	B	07 51 01.733	40 05 58.48					0.065	20.49			
	A	07 51 01.813	40 06 06.50	0.120	0.110	0.163	1.266	0.132	47.14	0.130	2017.075	iT24 1x60s I-filter. SNR B <20. Spc based on V-I color index
	B	07 51 01.742	40 05 59.18					0.152	13.16			
J0754+1305	A	07 54 04.627	13 05 53.75	0.120	0.110	0.163	0.825	0.074	24.54	0.060	2017.076	iT24 1x60s V-filter. Star disk A overlaps with background star
	B	07 54 04.129	13 05 45.09					0.066	39.55			
	A	07 54 04.715	13 05 52.79	0.120	0.110	0.163	0.795	0.127	25.12	0.120	2017.076	iT24 1x60s I-filter. Star disk A overlaps with background star. Spc based on V-I color index
	B	07 54 04.126	13 05 44.82					0.121	75.13			
J0858+5227	A	08 58 09.974	52 27 14.26	0.100	0.110	0.149	1.522	0.070	21.49	0.050	2017.084	iT24 1x180s V-filter
	B	08 58 09.377	52 27 15.50					0.067	24.24			
	A	08 58 10.025	52 27 14.31	0.120	0.110	0.163	1.628	0.104	39.32	0.100	2017.076	iT24 1x60s I-filter. Spc based on V-I color index
	B	08 58 09.410	52 27 15.41					0.112	20.97			
J0914+1806	A	09 14 44.504	18 06 15.19	0.070	0.080	-	-	0.061	107.01	0.060	2017.210	iT24 1x300s V-filter. No resolution of B, has to be fainter than 19.1Vmag
	B	-	-					-	-			
	A	09 14 44.512	18 06 15.36	0.060	0.090	0.108	0.566	0.100	197.22	0.100	2017.210	iT24 1x300s I-filter. Spc based on V-I color index. Vmag2 estimated 19.2
	B	09 14 45.221	18 06 11.17					0.109	24.36			

Table 2 concludes on next page.

CPM Pairs from LSPM so Far Not WDS Listed – Part IV

Table 2 (conclusion) Error estimations for the in table 1 provided measurements for the given objects

Name		RA	Dec	dRA	dDec	Err Sep	Err PA	Err Mag	SNR	dmag	Date	Notes
J0925+2102	A	09 25 27.680	21 02 30.85	0.060	0.120	-	-	0.031	164.66	0.030	2017.209	iT24 1x300s V-filter. No resolution of B, has to be fainter than 19.5Vmag
	B	-	-					-	-			
	A	09 25 27.680	21 02 31.03	0.070	0.080	0.106	0.352	0.120	240.45	0.120	2017.209	iT24 1x300s I-filter. Spc based on V-I color index. Vmag2 estimated 19.6
	B	09 25 27.989	21 02 47.79					0.124	32.64			
J0947+3820	A	09 47 43.280	38 20 07.72	0.110	0.110	0.156	1.676	0.069	22.41	0.050	2017.084	iT24 1x180s V-filter. SNR B <20
	B	09 47 42.856	38 20 09.56					0.109	10.77			
	A	09 47 43.270	38 20 06.21	0.040	0.010	0.041	0.436	0.131	69.60	0.130	2017.076	iT24 1x60s I-filter. Spc based on V-I color index
	B	09 47 42.835	38 20 08.00					0.132	42.50			
J0954+2427	A	09 54 39.922	24 27 54.12	0.070	0.090	-	-	0.061	20.05	0.030	2017.210	iT24 1x300s V-filter. SNR A <10. No resolution of B, has to be fainter than 19.5Vmag
	B	-	-					-	-			
	A	09 54 39.921	24 27 53.96	0.080	0.090	-	-	0.131	57.69	0.130	2017.210	iT24 1x300s I-filter. No resolution of B, has to be fainter than 18.9 Imag. Spc based on V-I color index
	B	-	-					-	-			
J1001+3627	A	10 01 19.914	36 27 22.43	0.070	0.060	0.092	0.933	0.089	14.17	0.050	2017.081	iT24 1x60s V-filter. SNR A and B <20
	B	10 01 19.987	36 27 28.02					0.093	13.33			
	A	10 01 19.929	36 27 22.25	0.080	0.060	0.100	1.053	0.148	21.73	0.140	2017.081	iT24 1x60s I-filter. Spc based on V-I color index
	B	10 01 19.938	36 27 27.69					0.154	16.43			
J1023+5440	A	10 23 15.554	54 40 06.53	0.080	0.100	0.128	0.823	0.042	92.13	0.040	2017.155	iT24 1x180s V-filter
	B	10 23 14.544	54 40 04.88					0.051	34.32			
	A	10 23 15.555	54 40 06.53	0.110	0.110	0.156	0.992	0.112	55.67	0.110	2017.081	iT24 1x60s I-filter. Spc based on V-I color index
	B	10 23 14.545	54 40 04.55					0.117	26.57			
J1034+0158	A	10 34 49.152	01 58 40.18	0.070	0.080	0.106	0.677	0.062	69.36	0.060	2017.305	iT24 1x60s V-filter
	B	10 34 49.642	01 58 34.98					0.062	73.92			
	A	10 34 49.158	01 58 40.33	0.090	0.110	0.142	0.906	0.130	126.17	0.130	2017.305	iT24 1x60s I-filter. Spc based on V-I color index
	B	10 34 49.645	01 58 35.09					0.130	139.16			
J1111+0221	A	11 11 09.649	02 21 06.59	0.120	0.120	-	-	0.046	47.22	0.040	2017.324	iT24 1x300s V-filter. No resolution of B, has to be fainter than 19.1Vmag
	B	-	-					-	-			
	A	11 11 09.671	02 21 06.17	0.120	0.120	0.170	1.374	0.131	56.67	0.130	2017.324	iT24 1x300s I-filter. Touching star disks. Spc based on V-I color index with Vmag2 assumed 19.2
	B	11 11 09.220	02 21 08.26					0.175	8.81			
J1139+3454	A	11 39 58.101	34 54 20.81	0.090	0.080	0.120	0.848	0.061	85.55	0.060	2017.305	iT24 1x60s V-filter
	B	11 39 58.752	34 54 19.38					0.073	25.84			
	A	11 39 58.088	34 54 20.92	0.080	0.090	0.120	0.833	0.120	165.32	0.120	2017.305	iT24 1x60s I-filter. Spc based on V-I color index
	B	11 39 58.750	34 54 19.40					0.121	75.03			
J1150+3142	A	11 50 38.803	31 42 24.34	0.120	0.120	0.170	1.953	0.130	157.75	0.130	2017.330	iT24 1x300s V-filter. Heavily overlapping star disks. SNR B <10
	B	11 50 38.424	31 42 23.17					0.231	5.21			
	A	11 50 38.808	31 42 24.26	0.110	0.090	0.142	1.638	0.140	106.20	0.140	2017.330	iT24 1x300s I-filter. Overlapping star disks. SNR B <20. Spc based on V-I color index
	B	11 50 38.429	31 42 23.12					0.170	10.69			
J1207+0012	A	12 07 03.533	00 12 51.64	0.120	0.090	0.150	1.214	0.100	123.07	0.100	2017.330	iT24 1x300s V-filter. Barely resolved, SNR B <5
	B	12 07 03.412	00 12 44.80					0.472	1.89			
	A	12 07 03.514	00 12 51.86	0.120	0.100	0.156	1.188	0.150	102.27	0.150	2017.330	iT24 1x300s I-filter. SNR B <20. Spc based on V-I color index
	B	12 07 03.440	00 12 44.41					0.162	17.38			
J1245+0101	A	12 45 22.922	01 01 04.67	0.100	0.100	0.141	1.578	0.061	120.61	0.060	2017.305	iT24 1x60s V-filter. SNR B <10
	B	12 45 22.770	01 01 09.27					0.121	9.88			
	A	12 45 22.932	01 01 04.52	0.080	0.090	0.120	1.180	0.130	194.45	0.130	2017.305	iT24 1x60s I-filter. Spc based on V-I color index
	B	12 45 22.754	01 01 09.72					0.131	59.25			

Counter-Check of 4,937 WDS Objects for Being Physical Double Stars

Wilfried R.A. Knapp

Vienna, Austria
wilfried.knapp@gmail.com

T. V. Bryant III

Little Tycho Observatory
703 McNeill Road, Silver Spring, Md 20910
mainsequence@verizon.net

Abstract: The WDS catalog contains (as of August 2017) more than 20,000 V-coded objects which are considered to be physical pairs because of their common proper motion (CPM) or other attributes. For 4,937 of these objects both components were identified in the UCAC5 catalog and counter-checked with UCAC5 proper motion data using a CPM assessment scheme according to Knapp and Nanson 2017. A surprisingly large number of these pairs seem to be optical rather than physical. Additionally GAIA DR1 positions are given for all components, and precise separation and position angle based on GAIA DR1 coordinates were calculated for all of the 4,937 pair

1. Introduction

The WDS catalog contains (per the August 2017 release) more than 20,000 double stars listed with their V-code declaring them as possibly physical pairs, usually based on assumed common proper motion or other indicators. The most recently available precise proper motion data in the GAIA DR1 catalog allows for a very reliable counter-check of this assumption, but the TGAS subset of GAIA DR1 with only about 2,000,000 stars covers only a small number of the WDS stars. The next reliable source of precise proper motion data we consulted is the UCAC5, as it contains data for more than 100,000,000 stars with data based on reduction of the UCAC images which used the TGAS objects as positional references and compared these positions with those in the GAIA DR1. This gave us a huge increase in the number of objects available to check against the WDS V-code entries.

2. Selection and Identification of the Objects

Given the above, a program to scan the WDS for "V" type objects that were likely to be included in the UCAC5 was written. This program eliminated all pairs whose primary was brighter than 6.0mv (the halation spot on the image being large enough to throw off the scanning software that creates the UCAC5 catalog) or fainter than 16.0mv (the approximate limit of the UCAC5). It also eliminated pairs that were less than 4 arc seconds in separation or greater than 60 arc seconds in separation, as the former are likely to be within the primary's halation spot and the latter are more likely to be optical. Of the 20,000+ "V" pairs listed in the WDS, this program found 6,742 pairs that met these criteria.

A second program was written that takes the 6,742 "V" pairs and tries to find stars in the UCAC5 that correspond to both the primary and secondary of the WDS pair. Of the 6,742 pairs only 4,937 were found that had UCAC5 stars associated with them. The criteria used to select these were:

- The UCAC5 stars could only be brighter than the WDS star by one magnitude, or fainter by two magnitudes.
- The separation of the UCAC5 stars needed to be within 4" of that listed by the WDS's most recent measurement.
- The position angle of the UCAC5 stars needed to be within 4 degrees of that listed by the WDS's most recent measurement.

Similar to visual observations there is the question of possible false positives. We did a counter-check with two different approaches: First we selected the

Counter-Check of 4,937 WDS Objects for Being Physical Double Stars

objects with the largest difference in separation and position angle between WDS and GAIA DR1 as such differences are either the result of very different proper motions as reported by the WDS and UCAC5 or of a misidentification. Second, we ran a program that searched all 4,937 pairs with UCAC5 stars associated with them, looking for objects close to these pairs as potential sources for misidentifications. We then checked these suspect objects manually with the help of Aladin using 2MASS images with WDS and UCAC5 catalog overlays and found a few misidentifications of primaries and secondaries. However, we kept the data set, as the error rate was less than one in a thousand, and further refinement of our search programs would not yield significantly better results. The misidentifications that we found are listed in "Appendix A - Errata" and include the correct data for these objects.

These 4,937 pairs were then analyzed by a spreadsheet that implemented the CPM assessment (see Appendix B) and calculated separation and position angle from the GAIA DR1 positions provided with the UCAC5 data rows.

3. Results

290 objects were found to be listed in the UCAC5 catalog with an unexpected large proper motion error range for at least one component. To avoid questionable CPM ratings we decided to split the results into two subsets to isolate the objects with pm data considered suspect. The spreadsheet with the results is far too large to be given here in print so we list only the first 25 items in table 1 as an example. The full data set with all data for all objects, including content description can be downloaded as spreadsheet from http://www.jdso.org/.

The programs used to find V pairs in the WDS, and then couple those stars with ones in the UCAC5, and then check for misidentifications are posted here: https://sourceforge.net/projects/codefromwdsvsucac5/files/?source=navbar.

The following data are given in Table 1:

- WDS ID
- Name = Discoverer ID
- GAIA DR1 coordinates for the primary (observation epoch 2015)
- Separation and position angle calculated from the GAIA DR1 positions for primary and secondary
- Proper motion vector direction for both components calculated from UCAC5 proper motion data in degrees.
- Proper motion vector length for both components calculated from UCAC5 proper motion data in mas/yr
- CPM rating (see Appendix B)
- Notes with comments.

The full data set available for download also contains additional columns to provide full information on all counter-checked objects.

4. Summary

From 4,937 V-coded WDS objects counter-checked with UCAC5 proper motion data (using the CPM assessment scheme according to Appendix B):

- Only 68 qualified as perfect AAAA CPM candidates with (within the given error range) ident proper motion vector direction and length, a PM error size of less than 5% of the PM vector length and a relationship of angular separation to PM speed of less than 100 years. This means the pair is almost certainly physical.
- 1,880 qualified as solid CPM candidates with (within the given error range) ident proper motion vector direction and length but with minor issues regarding PM error size and relationship of angular separation to PM speed. These are almost certainly physical.
- 1,005 qualified as good CPM candidates with proper motion vector direction and length differences within twice the given error range and with only minor issues regarding their PM error size and relationship of their angular separation to PM speed. Some differences in PM vector length and direction might be caused by an orbit depending on the plane of the orbit with respect to the sky so this class of objects might contain doubles with orbit. Overall there is a good chance that these pairs are physical.
- 168 objects qualified as weak CPM candidates, as they have a rather small probability for being physical.
- 197 objects are probably optical as their proper motion vector is more than twice but less than triple the given error range, as well as showing some PM vector length differences
- 1,329 objects (nearly 30% of the total number) are almost certainly optical pairs. Over 600 of them are UC pairs demonstrating the remarkable change of proper motion data from UCAC4 to UCAC5 by rendering these pairs from "probably physical" based on UCAC4 proper motion data to "almost certainly optical" based on the UCAC5 proper motion data.
- Additionally we have 290 objects with somewhat suspect UCAC5 proper motion data to be considered separately (see Addendum).

We would have expected that all V-coded WDS

(Text continues on page 392)

Table 1. The first 25 objects from the data set

WDS ID	Name	RA A	DE A	GAIA Sep	GAIA PA	PMVD° A	PMVD° B	PMVL A	PMVL B	CPM Rat	Notes
00001-2432	UC 301	0.02117861	-24.52940000	47.024	283.37	231.49	232.05	92.66	89.92	ABAB	Good CPM candidate
00004+3549	CRB 23	0.09759917	35.81139000	37.243	154.53	84.38	84.40	67.42	67.62	AABB	Solid CPM candidate
00006+4539	UC 303	0.14172670	45.65775000	52.176	311.43	79.36	77.91	65.53	69.24	ABBB	Good CPM candidate
00013+0504	UC 304	0.32828920	5.07007700	15.342	53.63	247.39	244.64	67.38	67.95	BAAB	Good CPM candidate
00013+0742	DU 4AB	0.33342190	7.70133900	15.209	264.10	205.54	205.15	80.24	79.76	AAAB	Solid CPM candidate
00020+2347	TVB 2	0.50731720	23.78087000	28.116	292.27	76.57	74.94	27.55	25.79	ABBC	Good CPM candidate
00020+4530	J 864AC	0.50702940	45.52219000	18.012	8.37	20.56	255.00	1.71	10.04	DDDC	Almost certainly optical
00023+1609	BPM 1	0.58341170	16.14635000	30.686	185.11	168.27	104.44	5.41	20.86	DDDC	Almost certainly optical
00029-7436	BVD 30AB,C	0.71324250	-74.59810000	37.832	11.44	172.63	152.18	67.86	59.14	DDAB	Almost certainly optical
00042+3732	UC 310	1.04570400	37.53939000	30.980	14.80	76.06	88.31	72.23	64.43	DCAB	Almost certainly optical
00043-4304	UC 311	1.07507200	-43.07456000	8.686	141.95	54.01	55.37	74.03	74.26	AAAB	Solid CPM candidate
00047+4049	UC 312	1.18156600	40.81849000	39.448	157.18	97.99	101.85	47.46	54.05	BCAB	Weak CPM candidate
00049-1811	UC 313	1.23707800	-18.17912000	18.133	239.72	191.08	191.42	96.29	96.00	AAAB	Solid CPM candidate
00053-0523	UC 315	1.32045300	-5.37600800	19.679	257.19	203.84	208.22	66.80	65.14	BABB	Good CPM candidate
00053-1857	UC 316	1.31539700	-18.95130000	25.494	278.04	35.31	50.47	63.84	46.03	DDBB	Almost certainly optical
00063+6851	CBL 559	1.58039100	68.85215000	19.432	209.67	92.65	95.48	58.46	57.56	AAAB	Solid CPM candidate
00070-1837	UC 322	1.73973600	-18.61536000	44.707	63.35	211.58	211.42	71.60	73.47	AAAB	Solid CPM candidate
00081+2029	AZC 2	2.02307600	20.47806000	25.761	146.83	106.95	106.01	86.45	83.02	AAAB	Solid CPM candidate
00085-0419	UC 324BC	2.14046700	-4.29685400	53.485	117.77	103.12	102.15	62.12	64.14	AABB	Solid CPM candidate
00091-5649	UC 327	2.27667000	-56.80847000	44.487	181.99	102.04	102.31	67.59	70.83	ABAB	Good CPM candidate
00092+3201	UC 328	2.30533600	32.01432000	9.955	172.25	243.01	237.65	65.65	60.37	BBBB	Good CPM candidate
00093+2517	GIC 2AB	2.31640300	25.28135000	29.602	237.15	131.84	130.82	230.87	223.33	BCAB	Weak CPM candidate
00099+0827	STF 4	2.46544400	8.45311900	5.232	275.69	103.17	101.52	59.26	65.62	ACBA	Weak CPM candidate
00100-5028	CBL 561	2.50342600	-50.47068000	21.011	83.90	240.87	238.52	149.97	152.43	BAAB	Good CPM candidate
00105+4524	CBL 1	2.62025200	45.39443000	22.982	229.57	323.13	322.85	85.00	86.94	AAAB	Solid CPM candidate

objects show significantly large proper motion but 260 from the 1,526 objects rated as probably or most certainly optical are listed in the UCAC5 catalog for both components with proper motion values far too small to allow for an assessment as “common”. As a threshold we used the root mean square over all e_pm values larger than 30% of the proper motion vector length of both components - this means that the given proper motion values are insignificant in comparison with the large proper motion error range. In some cases the UCAC5 proper motion errors are even larger than the proper motion values themselves.

This result shows the need for a critical CPM assessment of the remaining ~16,000 WDS objects not covered by our report. If our sample is representative, then there are about 5,000 V-coded objects that are probably optical pairs.

References

Buchheim, Robert, 2008, “CCD Double-Star Measurements at Altimira Observatory in 2007”, *Journal of Double Star Observations*, **4**(1), 28: Formulas for calculating separation and position angle from RA and Dec coordinates and proper motion vector direction and length from proper motion data

Knapp, Wilfried R.A. and Nanson, John, 2017, “A New Concept for Counter-Checking of Assumed CPM Pairs, *JDSO*, **13**(2), 139.

Hartkopf, William I., Mason, Brian D., Finch, Charlie T., Zacharias, Norbert, Wycoff, Gary L. and Hsu, Danley, 2013, “Double Stars in the USNO CCD Astrographic Catalog”, *The Astronomical Journal*, **146**:76 (8pp).

Gavras, P., Sinachopoulos; D., Le Campion, J.F. and Ducourant, C. – The CPMDS catalogue of common proper motion double stars in the Bordeaux Carte du Ciel zone, Astronomy & Astrophysics 521, A4

Acknowledgements

The following tools and resources have been used

Appendix A - Errata:

Checking about 50 of the most suspect objects regarding identification with unusual large difference in separation or position angle compared with the WDS catalog we found the following errors in the data set:

Table 2. Errors found in the data set

WDS ID	Name	RA A	DE A	RA B	DE B	CPM Rat	Notes	Error
15079-4019	UC 2935	226.980500	-40.319590	226.960600	-40.320340	DDDC	Almost certainly optical	Wrong secondary
09024+1226	GWP 1131	135.599300	12.432740	135.605800	12.434150	DADB	Almost certainly optical	Wrong secondary
17197-8520	UC 3324	259.912700	-85.337790	259.832700	-85.339490	DDDB	Almost certainly optical	Wrong secondary
17329-0129	UC 3366AC	263.225800	-1.490887	263.224900	-1.504463	DDDC	Almost certainly optical	Wrong primary

Table 3. Correct data for objects listed in Table 1.

Name	RA	Dec	Sep "	PA °	M1(G)	M2(G)	pmRA1	pmDec1	e_pm1	pmRA2	pmDec2	e_pm2	Ap	Me	Date	CPM Rat	Source/Notes
UC 2935	226.9805089	-40.3195914	58.545	268.682	15.855	16.049	-35.80	-11.20	5.445	-19.20	-7.90	11.322	0.96	Hg	2015	BCCC	GAIA DR1. M1 and M2 GAIA DR1 Gmag. PM data from UCAC5 catalog
GWP 1131	135.5992506	12.4327389	26.345	80.871	12.432	15.705	14.70	-47.50	1.414	32.20	-49.50	30.689	0.96	Hg	2015	CCCB	GAIA DR1. M1 and M2 GAIA DR1 Gmag. PM data from UCAC5 catalog
UC 3324	259.9127372	-85.3377903	25.788	263.364	14.016	16.119	-31.00	22.60	1.838	9.90	9.60	10.615	0.96	Hg	2015	CCCC	GAIA DR1. M1 and M2 GAIA DR1 Gmag. PM data from UCAC5 catalog
UC 3366AC	263.2254975	-1.4901794	51.462	182.249	10.298	15.138	-62.30	-4.00	1.414	-2.70	-4.40	3.471	0.96	Hg	2015	CCCC	GAIA DR1. M1 and M2 GAIA DR1 Gmag. PM data from UCAC5 catalog

Counter-Check of 4,937 WDS Objects for Being Physical Double Stars

The AB pair of UC3366 is J 453, obviously a good CPM candidate:

Table 4. Data for J 435

Name	RA	Dec	Sep "	PA °	M1(G)	M2(G)	pmRA1	pmDec1	e_pm1	pmRA2	pmDec2	e_pm2	Ap	Me	Date	CPM Rat	Source/Notes
J 453 AB	263.2254975	-1.4901794	2.789	155.933	10.298	10.761	-62.30	-4.00	1.414	-66.70	-5.80	3.536	0.96	Hg	2015	ABBA	GAIA DR1. M1 and M2 GAIA DR1 Gmag. PM data from UCAC5 catalog

It is remarkable that the errors found did not have a real impact on the CPM rating of the objects in question. A few more errors might still exist but we would not expect them to be more than one or two if any. On the other hand we found several UC objects from Hartkopf et al. 2013 as well as one BPM object from Gavras et al. 2010 with incorrect or at least unclear positions for the primary or secondary caused by very close objects covered by the data range between first and last observation:

Table 5. Data for correctly identified WDS objects with questionable data.

WDS ID	Name	RA A	DE A	RA B	DE B	CPM Rat	Notes	Error
07599-7511	UC 1632	119.9753	-75.18118	119.9733	-75.18758	DADB	Almost certainly optical	Correctly identified according to WDS, but most probably WDS error for primary - see difference first/last observation
14574-3908	UC 2879	224.3548	-39.13891	224.3479	-39,14464	DDDC	Almost certainly optical	Correctly identified according to WDS, but most probably WDS error for primary - see difference first/last observation
18375-4736	UC 3627	279.3780	-47.5943	279.3886	-47.60707	DDDC	Almost certainly optical	Correctly identified according to WDS, but most probably WDS error for primary - see difference first/last observation
15314-2908	UC 3020	232.8475	-29.14083	232.8366	-29.14693	DDCB	Almost certainly optical	Correctly identified according to WDS, but most probably WDS error for secondary - see difference first/last observation
18349-4746	UC 3617	278.7222	-47.7727	278,7324	-47.78019	DDDC	Almost certainly optical	Correctly identified according to WDS, but most probably WDS error for primary - see difference first/last observation
19400+1542	BPM1269	295.0003	15.70334	294,9916	15.69306	DDDC	Almost certainly optical	Correctly identified according to WDS, but most probably WDS error for secondary - see difference first/last observation

To avoid such unclear situations we suggest that the nearby objects be included in the WDS catalog as additional components of these objects, even if they are only optical.

As a side effect of our error search we found the primary of UC 3020 to be a common proper motion pair:

Table 6. Data for a newly detected CPM pair

Name	RA	Dec	Sep "	PA °	M1(G)	M2 (G)	pmRA1	pmDec1	e_pm 1	pmRA2	pmDec2	e_pm2	Ap	Me	Date	CPM Rat	Source/Notes
UC 3020 Aa/Ab	232.8474981	-29.1408275	3.093	267.445	12.062	13.928	-47.30	-45.70	1.345	-51.30	-45.30	3.607	0.96	Hg	2015.000	AABA	GAIA DR1. M1 and M2 GAIA DR1 Gmag. PM data from UCAC5 catalog
	232.8477345	-29.1406278	3.030	267.255									0.20	Eu	1999.270		UCAC5

Appendix B - Description of the CPM Rating Procedure

Four rating factors are used: Proper motion vector direction, proper motion vector length, size of the position error in relation to the proper motion vector length according to Knapp and Nanson, with an extension for relating separation to proper motion speed

- Proper motion vector direction ratings: “A” for identical direction within the error range (calculated by assuming the worst case of the position error pointing in the right angle to the PM vector), “B” for similar direction within the double error range, “C” for similar direction within the triple error range, and “D” for outside the triple error range.
- Proper motion vector length ratings: “A” for identical length within the error range (calculated by assuming the worst case of the position error pointing in the direction of the PM vector), “B” for similar length within the double error range, “C” for similar length within the triple error range, and “D” for errors outside of this.
- Error size ratings: “A” for an error size of less than 5% of the proper motion vector length, “B” for less than 10%, “C” for less than 15%, and “D” for an error size larger than 15%.
- Relation of separation to proper motion speed: "A" for less than 100 years, "B" for less than 1,000 years, "C" for less than 10,000 years and "D" for greater than 10.000 years.

To compensate for excessively large position errors resulting in an “A” rating despite high deviations proper motion direction and/or angle, an absolute upper limit is applied regardless of the calculated error size:

- Proper motion vector direction: Upper limit 2.86° difference for an “A”.
- Proper motion vector length: Upper limit 5% difference for an “A”.

Addendum Regarding UCAC5 Proper Motion Data

After finishing the first draft of this report we became aware of a reasonably large number of UCAC5 objects identified with WDS binaries having a surprisingly large proper motion error range making CPM assessment with UCAC5 proper motion data less reliable than assumed. While most UCAC5 objects are listed with e_pm values around 2mas/yr some are listed with a tenfold or even higher error size. These were initially considered as rare outliers but with more detailed checking it became clear that the number of such objects is larger than assumed. This is somewhat surprising as the UCAC5 data is based on re-reduction of UCAC image data with TGAS reference stars and the proper motion data is calculated by comparing UCAC5 and GAIA DR1 positions – this setup suggests a very high data quality. But as proper motion data calculated from comparison of 2MASS to GAIA DR1 positions is in many cases within an e_pm range of less than 6mas all UCAC5 objects with e_pm larger than that are to be viewed with caution.

As an example of this we checked a small sample of our data in Table 1 in detail.

Table 7: Counter-check UCAC5 based CPM rating for some of the objects with RMS e_pm larger than 12mas

					Rating with UCAC5		Rating with 2MASS to GAIA DR1	
Name	**RA A**	**DE A**	**Sep**	**PA**	**CPM Rat**	**Notes**	**CPM Rat**	**Notes**
UC 317	1.39717000	-47.5694100	10.564	176.88	DDCB	Almost certainly optical	CBBB	Probably optical
MRI 53	1.68339000	57.27257000	6.624	307.50	BACB	Good CPM candidate	AABB	Solid CPM candidate
UC 329	2.33485900	-41.5343300	31.526	326.12	DDCB	Almost certainly optical	CACB	Probably optical
UC 3968	292.969700	52.01293000	11.412	159.54	DBDB	Almost certainly optical	CCCC	Almost certainly optical
GRV1087	200.531300	67.81200000	28.268	8.30	BDCB	Almost certainly optical	AABC	Solid CPM candidate
GWP2029	202.026600	16.31330000	10.401	265.24	DDCB	Almost certainly optical	CBBB	Probably optical

This comparison shows that in most cases the difference in the CPM assessment might be minor but that there are also a few cases with very different results. For example we have changed an “Almost certainly optical” designation to “Solid CPM candidate”. These counter-checks are easily done manually for a few pairs, but this is impracticable for larger data sets. The only solution for this current work is to simply eliminate such suspect objects from the data set and postpone for these objects the CPM assessment for a subsequent paper probably based on GAIA DR2 proper motion data.

TYC 5780-308-1 Discovery of Stellar Duplicity During Asteroidal Occultation by (834) Burnhamia

Brad Timerson, IOTA North American Coordinator

T. George, IOTA Analyst

Ted Blank, Paul Maley, Steve Messner, John Moore, observers

Abstract: An occultation of TYC 5780-308-1 by the asteroid (834) Burnhamia on August 23, 2017 (UT) showed this star to be a double star. Both components of the double star were occulted as recorded by four observers. The separation of the two components is 0.0143 ± 0.0004 arcseconds at a position angle of 73.8 ± 2.7 degrees. The magnitude of the primary component is estimated to be 9.8 +/- 0.03 (Tycho2 VT). The magnitude of the secondary component is estimated to be 9.92 +/- 0.03 (Tycho2 VT).

Observation

On August 23, 2017 (UT), four observers occupying or operating sites across the United States observed the asteroid (834) Burnhamia occult the star TYC 5780-308-1. See Figure 1 for the path map of the event. All four sites observed two step events. All recorded occultation times and data from the observers can be found in archived IOTA records for the event. The observations were made by the observers located at the sites and with the equipment shown in Table 1.

The target star is magnitude 9.103 (Tycho2 VT). This magnitude is derived from the Tycho system magnitude VT given in the Tycho-2 Catalogue contained in the VizieR database [1]. The asteroid magnitude as predicted by the Minor Planet Center as reported in Occult4 [2] was 13.1 (V). The combined magnitude of the asteroid and the star was calculated to be 9.08 (using both Tycho2 VT and MPC V). The expected magnitude drop at occultation was calculated to be 4.02 magnitudes. The star is not listed in the Washington Double Star Catalog. The star is listed the Fourth Catalog of Interferometric Measurements of Binary Stars [3]. The data from that inquiry are shown in Table 2 [headings were derived from format descriptions].

Analysis

The observations were analysed in the standard manner described by IOTA [4].

The finished plot of the double star fit to the data is shown in Figure 6. The double star has a separation of 0.0143 ± 0.0004 arcseconds at a position angle of 73.8 ± 2.7 degrees.

Of the data sets that recorded the occultation, Blank

Table 1. Observers, site locations, equipment, methods, and results

Chords	Observer(s)	City/ Location	State	Country	Telescope Type	Telescope Dia (cm)	Method	Result
1,2	S Messner	Big Lake	MO	USA			Video+GPS Time Inst	Two Events
3,4	P Maley	Hiawatha	KS	USA	Ref	8	Video+GPS Time Inst	Two Events
5,6	J Moore	Turpin	OK	USA			Video+GPS Time Inst	Two Events
8,9	T Blank	Tipton	IA	USA			Video+GPS Time Inst	Two Events

TYC 5780-308-1 Discovery of Stellar Duplicity During Asteroidal Occultation by (834) Burnhamia

Table 2

211225.82-114906.7 BD-125932 SAO 164213 HD 201827 TYC 5780 0308 1 21124-1149								
Observation Date	**PA (deg)**	**Separation (as)**	**Sep. Error (as)**	**Filters (nm)**	**Telescope Aperture (m)**	**Num. Obs.**	**Orig. Ref. Code**	**Tech Code**
1974.7384	V45.1					1	Bvr1979b	O
1975.7153	V302.3	0.003	0.003	430		1	Afr1976	O
1994.8671		<0.038		558	3.6	1	Msn1996b	Sc

Table 3

Observer	Baseline	1st Drop	Bottom	1st Reapp	Baseline
Blank	181.56	100.54	4.77	86.66	183.07
Maley	115.14	47.73	2.75	44.4	114.98
Maley Normalized	181.56	75.26	4.34	70.01	181.31
Average	181.56	87.90	4.55	78.34	182.19

Table 4

Observer	Magnitude Change				Total Magnitude Change	
	1st D	2nd D	1st R	2nd R		
Blank	0.64	3.31	3.15	0.81	3.95	3.96
Maley	0.96	3.10	3.02	1.03	4.05	4.05
Average	0.80	3.20	3.09	0.92	4.00	4.01

and Maley recorded video without saturated stars. Therefore, the Blank and Maley events were suitable for calculating the stellar component magnitudes. The original videos for both observers were recorded with cameras using 0.45 gamma brightness compensation. This makes dim objects brighter and bright objects dimmer. This also affects the linearity of the light curve which also affects the magnitudes derived from the data. As a result, both videos were processed with inverse gamma correction to make the resulting light curve linear [5, 6]. Using the light curve data from these two observers, the magnitude drops of the two events were calculated using the brightness measurements derived by R-OTE [7], the Magnitude calculator routine in Occult4[2] (Method 3 – Magnitudes from light curve values), the combined VT magnitude from the Tycho-2 Catalogue and the predicted V magnitude of the asteroid as explained above. The results are shown in Table 3 and Table 4. Note that the measured brightness are ADU[†] values with no filters. The assumption is they are not much different from those in VT in calculating the magnitude of each component of the double star.

Magnitude Drops from R-OTE analysis

Based on the total magnitude drop estimates for the two components shown in Table 4, the average magnitude drop measured by both observers is within 0.015 of the predicted magnitude drop. This is excellent agreement from both observer light curves.

The magnitudes of the two component stars were derived by inputting the 'average' ADU brightness values into the Occult4 Magnitude Calculator. The results of this analysis are shown in Table 5.

The magnitudes of the two stars are estimated to be 9.8 ± 0.03 (VT) primary star and 9.92 ± 0.03 (VT) secondary star, and their magnitude difference is estimated to be 0.12 ± 0.04 (VT). The event was a BABA, with the secondary occulted first, then the primary, then the secondary reappearing and then the primary.

Based on the data presented in this report, the double star characteristics as shown in the plot in Figure 6 are shown in Table 6

† Analog-to-Digital-Unit – the digital equivalent of the brightness of the analog star on the video screen as process through Limovie.

Table 5. Occult4 Analysis of Average Brightness Changes

Assuming:
* a combined magnitude of 9.10
*Light levels at D of 182 => 88 => 5
Magnitudes for sequence B-A-B-A:
Mag B = 9.92, Mag A = 9.80

(Text continues on page 400)

TYC 5780-308-1 Discovery of Stellar Duplicity During Asteroidal Occultation by (834) Burnhamia

Table 6. Double Star Characteristics

Star	TYC 5780-308-1 SAO 164213 GaiaSrc6892019327085654272 2UCAC 27763256 3UC 157-284904 UCAC4 391-130067 UCAC5 6892019327085654272 URAT1 391-172137 PPMXL 1310283915415980810 000 PPMX 211225.8-114906 NOMAD1 0781-0799491 Spectral type G
Coordinates (UCAC5)	RA 21h 12m 25.8435s Dec -11d 49m 7.219s Current Epoch 2017.64)
Mag A	9.8 ± 0.03
Mag B	9.92 ± 0.03
Mag Difference	0.12 ± 0.04
Separation	0.0143 ± 0.0004 arcseconds
Position Angle	73.8 ± 2.7 degrees

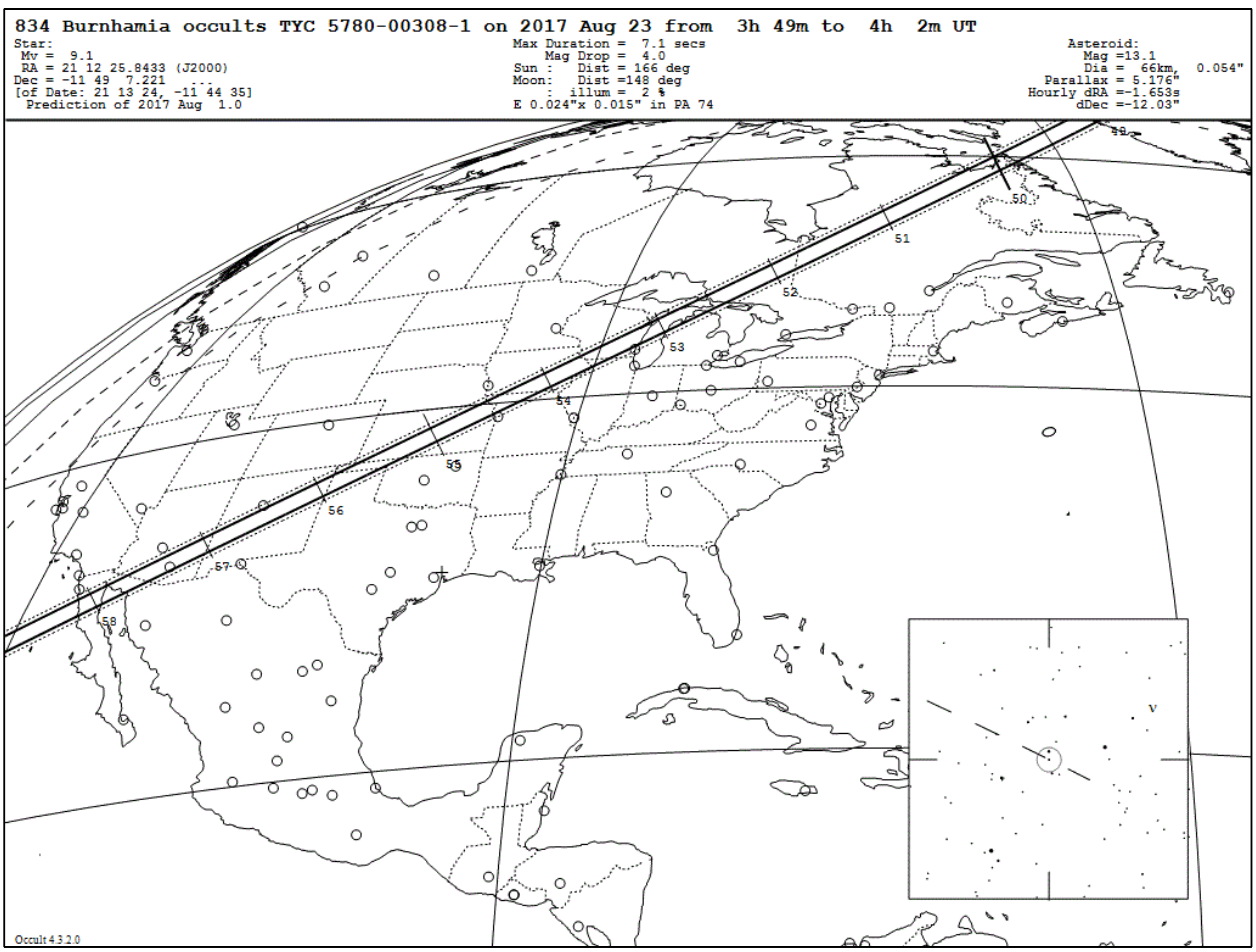

Figure 1. Occultation Path

TYC 5780-308-1 Discovery of Stellar Duplicity During Asteroidal Occultation by (834) Burnhamia

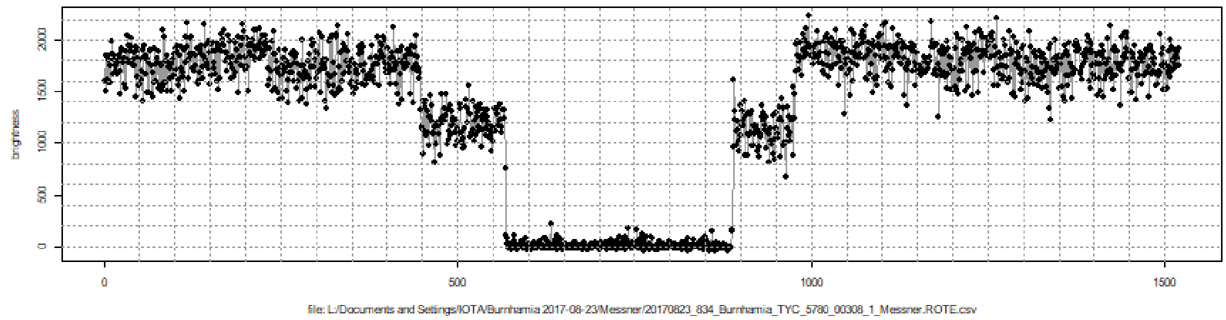

Figure 2. S. Messner light curve. Star was saturated, causing brightness fluctuations in the baseline and abnormal noise in the event bottom. Figure 2 – S. Messner light curve. Star was saturated, causing brightness fluctuations in the baseline and abnormal noise in the event bottom. Figure 2 – S. Messner light curve. Star was saturated, causing brightness fluctuations in the baseline and abnormal noise in the event bottom.

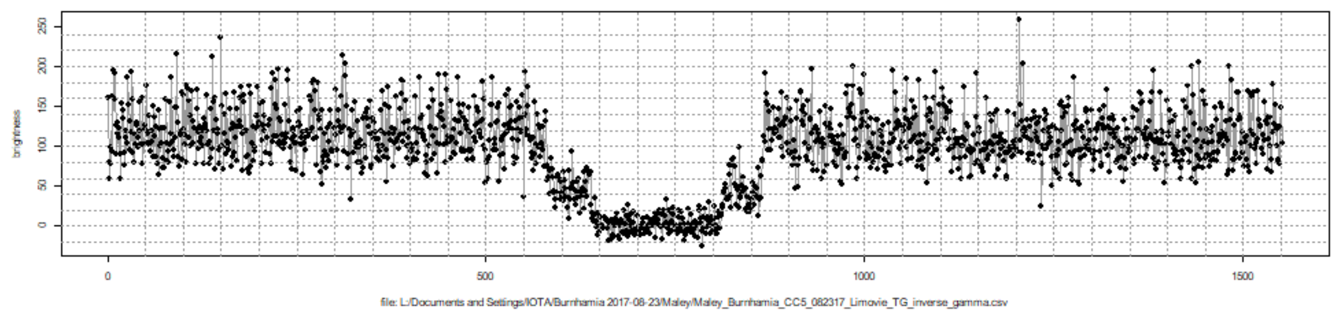

Figure 3. P. Maley light curve. Star was not saturated. Light curve is inverse gamma corrected. First step down is brighter than third step up. Noise in baseline and event bottom is normally distributed.

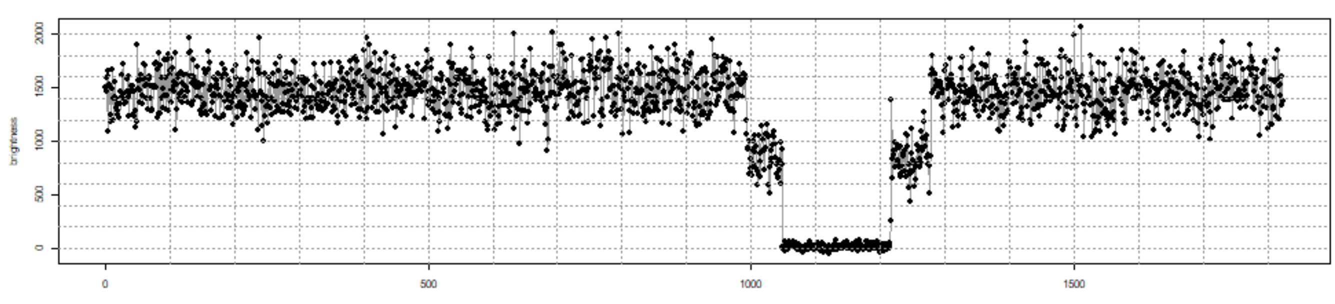

Figure 4. J. Moore light curve. Star was saturated, causing brightness fluctuations in the baseline and abnormal noise in the event bottom.

TYC 5780-308-1 Discovery of Stellar Duplicity During Asteroidal Occultation by (834) Burnhamia

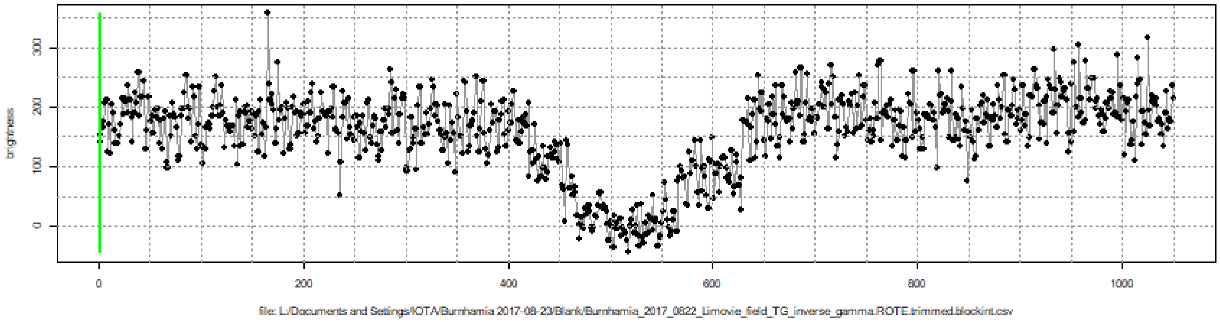

Figure 5. T. Blank light curve. Star was not saturated. Light curve is inverse gamma corrected. First step down is brighter than third step up. Noise in baseline and event bottom is normally distributed.

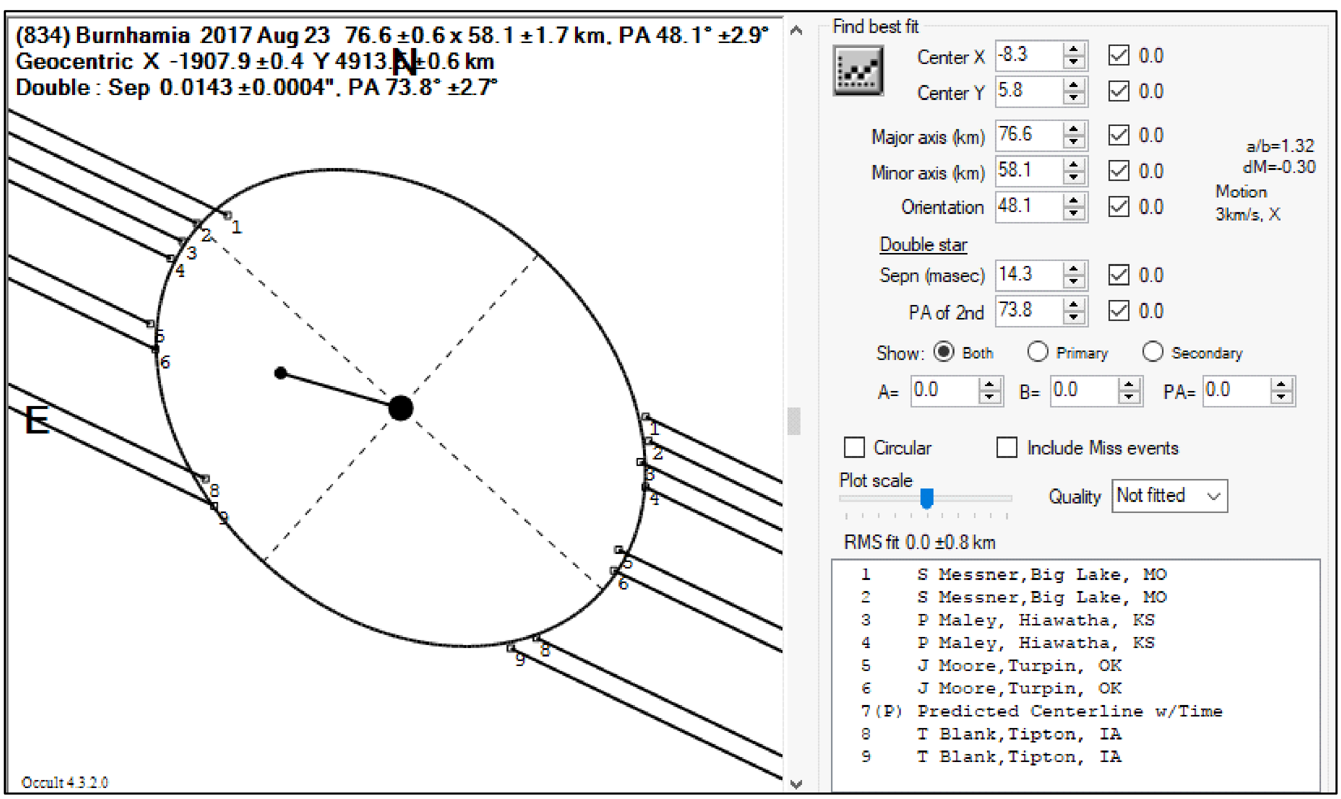

Figure 6. Occultation of TYC 5780-308-1 by (834) Burnhamia

TYC 5780-308-1 Discovery of Stellar Duplicity During Asteroidal Occultation by (834) Burnhamia

(Continued from page 396)

References

1. Ochsenbein F., Bauer P., Marcout J., *A&AS*, **143**, 221, 2000.
2. Occult v4.1.0. Occultation prediction software by David Herald, http://www.lunar-occultations.com/iota/occult4.htm
3. Hartkopf, W.I., Mason, B.D., Wycoff, G.L., & McAlister, H.A. 2001b, "Fourth Catalog of Interferometric Measurements of Binary Stars", http://www.ad.usno.navy.mil/wds/int4.html.
4. Herald, Dave, et al., "New Double Stars from Asteroidal Occultations, 1971 – 2008", *Journal of Double Star Observations*, **6**(1), 88-96, 2010.
5. RunCam Night Eagle Astro Edition linearity analysis using ArtStar by Bob Anderson.
6. Limovie (Light Measurement tool for Occultation observation using Video recorder) [Limovie 0.9.98.21], Kazuhisa Miyashita, Japan.
7. ROTE – R-Code Occultation Timing Extractor – Presentation at the 2013 Annual IOTA Meeting, October 4-6, 2013; Toronto, Ontario, Canada. http://www.asteroidoccultation.com/observations/NA/2013Meeting/R-OTE%202013%20IOTA%20Conference.pdf

Journal of Double Star Observations

April 1, 2018
Volume 14, Number 2

The Journal of Double Star Observations (ISSN 2572-4436) is an electronic journal published quarterly. Copies can be freely downloaded from http://www.jdso.org.

Questions, comments, or submissions may be directed to rclark@southalabama.edu or to rmollise@bellsouth.net

The *Journal of Double Star Observations* (*JDSO*) publishes articles on any and all aspects of astronomy involving double and binary stars. The *JDSO* is especially interested in observations made by amateur astronomers. Submitted articles announcing measurements, discoveries, or conclusions about double or binary stars may undergo a peer review. This means that a paper submitted by an amateur astronomer will be reviewed by other amateur astronomers doing similar work.

Submitted manuscripts must be original, unpublished material and written in English. They should contain an abstract and a short description or biography (2 or 3 sentences) of the author(s). For more information about format of submitted articles, please see our web site at http://www.jdso.org

Submissions should be made electronically via e-mail to rclark@southalabama.edu or to rmolise@bellsouth.net. Articles should be attached to the email in Microsoft Word, Word Perfect, Open Office, or text format. All images should be in jpg or fits format.